Seismic stratigraphy of the offshore basins of Argentina : characterization and modeling of the South Atlantic passive margin dynamics

Juan Pablo Lovecchio

Universidad de Buenos Aires

Sorbonne Université

Ecole doctorale 398 : Géosciences, Ressources Naturelles et Environnement

IFP Energies Nouvelles: Direction Géosciences

Seismic stratigraphy of the offshore basins of Argentina: characterization and modeling of the South Atlantic passive margin dynamics

"Estratigrafía sísmica de las cuencas costa afuera de Argentina: caracterización y modelado de la dinámica de los márgenes pasivos del Atlántico Sur"

Juan Pablo Lovecchio

Thèse de doctorat de Géologie

Tesis para optar por el título de Doctor en Geología de la Universidad de Buenos Aires

Sous la direction de :

Dr. Philippe Joseph	IFP Energies Nouvelles	Directeur de Thèse
Dr. Víctor A. Ramos	IDEAN, UBA-CONICET	Directeur de Thèse
Dr. Sébastien Rohais	IFP Energies Nouvelles	Promoteur de Thèse

Présentée et soutenue publiquement le 10 Décembre 2018

Devant un jury composé de :

Dr. Sierd Cloetingh	Professeur	Rapporteur
Dr. Dominique Frizon de Lamotte	Professeur	Rapporteur
Dr. Loïc Labrousse	Professeur	Examinateur
Dr. Ernesto Cristallini	Professeur	Examinateur
Dr. Vitor Abreu	Professeur	Examinateur
Dr. Philippe Joseph	Professeur	Directeur de Thèse
Dr. Víctor A. Ramos	Professeur	Directeur de Thèse
Dr. Sébastien Rohais	Ingénieur	Promoteur de Thèse

A mis viejos

que me bancan en todas,

siempre.

A mi abuela querida

que me cuida desde arriba.

Acknowledgements

This project would not have been possible without Sébastien, who put together the pieces to make the engine work and walked with me through these four years of reading, learning, working, thinking, discussing, writing and drawing. Merci Séb for sharing your ideas, and triggering the wright discussions; your capacity to see the little details that turn the geology upside down is a great strength I wish to continue to learn from.

Victor and Philippe, thank you for your continuous presence and support and for all your dedication during the last month of corrections of the manuscript. Victor I enjoyed our discussions and your huge knowledge of the geology of South America that we tried to fit in our models. You helped me a lot with all the UBA paperwork and procedures and I could not have done this cotutelle without your help. Philippe thank you for your help with the strati seq, your meticulous corrections on the manuscript (you find errors nobody see). Your concern on the evolution of the project allowed us to finish just in time.

Projects are not possible without sponsors, and this one would not have been possible without YPF. Ricardo Veiga was my boss when we started to discuss this project in 2013. Carlos Colo, who promoted the continuous formation and technical development of the staff, supported this project with the signature of the agreement with IFPEN. Gracias. Néstor Bolatti was key in the development of the whole project. As the Offshore Exploration Manager he continuously supported me and this study, and promoted many of the tasks that are now part of this thesis. Gracias Néstor. Claudio Haring, Executive Exploration Manager, supported me and this project in front of the hierarchy throughout these years and assured the accomplishment of this thesis. Gracias Claudio. Ignacio Brisson has been my boss during this last year, but has been my mentor since my first days in YPF. I always enjoy our unconventional discussions that give sense to many non-sense things. Finally, my trips to France would not have been possible without the continuous assistance of Silvita and Amanda. Thank you for making the machinery work and sorry for the endless expenses sheets.

Guadalupe Hernández-Fuda helped me geopositioning many structural maps and digitalizing uncountable faults. Viviana and Daniela where key for scanning and describing the thin sections of the Malvinas basin. Our last minute whatsapp communication from Avellaneda to Paris was very important to close he Malvinas chapter. We spend many, many days working

on Opendtect with David Epelboim from Geoinfo. We sorted many hardware, software, and workflow problems to try to build wheeler charts. Thank you David for your patience.

I also want to thank my colleagues at YPF that collaborates is some of the side projects, the Offshore Team in YPF: Ricardo, Pedro, Eric, Gonzalo, Sebastián and David; and the Y-TEC Team: Diana, Gladys, Juan, Guillermo, Eli, Daniel, Luciana, Lydia, Leo and Beto, among others. At IFPEN, my work would not have been possible without the help of the secretaries Odile et Djamela who helped me filling la feuille de temps. Merci.

Finally, and more important, I could not have accomplished this goal without the support of my family and friends. Gracias a todos.

Abstract

The multi-stage character of rifting observed in the evolution of the Mesozoic extensional basins offshore Argentina was integrated into a more regional framework of Gondwana, with a review of the chronology of rifting of the main Mesozoic basins in southern South America and Africa. The focus of the study was placed on the pre-Cretaceous rifting events that ended with the Early Cretaceous opening of the South Atlantic Ocean.

Three independent rifting events were identified in the Colorado/Salado basins area. A first rifting event was associated with the Late Triassic-Early Jurassic extensional reactivation of Late Paleozoic thrusts of the Ventania-Cape fold belt. This first set of faults is transected by a new set related to the main depocenters of the Colorado and the adjacent Salado basin. The second and main rifting stage is correlated with the Early-Middle Jurassic Karoo rifting. In the Early Cretaceous, WNW-ESE oriented extension produced a new rifting setting, emplacement of SDRs and finished with the South Atlantic breakup.

Further South, in the Malvinas basin, two rifting events were recognized and seismically characterized, and the synrift units were dated using U-Pb in zircon. The oldest rifting event was dated Late Triassic, while the second and main rifting event was dated Middle Jurassic and correlated to the Chon Aike magmatic province.

The post-breakup evolution of the Argentinean South Atlantic margin (Rawson-Colorado-Salado area) was also studied. Seismic stratigraphic characterization was carried out, with the preparation of chronostratigraphic charts and isopach maps. Three stages of drift evolution were identified. The first drift stage starts with the Late Hauterivian/Barremian breakup and lasts until the Top Cretaceous. Subsidence during this stage is conditioned by the thermal sagging over the main depocenters, which remained disconnected. With the Maastrichtian-Danian regional transgression, as the basement highs between basins are flooded, the margin becomes a single continental platform. The Paleogene drift stage two is characterized by subsidence and sedimentary input centered in the Salado area. The Rawson and southern Colorado area act as a high. Finally, during the Neogene, drift stage three is characterized by increased cylindrical subsidence (possibly related to Andean dynamic processes) and the remarkable interaction of contour currents (after the Drake Passage opening).

Resumen

Estratigrafía sísmica de las cuencas costa afuera de Argentina: caracterización y modelado de la dinámica de los márgenes pasivos del Atlántico Sur

El carácter multi-episódico del rifting observado en la evolución de las cuencas extensionales mesozoicas del sector costa afuera Argentino fue integrado en un marco regional del desmembramiento del supercontinente de Gondwana, con una revisión de la cronología del rifting para las principales cuencas mesozoicas en el sector austral de Sudamérica y África. El objetivo del estudio se focalizó en los eventos de rift pre-Cretácico que culminaron en el Cretácico temprano con la apertura del océano Atlántico Sur.

En el sector costa afuera de Argentina, particularmente en la zona de las cuencas del Colorado/Salado, se identificaron a partir de interpretación sísmica tres eventos de rift independientes. Un primer evento de rift se asoció con la reactivación extensional, ocurrida durante el Triásico tardío a Jurásico temprano, de antiguos cabalgamientos de la faja plegada y corrida de Ventania-Cabo del Paleozoico superior. Este primer conjunto de fallas es cortado transversalmente por otro set de fallas, formadoras de los principales depocentros de la cuenca del Colorado, y posiblemente la adyacente cuenca de Salado. Esta segunda etapa de rifting (la principal en cuanto a formación de cuencas para la zona de estudio) está relacionada con un evento de rift de edad Jurásico temprano y medio, correlacionable con el rifting de Karoo. En el Cretácico temprano, un nuevo evento extensional orientado WNW-ESE es responsable de la formación de depocentros en la zona más externa de la plataforma, el emplazamiento de SDRs (Seaward Dipping Reflectors) y finalmente la apertura del Océano Atlántico Sur entre Sudamérica y África.

Más al sur, en la cuenca de Malvinas, se reconocieron dos eventos de rift que fueron caracterizados sísmicamente, y para los que se obtuvieron dos edades absolutas mediante el método U-Pb en circón. El evento de rift más antiguo fue fechado Triásico superior, mientras que el segundo evento (el más importante en cuanto a formación de depocentros en la cuenca) fue datado Jurásico medio y correlacionado a la provincia magmática de Chon Aike.

La caracterización sismo-estratigráfica de la evolución post-ruptura del margen Atlántico de Argentina (segmento Rawson-Colorado-Salado) se llevó a cabo con la interpretación de secciones sísmicas y preparación de mapas isópacos para las principales secuencias. Se identificaron tres etapas de evolución de la deriva continental. La primera etapa comienza con la ruptura continental en el Hauteriviano tardío a Barremiano y se extiende hasta el Cretácico superior. La subsidencia en esta etapa está condicionada por la subsidencia termal sobre los principales depocentros, que fueron conectándose progresivamente. Los altos de basamento entre cuencas son cubiertos recién en el Maastrichtiano-Daniano, con una transgresión de carácter regional que integra finalmente a las cuencas del margen en una sola plataforma continental abierta. Durante el Paleógeno, la subsidencia y el aporte sedimentario se concentran en el área norte (cuenca del Salado). El sector sur (cuenca de Rawson y sector sur de la cuenca de Colorado) actúa como un alto relativo, sin acomodación. Finalmente, el ciclo Neógeno se caracteriza por subsidencia cilíndrica continua en la zona de plataforma (posiblemente relacionado con procesos geodinámicos andinos) y la participación notable de las corrientes de contorno en la dinámica sedimentaria (reforzada luego de la apertura del pasaje de Drake en el Eoceno).

Résumé étendu

Contexte général

Ce travail s'intègre dans le cadre d'une collaboration entre YPF S.A. et IFPEN, avec l'établissement d'une cotutelle entre les universités de UPMC – Paris 6 (désormais Sorbonne Université) et de Buenos Aires UBA. Cette thèse s'intitule « Stratigraphie sismique des bassins offshore de l'Argentine: caractérisation et modélisation de la dynamique des marges passives dans l'Atlantique Sud » et a été réalisée entre 2014 et 2018 par Juan Pablo Lovecchio.

Contexte industriel, scientifique et problématique

Les marges passives ont été, et sont toujours de nos jours le centre d'intérêt de très nombreux travaux scientifiques et industriels. Historiquement, les études sur les marges passives se sont concentrées sur la caractérisation de la structure de la croûte terrestre, leur historique de rupture (reconstructions cinématiques, modélisation analogique et numérique) ou leur évolution stratigraphique (en utilisant des techniques de stratigraphie séquentielle où d'ailleurs les principaux concepts ont été établis). La découverte d'importantes ressources d'hydrocarbures dans les eaux profondes et ultra profondes a suscité l'intérêt de l'industrie pétrolière. Les techniques d'acquisition sismique ont alors fait un bon technologique, ce qui a permis de mieux visualiser la structure de la marge passive et le remplissage des bassins associés.

L'Atlantique Sud est un laboratoire idéal pour comprendre l'évolution des marges passives, car les différents types de marges passives y sont présentes, et d'énormes ressources pétrolières incitent les compagnies à acquérir beaucoup de données (puits et sismique). Au Sud, la marge d'Argentine et les marges conjuguées de la Namibie et de l'Afrique du Sud restent des zones « frontières », avec un potentiel pétrolier énorme. Au cours des dernières années, l'Atlantique Sud a été la cible de plusieurs projets scientifiques (SAMPLE notamment) et de stratégies d'exploration d'hydrocarbures, augmentant le nombre de données sur le secteur et initiant de nouveaux débats scientifiques.

L’histoire complexe qui a précédé l’extension ayant conduit à l’ouverture du nouvel océan au Crétacé, en l’occurrence l’Atlantique Sud, a jusqu’à présent été peu traitée. Ce point est tout à fait crucial puisqu’il peut faire ressortir des géométries et des hétérogénéités dans la croûte, antérieures au processus de rifting final. Aussi, les amincissements du Moho visibles sur les données sismiques sous certains bassins préservés sur la marge d’Argentine (par exemple le bassin de Colorado) ne sont pas forcément contemporains et donc reliés au processus d’extension finale de la marge passive. C’est le point de départ de ces travaux de thèse. La problématique de la thèse était donc de comprendre et de caractériser la dynamique de la marge passive d’Argentine depuis son initiation via son héritage structural jusqu’à son évolution vers un stade mature.

Démarche, approche et données

Dans ce travail de thèse, la dynamique de la marge passive est analysée à travers les yeux d'un stratigraphe, impliquant (1) une phase de caractérisation et de quantification de l’architecture structurale et stratigraphique des bassins sédimentaires, suivie (2) d’une phase d’intégration régionale puis finalement (3) d’une phase de modélisation pour discuter la dynamique de la subsidence.

Ce travail repose sur l’interprétation de plus de 300.000 km de lignes sismiques, de 25 puits et d’une synthèse bibliographique de plus de 400 références. Des analyses paléontologiques et de datation sur zircon ont également été réalisées en collaboration avec M. Naipauer (UBA) and Víctor Valencia (Washington State University) afin de mieux contraindre le calendrier des évènements.

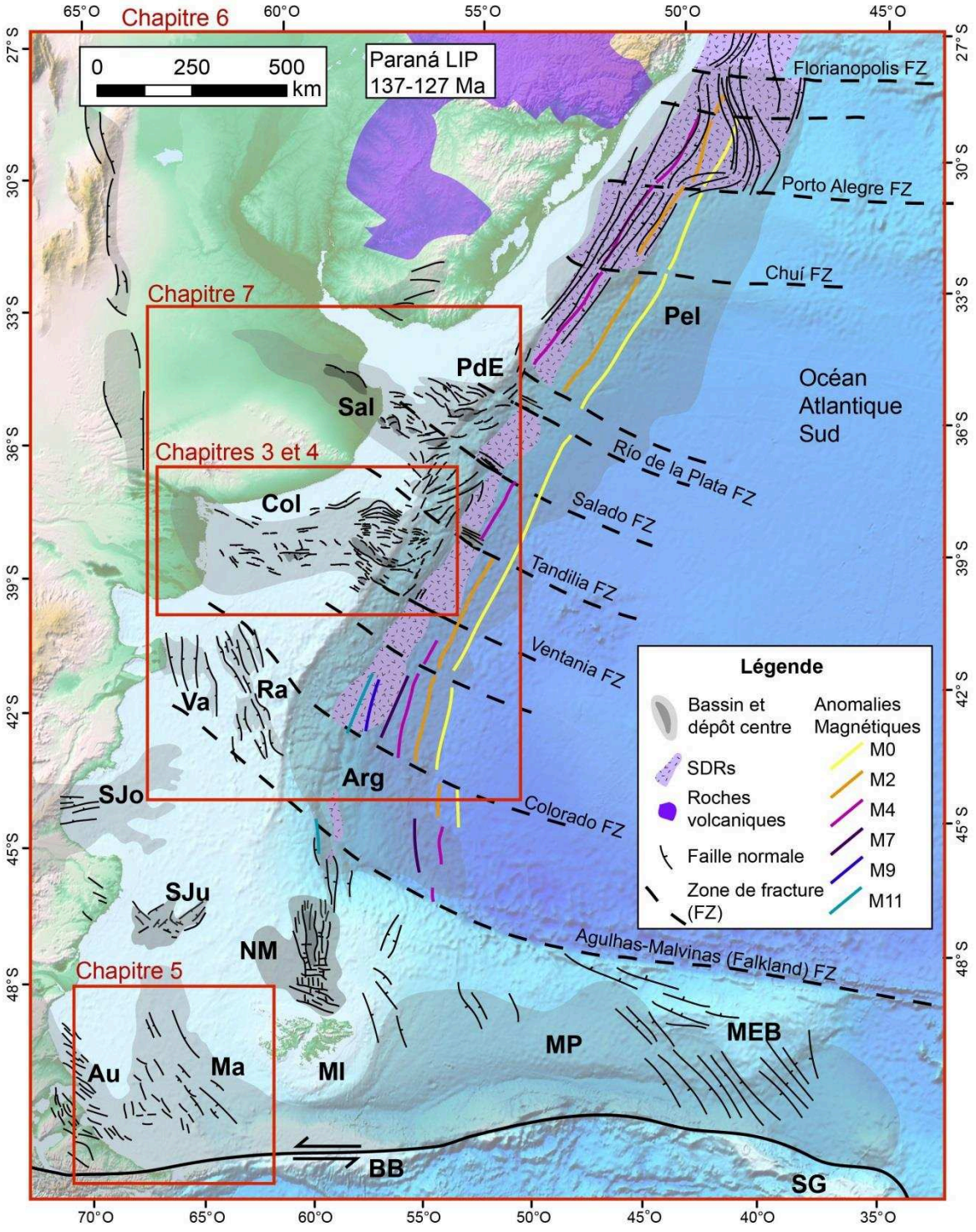

Figure I: Carte de localisation des bassins sédimentaires le long de la marge d'Argentine. Pelotas (Pel), Punta del Este (PdE), Salado (Sal), Colorado (Col), Valdés (Va), Rawson (Ra), Bassin du Golfe de San Jorge (SJo), San Julián (SJu), Bassin Austral (Au, Magallanes), Malvinas (Ma), Bassin de Malouines Nord (NM, North Falkland), Bassin Argentin (Arg). Voir le texte complet de la thèse pour un détail complet. Les principaux résultats de cette thèse sont présentés de manière géographique avec les rectangles rouges (Chapitres 3, 4, 5, 6 et 7).

L'évolution des principaux bassins mésozoïques de la marge d'Argentine est reconstituée (en particulier les bassins de Colorado, Salado et de Malvinas), et intégrée dans le cadre régional (sud-ouest du Gondwana) afin d'améliorer la compréhension des différentes phases d'extension et d'amincissement ayant abouti à l'ouverture de l'Atlantique Sud au Crétacé inférieur. La corrélation des événements de rifting anté-crétacés entre les bassins sud-américains et africains est également explorée. L'évolution post-rupture de la marge est examinée à partir de l'inversion des enregistrements sédimentaires et stratigraphiques des bassins de Colorado et de Salado. Ces résultats ont servi de données d'entrée pour une modélisation stratigraphique 3D à l'aide du logiciel DionisosFlow. La restauration de l'architecture stratigraphique a alors permis de quantifier la dynamique de la subsidence et de la confronter avec d'autres types de méthodes de calcul de la subsidence (« backstripping »).

Ce manuscrit est rédigé en anglais et est structuré en (1) une introduction, (2) sept chapitres et (3) des conclusions et perspectives (Figure I). Deux appendices présentent des résultats complémentaires ayant été réalisés en collaboration avec des collègues de YPF S.A. durant ces travaux de thèse.

Résultats

Trois résultats principaux peuvent être synthétisés de cette étude.

La première question abordée dans cette thèse était consacrée à l'initiation de la marge passive. De nombreuses controverses subsistent encore concernant l'intégration des bassins argentins dans la dynamique d'ouverture de l'Atlantique Sud. L'interprétation des données sismiques calibrées avec les puits du bassin du Colorado, a conduit à l'identification de plusieurs générations de failles avec des relations de recoupement. Trois étapes d'extension successives ont été identifiées dans la région du bassin du Colorado. L'événement d'extension le plus ancien correspond à une réactivation des structures permo-triassiques précédemment liées à la phase compressive de Ventania-Cape. Un deuxième événement est représenté par des failles recoupant les précédentes, et contrôlant des dépocentres orientés E-W à NW-SE. Nous avons corrélé ce deuxième et principal événement de rifting dans le bassin de Colorado au cycle du Jurassique inferieur-moyen « Cuyano » du bassin de Neuquén, et au rifting Karoo en Afrique.

Le troisième évènement est enregistré par des failles NNE-SSO parallèles aux structures de SDR. Elles ont été reliées au rifting du Crétacé en lien avec l'ouverture de l'Atlantique Sud.

Le rifting polyphasé est courant dans l'évolution des bassins sédimentaires, mais l'identification pour la première fois de trois stades superposés de rifting en Atlantique Sud, nous a motivé à explorer les bassins à proximité du bassin de Colorado. Le deuxième résultat principal de cette thèse est lié à l'extrapolation des résultats précédents sur toute la marge d'Argentine et sur la partie Sud de l'Afrique. Dans l'extrême sud, l'ouverture du bassin de Malvinas a été précisée et intégrée dans un schéma d'évolution à l'échelle des plaques. L'intégration des événements anté-atlantiques a été proposée en lien avec l'histoire du démantèlement mésozoïque du sud-ouest de Gondwana. En réalisant ces reconstructions paléo-tectoniques, il a été possible de corréler, par exemple, les bassins de Colorado et Salado, avec le rift Karoo II en Afrique de l'Ouest (par exemple, le bassin du Kalahari). L'ouverture de l'Atlantique Sud se focalise à l'endroit où les trois grandes phases d'extension ont été profondément marquées.

Le troisième point principal abordé dans cette thèse était de caractériser l'évolution de la marge après la « breakup », c'est-à-dire l'évolution de la marge passive mature. Le bassin de Colorado a d'abord été caractérisé et modélisé pour quantifier la dynamique de la subsidence, puis intégré à l'évolution de la marge passive dans le segment allant du bassin de Rawson à celui de Punta del Este. Le résultat majeur est que la marge passive, même à son stade mature n'a pas un comportement cylindrique. La comparaison avec des résultats déjà publiés a également montré qu'une approche basée sur l'inversion des architectures stratigraphiques pour quantifier les vitesses de subsidence parait absolument nécessaire pour mieux contraindre les modèles basés sur la dynamique des processus profonds.

Valorisation des travaux

Ce travail a fait l'objet de trois présentations à congrès, d'un papier accepté (Terra Nova, Chapitre 4), de deux papiers soumis (Chapitres 5 et 6). Il va faire également l'objet d'un autre papier (Chapitre 7). Deux autres papiers déjà publiés sont également présentés en appendices.

Ce travail est original dans le sens où la dynamique des marges passives est généralement traitée via un œil de structuraliste, alors qu'ici c'est le stratigraphe qui a inversé les architectures stratigraphiques pour caractériser l'évolution des bassins. On peut parler d'une approche à travers les processus de « surface ». L'identification de plusieurs phases d'extension, avant le mécanisme d'ouverture de l'atlantique du Sud est un résultat important de ce travail. L'intégration de ces résultats à plus grande échelle et la quantification de la subsidence ont ensuite montré l'importance des approches de processus de « surface » pour aller plus loin dans les approches « profondes ».

Pour continuer ces travaux, il faudrait détailler l'architecture stratigraphique à plus haute résolution afin de mieux caractériser les tendances identifiées. Ensuite, une modélisation stratigraphique à plus grande échelle (DionisosFlow) devrait permettre de mieux comprendre l'évolution non cylindrique de la marge.

Index

Introduction

The needs of new sources of energy have pushed offshore hydrocarbon exploration into deeper waters. The discovery of large reserves in the South Atlantic, in deep and ultra-deep waters offshore Brazil and Guyana, and in the conjugate African margin (e.g. Ghana, Angola) increased the necessity of better understanding the crustal and stratigraphic architectures, and their relations in the complex evolution of passive margins. The stratigraphic architecture controls the deposition of source rocks and reservoirs, and the configuration of stratigraphic and combined traps; while the calibration of the crustal structure is key in the prediction of the thermal evolution of the potential source rocks. Working on both deep and surface processes are nowadays the key challenge in scientific and applied approaches.

During the 1960's, passive margins were studied using gravimetric inversion, magnetic data, and refraction seismic to assess the crustal structure and the transition between the continental and oceanic crust domains. In the next four decades, these studies continuously improved our understanding of passive margins, by integrating the increasing amount geophysical and geological, scientific data being acquired around the world. The discovery of hydrocarbon resources in deepwater settings and the development of technology that allows their production at those water depths, focalized the industry attention on the evolution of passive margins. With the industry interest, came the possibility of acquiring large surveys of high resolution, deep, 2D PSTM and PSDM seismic data that allowed the characterization of the whole crust interval, down to the Moho. The development of numerical models provided new findings throughout the last two decades and especially in the last ten years, when thermo-mechanical modelling has been able to reproduce rifting and continental breakup.

However, most studies so far have focused on the breakup, either magma-poor or magma-rich, and have disregarded, or just briefly addressed the influence of the complex rifting histories in the breakup and in the successive passive margin evolution. Furthermore, most studies have looked at the rifting and breakup evolution in a 2D perspective, with transects across the area under extension. Older rifting events might induce or re-enforce not only heterogeneities in the mechanical structure of the crust, but also its thermal state, and could have an impact in the drift phase evolution and the stratigraphic architecture. So far, the complex polyphase evolution of passive margins has not been deeply addressed.

The South Atlantic Ocean opened in the Latest Jurassic to Early Cretaceous between South America and Africa as the final stage of the breakup of the supercontinent of Gondwana. In this study, the complex Mesozoic rifting history of the Southern South Atlantic realm is put into focus, to elucidate the influence of the pre-Cretaceous rifting events in the configuration of the Atlantic conjugate passive margins. Stratigraphic techniques are used to assess the complex evolution of passive margins. Some key parameters were interpreted from the stratigraphic record to constrain the Argentinean passive margin evolution. Most available models are based on 2D cross-sections illustrating one margin segment at the time. Nevertheless, passive margins have no reason to behave in a cylindrical manner, and thus a 3D characterization perspective, of both surface and deep processes, becomes necessary to establish major advances in the understanding of passive margins dynamics. The originality of the present study is then to bring the eyes of a stratigrapher onto basin scale dynamics using a 3D regional approach.

This manuscript is composed of three parts. Part I presents the state of the art and is formed of two chapters. Chapter 1 introduces the problematics with a review of rifting processes, continental breakup and passive margin evolution. The approach used in this study is then presented to assess the impact of polyphase rifting history on passive margin evolution. Chapter 2 introduces the geological framework of the South Atlantic Ocean with some generalities and a brief description of the South Atlantic opening. Generalities on the Argentinean offshore basins are also summarized.

Part II presents the results of this study regarding the rifting history of the Argentinean offshore basins. It is subdivided into four chapters. In Chapter 3 the geological framework for the Colorado basin is presented, together with the methodology followed for the seismic interpretation, and a characterization of the main depocenters. Chapter 4 is a paper recently published in Terra Nova that displays the elements to support the identification of three superimposed extensional stages in the Colorado basin. Some of these results are also correlated to the adjacent Salado and Punta del Este basins. We demonstrate how complex the rifting history of a passive margin basin can be, by introducing heterogeneities that have previously been neglected. These induced heterogeneities may or may not condition breakup, but play an important role in the passive margin evolution.

Chapter 5 is a paper about the Malvinas basin, emplaced in the southern end of the South American plate, that was considered for a special publication of the Journal of South American

Earth Sciences on Patagonian basins. The Malvinas basin is not a common passive margin basin. It initiated as an extensional basin in the Jurassic, but evolved to a foreland marine basin since the latest Cretaceous, related to compression of the South American-Scotia plate boundary to the south. Two new U-Pb zircon ages are used to date prerift and synrift units. Rifting in the Malvinas basin is analyzed in association with the emplacement of the Chon Aike Magmatic Province. The Chon Aike Magmatic Province is interpreted to have developed in a retroarc setting under extension. Several regional elements are integrated into a model that introduces a slab tear between South America and Antarctica, to explain extension associated with rotation, and the successive opening of the Weddell Sea between East and West Gondwana.

Chapter 6 is a regional integration of the different rifting events associated with the breakup of the supercontinent of Gondwana throughout the Mesozoic. After having identified multiple rifting stages in the Colorado basin, and characterized the extension associated with the emplacement of the Jurassic magmatic provinces (e.g. Chon Aike), the extrapolation of these external episodes to other basins in SW Gondwana was intended. The retroarc Subandean basins were also considered into the plate scale picture, to assess the influence of subduction processes related to the SW Gondwana margin on the generation of far-field stresses, which are responsible for the opening of rift basins in a passive rifting mode. The Mesozoic evolution of SW Gondwana is integrated to assess the formation of the offshore Argentinean basins, thirty years after the pioneering work leaded by Uliana (e.g. Uliana et al., 1985, 1989, 1995; Biddle et al., 1996; Fitzgerald et al., 1990), and Urien (e.g. Urien et al., 1981; Urien and Zambrano, 1973; Zambrano and Urien, 1970).

Part III is dedicated to the post-break evolution of the Argentina margin, with a special focus on the Colorado basin area. Chapter 7 characterizes the sedimentary infill of the Colorado and Salado basins throughout the main tectono-stratigraphic phases, using a sequence stratigraphy approach. The geodynamic evolution of the passive margin is interpreted, and forward stratigraphic modelling is used to quantify the subsidence history of the Colorado basin, throughout the passive margin phase.

In the last section Conclusions and Perspectives, the main results of this work are summarized and the perspectives for future work are presented.

PART I: STATE OF THE ART

Chapter 1. Problematics, objective and approach

1.1 Introduction

Offshore exploration has been key for incorporation of resources into the portfolios of major oil and gas companies in the last few decades. Deepwater plays, in particular, have become the main source of new discoveries as technology allows the displacement of the water depth frontier towards the ocean. Deepwater plays are also interesting because of the large, generally commercial, volumes of discovered hydrocarbons and the good reservoir quality. Even with the global industry downturn of the last years, a strong growth is forecasted for offshore E&P, making deepwater a key contributor to reserve replacement (Nelson et al., 2013). And particularly, recent success in deepwater exploration (Ghana, Brazil, Mozambique) encourages oil and gas companies to go into deeper waters and frontier areas. The southern South Atlantic is nowadays the next frontier. Argentina has the least explored continental margin in the peri-Atlantic realm (Davison and Steel, 2016). With the recent exploration activity carried out in Uruguay and a bidding round for the offshore areas taking place in Argentina in 2018, there is a great interest of the industry main players in the potential results that this exploration activity could provide.

Among deepwater plays, passive (rifted) margins are core areas for petroleum exploration and production (Mann et al., 2001), with the peri-Atlantic realm being mainly an oil-prone area (Guyana, Brazil, Angola, Ghana), and the peri-Indian a more gas-prone realm (Mozambique, Tanzania, Australia). Figure 1.1 is a schematic map showing passive margins with proven reserves and unproven resources (underexplored). The Brazilian and West Africa margin are shown as areas with proven reserves. The discovery of hydrocarbons in the sub-salt of the Santos basin (offshore Brazil) was a major turning point in the exploration of passive margin, which was possible thanks to the improvement of sub-salt seismic imaging and the development of technology for drilling and producing in deepwater and ultra-deepwater

settings. Further south, the Uruguayan and Argentinean, and the conjugate Namibian and South African margins remain underexplored. Not only geopolitical aspects make these environments different, but also Geology marks a sharp difference in margin architecture and play development between the Brazilian/Angolan margins and the conjugate margins to the south.

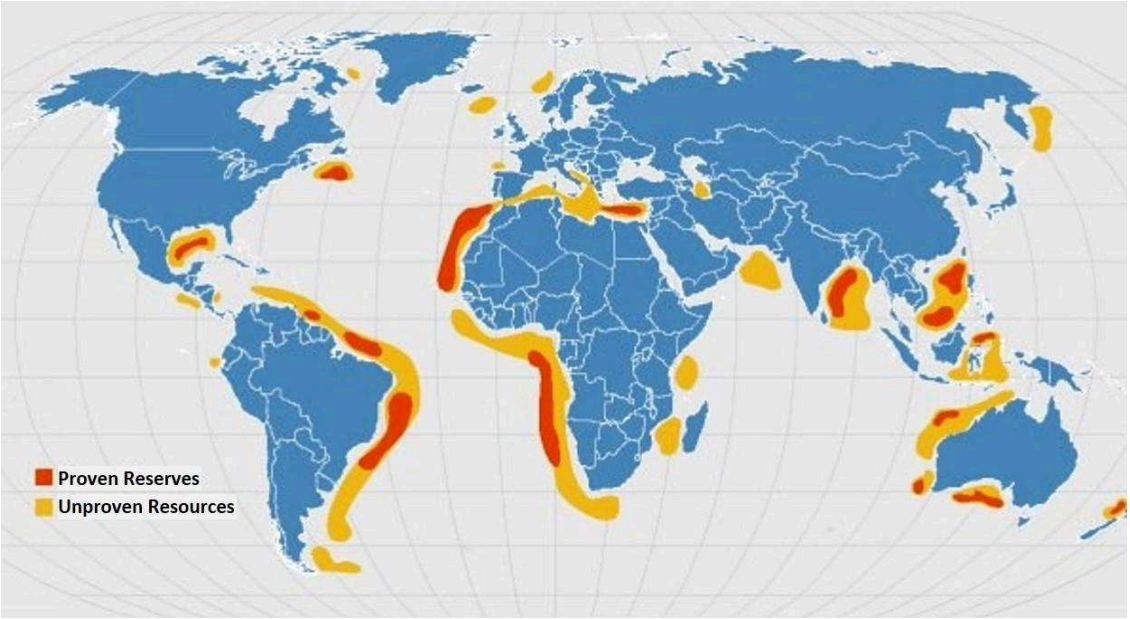

Figure 1.1: Schematic map of explored versus underexplored passive margins (after Shirley, 2010 and references therein).

The understanding of passive margins formation and evolution is key in the identification of potential exploratory plays and strategies. Passive margins form through rifting of continental plates. The South Atlantic rift, for example, opened in the Early Cretaceous as South America and Africa broke apart, disaggregating the supercontinent of Gondwana. Rifting is a complex process, as it can take place in multiple stages associated with different stress regimes through time. Rifting can take advantage of previous weakness zones in the lithosphere or can develop across them (Buiter and Torsvik, 2014; Will and Frimmel, 2018). The sedimentary basins in the Argentinean offshore record several of the Mesozoic rifting stages that SW Gondwana experienced, of which the South Atlantic opening in the Early Cretaceous was only the final stage (Uliana et al., 1989). Unravelling the Mesozoic rifting evolution of these basins (rifting stages that are precursor of the South Atlantic opening) is important for understanding the early steps of the complex geological evolution of passive margins. The infill of these sedimentary basins (pre- and post-breakup) records the interaction between (1) deep lithospheric processes such as rifting, mantle exhumation, oceanic breakup, long-term subsidence and (2) surface processes such as erosion, eustasy, transport and deposition of

sediments. Thus, these factors can be inverted from the study of the sedimentary record of basins.

Integrated studies combining characterization of both surface and deep lithospheric processes are nowadays a key milestone in both academic and industrial studies (e.g. Aslanian et al., 2009; Braun et al., 2013; Burov and Toussaint, 2007; Cloetingh and Burov, 2011). In the context of petroleum exploration, such integration is expected to provide critical information for petroleum system characterization (potential reservoirs and source rocks distribution, traps formation, thermal regime and timing of hydrocarbon generation and migration).

The study of the coupling between deep and shallow processes requires basin-scale characterization (potential field methods, seismic stratigraphic interpretation, well calibration) together with geodynamic and basin modeling tools (e.g. FLAMAR for the modelling of mantle and lithosphere dynamics and thermal regime, Burov and Poliakov, 2001; DionisosFlow for the sedimentary infill, Granjeon, 1997; TemisFlow for the modelling of the petroleum systems) that are in themselves very consistent. In this context, the main scientific and technical gap to be filled is to establish a comprehensive workflow that could result in both (1) the understanding of basin dynamics (rifting, breakup, drift) and (2) the characterization of the stratigraphy and potential petroleum systems.

In this study, the multi-stage rifting evolution of the Colorado and Salado basins area, and the Malvinas basin, were investigated and then integrated into the more regional SW Gondwana Mesozoic rifting evolution. The passive margin evolution of the Argentinean South Atlantic margin was then characterized through seismic stratigraphic techniques and the Colorado basin was modelled to highlight the main factors controlling its particular rift-to-drift evolution.

1.2 Rifting and the origin of extensional basins

Rifting is the process through which lithosphere thins, ultimately leading to the rupture of a continent and the formation of a new ocean (Merle, 2011). Rifting is also a very important mechanism for sedimentary basin formation and plays a key role in thermal regime, with immediate importance in petroleum exploration (Cloetingh et al., 2013). The thinning of the brittle crust is achieved through normal dip-slip faulting, while the lower crust and lithospheric mantle can behave with a more ductile rheology. The mechanisms responsible for producing

rifting have long been discussed. Two end-members rifting modes have been identified (Fig. 1.2): active and passive rifting. In active rifting (Fig. 1.2a), lithospheric thinning is associated with the impingement at the base of the lithosphere (1330°C isotherm) of a thermal plume, producing an asthenosphere upwelling which drives rifting (Dewey and Burke, 1974). In other words, lithospheric mantle is thinned by thermal erosion, but continental crust preserves its original thickness. Other notable characteristics of active rifting are regional uplift (doming) of the area affected by the plume, and volcanic activity since the early stages of rifting or event preceding rifting (Merle, 2011; Frizon De Lamotte et al., 2015).

In passive rifting (Fig. 1.2b), stretching is produced by the horizontal extension of continental lithosphere, in which far field stresses generated within or at the boundaries of plates, produce an extensional field (McKenzie, 1978). In passive rifting, the crust and lithospheric mantle are simultaneously thinned (Merle, 2011), producing a passive asthenosphere upwelling in response to the separation of the overlying layers, controlled by regional tectonic extension (see Nemcok, 2016).

Several parameters exert a control on rifting dynamics, conditioning how the lithosphere thins. The main controlling factors, summarized by Merle (2011), are: rate of extension, geothermal gradient, the rheological profile of the lithosphere, the thickness ratio between the crust and the lithospheric mantle, previous lithospheric discontinuities and heterogeneities and magmatic intrusions.

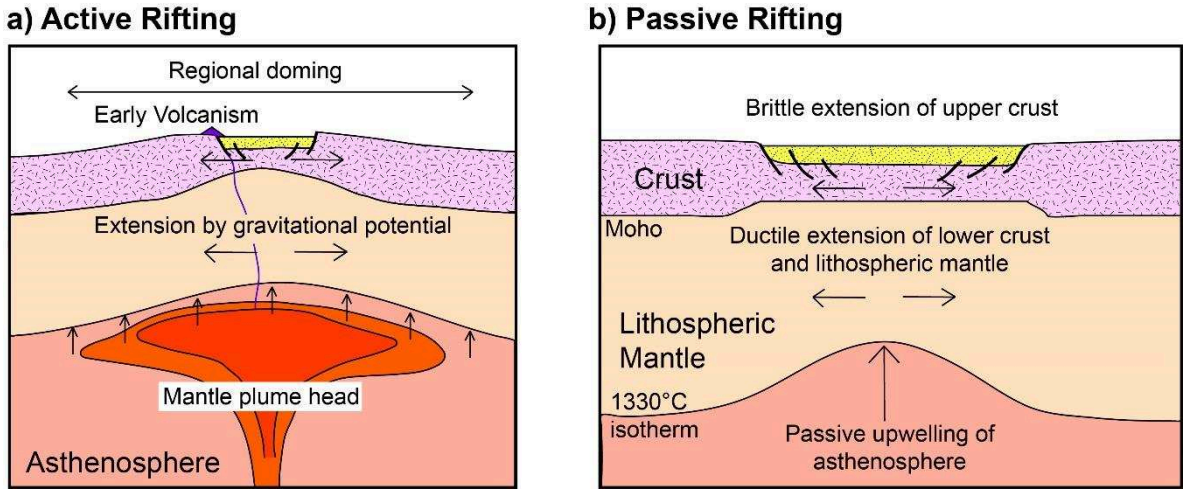

Figure 1.2: Schematic representation of a) Active; and b) Passive rifting end-members (after Allen and Allen, 2005; and Merle, 2011).

Nemcok (2016) differentiates between three rifting styles end-members: narrow, wide and core complex rift modes. Narrow rifts concentrate the lithospheric thinning in a 100-150 km wide zone. This localized extension can be the product of local weakening factors favoring the canalization of strain, such as local heat flow or magmatic activity, or can be related to crustal heterogeneities. The Gulf of Suez-Red Sea rift, and East African rifts are examples of narrow rifts. In wide rifts lithospheric thinning is more widely distributed, over an area that can exceed 1000 km (e.g. the Basin and Range province of North America). The high extensional strain that characterize these rifts, is usually not uniformly distributed. Finally, Core complex rifts typically present localized extension in the upper crust, accompanied by the broadly distributed extension of the lower crust, resulting in the exhumation of high-grade metamorphic rocks from the middle-lower crust. Core complexes require a ductile lower crust, which is common in regions that underwent previous orogenic thickening, or might be associated with ultra-slow extension.

Another characteristic useful in rift classification is symmetry. Symmetric rifts are the result of uniform stretching of the crust and the underlying lithospheric mantle (equal degree of extension of both layers, Fig. 1.3a). Mckenzie (1978) considered extension to be instantaneous, and with symmetrical extension and no solid block rotation involved, respected the conditions for pure shear (Allen and Allen, 2005).

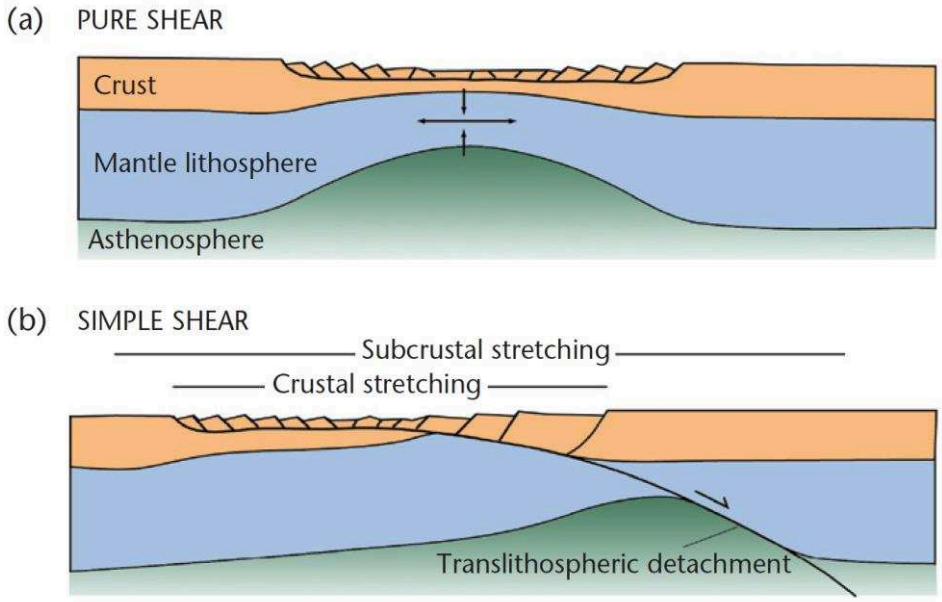

Figure 1.3: Models of strain geometry in rifts: a) symmetric rifts formed by pure shear and; b) asymmetric rifts produced by simple shear (from Allen and Allen, 2013, after references therein).

Alternatively, the lithosphere may extend asymmetrically. In asymmetric rifts the area affected by crustal brittle stretching is displaced from the area where the ductile subcrustal lithosphere is deformed (Fig. 1.3b). Wernicke (1981, 1985) proposed this simple shear model first for the Basin and Range province, where a large-scale shear zone (Fig. 1.3b) cutting through the entire lithosphere is responsible for relaying the brittle extension of the crust from the zone of upwelled asthenosphere. At lithospheric scale, the main decoupling horizons operating at plate boundaries are the Moho (crust-lithospheric mantle boundary) and the ductile lower crust, as well as pre-existing tectonic fabrics preserved in the brittle upper crust, such as older low-angle detachments or thrust systems which are prone to go through positive or negative inversion (Cloetingh et al., 2013). Coward (1986) introduced a more complex scenario by suggesting that the upper crust may deform by simple shear, and the lower crust and lithospheric mantle by pure shear.

Another important point to mention is the origin of the extensional forces that produce rifting in the different possible tectonic scenarios. In the case of active rifting, crustal thinning might be triggered by the impingement of a thermal plume (see Sengör and Burke, 1978; Fig. 1.2a). Thermal plumes sensu stricto, according to Merle (2011), are not so common. The only present day rift associated with a thermal plume is the East African Rift (see Corti, 2009), where a mantle plume rises from the mantle/core boundary (Ritsema et al., 1999). Merle (2011) suggests that active upwelling of the asthenosphere can alternatively be triggered by subduction-related processes by detachment of the subducting slab (slab break-off) and upwelling of hot asthenospheric material towards the base of the crust in the retroarc (Fig. 1.4a). In an alternative scenario, Zou et al. (2008) suggest that accumulation and thickening of a stagnant slab at the mantle transition zone may also initiate the active rise of the asthenosphere (Fig. 1.4b).

For the case of rift basins formed as a result of passive rifting, the far-field stress regime is usually related to sub-horizontal crustal forces. Many of these processes deal with effects of changes in subduction dynamics at convergent plate boundaries. Lithosphere is produced at oceanic ridges and consumed at subduction zones. These are the fundamental drivers of plate tectonics. According to Allen and Allen (2005), the subduction velocity (Vsub, Fig. 1.5a) results from a balance between driving forces (the gravitational body forces of the cold subducting slab, the slab pull force, Fsp in Fig 1.5b) and resistive forces (the viscous resistance of the mantle, also known as the anchoring force, Fa in Fig. 1.5b). Heuret and Lallemand (2005)

introduce two additional forces: the suction/pushing force related to the upper plate absolute motion that acts on the plate interface and conditions the trench dynamics (Fup in Fig. 1.5b), and the force generated by the mantle flow on the back-side of the subducting slab in the trench-normal direction (Fm in Fig. 1.5b).

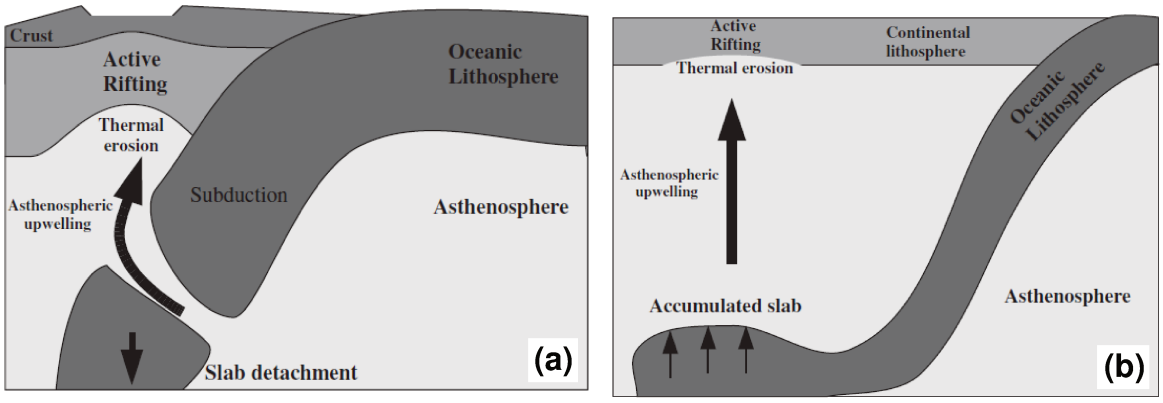

Figure 1.4: Two examples of triggering mechanisms for active rifting: a) slab detachment; b) accumulated stagnant slab (from Merle, 2011).

The convergence velocity results from the balance of the absolute motion velocities of the interacting plates (Vcon= Vup – Vlw). When the convergence rate is less than the subduction velocity, extension is observed in the retroarc (Fig. 1.6a), a process known as trench retreat, or upper plate retreat (if a fixed-trench is considered sensu Heuret and Lallemand, 2005).

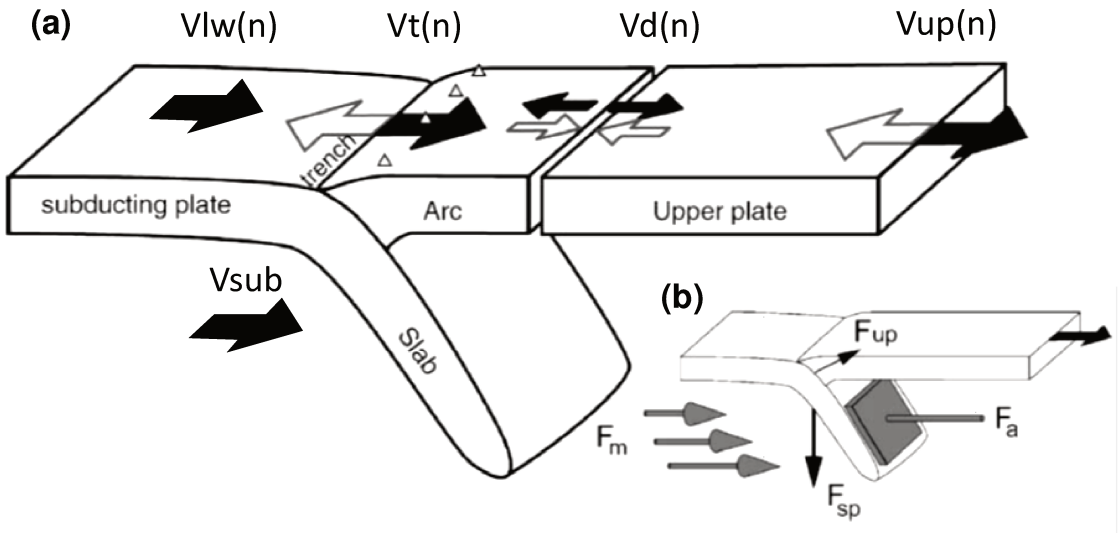

Figure 1.5: Schematic representation of a subduction zone. Vup: upper plate motion, Vlw: subducting plate motion, Vt: trench absolute motion, Vd: back-arc deformation rate, (n) refers to the trench-normal component of the absolute motion (modified from Heuret and Lallemand, 2005).

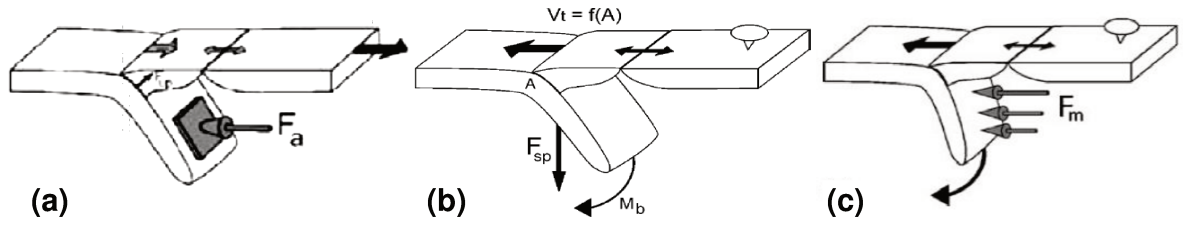

Figure 1.6: Different mechanisms responsible for producing extension in retroarc settings: a) upper plate retreat; b) slab-rollback; c) mantle flow induced extension (modified from Heuret and Lallemand, 2005).

The angle of subduction is a function of the buoyancy of the subducting plate regarding the sub-lithospheric mantle. Buoyancy will be a function of the plate's thickness as well as plate's density. Density at the same time is conditioned by the mineral composition (i.e. oceanic crust, continental crust) and by temperature (which in the case of oceanic crust is a function of crustal age). Old 'cold' oceanic crust has less buoyancy and thus sinks with a larger angle than young 'hot' oceanic crust. Changes in plate buoyancy of the subducting plate, produce changes in the subduction angle. A decrease in the subduction angle, due to the arrival of a more buoyant (thicker, less dense, or hotter lithosphere) will produce the migration of the magmatic arc away from the trench together with the advancement of compression in the retroarc (Fig. 1.7a). Flat-slab subduction will be the final stage of this process. An increase in the subduction angle (slab-steepening), on the other way, will produce a trench-ward migration of the volcanic arc and the onset of retroarc extension, with the formation of retroarc or back-arc basins (Fig. 1.7b). This process is known as slab rollback (Fig. 1.6b). Another possible source for slab/trench migration is related to mantle dynamics (Fig. 1.6c). This will depend on the direction of subduction and the global eastward mantle flow pattern (see Heuret and Lallemand, 2005).

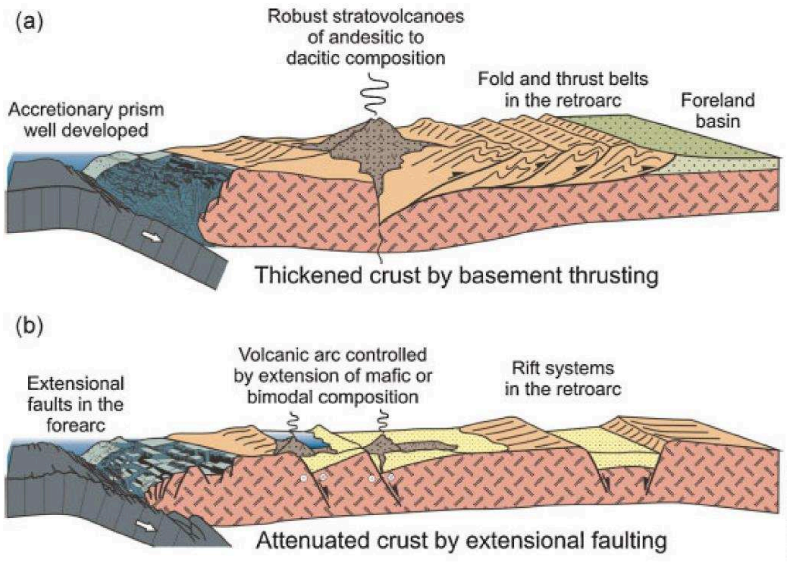

Figure 1.7: Contrasting models of subduction zones under (a) compression and (b) extension (from Ramos, 2010, after references therein).

Subduction along a convergent plate margin is not homogenous and uniform. Plates might have different shapes, the stress regime can rotate, and thus the absolute convergence can vary from one region to another. Slab tearing plays a major role in segmented subduction zones, particularly separating segments with different convergence regimes (e.g. retroarc extension, stagnation or compression, Fig. 1.8). Slab tear faults are likely to link two adjacent segments of the subduction zone and to accommodate horizontal movements if different roll-back velocities operate in the two segments (Rosenbaum et al., 2008). Slab tearing is also a way to explain the lateral passage from normal to flat-slab subduction. Slab tearing is expected to produce an asthenosphere window and volcanism.

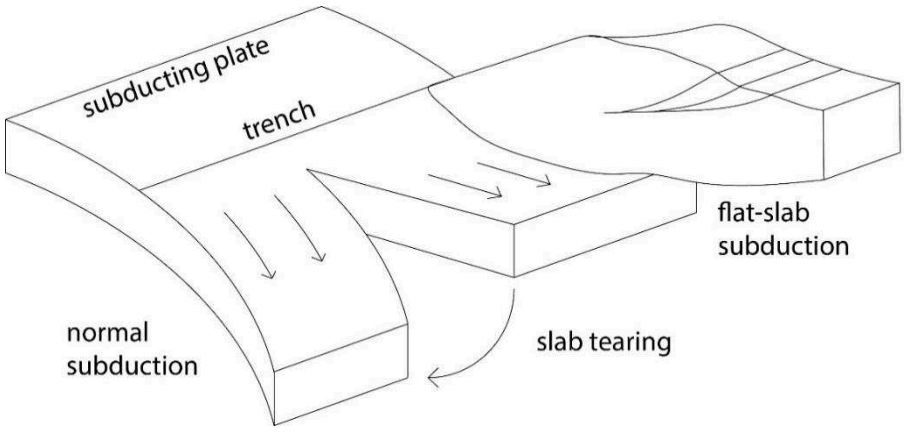

Figure 1.8: Schematic representation of the slab tearing mechanism, with a vertical tear separating segments of flat-slab and normal subduction.

1.3 Breakup of supercontinents

Successful rifting leads to continental breakup and the onset an oceanic basin. When a piece of continental crust is split in two by rifting, volcanic rocks are extruded from the asthenosphere and form ultimately a mid-ocean ridge, where oceanic crust will accrete and push the continents apart. Today the different continents are separated by oceanic basins. Even if the different oceans formed at different ages (Fig. 1.9), most of the oceanic crust on earth is of Mesozoic age. Consequently, if we went back in time to the Late Paleozoic, before the time when most of the present-day Earth oceans opened, we would find a supercontinent, a large mass of continental crust formed by welded cratons and other tectonic blocs. The supercontinent of Pangea existed since the mid-Carboniferous (near 320 Ma) and was broken apart by several rifting episodes that affected the plate integrity (Moulin et al., 2010). Many rift basins were generated throughout the breakup history, but only some of them were successful and originated oceanic basins.

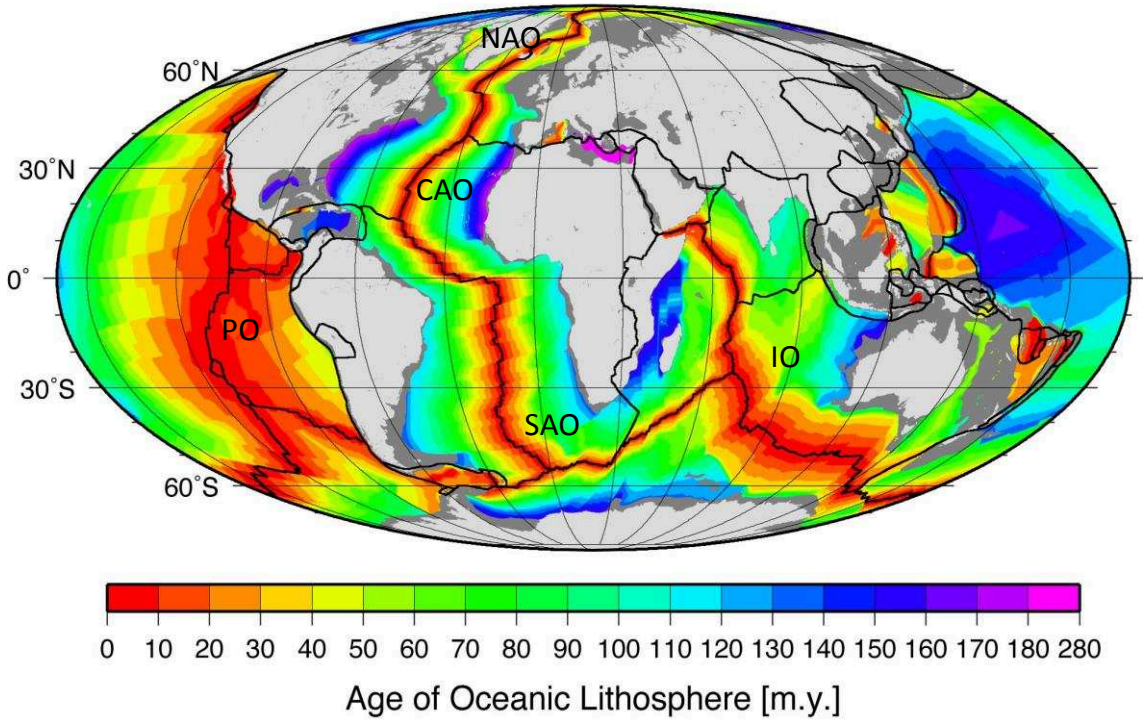

Figure 1.9: Age-area distribution of oceanic crust in the World (from Müller et al., 2008). PO: Pacific Ocean, NAO: North Atlantic Ocean, CAO: Central Atlantic Ocean, SAO: South Atlantic Ocean, IO: Indian Ocean

Then, the question that arises is: what triggers the breakup of supercontinents? This question has long been discussed since the proposal of the Wilson cycle theory. Internal Earth's heat was proposed to motorize plate tectonics. In this way it would also be a trigger for the opening of new oceans. Supercontinents are large masses of continental crust that would cause the insulation of the underlying mantle, producing abnormal heat concentrations and hot spots (hot-spots producing active rifting; see Anderson, 1994, and Trubitsyn et al., 2003). Dewey and Burke (1974) suggested that a new ocean would be born from the connection of several, more-or-less aligned, hotspots. The coincidence of new oceans and the presence of large igneous provinces (LIP) also supported this theory. Buiter and Torsvik (2014) reviewed the role of mantle plumes in continental breakup and note that although there is a relation, in many margins such as the Central or the South Atlantic, rifting had initiated long before the main phase of volcanism (e.g. CAMP and Paraná-Etendeka LIP respectively). Rifting and successive breakup of supercontinents is a process that has proved to be much more complex.

There is also an important role played by ancient sutures in localizing the extensional deformation. Supercontinents are intrinsically complex collages of cratons and shields bounded by sutures comprehended in metamorphic belts of former orogens produced during craton amalgamation. The structural grain of mobile belts introduces heterogeneities that, under extension, tend to guide fault emplacement and eventually breakup (Will and Frimmel, 2018). The orientation of the basement fabric and the stress-field also play an important role in the reactivation of old structures (Vergani et al., 1995).

In the case of Pangea, breakup of the supercontinent occurred in not one but several stages (Moulin et al., 2010, Fig. 1.10). The role of multi-stage rifting was evaluated by Frizon De Lamotte et al. (2015) who propose a combination of active and passive rifting processes to cause, in successive stages, the breakup of a large continental mass such as Pangea.

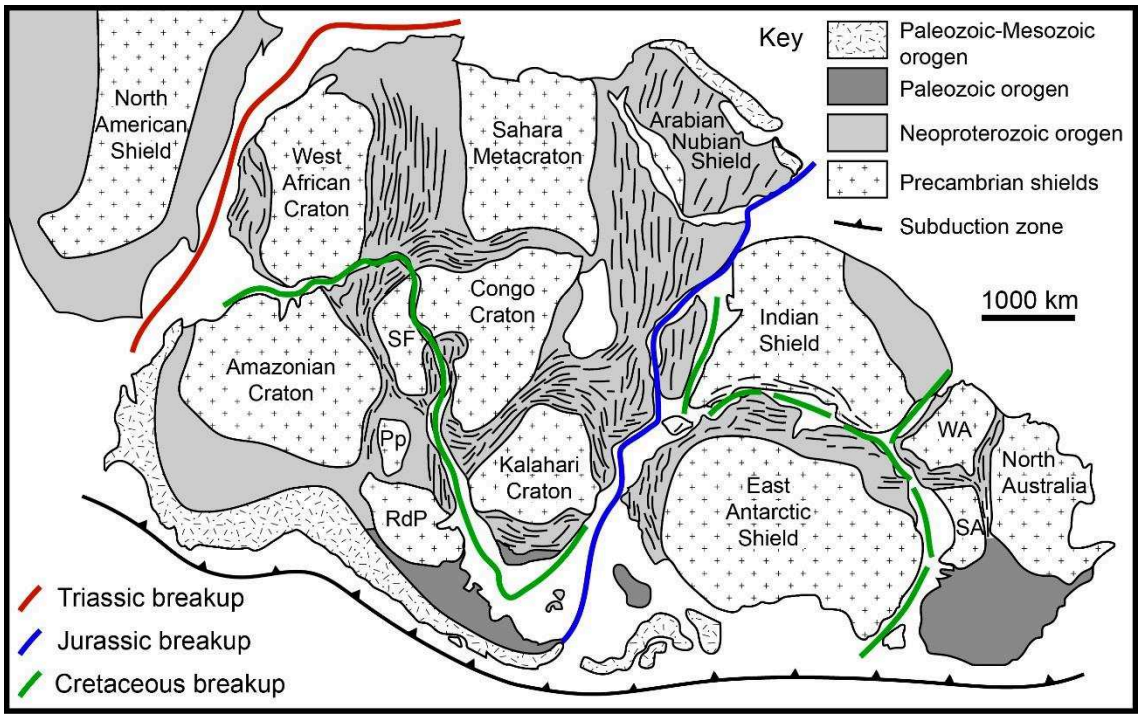

Figure 1.10: Pangea reconstruction at the end of the Paleozoic after Gray et al. (2008), showing the main breakup events modified from Moulin and Aslanian (2010) and Will and Frimmel (2018). Cratons: RdP: Río de la Plata, Pp: Paraná-Panema block, SF: Sao Francisco, WA: West Australia, SA: South Australia.

The thermal insulation and thus landmass instability expected to be produced by supercontinents on the underlying mantle seem not to be enough to produce overheated mantle, volcanism and active rifting (Heron and Lowman, 2011). Bercovici and Long (2014) suggest that it is subduction-related slab rollback instability that triggers continental landmass dispersal. This is still a matter of debate with some recent publication introducing mantle and lithospheric modelling.

Zhang et al. (2018) recently assessed the relative importance of these numerous processes in producing the breakup of a supercontinent, summarized in figure 1.11. After performing spherical 3D modeling for the mantle dynamics, they conclude that subduction retreat forces alone cannot produce breakup. Their modeled stress occurs above the subduction zone, but changes to compressional and then extensional again over the time. The models presented by these authors show that plume push stress (producing active rifting) seems three times larger than the one induced by subduction retreat, and concentrate the extensional stress induced by subduction in a zone up to 600 km from the trench.

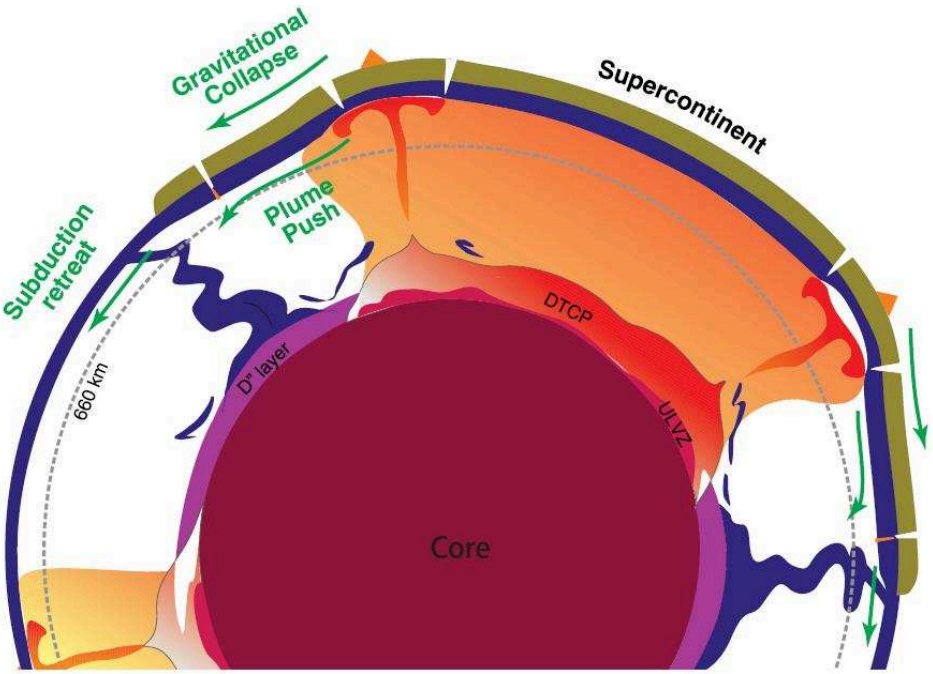

Figure 1.11: Simplified cartoon representing the main potential forces for supercontinent breakup (Zhang et al., 2018).

In a recent contribution, Dal Zilio et al. (2018) highlight the effects of subduction in inducing mantle flow near the subduction zone. As subducting slabs sink in the upper mantle, the counter flow of the mantle localizes divergent tractions at the base of the upper plate, and produce retro-arc rifting and eventually a back-arc basin. Following some of the ideas presented by Vaughan and Storey (2007), they use numerical models to simulate the effects of shallow and deep subduction on the upper plate. The basal drag and suction forces due to roll-back have commonly been invoked as responsible for the opening on back-arc basins (e.g. the Japan Sea, Jolivet et al., 1994). Marginal basins (Fig. 1.12a) are consistently located 250 km-500 km away from the trench while authors intended to understand how more distal basins can be produced by the same trench-ward tractions generated in the mantle by return flow associated with subduction. Dal Zilio et al. (2018) suggest that large-scale flow due to deep subduction (Fig. 1.12b) may have led to the long-lived extensional regime that experienced Western Pangea and ended with the opening of the South Atlantic. The authors were able to explain strain localization as far as 3500 km away from trench, this could be an explanation for triggering "mantle plumes" away from the trench, but still related to subduction dynamics.

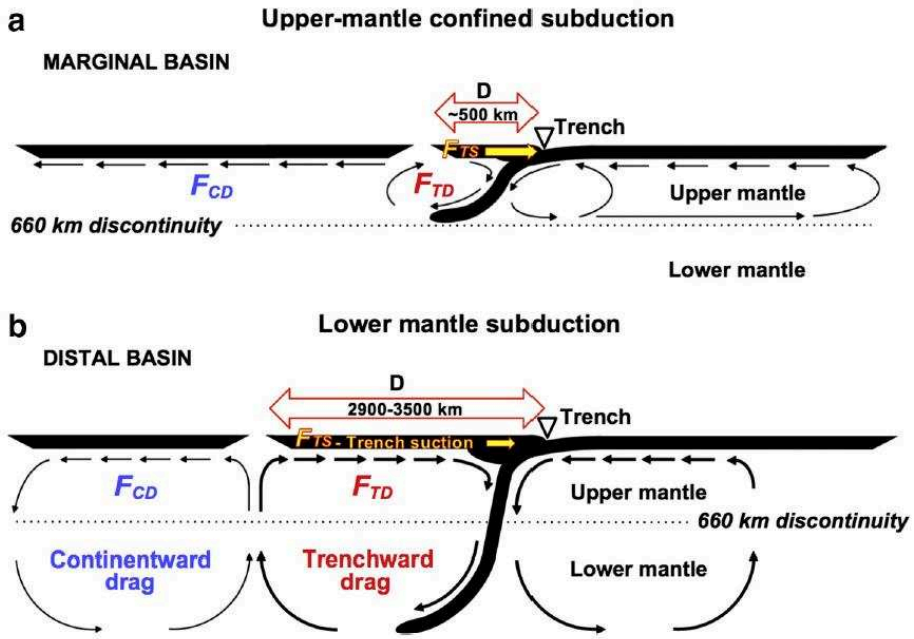

Figure 1.12: Two models for subduction-induced mantle flow and the effects on continental breakup (Dal Zilio et al., 2018): a) Upper mantle confined subduction model: large trench suction forces (yellow arrow) act on the upper plate within 500 km from the trench and generate a marginal back-arc basin; b) Whole mantle subduction model: the continental plate is subjected to compressional deformation and lithospheric thickening near the trench. The models show the formation of a distal basin, some 3000 km from the trench, produced by a subduction induced mantle convention cell.

In the case of the supercontinent of Pangea (Fig. 1.10), it took more than 100 Ma to break it apart. This process initiated in the Triassic, with rifting between Laurentia (North America) and Western Gondwana (Fig. 1.10), and the successive opening of the Central Atlantic (Withjack et al., 1999, 2012; Leleu et al., 2016). The emplacement of a Central Atlantic Magmatic Province (CAMP) would have occurred after the main phase of rifting (Frizon De Lamotte et al., 2015) and according to McHone (2000) it was not plume-induced. Triassic basins were not restricted to the Central Atlantic realm, rift basins developed across Gondwana (Uliana et al., 1989; Zerfass et al., 2003) and on the paleo-Pacific convergent margin (Ramos and Kay, 1991; Spikings et al., 2016).

On the other hand, the impact of the Karoo plume on East Africa in the Early Jurassic produced active rifting, with doming, volcanism and caused eventually continental breakup of Western Gondwana (South America + Africa) from Eastern Gondwana (Antarctica + Australia + India; Frizon De Lamotte et al., 2015). The continent dispersal process continued in the Early Cretaceous with the opening of the South Atlantic Ocean between South America and Africa and several other oceanic basins produced by the dispersal of Eastern Gondwana cratons

(Figure 1.9). As discussed by Frizon De Lamotte et al. (2015) and Will and Frimmel (2016), the South Atlantic is another case of passive rifting, triggered by far-field forces pulling the lithosphere apart, that was affected by massive volcanism, the Paraná-Etendeka LIP. In this scenario the opening would not have been triggered by a plume but the volcanism came when rifting was already established, and presumably oceanic crust was also being accreted in the southernmost segment (Franke, 2013; Stica et al., 2014). In this perspective, Gondwana breakup occurred as a combination of active and passive rifting modes (Frizon De Lamotte et al., 2015) and results as a great study case for understanding the influence of the different mechanisms. The different Mesozoic rifting events were crucial for the formation of the basins on the South American (Uliana et al., 1989; Urien et al., 1981) and African shelves (Broad et al., 2012; Jungslager, 1999; Macdonald et al., 2003).

1.4 Passive margins

The ultimate evolution of a successful rift is the opening of an ocean with development of conjugate passive margins. Passive margins present a complex structural and stratigraphic evolution. Typical passive margins are characterized by extensional faulting (at some stage), large scale gravitational tectonics (slumps and mass transport deposits -MTDs- associated with slope failure of the sedimentary prisms), and sometimes salt of shale tectonics (Allen and Allen, 2005). Extensional faulting during rifting produces the attenuation of the crust over the transition towards the oceanic crust. Once continental breakup occurs, the system passes from a rifting stage, to a drift stage. Different passive margin architectures will evolve from symmetric or asymmetric rifts (Fig.1.13). The simple shear model can explain the frequent asymmetry observed in conjugate passive margins as well as differences is subsequent thermal evolution (Fig. 1.3b and 1.13b, Cloetingh et al., 2013).

Cloetingh et al. (2013) presented numerical models that illustrate rifting and continental breakup. In their models, using a lithospheric extension velocity of 16 mm/yr, lithospheric extension is localized at the center of the domain on which a mantle weakness was imposed. If extension of both crust and mantle continue under constant velocity, breakup is achieved at 27 Ma. Their models show that when lithosphere is stretched at greater velocities, continental breakup is achieved faster, and with velocities bellow 8 mm/yr breakup is not achieved. Moreover, the tendency of lithosphere to neck (to concentrate strain in a particular area) is

weaker with decreasing extension velocities, producing wider rifts than at faster stretching velocities.

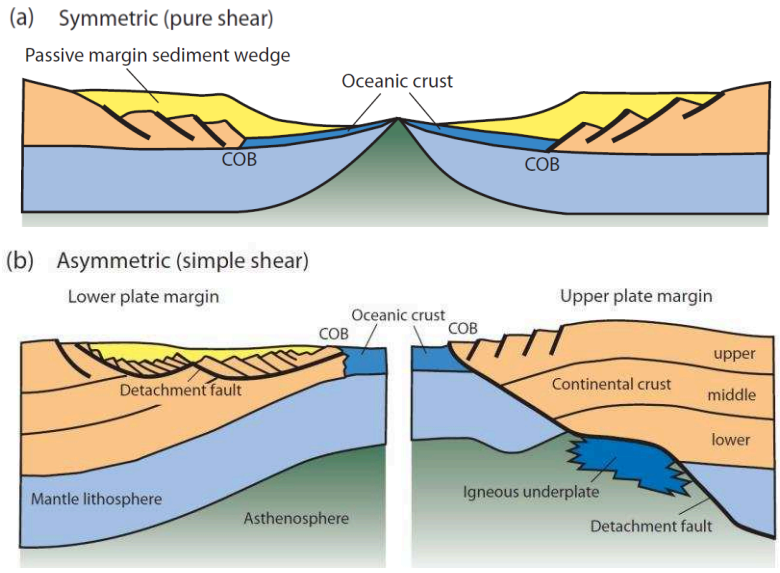

Figure 1.13: Schematic representation of symmetric and asymmetric passive margins: a) Symmetric passive margins derived from pure-shear rifting with a thermal anomaly placed below the area of maximum crustal thinning; b) Asymmetric conjugate margins derived from simple shear models, with the thermal anomaly displaced from the area with maximum crustal thinning. COB indicated the continent-ocean boundary, indicating the onset of the first truly oceanic crust (from Allen and Allen, 2013)

Besides symmetry, other characteristics are used in the classification of passive margins, e.g. abundance of sediments differ in sediment-nourished or sediment-starved margins, the presence or absence of gravitationally driven or salt tectonics in the drift phase (Allen and Allen, 2005).

The abundance of volcanic activity during breakup is also one of the key factors in passive margin classification. Magma-rich (volcanic) margins and magma-poor (hyper-extended) margins are the two end-members of this classification. Tugend et al. (2018) bring the question on the magmatic budget at the time of breakup. Magma-rich rifted margins have a high magmatic budget during rifting and at lithospheric breakup while magma-poor margins would have a very low magmatic budget. The most important factors controlling magmatic budget seem to be: mantle temperature, extension rates, mantle composition, preceding rift history and the presence or not of active upwelling. The magmatic processes occurring at the rift-to-drift transition (during lithospheric breakup) are recorded continentward of the first unambiguous oceanic crust. The area defined between normal continental crust on one side, and normal oceanic crust on the other, is referred to as the continent-ocean transition (COT).

The continent-ocean boundary (COB in Fig. 1.13) is defined at the external boundary of the COT, and the onset of normal oceanic crust.

Magma-poor margins (Fig. 1.14a) are typically hyper-extended margins. They show wide domains of extended crust (wide COT) with wide-ranging extensional features as rotated fault blocks and detachment surfaces near the base of the continental crust, and an anomalously small fraction of magmatism during breakup (Franke, 2013; Pérez-Gussinyé, 2013). Magma-poor margins are usually produced by passive asymmetric rifting (simple-shear) and usually preserve many of their characteristics. Exhumation of serpentinised lithospheric mantle is achieved through deeply rooted detachments. The Iberia-Newfoundland conjugate margins (Brune et al., 2017; Pérez-Gussinyé, 2013; Whitmarsh and Manatschal, 2012), the Labrador Sea (Chalmers, 2012), and the SE-India margin (Tugend et al., 2018) are some examples of this archetype. In a typical magma-poor margin section, as the one presented in figure 1.14a, Tugend et al. (2018) define several structural domains from continent to ocean: proximal, thinned, exhumed mantle, proto-oceanic (COT), and oceanic domains (see Peron-Pinvidic et al., 2013, for detailed terminology). The salt basins in the Brazilian South Atlantic and their conjugate in West Africa, even if some magmatism is present, are considered within the magma-poor margin class (Aslanian et al., 2009; Chaboureau et al., 2013; Kukla et al., 2018; Moulin et al., 2013; Peron-Pinvidic et al., 2013).

Transform margins are magma-poor, abrupt, margins that are intimately related to transform faults, which define a tangential movement between divergent plates (Roberts and Bally, 2012). The best-known transform margins are in the Equatorial Atlantic between, Guinea and Nigeria (Basile et al., 2005), and its conjugate along the conjugate margin of Northern Brazil, Suriname (Blaich et al., 2008), and the South America-South Africa (Broad et al., 2012) in the southernmost South Atlantic. In the last decade, transform margins became key areas of renewed margin research after the discovery of large hydrocarbon resources is stratigraphic traps associated with the abrupt nature of these margins offshore Ghana (Jubilée field, Dailly et al., 2013) and recent discoveries in French Guiana and Guyana (Liza discovery and satellites, Zborowski, 2018).

Magma-rich margins (volcanic margins, Fig. 1.14b) are characterized by extrusive, usually tholeiitic basalts forming wedges that thicken in the seaward direction. These packages identified on seismic data by high amplitudes are known as SDR or Seaward Dipping Reflectors (Hinz, 1981a; Mutter et al., 1982). Lower crustal igneous accretions (magmatic underplating,

sometimes called High Velocity Zones), especially near the COT, are another common characteristic of these margins. The nature of the basement in the COT below SDRs in magma-rich margins is poorly constrained. Interpretations arise from recent geophysical potential methods. It is usually referred to as transitional crust (Blaich et al., 2013). Tugend et al. (2018) and other authors discuss several potential scenarios as for example: intruded lower crust, intruded lithospheric mantle, and new magmatic crust. The most iconic examples of magma-rich passive margins are from Norway-Greenland (Mutter et al., 1982; Planke et al., 2000; Geoffroy, 2005), and the South Atlantic (Hinz, 1981; Gladczenko et al., 1998; Franke et al., 2007; Koopmann et al., 2014).

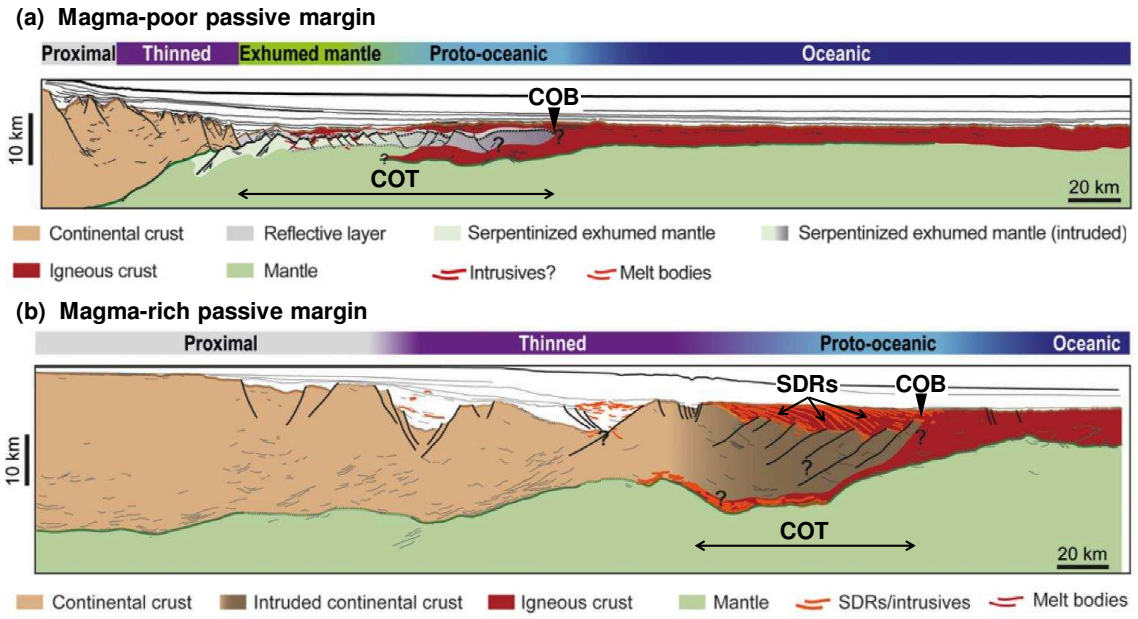

Figure 1.14: Examples of magma-poor and magma-rich rifted margins: a) Magma-poor SE Indian rifted margin; b) Magma-rich Uruguay South Atlantic margin (modified from Tugend et al., 2018). COT: Continent-Ocean Transition, SDR: Seaward Dipping Reflectors, COB: continent-oceanic boundary

Several authors such as Franke (2013), Nemčok (2016) and Tugend et al. (2018) make the distinction between crustal and lithospheric breakup. Lithospheric breakup is defined as a tectono-magmatic process recording the rift-to-drift transition at proto-oceanic domains, and is achieved through the emplacement of a steady-state, self-sustaining, sea-floor spreading system. Crustal breakup, on the other hand, refers to the separation of two blocks of continental crust (i.e. continental breakup) but does not necessarily imply the onset of oceanic crust accretion in between those two blocks (e.g. mantle exhumation can occur). In a nutshell, when crust breakup occurs prior to lithospheric breakup, magma poor margins develop, with a more 'ductile' lithospheric mantle preventing the ascent of the asthenosphere and the onset of oceanic

crust accretion. When lithospheric mantle occurs prior or at the same time that continental breakup, the abrupt ascent of the asthenosphere produces excess magmatism which is recorded in the SDR wedges.

Besides these two end-members, some rifted margins show complex and polyphased tectono-magmatic histories and can present features typical of both magma-rich and magma-poor archetypes. In the East Greenland-Mid Norway margin, for example, magma-poor rifting preceded magma-rich lithospheric breakup (Fig. 1.15). It is important to highlight however, that in this case, these two stages did not occur as part of a continuum process, but quite separate in time (Geoffroy, 2005).

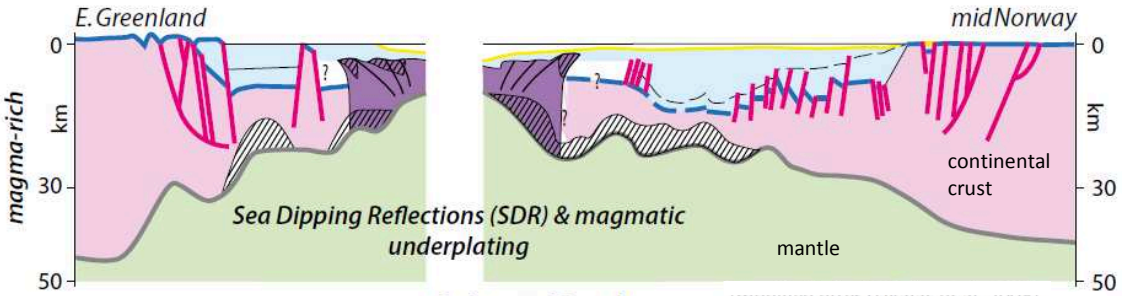

Figure 1.15: Schematic cross-section of the East Greenland-Mid Norway margin at the time of breakup. Magma-rich breakup was preceded by magma-poor rifting (modified from Doran and Manatschal, 2017).

One of the main features of magma-rich margins is the occurrence of SDRs, which were first identified on seismic data in the '80s (Hinz, 1981a; Mutter et al., 1982). Outcrops on the North Atlantic conjugate margins, in Greenland and Norway, have classically been used as analogs for SDRs, and observations made there have been used to support different proposed emplacement mechanisms (Geoffroy, 2005). For the South Atlantic in particular, the interpretation of margin structure during the 90's and 2000's was performed using seismic and gravimetric data that allowed the preparation of dip-sections with focus on crustal thickness and interpreted densities variations (Gladczenko et al., 1998; Franke et al., 2006; Schnabel et al., 2008; Blaich et al., 2009). SDRs are classically interpreted as volcanic flows emplaced in sub-aerial to shallow sub-aqueous conditions. SDR wedges have been drilled offshore Norway (Eldholm et al., 1987), southeast Greenland (Larsen et al., 1998). The well Kudu, drilled offshore Namibia found aeolian sandstones interbedded with shallow marine sediments and basalts, that have been interpreted as the top of SDR packages (McMillan, 1990). A big step forward in the knowledge of passive margins, and magma-rich margins in particular, was given in the last decade with the acquisition of deep seismic data, that made possible to depict the

whole crustal architecture, the Moho geometry, and to see below the SDRs (Koopmann et al., 2014a; Paton and Underhill, 2004; Stica et al., 2014; Horn, 2015). In a generalized dip-section across a magma-rich margin, as the one presented in figure 1.16, several typical features of this kind of margins are indicated. In the first place, the possible presence of previous sedimentary basins (as is the case of the NE-Atlantic, Fig. 1.15, or the Colorado basin, offshore Argentina, Franke et al., 2007), or eventual traps (large volcanic effusive plateaus, as is the case of the Serra Geral basalts in the pre-rift of the Pelotas basin, Stica et al., 2014). Another common feature in volcanic margins is the presence of high Velocity Zones (HVZ in Fig. 1.16), typically emplaced below the intruded transitional crust along the COT. HVZs might present velocities Vp of 7.2 to 7.7 km/s. Underplating of mafic and ultra-mafic magma is the main suggested process to produce this features (Kelemen and Holbrook, 1995; Geoffroy, 2005).

From the continental crust towards the oceanic domain, Geoffroy (2005) differentiates internal and external SDRs on the COT domain, and 'oceanic SDRs' (Fig. 1.16). Oceanic SDRs seem to be related to margins with a thick oceanic crust (of up to 40 km) as oceanic crust may reach up 40 km in thickness in Iceland and along the Greenland–Iceland–Faeroe aseismic ridge (Geoffroy, 2005). Internal and external SDRs are emplaced on the continent-ocean transition. There is not a clear criterium to differentiate them, rather than their relative location on the COT and the nature of the underlying crust (more magmatic for the outer SDRs). Sometimes inner and outer SDRs are separated by an external or outer high (of volcanic or exhumated lithosphere nature, see Planke et al., 2000).

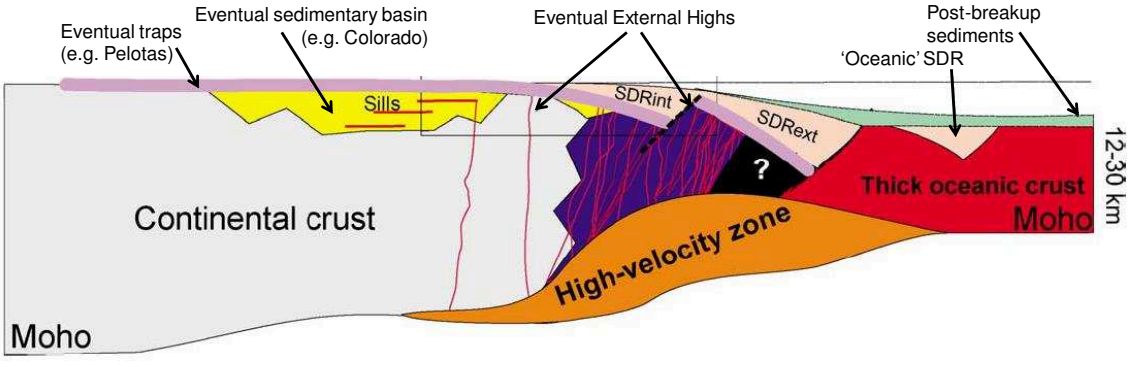

Figure 1.16: Schematic dip-section of a magma-rich passive margin, with the main features observed in different magma-rich margins (modified from Geoffroy, 2005).

SDR wedges are formed of subaerial to shallow subaqueous basalts, interbedded with usually continental (fluvial, aeolian) sedimentary packages. Their emplacement is interpreted to occur in a sustained environment near the sea level, and over a very short period of time. In

the North Atlantic, the chemistry of the basalts changed in time from alkaline to tholeiitic (Saunders et al., 1997), probably related to a decrease in contamination with continental crust with time towards a more MORB geochemistry closer to the onset of oceanic crust accretion. The wedge-shaped geometries of SDRs suggest a possible syn-magmatic fault activity during the process of crustal thinning and breakup.

Several mechanisms have been proposed for SDRs emplacement and remain until these days matter of discussion among the scientific community. One first and main difference highlighted by Talwani and Abreu (2000) is that there is no agreement regarding the time of onset of emplacement of SDRs, either during the rifting of continental crust or later (synrift), or as part of the early oceanic crust accretion (early drift). Authors such as Franke et al. (2010), Holbrook et al. (1994) and Talwani et al. (1995), following Hinz (1981) and Mutter et al. (1982), interpret emplacement during the early onset of oceanic crust accretion in a 'subaerial' ridge. In this way, the nature of the crust below the SDR is mostly magmatic, the surfaces bounding the wedges are interpreted as feeder dykes, and the subsidence is related to the loading of the younger SDRs. Recently Buck (2017) presented an update of this volcanic flexure model, introducing jumps in the location of the feeder systems (Fig. 1.17b). White and Mckenzie (1989) had suggested that SDRs formed during the rift phase under the influence of a hot spot. Although today we know that a hot spot is not required for SDR formation (e.g. the South Atlantic shows a wide range of SDRs previous to the Paraná-Etendeka plume impingement; Frizon De Lamotte et al., 2015; Will and Frimmel, 2018), SDR emplacement associated with subsidence created by active normal faulting remains valid. Eldholm et al. (1995) and Geoffroy (2001, 2005) explained SDR as syn-magmatic roll-over flexures accommodated by continentward-dipping normal faults (Fig. 1.17a). The presence of these continentward, or inboard dipping normal faults seems to be a key feature in volcanic margins, as they are not present in magma-poor margins (where normal faults tend to dip in a seaward direction). More recently Quirk et al. (2014) suggest an hybrid model of magma-assisted extensional growth for the emplacement of SDRs, where magma rises in the footwall of a normal fault as continental plates start to separate, and the weight of the younger flows trigger the subsidence.

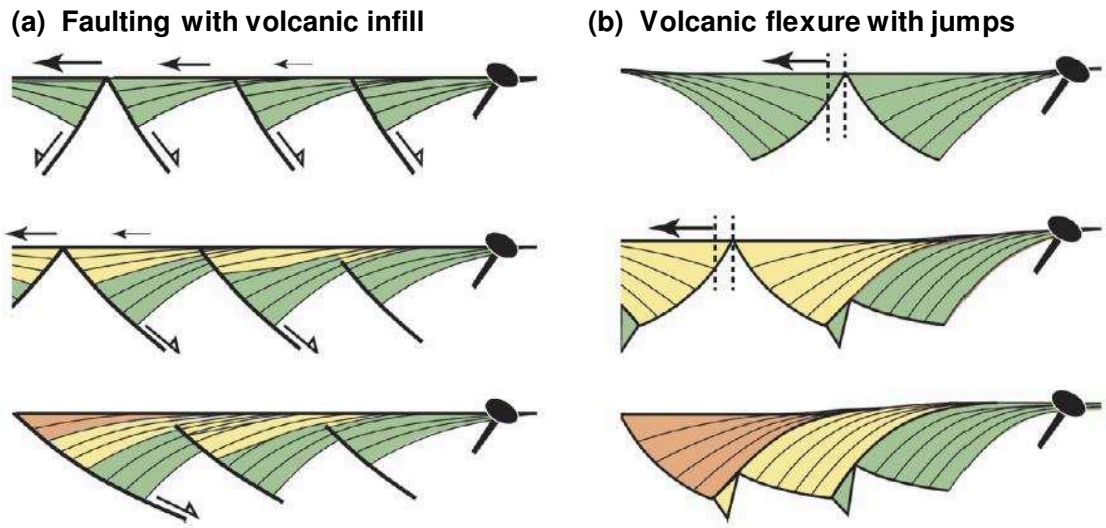

Figure 1.17: Generalized representation of two end-members emplacement mechanisms of SDRs: a) Normal fault model (after Eldholm et al., 1995, and Geoffroy, 2001); b) Volcanic flexure model, in this case with jumps (from Buck, 2017).

The increased resolution of the deep crustal levels in industrial seismic profiles of the last decade acquired along some rifted margins lead to the unraveling of an unexpected variety of structures and processes. Stica et al. (2014) highlighted, in the Pelotas basin (Brazilian South Atlantic margin), the sharp seaward SDR wedge-boundaries that they interpreted as syn-tectonic normal faults. Pindell et al. (2014) recognized in deep seismic lines not only the existence in many basins of fault-controlled SDRs (Fig. 1.18a), but also the occurrence of SDRs as long trains of convex-up SDRs (Fig. 1.18b), that seem to be welded with a magmatic lithosphere. This reflects that SDRs differ in the different basins and probably not one single mechanism should be used to explain all kinds of SDRs.

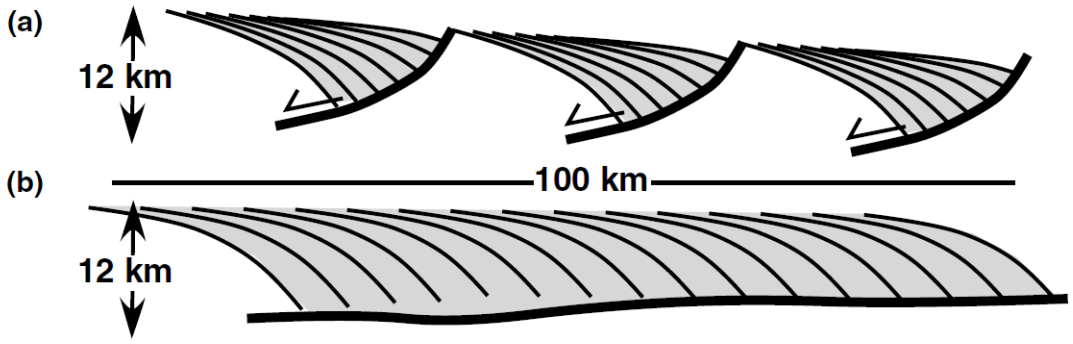

Figure 1.18: Models of (a) fault-controlled SDRs, and (b) trains of convex-up SDRs, have been identified in different basins (from Pindell et al., 2014).

Pindell et al. (2014) also introduced a model of outer marginal collapse for the evolution of rifted margins, where landward dipping shear zones at the base of a previously thinned crust,

produce rapid tectonic subsidence, an hypothesis that is similar to the active mantle model of Geoffroy (2005). More recently, Clerc et al. (2015, 2018) noticed that the lower crust appears much more intensely deformed in rifted margins than usually represented. They observed clear indications of ductile deformation of the deep continental crust along large-scale shallow dipping shear zones (similar to the one presented by Pindell et al., 2014), that sometimes define an anastomosed pattern, and that act as a decoupling surface for the deformation in the brittle upper crust and the more ductile lower crust and mantle. These shear zones generally show a top-to-the-continent sense of shear consistent with the activity of continentward dipping normal faults observed in the upper crust (Fig. 1.19).

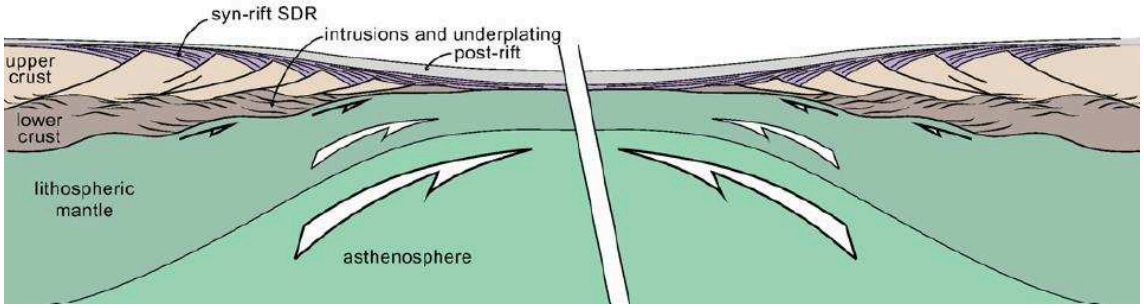

Figure 1.19: Schematic representation of magma-rich conjugate margins (from Clerc et al., 2018).

For the northern Argentinean margin, Paton et al. (2017) analyzed the gravimetric signature of the COT and interpreted a progressive increase of magmatic crust below the SDRs (similar to the oceanic crust) in the oceanward direction. Also, they did not observed faults at the wedges terminations (Fig. 1.20), but a diffuse termination off the SDRs oceanward. Their model (Fig. 1.21) invokes progressive rotation of originally horizontal volcanic flows with subsidence driven by isostasy in the center of the evolving SDR complex.

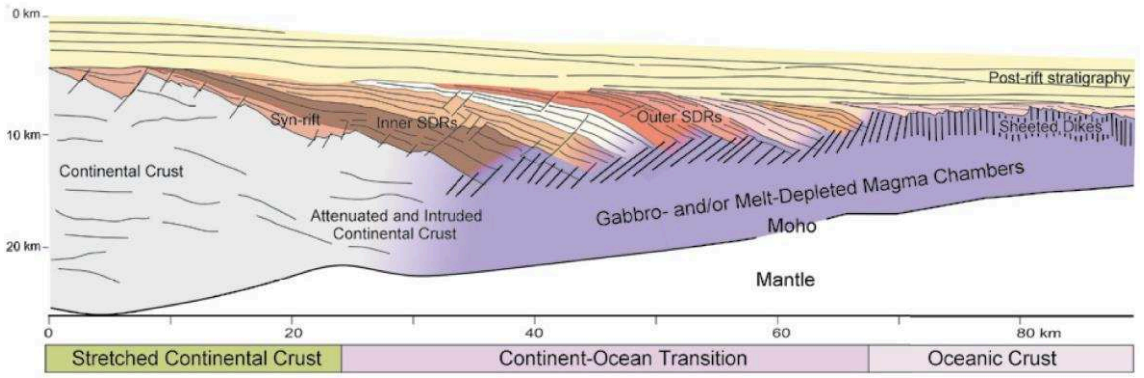

Figure 1.20: Sketch interpretation of the volcanic passive margin in the Salado segment, offshore Argentina (from Paton et al., 2017).

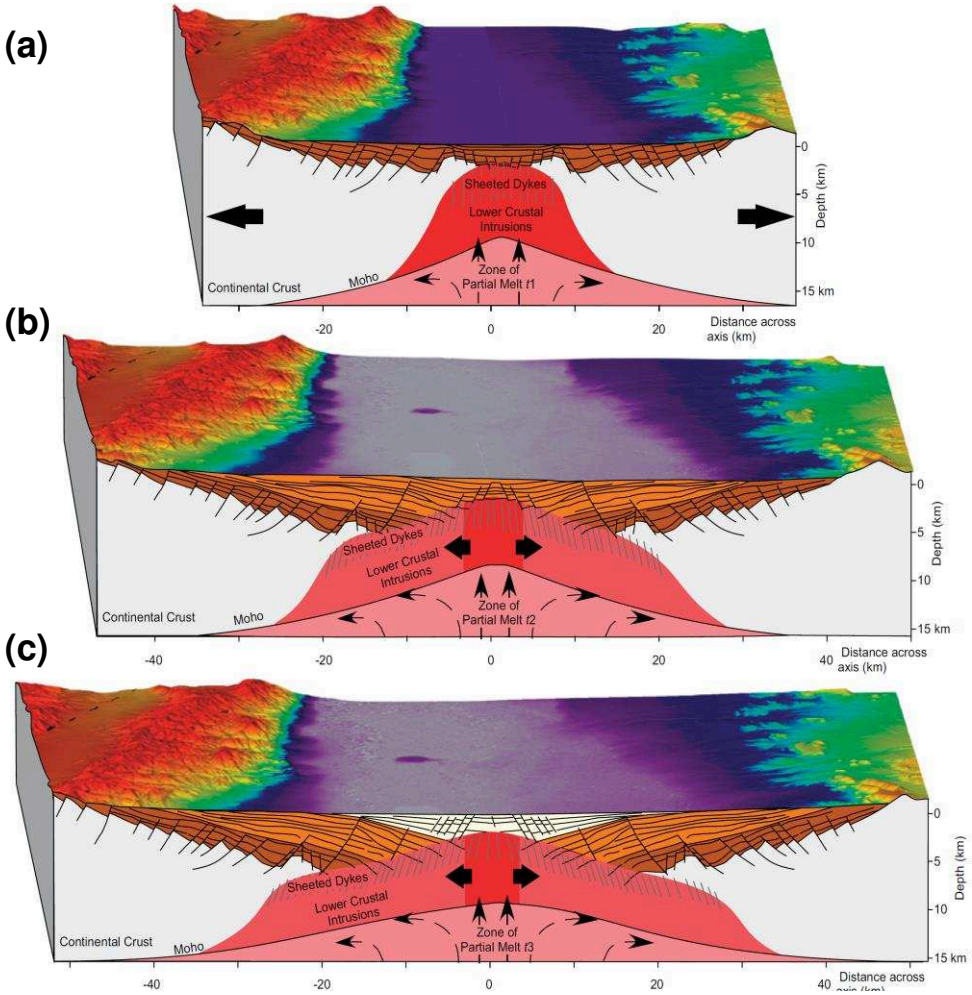

Figure 1.21: Model of the evolution of SDRs proposed by Paton et al. (2017): a) Mechanical processes dominate crustal stretching with lithospheric thinning resulting in magma generation in the center of the rift system; b) Strain is accommodated through diking. The dikes feed the subaerial magmatic flows on the surface. New magmatic crust is generated at the incipient spreading center; c) Breakup occurs and oceanic crust processes dominate the system.

In summary, the different SDR emplacement models are derived from some of the key magma-rich margins known, e.g. the outcrops in the NE-Atlantic, the magma-rich margins in the South Atlantic, etc. The models were progressively updated with the new data that was being acquired. The recent acquisition of deep seismic data allowed to see the structure of the SDRs and the crust underneath, in some cases fault-bounded SDRs are observed (Stica et al., 2014), in the other cases SDRs seem to merge with the transitional crust (Paton et al., 2017). Logically there is no need for having one unique model for SDR emplacement, because not all margins are the same, the nature and thickness of the continental crust that is breaking changes, the rate of extension, the temperature of the mantle could possibly change too, and so it seems rather probably to have SDRs displaying different architectures. The nature of the SDRs

themselves is transitional, because they record the breakup process of the lithosphere, they form during the last phase of rifting (inner SDRs on thinned continental crust), and the early onset of oceanic crust accretion in magma-rich margins (with outer SDRs on more magmatic crust, probably heavily intruded). The data to be acquired in the future in these frontier areas, and the continuous work will bring new insights and hopefully other models to better understand these margins.

Several authors have discussed the factors controlling if a rift system will break up in magma-poor or magma-rich mode. Franke (2013) suggests that passive margin evolution depends on the rheology of the lithospheric mantle. A magma-poor margin is created if, during extension, the brittle crust extends together with a 'ductile' lithospheric mantle. Magma-poor margins are defined by a wide area of highly attenuated hyper-extended crust, where the upper crust is deformed by deep listric faults that may sole out on a common detachment surface (eventually the Moho). If lithospheric mantle behaves in a more brittle way, it will also break together with the crust during extension and an asthenospheric window could arise, thus producing huge volumes of extrusive igneous rocks: the SDRs, typical of magma-rich margins.

The development of magma-rich margins has commonly been related to the presence of a mantle plume (e.g., White and Mckenzie, 1989; Eldholm et al., 1995). However, this idea has been challenged, in particular by Franke (2013) who shows that in the South Atlantic the SDR volumes increase systematically away from the plume impingement area (in the case of the South Atlantic, the plume related to the Paraná LIP, Fig. 1.22a). The relation between faster plate separation and magma-rich margins has also been established (Lundin et al., 2014) as well as the diachronism that can be observed in rifting and breakup. In areas with good magnetic data, diachronous break-up can commonly be demonstrated by magnetic isochrons that lengthen as sea floor spreading progresses. In these cases, older isochrons terminate against the COT and are "bypassed" by younger isochrons (Franke et al., 2007; Stica et al., 2014). This observation has long been considered to reflect propagation (e.g., Courtillot, 1982; Martin, 1984). An example is the northward propagation of the South Atlantic (e.g. Franke, 2013; Jackson et al., 2000; Nürnberg and Müller, 1991; Rabinowitz and LaBreque, 1979; Torsvik et al., 2009). Break-up usually takes place along segments, which may vary in sizes. The breakup model presented by Lundin et al. (2014) introduces a 'V-shaped' triangular map pattern with, at its apex, crustal stretching in an initiating phase, and with increasing extension towards the opposite end. Along the arms of the V the transition between coupling/decoupling and total

embrittlement can be observed at increasing distance from the apex. The apex works as a steadily-migrating 'pseudo-pole'. Close to the pole, the linear rate of plate separation is very small. At some farther distance, deformation will have progressed to the thinning phase (Lavier and Manatschal, 2006), where complete crustal embrittlement, fault penetration, and mantle serpentinization become probable. Mantle exhumation is predicted at a still greater distance. At some point, the pole is so distant that the linear half spreading rate exceeds the critical velocity for melting. This may lead first to production of an ultraslow hybrid mixture of peridotite and basalt, and eventually to Penrose 'typical and fully developed' oceanic crust. In map plane, a fully developed zonation from proximal rift to oceanic crust may have been completed far away from the pole while it is just beginning to initiate closer to the pole (Fig. 1.22b). Continental break-up around a single rotation pole cannot continue ad infinitum, but must progress by the eventual opening of a new segment. This model, presented by Lundin et al. (2014), predicts that architectural zonation will proceed sequentially along the conjugate lengths of an opening ocean following a series of moderately sized pole jumps (~1000-2000 km, Fig. 1.22c). For very large pole jumps (>2000 km) the rate of extension at the distal end may be so high that rapid necking is favored and possibly also magma-rich breakup. In such cases an along-strike transition from magma-rich to magma-poor may take place. This model has been used to explain the Red Sea, Labrador Bay, and could provide a guideline to understand the development of large scale architectural elements during the opening of the South Atlantic Ocean.

Numerical modelling has significantly contributed to the understanding of breakup and passive margin evolution (e.g. Huismans and Beaumont, 2008; Brune et al., 2014). But as the understanding of magma-rich margins is still under development, only some latest numerical models start to be successful in explaining the formation of volcanic margins (Geoffroy et al., 2015; Beniest et al., 2017) and there seems to be a long way to go in this debate.

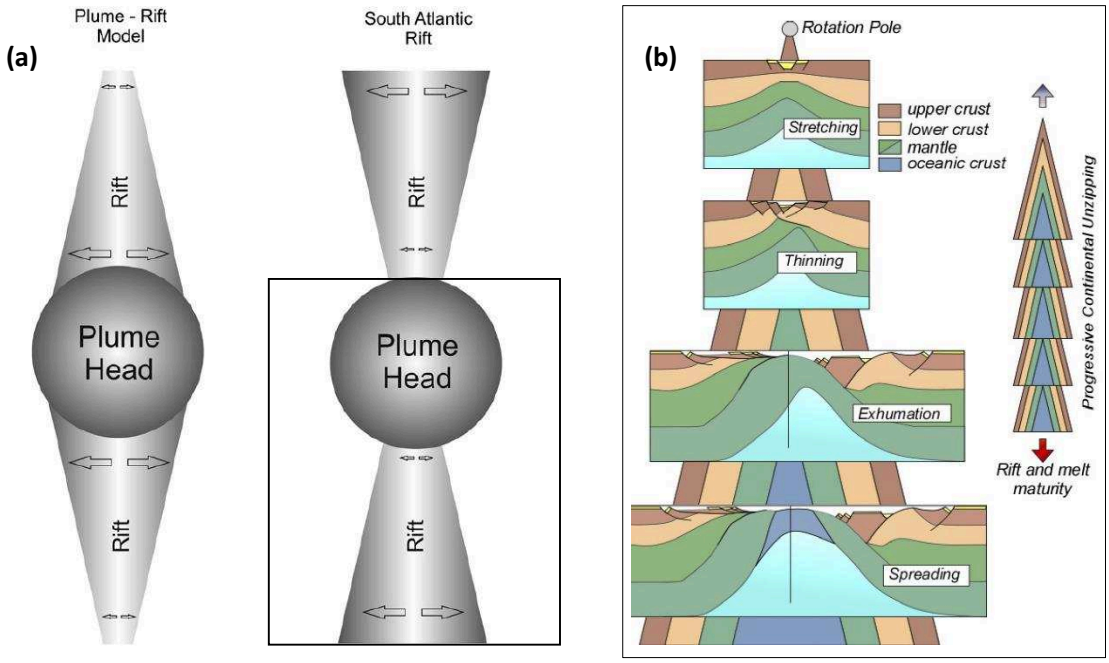

Figure 1.22: Selected models proposed for the opening mechanisms of the South Atlantic Ocean: a) Expected evolution of a rift that evolves in conjunction with a plume head (as the plume head triggers the rift evolution by a circular uplift, the earliest and widest rift is expected close to the plume head), but the contrary is observed in the southern South Atlantic (the rift started in the south, at the most distal point from the Paraná-Etendeka plume and rifting migrated towards the plume, from Franke, 2013); b) Diachronous breakup model presented by Lundin et al. (2014) after references therein, showing the V-shaped nature of each rift segment with more evolved facies away from the 'rotation' opening pole; c) Diachronous map patterns formed during 'unzipping' of the ocean, under stepwise pole propagation (Lundin et al., 2014).

1.5 Stratigraphic evolution of passive margins

Rifting, successive breakup and passive margin formation produce sedimentary basins that can be studied to invert their stratigraphic record as a tectonic evolution. The sedimentary infill of a basin records not only deep lithospheric processes such as rifting, mantle exhumation, oceanic breakup, but also the interaction of these processes with surface processes (Fig. 1.23). Surface processes are conditioned by the climate, erosion, that themselves control the sediment routing systems, the environmental conditions prevailing in the basin and base level changes (i.e. eustasy).

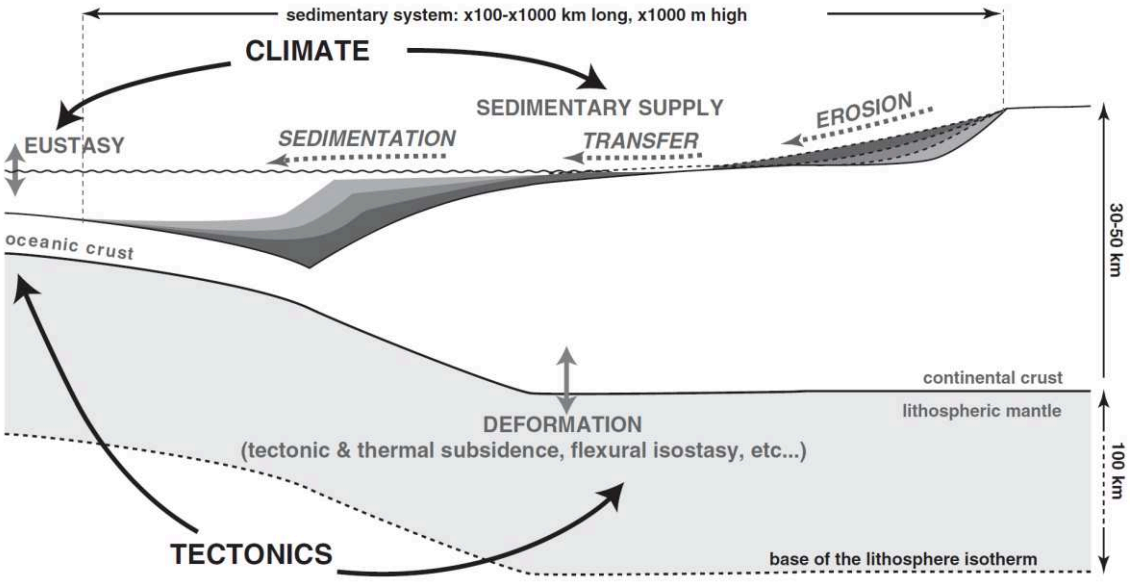

Figure 1.23: Summary sketch representing the main interacting processes determining the post-breakup evolution of a passive margin. Thermal subsidence, flexural isostasy and the load/unload effect of surface transfer are the main mechanism controlling the basin deformation (from Guillocheau et al., 2012).

In rift basins, stretching produces normal faulting of the brittle crust and subsequent thinning of the lithosphere, inducing subsidence and the formation of sedimentary basins. McKenzie (1978) proposed a method to compute subsidence in a rift basin with a pure-shear model that assumes uniform stretching of the crust and lithosphere. During rifting (synrift phase), depocenters will have a fault-controlled subsidence, which depends on the initial thickness of the crust compared to the initial thickness of the lithosphere, and the amount of stretching β factor (Allen and Allen, 2005). Regions with thick crusts should experience larger amounts of fault-controlled subsidence than those with thin crusts. Lithospheric mechanical stretching, and thinning, supposes the ascent of isotherms and an instantaneous increase in heat flow. After stretching has ceased (postrift phase), the new elevated geotherm relaxes as the lithosphere cools down and thickens. These regions experience thermal subsidence, caused by the relaxation of lithosphere isotherms to their pre-stretching position, with an exponentially decrease of heat flow with time. Regions with thick subcrustal lithosphere should experience greater subsidence and more prolonged post-rift thermal subsidence than those with thinned lithospheric mantles.

Passive margins are characterized by a seaward thickening prism of marine sediments that generally overlay a zone of faulted basement with rift basins usually filled with continental sediments, which record the rifting and breakup processes. Le Pichon and Sibuet (1981) applied

the uniform stretching model of McKenzie passive margins, as an approach to assess their subsidence history. But the subsidence history of nourished passive margins, with thick drift sedimentary covers is also affected by sediment load, which will add subsidence depending on the rigidity of the plate (Watts, 1989). Backstripping of the sedimentary cover is used to reconstruct the tectonic history of passive margins (Watts and Ryan, 1976; Steckler and Watts, 1978; Steckler et al., 1988), by removing the influence of sediment and water loading. Lavier et al. (2000) applied a similar backstripping method on 2D sections from the West Africa margin.

Elastic thickness is a proxy of the long-term strength of the lithosphere and exerts a strong control on the overall stratigraphic architecture of a passive margin. The most common approach for assessing the elastic thickness of the lithosphere is gravity modeling. Watts (1988) suggested a method of process-oriented gravity modelling, an alternative flexural backstripping method that can constrain the elastic thickness by comparing the observed crustal structure with the result of the combination of the restored rifted crust and the influence of the sediment load (see Fig. 1.24). In magma-rich margins, the effect of magmatic underplating and SDRs can also be included by computing their flexural loading effect (Watts, 2012).

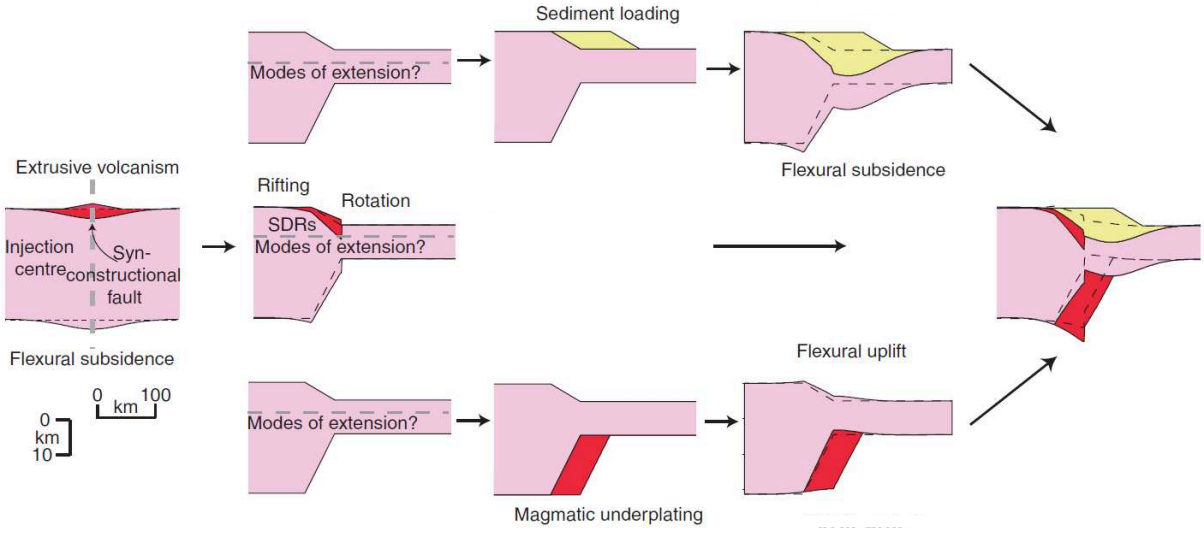

Figure 1.24: Key processes that condition the mechanical evolution of passive margins: rifting, sediment loading, SDR emplacement, and magmatic underplating have a strong influence on subsidence history (modified from Watts, 2012).

In the last decades, thermo-mechanical models have been used to assess the evolution of passive margins. These models combine the evolution of the thermal structure, that determines heat flow, and hence the amount of tectonic subsidence and uplift; with the

mechanical structure, that determines how it responds to sediment and other loads throughout the rift-to-passive margin evolution. Watts (2012) presents a complete synthesis of the use of thermo-mechanical models in passive margin studies. Kinematic models suggest that tectonics (thermal contraction, uplift and flexure) is a major control on the early stratigraphic evolution of passive margins, while at later stages, the sedimentary flux, and/or eustasy are the dominant controlling factors.

Another element that needs to be considered, together with the sediment load, is the unloading produced by erosion in the proximal part of the passive margin. There is a complex coupling effect that is recorded in the stratigraphy of sedimentary basins (Rouby et al., 2013). Classically the long-term regressive stratigraphic architecture of passive margins (with seaward migration of the shoreline) has been attributed to the exponentially decreasing rate of basement thermal subsidence, combined with the sedimentary supply, usually larger than the accommodation space. But the flexural component of subsidence may migrate in the seaward direction under the weight of a prograding sedimentary wedge. Cylindrical margins behave similarly along-strike, can be modeled with 2D sections and conclusions from that modeling can be extrapolated. But margins can also be non-cylindrical, present a strong 3D variability and thus need to be modeled in 3D for a correct assessment. Braun et al. (2013) introduced 3D modeling tool that was used to assess a non-cylindrical rifted margin, particularly for the case of two segments of a margin separated by a fracture zone, which incorporates variable elastic thickness, surface processes and 3D thermal subsidence. For the Western Africa Transform Margin, Braun et al. (2013) reproduce the subsidence patterns observed in the overlying passive margin sedimentary basin, and predict a relatively complex stratigraphic architecture, which is the result of varying sources and subsidence behaviors along the various segments of the margin.

A final comment on subsidence assessment comes from the recent progress made in the understanding of the influence of mantle convection and the resulting dynamic topography on passive margins. Müller et al. (2018) carried out sensitive modeling of these dynamics and obtained dynamic-induced subsidence values of up to 350±150 m for passive margins. These authors noticed that during the fragmentation of Pangea the most commonly observed process along passive margins is a gradual change from dynamic highs towards lows, reflecting the location of many passive margins over slabs sinking in the lower mantle. The understanding of these processes is still under development. Some observations are being made for South

America and contributing in the understanding of the influence of Andean processes on the South American platform (Dávila and Lithgow-Bertelloni, 2013; Flament et al., 2014; Davila et al., 2018). Paleodynamic models require accurate paleotectonic reconstructions. The southern South Atlantic reconstructions still need to be improved, especially considering the relations between South America, Africa and Antarctica during Gondwana breakup (König and Jokat, 2006).

Regional thermochronological studies have classically been applied to orogenic regions. Analysis on passive margins are still under development, since the post-breakup topographic evolution of passive margins (especially the onshore portion) remains poorly understood (Bigot-Cormier et al., 2005; Karl et al., 2013; Kollenz, 2015). Two end-members for the onshore part of passive margins are observed: elevated, versus low-lying passive continental margins. These areas observe episodic km-scale exhumation or burial events that still need to be addressed (Green et al., 2017; 2018).

In passive margins, the record of stratigraphic sequences is a function of the accommodation (the space available for sedimentation) and sedimentary influx (which provides the sediments to fill the space). Accommodation can be created either by subsidence, as previously detailed in the present manuscript, or by increasing the base level for sedimentation (the sea level in the case of passive margins). During the drift phase (post-breakup), eustasy is a key factor in controlling the stratigraphic architecture of passive margins, with variability at a higher frequency than subsidence (Vail et al., 1977a, 1977b; Van Wagoner et al., 1990).

In sedimentary basins, the sedimentary record can be divided in sequences, which are relatively conformable successions of genetically related strata, bounded by unconformities and their correlative surfaces (Mitchum et al., 1977). With the main surfaces in sequence stratigraphy (e.g. subaerial unconformities, transgressive surfaces, maximum flooding surfaces) being equivalent or approximatly equivalent to timelines, a sequence stratigraphic approach (Catuneanu et al., 2009) allows the preparation of a chronostratigraphic models that can be incorporated into larger models assessing the evolution of passive margins.

A synthesis of the stratigraphic response and the main unconformities from rifting to continental breakup was presented by Franke (2013). An adaptation of this model for magma-rich margins is presented in Fig. 1.25. In a rift basin strata can be grouped in pre-, syn- and post-rift sequences according to their relative chronology with respect to the extensional phase,

and the main factor conditioning subsidence. The pre-rift units correspond to older deposits that were preserved from erosion across the time between their deposition and the onset of rifting. The 'rift onset unconformity' (ROU) marks the top of the pre-rift unit and the base of the synrift (Fig. 1.25a). The synrift unit deposits during extension in fault-bounded prism usually presenting growth-strata (Fig. 1.25b). In aborted rift basins, cessation of mechanical extensional activity and the onset of the thermal sag phase of the basin is indicated by the synrift-postrift unconformity. In the case of successful rifting the formation of an oceanic basin enclosed by conjugate passive margins, the 'breakup unconformity' (BU) marks the onset of oceanic crust accretion (Fig. 1.25d). The BU separates the synrift strata from the drift phase strata. If magma-rich breakup occurs, SDRs are emplaced in an actively extensive area that will become the continent-ocean transition (COT). SDR emplacement occurs in the transition between the rifting of continental crust, and the onset of oceanic crust accretion (Fig. 1.25c). As 'normal' oceanic crust forms after the emplacement of SDRs, the BU can be tracked at the top of the SDR wedges and continued continentalward. It represented a diachronous hiatus, with a larger span of non-deposition towards the continent. The development of the BU can also be associated with rift-flank uplift.

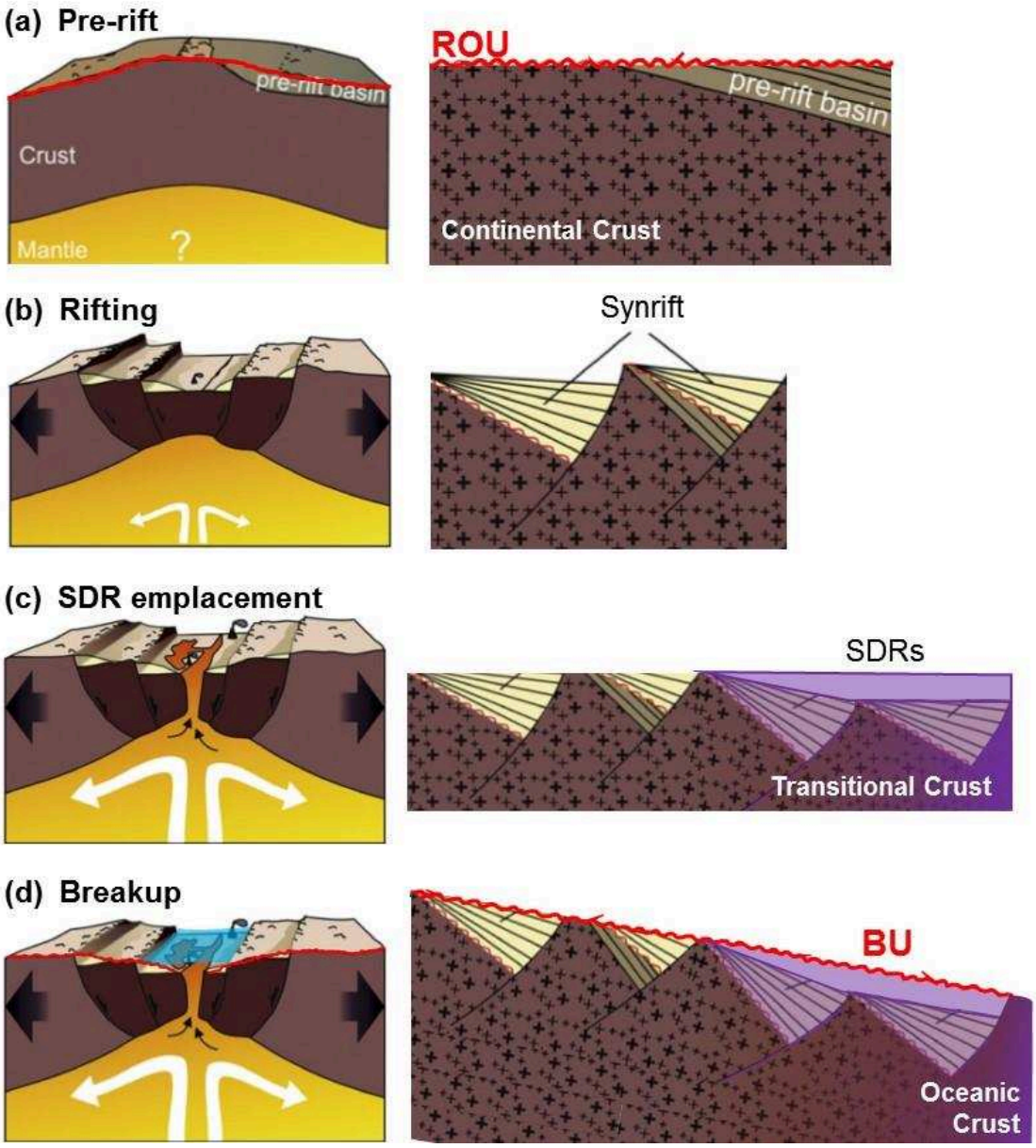

Figure 1.25: Formation of the main unconformities in rift-to-passive margin settings (drawings no to scale, modified after Franke, 2013). The Rift Onset Unconformity (ROU) marks the top of the pre-rift unit. ROU may form during doming preceding rifting (a). During rifting (b) grabens and half-grabens fill with sediments typically under continental conditions. In magma-rich margins, SDR emplacement occurs in the transition to breakup (c) under subaerial conditions. During SDR emplacement, the system shows a rapid seaward migration of the locus of extension, with a progressively thinner and more intruded continental crust (in 'transition' to full oceanic conditions). Just after breakup and the onset of oceanic crust accretion (d) the margin experienced erosion (possibly subaerial to lag-transgressive). The Breakup Unconformity (BU), tracked at the top of the SDRs and extended continentward, is a diachronic surface that marks the onset of the first post-breakup marine transgression.

In magma-poor margins, which lack SDRs, the BU is an unconformity at the top of the fault-bounded wedged sequences, and at the base of the drift phase sediments characterized by passive onlap on the previous relief.

After breakup, the continuous accretion of proto-oceanic crust and associated increasing subsidence allows the income of the sea and the formation of a proto-oceanic basin. Continental rim basins may develop on the conjugate margins according to their rifting history and symmetry (Fig. 1.26b). At the transition from rifting to proto-oceanic basin, subsidence (accommodation) commonly outpaces sediment supply, leading to the deposition of some typical facies indicative of sediment starvation in the basin depocenters: carbonates (carbonate factory enhanced by lack of siliciclastic supply), evaporites (require intermittent disconnection with the sea to allow evaporation), and black-organic shales (Allen and Allen, 2013). Black shales require high organic productivity and restricted water circulation to allow preservation of the organic-rich shales, which constitute major source rocks of hydrocarbons in passive margin settings.

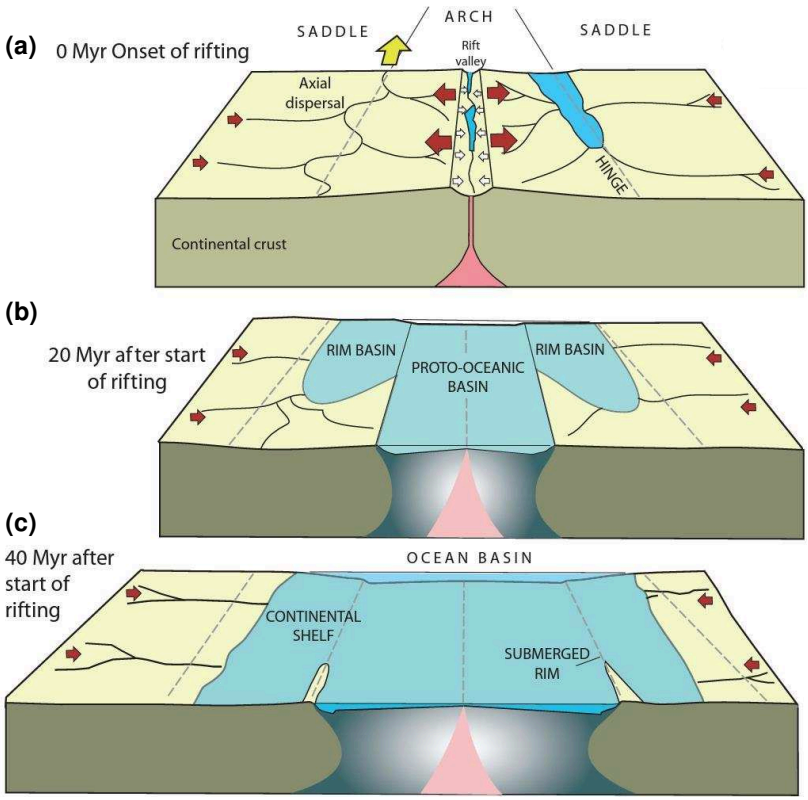

Figure 1.26: Formation of continental rim basins (from Allen and Allen, 2013, after Veevers, 1981): a) Rifting stage; b) 20 Myr after the onset of rifting the model predicts the flooding of rim basins under restricted ocean circulation, adjacent to a new ocean; c) 40 Myr after start of rifting, rim basins become fully connected to the oceanic trough.

Fully developed passive margins are characterized by sedimentary prisms including from proximal to distal: continental, transitional and fully marine environments (shallow and deepwater). Helland-Hansen et al. (2012) review the different typologies and genesis of marine shelve prisms and highlights that transgression is a pre-requisite for the formation of a shelf.

These authors differentiate three main types. Type 1 ‘sedimentary shelves’ (Fig. 1.27a) represent long-term constructional margins formed by overall progradation of a sedimentary wedge or prism. These shelves are formed by sedimentary nucleation and basinward progradation of the slope break. The accommodation is created by long-term subsidence of the margin (e.g. combination of thermal, flexure, sediment load, etc.). Deepwater settings are characterized by starved sedimentation. The basinward progradation of the slope break is balanced by sediment supply, slope failure processes and eventually the erosive action of contour currents in deepwater setting. Episodic transgression over the top of the prism triggers new progradation and the overall construction of the shelf.

Type 2 ‘combined structural-sedimentary shelves’ (Fig. 1.27b) are characterized by a direct structural nucleation and a sedimentary propagation of shelf-slope break. The slope location has a topography inherited from structure. The initial break is then blanketed by sediments, which may prograde with sufficient sedimentary supply.

Type 3 ‘structural shelves’ (Fig. 1.27c) represent tectonically controlled margins. They usually present a fixed slope break associated with the structural feature. According to Helland-Hansen et al. (2012), these shelves are usually sediment starved, with sediment passively filling a structurally-controlled topography. Basement may crop out on the slope.

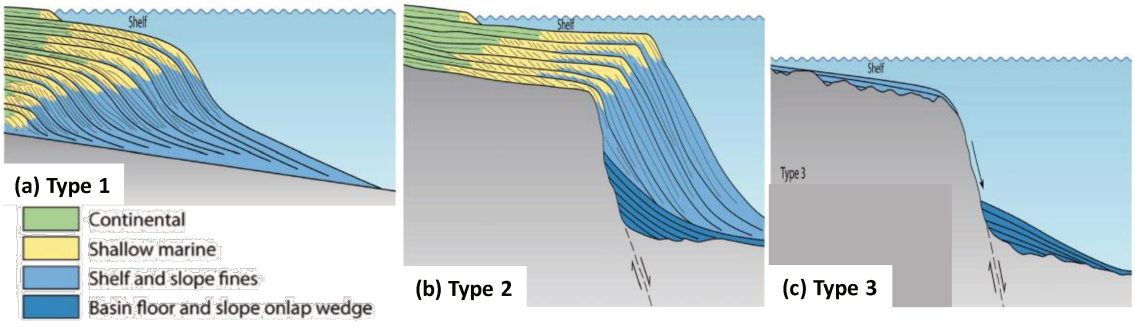

Figure 1.27: Main shelf types from Helland-Hansen et al. (2012): a) Sedimentary shelf, formed by nucleation and basinward propagation of the shelf-break; b) Combined sedimentary-structural shelf, with structural nucleation and propagation of the shelf-break in the slope; c) Structural shelf, with a structurally defined and fixed slope break.

Helland-Hansen et al. (2012) differentiate as well the term ‘platform’ from shelf. According to these authors, platform refers to a lower order feature with respect to a shelf. A platform may have a maximum relief of tens of meters and are formed during progradation of subaqueous deltas or coastal complexes (Fig. 1.28). Shelf is the whole constructed sedimentary prism of the passive margin.

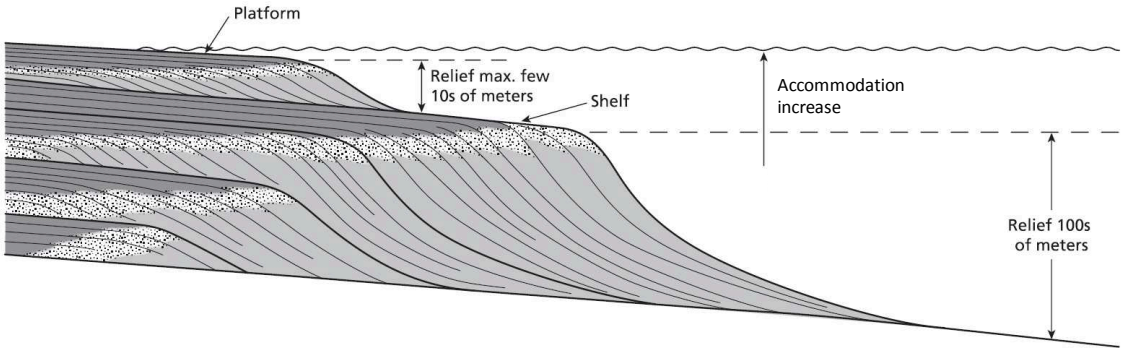

Figure 1.28: Sketch representing shelf and platform morphologies (modified from Helland-Hansen et al., 2012).

Besides the introductory morpho-dynamic character of passive margins described above, the stratigraphy of these basins can be assessed in terms of Sequence Stratigraphy. Although it has been used in the industry and academia for many years, Sequence Stratigraphy remains an 'informal' methodology with several lines of thinking. Much progress has been made in the recent years towards the standardization of sequence stratigraphic methods and building the bases for a common language among researchers (Catuneanu et al., 2009). The Depositional Sequence concept of Mitchum et al. (1977), particularly the Depositional Sequence III approach and nomenclature (see Catuneanu, 2006; Catuneanu et al., 2009) is used in this work. For seismic interpretation the approach of Vail (1987) and the update of Abreu et al. (2010).

During rifting, the grabens and half-grabens develop usually under continental conditions. The accommodation is controlled by subsidence and base level. Subsidence is mostly tectonic during synrift phase, and thermal during sag phase. The base level determines de sedimentation profile, could be within the basin if it is closed (with endorreic drainage), or outside if drainage connects several depocenters. In continental systems, if climatic conditions allow a positive water balance, a lake may form. The lake level will determine the (local) base level. Lacustrine source rocks are key in the hydrocarbon exploration of rift basins and may develop during synrift (e.g. the Bucomazi Fm of the Lower Congo Basin in West Africa) and/or sag (e.g. the Pozo D-129 Fm of the San Jorge Basin, Argentina). If water balance is negative, evaporation will produce playa-lake environments. Sediments will enter into the basin from all flanks, but the steeper slopes associated with the fault-bounded side of the rift will develop alluvial fan systems (or fan deltas), usually coarser than the systems with the not-faulted side.

The sequence stratigraphy of rift basins has been particularly studied by Martins-Neto and Catuneanu (2012), and Picarelli and Abreu (2015).

In the case of passive margins, particularly siliciclastic shelves have been the archetype where Sequence Stratigraphy was developed (Catuneanu et al., 2009). Some remarks need to be made before entering into the details of the Sequence model. Vail proposed that seismic reflectors represented timelines bounding strata. In seismic stratigraphic interpretation the character of the reflectors terminations is important (see Catuneanu, 2002). Above a key surface (discontinuity) reflectors may display onlap or downlap (Fig. 1.29). Onlap is a base-discordant relationship in which initially horizontal (or inclined) strata progressively terminate updip against a surface of greater initial inclination. Onlap can be of different nature depending on the facies that the termination is associated with. Catuneanu (2002) distinguishes between fluvial (landward shift of the upstream end), coastal (shoreface onlap on a ravinement or complex surface) and marine onlap (usually on the slope or abyssal plains and generally related to fine sediments). Downlap refers to the downdip termination of an inclined reflector towards a less inclined or horizontal surface downdip. Regarding the terminations against surfaces at the top of the sequence, offlap, toplap or truncation may occur (Fig. 1.29). Offlap is the depositional profile characterized by seaward down-stepping migration of the break, is a depositional angularity, not enhanced by erosion. Toplaps are terminations of strata (or the associated reflectors) against an overlying surface, representing the result of non-deposition and/or minor erosion. Truncation are related to deeper erosion of the underlying dipping strata along an unconformity.

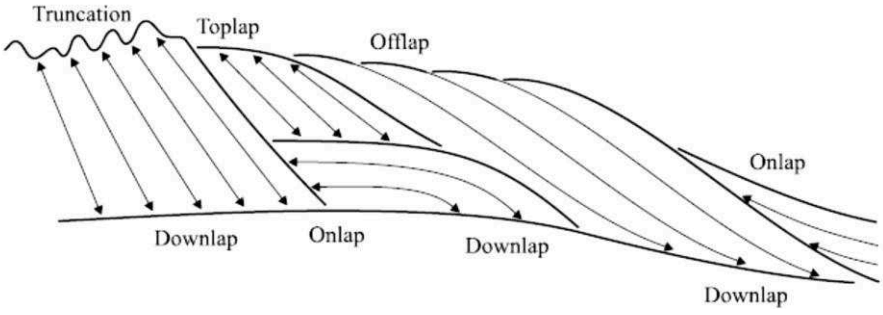

Figure 1.29: Main reflector terminations (from Catuneanu, 2002).

The terms transgression and regression refer to the displacement of the coast line in the continent or seaward direction respectively. The terms aggradation, progradation and retrogradation refer to the character of the stacking pattern (see Van Wagoner et al., 1990). In a progradational stacking pattern (Fig, 1.30a), sediments from more proximal environments

successively deposit over more distal environments indicating and overall migration of the facies trend and the shelf-break in the seaward (basinward) direction. In a retrogradational stacking pattern (Fig. 1.30b), sediments from more distal environments successively deposit over more proximal environments indicating and overall migration of the facies trend and the shelf-break in the continentalward (updip) direction. In an aggradational stacking pattern (Fig. 1.30c) the facies, thicknesses, and sandstone to mudstone ratios do not change significantly in a vertical profile and the shelfbreak remains approximately in the same position. Aggradation has been link with an equilibrium between accommodation and sedimentary supply, while progradation indicates sediment supply larger that generation of accommodation (sediment accumulation forces the system to migrate basinward), and retrogradation indicate larger generation of accommodation than sedimentary supply.

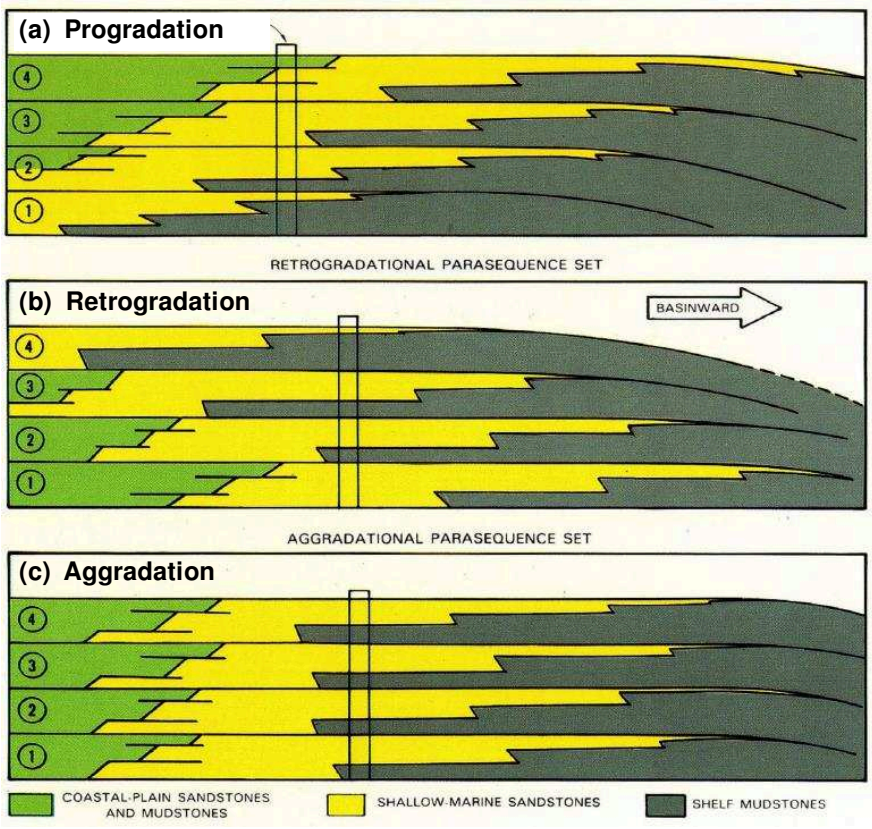

Figure 1.30: Main stacking patterns as illustrated by Van Wagoner et al. (1990): a) Progradation, b) Retrogradation, c) Aggradation

After the breakup unconformity, a marine transgression is necessary to initiate the nucleation of the continental shelf (Helland-Hansen et al., 2012). The deposition of organic rich transgressive shales is common at this stage. In the sequence stratigraphy approach, the stratigraphic record is divided into sequences (Fig. 1.31), separated by unconformities

(sequence boundaries, SB) and their correlative conformities. Each sequence records a cycle of increase and decrease of accommodation relatively to sedimentary influx. With an increase in accommodation, sediments prograde and aggrade, coastal onlap occurs at the continentalward end of strata. A Lowstand Systems Tract (LST, Fig. 1.319) is bounded by the SB at the base and a transgressive surface TS at the top. The TS marks a peak in the velocity of accommodation creation. A Transgressive Systems Tract develops on top of the TS, with a retrogradational stacking pattern, until the maximum level of accommodation is reached, the Maximum flooding surface (mfs, Fig. 1.31). After maximum flooding, accommodation starts to decrease relative to supply and the system will first aggrade and prograde during the Highstand Systems Tract (HST, Fig. 1.31). Strata of the HST displays downlap terminations towards the mfs. Accommodation decreases at higher rates, the system finally retrogrades in the late Highstand (this is equivalent to the falling stage system tract -FSST- of Depositional Sequence IV approach, see Catuneanu et al., 2009).

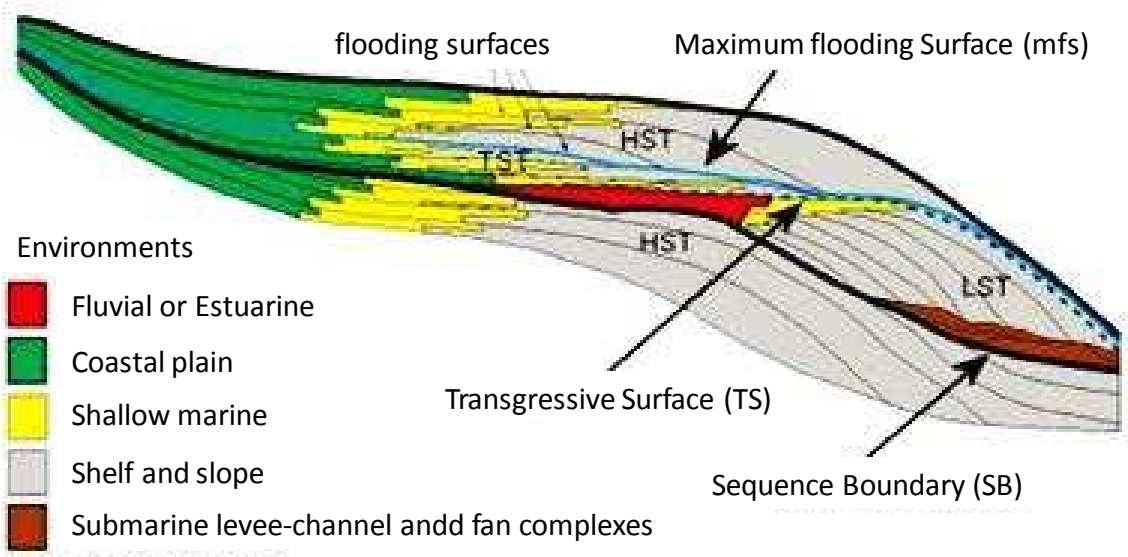

Figure 1.31: Depositional Sequence III approach to Sequence Stratigraphy (after Van Wagoner et al., 1990).

1.6 Objectives of the study and approach

Passive margin evolution has been strongly debated for many years as exposed in this State-Of-Art. The rifting and breakup evolution of supercontinents remain a matter of debate, especially in the case of the rifting and breakup of the supercontinents of Pangea and Gondwana throughout the Mesozoic. In the present PhD thesis, we will focus on the influence of previous inherited structures and deformation modes on the passive margin dynamic. Basin analysis, and more specifically seismic sequence stratigraphy will be used as the guideline approach.

Through the eyes of a stratigrapher, the structural and stratigraphic evolution of the main Mesozoic basins on the Argentinean shelf will be assessed (particularly the Colorado, Salado and Malvinas basins), and integrated into the regional (SW Gondwana) framework to better constrain the several rifting stages that ended with the opening of the South Atlantic Ocean in the Early Cretaceous. The correlation of pre-cretaceous rifting events between South American and African basins will also be explored to better constrain the pre-South Atlantic breakup evolution.

We used stratigraphic techniques to characterize and better correlate rifting stages by correlating their fillings. Absolute ages, biostratitraphic ages, detrital zircon ages, etc. were integrated to produce regional paleotectonic reconstructions. Sequence stratigraphic concepts and tools (e.g. reflector terminations, stacking patterns, unconformities), especially concerning seismic stratigraphy, were used in this thesis to characterize the sedimentary infill of the basins under study and the bounding surfaces in to reconstruct a tectono-stratigraphic framework.

The post-breakup evolution of the Colorado and Salado basins was characterized and modeled, and some controlling factors such as the subsidence, were inverted from the stratigraphic record. The sedimentary infill of a basin records the interaction between deep lithospheric processes (such as rifting, mantle exhumation, oceanic breakup, long term subsidence) and surface processes (climate, erosion, sediment transport and deposition). These parameters can be inverted from the stratigraphic record by performing sequence stratigraphy analysis and forward stratigraphic modeling in 3D with DionisosFlow. The restored basin infill (in nature and timing) was used to assess the passive margin evolution of the Colorado and Salado basins area, which are potentially representatives of the Argentinean South Atlantic margin.

Chapter 2. Geological Framework

2.1 The South Atlantic Ocean

The South Atlantic Ocean spans between South America and Africa (Fig. 2.1). This area attracts both scientific and industrial interests because it provides the full spectrum of phenomena related to continental breakup and passive margin formation. Besides, this sector hosts huge petroleum resources discovered in its conjugate margins, as for example the deepwater and pre-salt plays along the Brazilian and African margins, and the stratigraphic plays along the equatorial margins of Ghana and French Guiana. To the south, the Argentinean and Namibian/South African conjugate margins remain a frontier area still poorly characterized in term of petroleum resources. This area is nowadays the locus of both important scientific research and hydrocarbon exploration strategies.

The South Atlantic can be divided into four segments and is certainly a showcase of a wide range of processes controlling continental breakup. Following Moulin et al. (2010) and Torsvik et al. (2009), these four segments are from south to north: a) the Malvinas (Falkland) segment (to the South of the Agulhas-Malvinas Fracture Zone (AMFZ: 40-50°S, Fig. 2.1); b) the South Segment between the AMFZ and the Florianópolis FZ (FFZ, Fig. 2.1); c) the Central Segment, extends form the FFZ to the Romanche FZ (RFZ, Fig. 2.1); and d) the Equatorial segment, North of the RFZ, with a tectonic history signed by strike-slip processes between northeastern South America and Equatorial Africa.

Along the margin there are segments with presence of SDRs and others with a preponderance of saline deposits over volcanic rocks. An example of a volcanic margin (or magma-rich) is the South segment, with abundant volumes of igneous rocks extruded during the rupture along the COT (Franke et al., 2007; Koopmann et al., 2014b). Even if some volcanic eruptions have been described, the Central Segment is a predominantly magma-poor margin, hosting the Aptian salt deposits in the Brazilian and Angolan margin. The Equatorial and Malvinas Segments, enclosing the South Atlantic are described as transform margins.

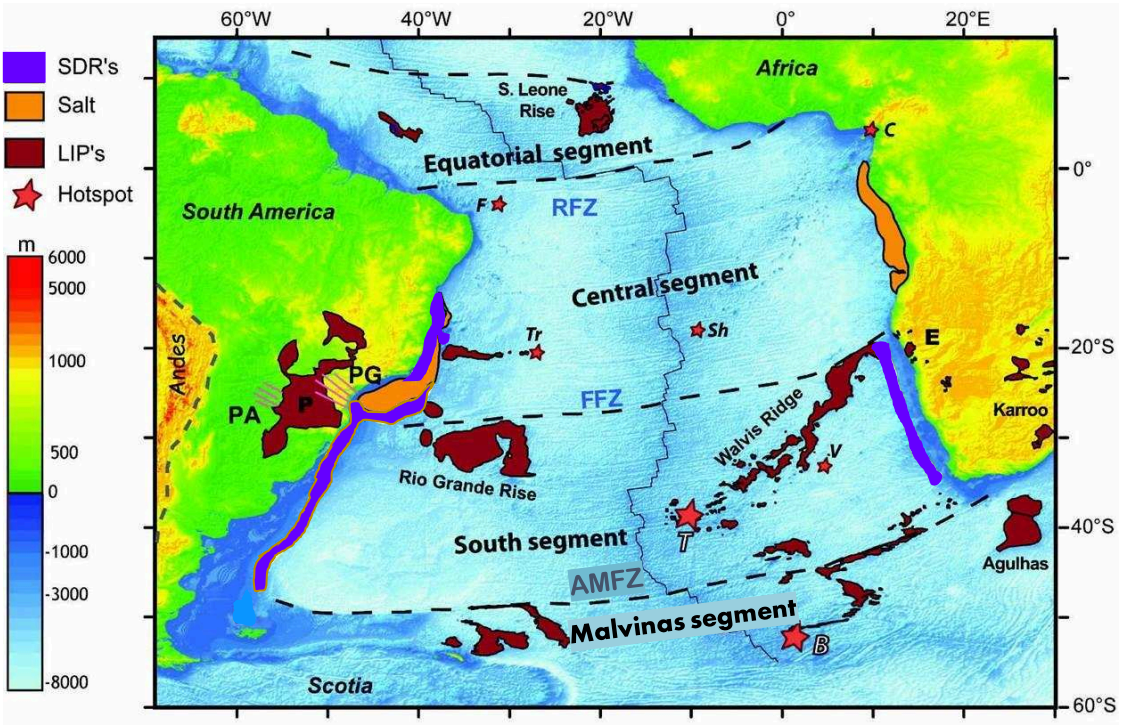

Figure 2.1: The South Atlantic Ocean and its segments (after Torsvik et al., 2009). Fracture Zones (FZ): RFZ (Romanche FZ), FFZ (Florianópolis FZ), AMFZ (Agulhas-Malvinas FZ). Large Igneous Provinces (LIP): P (Paraná), E (Etendeka). Dyke swarms: PA (Paraguay), PG (Ponta Grossa). Hotspots: F (Fernando), C (Cameroon), Tr (Trinidade), Sh (Saint Helena), T (Tristan da Cunha), V (Vema), B (Bouvet).

The similarity and apparent fit of the east coast lines of South America and West Africa was one of the signs that motivated Wegener to propose his theory of continental drift in 1915 as a mechanism to explain the opening of the ocean. Du Toit (1937, 1927), following ideas of Keidel (1916), contributed concrete elements that unequivocally demonstrated that Africa and South America were once united, as part of the supercontinent of Gondwana.

After going through different orogenies during the Paleozoic (Cawood, 2005; Blakey, 2008; Ramos, 2008; and references therein), the supercontinent of Pangea (Fig. 2.2) initiated a process of supercontinental breakup in the Triassic (Uliana et al., 1989; Macdonald et al., 2003; Moulin et al., 2010), and thus dismembered first in the 'smaller' supercontinents of Larentia and Gondwana, then by the Cretaceous in the present-day continents of South America, Africa, Antarctica, India and Australia.

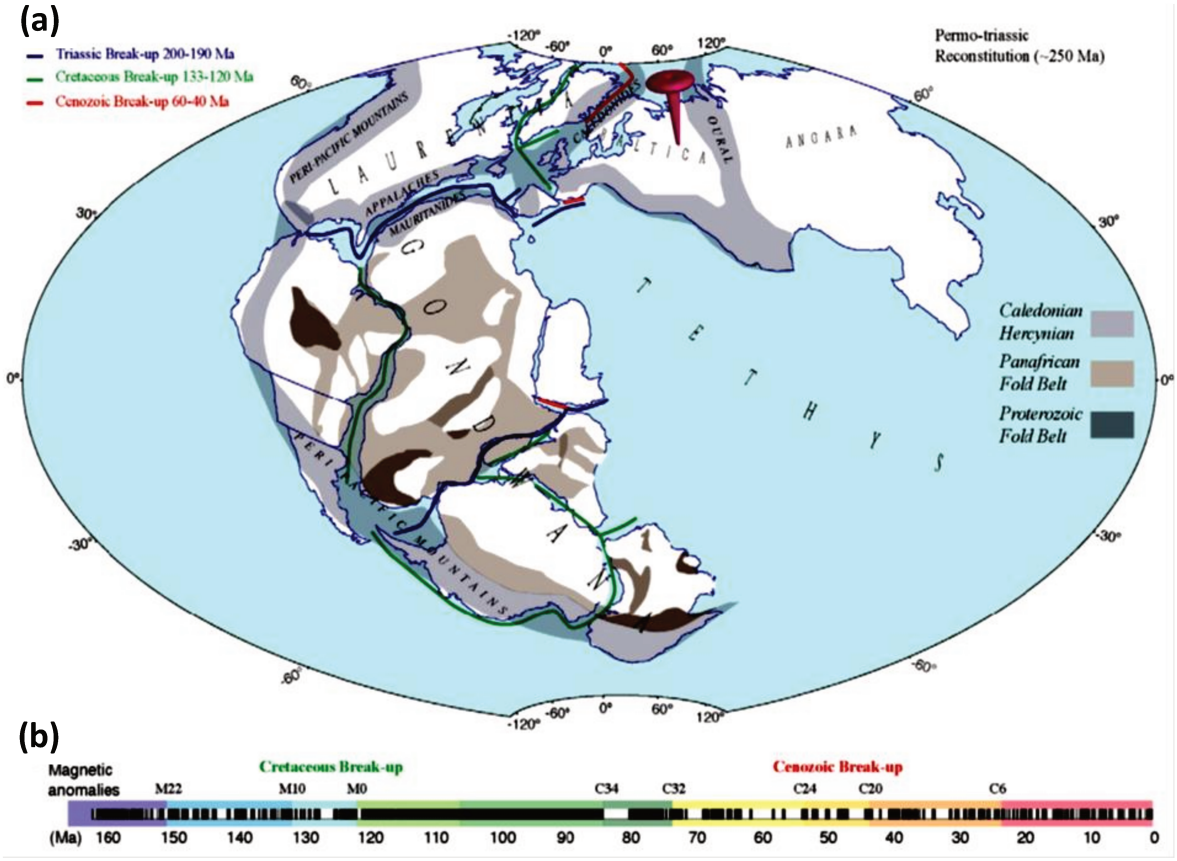

Figure 2.2: a) Paleotectonic reconstruction of the Pangea supercontinent (circa 250 Ma, pre-breakup), focused on Gondwana. Hammer projection. The opening occurred in three main episodes: The Triassic-Jurassic episode (in blue, 200-190 Ma) that divided Pangea into three supercontinents: (Laurentia, Baltica and Angara), (Africa and South America) and (Madagascar, India, Antarctica and Australia). The second episode (in green) occurred during the early Cretaceous (133-120 Ma), and the last (in red) during the Paleogene; b) Chronological scale of the different magnetic anomalies observed in oceanic crust since 160 Ma (from Moulin and Aslanian, 2010)

The apparent larger separation in the southernmost segments of the South Atlantic (Fig. 2.1), was the first observation that seemed to indicate a diachronism in the opening from south to north. The absolute ages of the opening were not known until the gravimetric and magnetic anomalies of the oceanic crust were detected, dated and correlated from the mid-Atlantic ridge to the continents. Rabinowitz and LaBreque (1979) proposed a model of reconstruction of the fit between South America and Africa adjusted with geophysical data, by integrating the pioneering works of John and Maurice Ewing, and collaborators (e.g. Ewing et al., 1963; 1964; 1971; Ewing and Ludwig, 1965; Dickson et al., 1968; Ewing and Lonardi, 1971), with the observations of Urien and Zambrano (1973), Ladd (1974), and the gravimetric and magnetometric measurements made during the 1970s by the Lamont-Doherty Geological Observatory. Alternative models of such insertion had been proposed by Bullard et al. (1965)

and followed by Pindell and Dewey (1982) and Unternehr et al. (1988) among others. Emery and Uchupi (1984) compiled much of the preexisting information in a "Geological Atlas of the Atlantic Ocean". Larson et al. (1985) takes the isochronous mapping initiated by Ladd (1974) and integrates it with bathymetric information, being able to determine more precisely the jumps between the different ridge segments between transform zones.

In the early 1980's, models seek to reconstruct the tectonic evolution in higher detail (Vink, 1982). The first full integration of the South Atlantic tectonic evolution, from a pre-opening position to the present, was proposed by Nürnberg and Müller (1991, Fig. 2.3). During the first decade of the 21st century, authors such as Eagles (2007) and Torsvik et al. (2009) introduced to the discussion, the importance of intracontinental deformation during the opening process. In parallel, many authors have focused on modeling the evolution of the opening of different segments of the South Atlantic (e.g. central segment, equatorial, etc.). The following works have significantly contributed to the better understanding of the conjugate margins, their crustal structure, architecture and evolution: Ford and Golonka (2003), Jokat (2003), Moulin (2003), Moulin et al. (2005, 2010), Blaich (2006); Blaich et al. (2013, 2011, 2009, 2008), Franke et al. (2010, 2007, 2006), Antobreh et al. (2009), and more recently Becker et al. (2012), Koopmann et al. (2014), Stica et al. (2014) and Arecco et al. (2016) among others.

The most recent kinematic models were introduced by Heine et al. (2013) and Pérez-Díaz and Eagles (2014), and it is on that basis that this description of the evolution of the South Atlantic Ocean is presented. These new studies allow us to reconstruct the current geometry of the ocean combining processes of extension of the crust, generation of oceanic crust, displacement of course through transformations, and using less intracontinental deformations than those interpreted by Eagles (2007) and Torsvik et al. (2009), especially for the southern portion of South America.

2.1 South Atlantic segments

To better integrate the kinematics of the opening and the nature of the processes that occurred at each stage, a general characterization of the conjugate margins along different segments of the South Atlantic (from south to north) is presented below.

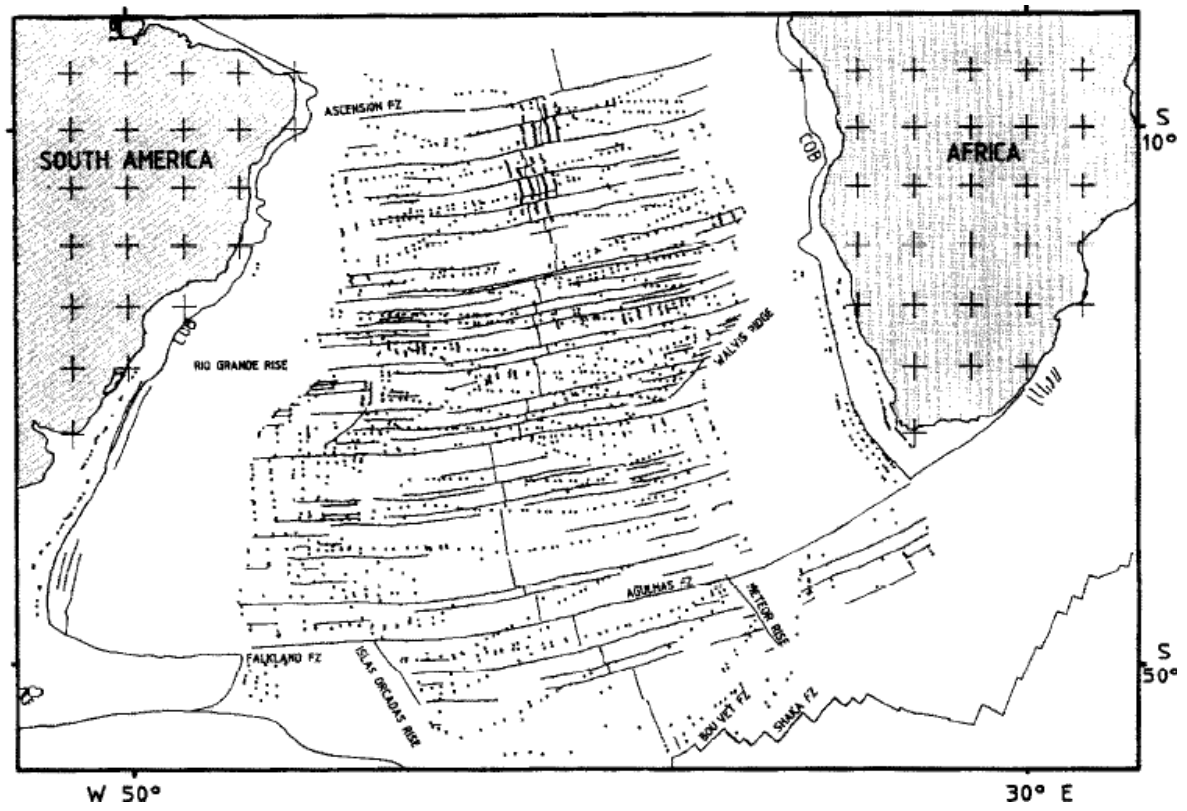

Figure 2.332: Tectonic map compiling the available magnetic anomaly data, with 'flow-lines' constructed using rotation poles, published by Nürnberg and Müller (1991).

Malvinas Segment

The Malvinas segment (Fig. 2.1) is the southernmost segment of the South Atlantic. It develops south of the Agulhas/Malvinas (Falkland) fracture zone. Lorenzo and Wessel (1997) investigated the Agulhas / Malvinas fracture zone along the Malvinas Plateau, focusing on flexural coupling through the continent-ocean fracture zone. At the same time Ben-Avraham et al. (1997) described the structure and tectonics of the Agulhas / Malvinas fracture zone in the southeast margin of Africa and divided it into four segments. Parsiegla et al. (2009) identified two rifting events in South Africa: one at 169 - 155 Ma (associated with the breakup between Africa and Antarctica) and a second since 136 Ma linked to the deformation along the Agulhas/Malvinas shear zone. Recently, Baby et al. (2018) assessed the evolution and uplift history of the African transform margin.

On the South American plate, the Malvinas segment is characterized by displaying appendix of continental crust that extends east from Patagonia (Fig. 2.4). This area of extended continental crust hosts the Jurassic Malvinas basin (Galeazzi, 1998), the Malvinas (Falkland) islands (Ramos et al., 2017, and references therein), the Malvinas (Falkland) Plateau (Biddle et

al., 1996; Ramos, 1996), and the Maurice Ewing Bank (Chemale et al., 2018). Since the latest Cretaceous, the South American plate been subjected to compression from the south, thus its compressional southern end, bounded by the southeastern extension of the Andes, given by the Fuegian Andes, the Burwood bank, and the North Scotia Ridge (Fig. 2.4).

The North Malvinas (North Falkland) basin (Fig. 2.4, Ross et al., 1996; Richards and Fannin, 1997) is characterized by two systems of normal faults. A first WNW-striking system in the southern rift has been correlated with WNW-striking Early Jurassic igneous dykes in the Malvinas (Falkland) islands (Ramos et al., 2017). The WNW-oriented faults in the North Malvinas basin are intersected by a second set of N-S striking faults that from depocenters of Early Cretaceous age (Lohr and Underhill, 2015).

The first movements of the Agulhas / Malvinas FZ occurred in the Valanginian from 138 Ma (Baby et al., 2018; and references therein). This shear zone would have been active until the Santonian (ca. 83 Ma), when the meso-oceanic ridge surpassed the bank Maurice Ewing (Lorenzo and Wessel, 1997).

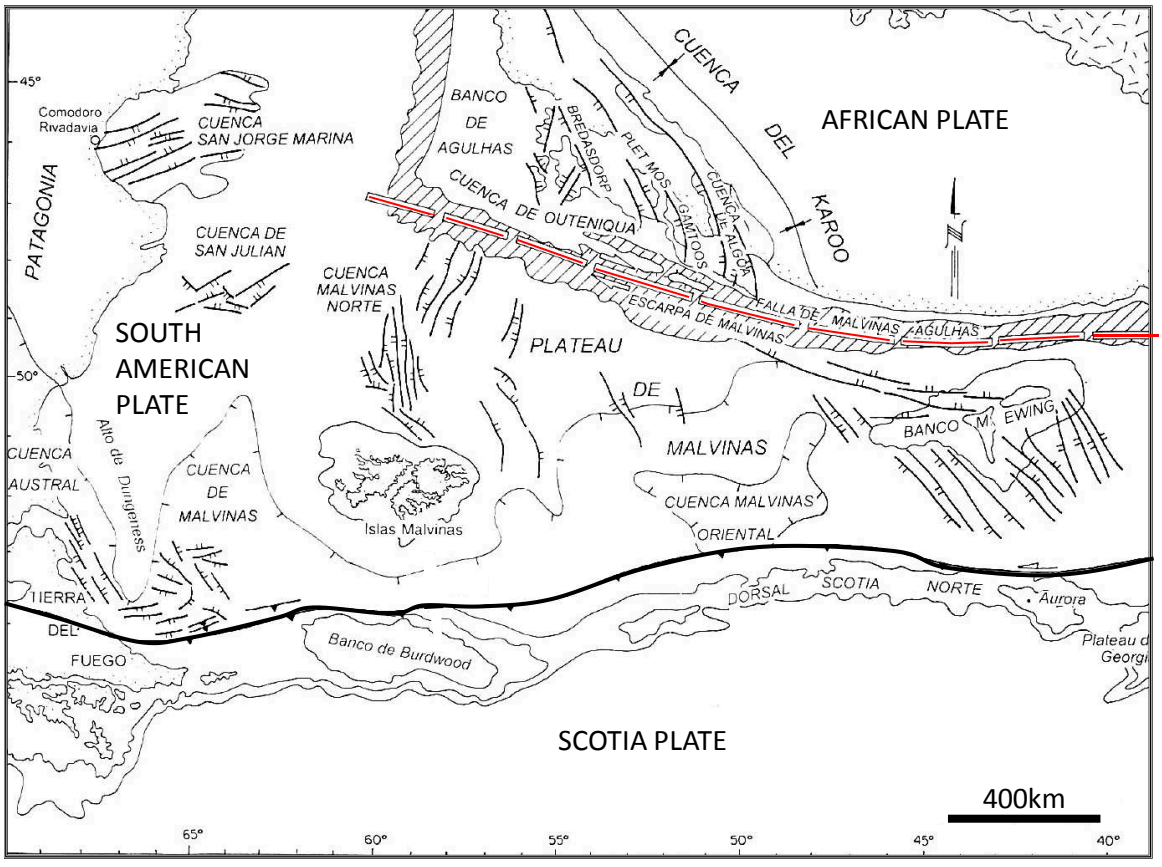

Figure 2.4: Main structural elements of the Malvinas Segment, with Africa at its Jurassic pre-breakup position (modified from Ramos, 1996).

South Segment

The South segment of the South Atlantic extends between the Agulhas / Malvinas FZ and Florianópolis FZ (Gladczenko et al., 1997). On the South American margin, it can be divided into a the southern part corresponding to the Argentinean/Uruguayan margin, and the Pelotas basin (offshore Brazil and northern (Uruguay). Franke et al. (2007) divided the Argentinean/Uruguayan margin into four subsegments separated by fracture zones (Fig. 2.5). Except for subsegment I (the southernmost), subsegments II to IV (north of the Colorado transfer zone) are characterized by the presence of large and thick wedges of SDRs.

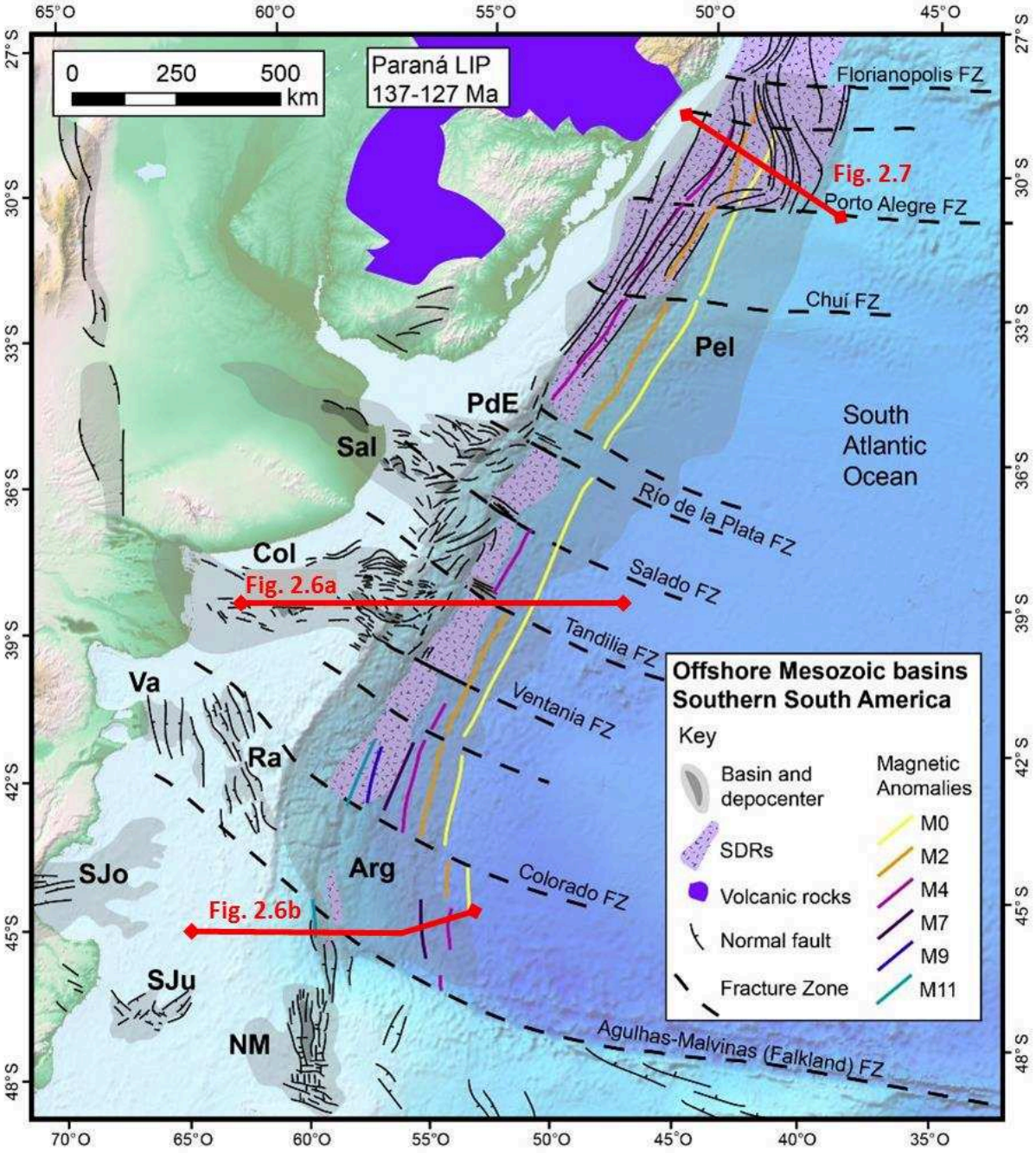

Figure 2.5 (previous page): Structural map showing the distribution of SDRs in the South Segment (after Franke et al., 2007; Gerster et al., 2011; Soto et al., 2011; Stica et al., 2014; Hall et al., 2018), onshore and shelf basins (after Ramos and Turic, 1996). Location of figures 2.6a and b and Fig. 2.7 is illustrated. Offshore basins: Pelotas (Pel), Punta del Este (PdE), Salado (Sal), Colorado (Col), Valdés (Va), Rawson (Ra), San Jorge Gulf basin (SJo), San Julián (SJu), North Malvinas (Falkland) basin (NM), Argentina basin (Arg).

Subsegment I, between the Agulhas-Malvinas FZ (Figs. 2.1, 2.4 and 2.5) and the Colorado FZ, is characterized by a sharp basement slope (abrupt margin, Fig. 2.6b) and scarce evidences of SDRs (Becker et al., 2012). This subsegment is the deepwater counterpart (Argentina basin) of the Valdés and Rawson basins present on the shelf (Fig. 2.5). It constitutes the transition zone between a transform Malvinas segment to the south and the volcanic margin described north of the Colorado FZ. Pull-apart basins related to the AMFZ are observed to the south, for which a volcaniclastic filling is inferred (Franke et al., 2007). This area was studied in more detail by Blaich et al. (2009) and Becker et al. (2012), who proposed that this southern subsegment (I) is related to the north extension of the Malvinas Norte basin fault system (Fig. 2.5).

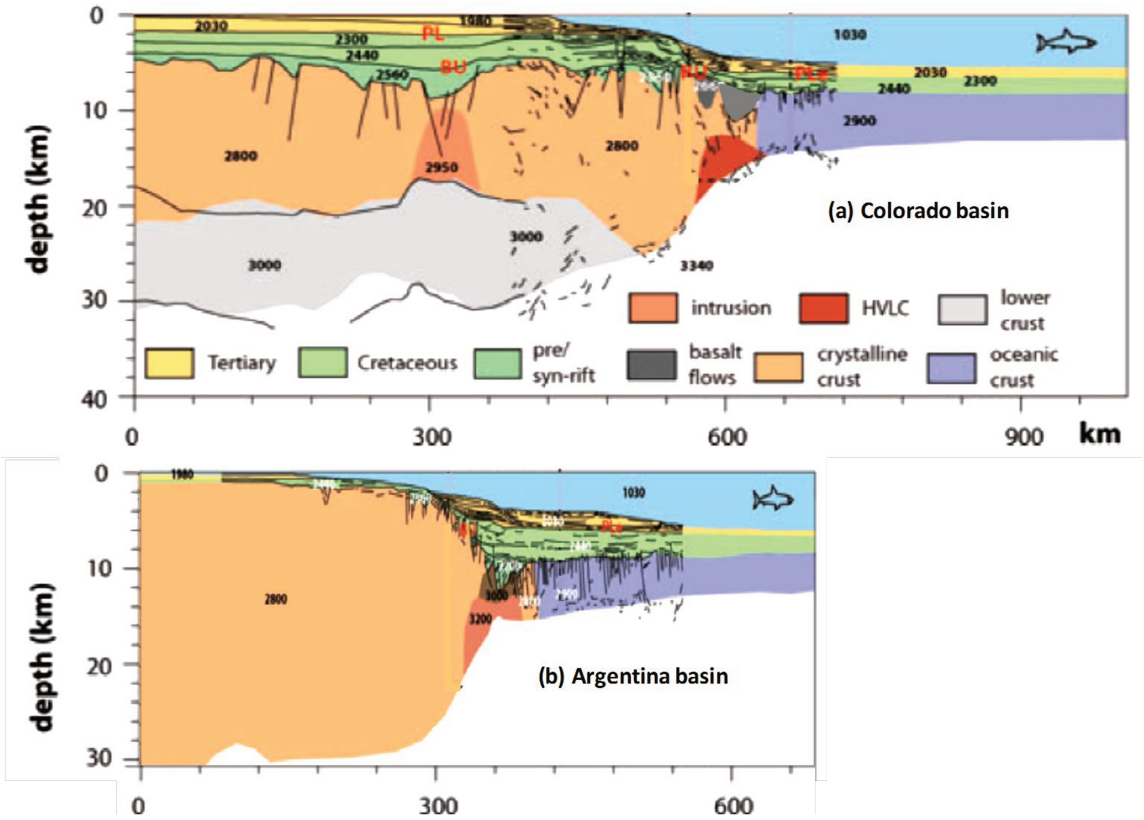

Figure 2.6: Crustal structure sections in the Argentina margin (modified from Blaich et al., 2009): a) Crustal structure section across de Colorado basin, subsegment II of Franke et al. (2007); b) Crustal structure section across subsegment I of Franke et al. (2007) and the Argentina basin. See Fig. 2.5 for location of the sections.

To the north of the Colorado FZ (Fig. 2.5) thick wedges of SDRs were described, emplaced in the COT. Franke et al. (2007) identified from gravimetric, magnetic and seismic data up to three juxtaposed major wedges of SDRs. The oldest, certain magnetic anomaly observed in the South American margin corresponds to M4 (Franke et al., 2007). Later works identified up to M9 (Gerster et al., 2011, see Fig. 2.5), and possibly M10, which has been recently reinterpreted by Hall et al. (2018) as M11. Subsegment III is comprehended between the Ventania FZ and the Salado FZ (Fig. 2.5), is also characterized by SDRs developed outboard the Colorado basin. In the Río de la Plata area, Soto et al., (2011) describe an area without clear indications of SDRs, possibly related to the development of the Río de la Plata FZ (Fig. 2.5). Subsegment IV of Franke et al. (2007) develops between the Salado and the Río de la Plata FZ, and is the outboard equivalent of the Salado/Punta del Este basins (Fig. 2.5). Further north, the Pelotas basin (northern Uruguay and southern Brazil) displays huge volumes of SDRs (Abreu, 1998). Stica et al. (2014) identified on seismic sections the volcanic sequences of Serra Geral (134-132 Ma, Paraná LIP, Fig. 2.5), preserved bellow the SDRs indicating a prerift character (Fig. 2.7). Stica et al. (2014) discuss that the SDRs in the southern subsegments are older and/or coeval with the Serra Geral volcanism, and that when breakup (that was advancing north) reaches the Pelotas latitudes, the SDRs postdate the Serra Geral flows.

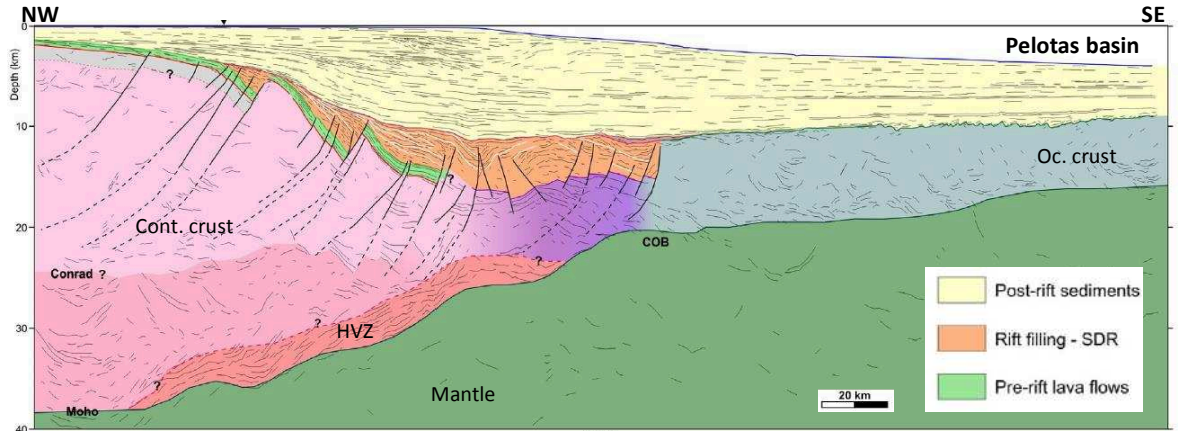

Figure 2.7: Interpretation of the regional dip seismic section of the North Pelotas basin (from Stica et al., 2014). See location in Fig. 2.5.

Regarding the conjugate African volcanic margin (Gladczenko et al., 1998, 1997; Elliott et al., 2009; and references therein), following the mapping criteria of Franke et al. (2007) for the South American margin, Koopmann et al. (2014) divided the Namibian/South African margin into four subsegments. Similarly to what happens in subsegment I offshore Argentina,

in South Africa the SDRs seem to be absent in the southernmost subsegment (Fig. 2.8) that here corresponds to the Cape basin and the Outeniqua basins on the continental shelf (see Broad et al., 2012). It is from the northern limit of this subsegment, marked by the Cape FZ, that SDR wedges are detected. The authors emphasize that the transition between the southernmost subsegment without SDR and the subsegment with SDR, immediately north of the Cape FZ, occurs abruptly in less than 50 km (Fig. 2.9a and b). For the South African margin Koopmann et al. (2014) report up to four major wedges of SDRs and magnetic anomalies up to M9 (Fig. 2.8). Recently, Hall et al. (2018) reported the discovery of the M11 magnetic anomaly, the oldest discovered so far in this area (Fig. 2.8).

Further north, many fracture zones have been mapped (Fig. 2.8), but the main FZ that seem to exert a control on SDR emplacement and establishment of the main subsegments are the Orange FZ and the Autseib FZ (Koopmann et al., 2014b). The Orange, Luderitz and Walvis basins are depocenters of the Early Cretaceous South Atlantic rift and seem to be controlled by the breakup kinetics and margin segmentation. Figure 2.10 presents a crustal section across the Orange basin, depicting not only the SDR wedges but also half-grabens of interpreted sedimentary infill inboard from the SDRs.

A comparison of the crustal structure of the conjugate southern South Atlantic margins carried out by Blaich et al. (2013) is presented in figure 2.11. Note that the northern transect relaying the Pelotas with the Walvis basin is rather symmetrical (Fig. 2.11a). Towards the latitude of the Colorado and the conjugate Orange basin the symmetry of the conjugate margins changes. The SDR wedges in particular are narrower than in the southern African margin (Fig. 2.11b and c). This asymmetry has been linked by Blaich et al. (2013) to asymmetric rifting at the time of breakup (simple shear mode).

This margin asymmetry has conditioned the passive margin evolution, particularly subsidence and thus accommodation. Marcano et al. (2013) presented a comparison of the conjugate margins. Figure 2.12 presents a zoom on the sedimentary cover of the Colorado-Orange transect (Fig. 2.11b). Note the differences in thickness of the Cretaceous (thicker on the African margin) and the Cenozoic (thicker on the South American margin). Considering eustasy is equal for both margins, differences will be related to sedimentary input and subsidence history depending on crustal architecture and tectonic/thermal evolution .

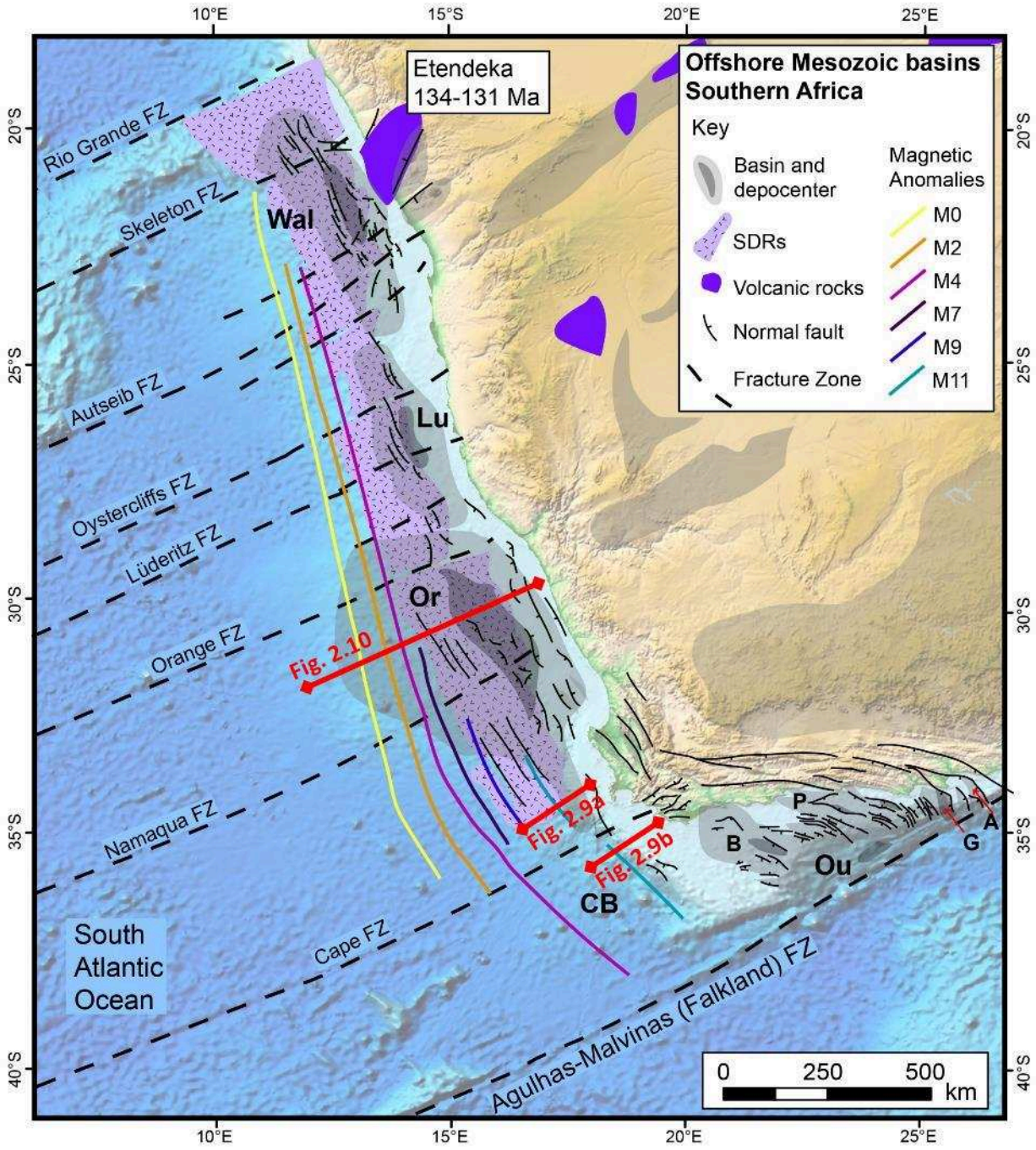

Figure 2.8: Structural map of the South African passive margin between the Agulhas-Malvinas (Falkland) FZ and the Florianópolis / Río Grande FZ (after Koopmann et al., 2014; and Broad et al., 2012; Hall et al., 2018). Note the distribution of SDR and magnetic anomalies.

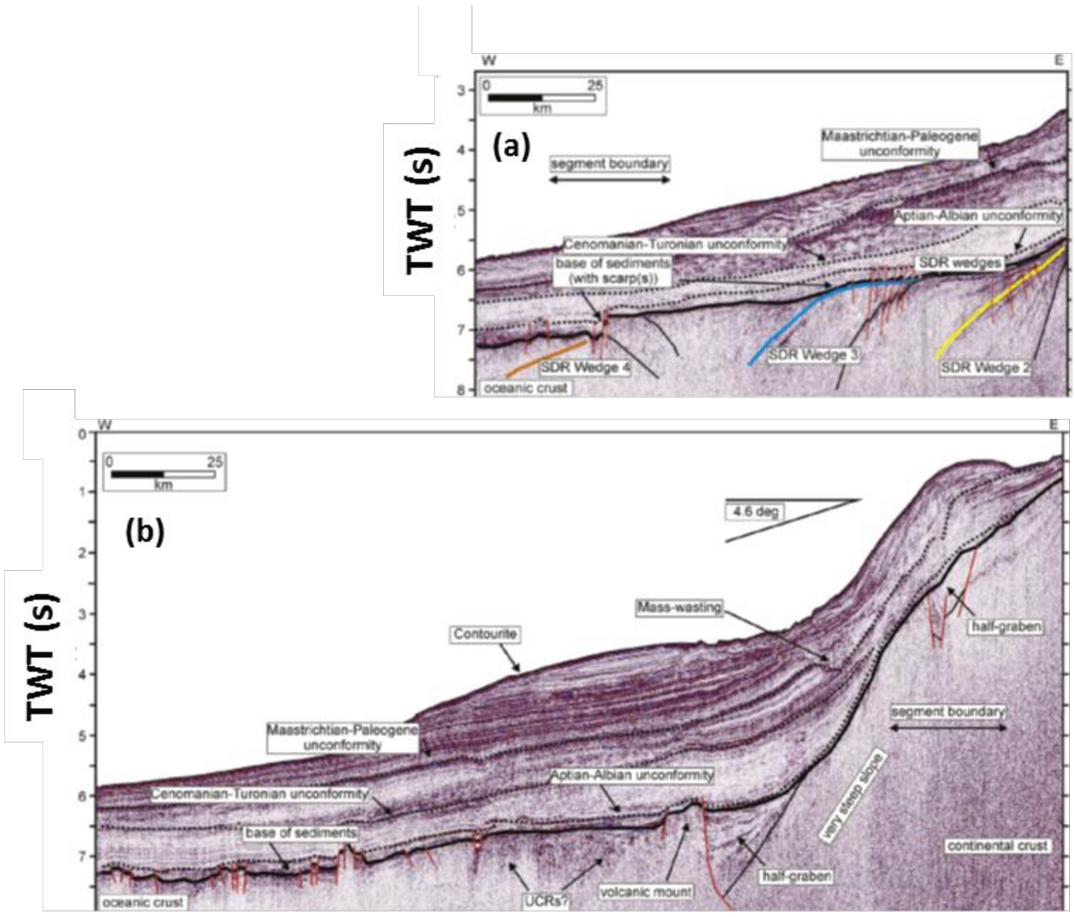

Figure 2.9: Seismic sections north (a) and south (b) of the Cape FZ (from Koopmann et al., 2014). Note the presence of several SDR wedges north of the Cape FZ (a); while to the south the margin is more abrupt and does not display obvious indications of SDRs. See location in Fig. 2.8.

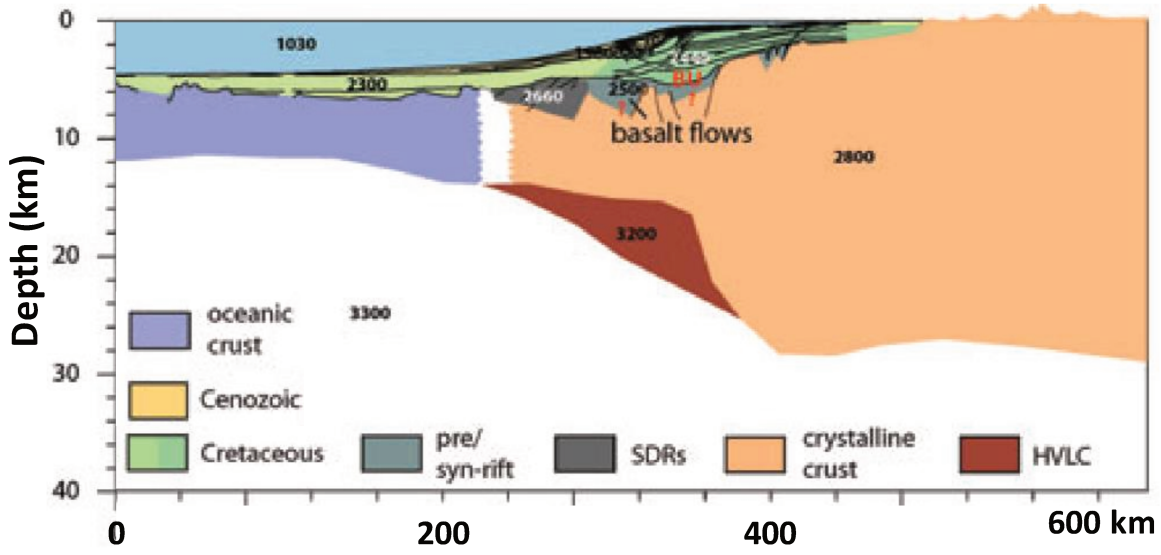

Figure 2.10: Crustal structure section of the Orange basin, offshore Namibia (from Blaich et al., 2009). See location in Fig. 2.8.

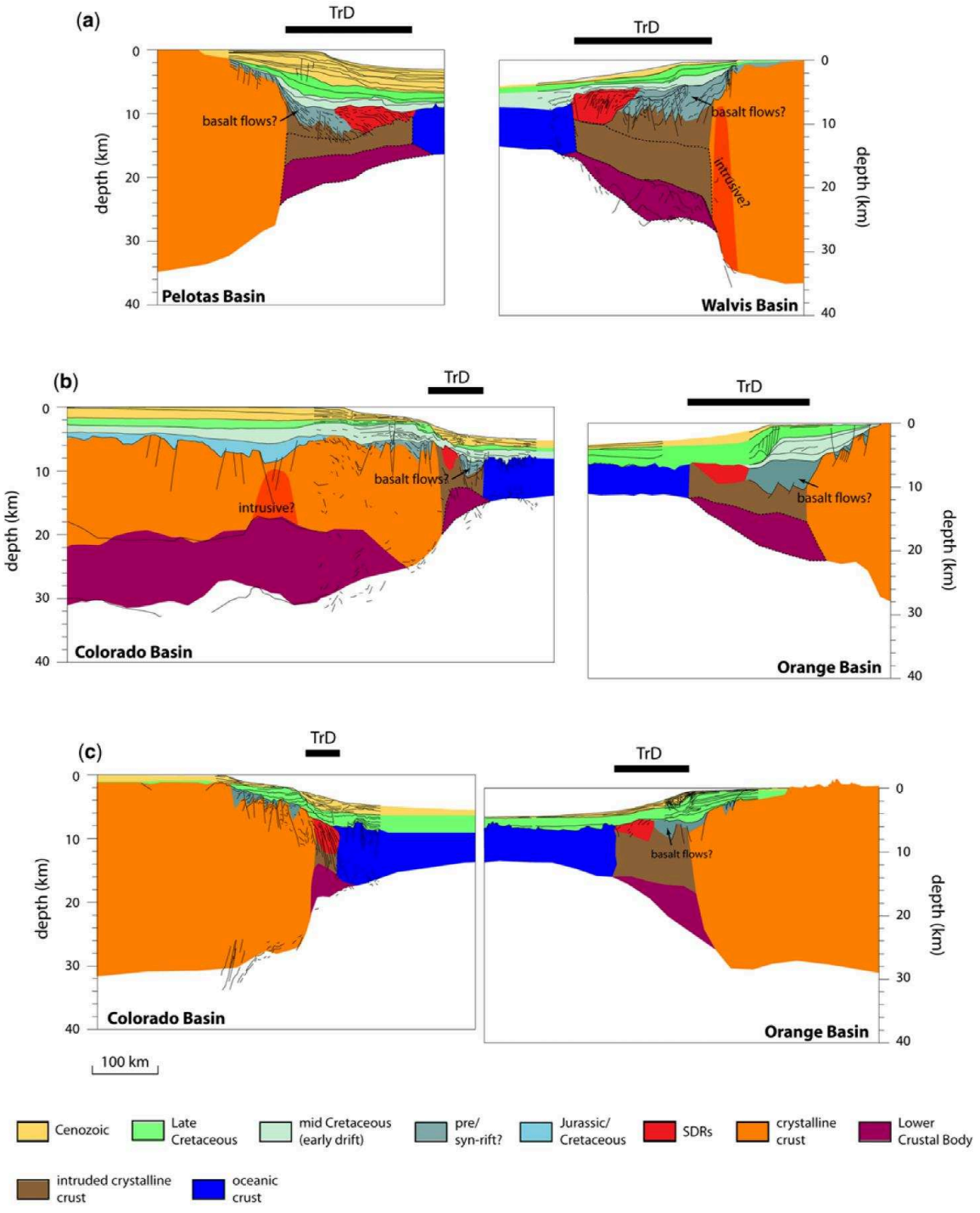

Figure 2.11: Conjugate transects along segments of the southern South Atlantic (from Blaich et al., 2013): a) Pelotas Basin (Brazil) – Walvis basin (Namibia); b) Colorado Basin (Argentina) – Orange Basin (South Africa); and (c) South of Colorado Basin (Argentina) – Orange Basin (South Africa).

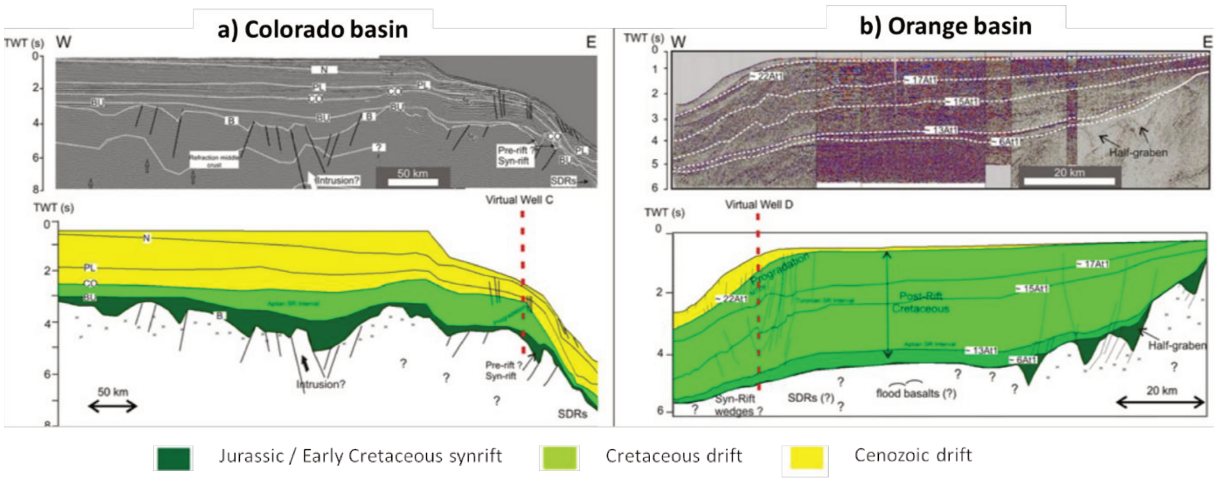

Figure 2.12: Seismic section and schematic interpreted transect of the Colorado basin (a) and the conjugate Orange basin (b) depicting the stratigraphic differences for the synrift, Cretaceous drift and Cenozoic (from Marcano et al., 2013). These sections are a zoom of the sedimentary cover of the conjugate margins presented in Fig. 2.11b.

Central Segment

The central segment of the South Atlantic is one of the most studied, given the discoveries of huge hydrocarbon reserves in both the Tertiary deep-water play and the pre-salt play. This segment is limited by the Rio Grande / Florianopolis FZ to the south and Romanche FZ to the north (Fig. 2.1). The Central segment is characterized by the presence of a thick cover of evaporites of Aptian age deposited "during" the opening, and preserved both in the Brazilian and in the Angolan / Congolese margins. (Fig. 2.1). The main references for this segment are Moulin (2003), Moulin et al. (2010, 2005), Blaich et al. (2011), Chaboureau (2012), Chaboureau et al. (2013). As the central segment would have been formed during the Cretaceous Magnetic Quiet Zone, there is an absence of magnetic anomalies with a defined orientation and a large zone of magnetic quiescence with chaotic patterns of anomalies (Fig. 2.13).

The crustal structural transects presented in Figures 2.14a and b were published by Blaich et al. (2011) and elaborated from 2D gravimetric inversion combined with seismic interpretation. The transect of the Espirito Santo basin (Brazil, Fig. 2.14a) has an extension of 400 km. Seismic interpretation allowed the detection of an abrupt shallowing of the Moho (from 30 to 15 km deep in less than 100 km) in a position close to the shelf break (Mohriak, 2003; Mohriak et al., 2008). In addition, continental crust is deformed by listric faults, which does not seem to affect the thick pre-salt sedimentary cover (Fig. 2.14b).

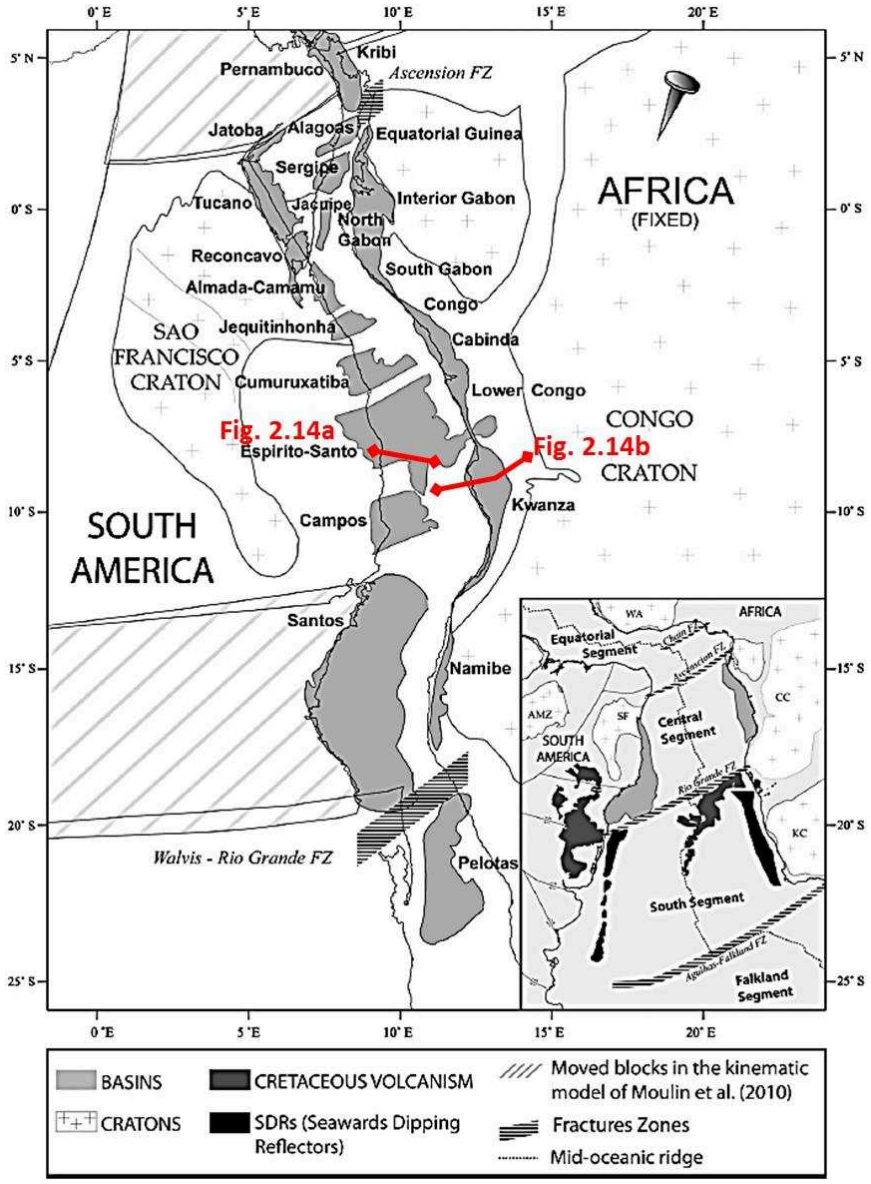

Figure 2.13: Paleotectonic reconstruction of the South Atlantic Central segment basins for the pre-breakup Berriasian configuration (from Chaboureau et al., 2013; after Moulin et al., 2010). Note the location of the transects presented in Fig. 2.14.

The transitional domain (COT) is characterized by failed and rotated blocks and synrift sedimentary wedges. The end of the transitional crust zone (the continent-ocean boundary, COB) is located approximately in the eastern limit of the saline basin, where a salt tongue is observed advancing towards the oceanic crust (Fig. 2.14a). In the Angolan margin (Kwanza basin, Fig. 2.13c) it has not been possible to identify the Moho with a high degree of certainty from seismic data. However, Blaich et al. (2011) propose a somerization of the Moho from the craton to the west (from 30 to 14 km deep in a range of 220 km). In the Angolan margin, inversion structures were also reported, for which Hudec and Jackson (2012) interpret a ridge-push effect, with plate reorganization and exhumation of the African continent as a result of

mantle dynamics. In addition, in both margins important salt tectonics is observed, with the development of diapirs (Fig. 2.14a and b).

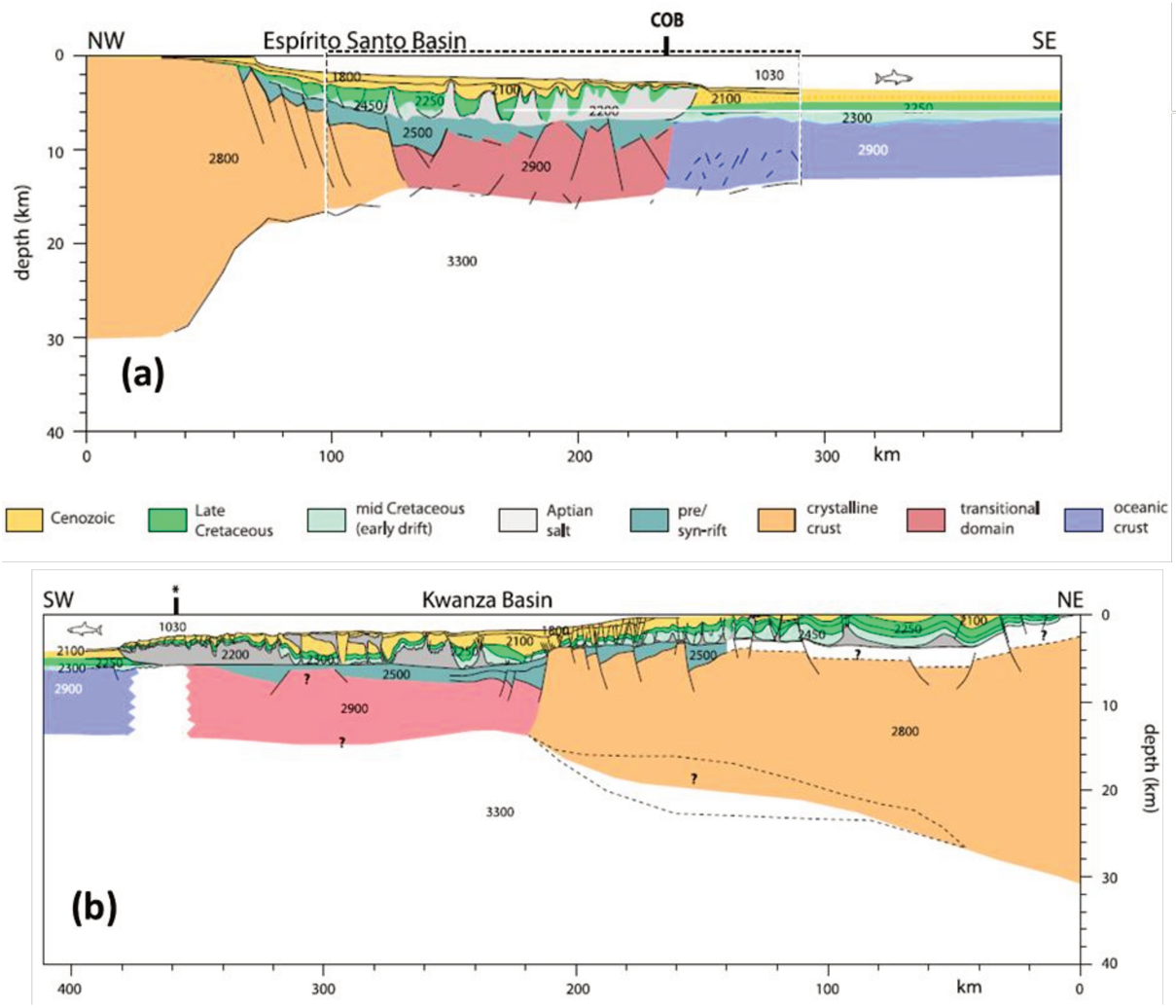

Figure 2.14: Structural crustal sections across the Central Segment of the South Atlantic Ocean: a) Brazilian Espirito Santo basin; b) and the conjugate Kwanza basin, offshore Angola (from Blaich et al., 2011).

Equatorial Segment

The equatorial segment, developed north of the Romanche FZ (Fig. 2.1), constitutes the transition between the South Atlantic and the Central Atlantic oceans. It is characterized by transform processes with absence of important volcanic volumes and salt. The discovery of large hydrocarbon reserves in stratigraphic traps in Ghana and French Guiana at the beginning of the 21st century led to a reassessment of this type of transform margins (Antobreh et al., 2009; Basile et al., 2005; Moulin et al., 2010).

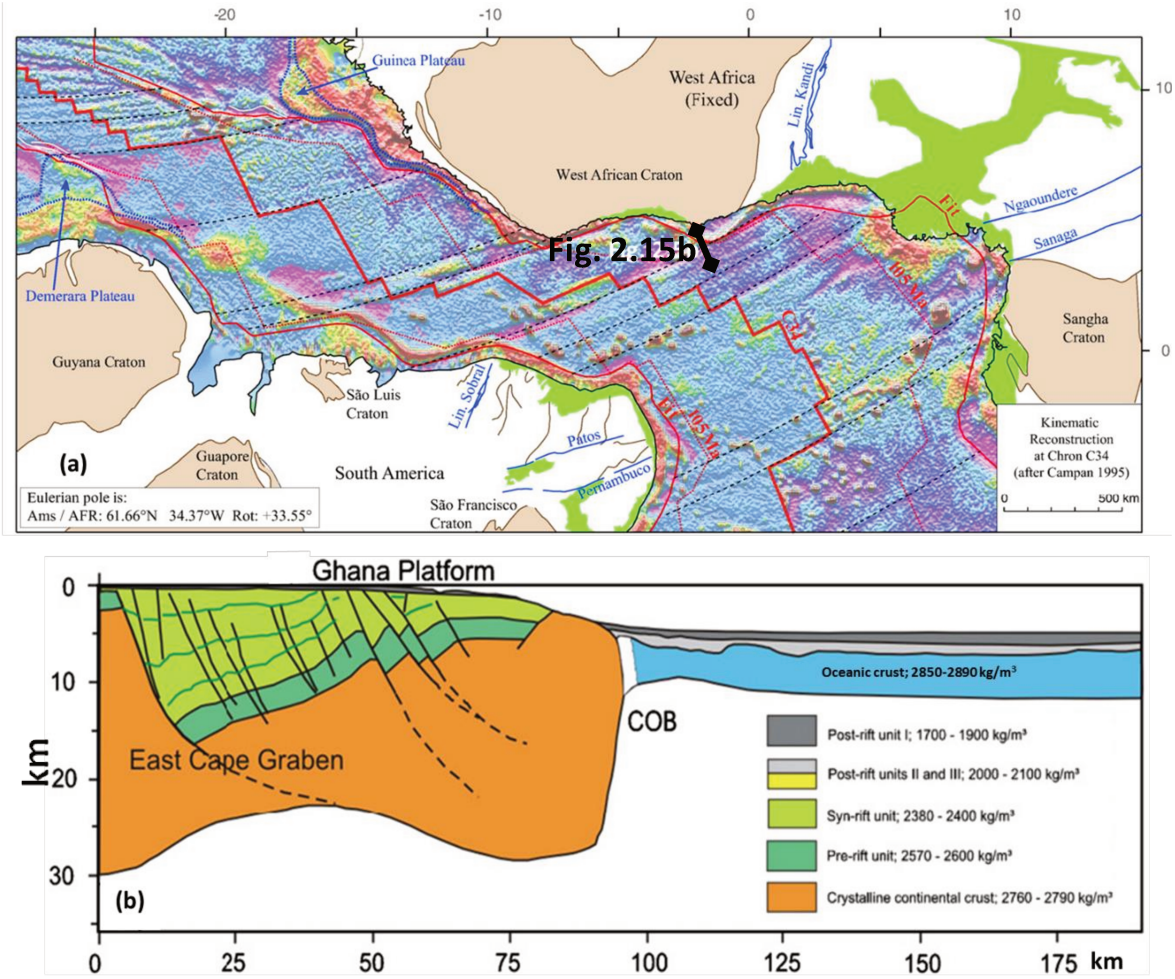

Figure 2.15: The Equatorial segment of the South Atlantic: a) Paleotectonic reconstruction at Chron 34 (84 Ma) of the Equatorial Atlantic Ocean (adapted from Moulin et al., 2010). The thick red line represents the meso-oceanic ridge for that time, the thin red lines indicate the position of the first ridge before the break (fit), the red dotted lines indicate the position of the ridge to 105 Ma; b) Structural transect of the Ghana transform margin (from Antobreh et al., 2009)

This type of transform margins is characterized by a more or less abrupt transition from continental to oceanic crust. In Figure 2.15b the Moho (base of crust) goes abruptly from 30 to less than 10 km deep in a very short distance. Pull-apart basins are commonly described on the shelf.

2.2 Synthesis of the southern South Atlantic opening: an overview

As originally proposed by (Rabinowitz and LaBreque, 1979) and later modeled by (Nürnberg and Müller, 1991), today it is generally accepted that the South Atlantic opening began in the south and propagated northward (Moulin et al., 2010; Franke, 2013; Heine et al., 2013; Pérez-Díaz and Eagles, 2014; Koopmann et al., 2016). However, these authors do not agree on many particularities, as for example about the role of intracontinental shear zones to accommodate plate deformation during rifting and drift (Eagles, 2007; Moulin et al., 2010; Fig. 2.16), the exact timing of rifting (Heine et al., 2013; Pérez-Díaz and Eagles, 2014), or the role of margin segmentation during rifting (Franke, 2013) among others.

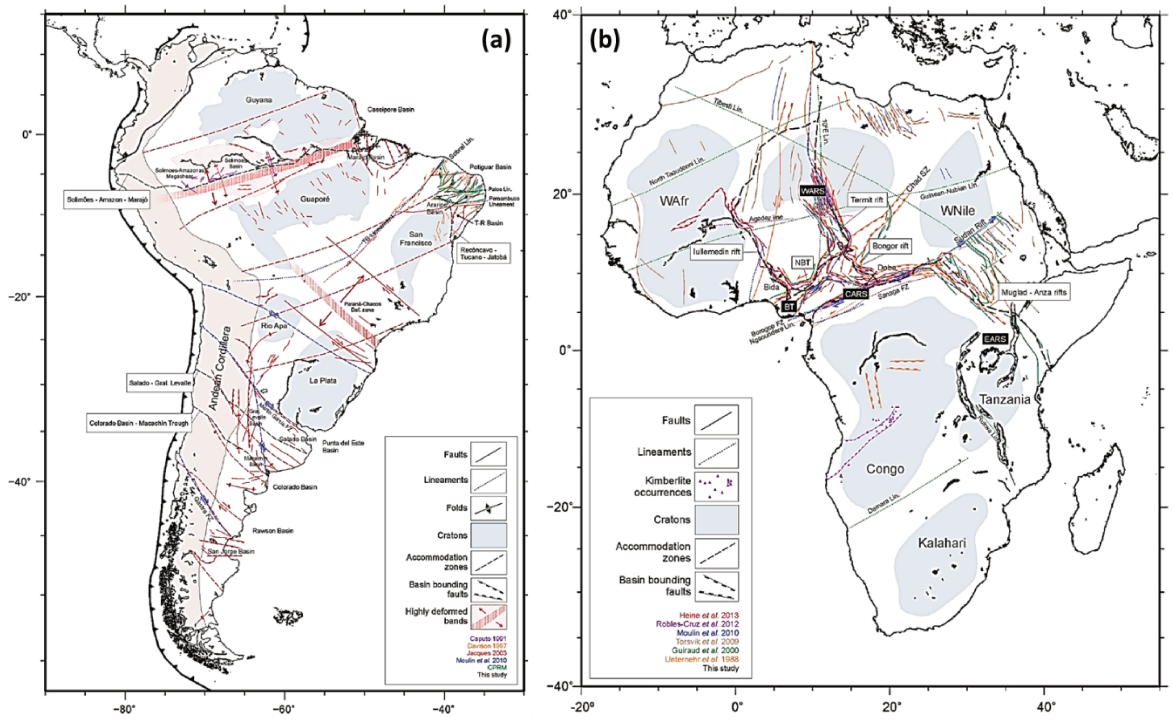

Figure 2.16: Compilation of intracontinental deformation zones in: a) South America, and b) Africa (from Pérez-Díaz and Eagles, 2014; after references therein. The activity of many of these intracontinental deformation zones is still matter of debate.

Rabinowitz and LaBreque (1979) had identified the M11 magnetic anomaly (~136 Ma, late Valanginian) on the African side as the oldest magnetic anomaly in the southern South Atlantic. However, on the South American margin, these authors had only identified up to M4 (130.6 Ma). Later Franke et al. (2007) and Gerster et al. (2011) identified up to M10 (~134 Ma) on the Argentinean offshore. Recently Hall et al. (2018) were able to establish the M11 anomaly on the South American margin (Fig. 2.5). 136 Ma is then the age of the oldest oceanic crust identified to date in this segment.

Figure 2.17 presents a model for the early evolution of the southern South Atlantic, presented by Franke in 2013. In this model, extension coincident with subsequent seafloor spreading following oblique and magma-poor rifting in the southernmost segment initiated in the late Valanginian or early Hauterivian (Fig. 2.17a).

The subsegment to the north of the Colorado FZ, defining the transition from magma-poor to volcanic rifting, initiates rifting at approximately 133 Ma (Franke, 2013). The strong margin segmentation displayed by the southern South Atlantic is interpreted to have been in place since at least the time of SDR emplacement. The chronological relation between the Tristan da Cunha plume impingement (accountable for the Paraná-Etendeka LIP) and the SDR emplacement along the southern South Atlantic margins is still debated. Stica et al. (2014) suggest that SDR emplacement in the southern subsegments occurs before plume impingement. Franke (2013) and Collier et al. (2017) propose a coeval evolution (Fig. 2.17b). Authors seem to agree, however, that the plume does not precede the opening (which would suggest active rifting mode) but is at least synchronous or impinged after rifting had already started (Frizon De Lamotte et al., 2015; Will and Frimmel, 2018). After stepping across the next fracture zone (subsegment boundary) seafloor spreading propagated fast to the north, reaching the transfer zone that bounds the southern to the central South Atlantic by the Barremian (Franke, 2013; Fig. 2.17c). Note that the extension of the fracture zone into the continents is not used by Franke (Fig. 2.17). However, the Agulhas-Malvinas (Falkland) fracture zone (AMFZ) accommodates the lateral displacement produced by plate separation. A major unconformity interpreted from seismic and well data offshore South Africa was assigned to the mid-Valanginian (Baby et al., 2018; and references therein) and related to shear activity along the AMFZ.

Note in Figure 2.17 that Franke (2013) already differentiates the sedimentary basins formed before the South Atlantic opening (San Jorge, Colorado, Salado; 2.17a), and the syntectonic basins actively formed at each stage.

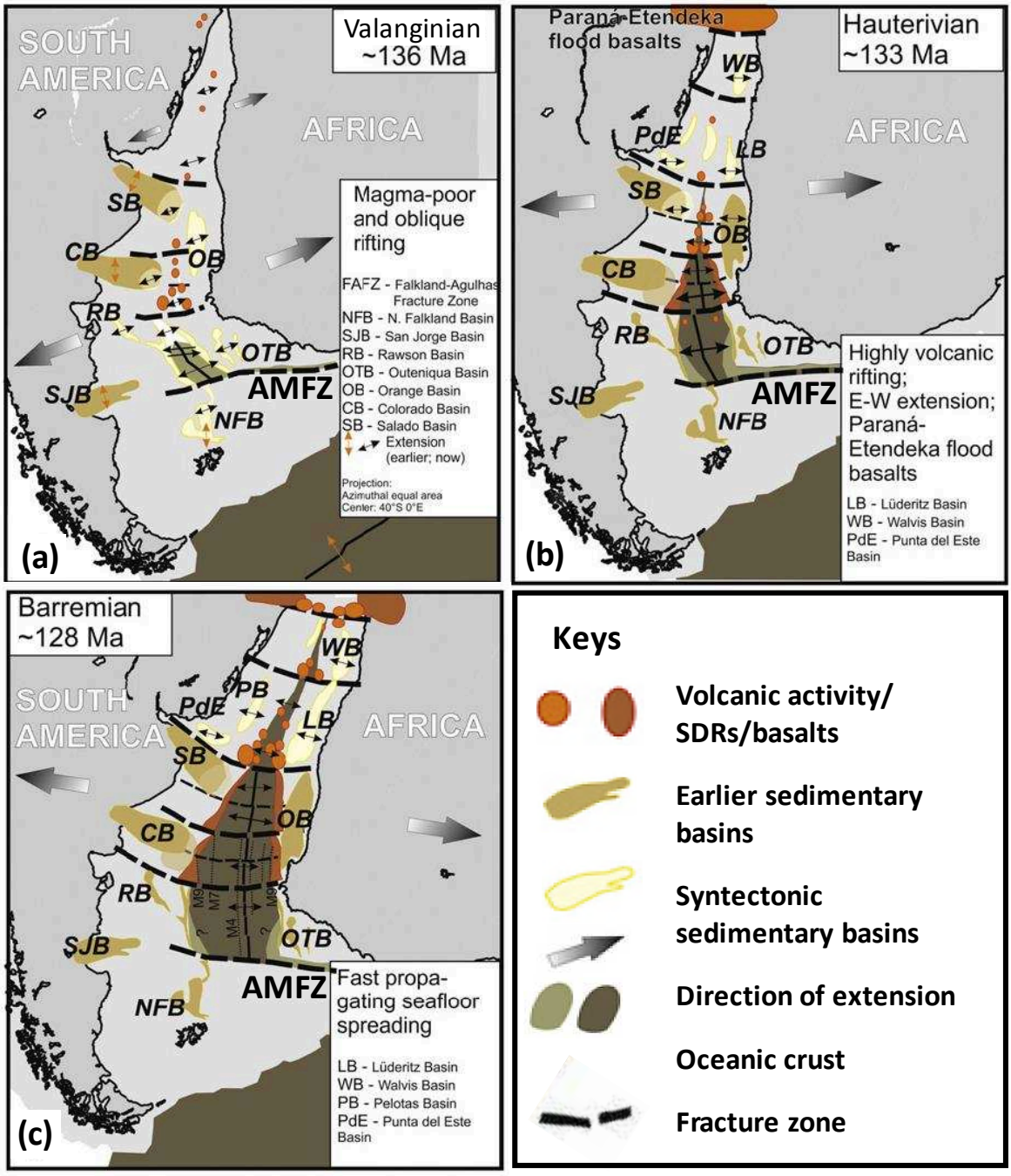

Figure 2.17: Sketches illustrating the early evolution of the southern South Atlantic at: a) circa 137 Ma; b) c. 133 Ma; and c) c. 128 Ma. (from Franke, 2013). Sedimentary basins: Pelotas basin (PB), Punta del Este basin (PdE), Salado basin (SB), Colorado basin (CB), Rawson basin (RB), San Jorge Gulf basin (SJB), North Malvinas (Falkland) basin (NFB), Outeniqua basin (OTB), Orange basin (OOB), Lüderitz basin (LB), Walvis basin (WB). AMFFZ: Agulhas-Malvinas (Falkland) Fracture Zone.

As the South Atlantic propagated from south to north, the age of the breakup unconformity (BU) displays also a strong diachronism. In the Outeniqua basin the BU was dated late Valanginian (Roux, 1997) as well as in the North Malvinas basin (Richards and Hillier, 2000; Ross et al., 1996), while a Barremian age was assigned south of the Walvis Ridge

(Brown et al., 1995; Jungslager, 1999); Hauterivian / Barremian in the San Jorge Basin (Baldi and Nevistic, 1996); Early-Middle Barremian in the Colorado basin (Fryklund et al., 1996; Juan et al., 1996). Hinz et al. (1999) proposed a minimum Hauterivian age for the BU in the Argentinean margin but noted that it may be time-transgressive. Stoakes et al. (1991) and Tavella and Wright (1996) interpreted a late Barremian/early Aptian age for the BU in the Salado basin, but it is probably not younger than Barremian.

In the central segment of the South Atlantic, rifting is interpreted to have occurred during the Barremian, with deposition of thick sections of lacustrine source rocks in the area between the Santos and Sergipe basins in the Brazilian margin and in the Namibe, Benguela, Kwanza, Congo and Gabon basins in the African counterpart (Fig. 2.13, (Aslanian et al., 2009; Chaboureau et al., 2013). The rifting propagates northwards at high speed rates.

The eastern end of the Malvinas Plateau (Maurice Ewing Bank, Fig. 2.4) separates from the Agulhas platform at 106 Ma (Pérez-Díaz and Eagles, 2014). However, the development of the Southern Ocean Large Igneous Province (SOLIP) in Albian/Cenomanian times, related to Bouvet's hot spot (Fig. 2.1), and possibly in subaerial conditions, could have produced semi-confined water circulation in the South Atlantic (Pérez-Díaz and Eagles, 2014). On the northern end, in the Equatorial Segment, Pérez-Díaz and Eagles (2014) propose that the breakup in this segment between the Cenomanian and the Turonian could have already allowed the communication of the Central and South Atlantic by deep sea currents. Wagner and Petsh (1999) suggest that only between the Turonian and the Danian (62-94 Ma), open marine conditions would have been established in the Equatorial Segment. Another important point to understand the beginning of the circulation of deep marine currents is the behavior of the Rio Grande High/Walvis ridge. According to Robinson et al. (2010) the subsidence of this region would have produced the exchange of deep waters towards only by the Campanian (83 Ma), and according to Voigt et al. (2013) only in the Paleocene (65-58 Ma).

2.3 The Offshore Argentinean Basins

As mentioned in the previous section, the sedimentary basins that developed on the Argentinean shelf seem to predate the Early Cretaceous South Atlantic breakup. Most of these basins, however, display a rifting evolution history intimately related to the Mesozoic extensional regimes responsible for the breakup of Pangea (Urien et al., 1981; Uliana et al., 1989;). After going through a process of continental accretion during the Paleozoic, which

ended up with the collision of Patagonia in the Permian (Ramos, 2008), the paleocontinent of Pangea changed to an extensional regime since the Triassic (Fig. 2.2). The formation of the Argentinean offshore Mesozoic basins responded first to these extensional regimes.

A structural map for the Mesozoic basins offshore Argentine is presented in Fig. 2.18. For the southern basins along the Malvinas segment of the South Atlantic (south of the AMFZ) note a strong structural grain (indicated by the orientation of the normal) mainly northwest. The North Malvinas and the San Julián basins are an exception (Fig. 2.18), North Malvinas displays a N-S axis, while the San Julián basins presents a more complex structure product of a complex Paleozoic evolution (Homovc and Constantini, 2001). The Rawson/Valdés basins, north of the AMFZ, display a similar orientation, with NNW-striking faults.

Further north, the Colorado and Salado/Punta del Este basins are largely oriented E-W to NW-SE. This highly oblique orientation regarding the NNE-striking COT (represented in Fig. 2.18 by the extension of the SDR wedges) has historically been explained in several ways: as aulacogenic basins related to triple junctions (Yrigoyen, 1975; Introcaso and Ramos, 1984; Franke et al., 2002); as trans-tensional basins associated with NW–SE dextral shear systems (Keeley and Light, 1993; Light et al., 1993; Tankard et al., 1995; Urien et al., 1995; Franke et al., 2006); as strongly conditioned by basement structural inheritance, with extensional reactivation along pre-existing crustal zones of weakness located obliquely to the direction of extension (Urien and Zambrano, 1973; Zambrano, 1980; Urien et al., 1981, 1995; Franke et al., 2006; Dominguez et al., 2011; Pángaro and Ramos, 2012); and finally, those who propose that the basin is actually older than the Early Cretaceous continental breakup, and its orientation responds to a previous rifting event (Autin et al., 2013; Gerster et al., 2011; Macdonald et al., 2003; Franke, 2013; Loegering et al., 2013), with a pre-Cretaceous rifting phase marked by NE–SW extension, that created basins at high angle to the Early Cretaceous COB on the Argentine margin.

The exact timing of rifting remains poorly constrained for several reasons. In the first place, these are frontier under-explored basins with tens of wells drilled. Second, hydrocarbon exploration wells are usually drilled on structural highs out depocenters making difficult the access to samples. When drilled, the synrift sequences tend to be of continental nature lacking datable fossils. Eventually volcanic rocks interbedded with the stratigraphic infill may allow absolute dating.

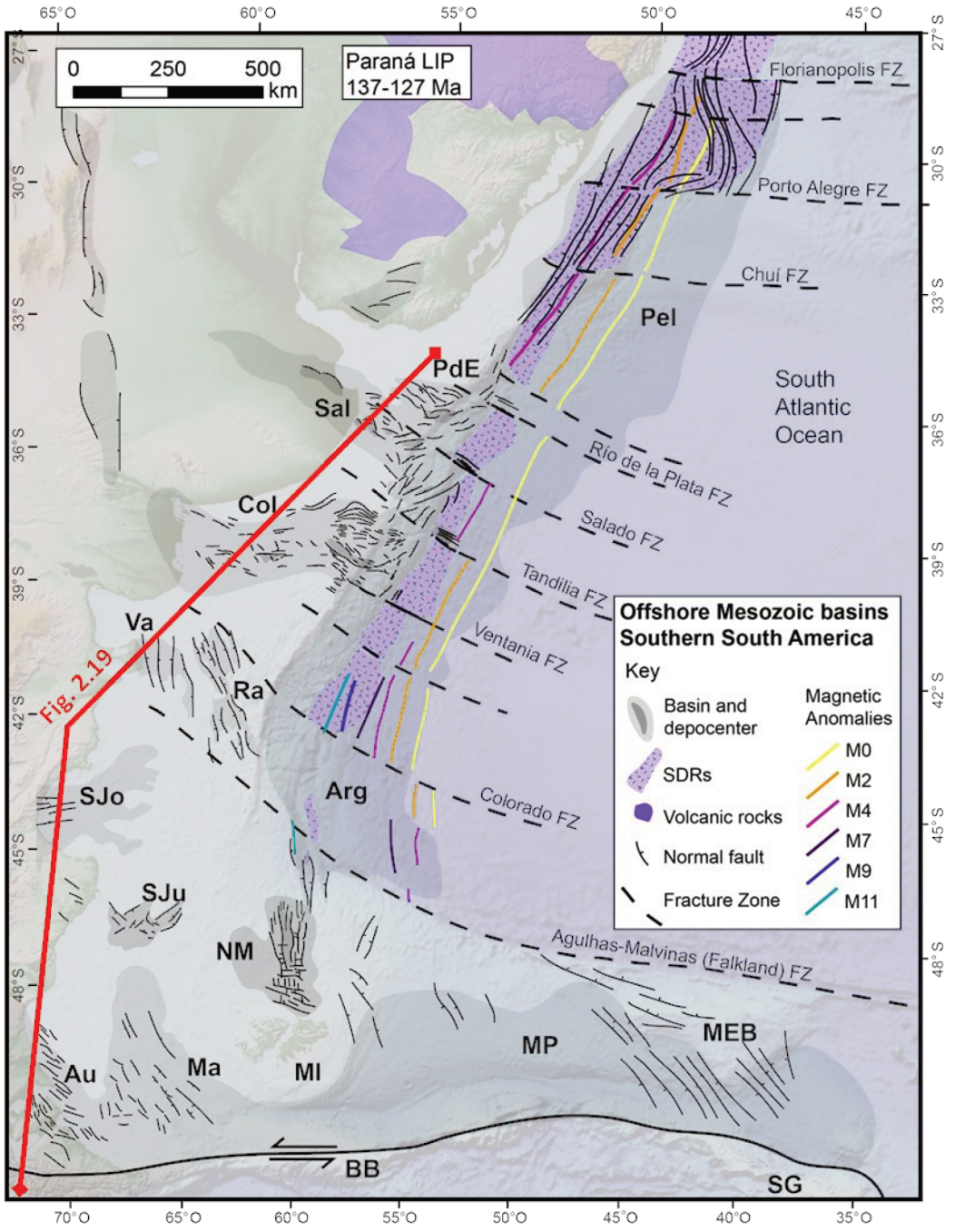

Figure 2.18: Structural map of the Atlantic basins along the Argentinean margin (after Franke et al., 2007; Lohr and Underhill, 2015; Mpodozis and Ramos, 2008; Uliana et al., 1989; Galeazzi, 1998; Gianni et al., 2015; Raggio et al., 2011b, 2011a; Soto et al., 2011).

However, one igneous event that characterizes the synrift infill of the southern offshore basins is the Chon Aike silicic LIP of Mid Jurassic age (Pankhurst et al., 1998, 2000). Since 170 Ma and until approximately 150 Ma, most of Patagonia was under extensional regime, with half-grabens oriented NNW-SSE to NW-SE and profuse volcanism (mainly rhyolitic ignimbrites) associated to the Chon Aike acidic LIP. Many lithostratigraphic names have been given to Chon Aike LIP representatives: Chon Aike Fm (in the Deseado massif), Serie Tobífera

(Austral and Malvinas basins), Lemaire Fm (onshore Tierra del Fuego island), Bahía Laura Gp, etc. El Quemado complex in the western Austral/Magallanes basins corresponds to a Late Jurassic late volcanic pulse (Pankhurst et al., 2000).

The stratigraphic evolution of the main basins offshore Argentina is presented in Fig. 2.19b (from Welsink, 2010), along a S-N section pictured in Fig. 2.18. Note the extension of the Chon Aike LIP in the Malvinas, San Julián and under the San Jorge Gulf basin (with a later, main rifting phase in the Neocomian). The extension associated with the Chon Aike LIP is responsible for the main rifting stage at the Malvinas basin. The San Julián basin also displays a more complex Paleozoic/Triassic rifting history note illustrated by Fig. 2.19. Towards the north, in the Rawson/Valdés, Colorado and Salado basins, the synrift infill of a presumably similar Jurassic age corresponds to sediments deposited in continental environments (which is consistent with the land-locked paleogeographic situation for that period, Macdonald et al., 2003; Uliana et al., 1989).

Note that the Malvinas basin in the south, develops a sag phase since the early Cretaceous under marine conditions. The basin was open to the sea towards the south (the Weddell sea; Ghidella et al., 2002) and not the South Atlantic Ocean. The San Jorge Gulf basin hosts continental environments in a land-locked basin (occasionally open to the Pacific in the Neocomian, not represented). The San Julián and Rawson/Valdés basins present a hiatus for most of the Cretaceous, while the Colorado and Salado basins display continental to marine conditions developed during the drift phase after the Late Hauterivian/Barremian diachronous South Atlantic breakup. These basins are then open to the South Atlantic Ocean.

The Cenozoic evolution displays a large variety of processes. In the south, the Malvinas basin goes through a foreland phase initiated with N-S compression since the latest Cretaceous. The San Jorge Gulf basin finally opens to the Atlantic (also because the Andean Cordillera is uplifted to the west since the Late Cretaceous (Fitzgerald et al., 1990). The Rawson/Valdés, Colorado and Salado basins display continental to marine environments throughout the Cenozoic, with several transgressive regressive cycles dated but yet poorly understood.

To summarize, the evolution of the Southern South Atlantic passive margin is complex both in time and space. In the first place, a superposition of Mesozoic rifting events is observed in this area, part of the SW margin of Gondwana. The area is intrinsically heterogeneous, formed as a collage of cratons, mobile belts and accreted terranes, and these heterogeneities

played a role in basin formation. Moreover, the South Atlantic Ocean opening, since the Latest Jurassic, buy taking place throughout the Early Cretaceous, occurred in a diachronous way, from south to north, with formation of different types of margins (i.e. magma-poor, magma-rich). A combination of the previous rifting events and the margin formation mechanism will have an impact on basin evolution, that will be assessed along the following chapter.

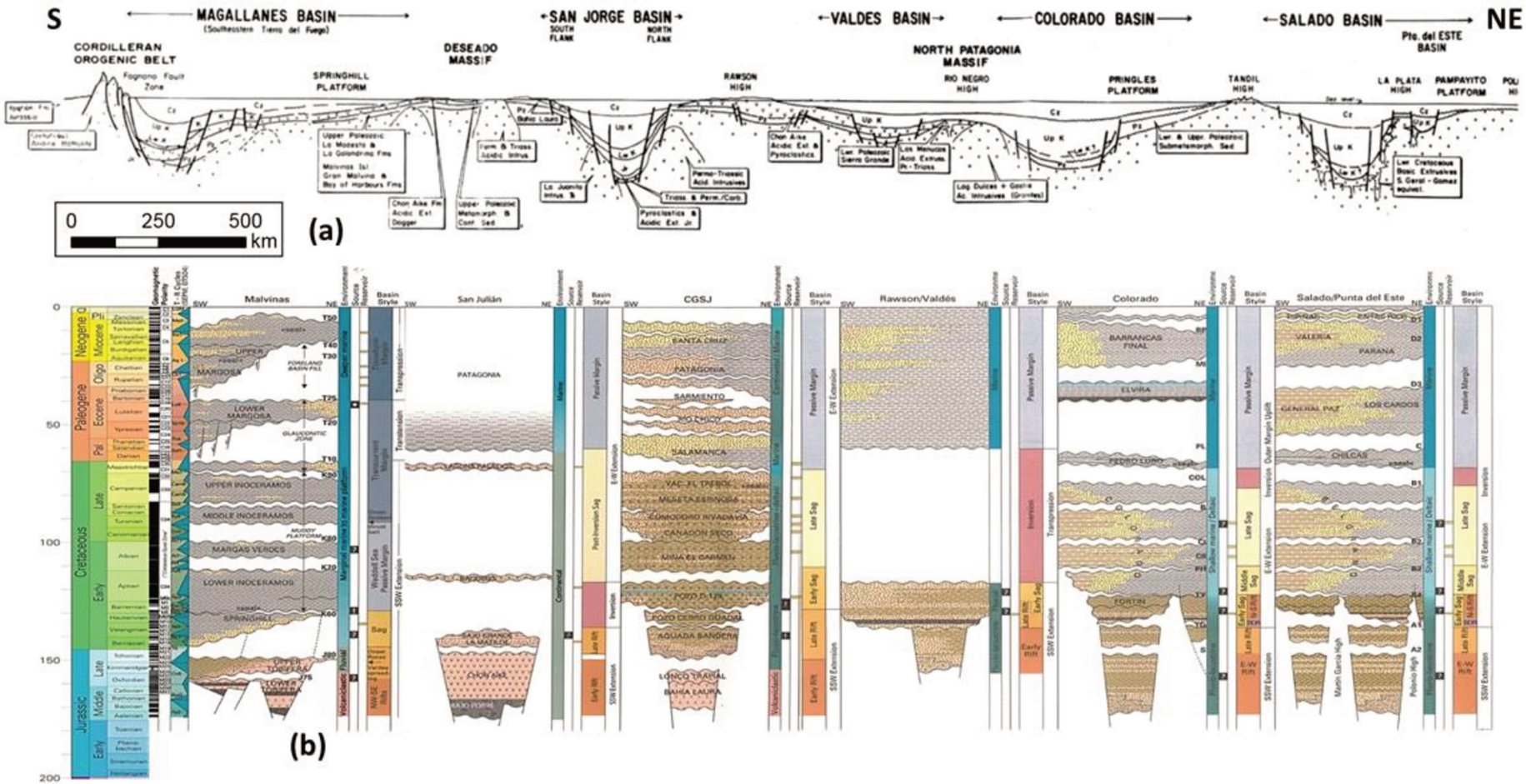

Figure 2.19: a) Schematic structural section across the Argentinean offshore basins (from Urien et al., 1981); b) Correlation of chronostratigraphic chart across the main offshore Argentinean basins (from Welsink et al., 2010).

PART II: RIFTING EVOLUTION OF THE ARGENTINEAN MARGIN

Chapter 3. Colorado basin

We present hereafter the results of the work carried out on the Colorado basin to support the publication presented in Chapter 4. The seismic interpretation and the structural and isopach maps presented here have also been used in the characterization and forward stratigraphic modeling of the post-breakup evolution of the Colorado basin, presented in Chapter 6.

3.1 Introduction

The Colorado basin is an extensional basin located in the Argentinean margin in the South Segment of the South Atlantic (Fig. 3.1). It is largely oriented E-W, spanning 200 km in the N-S direction, between 39° and 41° S, and more than 600 km in the E-W direction amid 56° and 63° W) covering an area of more than 150,000 km^2 (Fig. 2). Dated Mesozoic, the basin formation is known to be related to the breakup of Gondwana, which broke apart South America from Africa and ended up with the opening of the South Atlantic in the Early Cretaceous. Most of the Colorado basin is emplaced offshore on the Argentinean shelf, although its western border reaches the shore and some of the first exploration wells in the basin were drilled onshore in the 1940's and 1960's (Fig. 3.1).

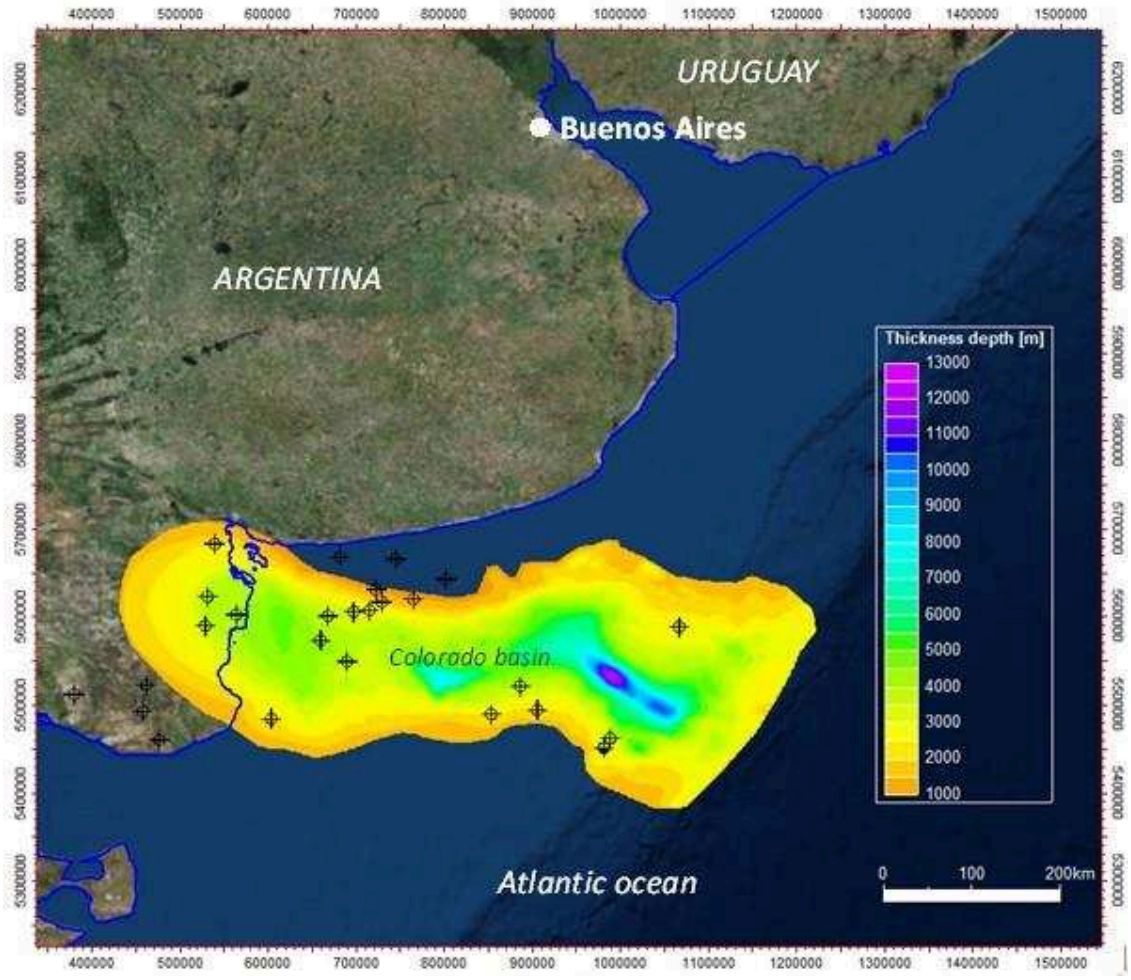

Figure 3.1: The Colorado basin on the Argentinean shelf. Colors correspond to total sedimentary thickness (meters) outlined by the extension of the Cretaceous basin. Hydrocarbon exploration wells are displayed. Projection UTM20S.

The Colorado basin occupies an area of more than 150,000 km^2 on the Argentinean shelf. It is limited to the north by the Ventania and Tandilia systems (Gerster et al., 2011; Fig. 3.2). The Ventania system is a Late Paleozoic fold-and-thrust belt exposing from SW to NE: lower, middle and upper Paleozoic rocks. The Claromecó basin is enclosed between the Ventania and Tandilia systems and records Late Paleozoic sedimentation. Proterozoic igneous-metamorphic basement, part of the Rio de la Plata craton, outcrops in the Tandilia system, and is covered by Precambrian sedimentary rocks. Tandilia extends to the east acting as a basement high that separated the Colorado and Salado basins until the latest Cretaceous. Further offshore, on transitional and oceanic crust, the northern limit of the basin is given by the Tandilia shear zone (Fig. 3.2).

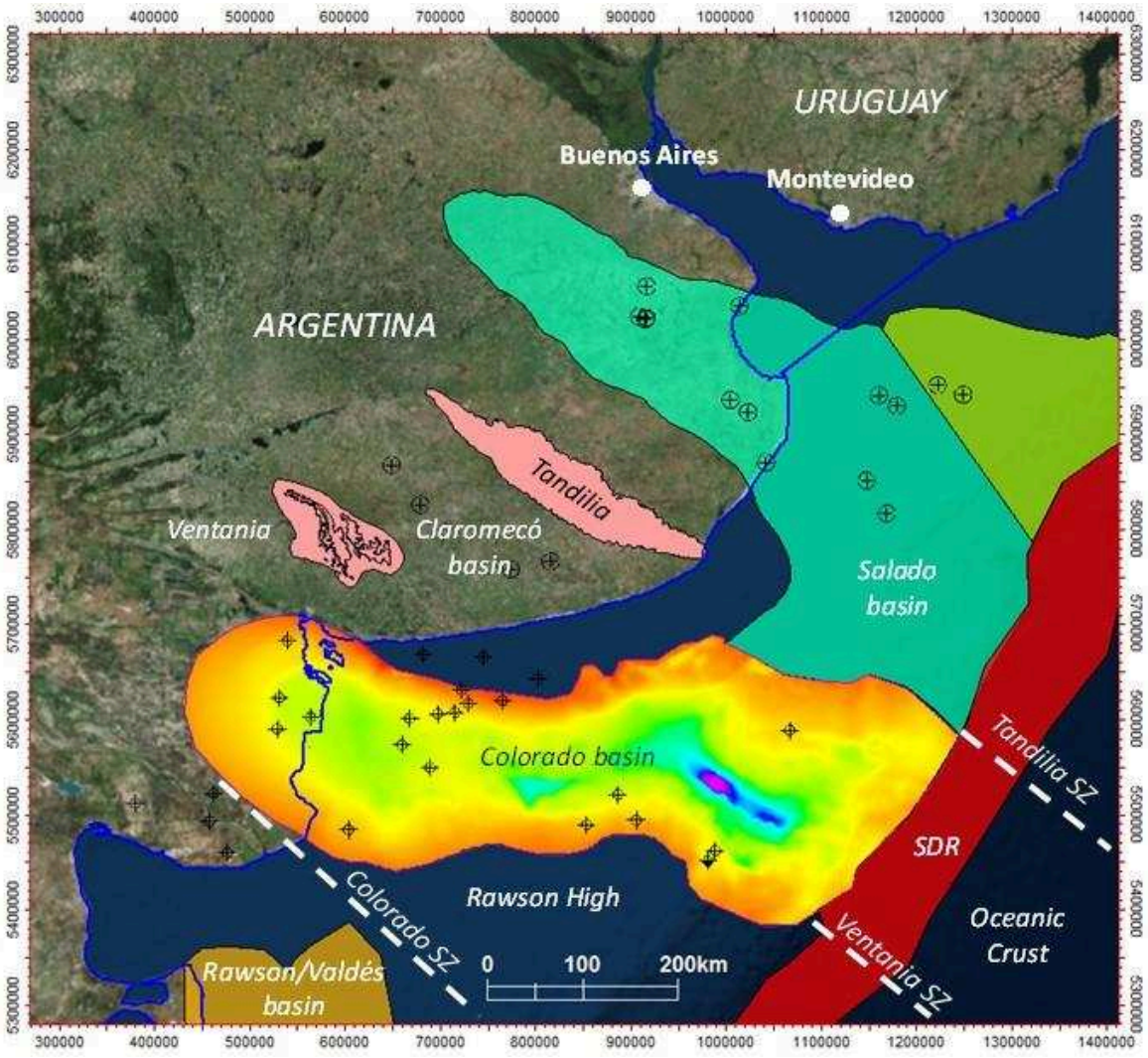

Figure 3.2: Main tectonic features limiting the Colorado basin. Shear Zones after (Franke et al., 2007; Gerster et al., 2011). The color scale in the Colorado basin indicate total sedimentary thickness, see Fig. 3.1. Hydrocarbon exploration wells are depicted.

To the south it is bounded by the Rawson high, an extension of the North Patagonian massif which also limits the basin to the west, where the Paleozoic rocks of the North Patagonian Massif crops out. Further offshore on the oceanic crust, the southern limit of the Colorado basin is the Ventania shear zone. To the east, the basin boudary was established at the eastern limit of continental crust, interpreted as the limit of the first SDR in the segment. The sedimentary basin developed on transitional and oceanic crust further east, is referred to as the Argentina basin (Rabinowitz and LaBreque, 1979).

The existence of three main and independent depocenters in the Colorado basin was first recognized in the basin by Gerster et al. (2011) and then supported by Pángaro and Ramos (2012) and Loegering et al. (2013), who named them Western, Central and Eastern Colorado,

a nomenclature that persisted and that we use in this study (Fig. 3.3). All depocenters are disposed on a stripe between 39° and 41° S. The Eastern Colorado depocenter (ECol) is located between 55° and 58° W. It has a strong SE-NW orientation, extending 200 km in that direction and approximately 30 km in the SW-NE direction (Fig. 3.3). It is also the deepest depocenter of the basin, reaching more than 12 km of total sedimentary thickness (Fig. 3.3). The Central Colorado depocenter (CCol) extends between 58° and 60°30' W. It is oriented E-W, 80 km long and 30 km wide, and is placed on the southern portion of the basin, not centered with respect to the total thickness map. Sedimentary thickness reaches 7 km in the axis of the depocenter (Fig. 3.3). The Western Colorado depocenter (WCol) is located between 60°30' and 63°30' W. It has a more irregular shape, gently oriented SE-NW, 160 km long by 80 km in the SW-NE direction. It has a maximum sedimentary thickness of approximately 5 km.

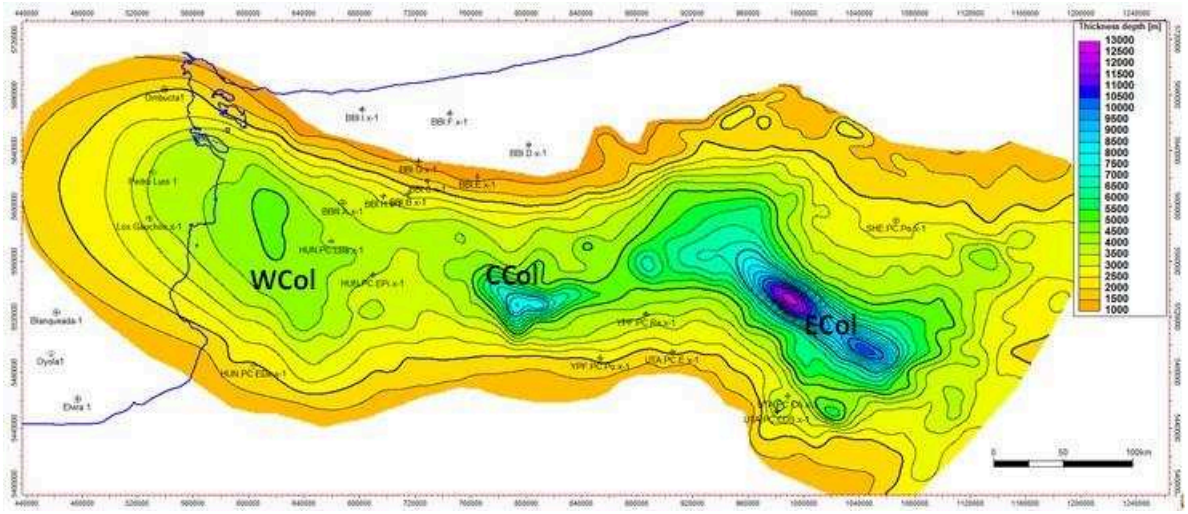

Figure 3.3: Total sedimentary thickness map (in meters) of the Colorado basin. The three main depocenters are depicted. WCol: Western Colorado, CCol: Central Colorado, ECol: Eastern Colorado.

3.2 Geological Framework

3.2.1 Prerift Geology

The prerift geology is important to the Colorado basin as (1) it has been said to influence the basin structure (Dominguez et al., 2011; Pángaro and Ramos, 2012; Autin et al., 2013) and (2) there is still debate on the synrift or Paleozoic prerift nature of sections drilled by hydrocarbon exploration wells (i.e. the Cruz del Sur well; Fryklund et al., 1996; Pángaro et al., 2016).

The oldest rocks known in Argentina are Paleoproterozoic and outcrop in the Tandilia system (Fig. 3.2 and 3.4). These rocks form an calc-alkaline igneous-metamorphic complex named the Buenos Aires Complex. It is mainly composed of granitic-tonalitic gneisses, migmatites, amphibolites, with minor ultramaphic rocks and some granitoid intrusives (Cingolani, 2011). The origin of this complex is related to an orogenic event (2.12-2.25 Ga) followed by continental collision (2.08-2.1 Ga). The Paleoproterozoic basement is overlain by the Neoproterozoic Sierras Bayas group, a mixed passive margin succession containing siliciclastic and carbonate sediments, covered by the quartz-arenites and shales of the Silurian Balcarce Fm (Cingolani, 2011).

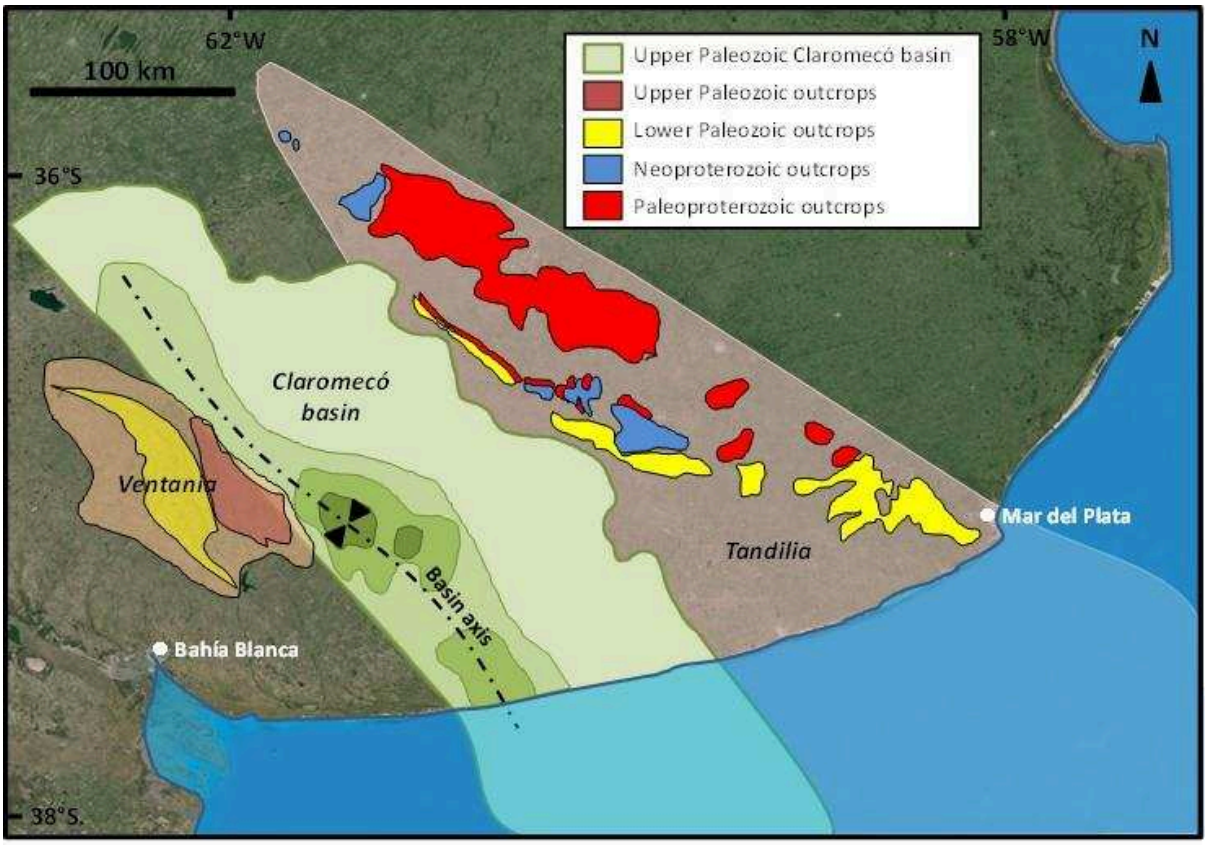

Figure 3.4: Schematic map showing the prerift units related to the Colorado basin, outcropping onshore Argentina (after Ramos, 2008; Cingolani, 2011). Contours in the Claromecó basin represent a relative trend derived from gravimetric data

The Ventania system is a fold-and-thrust belt with NE vergence (top to the NE), involving lower and upper Paleozoic series (Harrington, 1980; Fig. 3.4). The whole sedimentary succession reaches around 4500 m in thickness (Ramos et al., 2014). The oldest units crop out on the western flank, becoming younger to the east. The sedimentary rocks in the

Ventania system display low to medium grade of metamorphism, being more intense in the oldest units to the west.

The Cambrian-Ordovician Curamalal Gr cropping out in Western Ventania represents a siliciclastic passive margin. After a conglomeratic base, the succession is dominated by fine-grained quartz rich sandstones with some shaly intervals towards the top. Detrital zircon data point towards two sediment sources: one in the north, Tandilia, mainly for the basal conglomerates; and one in the northwest, with Cambrian ages associated with the Pampean orogen (Ramos et al., 2014).

In Ventania, the Curamalal Gr is unconformably overlaid by the Ventana Gr, which starts with the Bravard Fm coarse to conglomeratic sandstones, followed by the Napostá/Providencia/Lolén succession which exceeds 1 km in thickness and is composed mainly of medium-to-fine grained quartz-arenites. Shaly intercalations are common towards the top of the Lolén Fm (Harrington, 1980). The Ventana Gr has been interpreted as an open marine environment in a passive margin setting, with a complete transgressive-regressive cycle recorded. Ramos et al. (2014) dated the whole Ventana Gr as Silurian-Devonian, as containing Cambrian and Ordovician zircons of Pampean age, which indicate paleosedimentary sourcing from the W-NW, indicating a provenance area from the Eastern and Western Sierras Pampeanas. Brachiopod casts in the bottom section of Lolén Fm date it Emsian (Benedetto, 2012; Harrington, 1980). The Ventana Gr correlates with the Bokkveld Gr and partially with the upper section of the Table Mountain Gr (Cape Supergroup) of South Africa. The correlation between the successions present in Ventania and those of the Cape fold belt and the Karoo basin in South Africa basin was proposed by Keidel (1916) and followed by du Toit (1927). The Ventana Gr correlates with the Bokkveld Gr and partially with the upper section of the Table Mountain Gr (Cape Supergroup) of South Africa (Flint et al., 2011).

Late Paleozoic rocks are grouped in the Pillahuincó Gr, a glacial and late glacial succession recording the Gondwana glaciation that unconformably covers the Ventana Gr. It crops out in eastern Ventania system and spans to the NE in the subsurface of the Claromecó basin (Fig. 3.4).

The Pillahuincó Gr starts with the Sauce Grande Fm, up to 900 m thick, formed of interbedded diamictites, conglomerates, sandstones and shales. The basal section is richer in diamictites, with shaly matrix and drop-stones, with boulders of up to 3m in diameter, many

striated. The middle section hosts thick quartz-rich, normally graded and cross-bedded sandstones. Interbedded greenish conglomeratic 1-2 m thick lenses are common. The top section of the Sauce Grande Fm is again rich in diamictites (Fig. 3.5a), with a higher content of shaly matrix and drop-stones which become scarcer towards the top, where it gradually passes into the Piedra Azul Fm (Harrington, 1980).

The Piedra Azul Fm reaches 290 m in thickness and hosts bluish to black slates with Murchinsonia sp. casts and scarce cross-bedded sandy lenses. The Bonete Fm conformably overlies Piedra Azul and consists of up to 400 m of interbedded sandy and shaly beds. It is rich in paleoflora, especially that of the Upper Paleozoic NBG biozone, and hosts fossil elements of the Eurydesma bivalve fauna (Benedetto, 2012). Fossil content details can be found in Harrington (1980) and further references mentioned therein. The last unit of the Pillahuincó Gr known in the onshore area is the Tunas Fm. The Tunas Fm crops out on the eastern flank of the Ventania system and continues in the Claromecó basin. Purple and green shales and mudstones with Gangamopteris flora are common especially in the bottom section, whereas towards the top, fine- to coarse-grained, reddish to brownish sandy beds become more frequent (Harrington, 1980). The Tunas Fm can reach up to 2,000 m in thickness.

The diamictites of the Sauce Grande Fm have been interpreted as deposited in a glaciomarine environment. Ramos et al. (2014) suggest that the recent discovery of clasts with archeocyathids derived from Eastern Antarctica within the Sauce Grande diamictites (Gonzalez et al., 2013) support a correlation with the Lafonia Fm of the Malvinas islands and the Dwyka Gr tillites present in the Karoo basin of South Africa (Fig. 3.5a and c). The Piedra Azul Fm represents early postglacial transgressive deposits, covered by the marine to deltaic deposits of Bonete Fm and Tunas Fm. The Tunas Fm has been interpreted as deposited in an estuarine–tidal flat environment (Andreis and Japas, 1996).

Another point to highlight is the change in polarity of paleocurrents observed in the Pillahuincó Gr, consequence of the inception of a foreland basin with sediment sourcing from the arc/fold belt to the south (Lopez-Gamundi and Rosello, 1998) at the time of deposition of the Tunas Fm. Growth strata have been identified in the Tunas Fm, supporting its interpretation as syntectonic deposits (Lopez-Gamundi et al., 1995). Ash-fall deposits interbedded with the Tunas Fm were first described by Iñiguez et al. (1988). Absolute dating gives a middle Early Permian age for this unit (Alessandretti et al., 2013). Ramos et al. (2014) propose that the source of these volcanic ashes is the Somún Curá/North Patagonian Massif.

The Piedra Azul, Bonete and Tunas succession has been correlated with the base of the Ecca Gr of the Karoo basin (South Africa, Fig. 3.5c): Prince Albert, Whitehill and Collingham Fms respectively.

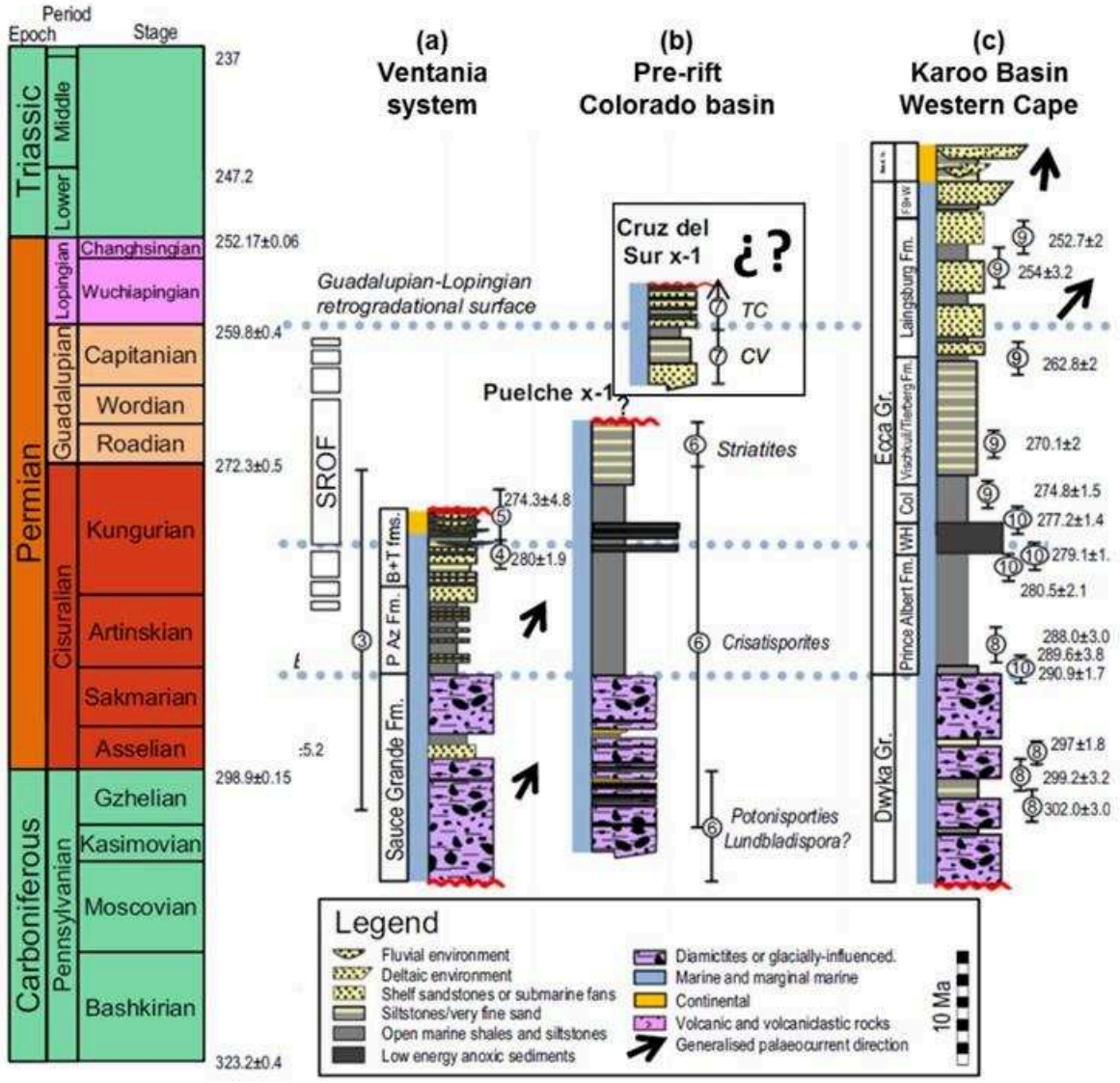

Figure 3.5: SW Gondwana upper Paleozoic to Lower Triassic correlation chart (modified from Pángaro et al., 2016). The interpretation of the sequences in Cruz del Sur x-1 is debated.

The drilling of exploration wells in the Claromecó basin (Fig. 3.4), confirmed the extension of the Paleozoic basin to the North of the Ventania system with similar facies. A major unconformity tops the Paleozoic, above which Tertiary sediments overlie. Schiuma (2012) reports an average vitrinite reflectance (Ro) of 1.58% average (min: 1.34; max: 1.857; n: 80) for a coal seam sample taken from one exploration well (named PANG) at approximately 700 m MD (measured depth). Schiuma's calculations indicate that with a normal thermal

gradient, the sequences containing these coal seams should have reached depths of about 4,000-4,500 m. The fact that they are nowadays at approximately 700 m below ground level, together with the advanced degree of metamorphism of the Curamalal, Ventana and Pillahuincó Grs in the Ventania system outcrops, suggests an important exhumation and denudation event since the earliest Mesozoic. This hypothesis is supported by recently published AFTA data (Kollenz, 2015).

In the offshore, to the south of Ventania and the Claromecó basin, the presence of Paleozoic strata has been known since the early steps of offshore exploration (e.g. Pingüino well, Fig. 3.6). However, it was not confirmed until the drilling of the Puelche well in 1977, when diamictites were described in the Colorado basin prerift tilted blocks and correlated with the Sauce Grande Fm (Lesta et al., 1978; Fig. 3.6). Then other wells drilled this Paleozoic prerift such as Estrella, Cruz del Sur, etc.

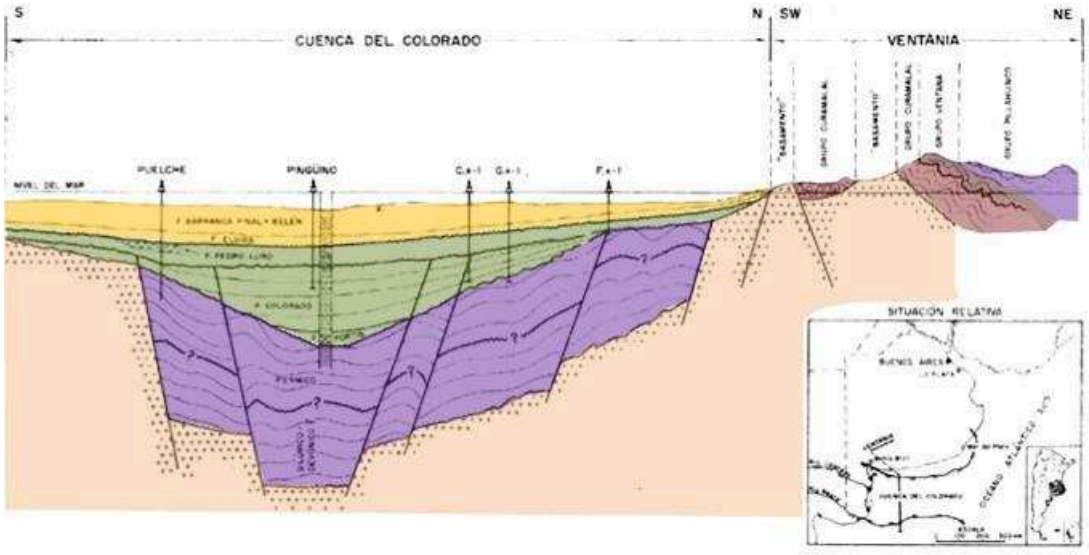

Figure 3.6: Regional schematic section of the Western depocenter of the Colorado basin, with interpretation of the folded Paleozoic series bellow the Mesozoic strata (after Lesta et al., 1978).

The extension of the Claromecó basin to the SE in the prerift of the Colorado basin (Fig. 3.4) has been addressed by Pángaro and Ramos (2012), Pángaro (2013) and Pángaro et al. (2016), and was named by these authors as the Hespérides basin. Biostratigraphy of these sequences has been studied by Archangelsky and Gamerro (1980) and recently by Balarino (2012, 2009). Pángaro et al. (2016) correlate the section drilled in Puelche as equivalent to the Pillahuincó Gr of Ventania (Fig. 3.5) and propose that the section drilled by Cruz del Sur.x-1 would be younger than that tested by Puelche, and equivalent to the Laingsburg Fm in the Karoo

basin (Fig. 3.5). Recent analysis carried out on palynological samples from the Cruz del Sur well point to a Mesozoic age for this series (Ottone and Angelozzi, 2015), which is consistent with the seismic interpretation of a synrift originally proposed for this segment (Fryklund et al., 1996).

A schematic view of the prerift paleotectonic framework is presented in Figure 3.7. The area of influence of the Gondwanides orogen is illustrated, covering the Northern volcanic arc and an area in central Argentina with Paleozoic rocks including San Rafael and Carapacha basins (Pángaro et al., 2016). The extension of the Claromecó basin under the Colorado basin is also illustrated.

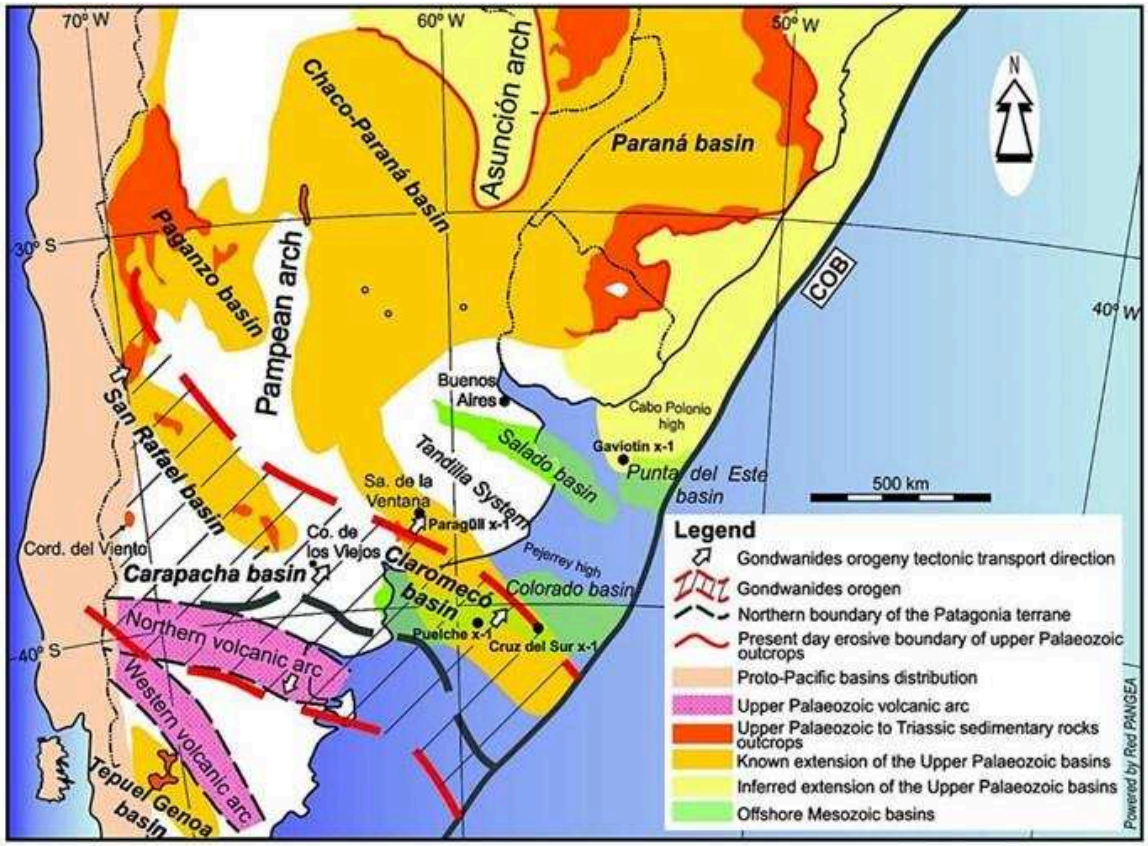

Figure 3.7: Distribution of upper Paleozoic to Lower Triassic basins of southern South America (from Pángaro et al., 2016, after references mentioned therein).

A reconstruction of the Ventania fold-and-thrust belt and its continuation, under the Colorado basin, with the Cape fold-and-thrust belt is shown in Figure 3.8. Their existence has been interpreted to be a consequence of a buttressing effect of the Río de la Plata and Kalahari cratonic blocks applied to the more 'ductile' Dom Feliciano metamorphic belt (Pángaro and Ramos, 2012; Fig. 3.8). The red and blue lineaments were deducted by the authors from

gravimetric anomalies, and the ones located on the South American continent have their counterpart on the African continent in the Saldania belt (SB).

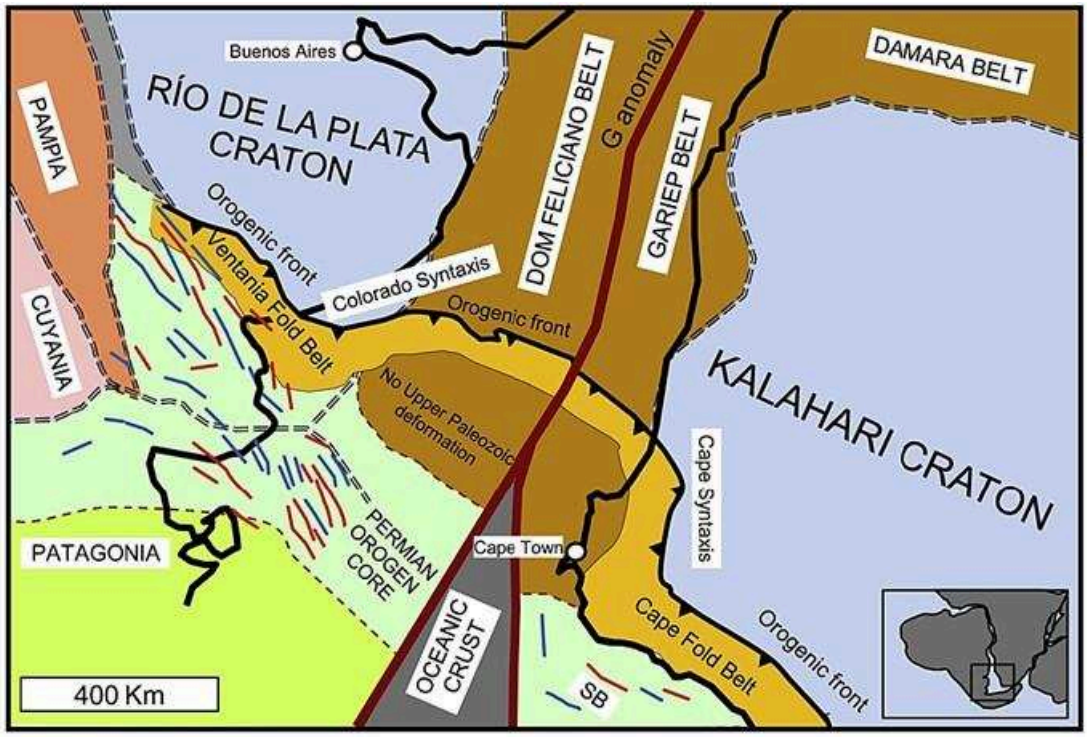

Figure 3.8: Paleogeographic restoration of the Permian orogen at a pre-breakup geometry (from Pángaro and Ramos, 2012).

3.2.2 Mesozoic evolution

After the Gondwanides orogeny at the end of the Paleozoic (du Toit, 1927; Ramos, 2008; Vaughan and Pankhurst, 2008; Pángaro and Ramos, 2012), Pangea, and particularly West Gondwana, went through a complex rifting process that ended with the dismembering of the ancient supercontinent (Uliana et al., 1989; Frizon De Lamotte et al., 2015). The South Atlantic Ocean opened in the Early Cretaceous between South America and Africa (Chapter 2.2) and changed since then, the basin dynamics in the peri-Atlantic realm.

The Colorado and Salado/Punta del Este basins, located off the Atlantic coasts of Argentina and Uruguay, are largely oriented E-W to NW, at high angles with the Atlantic continent-ocean transition (COT). This highly oblique orientation regarding the NNE-striking COT (represented in Fig. 2.18 by the extension of the SDR wedges, and in Fig. 3.8 by the G anomaly, see Rabinowitz and LaBreque, 1979) has historically been explained in several ways, i.e. as aulacogenic basins related to triple junctions (Franke et al., 2002; Introcaso and Ramos, 1984; Yrigoyen, 1975); as trans-tensional basins associated with NW–SE dextral shear systems

(Keeley and Light, 1993; Light et al., 1993; Franke et al., 2006; Tankard et al., 1995; Urien et al., 1995); as strongly conditioned by basement structural inheritance, with extensional reactivation along pre-existing crustal zones of weakness located obliquely to the direction of extension (Urien and Zambrano, 1973; Zambrano, 1980; Urien et al., 1981, 1995; Ramos, 1996; Franke et al., 2006; Dominguez et al., 2011; Pángaro and Ramos, 2012). More recently several authors support a two-stage rifting evolution, with a first rifting stage, characterized by overall N-S extension and the formation of the Colorado and Salado basins, and a second rifting stage with approximately E-W extension, responsible for the opening of the South Atlantic Ocean (Fig. 3.9; Macdonald et al., 2003; Gerster et al., 2011; Franke, 2013; Loegering et al., 2013; Autin et al., 2013; Koopmann et al., 2016). A more detailed evolution and the integration of the rifting evolution of the Colorado and Salado basins in the Gondwana breakup framework is presented in Chapter 6.

The synrift infill age and nature in the Colorado basin is poorly constrained. Most of the exploration wells have been drilled on structural highs out of the main depocenters, so they found sag facies on top of basement or Paleozoic prerift units (e.g. the Pejerrey well, Juan et al., 1996). The Ranquel well did penetrate some synrift equivalent units and found red beds (conglomerates, sandstones and reddish siltstones; Lesta et al., 1978). By correlation with the synrift drilled in the Salado basin (Tavella, 2005; Tavella and Wright, 1996), the synrift has been interpreted to consist of continental red beds (Fig. 3.10). However, the discovery of organic grey shales in the synrift section in the Cruz del Sur.x-1 well (Fryklund et al., 1996) points towards the development of lacustrine facies within the depocenters. A detailed discussion on the Cruz del Sur depocenter is given later in this chapter. The continental facies in the synrift section make these units poorly constrained in age. Palynoelements have large biochrons and are scarce or not preserved (e.g. in the red beds). Volcanic rocks have been described in the basal section of the Corona Austral. These rocks are andesites and yielded a K/Ar age of 130.1±2.3 Ma (Aguirre et al., 2001). These volcanic rocks are interbedded with sandstones. It remains uncertain if these volcanic rocks are intrusive or extrusive, and whether they are interbedded with sediments of the prerift or synrift section. A schematic a priori illustration of the Colorado basin stratigraphy is presented in Figure 3.10.

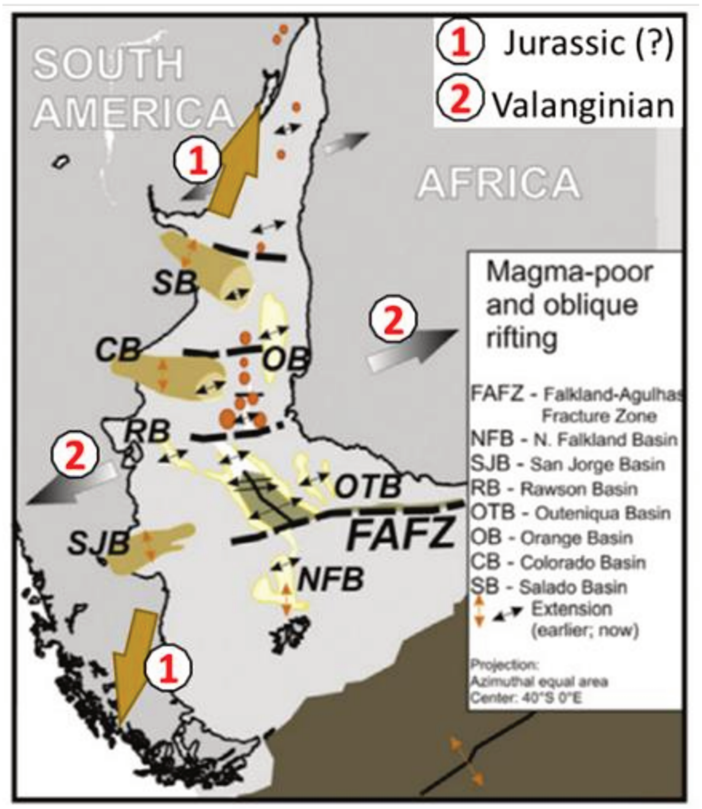

Figure 3.9: Formation of the highly oblique basins on the Argentinean margin (after Franke, 2013).

South Atlantic breakup at the latitude of the Colorado basin is interpreted to have taken place in Late Hauterivian times (Franke et al., 2007; Heine et al., 2013). The post-breakup evolution of the basin is marked by a rising sea-level and thermal subsidence over the largely EW-oriented Jurassic depocenters. Since the Aptian-Albian and through all the Late Cretaceous, major progradation and aggradation of the shelf is observed in the Colorado basin. Deposition is restricted to the Colorado 'trough' as sequences laterally onlap the southern Rawson and northern Tandilia highs. The presence of these exhumed highs throughout the mid-late Cretaceous is believed to have produced a complex coastline with huge E-W elongated estuaries flooded during transgressions in the Colorado and Salado basin depocenters (Fig. 3.11). These features are believed to have been completely flooded by the latest Cretaceous. Fluvial to coastal systems occupy the Colorado trough throughout the Late Cretaceous. The Colorado Fm was defined in the wells drilled on the shelf that penetrated mostly fluvial facies

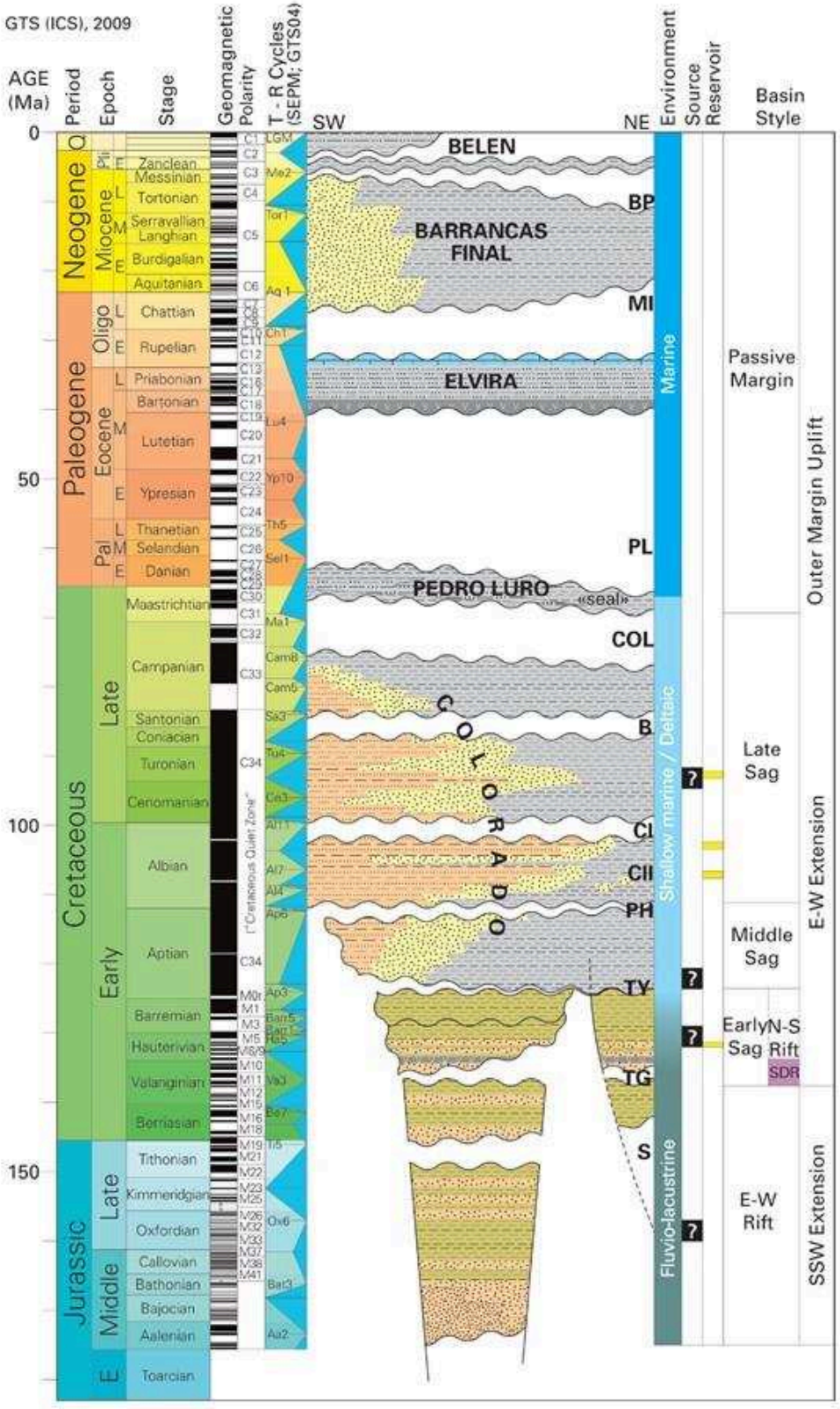

Figure 3.10: Generalized chronostratigraphic chart of the Colorado basin, showing stratigraphy, constraining ages, and main regional tectonic events. It is a zoom of Fig. 2.19 (from Welsink, 2010).

(Fig. 3.10). Sediments were sourced from the west, with Andean orogenic events producing uplift and erosion (Fennell et al., 2015; Andres Folguera et al., 2015), generating sediments that are transported from the Andes to the Atlantic basins by river systems. Seismic data indicate coastal to marine environments develop towards the east and the shelf-break is located neat COT (that marks a structural step on the margin).

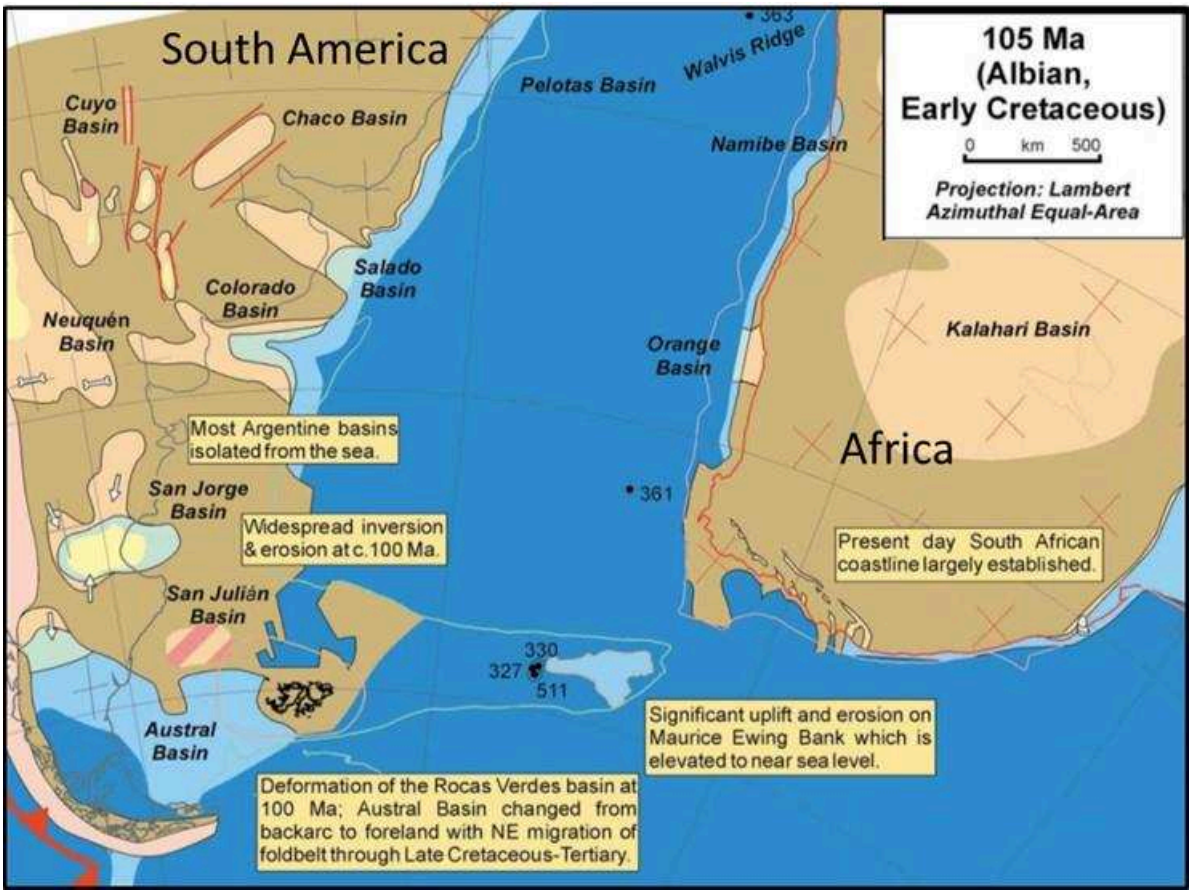

Figure 3.11: Paleogeographic reconstruction of the South Atlantic for the Albian (~105 Ma). Most of the margins are now in the thermal sag phase and have been transgressed (from Macdonald et al., 2003).

A major Atlantic transgression associated with a regional sea level rise produced the complete flooding of the Colorado basin since the Campanian. A paper on this transgression and the communication of a palynomorph species was published as part of this thesis (Ottone et al., 2018; Appendix 1), and even the flooding of the Neuquén basin from the Atlantic (Figs. 3.11 and 3.12) in Maastrichtian-Danian times (Aguirre-Urreta et al., 2011). In the Colorado basin, the transgression deposited the marine shales of the Pedro Luro Fm (Fig. 3.10).

The drilling of Puelche and Ranquel wells in the late 1970's allowed the recognition of a volcanic field interbedded with the transgressive shales of the Pedro Luro Fm on the southern

margin of the Colorado basin (Lesta et al., 1978). Tuffs and peperite facies are described in these wells, interbedded with shales, volcanic agglomerates and basalts top the section. An absolute K-Ar age of 70±3 Ma (Linares, 1978) was assigned to a basalt in the Puelche well. A review of the facies and a general seismic characterization of the 'Ranquel volcanic field' was in an extended abstart at the Argentinean Geological Congress in 2017 and is included in this manuscript in Appendix 2.

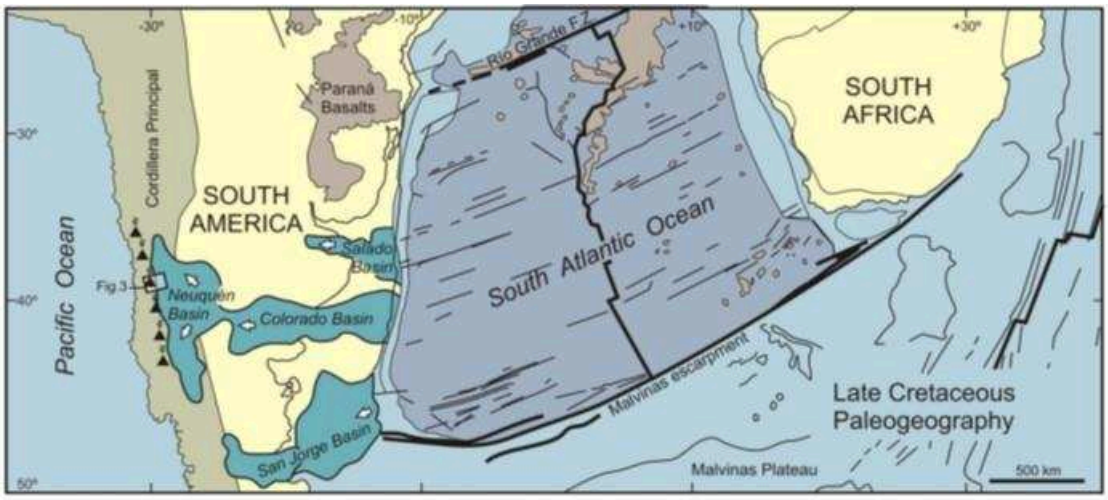

Figure 3.12: Paleogeographic reconstruction for the Late Cretaceous (from Aguirre-Urreta et al., 2011).

A major erosional event is detected on seismic data close of the top of the Cretaceous in the Colorado and Salado basins (the NTK marker, Near Top Cretaceous, in YPF internal reports), also recognized on the African conjugate margins (Jungslager, 1999; Broad et al., 2012).

3.2.3 Cenozoic evolution

The northern and southern bounding highs of the Colorado trough become flooded with the Campanian-Danian transgression and normal passive margin conditions on a broad open marine environment settled in the Colorado basin during the Cenozoic. In the exploration wells, on top of the Pedro Luro lies the Elvira Fm (Fig. 3.10), transgressive fine- to very fine-grained glauconitic sands of late Eocene to early Oligocene age (Lesta et al., 1978). On top of the later, lies the Barranca Final Fm (Fig. 3.10), corresponding to fine-grained clastics with few carbonate beds and tuff. Barranca Final Fm has been assigned to the late Oligocene to Miocene. Finally, coquinas, sands and shales of the Belén Fm deposited in the Colorado during the Pliocene (Gerster et al., 2011).

Renewed orogenic events in the Andes occurred during the Tertiary. Folguera et al. (2015) identified two main Neogene foreland basins in the central Pampas, that developed across several morphostructural blocks and basins. To the north of the Colorado river, a late Miocene depocenter records low-energy sedimentary environments in a gentle slope paleorelief, which suggest uniform accommodation in a distal foreland. Evidence point to the presence of a forebulge of a broken foreland that remained until these days (Fig. 3.13).

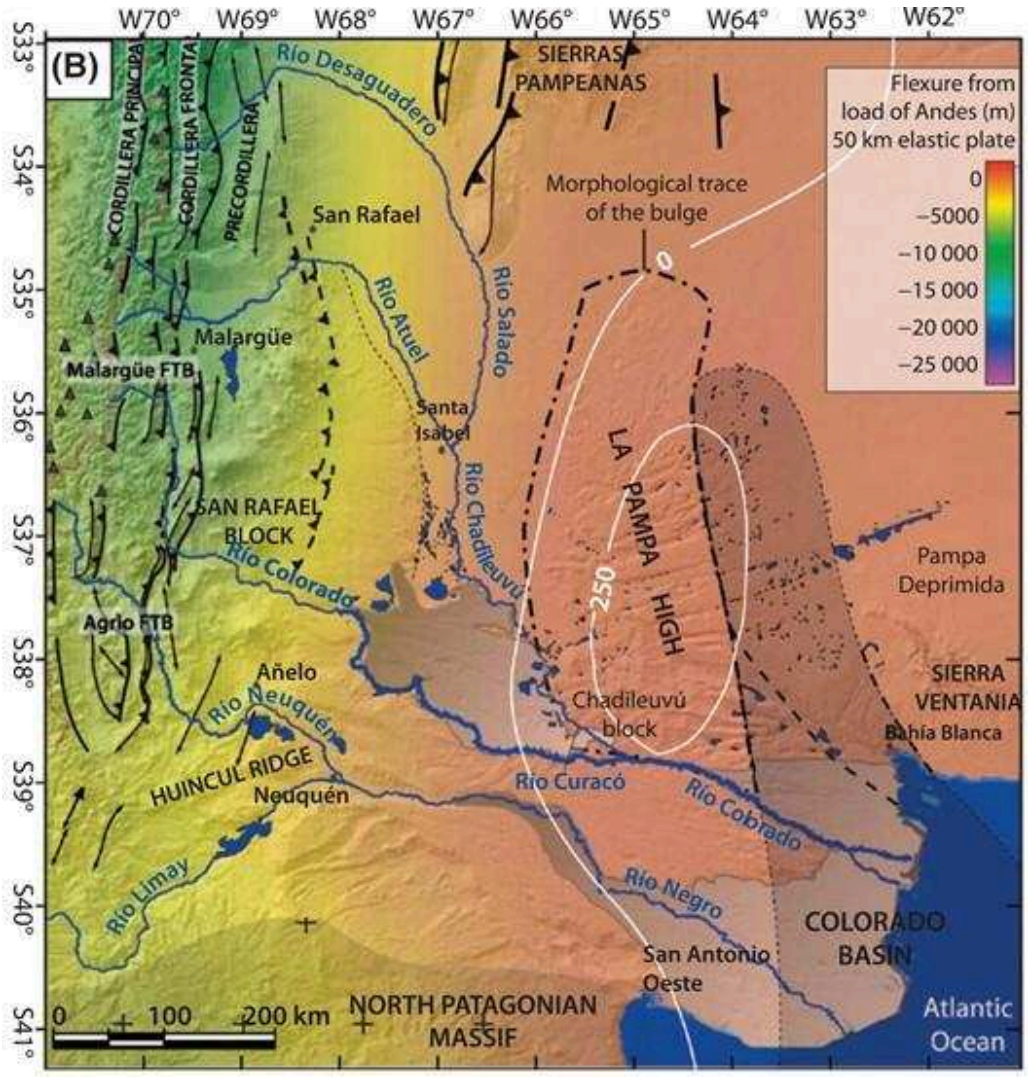

Figure 3.13: Main geomorphologic elements of the Central pampas west of the Colorado basin, showing supply areas and drainage systems to the Colorado river (from Nivière et al., 2013). Note the white contours in meters showing their interpreted Andean forebulge.

South of the Colorado river, the foreland basin units show a progradation from the orogenic front towards the east. The characteristics of the deposits and the thickness of the successions suggest that the foredeep depocenter might have been located to the west of 65°W (towards the Colorado basin), the forebulge was interpreted as the 'La Pampa High'

(approximately 65°W, Fig. 3.13) and the backbulge is located to the east, towards the Colorado basin. Folguera et al. (2015) propose for this area a model with discontinuous subsidence (active during orogenic periods). These authors hypothesize that the changes in accommodation space were controlled by tectonic dynamics, while the volume of sediment supply delivered to the basin was related to increased denudation of the source areas during pulses of uplift in the late Miocene, and likely regulated by climatic conditions during the latest Miocene – Pliocene.

3.3 Exploration History and Dataset

Hydrocarbon exploration in the Colorado basin is summarized in figure 3.14. YPF did pioneering studies with the drilling of Pedro Luro and Ombucta wells in 1945 and '46. Shell Production Company of Argentina followed in the onshore exploration through 1958 to '61, when they acquired 2684 km of 2D seismic and drilled a total of 7 wells (5 shallow and 2 "deep" tests). Concluding remarks of the onshore exploration and the results of the Shell campaign were summarized by (Kaasschieter, 1963, 1965). The first onshore wells detected the presence of a major Paleogene transgression, the Pedro Luro shales, overlying a sandy unit named the Colorado Fm assigned to the Late Cretaceous (see Fig. 3.10). The investigated play was the Colorado continental to littoral sandstones in fault-related structural closures. Some of the deepest wells also detected a sequence with more shaly intercalations, sometimes grey-colored, named the Fortín Fm, interpreted at that time as synrift.

Offshore exploration in the basin then start again at the end of the sixties, with Phillips drilling 9 wells back-to-back in shallow waters on the northern flank of the western depocenter (Fig. 3.14). They were chasing the stratigraphic pinch-out of the Colorado Fm on the basin margin, between the basement and the transgressive Pedro Luro shales. Hydrocarbon shows were detected only in the deepest well A.x-1 (Gebhard, 2005). During the same period, Hunt Oil Co. drilled 3 more wells in the central and southern part of WCol. 'La Ballena well (HUN.PC.LBa,x.1) was proposed to test the synrift section of the Western depocenter in a deeper position, while 'El Delfín' (HUN.PC.Ede.x-1) and 'El Pingüino' (HUN.Epi.x-1) wells targeted the top of the Colorado Fm.

The Central depocenter (CCol) was only explored since 1977. YPF drilled the Puelche (YPF.PC.Pu.x-1) and Ranquel (YPF.PC.Ra.x-1) wells back-to-back in 1977 (Fig. 3.14) to test seismic anomalies in the early Tertiary, that were interpreted at the time as possible carbonate buildups and turned out to be volcanic rocks forming a large volcanic field on the southern

flank of the basin. Below the Mesozoic section, these wells confirmed the presence of Paleozoic sediments further east from the well-known series of the Ventania system and the Claromecó basin (Lesta et al., 1978).

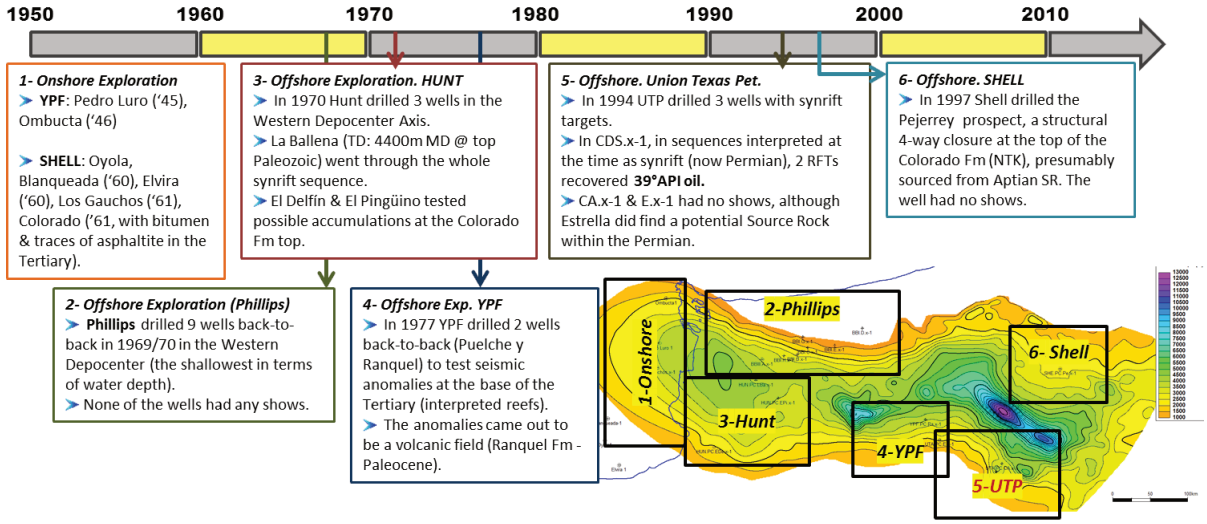

Figure 3.14: Colorado basin exploration summary timeline.

With negative results so far, exploration resumed in the 1990's. In 1994, Union Texas drilled three wells with targets in what was interpreted as synrift of the Central and Eastern depocenters (Fig. 3.14). The 'Cruz del Sur' well (UTA.PC.CDS.x-1) was the first well to be drilled and found oil in good quality reservoirs interpreted by the operator as synrift series. These sequences containing the reservoirs where interpreted by Pángaro et al. (2016) as Paleozoic prerift, but following the recent review of Ottone and Angelozzi (2015) that report Classopolis sp. (palynoelements of Mesozoic age) from side wall cores, the original interpretation of Union Texas regarding its Mesozoic age is retained. Two RFT (Repeat Formation Tester, Schlumberger) recovered oil from the rock formation. One RFT at 3487.45 m MD recovered 2 gallons of fluid with 5% oil cut. The other RFT tested 3 gallons with 10% oil cut of light oil (39° API; Fryklund et al., 1996; Gebhard, 2005). The 'Corona Austral' (UTA.PC.CA.x-1) and 'Estrella' (UTA.PC.E.x-1) wells also investigated the synrift section and reached the prerift, with no hydrocarbon shows. However, 'Estrella 'drilled a potential source rock in the Permian prerift section.

In 1997 Shell drilled the Pejerrey well (SHE.PC.Pe.x-1, Fig. 3.15), on the northern flank of the Eastern depocenter (ECol). The target reservoir was the Colorado Fm, at a four-way dip closure detected with 2D seismic data. The expected source rocks were Aptian marine shales of restricted shelf environment, deposited during the early sag phase along the basin axis.

Consequently, lateral migration from the source rock depocenter to the prospect location (further north) was necessary to charge the trap. The well presented no hydrocarbon shows and was plugged and abandoned.

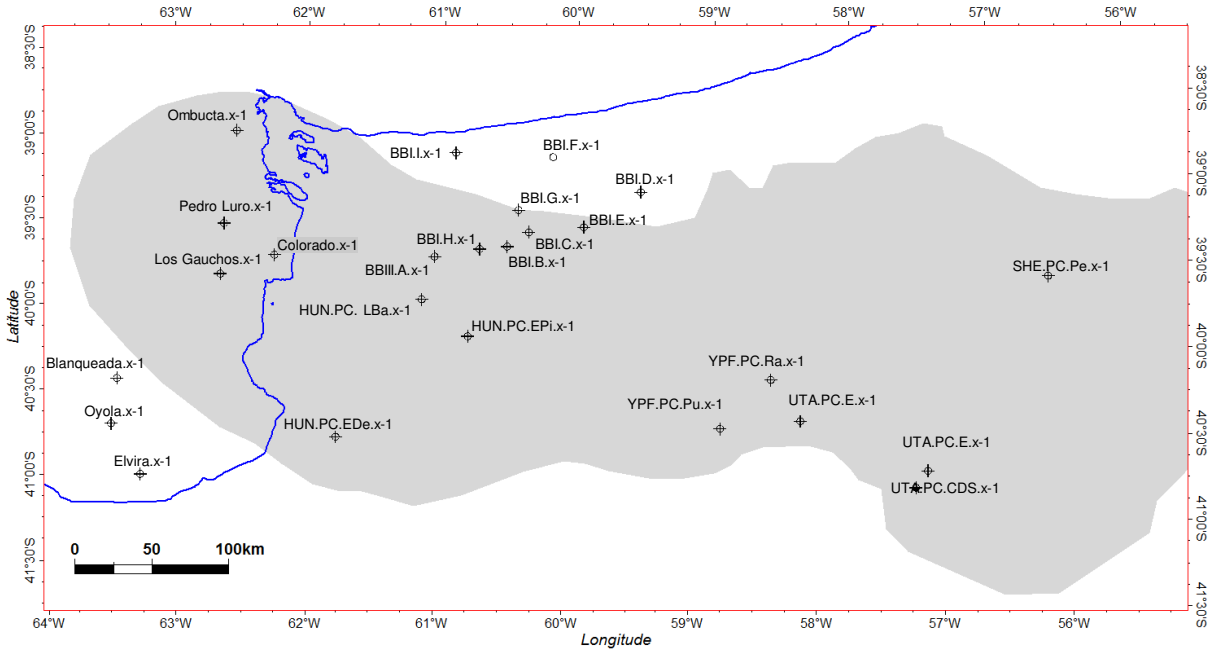

Figure 3.15: Map of the exploration wells used in the present study.

Between 1999 and 2001, YPF acquired 2D seismic data and later on in 2004-2005 a 3D survey in the shelf edge location. Also the BGR (German Bureau of Geology) acquired 2D seismic together with gravimetric and magnetometric data in 1998 and 2004 (Figueroa et al., 2005). COPLA (Argentinean Commission for the external limit of the Argentinean continental shelf) acquired as well 2D seismic, gravimetric and magnetometric data in 2001-2002 to better establish the external limit of the Argentinean shelf, but these latter data were not available for this study.

A multiclient 2D regional seismic survey was then acquired by GXT (ION Geoventures) in agreement with the Argentinean state-owned ENARSA. These 2D BasinSpan lines record as much as 16 seconds and illuminate the whole lithosphere including the Moho. A PSTM (Pre-Stack Time Migration) process result of this survey was available for this study.

Well data from the 25 exploration wells of the Colorado basin (Fig. 3.15) with different sets of well data were also available for this study. This study is supported by the seismic interpretation of approximately 300,000 km of 2D seismic (Fig. 3.16) of several vintages and varied seismic quality. The old seismic data acquired during the early stages of basin

exploration (before the 1990's) is usually or rather bad quality, although interpretation of major surfaces is possible. The newer seismic surveys (of acceptable seismic quality) were acquired since the 1990's on the eastern part of the shelf and slope.

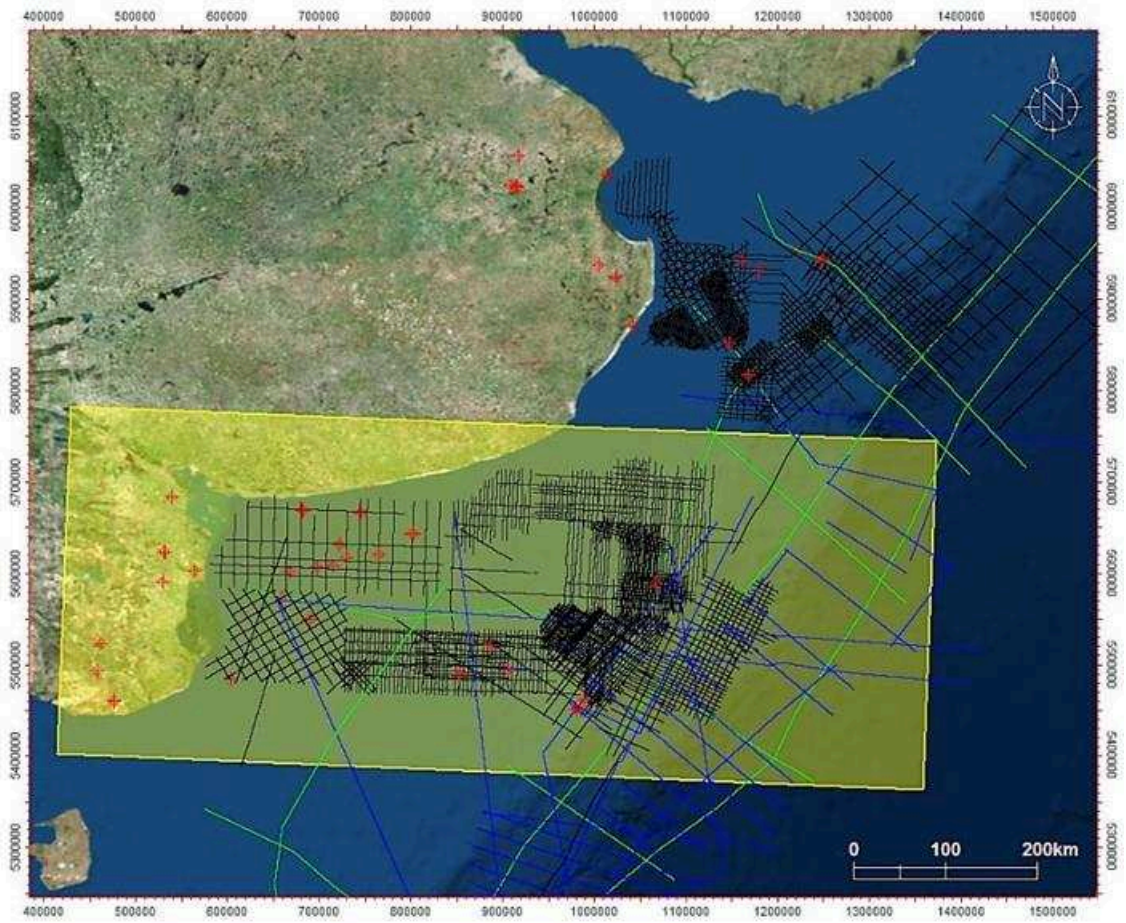

Figure 3.16: Map of the Colorado, Salado and Punta del Este basins with the 2D seismic surveys and exploration wells used un the present study. Study area depicted in yellow is for the Colorado Basin.

3.4 Methodology

Seismic stratigraphic and structural interpretation was carried out using Petrel software (Schlumberger). Seismic and well data were gathered in an integrated interpretation project. More than 300,000 km of 2D seismic were interpreted and the information was integrated to generate time structure maps for the main horizons. We used a gridding spacing of 1 km for the regional maps, and 300 m to 500 m for the detailed depocenters maps. Faults were interpreted in the seismic lines by interpretation sticks and then grouped to create 3D faults.

The main unconformities were detected and interpreted on 2D seismic as horizons. In this way, the sea bottom, near top Cretaceous, breakup unconformity, top synrift, rift onset unconformity (top prerift) were interpreted first on the regional span lines, and then extended throughout the dataset. See Table 3.1 and Fig. 3.17 for a detail of the horizons interpreted in this study. Further horizons within the post-breakup succession were interpreted and are introduced in Chapter 7. The basin span lines with recording times of up to 16 seconds, and some of the BGR lines, allowed the seismic interpretation of the seismic Moho and the base of the SDR wedges in the study area.

Horizon	Name	Age
000_sea_bottom	Sea bottom	~0 Ma
NTK	Near Top Cretaceous	~61 Ma
100_intracret2	Intra-Cretaceous SB	~100 Ma?
112_Top Aptian	Top Aptian (source rock)	~112 Ma?
125_BUU	Breakup unconformity	~125 Ma?
135_base SDR	Base of SDRs	~135 Ma?
Top SR 3b	Top synrift 3	~Late Jurassic?
Top SR 3a	Intra synrift 3 unc.	~Late Jurassic?
Top SR 2b	Top synrift 2	~Mid Jurassic?
Top SR 2a	Intra synrift 2 unc.	~Mid Jurassic?
Top SR 1	Top synrift 1	~Triassic?
250_TopPreRift	ROU	~Top Paleozoic
Moho	Seismic Moho	

Table 3.1: Main seismic horizons interpreted for the Colorado basin

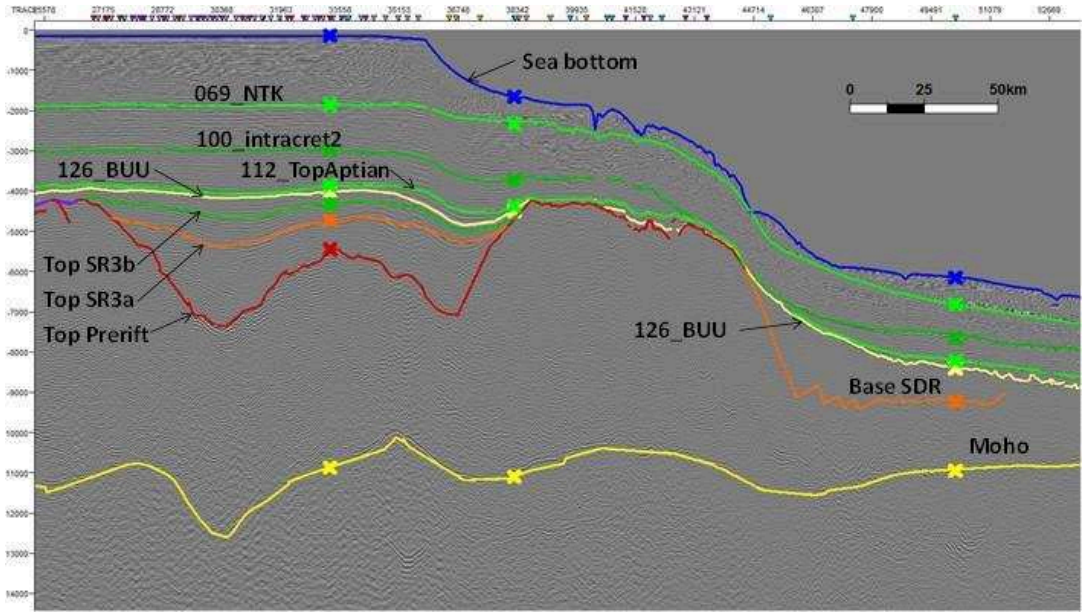

Figure 3.17: Example of seismic line (TWT) across the Colorado basin (ECol and slope), showing some of the main seismic horizons interpreted.

Wells were tied to seismic using VSP (Vertical Seismic Profile, or check-shots) data when available. For the other wells, we used sonic logs to compute interval velocities and convert depth to time, or used average velocities from neighboring wells. A 3D regional velocity model was built from 7 wells. Figure 3.18 shows the depth (Z) versus Average velocity for the 7 wells used to build the velocity model. TDR (Time-Depth Ratios) were obtained and then gridded in the study area.

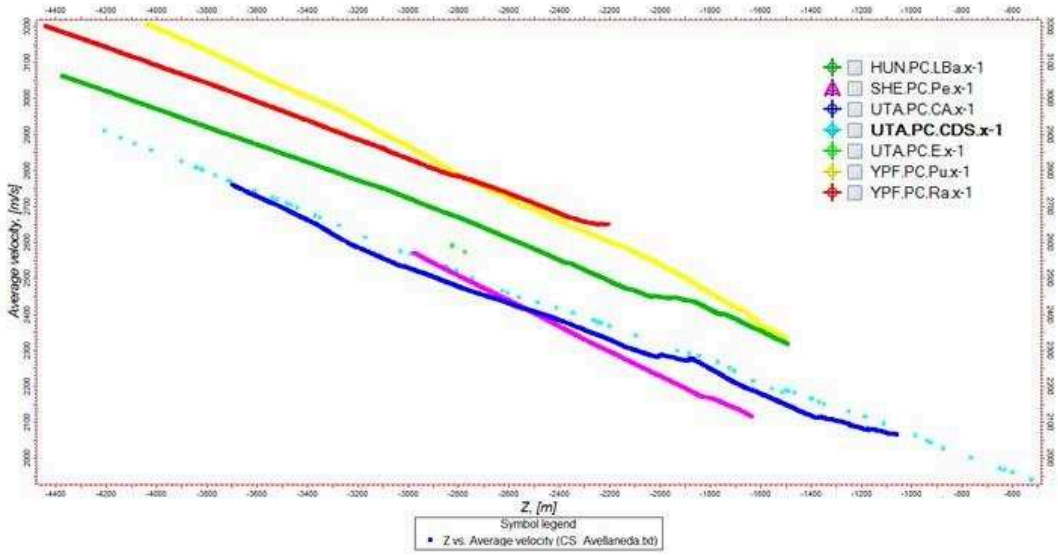

Figure 3.18: Time-Depth Ratios (TDR) for the wells used to build the velocity model.

A five-layer velocity model was created to convert time to depth maps. The five main horizons used to prepare the 3D velocity model were: sea bottom, NTK, BU, Top prerift and Moho.

- Layer 1 is in between the reference datum (sea level) and the sea bottom. It represents water depth (with sea water constant velocity of 1500 m/s).
- Layer 2 is in between the sea bottom and the top of the Cretaceous (horizon NTK). It corresponds to the Cenozoic interval.
- Layer 3 is in between NTK and the breakup unconformity (horizon BU). It corresponds to the Cretaceous drift unit.
- Layer 4 corresponds to the Synrift, between the Top prerift and the BU horizons.
- Finally Layer 5 corresponds to the Paleozoic Prerift + Crust + SDR, it goes between the Top Prerift and the interpreted Moho. A constant interval velocity of 6,000 m/s was assigned to this layer to build the Velocity Model.

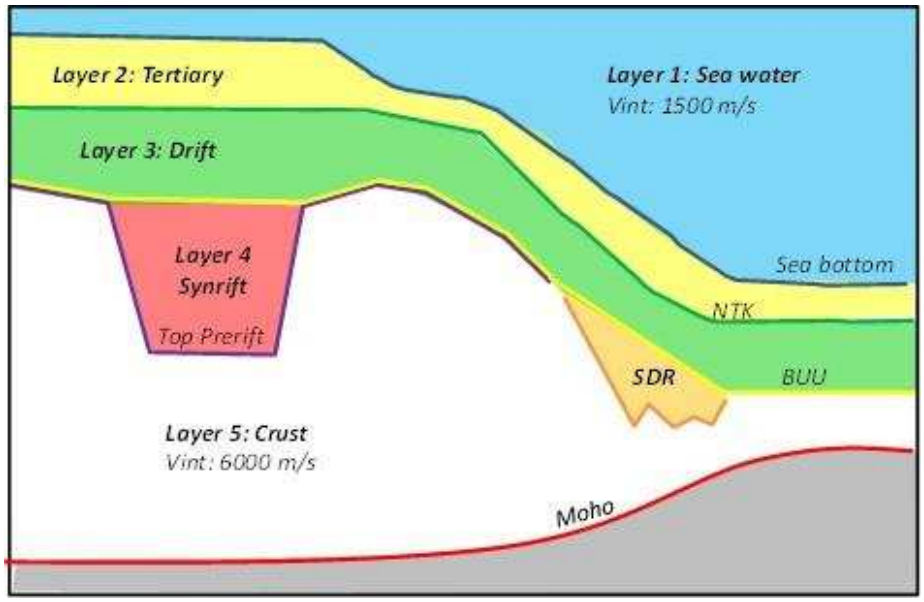

Figure 3.19: Sketch showing the layers used to build the velocity model.

As pointed out above, velocities for Layers 1 and 5 were constant. In order to grid velocity maps to reflect changes in interval velocities across the basin, a first automated velocity gridding was carried out with Petrel, extracting interval velocities from the well TDRs (Time/Depth Ratios). Even if there are only seven wells available, they are rather well-distributed in the study area, which allowed obtaining rather simple initial velocity grids. Velocity grids were then adjusted using layer time thickness maps to show higher interval

velocities in the areas where the sedimentary packages are thicker. The calibration of the interval velocity grids was carried out from top to bottom, adjusting at each time the velocities to match the obtained depth maps with the well tops. The interval velocity maps obtained through this method, and that were used in the velocity model in order to accomplish time-to-depth conversion, are shown in figures 3.20, 3.21 and 3.22.

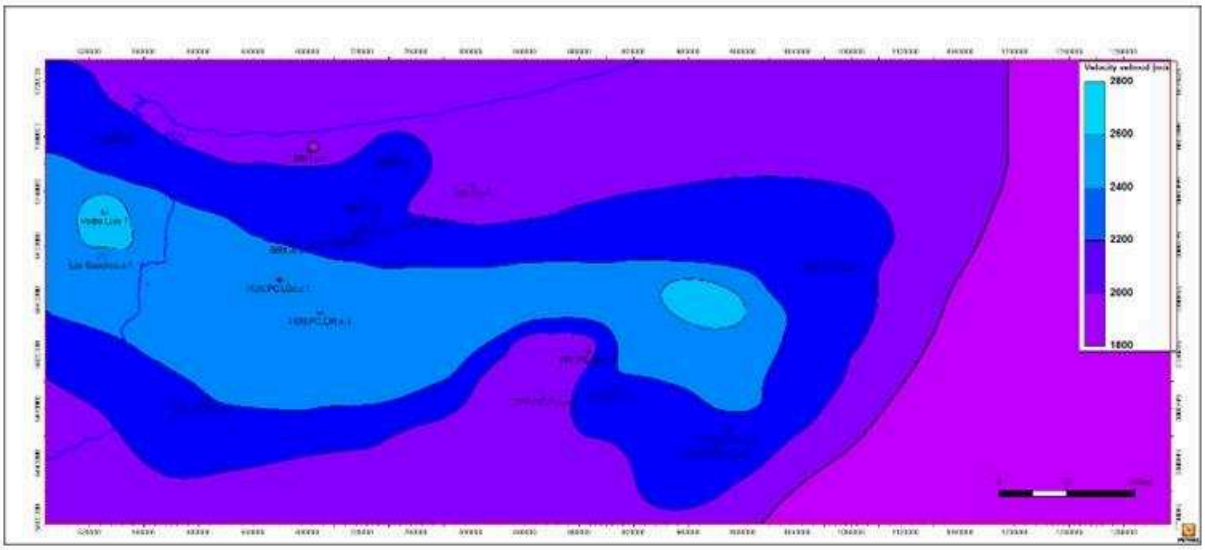

Figure 3.20: Layer 2 Interval Velocity: Sea floor – NTK. Note higher velocities in the trough axis.

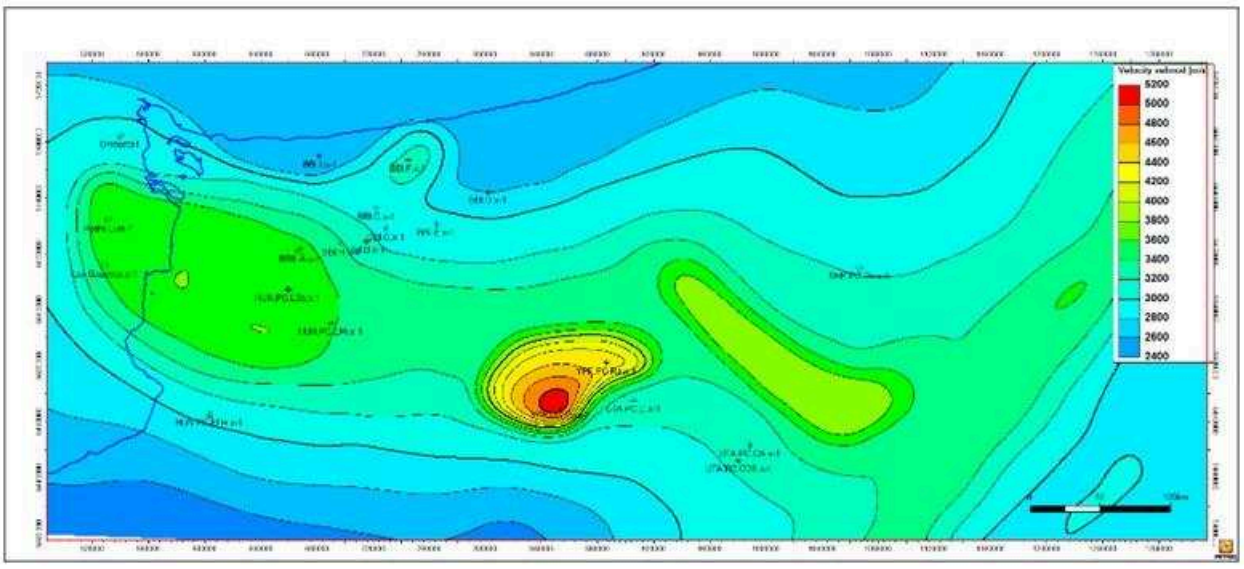

Figure 3.21: Layer 3 Interval Velocity: NTK to BUU. Note higher interval velocities in the depocenters, and a strong anomaly in the central southern sector, corresponding to a Late Cretaceous volcanic field.

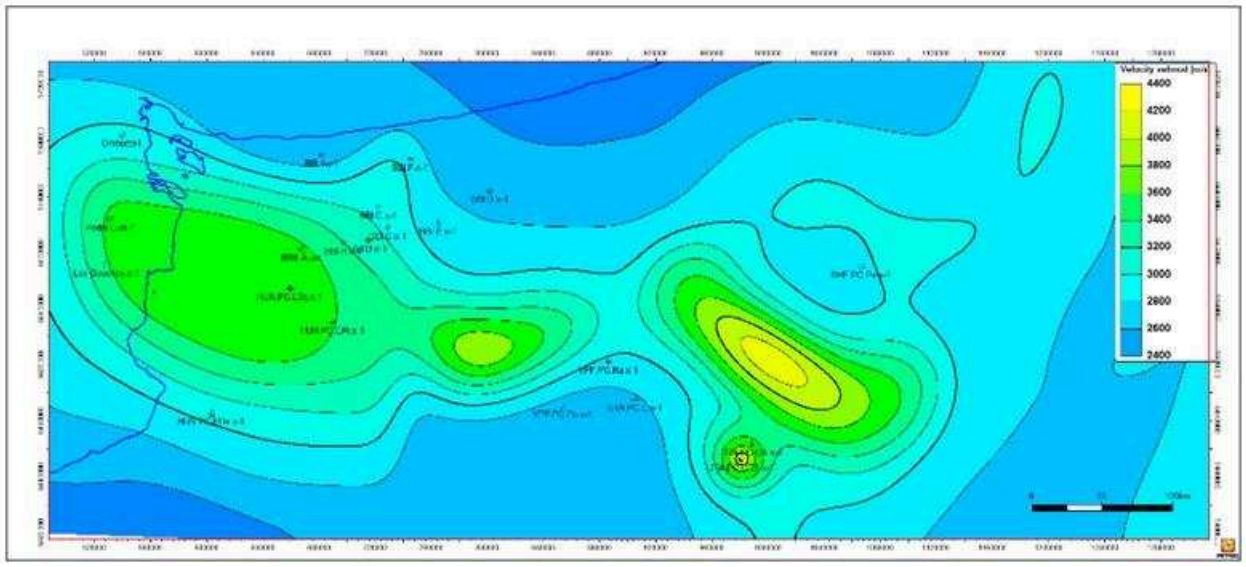

Figure 3.22: Layer 4 Interval Velocity: BUU to Top prerift. This map corresponds to the velocities of the synrift sequences. Note higher average velocities in the depocenters, where units are thicker and bases reach deeper levels.

Once the model was built, all time horizons (not only the ones used to build the velocity model) can be converted to depth using the 3D velocity model. Depth grids obtained with this velocity model were then used to create isopach maps (thickness) of each unit.

3.5 Results

The results are presented starting with generalities at a large scale on the Colorado basin and then focusing with more detail on the different depocenters.

3.5.1 Sedimentary envelopes

The main unit tops, used to build the velocity model, are presented in this section together with isopach (thickness) maps.

Figure 3.23 shows the bathymetry computed from seismic interpretation. A large shelf (approximately 300 km wide) is illustrated, with all exploration wells drilled in shallow waters (<100 m). To the east the shelf break is oriented NNE. The slope can be divided into three sections (see the spacing in contour lines). Between 200 and 1,000 m water depth, a first slope is detected with a 4% inclination. Then between 1,000 and 2,000 m depth there is a 'flat' with 1.4% slope and finally between 2,000 and 4,000 m there is a new increase in slope with a 5%

inclination, leading to the basin floor below the 2,000 m water depth. These two slope steps represent the Miocene and the fossilized Cretaceous shelf (further seaward).

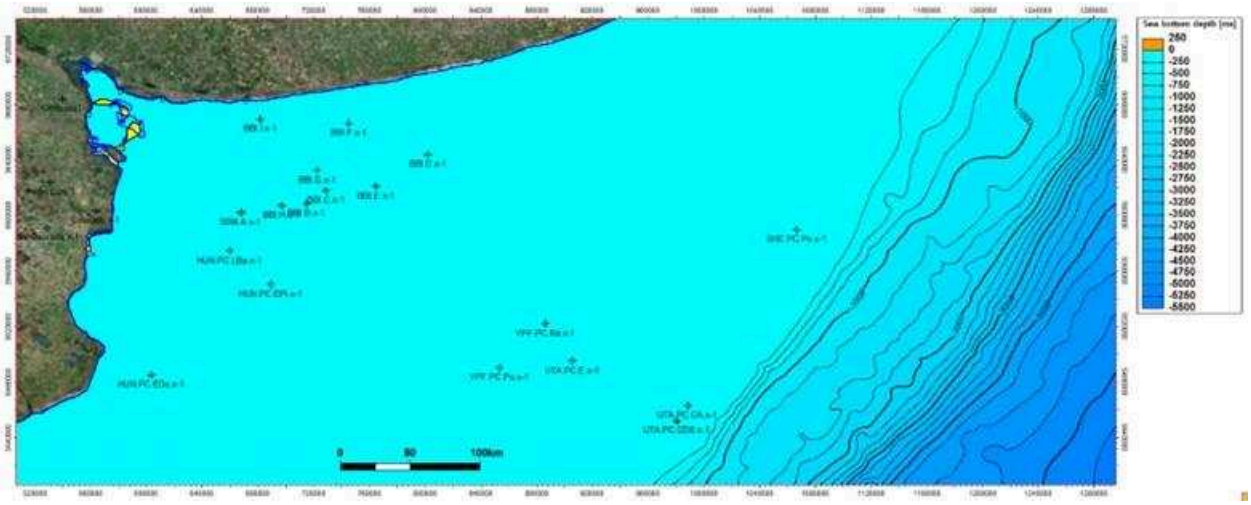

Figure 3.23: Bathymetry of the study area as derived from seismic interpretation (sea bottom horizon, depth in meters). Contour interval (C.I.): 250 m.

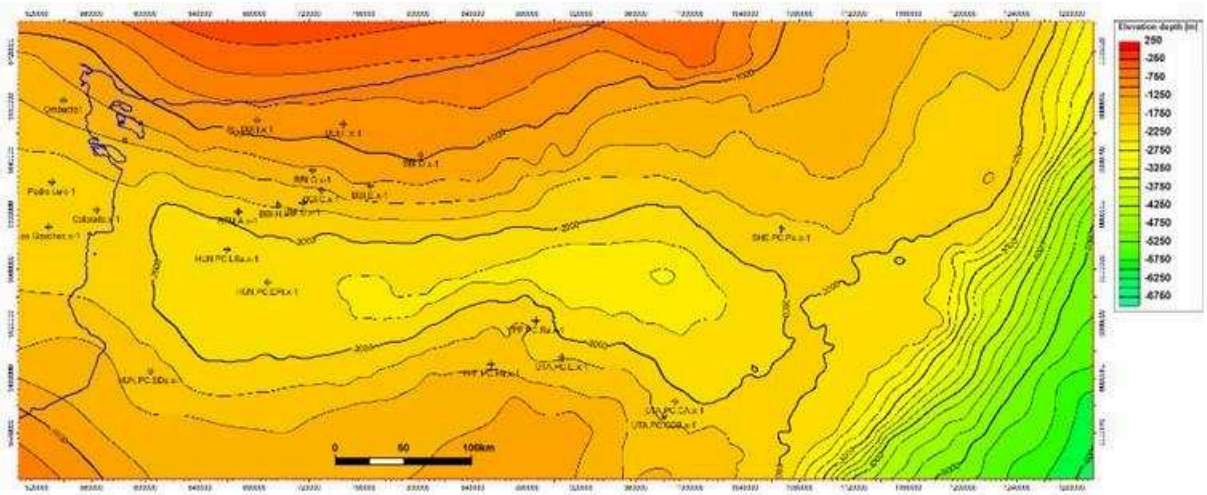

Figure 3.24: Depth structural map of the NTK horizon (near top Cretaceous). C.I.: 250 m

Figure 3.24 shows the structural map corresponding to the NTK horizon (near top Cretaceous). The Colorado basin depocenter is illustrated with depths higher than 2000m. The isopach map between the Sea Bottom and NTK horizons, corresponding to the total Cenozoic thickness, is presented in Fig. 3.25. The Cenozoic depocenter extends E-W along the Colorado basin axis. There is a sharp N30°-directed border that corresponds to the shelf break (see Fig. 3.23). There is less Cenozoic thickness on the slope and it is even completely eroded at some location at the base of the present-day slope (see the red spots in Fig. 3.25).

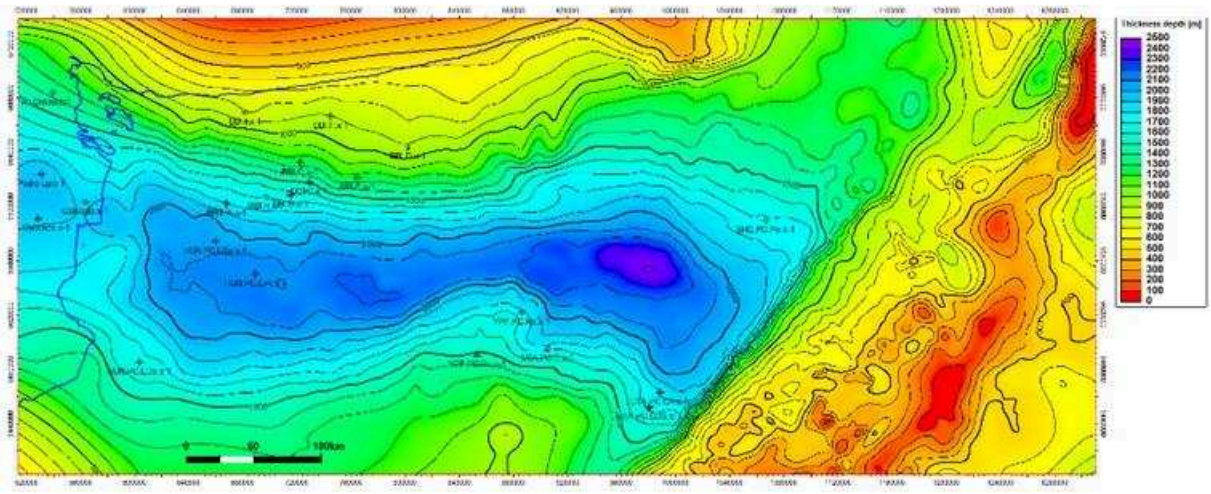

Figure 3.25: Cenozoic Isopach (thickness) Map, computed between sea bottom and NTK. C.I.: 100 m

Figure 3.26 presents a structural map for the breakup unconformity (BU horizon). The three main depocenters of the Colorado Basin can now be identified, the most prominent being the Eastern Colorado (ECol). The BUU horizon is a complex unconformity that corresponds to the exposed surface at the time of the first normal oceanic crust accretion followed by marine transgression. It can be correlated from the top of the oceanic crust, to the top of the SDR wedges, and then landward, the BUU passes to the top of the prerift (basement) or top synrift (in the depocenters). The isopach map shown on Fig. 3.27 corresponds to the thickness of the first drift sequence that started depositing from the breakup and lasted until the NTK unconformity. In the isopach map, the Cretaceous Drift deposition is restricted to the Colorado trough. This meaning that sedimentation took place along the Colorado basin axis and the northern and southern margins, Tandilia and Rawson highs respectively, were subaerially exposed. The highs were completely flooded by the latest Cretaceous, during the Campanian-Maastrichtian-Danian transgression, and since then sedimentation took place along and across the whole Argentinean shelf (Colorado, Salado, Rawson, etc.).

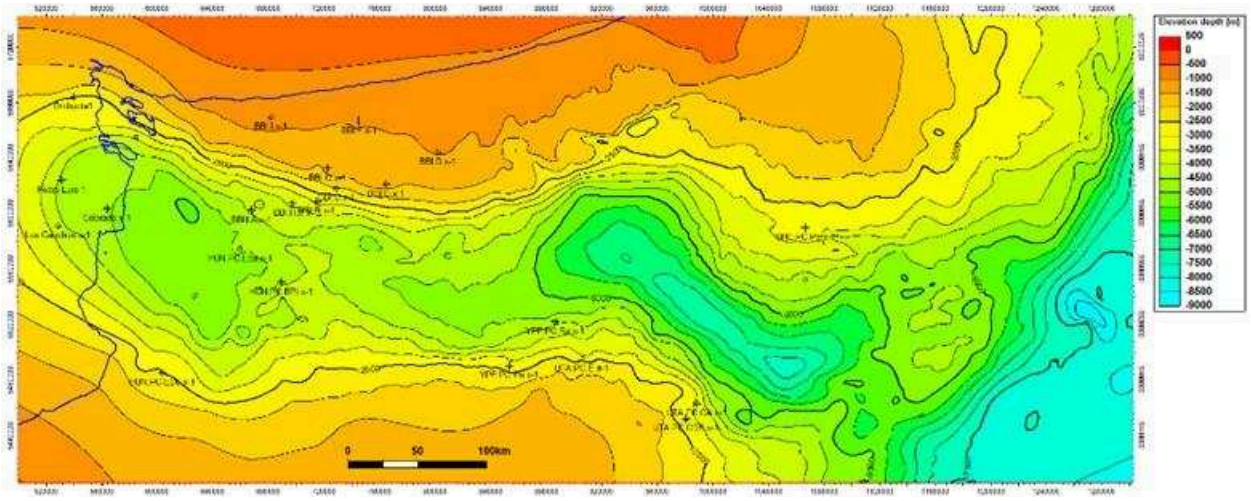

Figure 3.26: Depth structural map of the BUU horizon (breakup unconformity). C.I.: 500 m

The thickness of the Cretaceous Drift megasequence reaches 3,000 m in Western Colorado (WCol) and more than 5,000 m in Eastern Colorado (ECol). In Central Colorado (CCol), the depocenter is less defined, but thickness reaches at least 2,500 m (Fig. 3.27).

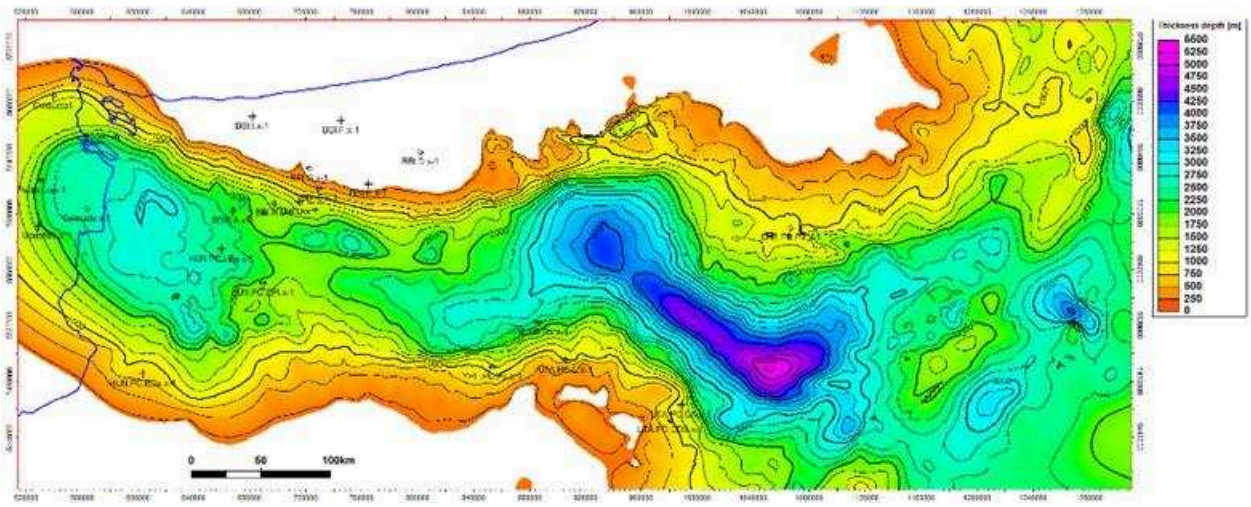

Figure 3.27: Cretaceous Drift Thickness Map, computed between NTK and BUU. C.I.: 250 m

Figure 3.28 is a depth structure map of the Top Prerift (being basement or Paleozoic prerift accordingly). Oceanward, the Top Prerift has been interpreted at the top basement on continental crust. In the COT transition, this horizon follow the Top SDRs, thus the BU. The three Colorado basin depocenters can be identified. ECol, NW-oriented, is the deepest depocenter exceeding 12 km of total depth. ECol is controlled by a master fault dipping to the NE. CCol is oriented E-W, controlled by a master fault dipping to the south, and exceeds 7,500 m of total depth. WCol is largely oriented NNW, it does not seem to be bounded by faults, it reaches 5,000 m depth. It is worth to note that seismic quality in the WCol area is rather bad,

as seismic surveys date from the 1960's. There are several smaller fault-controlled depocenters in the central part of the basin, associated with NW-directed faults, and along the margins, especially the northern one. A detailed description of the main depocenters, together with a seismic stratigraphic interpretation will be presented in the following sections.

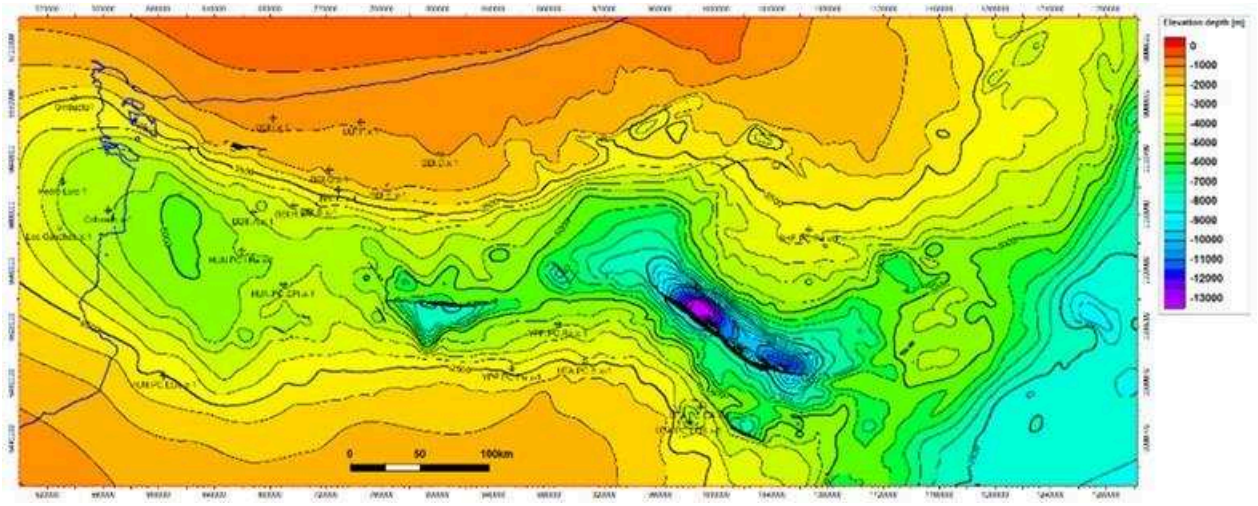

Figure 3.28: Depth structural map of the Top Prerift horizon (Top prerift: ROU). C.I.: 500 m.

The isopach map for the synrift megasequence (pre-breakup ~126 Ma) is presented in figure 3.29. This map was prepared from seismic interpretation (available only offshore, see Fig. 3.16) so it may not represent well the synrift present in the onshore part of the basin. Nevertheless, the other major and minor depocenters are depicted.

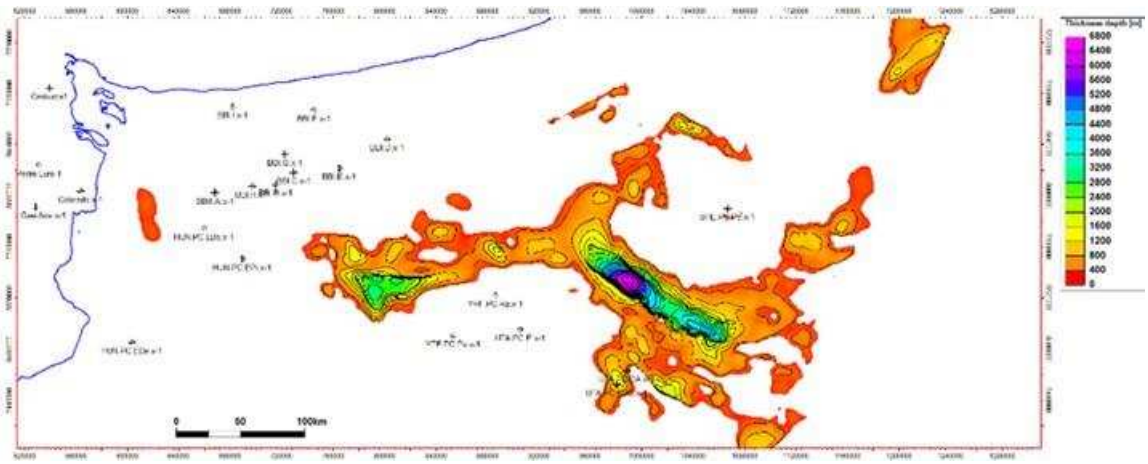

Figure 3.29: Total Synrift thickness Map, between BUU and Top Prerift. CI: 400 m.

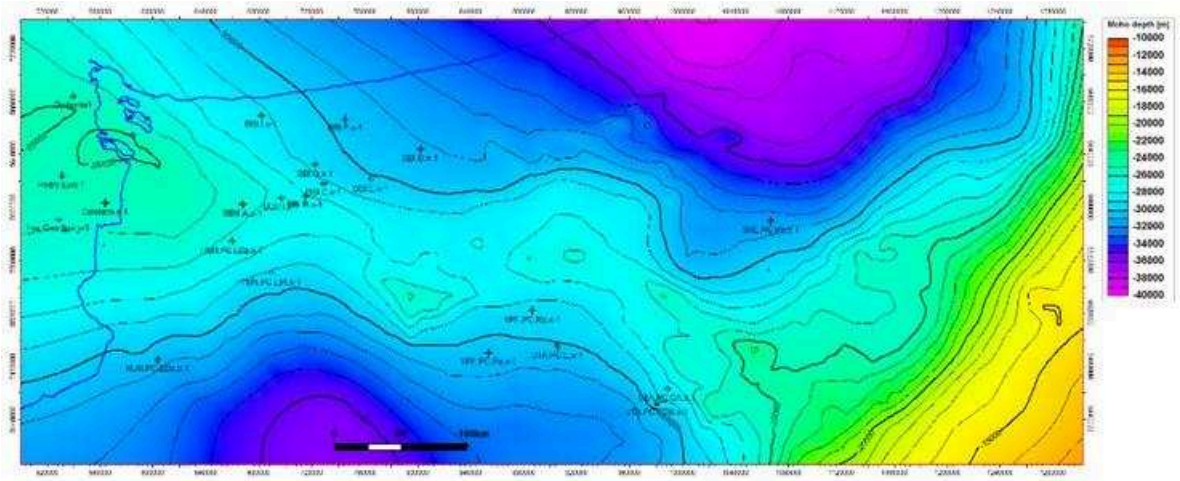

Figure 3.30: Depth structural map of the seismic Moho. C.I.: 1000 m

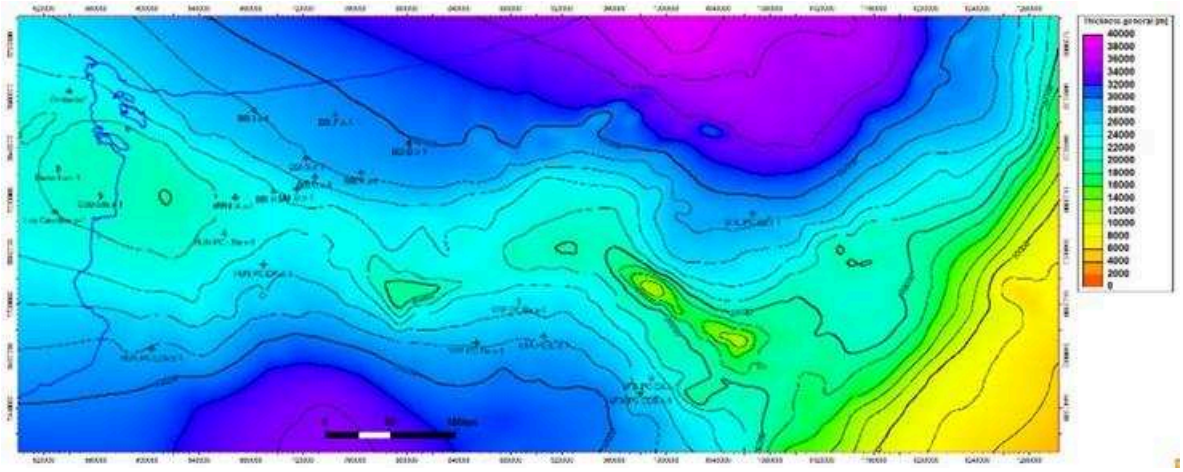

Figure 3.31: Crustal thickness map (between Top Prerift and seismic Moho). C.I.: 2,000 m

Figure 3.30 depicts the depth structure of the Moho (with increasing uncertainty to the west). The eastern area is better constrained with deep and recent seismic data. The crustal isopach map presented in Fig. 3.31 shows crustal thinning especially for the Central and Eastern depocenters (the western depocenter is not covered with deep seismic and interpretations should be disregarded).

3.5.2 Structural Framework

Besides the three main depocenters already described in the introduction, another main tectonic feature observed in the Colorado basin is what has been called the 'external high' (Figueroa et al., 2005; Gerster et al., 2011), a crustal block that separates (as a threshold) the ECol depocenter from the inner SDR wedges. The external high is a block elongated in the ENE direction that hosts several 4-way closures at the basement level.

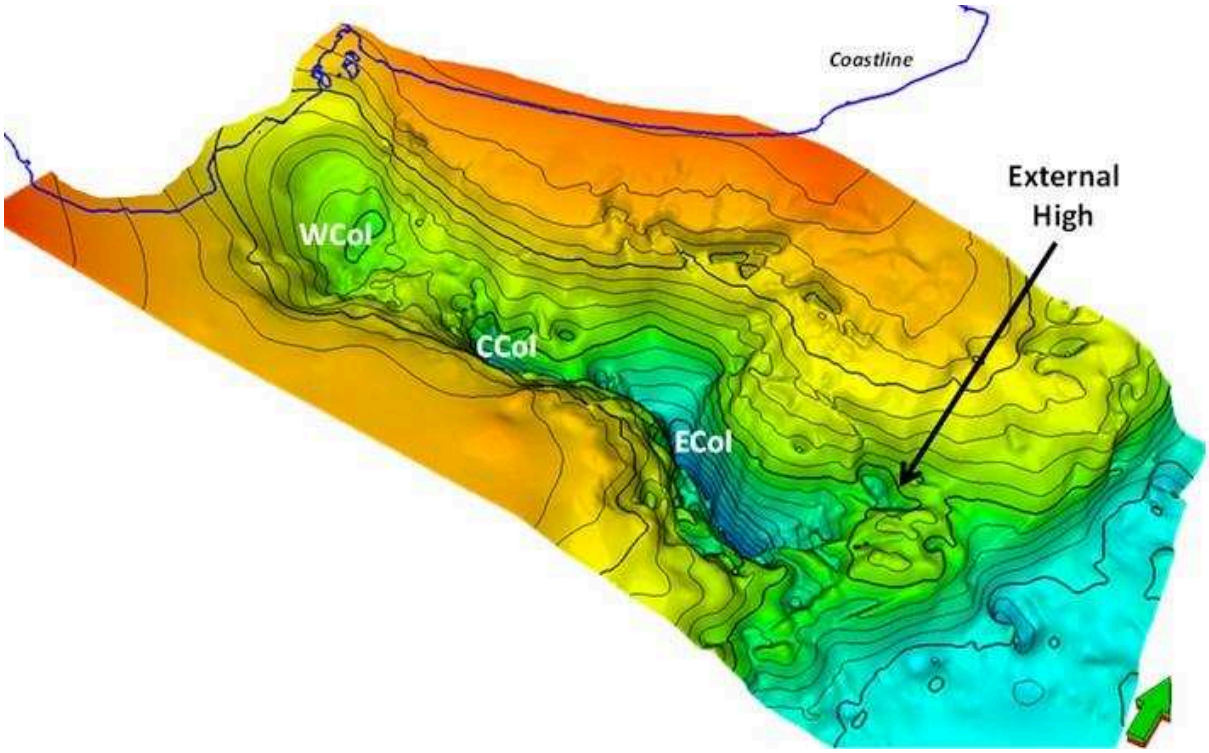

Figure 3.32: 3D view of the Top Prerift horizon in the Colorado basin. The three main depocenters and the External high block are depicted.

In order to assess the structural framework of the basin, figure 46 is introduced: a depth structure map for the Top Prerift level with all faults affecting prerift. The difference between figure 3.33 and the map presented in figure 3.28, is that Fig. 3.28 shows only the faults that displace the top of the prerift, but Fig. 3.33 shows all faults, not only those affecting the top of the prerift but also older faults, that were 'fossilized' and subject of erosion before the onset of sedimentation.

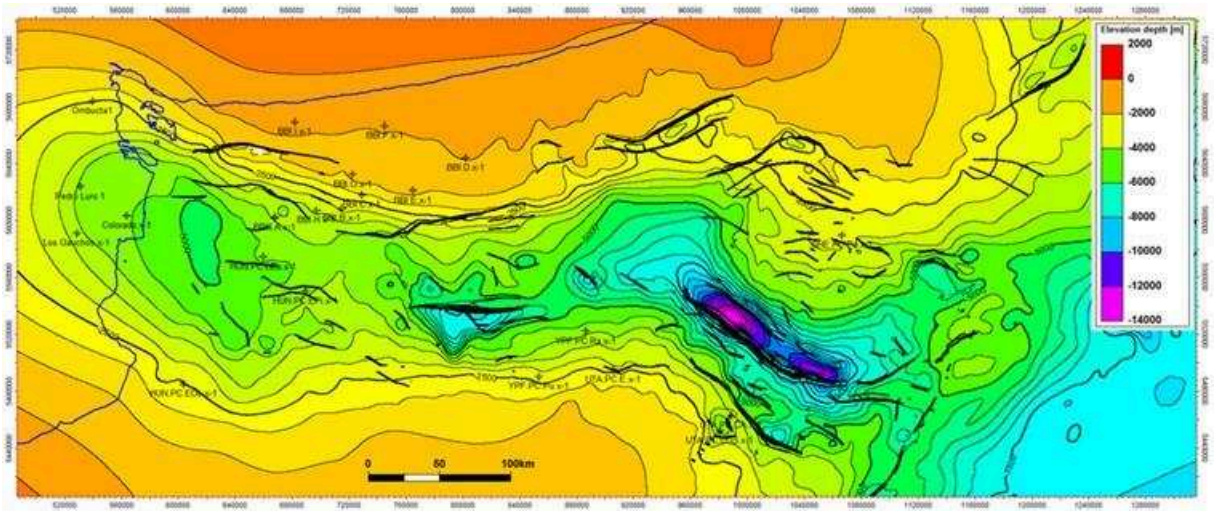

Figure 3.33: Depth structure map of the Top Prerift, with all faults affecting the prerift unit.

A closer analysis of the fault pattern allowed the classification of faults into several fault groups according to their orientation, cross-cutting relationship, and their distribution in the basin. This analysis is presented in Chapter 4, together with a discussion on rifting evolution.

A brief description of each depocenter is presented hereafter.

3.5.2.1 Eastern Colorado Depocenter

The Eastern Colorado depocenter (ECol) is a half-graben striking SE-NW. It is the deepest of the three main depocenters of the Colorado basin, reaching more than 12 km of total sedimentary thickness (Fig. 3.3). It is bounded on the SW, by a NE-dipping normal fault that extends more than 130 km in the strike direction (fECol, Fig. 3.34).

ECol is depocenter formed by two main fault-bounded depocenters separated by a saddle. The NW depocenter is the deepest, reaching a total depth to the Top Prerift of more than 12,000 m. The NW depocenter is bounded to the SW by fECol, and to the NE by an antithetic fault here named a1 (Fig. 3.34 and 3.35a). This depozone extends 60 km in the NW-SE direction and 20 km in the SW-NE direction. Two main synrift units were interpreted: Top Synrift (SR) and a Top Late Synrift (LSR, Fig. 3.35a). Top SR (interpreted in orange in Fig. 3.35) is an unconformity bounding the synrift unit. Top LSR (dark green in Fig. 3.35) is another unconformity at the top of the late synrift unit, still displaying some active fault controls.

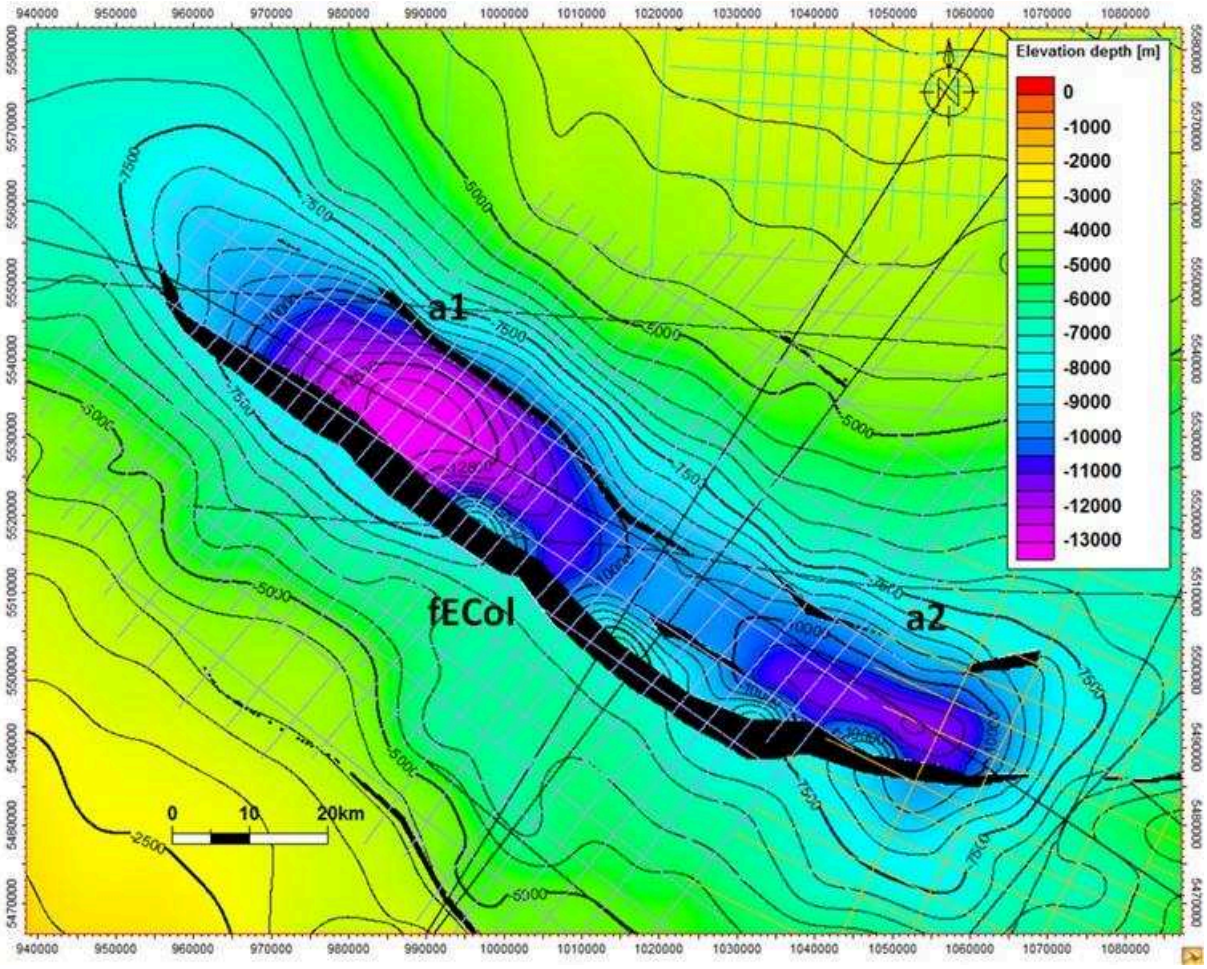

Figure 3.34: Depth structural map for the Top Prerift in the ECol depocenter. Note the two depocenters separated by a saddle structure

Above Top LSR, a thermal sag phase was identified, topped by the BUU (breakup unconformity). The BUU horizon was interpreted from the top of the SDRs on the COT, passing by the external high and finally into the ECol depocenter (see figure 3.17). The preservation of a sag phase bellow the BU indicates that the rifting phase responsible for the formation of ECol has already stopped. A previous rifting stage is then interpreted for the creation of ECol, since in a normal rift-to-drift transition, the BU marks the synrift-postrift unconformity.

The SE depocenter is located closer to the southeastern tip of fECol, where it turns toward and strikes WNW-ESE. It reaches a maximum depth of 11,500 m and measures 35 km long by 15 km wide. This depocenter is also bounded by an antithetic fault (a2 in Fig. 3.35c), which gives it a more graben-like geometry.

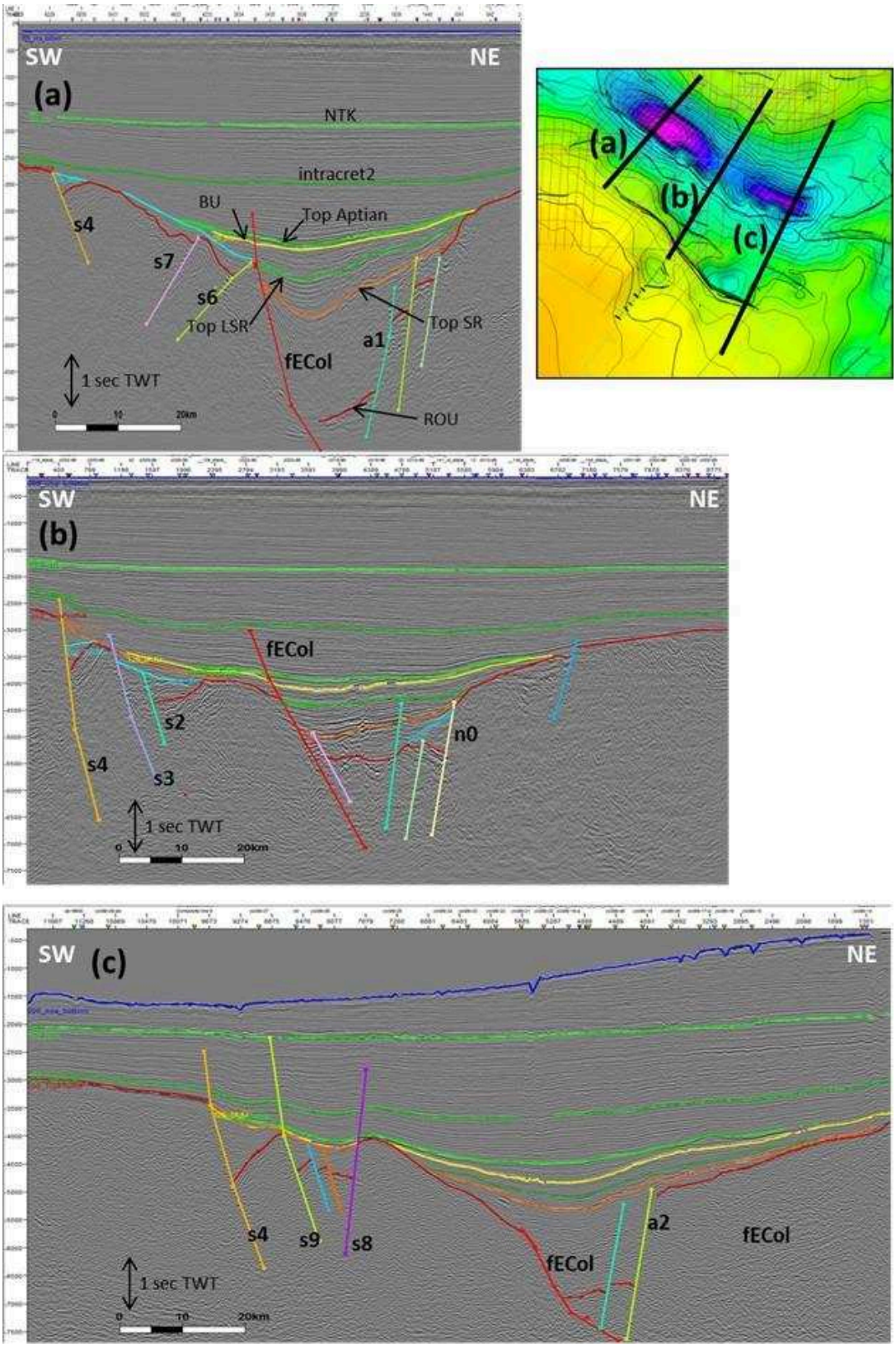

Figure 3.35: Seismic sections across the ECol depocenter (PSTM, TWT): a) Line c023-96 across the NW depocenter; b) C047-96 across the central saddle; c) Line ycc99-09ab across the SE depocenter of ECol.

The saddle separating both depocenters, is a relative high oriented along the fECol fault. A seismic section across this area is shown in figures 3.35b. At this position, ECol is a half-graben, bounded by fECol on the SW, and the antithetic fault here is n0, which bounds an older synrift wedge. A seismic line along the strike of ECol is presented in Fig. 4.6 (Chapter 4). Figure 3.36 shows a thickness map for units SR3a + SR3b. The two depocenters are clearly identified, separated by the saddle.

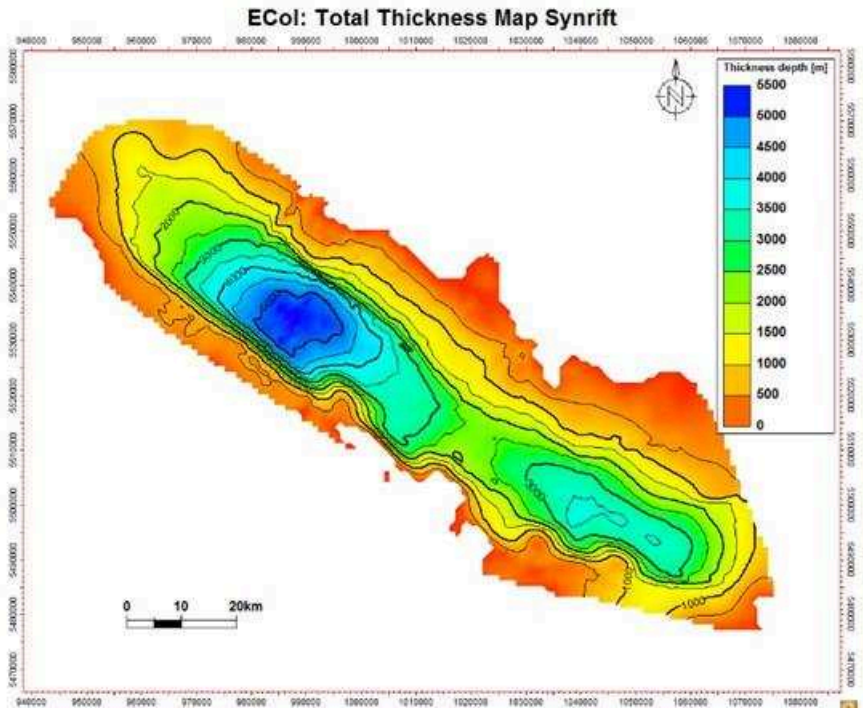

Figure 3.36: Thickness map of the Synrift + Late Synrift units in the ECol depocenter.

A sketch depicting interpreted evolution of the ECol depocenter is presented in figure 3.37. At an Early Rift stage (Fig. 55A), two independent grabens are form (NW and SE depozones respectively). With the rifting progress, faults $fECol_1$ and $fECol_2$ become linked a single larger depocenter develops (ECol, Fig. 55B). At the former relay ramp region between both depozones, the saddle structure is established, with subsidence controlled by the fECol fault to the SW. For some reason antithetic faults a1 and a2 remained disconnected.

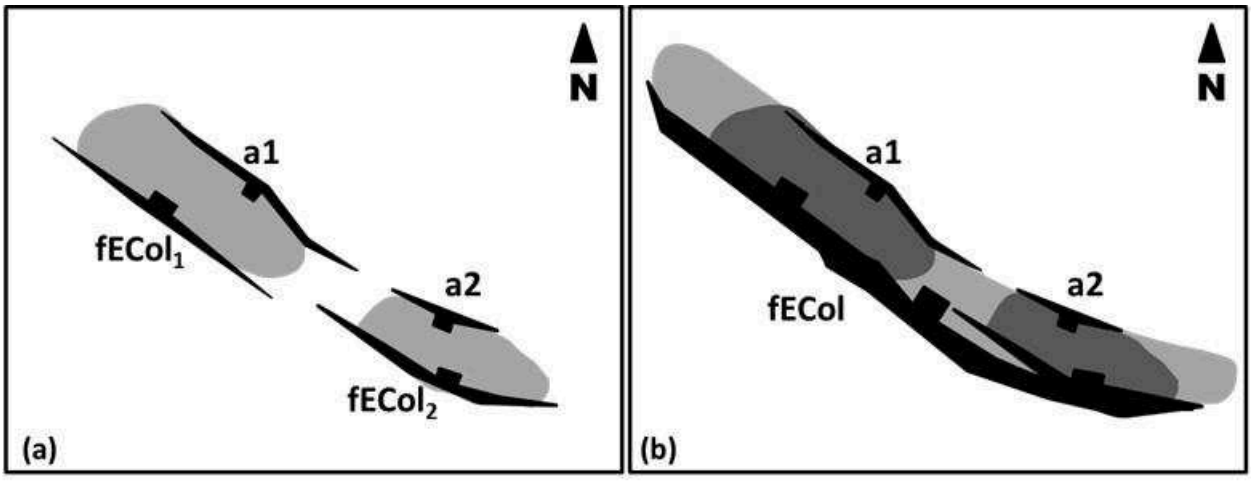

Figure 3.37: Evolution sketch for the ECol depocenter: a) Early rift stage, two independent grabens; b) Faults $fECol_1$ and $fECol_2$ link and the ECol depocenters becomes a half-graben with a controlling master-fault to the SW (fECol).

3.5.2.2 Central Depocenter

The Central Colorado depocenter (CCol) extends between 58° and 60°30' W. It is oriented E-W (80 km long and 30 km wide) and is located on the southern portion of the Colorado trough (Fig. 3.33). In the depth structure map for the Top Prerift presented in Fig. 3.38, a group of NNW-oriented faults are illustrated, following the E-W-striking master fault that forms CCol (fCCol).

The CCol depocenter is a half-graben, formed by a southward-dipping master fault (fCCol) that creates a large roll-over structure affected by antithetic faults. In CCol, two main synrift phases were identified. Figure 3.39 shows several horizons interpreted in the depocenter. Top SR (dark blue) depicts the top of the synrift unit. Aprons were detected on the faulted northern border of the depocenter. Within the Synrift unit, a feature interpreted as a possible carbonate buildup was also identified and small scale clinoforms were observed, prograding from the buildup towards the master fault (Fig. 3.40a). Alternatively, this build-up could also be a related to volcanism.

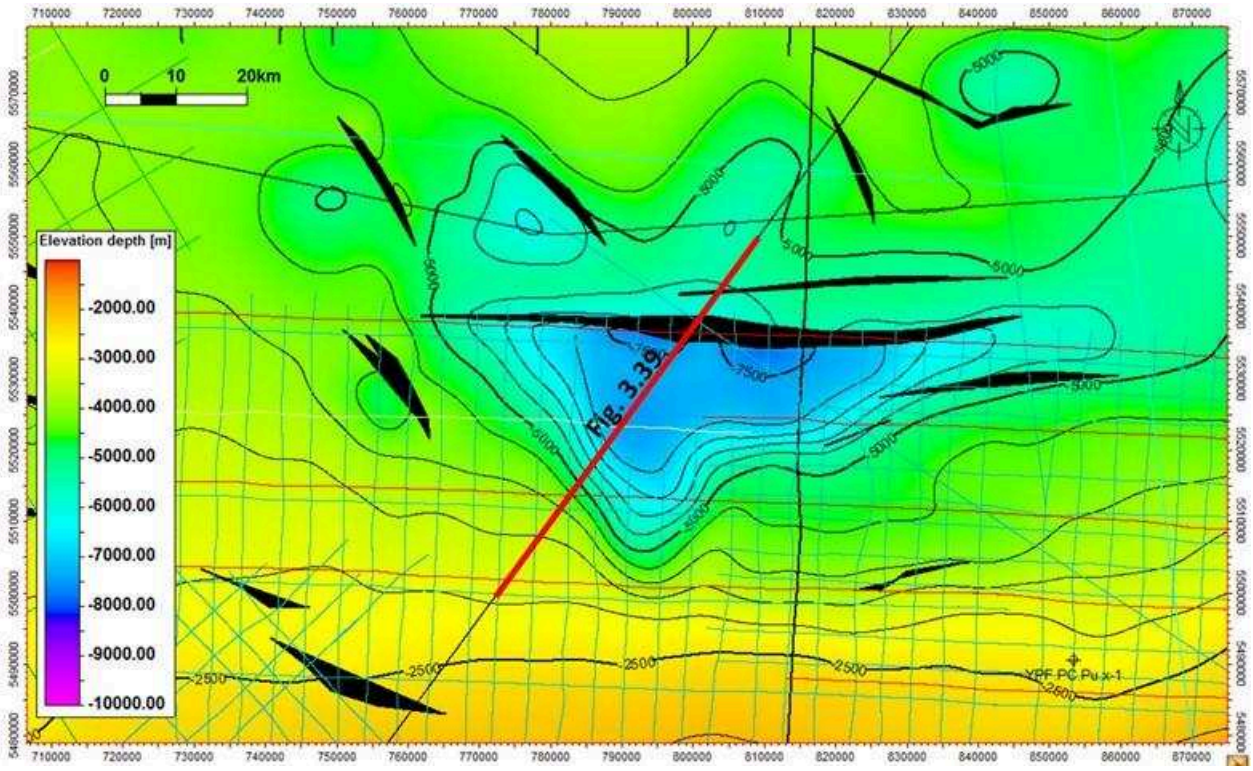

Figure 3.38: Depth structural map for the Top Prerift in the CCol depocenter area.

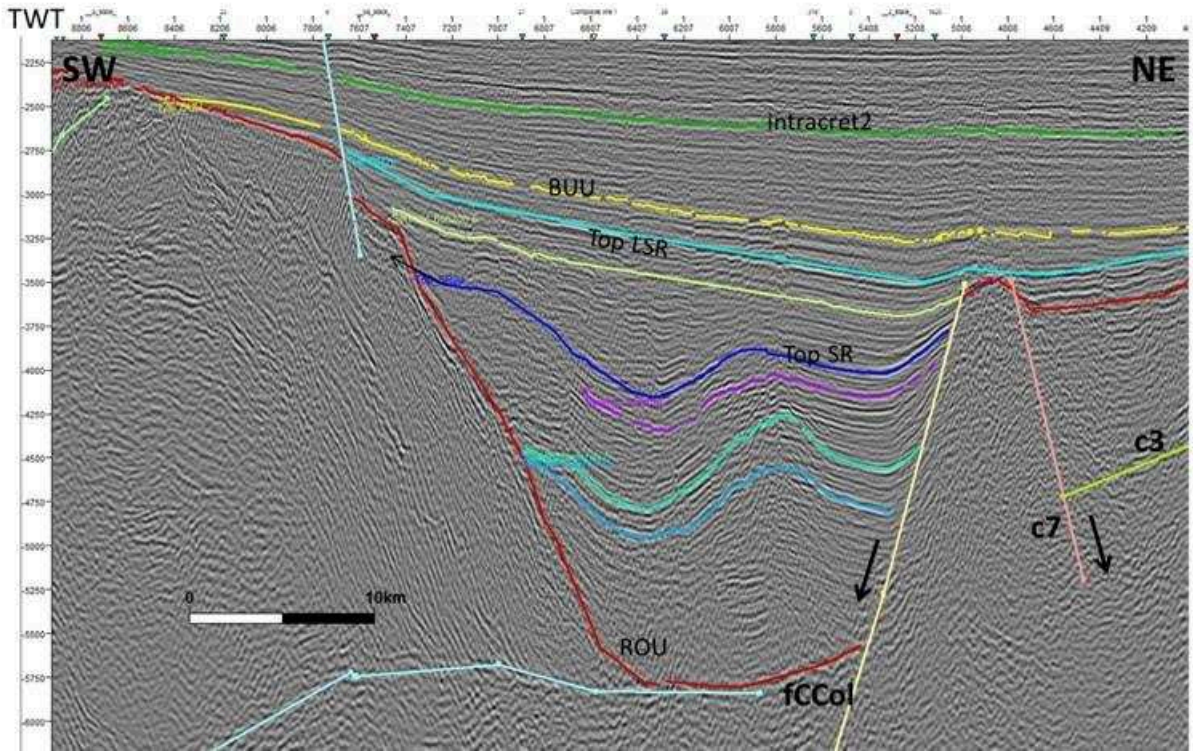

Figure 3.39: Seismic line as19200 (PSTM) across the CCol depocenter.

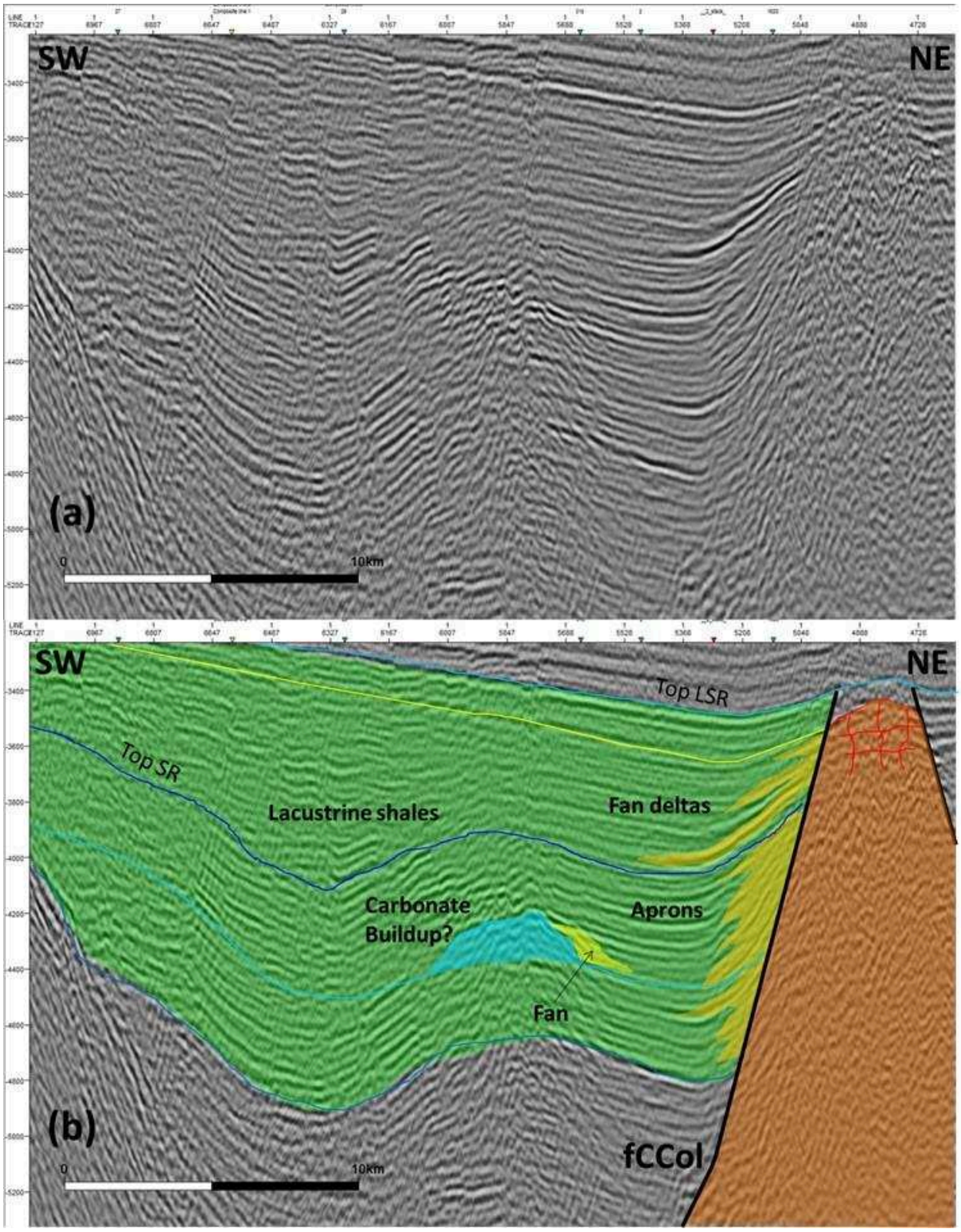

Figure 3.40: Zoom of sesimic line as19200 (PSTM, TWT) across the CCol depocenter: a) Uninterpreted line; b) Interpreted line with main geologic bodies.

A Late Synrift unit was also interpreted for CCol, between Top SR and Top LSR. The transition from the Top SR to the Top LSR units is characterized by large fans supplied from the faulted border (lower tectonic subsidence, or pulse in sediment supply?). Then, during the deposition of LSR, the fan deltas show an overall retrograding pattern. Above the Late Synrift unit (LSR), a thermal sag unit was interpreted (between Top LSR and BU in Fig. 3.39)..

Figure 3.41 shows a paleoenvironmental reconstruction for the sedimentary environments in the synrift stage of the CCol depocenter. The reconstruction comes from an analog, the Early Jurassic Cañadón Asfalfo Fm of the homologous basin (located in northern Patagonia). The Cañadón Asfalto Fm represents a mixed environment with development of palustrine environments and deposition of black shales, black mudstones and evaporates, surrounded by littoral sequences. In the marginal environment, a wide biohermal buildup belt developed (laminated and stromatolithic carbonates).

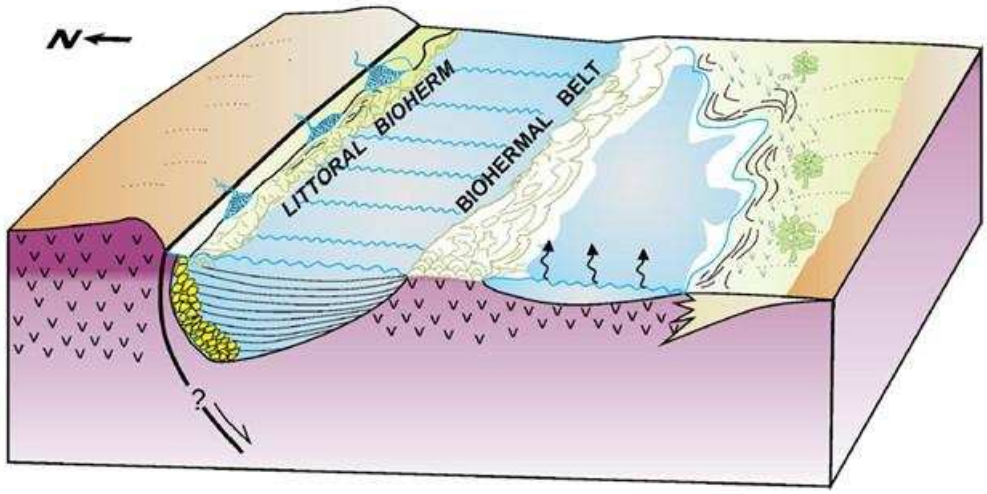

Figure 3.41: Analog depositional model for the CCol depocenter (modified from Volkheimer et al., 2015).

3.5.2.3 Western Depocenter

The Western Colorado depocenter (WCol) is located between 60°30' and 63°30' W. It has a more irregular shape, gently oriented SE-NW (160 km long by 80km in the SW-NE direction). It has a maximum sedimentary thickness of approximately 5 km.

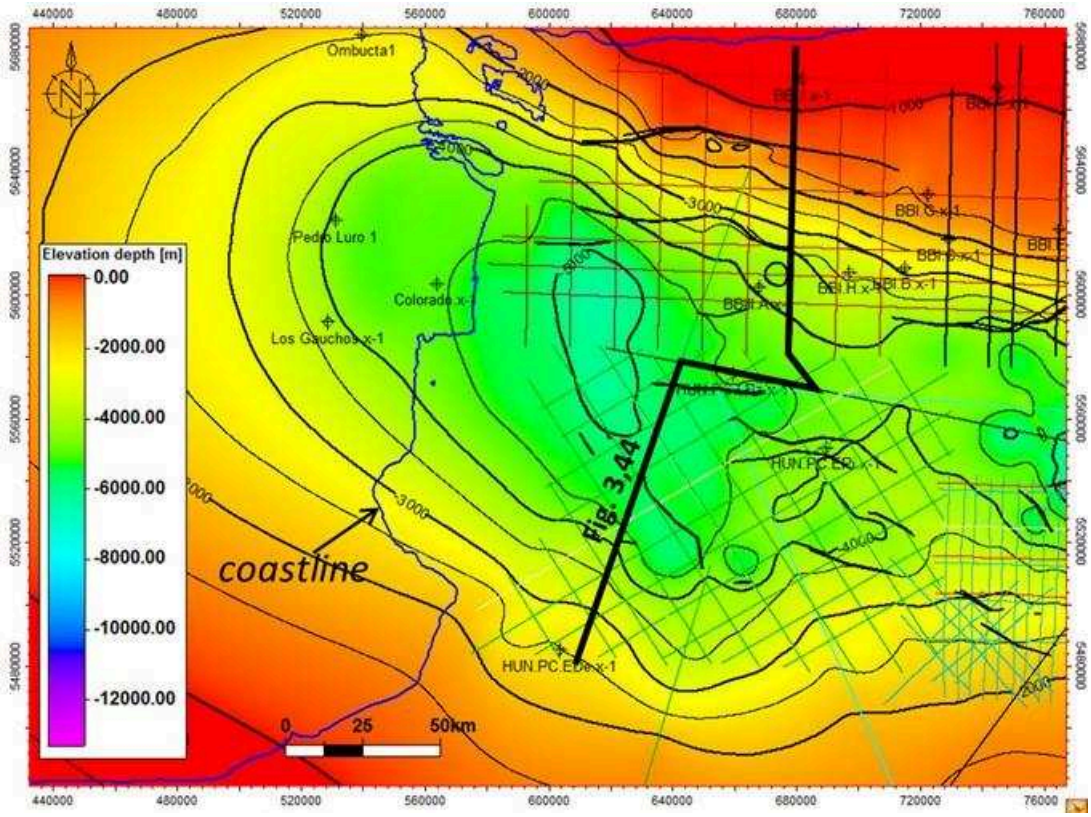

Figure 3.42: Depth Structure map at the Top Prerift horizon in the WCol depocenter. 2D seismic data available are indicated and the location of Fig. 3.44 is highlighted. Present day coastline is shown in blue.

WCol develops partly onshore. Wells Colorado, Pedro Luro, Los Gauchos, Ombucta and Blanqueada drilled the Cretaceous section (Fortín and Colorado Fm). The wells drilled onshore on the SW border (Lagunas Dulces, O'Connor, Oyola) found Cenozoic on top of basement (Fig. 3.43). There is not seismic data available for the onshore part of the basin. The contours for the Top Prerift horizon have been drown respecting the TDs of the wells, although none reached the basement, then Top Prerift values larger than TD were used to 'close' the contours with geological criterion following also the trends indicated in the maps presented by Kaasschieter (1963).

Seismic data available for WCol are some of the oldest seismic data in the basin, acquired in the 1960s, when the Philips and Hunt exploration wells were drilled in this shallow

water area. Figure 3.44 depicts a seismic transect created with the available seismic. The seismic data (scarce, of bad quality and short recording times) just allowed the interpretation of the Top Prerift, Top intracret2 and NTK unconformity (Top Cretaceous).

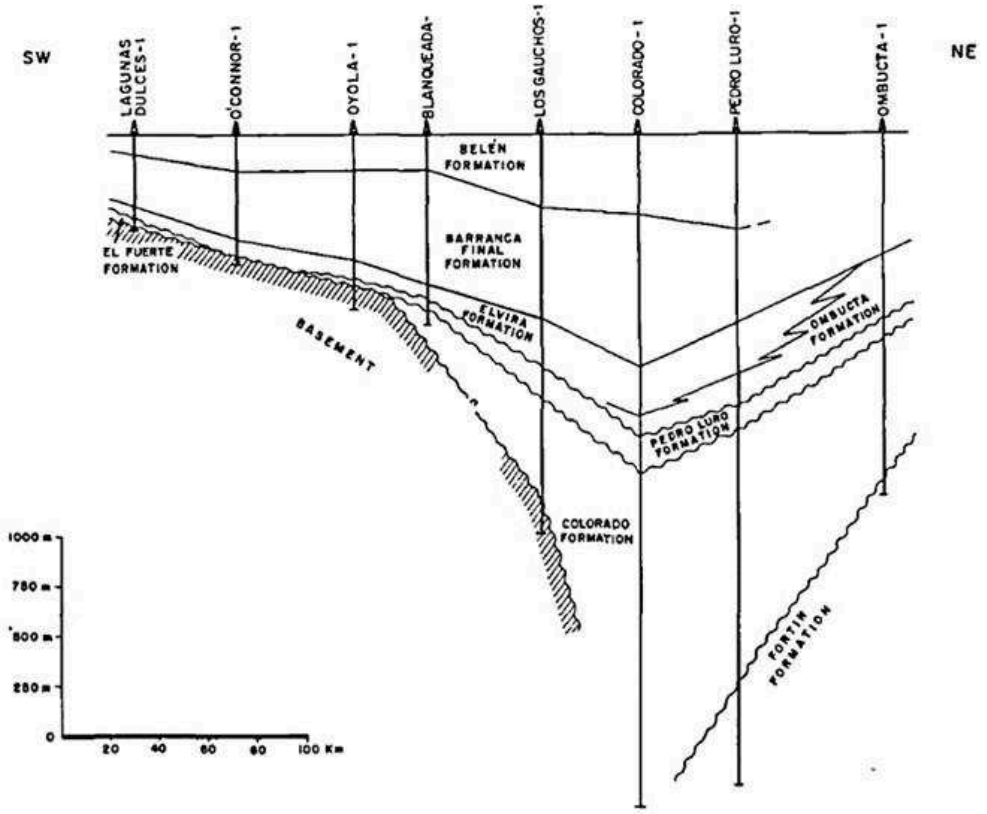

Figure 3.43: Well cross section across WCol (from Kaasschieter, 1963).

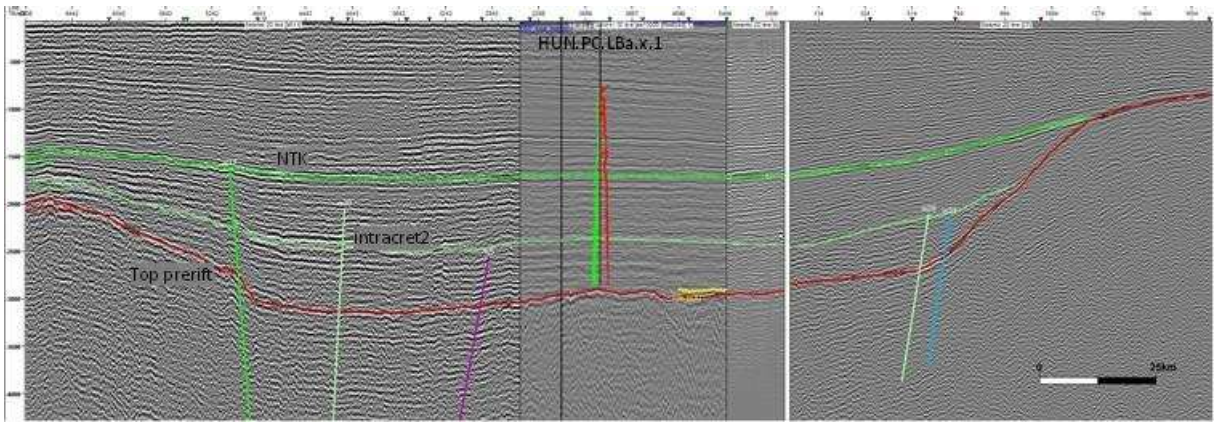

Figure 3.44: Seismic transect across WCol (several vintages, TWT). See location in Fig.3.42.

Some aspects about this depocenter remain unclear. The contours for the Top Prerift seem to follow a NNW-direction (Fig. 3.42) as some of the interpreted faults (Fig. 3.33). This alignment is independent from the artificial closing of the contours in the onshore area. Pángaro

and Ramos (2012) noticed this direction but interpret larger faults of this strike, that could not be interpreted on seismic data in this study.

What was interpreted is a Top Prerift (red horizon in Fig. 3.44) that coincides at this position with the breakup unconformity (BUU), meaning subaerial exposure of the basement at the time of continental breakup. No clear synrift wedges were interpreted in WCol (probably due to bad quality seismic data) and faults do not seem to have large throws.

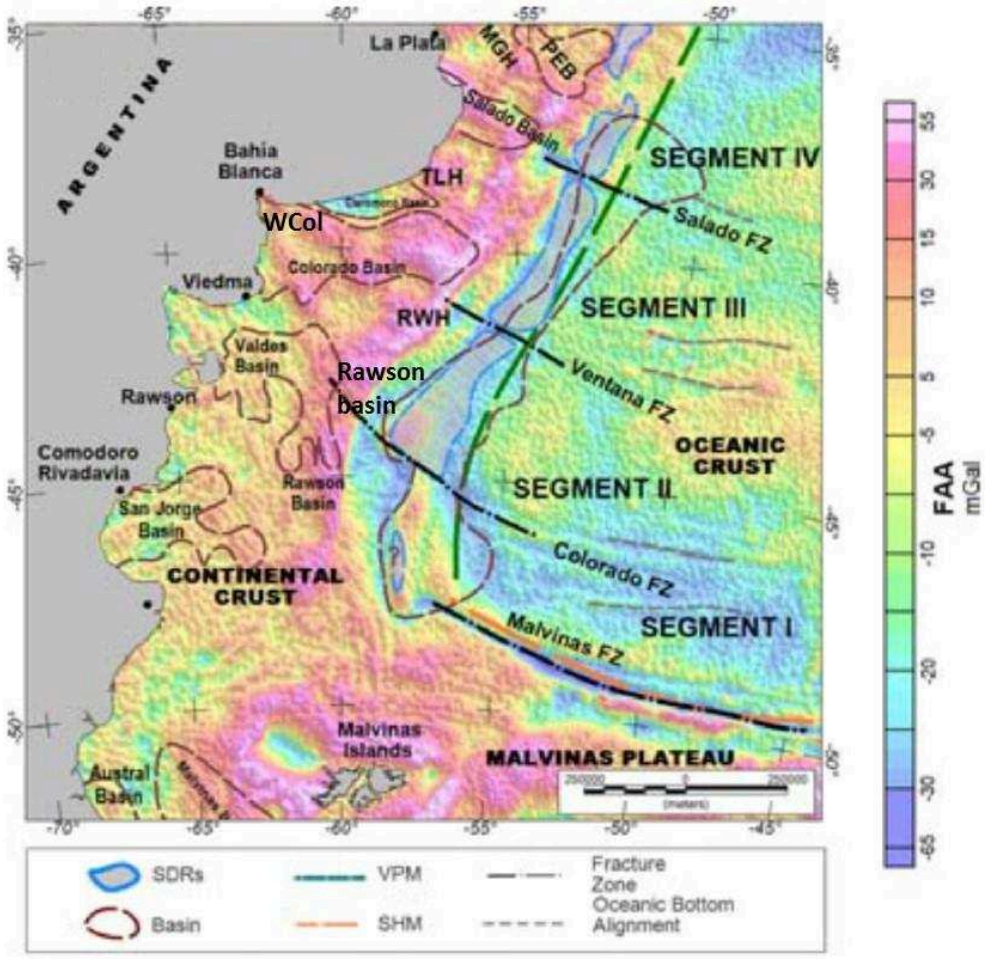

Figure 3.45: Free Air Anomaly Map for the Argentinean Offshore (from Arecco et al., 2016).

On top of the basement, two drift units were interpreted on the seismic data (Fig. 3.44), with clear onlap and pinch-out terminations towards the southern and northern shoulders. The lack of synrift deposits (fault-bounded) and the thick sag-related drift, is a point which remains to be explained. The lack, bad quality and short recording times of seismic data could be the reason why we are not being able to interpret the synrift. Another possibility is that the synrift depozones are located onshore (around Pedro Luro and Colorado wells) and are not covered with seismic data. The recent publication of gravimetric data seems to indicate an alignment

between the WCol depocenter and the Rawson basin located further south (Fig. 3.45, Arecco et al., 2016). Finally, it is possible that the mechanism responsible for thermal subsidence during the Cretaceous was not postrift thermal sagging, but rather mantle-related dynamic subsidence.

3.5.2.4 Cruz del Sur depocenter

The well Cruz del Sur (UTA.PC.CDS.x-1) was drilled in 1994. The operator Union Texas was targeting a hanging graben on the southern shoulder of ECol. It is a small depocenter (25 km in the NW direction by 15 km in the SW direction) bounded by faults (Fig. 3.46), and affected by many smaller faults that create an antiform structure at the 'synrift' level.

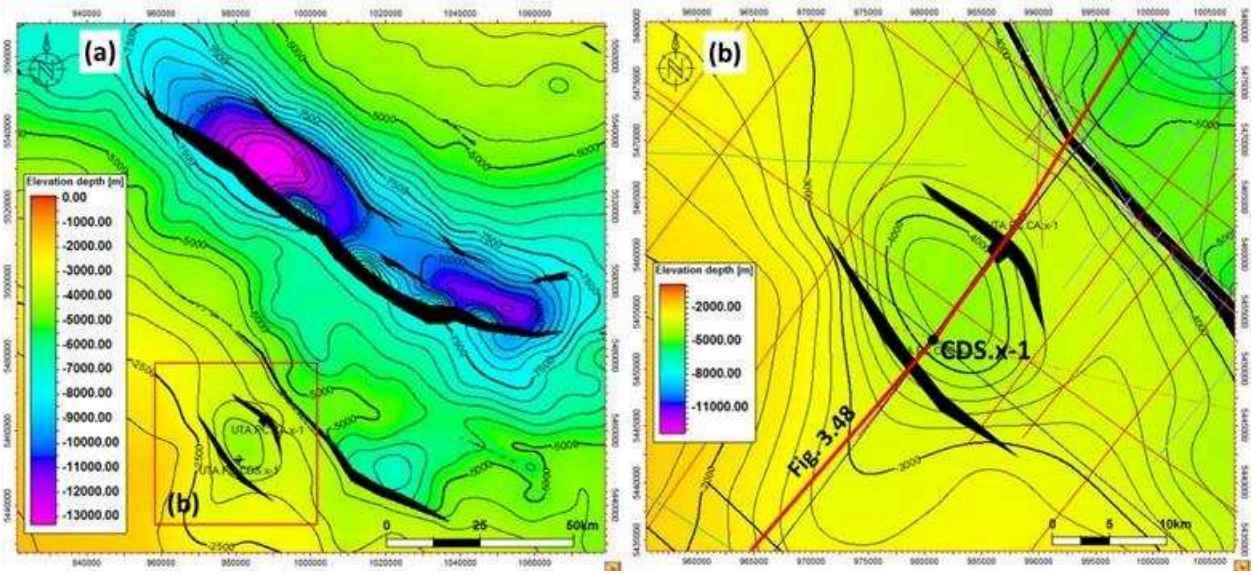

Figure 3.46: Depth Structure Map for the Top Prerift horizon at the Cruz del Sur (CDS) depocenter: a) Location map to the south of ECol; b) Detail map of the CDS depocenter.

The Cruz del Sur well is important in the Colorado Basin because it is the only well to date to test oil. The results of two RFT tests are shown in Table 3.2.

Depth (MD)	Fm Pressure (PSIG)	Fm Temperature °F (°C)	Fluid Recovery
3,438.54 m	5205.58	262°F (127.8°C)	15% oil / 85% Fm fluid (2 gallon chamber)
3,489 m	5280	261°F (127.2°C)	5% oil / 95% Fm fluid (1/2 pint recovered)

Table 3.2: RFT results. Cruz del Sur well. Run 2 (June 19th, 1994; Fryklund and Stevens, 1994).

The bottom hole section drilled by Cruz del Sur is presented on Fig. 3.47. The depths of the two RFTs that tested oil (Table 3) have been pointed out by green circles. The section starts from the bottom with medium-grained sandstones, occasionally coarse, with minor shale content (Fryklund and Stevens, 1994). A peak in the Gamma Ray (GR) response can be observed at 3,980 m MD and from then on two prograding coarsening-upward cycles can be determined (Fig. 3.47). At 3,500 m MD a sharp surface marks the base of a fine- to very fine-grained sandstones body on top of grey shales. The sedimentary body between 3,400 m and 3,500 m MD has an overall blocky GR pattern and was the reservoir where oil was tested. Between 3,300 m and 3,350 m MD another sand body was detected, and consists of medium-to-coarse grained sandstones, also interbedded with shales. Grey shales become dominant above 3,225 m MD, and are described as occasionally silty. A limestone bed was drilled at 3,010-20 m MD and traces of oil stain are described in the mudlog. White tuff layers have been described at 2,980-90 m MD and 2,810-20 m MD. At 2,790 m MD a new sharp sequence boundary puts medium-to-coarse and conglomeratic sandstones (Mesozoic) in contact with underlying grey-to-green claystones.

The well Corona Austral (UTA.PC.CA.x-1) drilled 15 km to the NE of CDS.x-1 did not find this section (it was drilled on a basement high bounding the Cruz del Sur depocenter).

In CDS.x-1, the operator used seismic interpretation, biostratigraphic data and mudlog to provide a Permian age for the bottom section (4,288-3,994 m MD), Late Jurassic to the Lower Synrift section (3,994-3,225 m MD), Berriasian-Valanginian to the Mid-Synrift section (3,225-3,010 m MD), Hauterivian-Aptian for a ‘Top Synrift Formation’ (3,010-2,850 m MD).

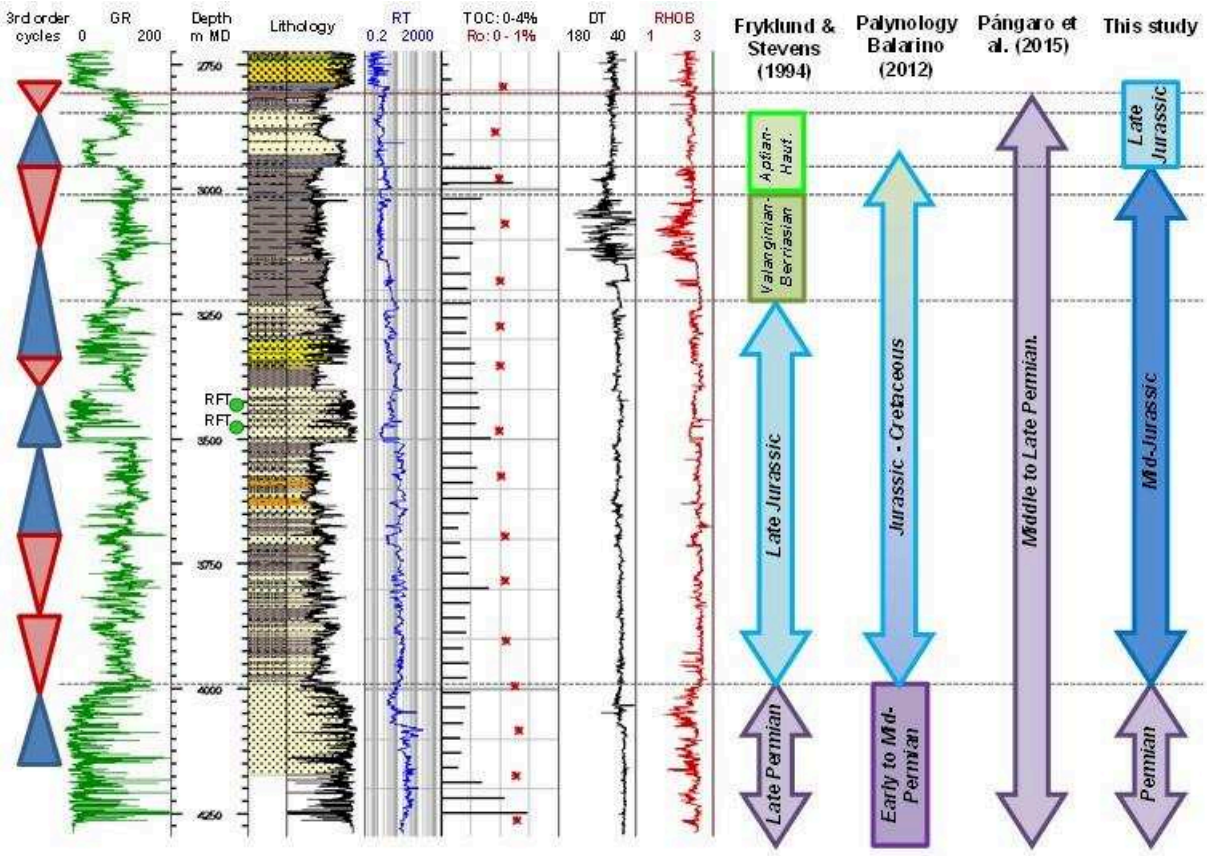

Figure 3.47: Bottom section of well Cruz del Sur (UTA.PC.CDS.x-1) between 2750 to 4250 m MD.

A palynological review carried out by Balarino (2012) from the prepared samples obtained from SWC (Side Wall Cores) pointed to a Cisularian to Early Guadalupian age (Early-Middle Permian) for the section below 3,995 m MD.

The presence of Permian palynological elements in the whole section lead to different interpretations of the age of the section between 2,800 and 4,000 m; and there has been debate on whether the section is part of the Mesozoic synrift (as interpreted by UTAL; Fryklund et al., 1996; Fryklund and Stevens, 1994) or is the Paleozoic prerift (Pángaro et al., 2016).

A biostratigraphic review of several wells in the Colorado basin, performed by GEMA (2000) by request of YPF, also provided a Permian age for this section. Since then, reinterpretation of seismic data carried out by Pángaro and Ramos (2012) or Loegering et al. (2013) lead them to postulate a Permian age for this unit. Pángaro et al. (2016) provides a Middle-to-Late Permian age for this section (Fig. 3.5).

The structure drilled by CDS.x-1 is a complex structure (Fig. 3.48) affected by several faults. The structure is poorly covered with seismic data (Fig. 3.46b), and seismic interpretation is arguable. Figure 3.48 shows, at a first glance, that the light blue marker (Top SRa) is largely parallel to the Top Prerift (ROU horizon). It would be possible to interpret the SRa unit as part of the prerift in the CDS depocenter, because it is deformed consistently with the underlying prerift. The Top SRb (orange horizon) is more clearly interpreted as a top synrift, as it defines a wedge-shaped package beneath it (between Top SRa and Top SRb) in all depocenters.

A recent biostratigraphic review conducted by specialists from YPF Laboratories Y-TEC (Ottone and Angelozzi, 2015) on the prepared samples from SWC that had been preserved in the MACN (Argentinean Museum of Natural Sciences, Buenos Aires) highlighted that presence of Classopollis spores in the SWC, pointing to a Mesozoic age. The biochron of Classopollis is (Late Triassic to Paleocene). Moreover, the lack of angiosperms pollen would point to a Jurassic/Early Cretaceous age for this sequence (at least between 2,900 and 3,636 m MD). The Permian species also found in this section, would then be reworked material redeposited in the Mesozoic.

Given that the section in debate is interpreted as Synrift, a detailed seismic interpretation and flattening of the seismic at the interpreted synrift tops was carried out to better assess the depocenter evolution. Figure 3.49 shows a zoom of the CDS structure. Figure 3.49c presents the seismic data flattened to horizon Top SRa (light blue). Extension and faults activity of s6 and especially s5 faults (to the NNE) in interpreted at this stage. Figure 3.49d shows the seismic line flattened to horizon Top SRb (orange). Extension and fault activity of s6 and s6b faults, forming a small graben, is interpreted at this stage. Fault s5 was not active in this second rifting stage. In this interpretation, fault s6 is intersects and displaces fault s5.

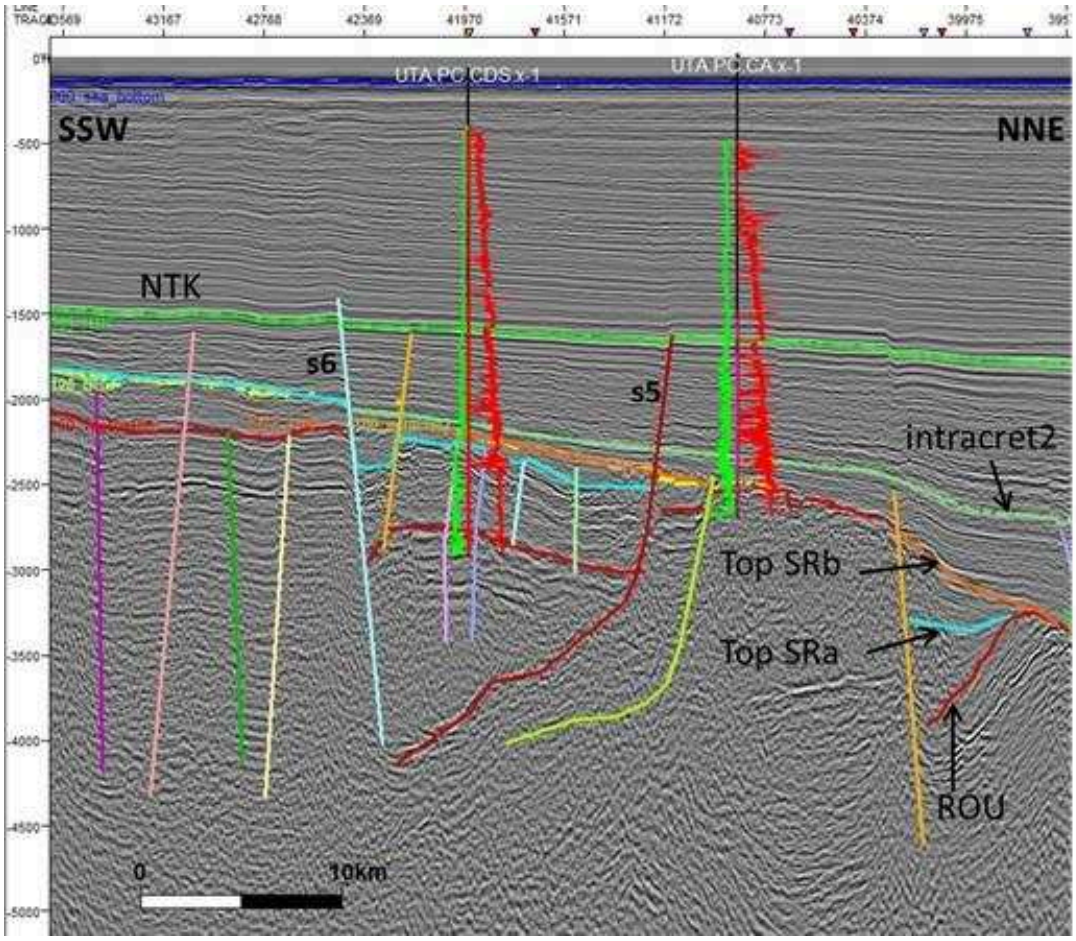

Figure 3.48: Seismic line as19400 across the CDS depocenter. See Fig. 48 for a larger view of the depocenter location. See Fig. 3.46b for seismic line location on the map.

We use the results of the latest analysis produced by Ottone and Angelozzi (2015), that highlight the presence of Classopollis and give a tentative Early-Jurassic age to the unit between 2,950 and 4,000 m MD, considering Classopolis is reported to be very abundant in the Early-Middle Jurassic Cuyo Group of the Neuquén basin (Volkheimer et al., 2015).

Regarding the sedimentary environments, Pángaro et al. (2016) interpret this section as an equivalent of the Late Permian turbidite lobes of the Laingsburg Fm in the Karoo basin (Fig. 3.5). If we follow the latest palynologic data review (Ottone and Angelozzi, 2015) and the regional information, these fine- to medium-grained sandy packages, with a blocky GR pattern and sharp bases and tops interfingered with dark shales (Fig. 3.47), could well be lacustrine turbidites deposited in a Jurassic fault bounded lake during the synrift stage.

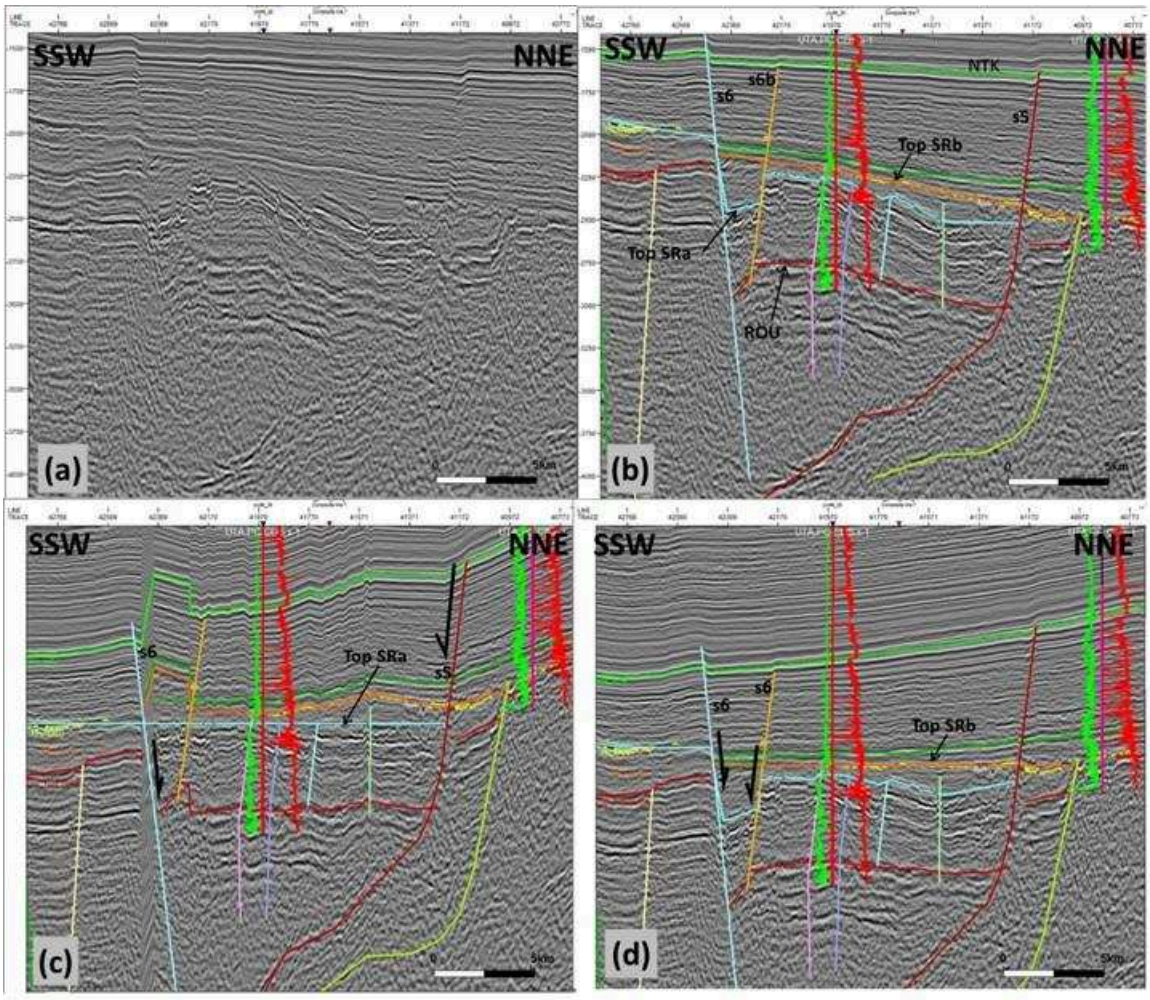

Figure 3.49: Zoom of seismic section as19400 on the CDS structure: a) Uninterpreted seismic line; b) Interpreted seismic line; c) Interpreted seismic line flattened at Top SRa; d) Interpreted seismic line flattened at Top SRb.

3.5.3 Breakup evolution

The area known as External high (Fig. 3.32) is the easternmost region of the Colorado basin before passing eastward to the SDRs and oceanic crust. It is located to the east of ECol (Fig. 3.50) and is characterized by the presence of largely NE-oriented changing in strike from E-W closer to the ECol depocenter, to NNE towards the east.

A seismic section across the external high is shown in Fig. 3.51. Part of a the ECol depocenter and the fault fECol is shown on the NW end. In the center of the figure, the External High is affected by normal faults. Further east, the SDRs are emplaced on the COT. The horizon interpreted in orange in Fig. 3.51 is the Base SDR. Several wedges of SDRs were identified

(Fig. 3.52). The horizon interpreted as the base of the SDRs (orange in Figs. 3.51 and 3.52) is a composite horizon which (following Stica et al., 2014) that connects the bases of different SDR wedges through 'faults' or discontinuities (poorly imaged). A thickness map of SDRs was prepared for the unit between the base of the SDRs horizon and the breakup unconformity (BU), using a constant interval velocity of 5,000 m/s. This isopach of the SDRs is presented in Figure 3.53. According to this interpretation, SDR can reach maximum thickness of around 6 km in the study area.

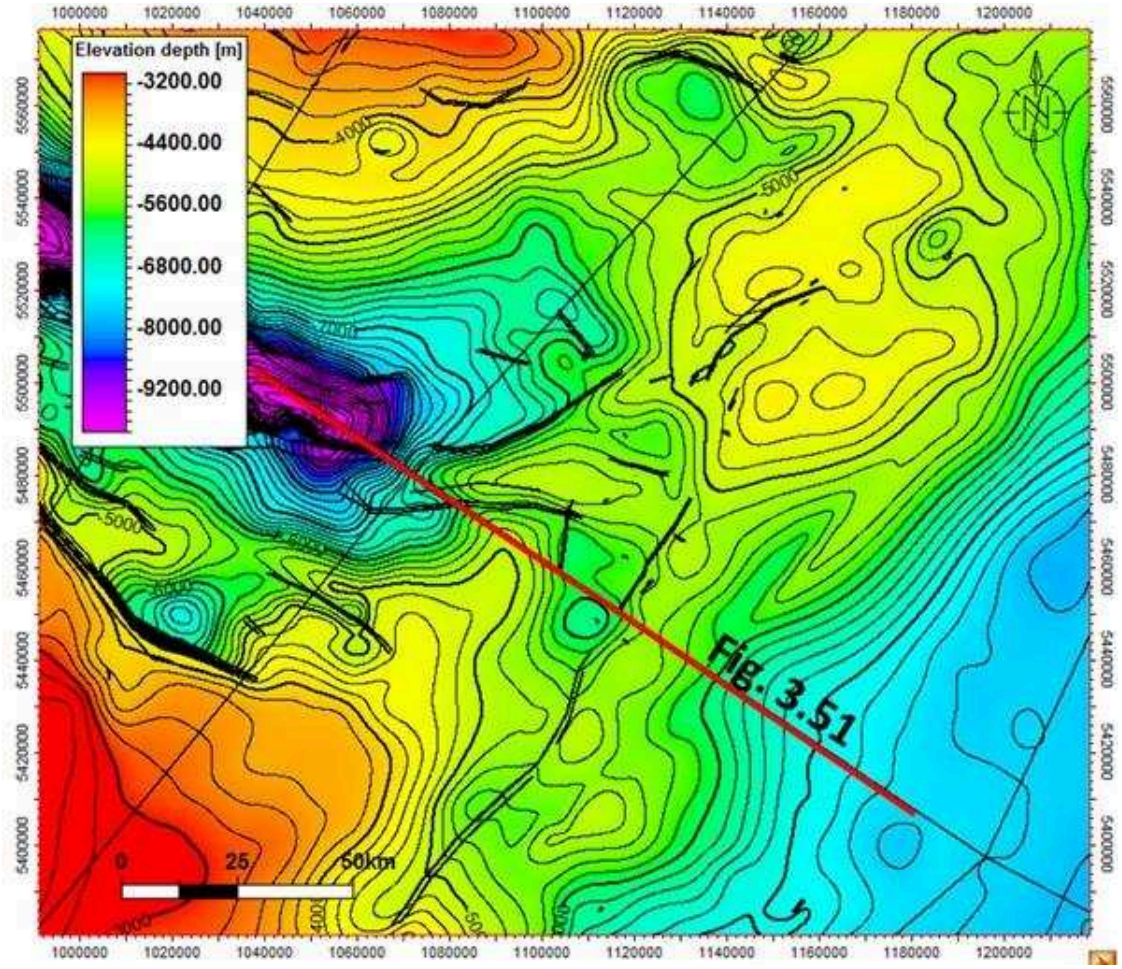

Figure 3.50: Depth structure map for eastern ECol and the External High area.

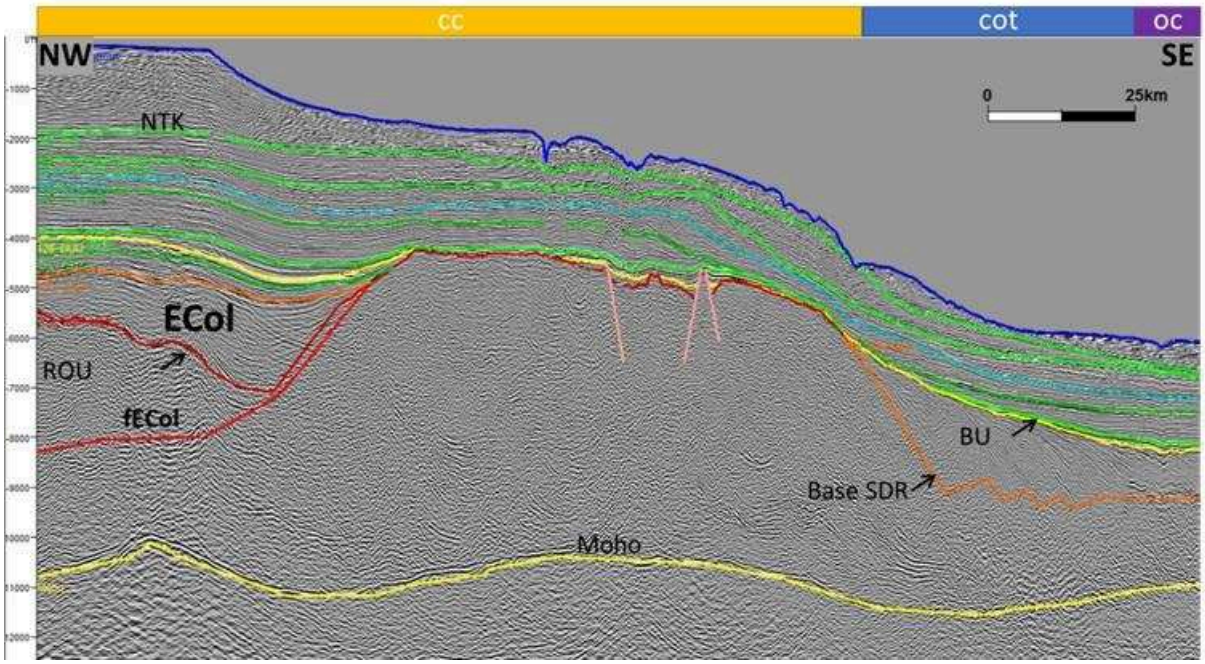

Figure 3.51: Seismic line as13000 (PSTM, TWT) across the ECol depocenter, the external high and the SDRs (cc: continental crust; cot: continent-ocean transition, oc: oceanic crust).

The SDRs are not dated in this segment of the margin, but they are interpreted to be emplaced at between 132 and 134 Ma (Late Hauterivian, Franke, 2013). The breakup unconformity (BUU) develops during the process of generation of normal oceanic crust, with uplift and erosion of the basin margins (Allen and Allen, 2005). Above the BU, a transgressive marine sequence usually occurred. In the study area, the post-breakup transgression is interpreted to have flooded the Eastern Colorado depocenter and parts of the external high (Gerster et al., 2011). In the extensional depocenters observed on the external high (Fig. 3.51), the BUU (as interpreted from the top of the SDRs continentward) marks the change from synrift to postrift regime, whereas ECol and the other depocenters were already under 'thermal subsidence'. A discussion on this point is presented in Chapter 4.

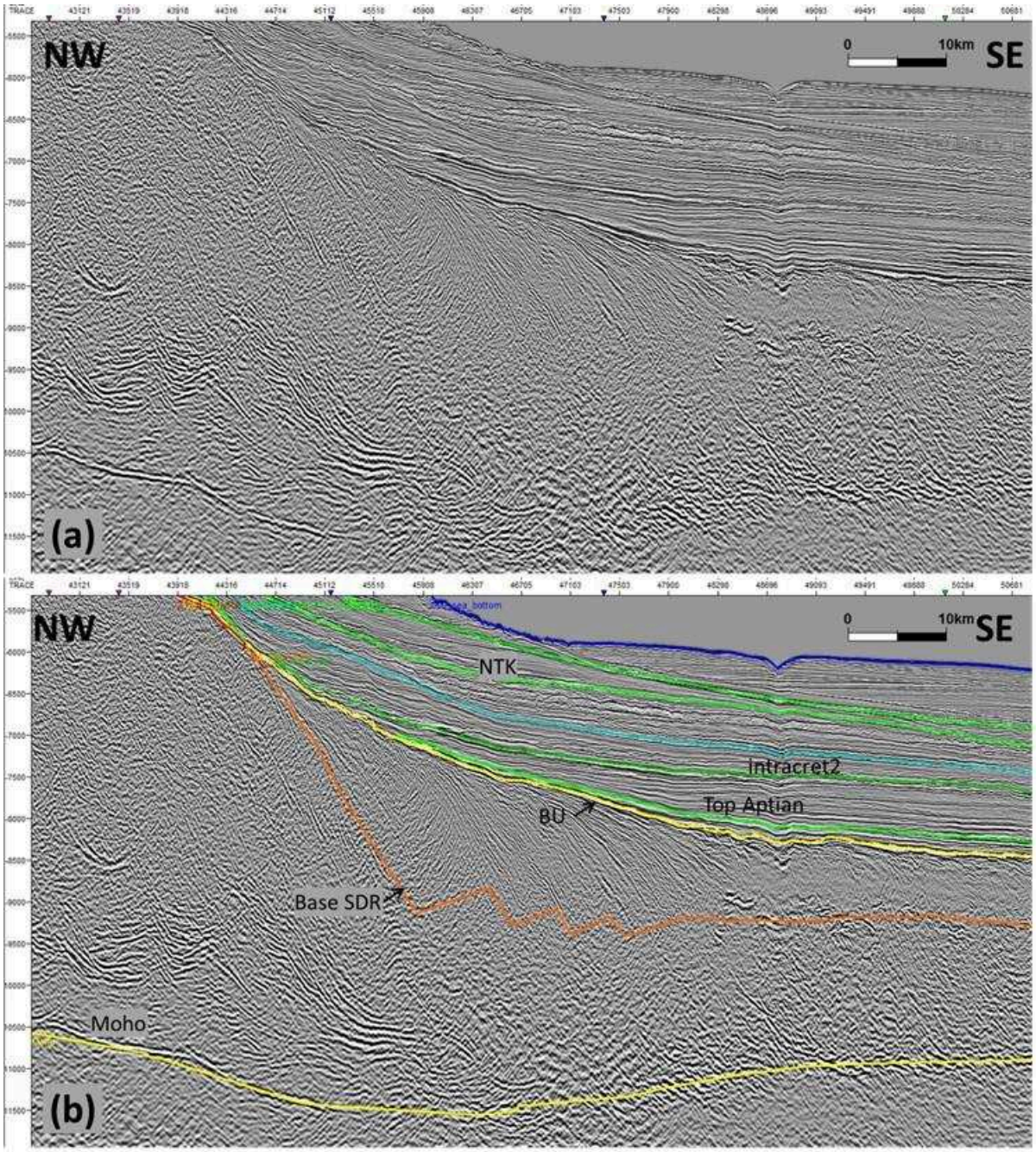

Figure 3.52: Zoom-in of seismic line as13000 (PSTM, TWT) across the SDRs wedges east from the Colorado basin: a) Uninterpreted seismic section; b) Interpreted seismic section.

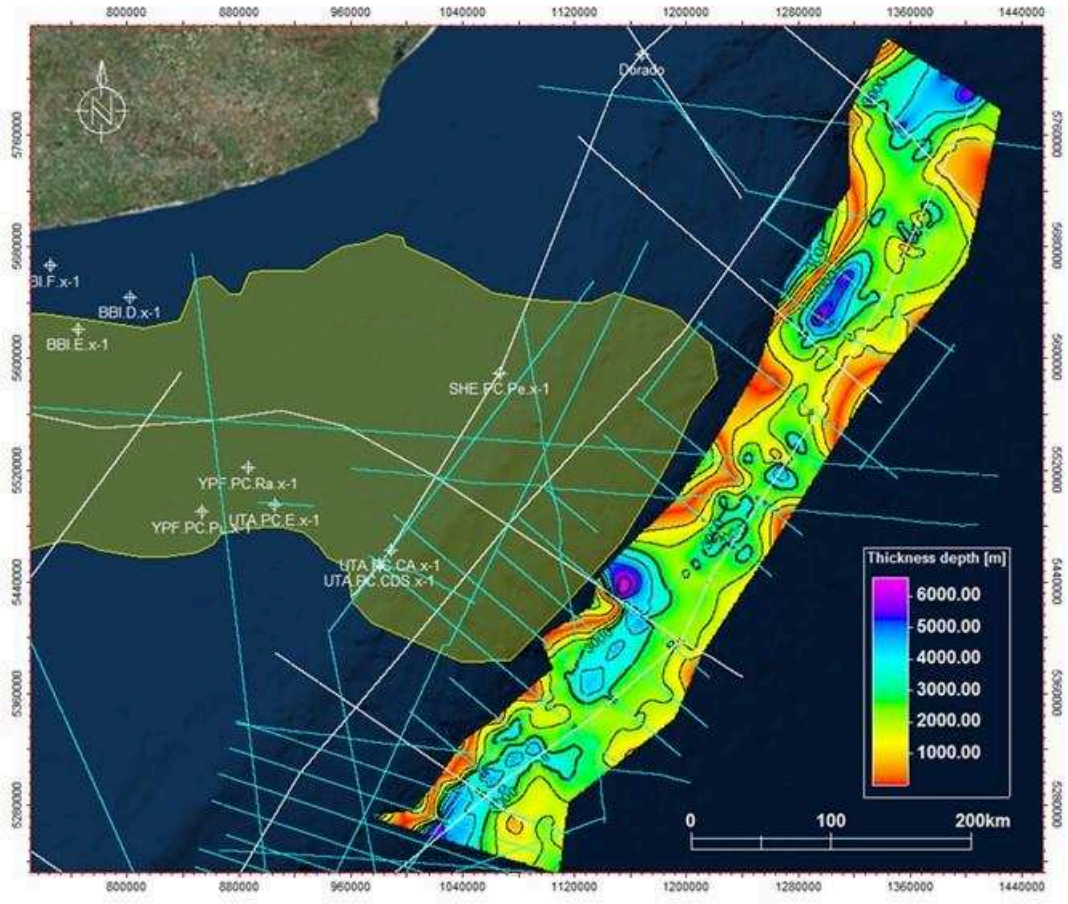

Figure 3.53: Total Thickness map of the SDR wedges (depth converted using a constant interval velocity of 5,000 m/s).

A structural framework of the Colorado basin was presented in this chapter. It was prepared by carrying out extensive seismic interpretation of the 2D seismic data available in the study area. The main basins depocenters have been described and characterized and the cross cutting relationships of some of faults have been used to interpreted multiple rifting stages throughout the evolution of the Colorado basin. The discussion of these interpretations is presented in Chapter 4.

Chapter 4. Multistage rifting evolution of the Colorado basin (offshore Argentina): Evidence for extensional settings prior to the South Atlantic opening

This chapter presents the discussion on the structural evolution of the Colorado basin area has been published as part of this project in Terra Nova in collaboration with my colleagues at YPF SA: Lovecchio, J.P.; Rohais, S.; Joseph, P.; Bolatti, N.; Kress, P.; Gerster, R.; Ramos, V. 2018. Multistage rifting evolution of the Colorado basin (offshore Argentina): Evidence for extensional settings prior to the South Atlantic opening. Terra Nova, v. 30, 359-368.

4.1 Abstract

The identification of three independent rifting events in the Colorado basin area highlights the complexity of its Mesozoic rifting history, which ended in the Early Cretaceous with the opening of the South Atlantic Ocean. A first rifting event, associated with the extensional reactivation of previously compressive thrusts of the Ventania-Cape fold belt, is transected by faults forming the main depocenters of the Colorado and possibly the adjacent Salado basin. The second and main rifting stage is correlated with the Early Jurassic Karoo rifting. In the Early Cretaceous WNW-ESE extension produced NNE-trending landward-dipping faults, concentrated in the outer 100-200 km of the continental crust domain, possibly coeval with SDR emplacement. This is the first identification of three superimposed rifting settings in the southern South Atlantic realm and is key to understanding the complex Mesozoic breakup history of SW Gondwana.

4.2 Introduction

Understanding the evolution of volcanic passive margins, especially the crustal architecture and related rifting mechanics, has been greatly enhanced thanks to high resolution and deep seismic data (Franke et al., 2006, 2007; Blaich et al., 2013;Stica et al., 2014) as well as to major advances in numerical modeling (Beniest et al., 2017; Geoffroy et al., 2015). However, most of the proposed models were built based on 2D cross sections, without considering the basement heterogeneities on either conjugate margin in a 3D perspective. Will and Frimmel (2018) analyzed the factors conditioning the emplacement of the South Atlantic Ocean focusing on intrinsic basement heterogeneities associated with the Neoproterozoic Brasiliano-Panafrican orogeny, disregarding other heterogeneities introduced by previous rifting events.

The opening of the South Atlantic in the Early Cretaceous was only the final stage of a complex rifting process (Uliana et al., 1989) that initiated after the Mid-Permian to Early-Triassic Gondwanan orogeny (Hälbich, 1983; Hansma et al., 2016). The Central Atlantic was the locus of the Triassic rifting. Intracontinental rifts also developed in Africa and South America at this time (Zerfass et al., 2004). The Karoo rifting on Eastern Africa since the Early Jurassic (Delvaux, 2001), is associated with breakup of Africa from Antarctica and India and the opening of the Weddell Sea (Ghidella et al., 2002). In the Early Cretaceous E-W directed extension is responsible for the South Atlantic opening. Frizon De Lamotte et al. (2015) review rifting processes in the Pangea breakup and suggest that, oppositely to the active Karoo rifting, the Early Cretaceous rifting (responsible for the opening the South Atlantic) was passive rifting, related to far-field forces controlling the initiation of rifting diachronically from south to north (Nürnberg and Müller, 1991).

On the Argentinean South Atlantic margin, prerift is composed of Late Paleozoic glacial and marine successions that were involved in a Permian-Early Triassic Ventania-Cape fold belt (Pángaro and Ramos, 2012; Pángaro et al., 2016), which has been traced across the South Atlantic to the Namibian margin (Paton et al., 2016).

The Colorado and the Salado basins (Fig 4.1) are troughs oriented largely E-W, at high angle with the NNE-oriented continent-ocean boundary (COB). Magma-rich rifted margins as the southern South Atlantic are characterized by the presence of SDRs (Seaward Dipping Reflectors; Hinz, 1981; Gladczenko et al., 1997; Hinz et al., 1999; Stica et al., 2014; and Paton

et al., 2017) on the continent-ocean transition (COT). We define the COT as the area with SDR development on thinned transitional crust (sensu Blaich et al., 2013). The external boundary of the COT, passing to the normal oceanic crust domain is the continent-ocean boundary (COB in Fig. 4.1).

The chronology of rifting in the Colorado and Salado basins is poorly constrained. Hydrocarbon exploration wells were drilled on structural highs outside the main depocenters and the few wells that investigated the synrift section mostly found red beds, where datable fossils are scarce.

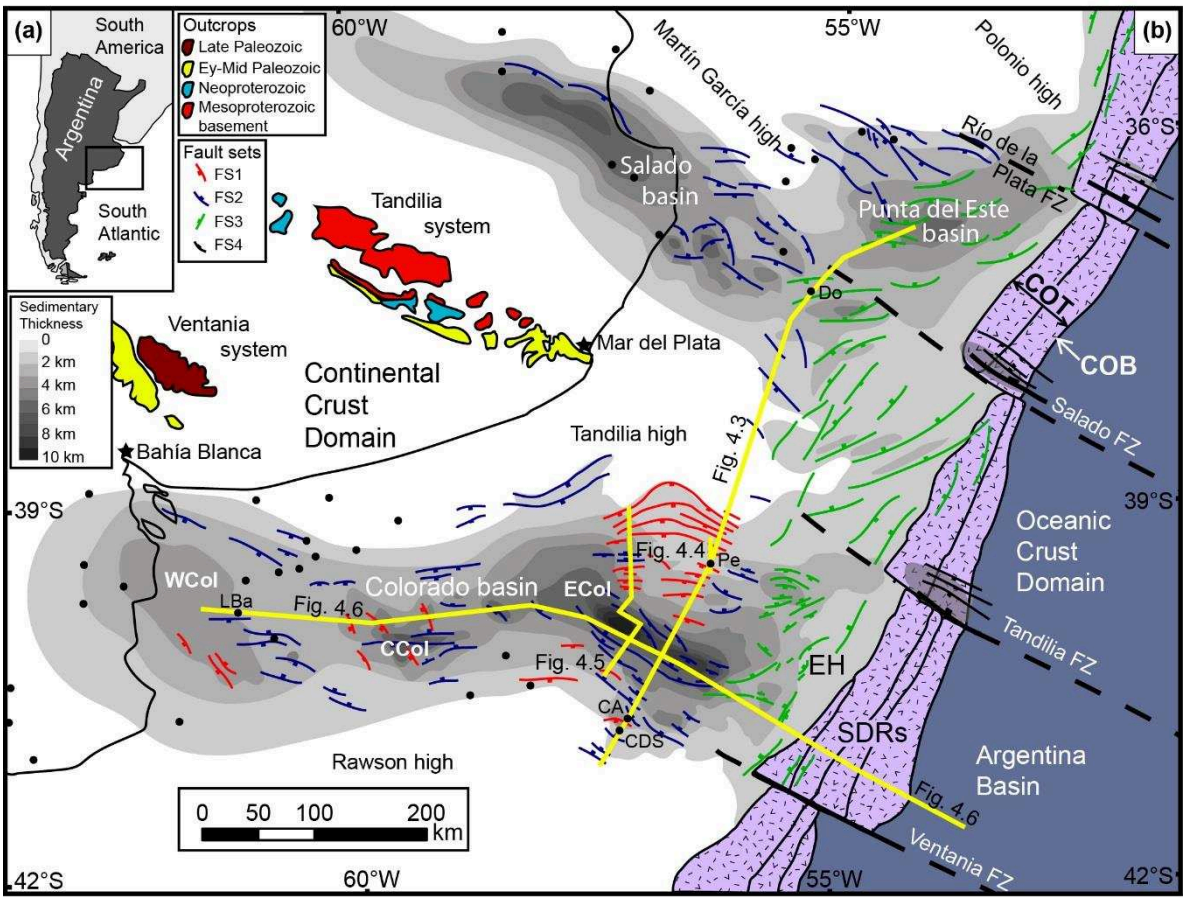

Figure 4.1: Structural map of the Colorado and Salado basins (offshore Argentina) and the Punta del Este basin (offshore Uruguay). A: Map showing the location of the study area. B: Total sedimentary thickness on the continental crust domain (CCD). Colorado basin depocenters: WCol (western), CCol (central), ECol (eastern). Faults have been gathered into four fault sets (FS) according to their relative chronology. SDR wedges (mapped after Franke et al., 2007; and Soto et al., 2011). COT: continent-ocean transition, COB: cont.-ocean boundary, OCD: Oceanic crust domain, FZ: fracture zone, EH: External High. The black dots show the location of the exploration wells. Yellow lines indicate the location of seismic transects presented in this contribution.

Several hypotheses were proposed to explain the high obliquity between these basins and the NNE-oriented COB. At first, studies implied the development of both basins synchronously leading to the opening of the South Atlantic in a single and continuous rifting event. Obliquity was explained either by aulacogens (Yrigoyen, 1975, Introcaso and Ramos, 1984) controlled by Paleozoic or previous sutures (Ramos, 1996), transtensional basins associated with NW–SE dextral shear systems (Keeley and Light, 1993; Tankard et al., 2009; Franke et al., 2006), or as due to structural inheritance (Urien et al., 1995; Dominguez et al., 2011; Gebhard, 2005).

More recently, two superimposed rifting stages were used to explain the obliquity: a first Jurassic event with a NE-SW oriented extension, forming the Colorado and Salado basins, and a second E-W oriented extensional event forming the South Atlantic rift in the Early Cretaceous (Macdonald et al., 2003; Gerster et al., 2011; Pángaro and Ramos, 2012; Autin et al., 2013; Franke, 2013).

In this paper, after having carried out seismic interpretation and identified cross-cutting relationships between different generations of faults, we present evidence for not only two but three independent extensional stages. An older, previously unknown event was identified in the study area. This event is evidenced by the extensional reactivation of previously compressive thrusts of the Ventania-Cape fold belt. Extensional reactivation of thrusts has been described in other locations in Gondwana (De Wit and Ransome, 1992; Aldiss and Edwards, 1999; Franzese and Spalletti, 2001; Paton, 2006).

4.3 Materials and Methods

The database made available by YPF SA comprised 25 exploration wells (Fig. 4.1) and more than 30,000 km of 2D multichannel reflection PSTM seismic lines in the Colorado and Salado basins. Petrel software was used for interpretation. Time structure maps were generated for selected horizons (Fig. 4.2) to delineate the main depocenters. Wells were tied to seismic lines using synthetic logs or VSP data when available, producing new velocity laws that were integrated into a 3D regional velocity model used to convert the time structure maps and 2D TWT seismic sections into depth. Faults were interpreted on seismic lines and a structural model was prepared. Faults were then grouped into sets according to their orientation, dip, displaced reflectors, detachment level and cross-cutting relationships.

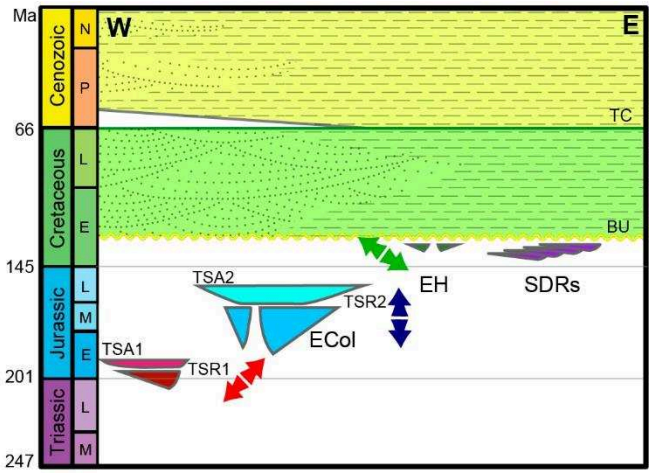

Figure 4.2: Schematic chronostratigraphic chart depicting chronology of rifting events and the main horizons used in seismic interpretation. TSR1: Top Synrift 1, TSA1: Top Sag 1, TSR2: Top Synrift 2, TSA2: Top Sag 2, BU: Breakup Unconformity, TC: Top Cretaceous. Arrows indicate the main direction of extension for each rifting stage (respect to present day South America). Late Triassic-Early Jurassic rifting (FS1): SW-NE extension; Early-Mid Jurassic rifting (FS2): N-S extension; Early Cretaceous rifging (FS3) and SDR emplacement: WNW-ESE extension.

4.4 Results

A structural map of the Colorado and Salado basins is presented in figure 4.1. The deepest Eastern Colorado (ECol) depocenter is a half-graben controlled by a NW-striking, NE-dipping master fault (Figs. 4.3, 4.5 and 4.6). In a structural section across ECol (Fig. 4.3) two sets of faults were identified. Tilted blocks on the northern flank of ECol are associated with a first set of faults (FS1), dipping to the S-SW and detaching at a level within the crust (at depths of approximately 10-15 km. Paleozoic strata are preserved in the tilted blocks but the synrift deposits associated with the rotation of these blocks are mostly eroded (Fig. 4.4, Pángaro and Ramos, 2012).

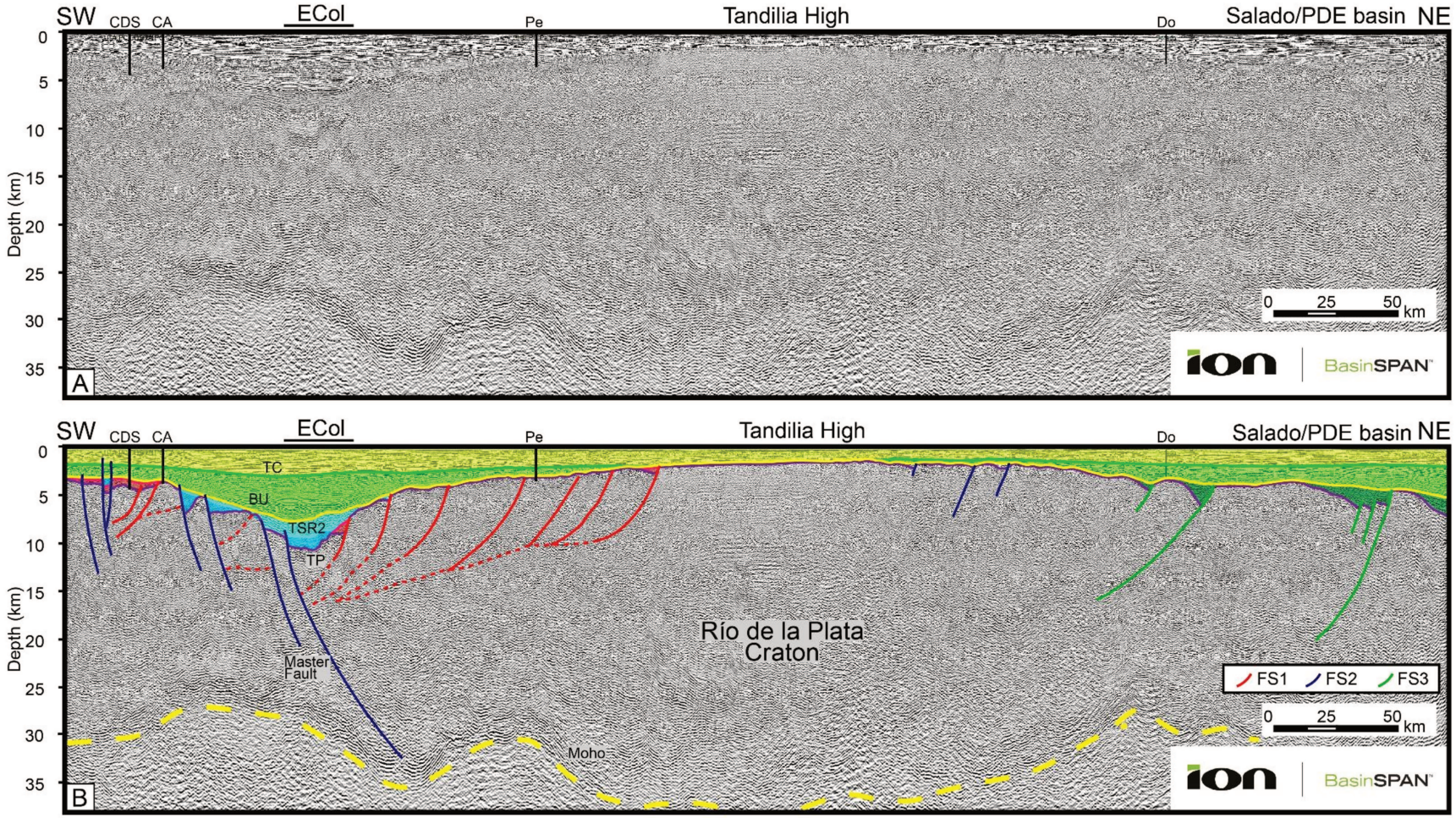

Figure 4.3: Depth-converted seismic line across the ECol depocenter (location in Fig. 4.1b): a: uninterpreted and; b: interpreted section. Note the tilted blocks on the northern flank of ECol formed by FS1 faults detaching at 10-15 km (a detail of the tilted blocks is presented in Fig. 4.4). The main ECol depocenter is formed by FS2 faults detaching at the Moho (25-30 km deep approx.). The location of the Cruz del Sur (CDS), Corona Austral (CA), and Pejerrey (Pe) hydrocarbon exploration wells is depicted. A key for seismic horizons is presented in Fig. 4.2. Note the increase in crustal thickness across the Tandilia High, an offshore extension of the Río de la Plata craton.

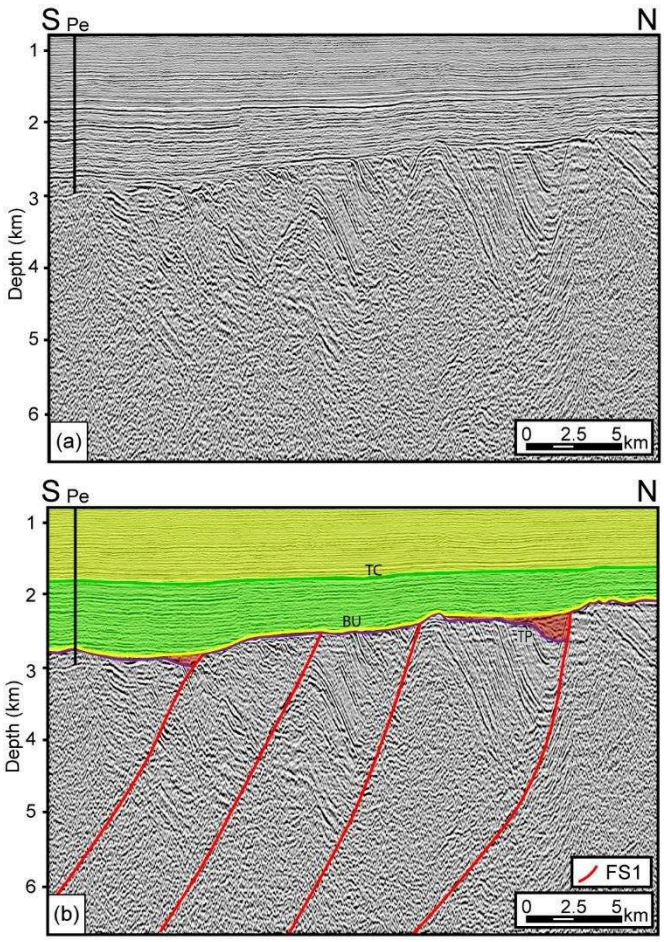

Figure 4.4: Depth converted seismic line on the northern flank of the ECol depocenter. A: uninterpreted and, B: interpreted section. Tilted blocks associated with FS1 faults are shown in detail. Note that most of the synrift associated with this rifting has not been preserved. The location of the Pejerrey (Pe) well is shown.

A second set of faults (FS2), including the master fault forming ECol and conjugates, intersects FS1 faults. FS2 faults are steeper and more deeply rooted, with the master fault possibly detaching at deep crustal levels close to the Moho (at a depth of about 30 km, Fig. 4.3). By extrapolating these observations across the study area, we classified the observed faults into four fault sets according to their relative chronology. Besides FS1 and FS2 already presented, FS3 faults are largely oriented NNE parallel to the SDRs and continent-ocean boundary and restricted to the outer 100-200 km of the continental crust domain and COT (Fig. 4.1 and 4.6). Finally, FS4 faults were interpreted in the areas affected by fracture zones. Although the fracture zones appear to have an impact on the shelf structure and onshore geology, FS4 faults are restricted to the COT affecting SDRs wedges (Fig. 4.1).

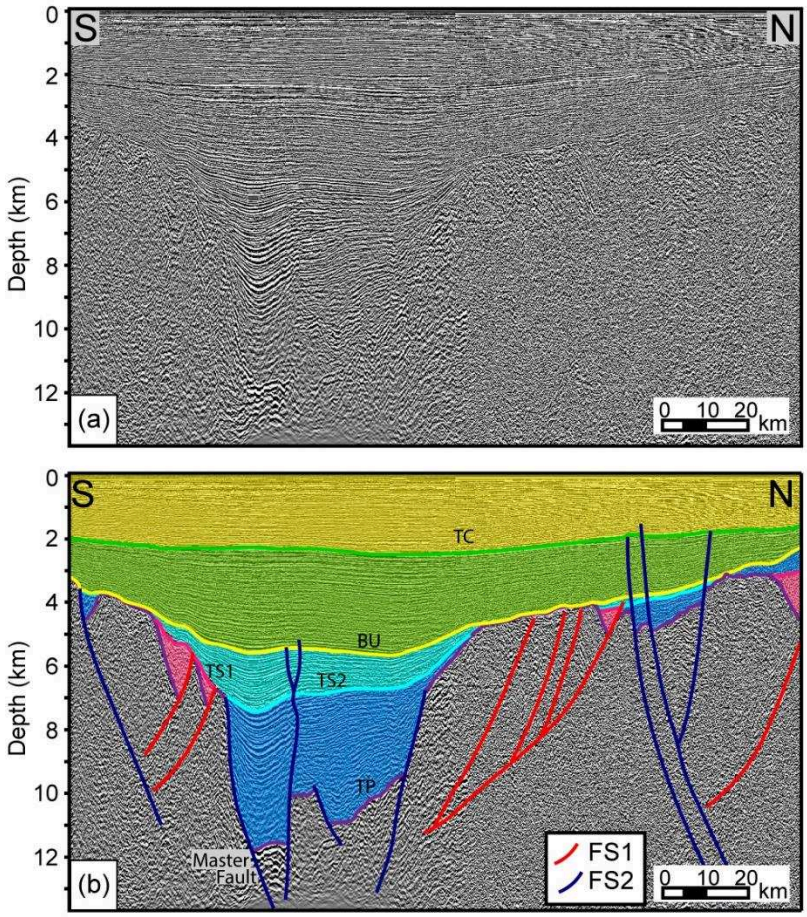

Figure 4.5: Depth converted seismic transect across the ECol depocenter. A: uninterpreted and, B: interpreted transect. Note preserved half-grabens of rifting stage 1 on the southern flank of ECol and transection of FS1 and FS2 faults.

On another seismic transect across ECol, tilted blocks were identified both on the northern and the southern flank of the depocenter, forming relict half-grabens 'hanging' on the footwall of the ECol master fault (Fig. 4.5). Some FS2 faults show reactivation reaching the top Cretaceous horizon, probably associated with strike-slip movement during the drifting phase. FS1 faults do not present Late Cretaceous reactivation.

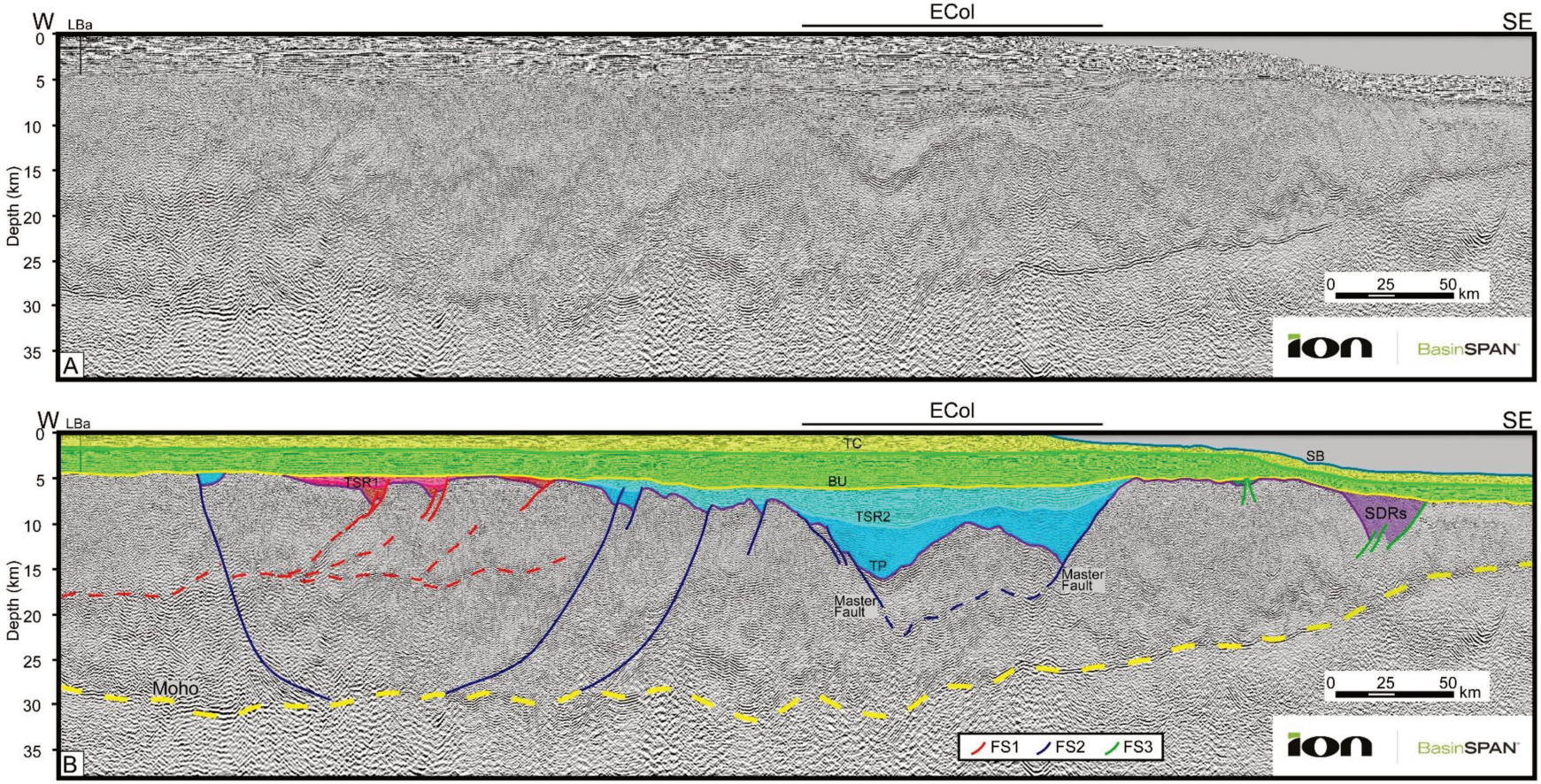

Figure 4.6: Depth-converted seismic line across the Colorado basin (location in Fig. 4.1b). A: uninterpreted and, B: interpreted section. After Horn (2015). FS1 faults form half-grabens to the west of the line and seem rooted at intra-crustal level near 15 km. FS 2 faults are responsible for the formation of the ECol depocenter and are rooted at deeper lithospheric levels (25-30 km deep.). Our seismic interpretation of the Moho is consistent with the Moho derived from gravity methods presented by Franke et al. (2006) and Blaich et al. (2009). The location of the La Ballena (LBa) well is depicted. A key for seismic horizons is presented in Fig. 4.2.

In the central area, north of the CCol depocenter, a set of NNW-striking listric faults forming tilted blocks and half-grabens, with an intra-crustal detachment level (approx. 17-20 km deep, Fig. 4.6) are intersected by the E-W-oriented, S-dipping, master fault forming the Central Colorado half-graben (CCol, see Fig. 4.1 for location, CCol spans south of the seismic line presented on Fig. 4.6). Similarly to the he ECol-master fault, the CCol-master fault presents a steep geometry and detachment at a deep lithospheric level (~25 km).

Thick synrift seismic sequences (fault-bounded wedges with divergent reflectors towards the active fault) were interpreted for the Central and Eastern depocenters. Data quality in WCol did not allow synrift interpretation. A postrift package (reflectors passively onlapping the basement highs around the depocenters beyond the synrift-bounding faults) was also interpreted. In passive margin-related basins, the synrift-to-postrift unconformity typically marks the breakup event (Franke, 2013). The breakup unconformity (BU in Fig. 4.2) marks the onset of oceanic crust accretion and is interpreted in volcanic margins at the top of SDR wedges (Fig. 4.6). In the Colorado basin, however, a postrift package was identified between the top of the synrift (TSR2) and the breakup unconformity, tracked from the COT domain (Fig. 4.6).

The NE-NNE striking faults of FS3 are restricted to a strip covering the easternmost 100-200 km of the continental crust domain. They form half-grabens on the northern flank of the Tandilia high and are responsible for structuring the external high (EH), a block formed of continental crust that separates the ECol depocenter from the COT-SDR domain (Franke et al., 2006; Gerster et al., 2011; Fig. 4.1). For depocenters formed by FS3 faults, the BU is indeed the synrift-postrift unconformity (sensu Franke, 2013). Therefore we interpret this extensive event as being part of the South Atlantic opening and largely contemporaneous with the emplacement of SDRs further east (sensu Stica et al., 2014). FS3 faults may present extensional reactivation across the BU indicating extensional activity during and slightly after the breakup.

4.5 Discussion

Based on the data analyzed, and by integrating the relative chronology of faulting within the regional tectonic framework, we propose a model for basin evolution with three rifting stages (Fig. 4.7).

The final stage, Early Cretaceous rifting, is the best constrained in age as it is directly associated with SDR emplacement and breakup. Neither the SDRs nor the oceanic crust have

been drilled in this part of the South Atlantic. Plate kinematic models are useful to integrate data on both margins and are calibrated with oceanic crust magnetic anomalies (Moulin et al., 2010; Heine et al., 2013). SDRs have been drilled however, on the conjugate Namibian margin (Kudu well) and sedimentary packages interbedded with the volcanics were dated Barremian (McMillan, 1990). Faults grouped in FS3 are subparallel to the SDR wedges bounding reflectors and the COB and are restricted to the outer 100-200 km wide fringe of the continental crust domain (Fig. 4.7c). We interpret FS3 as genetically linked to the Early Cretaceous rifting stage, and their development in a narrow fringe as due to a concentration of strain around the incipient ridge. FS4 faults also developed as part of the Early Cretaceous rifting event, but associated with margin segmentation during SDR emplacement (see Franke, 2013).

However, the main rifting event for the area of study is older and is associated with FS2 faults forming the ECol and CCol depocenters in Colorado, and the adjacent Salado basins (Fig. 4.7b). From the presence of a thick postrift unit preserved in ECol (between TSR2 and BU, Fig. 4.2), we infer that thermal subsidence had already started before the Early Cretaceous breakup, confirming at least two independent rifting settings. We interpret Early-to-Mid Jurassic, largely oriented N-S extension for this event and correlate it with the Karoo rifting.

Cross cutting of FS1 faults by FS2 faults identified in the ECol and CCol depocenters point to the presence of a previously unknown rifting stage. We associate the NW-striking, S-SW dipping listric faults with the extensional reactivation of thrusts of the Permian to Early Triassic Ventania-Cape fold belt. Seven of these former thrusts were identified in the study area (Fig. 4.7a). Figure 4.8 is a seismic transect across the former Ventania-Cape fold belt in the Colorado basin area, formed by a combination of the seismic lines presented in figures 4.6 and 4.3. The detachment for FS1 faults follows the detachment of the former thrusts and shallows towards the NE, away from the Gondwanides orogen (Mosquera et al., 2011). Note the transection of the extensionally reactivated thrusts (FS1) with the master fault forming ECol (FS2) in the central area. A Late Triassic-Early Jurassic age for this initial rifting stage is interpreted by association with the Precuyano rifting event in the Neuquén basin (D'Elia et al., 2015) that has also been related to reactivation of Late Paleozoic structures (Mosquera and Ramos, 2006). FS1 faults do not seem to be present in the Salado basin area as this region was north of the area of influence or the Permian-Early Triassic Ventania-Cape fold belt.

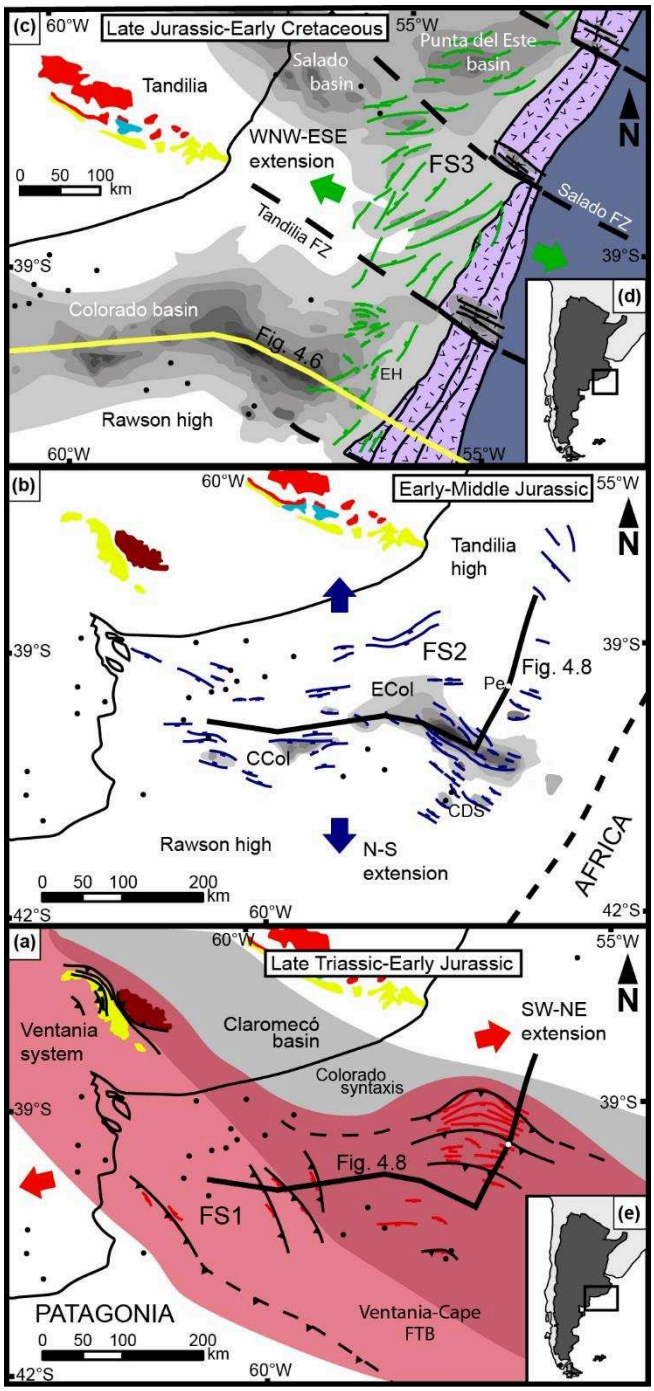

Figure 4.7: Tectonic evolution of the Colorado basin: a) Late Triassic-Early Jurassic rifting stage associated with FS1 faults, extensionally reactivated thrusts of the Late Permian-Early Triassic Ventania-Cape fold belt. Main reactivated thrusts are drawn in black; b) Main rifting stage (Early-Mid Jurassic) responsible for FS2 faults and the formation of the Colorado and Salado basins' main depocenters; c) Final rifting stage (Early Cretaceous) related to the South Atlantic breakup and emplacement of SDRs. FS3 faults are largely oriented NNE, parallel to the SDRs and COB; d) Location map for Fig. 4.7c; e) Location map for Fig. 4.7a and b.

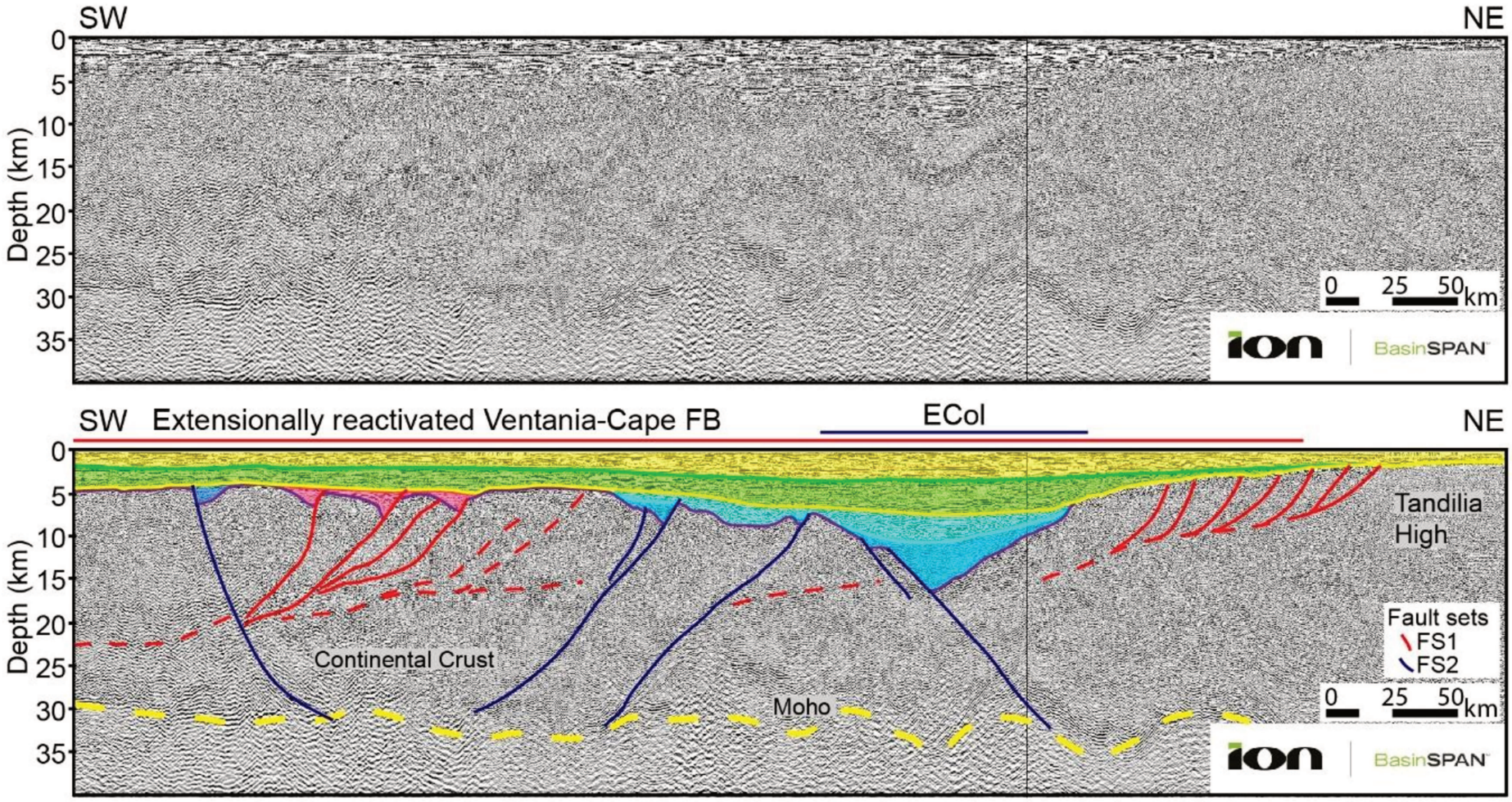

Figure 4.8: Depth-converted seismic transect across the Colorado basin. See location in Fig. 4.5b, formed by a combination of Figs. 4.3 and 4.6. Extensionally reactivated thrusts (FS1) form small half-grabens to the west (north of the CCol depocenter, see Fig. 4.1b) and tilted blocks on the northern flank of the ECol depocenter. The system is intersected by FS2 faults that detach at deeper levels (25-30 km), related to crustal thinning under Colorado basin depocenters.

The understanding of the complex rifting history of the southern South Atlantic segment is crucial to better model the conjugate margins. Most 2D models consider the Colorado main rifting even (Early-Mid Jurassic) as synchronous with SDR emplacement and the South Atlantic opening. We showed that it is not the case. Crustal thinning in the Colorado basin is oriented E-W, as a consequence of the Early-Mid Jurassic rifting related to N-S extension. Models attempting to explain this 3D complexity with a single event on 2D sections oversimplify the Gondwana breakup history along the Argentinean margin.

4.6 Conclusions

The identification of three rifting stages in the Colorado basin is key to understanding the complexity of long term continental breakup processes that affected the Paleozoic supercontinents. A previously unknown rifting stage was identified. Extensional reactivation of Late Paleozoic-Early Triassic thrusts of the Ventania-Cape Fold Belt was produced in Late Triassic-Early Jurassic times. A second rifting stage was responsible for the main depocenters of the Colorado and Salado basins. Faults associated with this stage cross cut older faults and are largely oriented E-W to SE-NW. An Early-Mid Jurassic age was assigned to this stage, in agreement with the Karoo rifting and the N-S extension responsible that ended with the opening of the Weddell Sea. The area went into a final rifting stage in the Latest Jurassic-Early Cretaceous. With extension oriented WNW-ESE, faults developed in the outer 100-200 km wide fringe parallel to the NNE-striking COB. This final rifting stage involved the emplacement of SDRs and produced the opening of the South Atlantic Ocean.

Chapter 5: Rifting evolution of the Malvinas basin, Offshore Argentina: new constrains from zircon U–Pb geochronology and seismic characterization

This chapter includes new insights in the understanding of the rifting in the Malvinas basin that have been obtained from seismic interpretation in collaboration with my colleagues at YPF SA. Moreover, two U-Pb zircon ages for the synrift and prerift units are presented, obtained in collaboration with M. Naipauer (UBA) and V.A. Valencia (Washington State University). The content of this chapter has been submitted for publication in the Journal of South American Earth Sciences, in a special number on Patagonian basins (Authors: Lovecchio, J.P.; Naipauer, M.; Cayo, E.; Rohais, S.; Ramos, V.A.; Giunta, D.; Gerster, R.; Bolatti, N.; Joseph, P.; Valencia, V.A.).

5.1 Abstract

The Malvinas basin, emplaced in southern South America, is an asymmetrical extensional basin affected by NNW-striking faults. In this contribution we present a review and updated structural framework for the Malvinas basin, as well as two new U-Pb zircon ages for the prerift and synrift series. A volcanic breccia within the prerift section, in the Río Chico High area, yielded a Late Triassic crystallization age (215 Ma, U-Pb in zircon), which is the first

Triassic age in the basin and was correlated with the El Tranquilo basin in the Deseado Massif. The synrift Serie Tobífera unit had been correlated to the Middle Jurassic Chon Aike large igneous province. We present the first U-Pb zircon age for Serie Tobífera in the Malvinas basin that confirms this interpretation. A tuff level within this unit yielded a crystallization age of 169 Ma (U-Pb in zircon). The synextensional emplacement of the retroarc Chon Aike Magmatic Province is associated with trenchward migration of the coetaneous volcanic arc (Pankhurst et al., 2000; Rapela et al., 2005). We propose the existence of a vertical slab tear towards the south of the Malvinas basin, and between the South American and Antarctic blocks to explain the rotational extension observed in the Chon Aike structural fabric at continental plate-scale. This slab tear would have initiated in the latest Triassic and it is believed to be active during the Early-Mid Jurassic. Differential slab roll-back of the subducting plate below Patagonia (Mpodozis and Ramos, 2008; Echaurren et al., 2017) would have been produced by this tear, inducing the rotational extension observed for the Chon Aike Magmatic Province and related volcanism. The slab tear model is a new alternative explanation to the origin of Weddell Sea. Once Eastern Antarctica was detached from Africa with the opening of the Mozambique channel, the thermal anomaly produced by an asthenospheric window opened by the slab tear would have triggered the opening of an oceanic basin between Eastern and Western Gondwana.

5.2 Introduction

The Malvinas basin originated as an extensional basin located at the southern edge of the South American plate, offshore southern Patagonia, on the Argentinean shelf (Ludwig et al., 1968). The basin displays a triangular shape, extending for about 500 km along the NNW-oriented basin axis, and approximately 400 km in the E-W direction in the widest segment towards the south (Fig. 5.1). The basin is bounded to the northwest by the Río Chico high (Dungeness arch) that separates the Malvinas from the Austral (Magallanes) basin to the west. To the east, the basin is limited by the Malvinas (Falkland) Islands High. An active margin is the natural basin boundary towards the south, characterized by the development of a submerged fold-and-thrust belt formed by N-S oriented compression since the Latest Cretaceous, and Neogene left-lateral strike-slip between the South American and Scotia plates (Galeazzi, 1998; Raggio et al., 2011b).

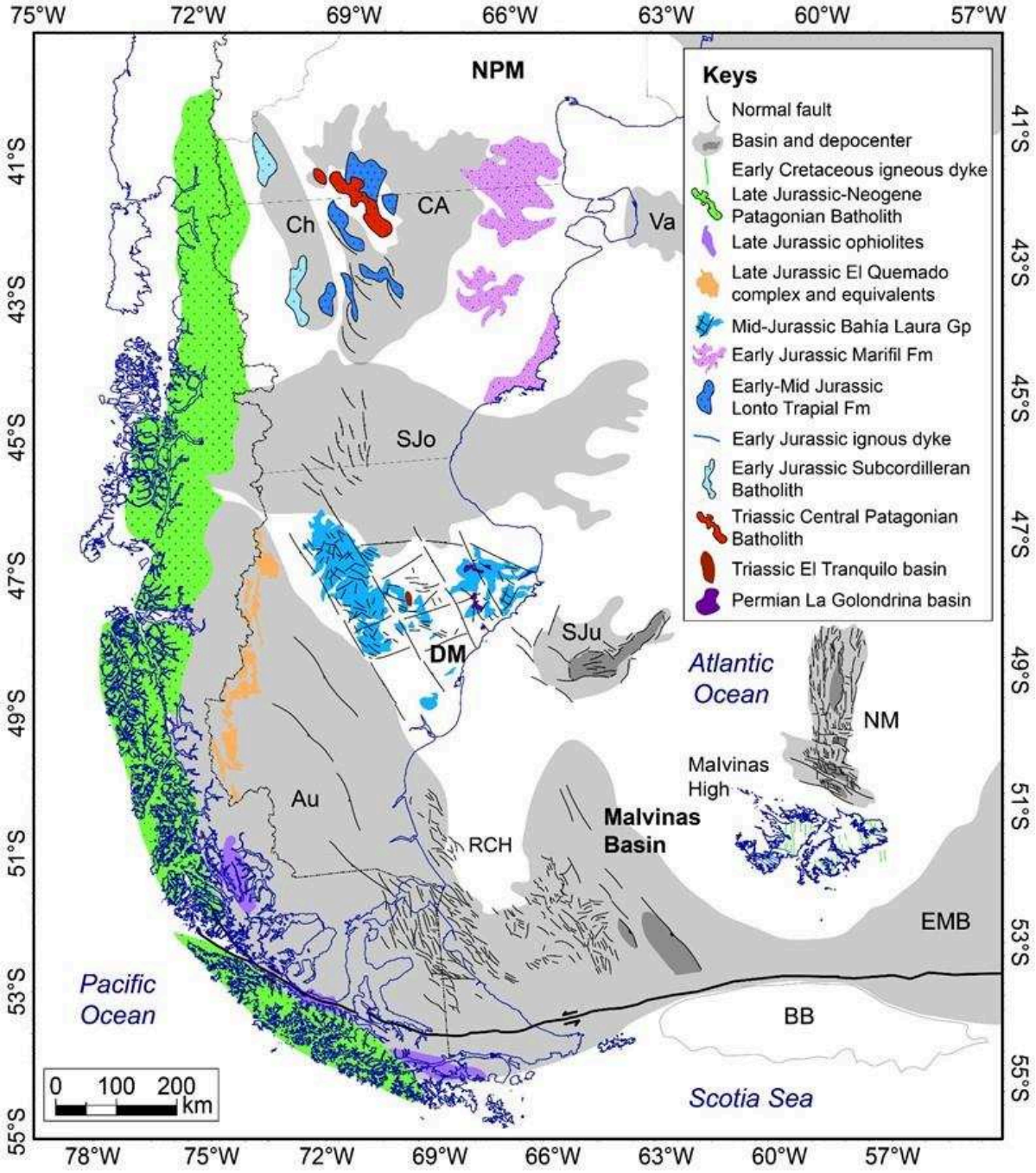

Figure 5.1: Mesozoic basins of Patagonia. Note the emplacement of the Malvinas basin bounded by the Río Chico High (RCH) to the northwest, the Malvinas High to the northeast and the transform plate boundary to the south. Other Mesozoic basins are illustrated: Austral/Magallanes basin (Au), North Malvinas (Falkland) basin, San Julián (SJu), San Jorge Gulf basin (SJo), Liassic Chubut basin (Ch), Cañadón Asfalto (CA), Valdés (Va). In northern Patagonia, the North Patagonian Massif (NPM) hosts Paleozoic rocks and a Mesozoic volcanic cover, with Mesozoic batholiths to west related to ancient volcanic arcs. Further south, the Deseado Massif (DM) hosts Permian and Triassic deposits and a Jurassic volcanic cover. Note the development of the ophiolitic complexes of the Rocas Verdes basin in the SW Austral basin (after Echaurren et al., 2017; Figari et al., 2015; Galeazzi, 1998; Lohr and Underhill, 2015; Malkowski et al., 2015; Micucci et al., 2011; Panza and Haller, 2002; Ramos, 2002).

The Malvinas basin evolution is known from seismic data interpretation and hydrocarbon exploration drilling. The basin evolved through three main tectonic phases: rift, sag and foredeep (Galeazzi, 1998). Rifting chronology is poorly constrained. The basin's main depocenter, a half-graben formed by a NNW-striking westerly-dipping fault, located towards the southeast of the basin (Fig. 5.1), remains undrilled. In the past, the age of rifting has been inferred from correlation with the neighboring Austral (Magallanes) basin. In both basins synrift infill is referred to as Serie Tobífera (Thomas, 1949), a subsurface equivalent of the Chon Aike Magmatic province (Kay et al., 1989; Pankhurst et al., 2000) and assigned to the Middle Jurassic. Hydrocarbon exploration was carried out in the basin since the late 1970's. Most wells were drilled at shallow water depths, on structural highs on the platform towards the Río Chico High. The synrift intervals investigated by those wells are very limited, and represented by volcanic facies. In this contribution we present a regional structural framework for the Malvinas basin's depocenters, seismic characterization of their infill, the first absolute U-Pb zircon ages to constrain a new rifting evolution model.

5.3 Geological Framework

The amalgamation of Gondwana ended in the Late Paleozoic with the accretion of Patagonia on the SW-margin (Ramos, 2008). The SW margin experienced intermittent subduction as evidenced by the presence of a Late Triassic, Early Jurassic, and Cretaceous migrating volcanic arc (Echaurren et al., 2017). Throughout the Mesozoic, the margin also went through generalized extension probably related to the western subduction dynamics, a process that ended with the breakup of the Gondwana supercontinent in the Early Cretaceous (Macdonald et al., 2003; Frizon De Lamotte et al., 2015).

The prerift units were described in the periphery of the basin. The oldest basement rocks in the area crop out in the Malvinas (Falkland) islands. The Cape Meredith Complex (Adie, 1952; Cingolani and Varela, 1976) is composed of Grenvillian granitic gneisses and amphibolites with ages of 1067±9 Ma (U-Pb in zircon; Jacobs et al., 1999). The complex is intruded by Neoproterozoic to Cambrian lamprophyre dykes (Thomas et al., 1998). A Paleozoic cover composed of Siluro-Devonian to Permian siliciclastic rocks is overlying the basement present exposed in the Malvinas islands. The sedimentary section starts with a basal conglomerate followed by a cross-bedded, coarse-grained, sandy succession of the Port Stephens Fm, followed by a marine transgression recorded by the Fox Bay Fm and the sandy

units assigned to the Port Philomel and Port Stanley Fms, that yielded Late Devonian palynomorphs (Marshall, 1994a). The Devonian succession is overlaid by the Permian Lafonia Group, that records the Gondwanan glaciation in a glacio-marine environment. The Paleozoic cover is intruded by at least two sets of Mesozoic igneous dykes (Fig. 5.1). A first set of WNW-oriented dykes, abundant in the southern Gran Malvina Island (West Falkland) yielded Early Jurassic ages (Cingolani and Varela, 1976). A second set of dykes, oriented N-S and more sparsely distributed, was described in northern Gran Malvina (West Falkland) and in Soledad (East Falkland) islands. Early Cretaceous (Valanginian-Hauterivian) ages have been determined for N-S oriented dykes (Hole et al., 2015; Richards et al., 2013; Stone et al., 2008). These two main directions of dykes of different age, were interpreted by Ramos et al. (2017) to indicate a change in the regional stress field and were correlated to the two rifting stages identified in the North Malvinas basin (N. Falkland, Brandsen et al., 1999). In the North Malvinas basin, a first set of WNW-oriented faults forming half-grabens in the southern rift are transected by the N-S oriented faults related to the Early Cretaceous half-grabens of the northern rift (Lohr and Underhill, 2015).

The Río Chico High (also known as Dungeness Arch) is the southern extension of the Deseado Massif and forms a southerly-plunging structural ridge that separates Malvinas from the Austral basin to the west (Fig. 5.1). The Río Chico high has been the locus of hydrocarbon exploration since the 1980's, with several discoveries on its western flank in the Austral basin (Arbe and Fernandez Bell Fano, 2002). Many of these wells penetrated granitic rocks forming the basement, but absolute ages for basement on the ridge were not available. Onshore, the basement of the southern Austral basin is given by the Tierra del Fuego Igneous and Metamorphic Complex. Hervé et al. (2010) obtained Cambrian crystallization ages (525-540 Ma, U-Pb SHRIMP on zircon) for the gneisses-granites within the basement rocks. These rocks also display high-grade metamorphism, which has been dated Permian (~270 Ma, Hervé et al., 2010).

The Deseado Massif displays a Neoproterozoic to Cambrian igneous-metamorphic basement. Two units were differentiated (Giacosa et al., 2002): the Río Deseado Complex (Viera and Pezzuchi, 1976) with low-to-medium grade metamorphic rocks intruded by Devonian granites (Chebli et al., 1976; Pankhurst et al., 2003) and Early Jurassic dykes; and the low-grade metamorphic rocks of La Modesta Fm, with a maximum Early Silurian age of sedimentation (446 ± 6 Ma; U-Pb detrital zircon; Moreira et al., 2013).

Overlying the basement, the fluvial deposits of La Golondrina Fm represent a rift basin infill (Ramos and Palma, 1996). Although Bellosi and Jalfin (1989) interpreted La Golondrina basin in an intra-arc setting, the retroarc basin setting proposed by Uliana et al. (1985) is followed in this work due to the geodynamic framework and the lack of Triassic volcanism to the east of this location. A Late Triassic cycle of alluvial plain sands and shales rich in palaeoflora (El Tranquilo Gr, Haller, 2002), was interpreted as a reactivation of the Late Permian rift. According to Giacosa (1998), brownish crystalline tuffs are interbedded with conglomerates towards the base of the sequence, but these rocks have not been dated. The Permo-Triassic succession is intruded by the La Leona Fm granite dated Latest Triassic (203±2 Ma and 202±2 Ma; Rb-Sr by Pankhurst et al., 1993) to Early Jurassic (198±3 Ma, Rb-Sr by Varela et al., 1992; 191±10 Ma, K-Ar in biotite; Chebli et al., 1976). Outcrops of Permian and Triassic rocks are scarce and only a few outcrops are known across the area (Fig. 5.1). Most of the Deseado Massif is covered by a Middle-Late Jurassic volcanic field (Fig. 5.1), referred to as the Bahía Laura Group (and equivalents), forming the Chon Aike Magmatic Province (Pankhurst et al., 2000; Panza and Haller, 2002; Fig. 5.2). The synextensional emplacement of the bimodal volcanism of the Chon Aike province in a retroarc setting was suggested by Uliana et al. (1985). Rapela et al. (2005) confirmed the coeval development of the Chon Aike magmatism with arc activity to the west, represented by the Subcordilleran Batholith, an elongated batholith oriented NNW cropping out in the North Patagonian Massif (Fig. 5.1). Depocenters filled with volcanic and volcaniclastic rocks of the Chon Aike province are usually related to NNW-trending faults (Gust et al., 1985). Another observation of Uliana et al. (1985) was the trench-ward migration of the Mid-Late Jurassic magmatic province, a process that ended with the opening of the Rocas Verdes back-arc in the Late Jurassic (Dalziel, 1981). Uliana et al. (1985) linked this extension with subducting slab-deepening during the Jurassic. Mpodozis and Ramos (2008), and more recently Echaurren et al. (2017), related the trenchward arc migration from the Early Jurassic Subcordilleran Batholoith position to differential slab rollback (a non-cylindrical slab rollback, accentuated towards the southern end). This mechanism also explains the development of the Cañadón Asfalto and Liassic Chubut basins in a migrating retroarc setting (see Fig. 5.1, Suárez and Márquez, 2007). Echaurren et al. (2017) suggest slab steepening in the Late Jurassic as the process responsible for continuous trenchward migration of the locus of volcanism in northern Patagonia to the north-south oriented Patagonian Batholith (Fig. 5.1). An older batholith is also present in the Northern Patagonian Massif, the Central Patagonian Batholith (CPB, Fig. 5.1; Rapela et al., 2005). The

CPB was emplaced in the Late Triassic (200-224 Ma, Rapela et al., 2005), in a NW direction and has been associated with an extensional setting (Kay, 1993).

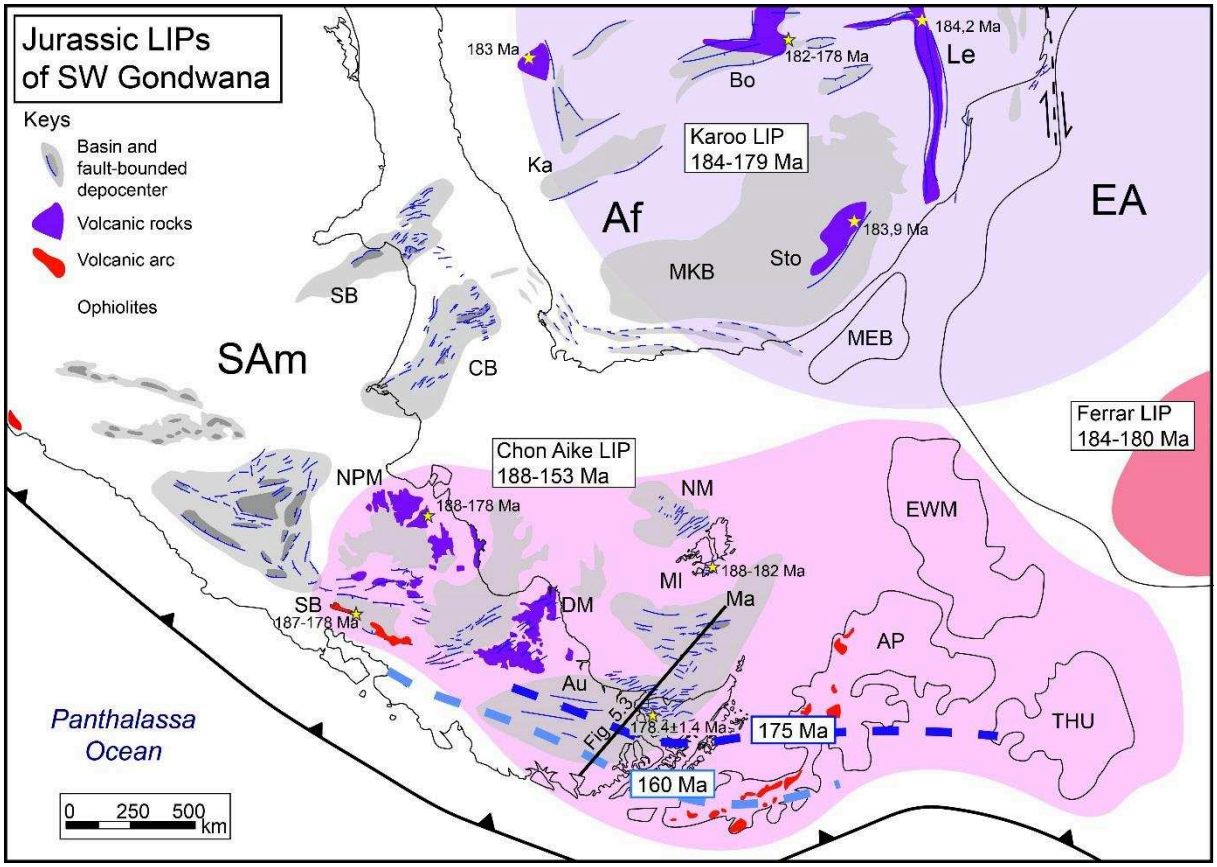

Figure 5.2: Jurassic Large Igneous Provinces of SW Gondwana (after Kay et al., 1989; Pankhurst et al., 2000; Rapela et al., 2005; Uliana et al., 1989, 1985; Vergani et al., 1995; Jourdan et al., 2005; Storey et al., 1992). Note the occurrence of the Karoo LIP in southern Africa (Af) and East Antarctica (EA), the approximately synchronous Ferrar LIP in Antarctica, and the Chon Aike silicic Magmatic Province in southern South America (SAm) and the Antarctic territories (Antarctic Peninsula: AP; Ellsworth-Whitmore mountains, EWM; and Thurston island, THU). Note the trenchward diachronism of the Chon Aike volcanism from Early to Late Jurassic indicated by the dotted lines. The location of the chart presented in Fig. 5.3 is indicated.

The Serie Tobífera represents the subsurface equivalent of the Large Igneous Chon Aike Magmatic Province (MP; Kay et al., 1989). Serie Tobífera particularly corresponds to the main synrift infill (penetrated so far by hydrocarbon exploration wells) for the Malvinas and Austral/Magallanes basins. In Malvinas it has not been dated. But some absolute ages of Serie Tobífera and equivalents have been presented by Pankhurst et al. (2000) for the Austral basin and for Chon Aike outcrops in Patagonia. An Early Jurassic U-Pb age (SHRIMP) of 178.4±1.4 Ma (Toarcian; Pankhurst et al., 2000) was obtained for the Serie Tobífera in the La Gaviota borehole (Fig. 5.2). A Late Jurassic U-PB age (SHRIMP) of 154.5 ± 1.4 Ma (Pankhurst et al.,

2000), was obtained for outcrop rocks of El Quemado Complex (a late Chon Aike representative from the Southern Patagonian Cordillera). Late Jurassic rifting seems to be restricted to the western sector of the Austral basin and crops out in the Southern Patagonia Cordillera. Within the western Austral basin, rifting and volcanism display a south-to-north diachronous behavior. Malkowski et al. (2015) present an acknowledgeable review of the rifting diachronism, with initiation of rift volcanism earlier in the south, successive onset of bimodal volcanism and finally opening of the Rocas Verdes marginal basin (Dalziel, 1981) in the Late Jurassic. The Malvinas basin seems to have already been in a thermal sag phase during the Late Jurassic, while the lack of deposits in the eastern Austral basin (western flank of the Río Chico High) are interpreted as a product of uplift and erosion. Figure 5.3 presents a chronostratigraphic chart to illustrate the diachronous rifting evolution from east to west in the Malvinas and Austral basins, and in the Rocas Verdes Late Jurassic Marginal basin.

The Springhill (Thomas, 1949) records a major transgression that flooded the Austral and the Malvinas basins during the sag phase. The Springhill Fm marks the base of the sag phase, as it usually overlies the synrift Serie Tobífera or the igneous-metamorphic basement. The transgression took place in several pulses, which are recorded in the Austral/Magallanes and Malvinas basins as several sedimentary cycles.

In the Malvinas basin, the Springhill flooding seems to have started in the Late Jurassic (Galeazzi, 1998), but as the main depocenters (where the oldest post-rift transgressive units are expected) remain underexplored, the onset of the thermal sag phase in the Malvinas basin could be as old as Mid-Jurassic (Fig. 5.3). The marine flooding that deposited the Springhill Fm entered the Malvinas basin from the south (main depocenter) and progressively transgressed over the Río Chico High to the NW and the Malvinas (Falkland) islands high to the NE.

In the Austral basin, particularly, the paleogeography associated with the Springhill Fm, typically of Early Cretaceous age, is characterized by structurally-controlled paleovalleys and depositional paleohighs (Schwarz et al., 2011). The older fluvio-estuarine cycles of the Springhill Fm (the Early Cretaceous Hydra cycle, Arbe and Fernandez Bell Fano, 2002) are preserved only in the paleovalleys and are absent on the paleohighs. The synrift depocenters seem to have exerted some control on the paleovalley distribution. The later Springhill cycles progressively cover the paleorelief (Fig. 5.3). The Rio Chico High was also progressively flooded, and by the Aptian it was almost fully covered.

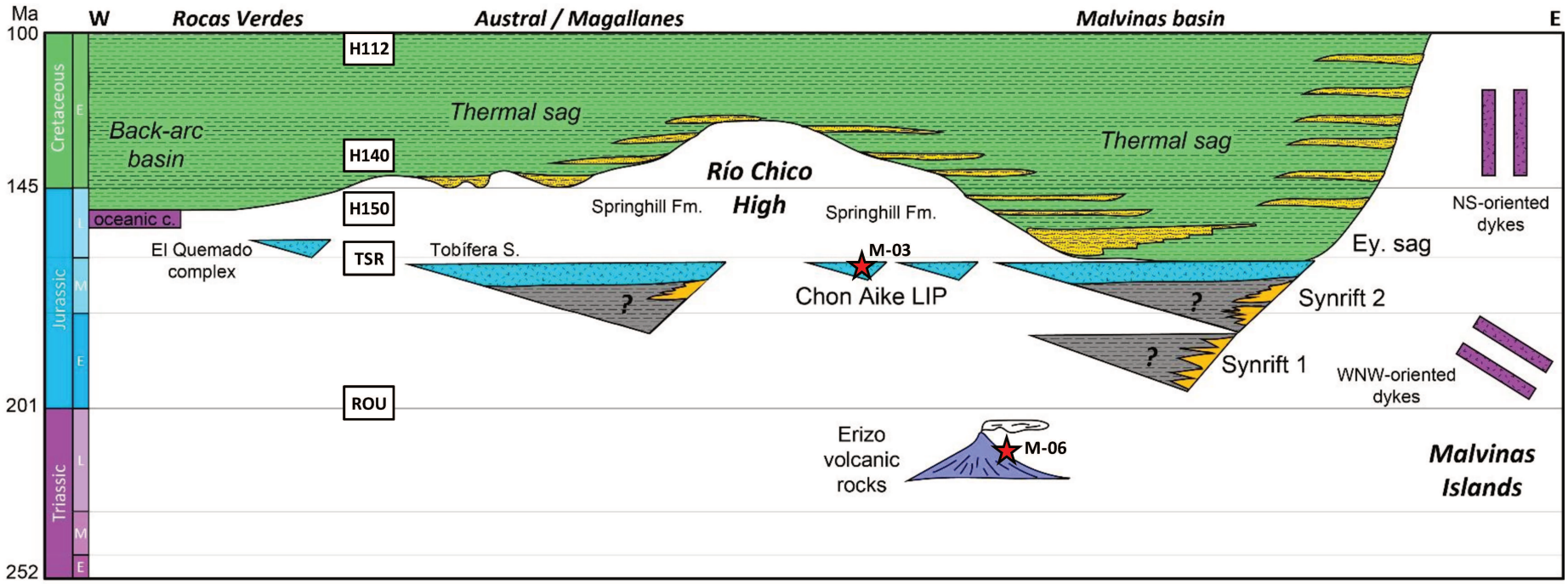

Figure 5.333: Schematic chronostratigraphic charts for the Triassic-to-Early Cretaceous time interval across the Rocas Verdes, Austral and Malvinas basins. The age of the intrusive igneous dykes of the Malvinas (Falkland) islands is indicated (ages after Ramos et al., 2017; and references therein). Note the interpreted rifting diachronism from east to west, with opening of the Rocas Verdes marginal basin in the Late Jurassic. Note also the diachronism of the Springhill Fm transgression successively covering the Río Chico High by the end of the Neocomian. The approximate location of samples M-03 and M-06 is shown with red stars.

Since at least the Cenomanian, the Austral basin entered in a Foreland tectonic phase, associated with subduction from the west, while the Malvinas basin continued under a thermal sag until the latest Cretaceous, when compression from the south produced tilting of the basin and the onset of a foreland tectonic phase.

5.4 Materials and Methods

A dataset for the Malvinas basin, composed of 2D TWT multi-channel seismic data and 20 hydrocarbon exploration wells, was made available by YPF SA. Seismic transects were prepared by connecting several seismic lines of different surveys. The main horizons associated with seismic stratigraphic surfaces were interpreted on the transects. A blend of amplitude and tecVA attribute (Bulhoes and Nogueira de Amorim, 2005) was generated to highlight structural features. Structural maps for the main horizons were prepared. We had access to well data, such as well reports, electric logs, mud logs, etc. and prepared well correlations.

Two rock samples were recovered from exploration well cores, one from the Erizo.x-1 well and one from the Calamar.x-1 well (Fig. 5.6). The Erizo.x-1 sample (M-06, Fig. 5.4a) is a volcanic breccia recovered from the prerift unit (1971,6-1971,8 m MD, measured depth). A thin-section microphotography is presented in Fig. 5.5. The sample from the Calamar.x-1 well (M-03), was obtained from a tuff level at the top of the synrift unit (1779,6 m MD, just below the synrift-postrift unconformity, Fig. 5.4b) and was used to constrain the crystallization age of the Serie Tobífera. Core samples weighted 2.280 Kg (M-06) and 1.779 Kg. (M-03). Zircon grains were concentrated and separated using standard preparation methods at the La.Te.Andes laboratory (Salta, Argentina). Final grains selection of the zircon populations for U-Pb analysis was undertaken by hand-picking using a binocular microscope at the laboratory of IDEAN (UBA-CONICET). Zircons in this study were analyzed for their U-Pb age at the Radiogenic Isotope and Geochronology Lab (RIGL) at Washington State University. Analytical methods and U-Pb (LA-MC-ICP-MS) age measurements of zircons are available in the Supplementary Material.

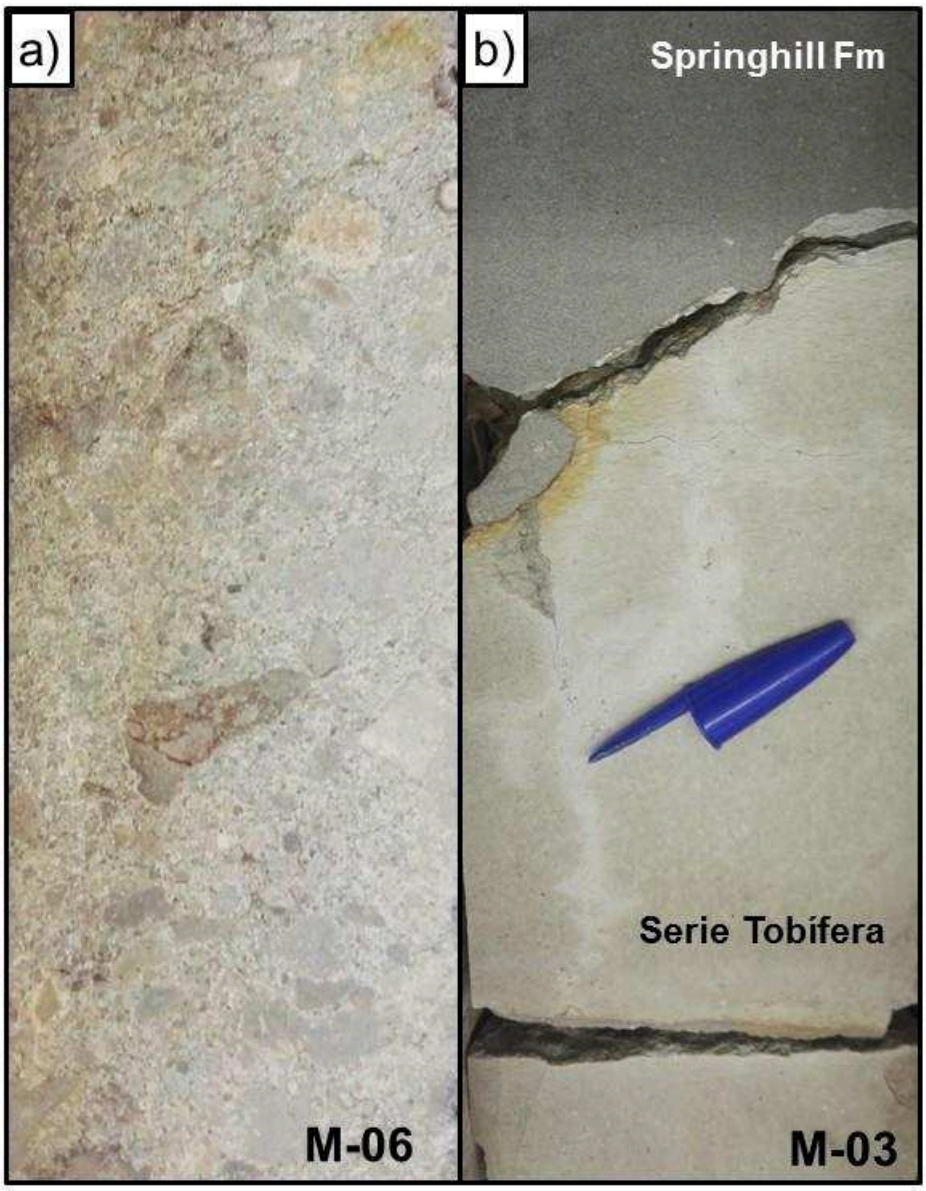

Figure 5.4: Core photos of the samples analyzed in the study: a) Sample M-06: a volcanic breccia sampled from the Erizo.x-1 well; b) Basal contact of the Springhill Fm (post-rift) overlying the Serie Tobífera, from which Sample M-03 was recovered.

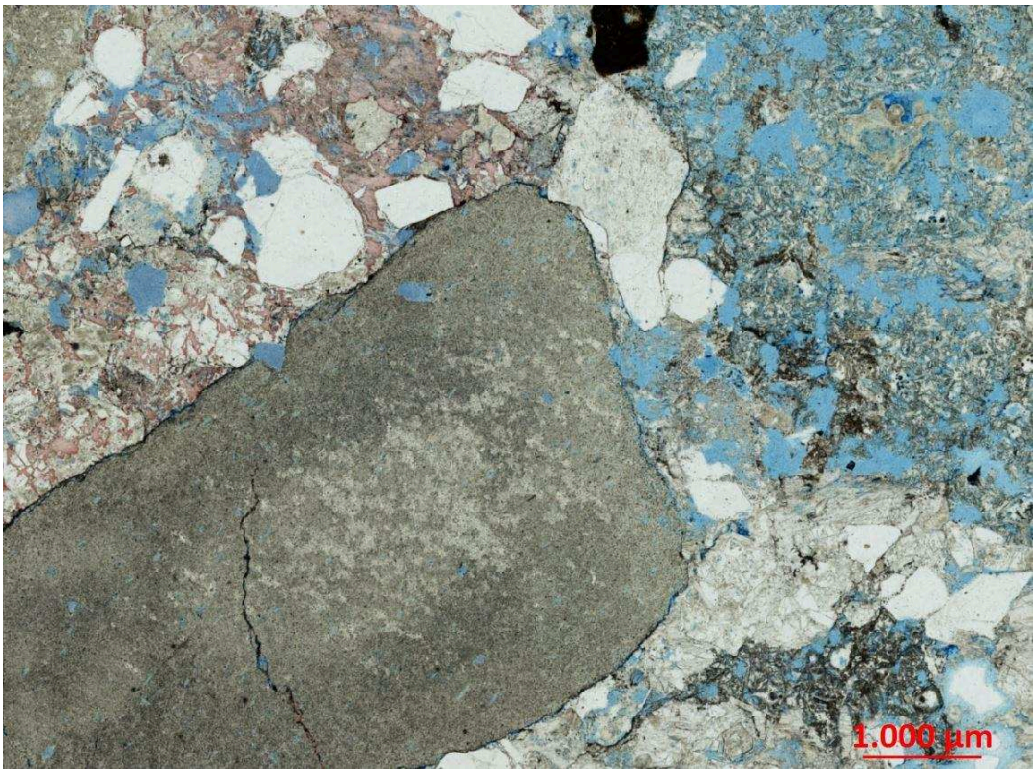

Figure 5.5: Thin section microphotography of the volcanic breccia of sample M-06. Note the large sub-rounded tuff clasts and the smaller sub-angular Quartz in a partially dissolved cemented tuffaceous matrix. Pink indicates Calcite, while light blue indicates porosity.

5.5 Results

5.5.1 Seismic characterization

A structural map for the Top Prerift is presented in figure 5.6. This surface corresponds to the unconformity at the base of the synrift unit, also referred to as ROU (Rift Onset Unconformity, sensu Franke, 2013). It represents the top of either the Precambrian/Paleozoic igneous-metamorphic basement, or any other unit deposited in the study area before the onset of rifting (e.g. Paleozoic series of the Malvinas Islands). The synrift units are detected on seismic data as wedges of fault-bounded sedimentary or volcano-sedimentary sequences. The map presented in figure 5.6 shows the development of the main depocenter asymmetrically displaced towards the southeast of the Malvinas basin. Baristeas et al. (2013) obtained a similar structural map for the top basement but did not map the faults. The main depocenter, known as Central Graben is in fact a half-graben extensional basin bounded to the NE, by a SW-dipping master normal fault (Figs. 5.6, and 5.7). Minor NE-dipping faults on the SW-flank give the apparent configuration of a graben and thus its name.

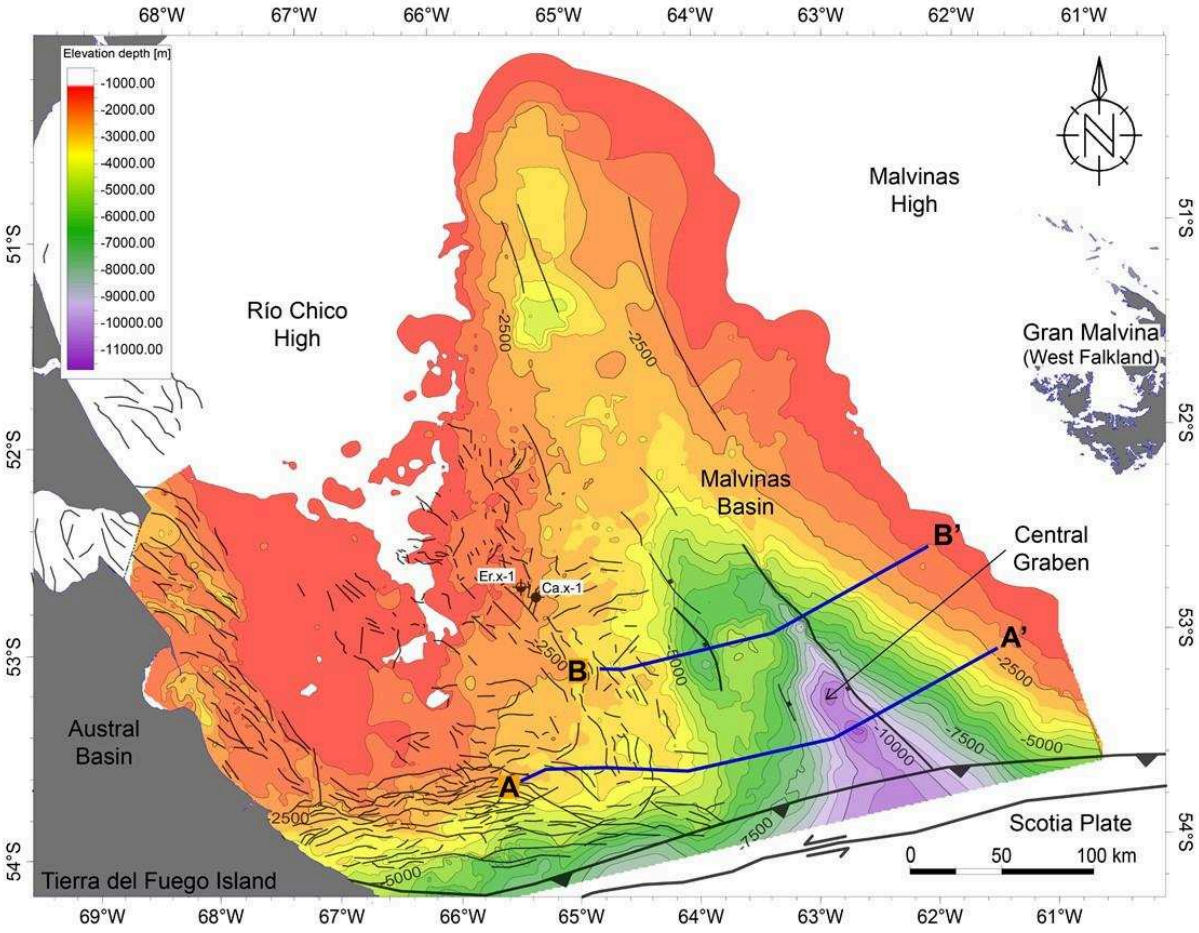

Figure 5.6: Depth structure map at the Top Prerift for the Malvinas basin, Río Chico High and the eastern Austral basin. The main depocenter of the Malvinas basin, the Central Graben, is displaced to the southeast. The main rifting-related faults are oriented NNW. Towards the south, the presence of near E-W oriented faults is due to deformation related to the Latest Cretaceous-Cenozoic compression from the south. Note the location of the present-day orogenic front (northern limit of the fold-and-thrust belt). The location of the studied wells and the transects of Figs. 5.7 and 5.8 are indicated.

The main direction of faults-strike associated with rifting is NNW, similarly to other Jurassic depocenters in Patagonia (Uliana et al., 1985). Half-grabens bracket both flanks of the Río Chico High (Fig. 5.6). As detected in several exploration wells and interpreted in seismic data, the Río Chico High itself is structured by NNW-trending faults, and presents a high degree of exhumation. Basement or relict Serie Tobífera deposits are preserved below the synrift to postrift unconformity and the transgressive Springhill Fm (Galeazzi, 1998). The southern flank of the Río Chico High is characterized by the development of E-W trending normal faults, associated with the flexural bending of the south American plate due to the onset of compression from the south (sensu Bry et al., 2004).

Two seismic sections were selected to illustrate the rifting structure of the Malvinas basin. Figure 5.7 is a seismic transect (transect A-A') located in the southern part of the basin (see Fig. 5.6), showing the deepest depocenter, known as the Central Graben. Figure 5.8 displays seismic transect B-B', located to the north of transect A-A', where the entire succession can be described, across the Central graben and the second deepest depocenter, these two main depocenters being separated by the Bouchard structural high.

The lowermost section is interpreted as the acoustic basement, represented by chaotic reflectors together with reflection-free zones, affected by normal faulting during rifting. Occasional continuous reflectors below Top Prerift (e.g. under the main depocenter) are interpreted as prerift Paleozoic sedimentary layers. The evolution of the Central Graben is controlled by a major normal fault to the northeast, and numerous minor faults affecting the synrift unit, defined between the ROU horizon (Top pre-rift/basement) and the TSR horizon (Top Synrift). The filling of this interval is recognized by weak and discontinuous reflectors, changing abruptly in the middle-upper section to a more continuous pattern, characterized by high amplitude, parallel and occasionally oblique reflections. Although the Central Graben remains undrilled, this section is interpreted to be formed of principally of sedimentary deposits.

The TSR horizon marks the synrift to postrift unconformity and the onset of the thermal sag phase. The unit between TSR and the H150 horizon is referred to as the Early sag. This unit is characterized by continuous and high-amplitude reflectors, filling the depocenters and progressively onlapping the lateral paleohighs towards the borders of the basin. The sequence is interpreted as a lacustrine succession (possibly containing marine flooding events), interbedded with eventual tuffaceous layers.

The H140 horizon (near Top Jurassic) is a strong and continuous positive reflector. This event it is mainly an unconformity that becomes sub-conformable towards to the depocenters. On the Río Chico High, this horizon coincides with the synrift-postrift unconformity between Serie Tobífera and the Springhill Fm (e.g. well Calamar, Fig. 5.4b). Strong and continuous reflectors follow the H140 horizon, mostly parallel to subparallel in character, and occasionally progradational. The Aptian maximum flooding surface can be recognized and interpreted on seismic data (H112 horizon). This horizon marks the flooding of the Río Chico High (Fig. 5.3). The basin remains under marine conditions and thermal subsidence until the near top Cretaceous, marked by the BTc horizon (Base Tertiary). The main extensional faults affecting the Jurassic-Cretaceous succession usually end below the BTc horizon.

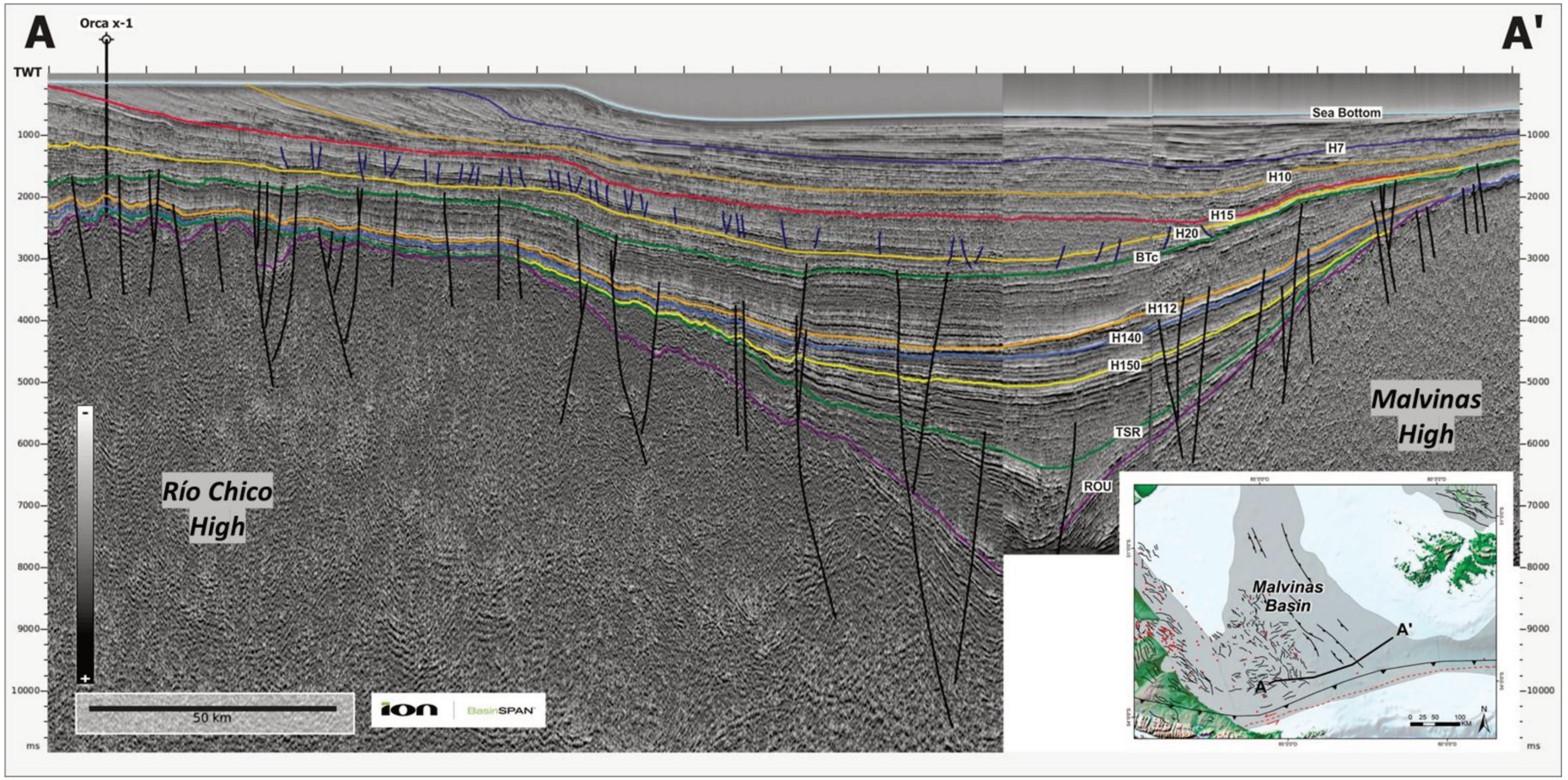

Figure 5.7: Seismic transect AA' (TWT) across the Central Graben of the Malvinas basin. Note the occurrence of a thick synrift wedge, interpreted to be bounded to the NE by a SW-dipping normal fault (not seen due to short seismic recording time).

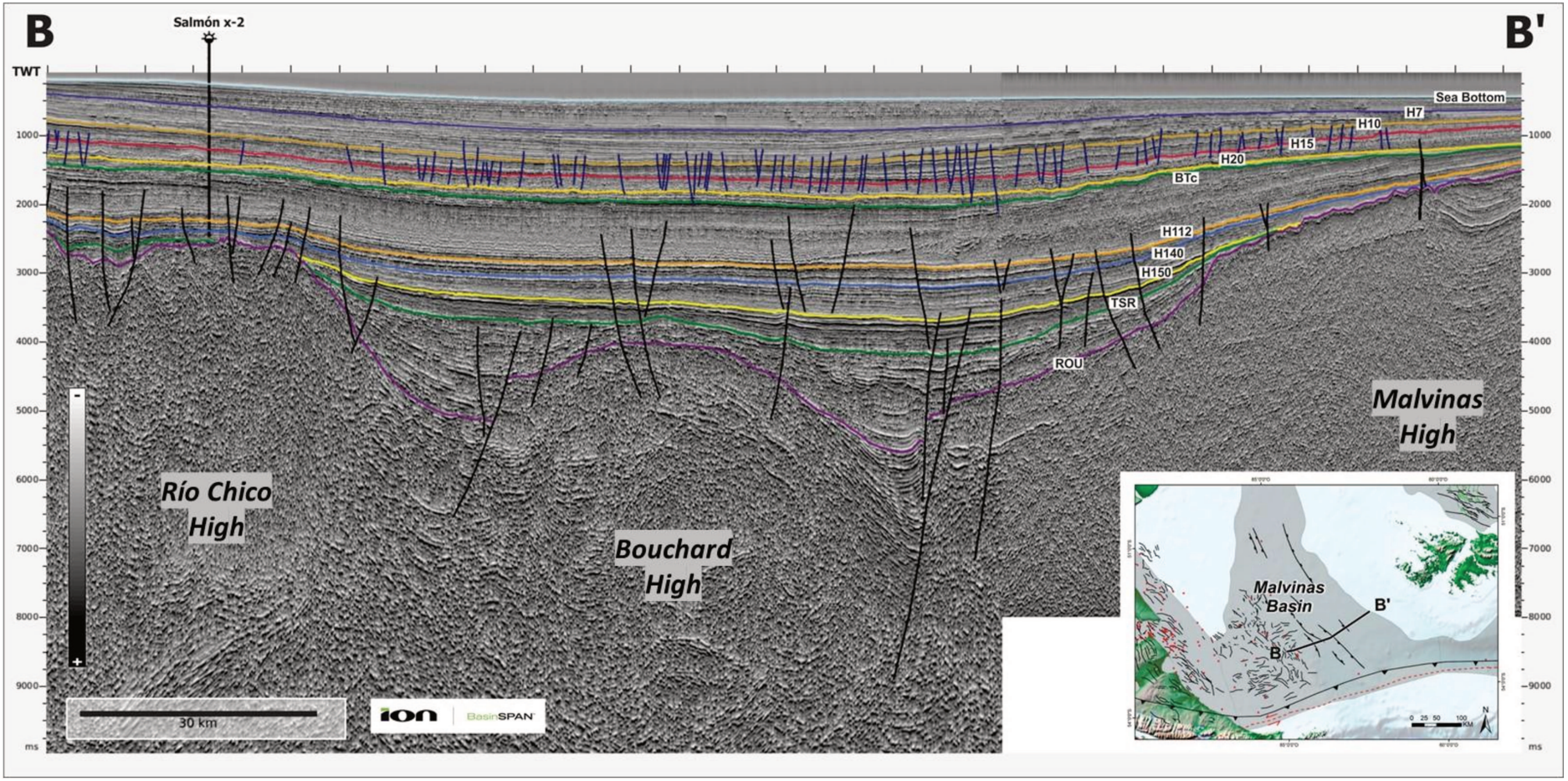

Figure 5.8: Seismic transect BB' (TWT) across the Malvinas basin. Note the occurrence of two half-grabens. The one on the right-hand side (East) is the central graben illustrated in Fig. 5.7 at a northern location. The half-graben on the left-hand side is another depocenter. Both half-grabens are separated by the Bouchard structural high.

The Cenozoic deposits correspond to the N-S oriented foreland basin (near orthogonal to the rifting direction and to the orientation of Transects A-A' and B-B'. Horizons: H20, H15, H10, H7 and Sea Bottom indicate different markers across the Cenozoic succession. Some polygonal extensional faults can be interpreted affecting the Tertiary cover, mainly the BTc-H15 sequence in the basin center (Fig. 5.7).

5.5.2 Zircon description and U-Pb geochronology

5.5.2.1 Zircon morphology analysis

Morphological analysis of zircon grains was conducted under binocular and cathodoluminescence images. Morphological populations were identified based on color, size, shape, habit, and elongation; the presence of internal cores, fractures, and inclusions was also recorded. Representative grains from the main morphological groups are shown in figures 5.9a and 5.9b.

In sample M-06 most of the separated zircons, approximately 300, are characterized by prismatic habit with elongations between 3 and 4 and idiomorphic form. They are mostly transparent or pink in color. Pyramidal faces are preserved and abundant inclusions were observed. A subordinate population of crystals presented long prismatic habit with elongation > 5 and idiomorphic shape indicating a volcanic origin (Figure 5.9a). Most of the grains from sample M-06 have, in the cathodoluminescence (CL) images, oscillatory zoning typical of plutonic and/or volcanic zircons.

Two hundred and fifty (250) zircon grains were separated from the sample M-03. Crystals present a long prismatic habit (elongation > 5) and idiomorphic form. Zircon grains are transparent, have many long inclusions and some of them present bi-pyramidal crystal face that indicate a possible volcanic origin. A minor amount of crystals presented short prismatic habit (elongation 2-3) and idiomorphic form (Figure 5.9b). The CL images show crystal with internal textures characterized by oscillatory zonation indicating a magmatic origin (Fig. 5.9b).

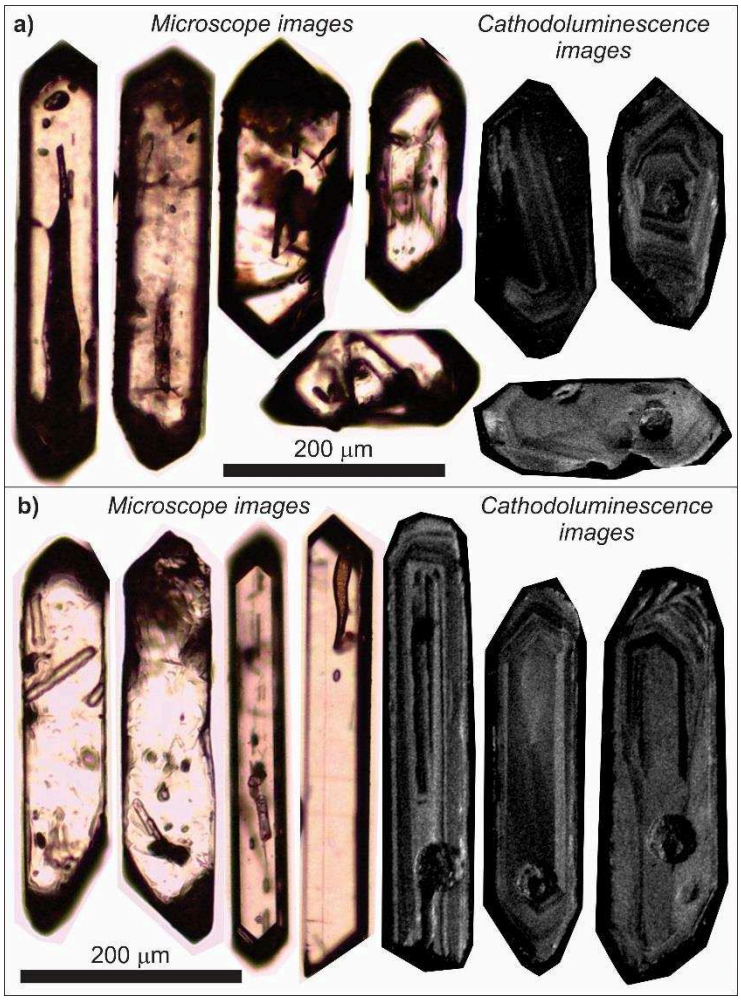

Figure 5.9: Microscope and cathodoluminescence images of the studied samples: a) Zircon grains from the M-06 sample (Prerift, Erizo.x-1 well); b) Long prismatic zircons recovered from sample M-03 (Serie Tobífera, Calamar.x-1 well).

5.5.2.2 U-Pb geochronology

In sample M-06, a total the 149 concordant ages were obtained in a range between ca. 203 Ma and 1,013 Ma (figures 5.10a and 5.10b). The distribution of the ages is bimodal with two maximum peaks at 215 Ma and 296 Ma. The most representative group has Triassic ages (63%) while the second group has Permian to Late Carboniferous ages (35%). Considering the morphological analysis of the crystals from sample M-06, with zircons of volcanic origin without evidence of transport, the maximum peak at 215 Ma (Late Triassic) is interpreted as the better age for the crystallization of the volcanic breccia in the prerift unit drilled by the Erizo.x-1 well. The older ages are interpreted as inherited zircons, probably from previous Late Paleozoic igneous rocks, very well represented in Patagonia (Pankhurst et al., 2006; Hervé et al., 2010).

In sample M-03, long prismatic zircons were analyzed and 109 concordant ages were obtained (Figures 5.10c and 5.10d). The analyzed zircons yielded a unimodal distribution of ages with a maximum peak at 169 Ma. Most of the zircons are between ca. 163 Ma and 186 Ma (93%). Single ages appear at 244, 250, 430, 479, 501, 504, 507, 514 Ma (Figure 5.10c). The age of the peak at 169 Ma (Bathonian) is interpreting as the crystallization age of the tuff sample M-03, obtained from the top of Serie Tobífera (synrift unit) from the Calamar.x-1 well.

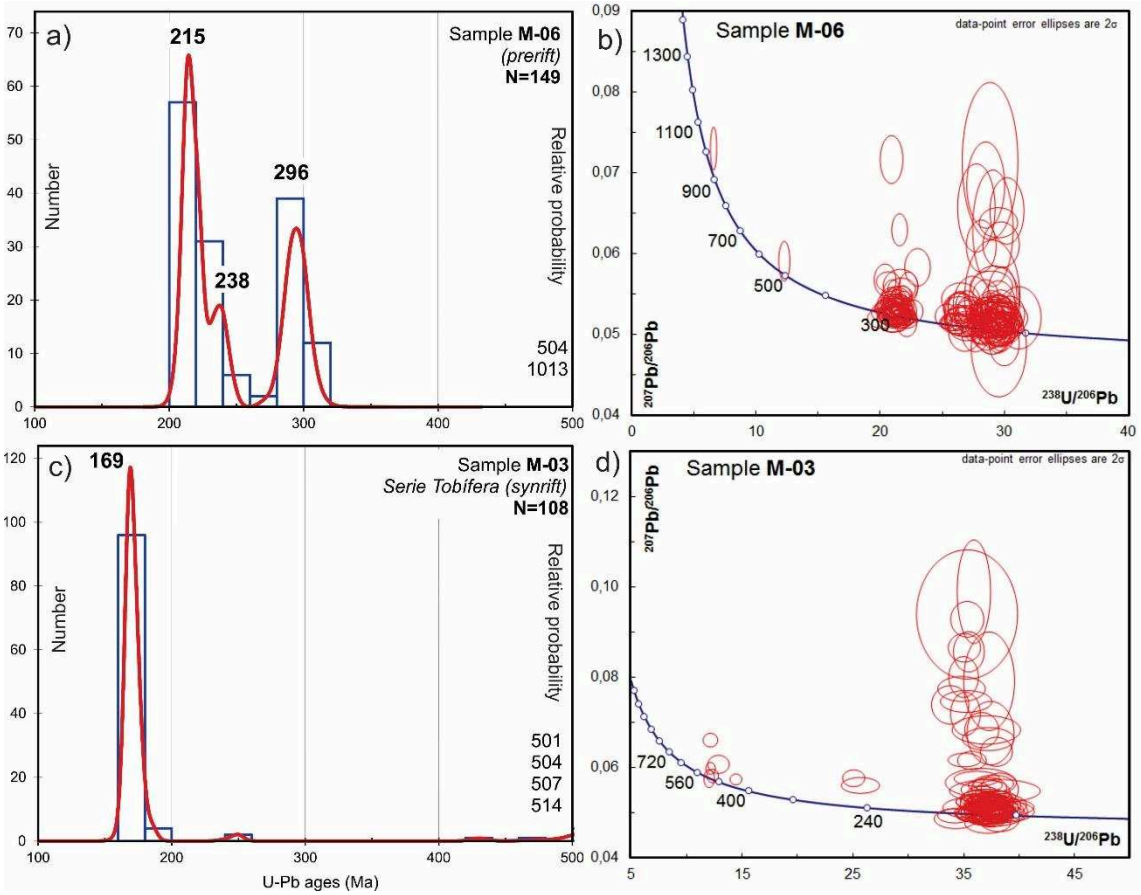

Figure 5.10: Frequency histogram and relative probability plots of U-Pb (LA-MC-ICP-MS) ages of zircons for the samples M-06 (a) and M-03 (c). Tera-Wasserburg diagrams for the dated samples M-06 (b) and M-03 (d).

5.6 Discussion

The crystallization age of 215 Ma interpreted for the volcanic breccia (sample M-06) in the Erizo.x-1 well is the first Triassic age in the Malvinas basin. Due to the complexity of seismic interpretation in the Erizo well area, it was not possible to validate whether the interval the sample was recovered from indicates synextensional emplacement (fault-bounded, wedged shape). If that was the case, this could indicate the first onset of Mesozoic rifting in the Malvinas

basin area. Regionally it correlates with the Late Triassic ages attributed to the Central Patagonian Batholith (Rapela et al., 2005; Zaffarana et al., 2014), the La Leona granites (Pankhurst et al., 1993) in the Deseado Massif; and the Late Triassic extensional basins in central Argentina (Cuyo, Bermejo, Precuyano cycle of the Neuquén basin) and the Deseado Massif (El Tranquilo basin). In the Erizo.x-1 well, this Triassic breccia underlies, via a sharp unconformity, the volcanic tuffs of Serie Tobífera, which are regionally, and as confirmed by the age of sample M-03 (Mid-Jurassic). Although the Triassic volcanic breccias in the Erizo well are probably associated with an extensional setting (Uliana et al., 1989), we consider this event different from the main rifting event associated with the formation of the Malvinas basin and thus put this unit within the prerift.

The Bathonian crystallization age (169 Ma) that we obtained for Serie Tobífera in the Malvinas basin (sample M-03) confirms the link between this basin and the Early to Middle Jurassic Chon Aike event. The Chon Aike MP has been associated with synextensional emplacement (Uliana et al., 1985; Gust et al., 1985). This extension has been related to a retroarc setting (at least for the Early Jurassic), by developing synchronously with the Subcordilleran Batholith that represented the arc at that time (Rapela et al., 2005; Fig. 5.2).

The WNW-directed Early Jurassic dykes in the Malvinas (Falkland) Islands (Cingolani and Varela, 1976) have been correlated to the WNW-striking normal faults of the southern rift of the North Malvinas (North Falkland) basin (Ramos et al., 2017; and references therein). Thomson et al. (2002) observed extensive cooling and uplift of the islands, which are part of the Malvinas High (Fig. 5.1), starting just before the Early Jurassic and synchronous with the emplacement of the dolerite dykes. Influenced by the paleogeographic models that placed this tectonic block, named Lafonia, west of South Africa (Adie, 1952), the authors attributed this uplift to the impingement of the Karoo plume. Adie's paleogeographic model has been challenged by new paleomagnetic data from the islands and an Early Mesozoic paleogeographic position with respect to the South American plate similar to present-day seems more reasonable (see the discussion in Ramos et al., 2017). This Early Jurassic uplift could be related, however, to shoulder uplift of the Malvinas basin. The Malvinas basin is largely asymmetrical, with a fault-bounded end to the NE, towards the Malvinas High. This fault-bounded border will produce a more abrupt flank to the NE that will condition the stratigraphic architecture Fig. 5.3).

Several authors have observed the diachronous development of the Chon Aike MP (Uliana et al., 1985; Gust et al., 1985; Pankhurst et al., 2000). The oldest Chon Aike ages are observed in towards present-day eastern Patagonia and the Malvinas (Falkland) Islands. The Middle Jurassic silicic volcanism characteristic of the Chon Aike MP is rather widespread in the North Patagonian Massif, the Deseado Massif, in the Cañadón Asfalto and San Jorge Gulf basins, and as the main synrift infill of the Austral and possibly the Malvinas basin. The Late Jurassic volcanism (El Quemado Complex and equivalents), however, is restricted to the present-day Andean foothills to the west. This Late Jurassic volcanism has been interpreted as preceding the opening of the Rocas Verdes marginal basin, and displays a diachronous behavior from south to north (see the compilation by Malkowski et al., 2015).

The diachronism of the retroarc volcanic activity is also reflected in volcanic arc migration. Several authors have noticed and highlighted the trenchward arc migration throughout the Jurassic. Echaurren et al. (2017) suggest a non-cylindrical arc migration to be produced by differential slab rollback. This rotational arc migration implies a clockwise rotation of the stress field of ~20° between the Early Jurassic Subcordilleran Batholith and Late Jurassic-to-Neogene, N-S-striking, Patagonian Batholith (PB, Fig. 5.1).

When observing the structural fabric of the Early-Middle Jurassic faults and structures across Patagonia (Fig. 5.1) a certain ‘fanning’ can be interpreted. WNW- to NW-oriented faults are observed on the east with the WNW-striking faults of the Southern Rift of the North Malvinas (North Falkland) basin, the WNW-oriented dolerite dykes in the islands, the NW-oriented Central Patagonian Batholith, the NW-striking structures of the Deseado Massif. The Malvinas and Austral basins are related to NNW-directed faults, while towards the west, structures display a more N-S strike, parallel to the Andean margin trench. If the migration of the volcanic arc in northern Patagonia is considered, the apex of this ‘fanning’ structures would be placed near the northern limit of Patagonia (present-day 40° LS). We attribute this ‘fanning’ character of structures associated with the synextensional Chon Aike MP to a clockwise rotation produced by the influence of a vertical slab tear towards the south of present-day Patagonia, between South America and Antarctica (Fig. 5.11a), active since the latest Triassic.

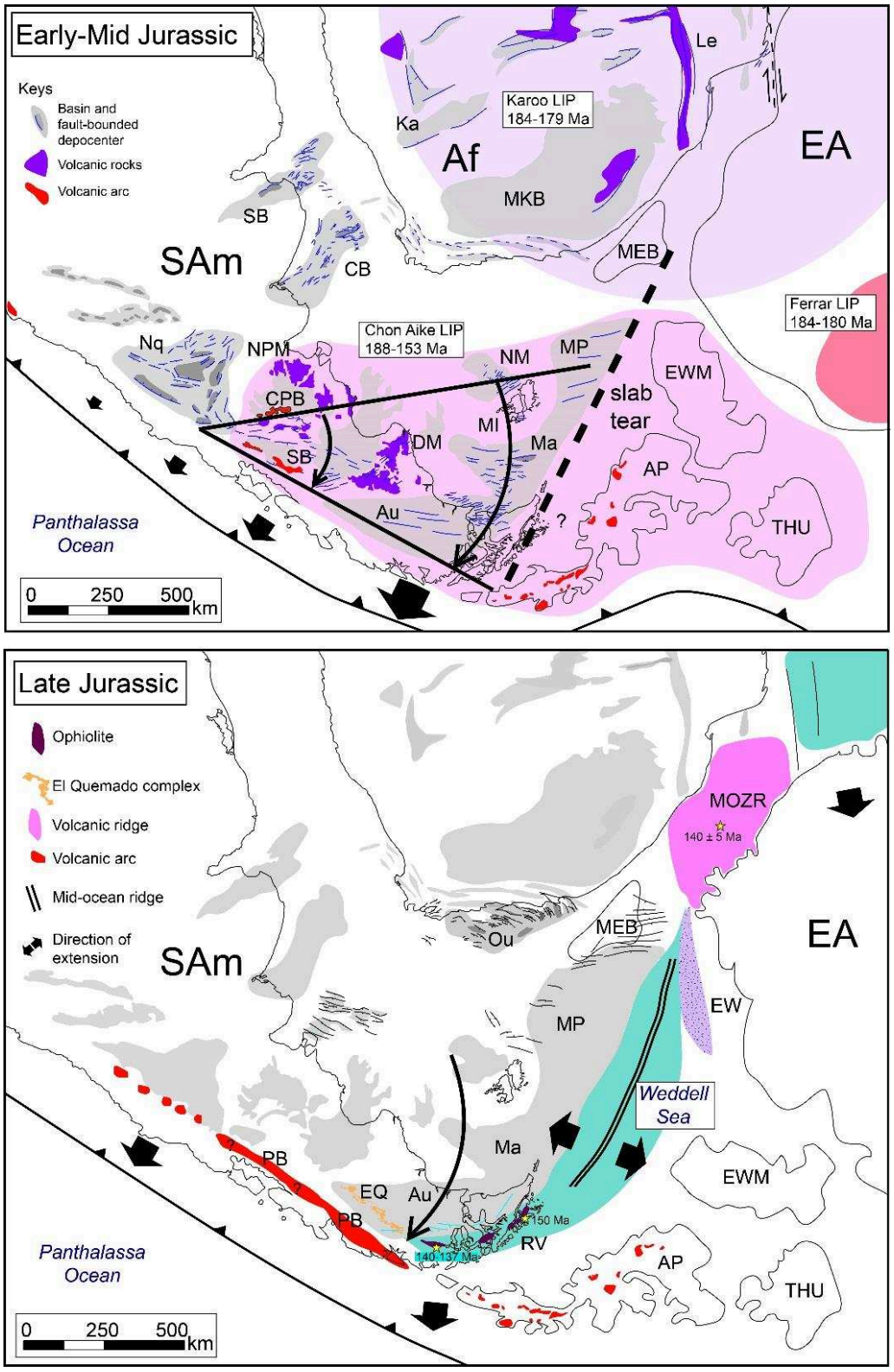

Figure 5.11: Rifting evolution of the Chon Aike MP: a) Early-Middle Jurassic rifting coeval with the Chon Aike MP emplacement; b) Late Jurassic extension is focalized in western Patagonia and produced the opening of the Rocas Verdes marginal basin (RV). The Weddell Sea opened in the Late Jurassic between Eastern and Western Gondwana (blue representd oceanic crust). Note the Late Triassic Central Patagonian Batholith (CPB), and arc migration (indicated by a curved black arrow) between the Early Jurassic Subcordilleran Batholith (SB, Fig. 5.11a) and the Late Jurassic Patagonian Batholith (Fig. 5.11b).

In our interpretation, the slab tear allows the rotational extension produced by the differential slab rollback suggested by Mpodozis and Ramos (2008) and Echaurren et al. (2017) and is necessary to explain the non-cylindrical behavior of the plate subduction below Patagonia. The rotational extension in Patagonia would have produced not only the change in the orientation of structures from present-day WNW to N-S in Patagonia, but also the rotational arc migration between the Early Jurassic (SB) and the Late Jurassic positions (PB), bracketing the time of emplacement of the Chon Aike MP.

A Neogene slab tear observed in the Mediterranean region, under the Aegean sea (Jolivet et al., 2015) could be considered a good recent analog to explain the geodynamic context. In the case of the Aegean, the slab tear is interpreted to being responsible for producing clockwise block rotation in the Hellenides (van Hinsbergen et al., 2005) and the counterclockwise rotation of blocks located across the tear. For SW Gondwana we interpret a maximum clockwise extensional rotation of ~40° for the Jurassic Chon Aike MP (Fig. 5.11a, 5.12). In this way, maximum extension, and thus maximum crustal attenuation are observed in southernmost Patagonia (Austral-Malvinas basins), an area heavily affected by the Gondwanides orogeny. Counterclockwise rotation is referred to having affected the Ellsworth-Whitmore Mountains (EWM) and other Antarctic blocks throughout the Mesozoic (Dalziel et al., 2013) which, in the slab tear model, is consistent with emplacement across the tear (Fig. 5.11a, Fig. 5.12).

It is interesting to note as well, the relation between this proposed slab tear and the Late Jurassic opening of the Weddell Sea (Ghidella et al., 2002; König and Jokat, 2006) emplaced between Western (South America + Africa) and Eastern Gondwana (Antarctica conjugate) in the Late Jurassic. Extension related to the Weddell Sea opening is interpreted to have started with the impingement of the Karoo plume in Eastern Africa in the Early Jurassic, that produced the opening of many Karoo-age basins in southern Africa and notably the Mozambique basin between SE-Africa and the Eastern Antarctica block (EA in Fig. 5.11). Separation of these two blocks is interpreted to have been achieved through the development of the large lateral shear zone between East Antarctica and West Gondwana (König and Jokat, 2006). These authors suggest that this shear zone was precursor of the Weddell Sea. A shear zone is indeed necessary to explain East-West Gondwana continental displacement. What was not explained by these authors were the reasons why the Weddell Sea opened in the Late Jurassic between Antarctica and the southern edge of the South American plate. The Weddell Sea roughly coincides with

the location of the slab tear (Fig. 5.11b). We suggest that the slab tear not only had an influence on geodynamics of the SW Gondwana blocks during the Early-Middle Jurassic, but the potential asthenospheric windows it might have opened (see Fig. 5.12) would have triggered the opening of the Weddell Sea, once East Antarctica was completely decoupled from Africa through the Mozambique basin and equivalents. It also explains the rapid and major flooding recorded by the Springhill Fm (Lower Cretaceous) while Patagonia loses its plate boundary conditions to the south.

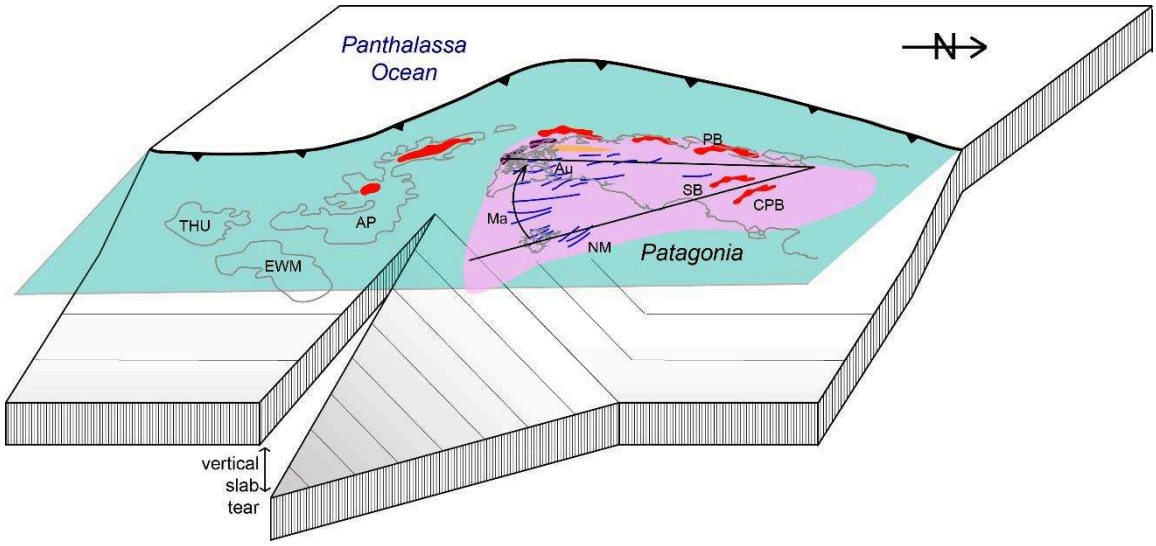

Figure 5.12: 3D sketch of the Jurassic vertical slab tear model for southern Patagonia, that explains the synextensional emplacement of the Chon Aike MP in Patagonia, associated with clockwise asymmetric extension and trenchward volcanic arc migration. The upper plate is indicated in the bluish color and coastlines of Present day Patagonia and the Antarctic territories are displayed. The North arrow indicates the present-day North for Patagonia.

5.7 Conclusions

In this contribution we presented new U-Pb zircon ages for Late Triassic and Middle Jurassic units in the Malvinas basin. The Late Triassic age (215 Ma, U-Pb in zircon) corresponds to a volcanic breccia that has been related to volcanic activity that correlates with the Central Patagonian Batholith and the La Leona granites. Although a possible synextensional character is attributed to this unit by correlation with the El Tranquilo basin in the Deseado Massif, this unit is interpreted within the prerift of the Malvinas basin, as its development is interpreted to correspond to a different stage of that of the Malvinas basin rifting. A

crystallization age of 169 Ma (U-Pb in zircon) was obtained for a tuff level within Serie Tobífera, which confirms the Middle Jurassic age of this unit, as part of the Chon Aike MP.

The Malvinas basin is an asymmetrical basin, affected by NNW-striking faults. The main depocenter located towards the SE end of the basin, is a half-graben bounded by a major NNW-striking, SW-dipping, normal fault. Rotational extension is observed for the retroarc Chon Aike MP, associated with trenchward volcanic arc migration (Pankhurst et al., 2000; Rapela et al., 2005). By reviewing the regional basin dynamics and related magmatic events, we propose the existence of a slab tear towards the south of the Malvinas basin, and between the South American and Antarctic blocks, that initiated in the Latest Triassic and that was active throughout the Early-Mid Jurassic. It could have produced the differential slab roll-back of the subducting plate below Patagonia noticed by Mpodozis and Ramos (2008) and Echaurren et al. (2017) that seems to have controlled the rotational extension observed for the Chon Aike MP and related basins. The slab tear model would also explain a thermal anomaly that might have triggered the opening of Weddell Sea.

Acknowledgements

The authors thank YPF S.A. for making available the database for this study and for the continuous support during research, La.Te.Andes for carrying out the zircon separation, and ION GeoVentures for permission to present seismic data from their Argentina SPAN program, that were used in the preparation of the transect. And a special thanks to Viviana Meissinger and Daniela Ancheta for scanning the thin section and discussing the interpretation of the breccia.

Chapter 6. Mesozoic breakup of SW Gondwana and basin formation along the Argentinean Atlantic margin

This chapter includes new insights in the Mesozoic rifting evolution of Gondwana, a complex process occurring in several stages that ended with opening of the South Atlantic Ocean in the Early Cretaceous. Mesozoic rifting in southern South America seems strongly related to retroarc extension. The content of this chapter has been submitted for publication in Basin Research (Authors: Lovecchio, J.P.; Rohais, S.; Ramos, V.A.; Joseph, P.; Bolatti, N.D.).

Highlights:

- Mesozoic rifting of Gondwana was a complex process occurring in several stages, and strongly related to retroarc extension.
- The Colorado and Salado basins are part of the Karoo Rift system.
- The South Atlantic Rift initiated in the southernmost segment, an area that was affected by a previous crustal thinning phase since the Late Jurassic, with rifting in the Rawson/Valdés and Outeniqua basins.

Abstract

The opening of the South Atlantic in the Early Cretaceous was only the final stage of a complex rifting process of SW Gondwana. In this contribution we review and reassess the chronology of Mesozoic basin formation in southern South America and Africa, and integrate in into the long-term breakup history of SW Gondwana. Triassic rifting evolution is associated with the Central Atlantic breakup (Karoo I), as well as retro-arc extension on the southwestern margin of Gondwana. In the Early Jurassic, rifting on Eastern Africa was triggered by the impingement of the Karoo plume, with development of the Karoo II depocenters. The Colorado and Salado basins on the Argentinean shelf formed during this stage. Rifting in East Africa ultimately produced the breakup of Eastern from Western Gondwana in the Middle Jurassic. In Patagonia, the Austral, Malvinas, and possibly the southern rift of the North Malvinas (Falkland) basin formed, associated with the silicic Chon Aike Magmatic Province in the Patagonian retroarc. In the Late Jurassic the Rocas Verdes back-arc basin opened as an ultimate consequence of retroarc extension in southernmost South America. Oblique rifting in the orogenic core of the former Gondwanides orogen produced the Outeniqua and Rawson/Valdés basins. The South Atlantic rift initiated in the Early Cretaceous associated with present-day E-W extension. Rifting occurred diachronically from south to north, initiating in the previously thinned Rawson/Valdés-Outeniqua segment. The presence of an older possibly continuous rifting in this segment could explain the lack of SDRs south of the Colorado-Cape fracture zones. To the north, rifting and SDR emplacement occurred progressively to the north, producing strongly asymmetric conjugate margins.

6.1 Introduction

What triggers the breakup of supercontinents? This question has long been discussed since the proposal of the Wilson cycle theory. Internal Earth's heat has been proposed to motorize plate tectonics. In this way it would also be a trigger for the opening of new oceans, with supercontinents causing the insulation of the underlying mantle, producing abnormal heat concentrations and hot spots. A new ocean was born from the connection of more-or-less aligned hotspots (Dewey and Burke, 1974). The coincidence of new oceans and the presence of large igneous provinces (LIP) also supported this theory. Buiter and Torsvik (2014) reviewed the role of mantle plumes in continental breakup and note that although there is a relation, in many margins such as the Central or the South Atlantic, rifting had initiated long before the

main phase of volcanism. Rifting and successive breakup of supercontinents is a process that has proved to be much more complex. Breakup of a supercontinent such as Pangea occurred in not one but several stages (Moulin et al., 2010, Fig. 6.1). Regarding the process, the thermal insulation and thus landmass instability expected to be produced by supercontinents on the underlying mantle is not enough to produce overheat mantle, volcanism and active rifting (Heron and Lowman, 2011). Bercovici and Long (2014) suggest that it is subduction-related slab rollback instability which produces continental landmass dispersal. And indeed, a recent review of the Pangea breakup by Frizon De Lamotte et al. (2015) proposes a combination of active and passive rifting to produce, in successive stages, the breakup of large continental masses. Active rifting is caused by the impact of a mantle plumes, producing doming, volcanism and extension (see Sengör and Burke, 1978). Passive rifting is related to lithospheric far-field forces pulling the lithosphere apart, notably related to subduction zones.

Supercontinents are intrinsically complex collages of cratons and shields bounded by metamorphic mobile belts (former orogens produced during craton amalgamation). The structural grain of mobile belts introduce heterogeneities that, under extension, can guide fault emplacement and eventually breakup (Buiter and Torsvik, 2014). The supercontinent of Pangea is no exception (Fig. 6.1). It took more than 100 Ma to break Pangea apart. This process initiated in the Triassic, with rifting between Laurentia (North America) and Western Gondwana (Fig. 6.1), and the successive opening of the Central Atlantic (Withjack et al., 1999, 2012; Leleu et al., 2016). The emplacement of a Central Atlantic Magmatic Province (CAMP) would have occurred after the main phase of rifting (Frizon De Lamotte et al., 2015) and would not be plume-related (McHone, 2000). Triassic basins were not restricted to the Central Atlantic realm, rift basins developed across Gondwana (Uliana et al., 1989; Zerfass et al., 2003) and on the paleo-Pacific convergent margin (Ramos and Kay, 1991; Spikings et al., 2016).

On the other hand, the impact of the Karoo plume on East Africa in the Early Jurassic produced active rifting, with doming, volcanism and caused eventually continental breakup of Western from Eastern Gondwana (Frizon De Lamotte et al., 2015). The continent dispersal process continued in the Early Cretaceous with the opening of the South Atlantic Ocean between South America and Africa and several other oceanic basins produced by the dispersal of Eastern Gondwana cratons (Fig. 6.1). As recently discussed by Frizon De Lamotte et al. (2015) and Will and Frimmel (2016), the South Atlantic is another case of passive rifting, triggered by far-field forces pulling the lithosphere apart, that was affected by massive

volcanism, the Paraná-Etendeka LIP. In this scenario the opening would not have been triggered by a plume but the volcanism came when rifting was already established. In this perspective, the South Atlantic opening was only the final stage of the long and complex Gondwana breakup.

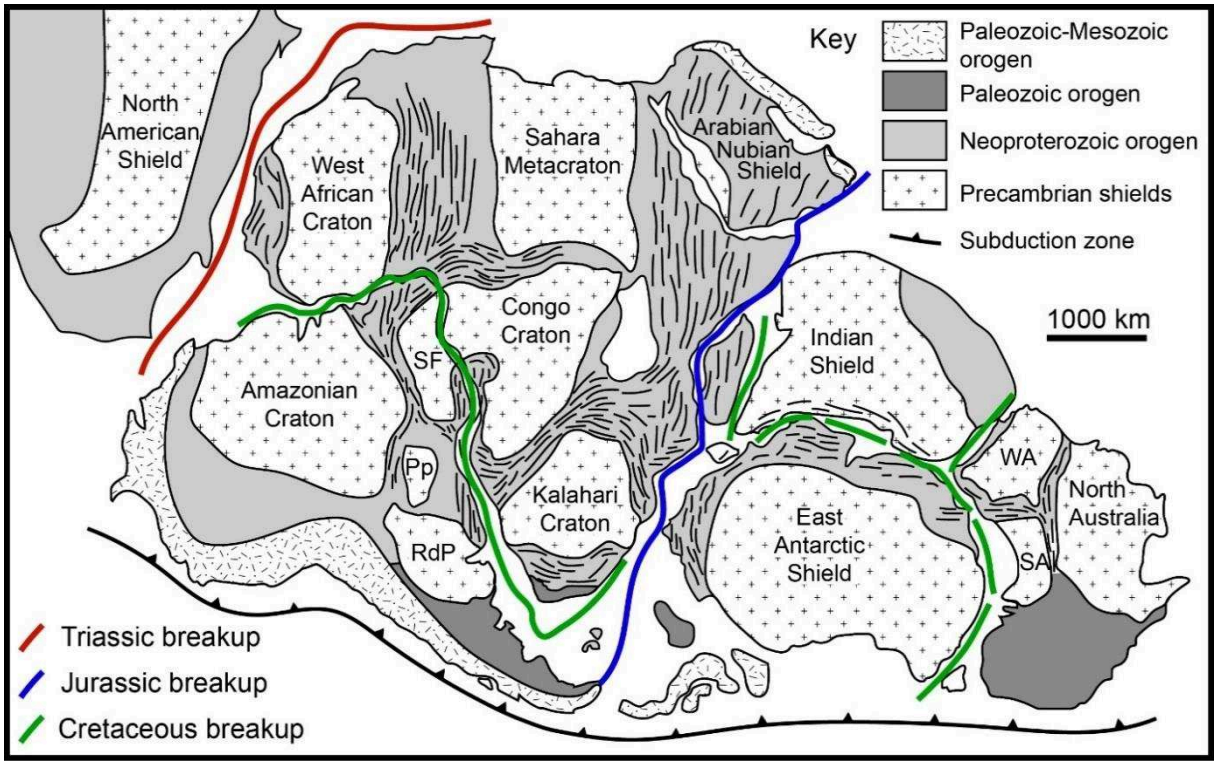

Figure 6.1. Gondwana view in a Pangea reconstruction at the end of the Paleozoic after Gray et al. (2008), showing the main breakup events modified from Moulin and Aslanian (2010) and Will and Frimmel (2018). Cratons: RdP: Río de la Plata, Pp: Paraná-Panema block, SF: Sao Francisco, WA: West Australia, SA: South Australia.

The different Mesozoic rifting events were crucial for the formation of the basins on the South American and African platforms. After having identified three super-imposed rifting stages in the Colorado basin (Argentinean margin, Fig. 6.3, Lovecchio et al., 2018), we review in this contribution the chronology of Mesozoic basin formation in southern South America and Africa, and integrate them into the long-term breakup of SW Gondwana. We focus on the southern South American offshore basins, and follow the pioneer integrations of Urien et al. (1981) and Uliana et al. (1989), later complemented by the contributions of Franzese et al. (2003), and Macdonald et al. (2003). We also incorporate recent absolute ages published by different authors, and present a new model that illustrated the different stages of SW Gondwana Mesozoic rifting.

6.2 Geological Framework: Pre-rifting configuration

Southwestern Gondwana is a collage of cratons limited by mobile belts and accreted terranes formed as a result of almost continuous subduction since the beginning of the Phanerozoic (Fig. 6.2). In the Neoproterozoic, the Panafrican orogeny welded the Rio de la Plata and African shields through the Dom Feliciano belt. Since the Cambrian, and throughout the Paleozoic subduction from the west produced the accretion of different allochthonous terranes: Pampia, Cuyania, Chilenia (Ramos, 1999; Victor A Ramos, 2010). Subduction was intermittently active throughout the Paleozoic. The terrane of Patagonia was the last to accrete, in this case from the SW, producing a Carboniferous-to-Permian volcanic arc in Northern Patagonia and a Permian-to-Early Triassic fold-and-thrust belt (Fig. 6.2) largely oriented E-W. This fold belt is recognized in South America: the Ventania System (see Ramos, 2008 and references therein), in Africa: the Cape fold belt (Hansma et al., 2016), and in the Ellswoth-Withmore Mountains in Antarctica (Curtis, 2001). In the Mesozoic, under an extensional stress regime, negative inversion of this fold belt occurred. This process has been described on the Argentinean shelf in the Colorado basin by Pángaro and Ramos (2012), and more recently by Lovecchio et al. (2018). On the African conjugate margin, structures at high angles with the margin orientation, and affecting older series have been described by Paton et al. (2016) and interpreted as an extension of the Cape fold belt in the prerift of the Orange basin.

At the end of the Paleozoic, with the accretion of Patagonia from the SW (Ramos, 2008; Miller et al., 2016) the amalgamation of Pangea was completed. But supercontinents are unstable, and soon after the final supercontinent configuration was achieved, different instabilities induced the onset of rifting since the beginning of the Mesozoic era.

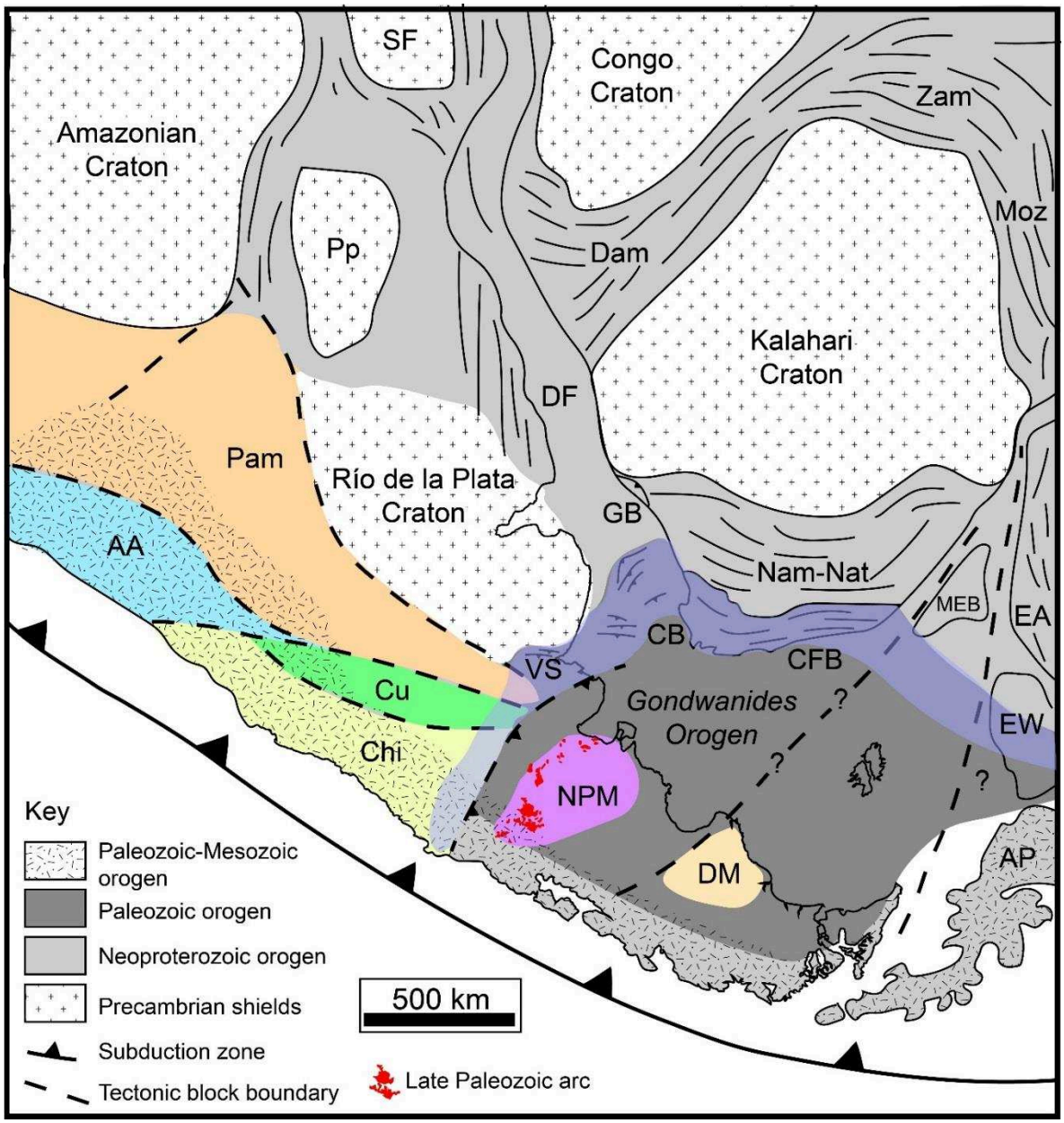

Figure 6.2: Simplified structural scheme of SW Gondwana at the end of the Paleozoic, with a detail of cratons, terranes and mobile belts, after Gray et al. (2008); Ramos (2010); Pankhurst et al. (2006); Pángaro and Ramos (2012); and Lovecchio et al. (2018). Main Precambrian mobile belts: Dom Feliciano (DF), Gariep (GB), Namaqua-Natal (Nam-Nat), Mozambique (Moz). Main Paleozoic accreted terranes: Pampia (Pam), Cuyania (Cu), Arequipa-Antofalla (AA), Chilenia (Chi). Other Tectonic blocks: Paraná-Panema (Pp), Sao Francisco (SF), North Patagonian Massif (NPM), Deseado Massif (DM), Eastern Antarctica (EA). Permian-Triassic mobile belt (in purple): Ventania system (VS), Prerift of the Colorado basin (CB), Cape Fold Belt (CFB), Ellsworth-Whitmore Mountains (EW). Projection UTM. Undeformed plates, continental fit modified after Dalziel et al. (2013).

6.3 Materials and Methods

After performing seismic interpretation in the Colorado basin area, and identifying three independent Mesozoic rifting events (Lovecchio et al., 2018), in this contribution we correlate and integrate these and other rifting stages into a comprehensive scheme of rifting forming the main Mesozoic basins around the South Atlantic realm, with special interest in the evolution of the Argentinean Mesozoic basins. We prepared structural maps, where we compiled published and newly generated data on fault-bounded depocenters and the main structures related to basin formation. We generated chronologic tectonic charts summarizing rifting stages for Mesozoic basins in southern South America and southern Africa. Absolute ages that constrain synrift infill age were obtained either from interbedded volcanics (e.g. lavas, ash beds), from paleontological content, and from detrital zircon data. However, age determinations from the synrift series are usually scarce. Depocenters are deeply buried and hydrocarbon exploration wells have commonly been drilled on structural closures out of the main troughs. Moreover, synrift series many times consist of red beds, which makes difficult the application of paleontological or biostratigraphic methods. Thermochronological methods allow the interpretation of exhumation events, which might be linked to rifting in the appropriate tectonic framework. Besides these difficulties, we present a synthesis of the main rifting episodes observed in the basins of the study area and surroundings.

Finally, we generated paleotectonic maps for the main rifting events, we color-coded faults according to the period of active rifting, and propose a model to explain the formation and evolution of the main basins in the study area throughout the Mesozoic finishing with the opening of the South Atlantic.

6.4 Mesozoic basins across the South Atlantic

6.4.1 Mesozoic basins in southern South America

South America is bounded to the west by the active margin resulting from the subduction of the oceanic Pacific plate from the west, under the continental South American plate (Fig. 6.3). Subduction has been intermittently active since the Cambrian and is associated with terrane accretion across the Paleozoic (Fig. 6.2; Ramos, 1999). This process is responsible for the largely oriented N-S structural fabric, which explains the abundance of N-S striking-structures in most of the Mesozoic basins to the west. The stress regime, related to subducting

slab dynamics, had an impact on structures generation and reactivation throughout basin evolution. This process, observed in the Neuquén basin by Vergani et al. (1995) can be extrapolated to other Subandean basins. The eastern limit of the South American plate is given by the Atlantic passive margin, with several rift basins emplaced on the continental shelf, notably at high angles with the Early Cretaceous Continent-Ocean Transition zone (COT).

Figure 6.3 depicts the main Mesozoic basins in southern South America, following the pioneer integration presented by Uliana et al. (1989). Additional references were used to established the map presented in Figure 6.3 (Urien et al., 1981; Caminos 1999; Chebli and Spalletti 1989; Turner, 1979, 1980; Turic et al., 1996, Chebli et al., 2005; Kozlowsky et al., 2011).

In this contribution the chronology of rifting was summarized in a chart presented in Figure 6.4. Hereafter, the rifting history is presented in a chronological order. The Cuyo and the Bermejo basins record synrift sedimentation in the Triassic. We gather in these two basins several aligned depocenters with a common rifting history. The Cuyo basin includes the Río Blanco, Santa Clara, Tupungato, La Esperanza-Divisadero and the General Alvear sub-basins. The Bermejo basin gathers the Ischigualasto, Marayes, Guayagas, Las Salinas and Beazley sub-basins (see Barredo et al., 2012). Vertebrate fossils and radiogenic ages of intruded subvolcanic rocks places rifting in the Early Triassic in the Bermejo and Middle Triassic in the Cuyo basin (Barredo et al., 2012; Stipanicic, 2001). The Triassic stratigraphy of southern South America was reviewed by Jenchen and Rosenfeld (2002), and Zerfass et al. (2004). For the Triassic basins, these authors highlight influence of previous structural fabric of the basement, with en-echelon depocenters produced by NNW trending faults associated to low-to-moderate angle detachment surfaces. Ramos and Kay (1991) linked the main detachments of the listric faults to the former suture between Pampia and Cuyania, two terranes accreted to the SW margin of Gondwana in the Early Paleozoic (Fig. 6.2).

The Neuquén basin, records two rifting events (Legarreta and Uliana, 1996; Vergani et al., 1995 and references therein). The Precuyano cycle, aged Late Triassic - Early Lias (early Hettangian), is associated with isolated half-grabens filled with volcanic rocks and continental sediments. Rifting diachronism was determined for the basin, with younger deposits towards the south (D'Elia et al., 2015). Later on, throughout the Lias, extension resumes with reactivation of older structures, and the later coalescence of depocenters. The sedimentary infill is formed of continental-to-marine sequences (Los Molles Fm), rich in paleontological and

detrital zircon content, covered by the prograding deltaic sediments of the Lajas Fm (see Naipauer et al., 2018).

Further south, the Cañadón Asfalto records back-arc rifting in a continental environment during the Early Jurassic (see Cuneo et al., 2013 and Figari et al., 2015). The westward migration of the arc, triggered the opening of the Liassic Chubut basin and the development of the marine systems of the Toarcian Osta Arena Fm (see Suárez and Márquez, 2007, and references therein).

In the San Jorge Gulf basin three rifting stages have been identified by Fitzgerald et al., (1990). A first rifting event poorly constrained was assigned to the Triassic-Early Jurassic by extrapolation from deposits in the Deseado Massif. These deposits are difficult to distinguish from the Middle Jurassic Volcano-Sedimentary Complex (Clavijo, 1986), part of the acidic to intermediate Chon Aike Magmatic Province (Pankhurst et al., 2000). In the Early Cretaceous, the Neocomian rifting stage is responsible for the development of half-grabens under continental-to-marine conditions (Figari et al., 1997). To the west, several NW-striking depocenters developed in the Rio Mayo embayment (see Iannizzotto et al., 2004) filled with marine deposits, rich in paleontological content (Olivero, 1987; Olivero and Aguirre-Urreta, 2002). Finally, a third rifting stage in the Late Cretaceous is recorded by E-W trending faults on the eastern part of the basin. These faults might have reactivated previous normal faults (affecting the basement) or detached within the sedimentary cover (Fitzgerald et al., 1990).

The San Julián basin's rifting chronology is yet poorly constrained, and its evolution is interpreted to be in close relation with the Deseado Massif basins. However the extension of the Deseado Massif deposits towards the depocenters of the San Julián basin has not been confirmed, as these beds have not been reached by hydrocarbon exploration wells (Micucci et al., 2011b). Various tectonic settings have been interpreted for the Permo-Triassic continental deposits of La Golondrina and La Juanita formations and El Tranquilo Group in the Deseado Massif. Bellosi and Jalfin (1989) support an intra-arc basin interpretation, while Ramos and Palma (1996) interpret an intracratonic rift. An Early-to-Middle Jurassic rifting event is confirmed across the area, with volcanic rocks and continental deposits rich in volcaniclastic content (Figueiredo et al., 1996).

Further south, the Austral (Magallanes) and the Malvinas basins record a main phase of rifting in the Early-to-Middle Jurassic, with half-grabens largely oriented NNW (Fig. 6.3). The

presence of Triassic rocks below the Malvinas basin was proposed by Uliana et al. (1989). The synrift was dated Mid-Jurassic in an exploration well in the Tierra del Fuego island (Pankhurst et al., 2000). This age is consistent with the Early Jurassic ages for NW-striking igneous dykes in the Malvinas (Falkland) islands (see recent review of Ramos et al., 2017) and thermochronological data (Thomson et al., 2002). The central graben of the Malvinas basin remains undrilled. Towards the west, extension produced in Late Jurassic the opening of the Rocas Verdes back-arc basin. This rifting is recorded by the bi-modal volcanism of El Quemado complex in Argentina (Pankhurst et al., 2000) and the onset of oceanic crust accretion, evidenced by the presence of ophiolite complexes (Fig. 6.3; Calderón et al., 2013; Malkowski et al., 2015).

Figure 6.3 (next page): Map of the main Mesozoic basins of SE South America (SAm). NOA: Northwest Argentina Cretaceous basin, SCh: Sierras Chicas, GL: General Levalle, Mac: Macachín, Be: Bermejo, Cu: Cuyo basin, Nq: Neuquén, Ch: Liassic Chubut basin, CA: Cañadón Asfalto, SJo: San Jorge Gulf basin, Au: Austral/Magallanes basin, Ma: Malvinas basin, NM: North Malvinas (Falkland) basin, SJu; San Julián, Va: Valdés, Ra: Rawson, Col: Colorado, Sal: Salado, PdE: Punta del Este basin, SL: Santa Lucía, Pel: Pelotas. Other features: MI: Malvinas (Falkland) islands, VB: Volunteer basin, FRB: Fits Roy basin, MP: Malvinas (Falkland) Plateau, MEB: Maurice Ewing Bank, SG: South Georgia, VS: Ventania system, TS: Tandilia system. FZ: Fracture Zone. Faults and depocenters after Uliana et al. (1995, 1989); Veroslavsky (1999); Franke et al. (2007); Micucci et al. (2011); Starck (2011) ; Becker et al. (2012); Bechis et al. (2014); Stica et al. (2014); Figari et al. (2015); Lohr and Underhill (2015); Gianni et al. (2015) and Lovecchio et al. (2018). Background topography from Etopo 1 (Amante and Eakins, 2009).

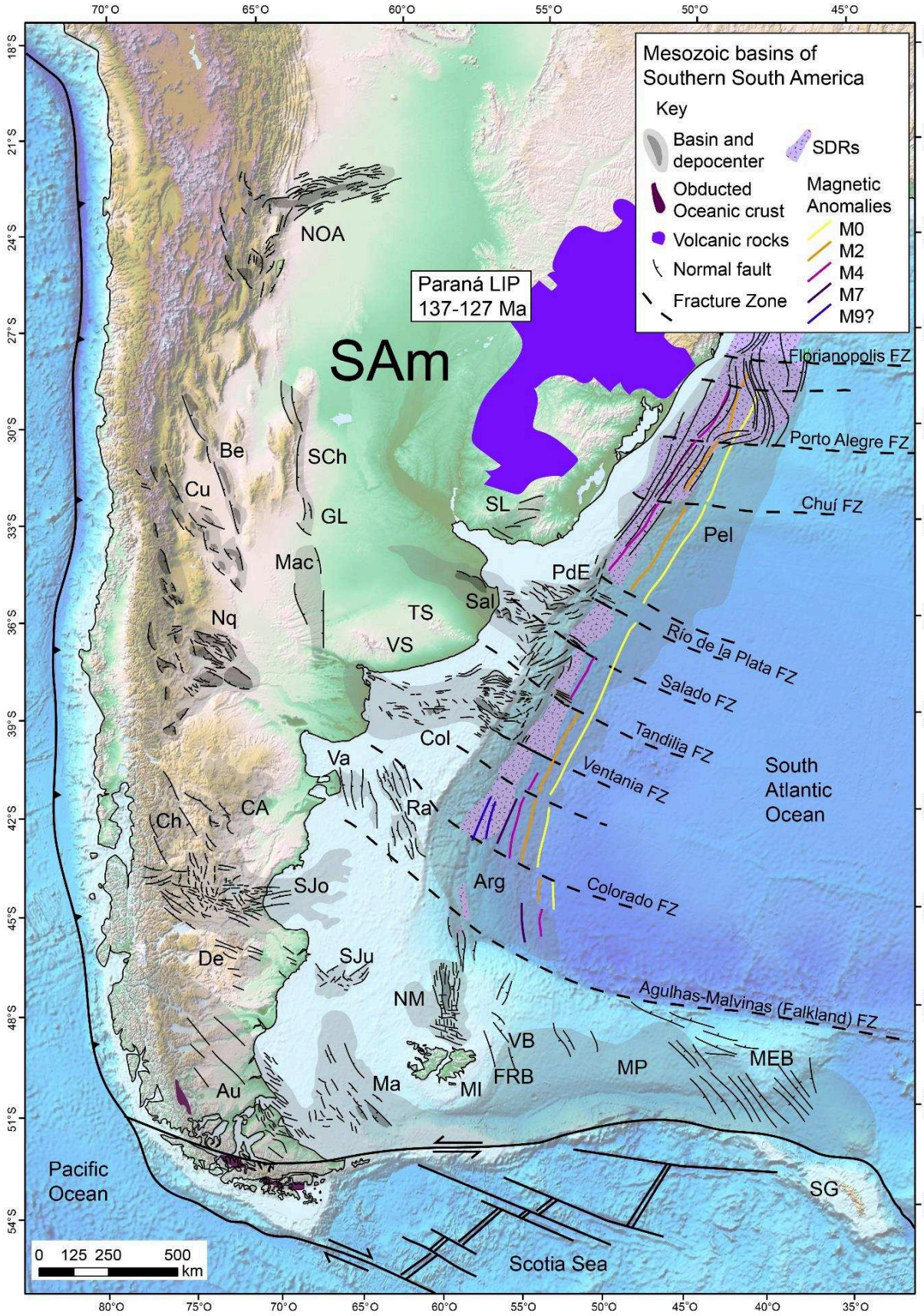
Mesozoic basins of
Southern South America
Key
Basin and depocenter
Obducted Oceanic crust
Volcanic rocks
Normal fault
Fracture Zone
SDRs
Magnetic Anomalies
M0
M2
M4
M7
M9?
Paraná LIP
137-127 Ma
SAm
NOA
Be
SCh
Cu
GL
Mac
Nq
TS
VS
SL
Sal
PdE
Pel
Florianopolis FZ
Porto Alegre FZ
Chuí FZ
Río de la Plata FZ
Salado FZ
Tandilia FZ
Ventania FZ
Colorado FZ
Agulhas-Malvinas (Falkland) FZ
Col
Va
Ra
Ch
CA
SJo
Arg
De
SJu
NM
VB
FRB
MP
MEB
Au
Ma
MI
SG
South
Atlantic
Ocean
Pacific
Ocean
Scotia Sea
0 125 250 500
km
70°O
65°O
60°O
55°O
50°O
45°O
40°O
35°O
80°O
75°O
18°S
21°S
24°S
27°S
30°S
33°S
36°S
39°S
42°S
45°S
48°S
51°S
54°S

Further east, in the North Malvinas (Falkland) basin (Fig. 6.3), two intersecting rift systems are observed (Brandsen et al., 1999). The Neocomian, N-S striking faults forming the Northern branch, intersect the NW-striking faults forming the older Southern rift system. The Southern rift system remains underexplored. A Late Jurassic rifting age was assigned by Lohr and Underhill (2015). However, an Early to Middle Jurassic age seems more consistent with regional data, as suggested by Ramos et al. (2017a). The presence of two transecting rift basins has been used to support a rotation of the Malvinas microplate during the Jurassic (Adie, 1952; Marshall, 1994b). More recently, this has been reinterpreted as a record of the change in the orientation of the stress regime between the Jurassic and the Early Cretaceous (Ramos et al., 2017).

The Malvinas (Falkland) Plateau is a projection to the east of the Argentinean continental shelf that extends between the Malvinas islands and the Maurice Ewing Bank (J. I. Ewing et al., 1971). The plateau limits to the south with the Scotia plate (via a transpressive margin) and is bounded to the north by the Agulhas-Malvinas (Falkland) Fracture Zone (FZ). The geology of the Malvinas Plateau is poorly constrained due to the lack of public seismic data. Biddle et al. (1996) published a map with the main interpreted faults and suggest a Jurassic rifting stage. Marine sedimentation since at least the Mid-to-Late Jurassic boundary is recorded in DSDP-511 well on the Maurice Ewing Bank (Price and Gröcke, 2002). Barker (1999) proposed the presence of oceanic crust under the plateau, but recent works point towards highly-extended continental crust (Chemale et al., 2018; Kimbell and Richards, 2008). Fraticelli et al. (2016) mention the development of two main sedimentary troughs: The Fitzroy and Volunteer basins (Fig. 6.3).

North of the Agulhas-Malvinas Fracture Zone (AMFZ) develops the Austral segment of the South Atlantic, that extends between the AMFZ and the Río Grande FZ north of the Pelotas basin (Moulin et al., 2010). This segment is characterized by the overall presence of Seaward Deeping Reflectors (SDR) on the Continent-Ocean Transition zone (COT, sensu Blaich et al., 2011). SDRs are volcanic wedges with interbedded continental sediments deposited in subaerial environments, emplaced during breakup on both conjugate margins (Hinz, 1981b). SDR development characterize volcanic or magma-rich passive margins such as the Southern South Atlantic. A general review of the Argentinean volcanic margin is presented by Hinz et al. (1999) and Franke et al. (2010, 2007).

The Argentinean shelf is one of the widest platforms in the world. It extends for up to 500 km and is characterized by the presence of several sedimentary basins perched on continental crust, notably the Rawson/Valdés, Colorado and Salado/Punta del Este basins. The Rawson/Valdés basins are two rift basins oriented NNW, and composed of several half-grabens formed mainly by western-dipping faults. The main depocenters remain undrilled. Otis and Schneidermann (2000) proposed a Mid-Jurassic age for the rifting, while Continanzia et al. (2011) suggest a Late Jurassic-Neocomian age.

Further North, the Colorado and Salado/Punta del Este basins display a general E-W to NW strike at high angles with the NNE-oriented COB. Several hypotheses were proposed to explain this obliquity. At first, studies interpreted the development of both basins synchronously leading to the opening of the South Atlantic in a single and continuous rifting event. Obliquity was explained either by aulacogenic basins (Introcaso and Ramos, 1984; Yrigoyen, 1975), transtensional basins associated with NW–SE dextral shear systems (Franke et al., 2006; Keeley and Light, 1993; Tankard et al., 1995), or as due to structural inheritance (Dominguez et al., 2011; Gebhard, 2005; Ramos, 1996; Urien et al., 1995).

Later, two superimposed rifting stages were used to explain the obliquity: a first Jurassic event with extension oriented NE-SW, forming the Colorado and Salado basins, and a second E-W oriented extensional event forming the South Atlantic rift in the Early Cretaceous (Macdonald et al., 2003; Gerster et al., 2011; Pángaro & Ramos, 2012; Franke, 2013; Autin et al., 2013). Lovecchio et al. (2018) postulated the existence of not two but three overprinted rifting stages in the Colorado area, with an older, previously unknown rifting event associated with the extensional reactivation of Permian thrusts of the Ventania-Cape foldbelt. This reactivation is interpreted to have taken place in the Late Triassic-Early Jurassic. The system was transected in the Early-to-Mid Jurassic by the main rifting event, responsible for the opening of the main depocenters in the Colorado and the adjacent Salado basin. Finally, in the Early Cretaceous, extension associated with the opening of the South Atlantic generated normal faults in a 100-km wide stripe of the outer continental crust, oriented parallel or slightly oblique to the COB, and with a main dipping towards the continent (inboard).

The Salado/Punta del Este and the Santa Lucía basin (onshore Uruguay) developed on of the Rio de la Plata Craton. The Santa Lucía basin has been interpreted as a pull-apart basin, initiated in the Late Jurassic (Veroslavsky, 1999), but no absolute ages are available.

The Pelotas basins spans offshore Uruguay and southern Brazil. Rifting in this basin is intimately related to the South Atlantic opening (Abreu, 1998). Rifting chronology is not only constrained by magnetic anomalies. The Paraná LIP (137-127 Ma) is part of the prerift and sets a maximum age for rifting (Stica et al., 2014). Faults are oriented largely parallel to the COB and tend to dip inboard, which is consistent with the Early Cretaceous rifting in the Colorado-Salado segment (Lovecchio et al., 2018).

Onshore, in central Argentina a N-S directed branch of Early Cretaceous rift basins is present along the western margin of the Rio de la Plata craton. From south to north, the Macachín basin (undrilled and only known from gravimetric and refraction seismic data, de Elorriaga, 2010; Kostadinoff and Llambías, 2002) displays a strong NNW direction. To the North, the General Levalle basin (Webster et al., 2004) is oriented N-S and a high-angle dipping master fault to the West, associated with reactivated basement structures. The Sierras Chicas basin in Córdoba is formed of different depocenters along the Córdoba hills. Similarly, to the General Levalle basin, is formed by the extensional reactivation of an east-dipping basement fault. The Sierras Chicas fault was then inverted in the Miocene with the Andean orogeny (see Schmidt et al., 1995). These basins are filled with red beds, interbedded with Early Cretaceous volcanic rocks (Lagorio et al., 2016).

In northern Argentina, the Northwestern Argentina Cretaceous basin (NOA in Fig. 6.3 and 6.4) is formed of three depocenters: Metán-Alemanía and Tres Cruces depocenters form a N-S directed branch, while the Lomas de Olmedo depocenter is oriented E-W (for general reference see Starck, 2011, and references therein). Synrift is composed of red beds interbedded volcanic rocks. Galliski and Viramonte (1988) report Early Cretaceous ages for the synrift Pirgua Group.

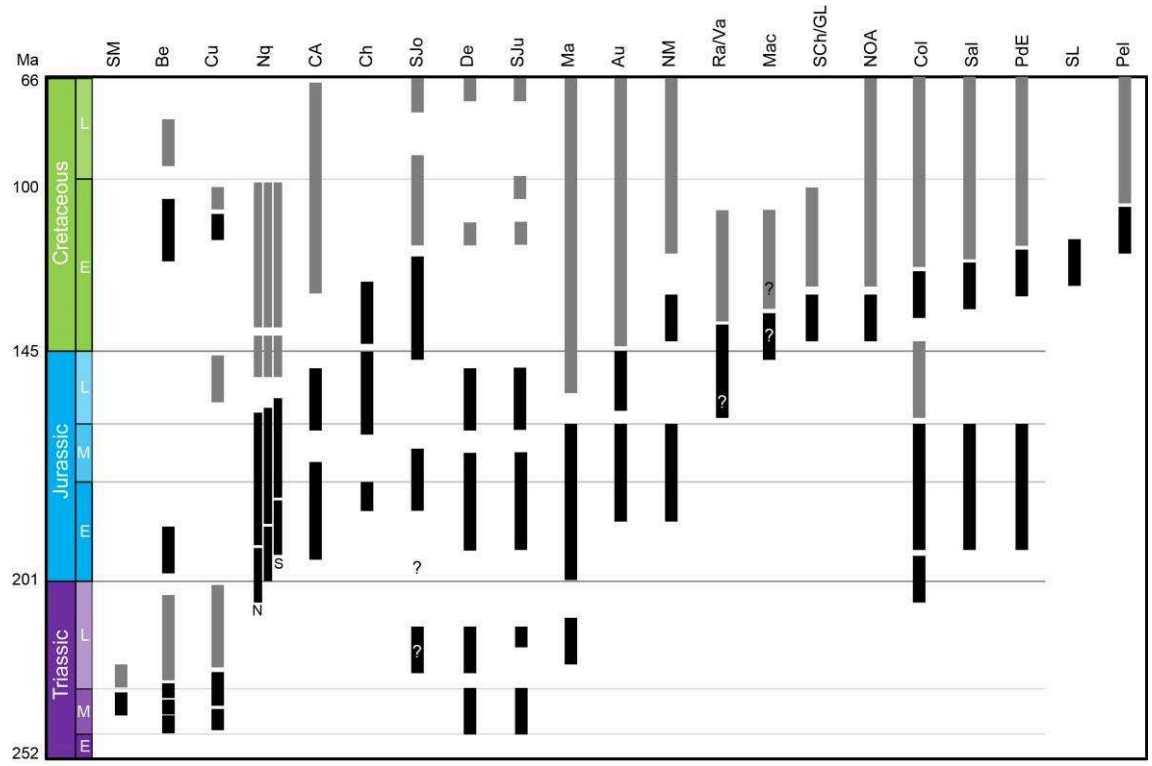

Figure 6.4: Rifting chronology chart for the main Mesozoic basins of SE South America. Black bars indicate perionds of active rifting, grey bars indicate postrift sedimentation. Santa María (SM), Bermejo (Be), and Cuyo basin (Cu) after Kokogian and Mancilla (1989); Zerfass et al. (2004); Barredo et al. (2012) and Colombi et al. (2015). Neuquén basin (Nq) after D'Elia et al. (2015) and references therein. Cañadón Asfalto (CA) after Cúneo et al. (2013) and Figari et al. (2015). Chubut Liassic basin after Suárez and Márquez (2007) and references therein, San Jorge Gulf basin (SJo) after Fitzgerald et al. (1990), and Iannizzotto et al. (2004). Deseado (De) and San Julián (SJu) basins after Figueiredo et al. (1996). Austral/Magallanes (Au) includes the Late Jurassic Rocas Verdes basin, ages after Pankhurst et al. (2000) and Calderón et al. (2013). Malvinas (Ma) and North Malvinas (North Falkland) basins after Galeazzi (1998); Ramos et al. (2017); and Lohr and Underhill (2015;). Rawson/Valdés basin (Ra/Va) after Continanzia et al. (2011). Macachín basin (Mac) is undrilled, thus rifting age is poorly constrained. Sierras Chicas and General Levalle basins in Córdoba (SCh/GL) after Lagorio et al. (2016); Schmidt et al. (1995); and Webster et al. (2004). Northwestern Argentina Cretaceous basin (Salta, NOA) after Starck (2011) and references therein, age after Galliski and Viramonte (1988). Colorado (Col), Salado (Sal), and Punta del Este (PdE) basins after Lovecchio et al. (2018); Gerster et al. (2011); and Loegering et al. (2013). Santa Lucía basin (SL) after Veroslavsky, (1999). Pelotas (Pel) after (Stica et al., 2014) and references therein.

6.4.2 Mesozoic basins in southern Africa

Although the African basins are not the focus of this study, we summarize their rifting chronology to better illustrate the framework for the evolution of the South American basins.

The collision of Patagonia against the SW margin of Gondwana in the Late Paleozoic, produced the Ventania-Cape foldbelt and changed the subsidence regime of the neighboring

Main Karoo basin of South Africa from intracratonic sag to a foreland configuration (see Veevers et al., 1994; Catuneanu et al., 2005; Linol and Wit, 2016). 'Karoo' is also used for all the coeval basins that developed across Africa since the Late Carboniferous regardless of the tectonic regime (see the discussion of Guillocheau et al., 2018). These basins record continental deposits interbedded with volcanic rocks and lack datable marine fossils. Thus the chronostratigraphic framework for these basins remains poorly understood. Frizon De Lamotte et al. (2015) suggest a two-step scenario, by splitting all the Karoo basins in two groups. The Karoo I basins gathers the Late Carboniferous to Triassic poly-phased depocenters, overall trending NE-SW; and the Karoo II basins the Jurassic depocenters associated with extension due to the impact of the Karoo plume (Bouvet hotspot) and breakup of East Africa from Madagascar and East Antarctica. In this study, to characterize the chronology of the Karoo rifting, we follow the rationale of Frizon De Lamotte et al. (2015) and compliment it with the work of Nairn et al. (1991), Smith et al. (1993), Zerfass et al. (2005), Mahanjane (2012), Mueller and Jokat (2017), Guillocheau et al. (2018), and the recent review for the East Africa region by Davison and Steel (2018).

We present in figure 6.5 a map of the Mesozoic basins in southern Africa. Onshore, besides the Main Karoo Basin (MKB) the other Karoo depocenters are distributed along two axes oriented ENE: 1) the Waterberg-Zambezi axis (Karoo I sensu Frizon De Lamotte et al., 2015); and 2) the Kalahari- Botswana-Limpopo axis (Karoo II). In East Africa, a group of N-S oriented grabens are observed, but they are consequence of two different origins: 1) the Lebombo monocline (Klausen, 2009) and its eastern extension in the Zululand basin (Broad et al., 2012), of Early Jurassic age (Karoo II); and 2) a group of grabens to the East of Early Cretaceous age in the area of Beira (Mozambique).

The southeast coast of Africa is an abrupt margin largely characterized by the dextral movement of Africa along the Agulhas-Malvinas FZ. However, the synrift of the Durban basin (Fig. 6.5), drilled offshore, produced Late Jurassic to Late Valanginian ages and was correlated to the red beds described in the Zululand basin by Visser (1998).

In southern South Africa, extensional reactivation of the Cape foldbelt throughout the Mesozoic has been described by De Wit and Ransome (1992); Paton (2006) and Paton et al. (2016). These reactivations are interpreted to have taken place intermittently during the different extensional events that Africa experienced in the Mesozoic, but so far, they are poorly constrained in age as many other Karoo basins.

Offshore, the Outeniqua basin is formed of several WNW-trending half-grabens, named from east to west: Algoa, Gamtoos, Pletmos and Bredasdorp sub-basins (Fig. 6.5). These half-grabens are bounded by SW-dipping, en echelon listric faults, coherent with the extensively-reactivated thrusts of the Cape foldbelt further north (Fourché et al., 1992; Paton and Underhill, 2004). These faults display an arcuate shape, changing strike from WNW to NNW towards the east as they approach the AMFZ (Fig. 6.5). It had been suggested that the arcuate shape is inherited from the Cape foldbelt (De Swardt and McLachlan, 1982), however, it seems more probably an effect of strike-slip along the AMFZ (Broad et al., 2012). For the chronology of rifting, we follow here the review of Broad et al. (2012) and the references therein.

Figure 6.5 (next page): Map of the main Mesozoic basins of southern Africa (Af). MKB: Main Karoo basin, Etj: Etjó, Wtb: Waterberg, MZa: Mid-Zambezi, Li: Limpopo, Bo: Botswana, Ka: Kalahari, MOZB: Mozambique basin, Le: Lebombo, Zu: Zululand, Du: Durban, , Wal: Walvis, Lu: Luderitz, Or: Orange, CB: Cape basin, CFB: Cape Fold Belt; Ou: Outeniqua basin. Outeniqua sub-basins: B: Bredasdorp, P: Pletmos, G: Gamtoos, A: Algoa. After Smith et al. (1993), Frizon De Lamotte et al. (2015), Nairn et al. (1991), Mahanjane (2012), Mueller and Jokat (2017), Stollhofen et al. (1998), Davison and Steel (2018), Broad et al. (2012), Clemson et al. (1999), Koopmann et al. (2014), and Paton et al. (2016). Background topography from Etopo 1 (Amante and Eakins, 2009).

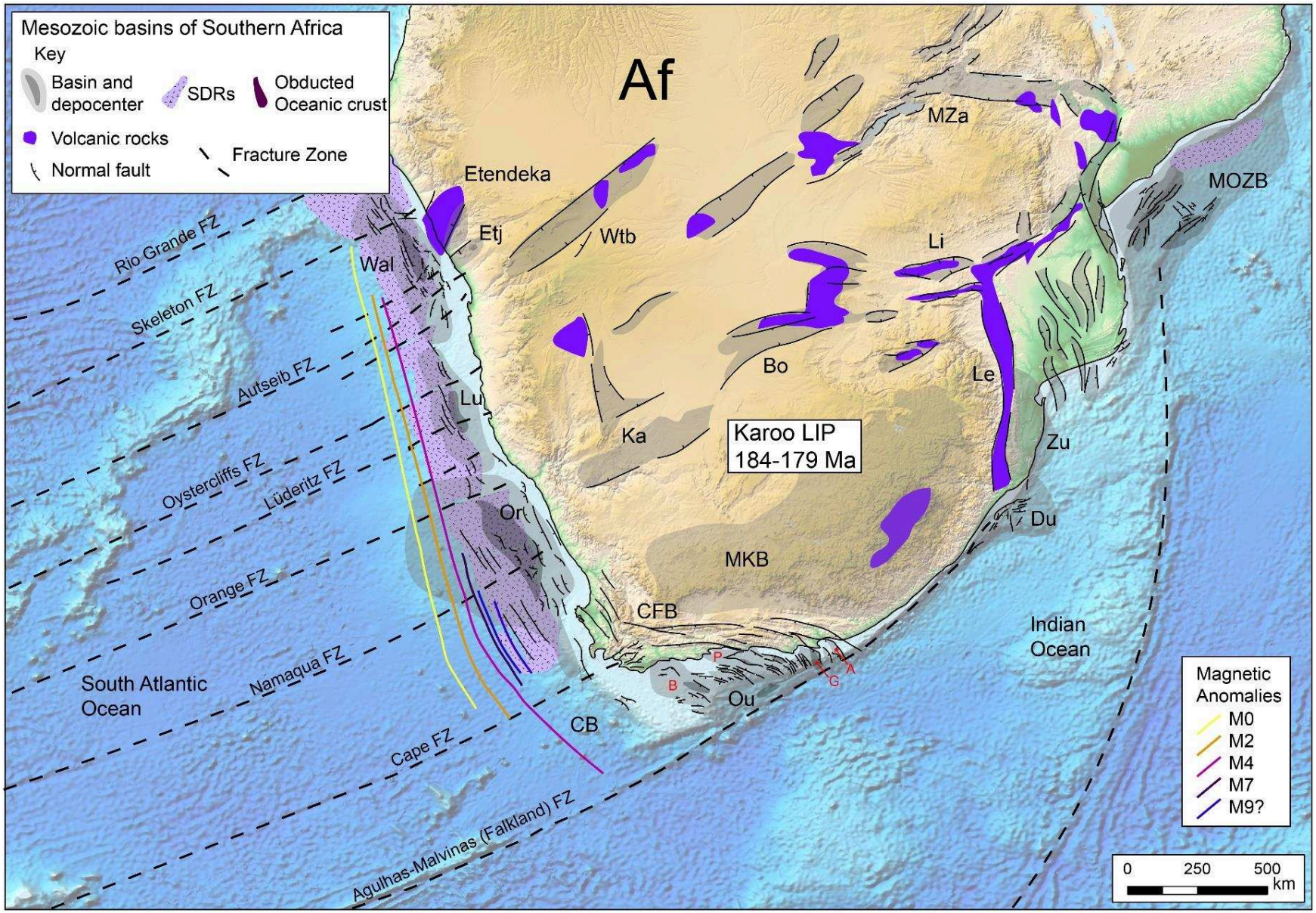
Mesozoic basins of Southern Africa
Key
Basin and depocenter
SDRs
Obducted Oceanic crust
Volcanic rocks
Fracture Zone
Normal fault
Af
Etendeka
Etj
Wtb
Wal
MZa
MOZB
Li
Bo
Le
Zu
Du
Lu
Ka
Karoo LIP
184-179 Ma
Or
MKB
CFB
Ou
CB
Indian Ocean
South Atlantic Ocean
Rio Grande FZ
Skeleton FZ
Autseib FZ
Oystercliffs FZ
Lüderitz FZ
Orange FZ
Namaqua FZ
Cape FZ
Agulhas-Malvinas (Falkland) FZ
Magnetic Anomalies
M0
M2
M4
M7
M9?
0
250
500
km

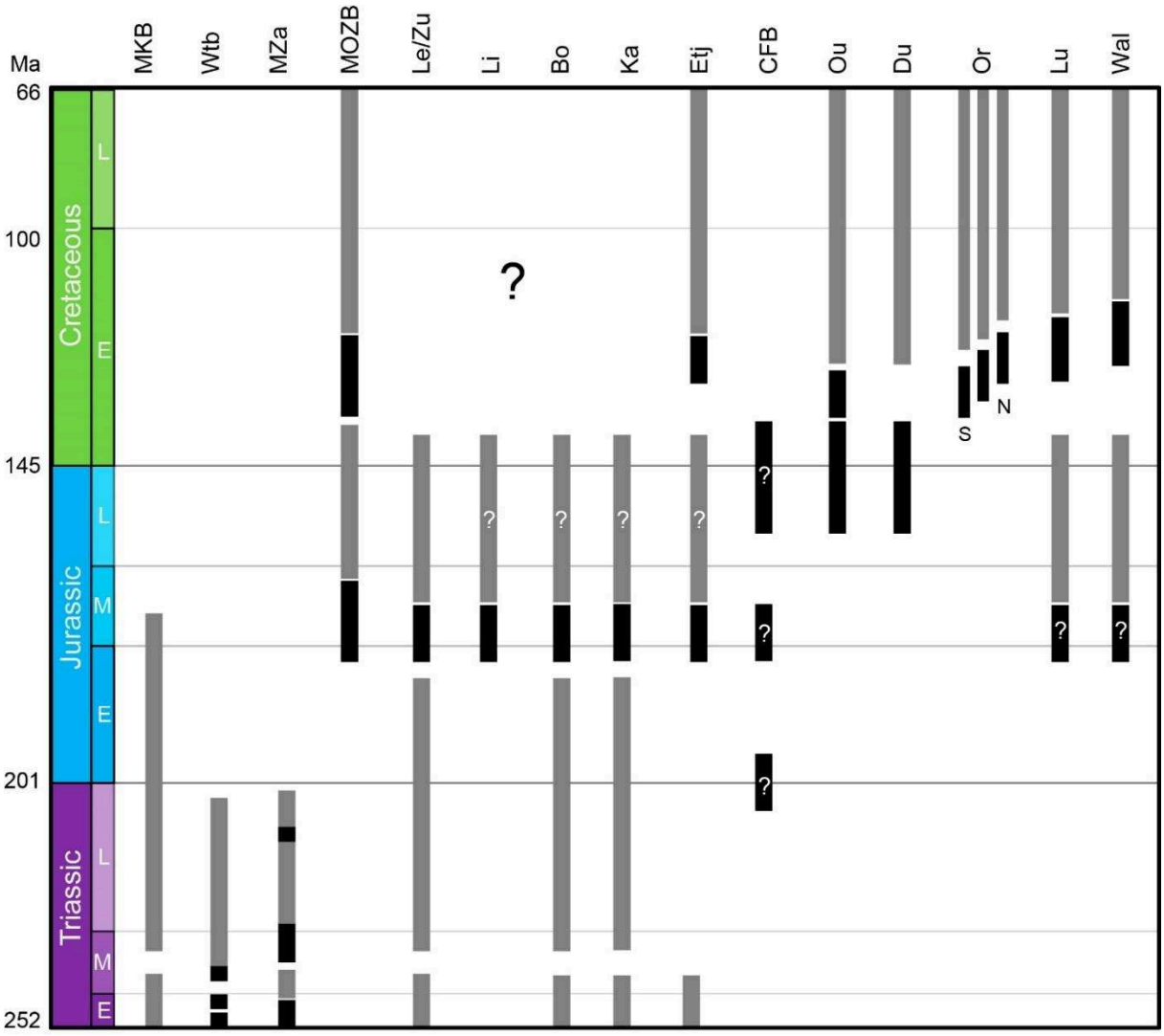

Figure 6.6: Rifting chronology chart for the main Mesozoic basins of southern Africa. Black bars indicate perionds of active rifting, grey bars indicate interpreted postrift sedimentation. Main Karoo Basin (MKB) after Catuneanu et al. (2005), and Duncan et al. (1997). Waterberg (Wtb) and Mid-Zambezi (MZa) after Zerfass et al. (2005) and references therein. Mozambique basin (MOZB) after Mueller and Jokat (2017). Limpopo (Li) and Lebombo (Le) monocline ages after Jourdan et al. (2007), and Klausen (2009). Botswana (Bo), Kalahari (Ka) and Etjó (Etj) basins after Catuneanu et al. (2005) and Smith et al. (1993). Etjó also records the Etendeca Zululand (Zu) and Durban (Du) after Broad et al. (2012). Etjó basin (Etj) after Renne et al. (1996).

Two synrift units are identified across the different Outeniqua sub-basins. The first synrift package starts with fluvial sediments, overlaid by a shallow marine succession (dated Kimmeridgian/Tithonian), topped by a fluvial section. The unconformity between synrift I and II is a regional unconformity of intra-Valanginian age, named 1At1 offshore South Africa (Broad et al., 2012; Jungslager, 1996), that was interpreted to mark the onset of strike-slip movement along the AMFZ (du Toit, 1979). The synrift II varies considerably across the Outeniqua basin: shallow marine Valanginian-Hauterivian beds deposited in the Algoa sub-

basin (Valicenti and Stephens, 1984), while deep-water Hauterivian shales are present in the Bredasdorp sub-basin (Broad et al., 2012).

The structure of the western Atlantic margin of Africa, is marked by development of Early Cretaceous basins oriented NNW, parallel to the present-day coastline and a volcanic margin with abundant SDRs, conjugate to the Argentinean margin. The Orange basin is the most prominent basin of the margin, occupying the eastern coast of South Africa and southern Namibia. Several half-grabens developed on continental crust, three of which have been drilled. The oldest dated sediments are Hauterivian lacustrine shales (Broad et al., 2012). Several SDR wedges develop to the west, on the continent-ocean transition. Absolute ages have not been published, but SDRs were interpreted to emplace in the Hauterivian (Broad et al., 2012). A Barremian biostratigraphic age is reported for some sedimentary packages interbedded with volcanics in the Kudu well (McMillan, 2003). The breakup unconformity (named 6At1) is dated late Hauterivian and deeply erodes the more proximal eastern depocenters (Broad et al., 2012). A complete review of the Atlantic volcanic margin was presented by Gladczenko et al. (1998) and Jungslager (1999), and more recently by Koopmann et al. (2014). The margin is transected by several E-W oriented fracture zones (FZ, Fig. 6.5) which, similarly to what is observed on the Argentinean shelf, affect the COT and the outer continental crust domain. The formation of FZ is a process interpreted to be deeply related to breakup in volcanic segmented margins and SDR emplacement.

The distribution of SDRs, however, is not the same along the margin. Similarly to what is observed on the conjugate Argentinean margin, the southernmost segment of the African Atlantic margin, between the AMFZ and the Cape FZ seems to be lacking SDRs (Koopmann et al., 2014b), this segment is referred to as the Cape basin. The southernmost segment corresponds to the Outeniqua basin developed on continental crust, but the crustal structure of the COT remains poorly constrained. To the north, the different FZ segmenting the margin present a dextral component. The oldest magnetic anomalies (M9 to M7, according to Koopmann et al., 2014) were determined in the southernmost segment with SDRs (just north of the Cape FZ) and disappear to the north, illustrating diachronism in the South Atlantic opening as it was demonstrated in the Pelotas basin by Stica et al. (2014).

To the north of the Orange basin, two other basins are described on the Namibian margin south of the Walvis Ridge, these are the Luderitz and Walvis basins (Fig. 6.5), which are also characterized by faults largely oriented parallel to the COT and to the present-day coastline

(Clemson et al., 1997). These basins are also interpreted to be of Neocomian age and conjugate with the Pelotas basin (see Cartwright et al., 2012). A thick pre-rift unit is interpreted on seismic data and correlated with Karoo-age sediments of the Namib rift and volcanics of the Etendeka Group (Clemson et al., 1999). The Etendeka basalts are equivalent to the Serra Geral basalts (onshore South America) and form part of the Paraná-Etendeka LIP (Milner et al., 1995). A 132 Ma age, close to the Valanginian-Hauterivian boundary, was produced by Renne et al. (1996).

6.5 MESOZOIC RIFTING IN SW GONDWANA

Mesozoic was an era of continental dispersion following the amalgamation of Pangea, which ended in the Permian with the collision of Patagonia against the southwestern margin of Gondwana. In this section we present, in a set of four paleo-tectonic maps, the rifting evolution of the different Mesozoic basins of SW Gondwana (Figs. 6.7 to 6.10). Besides the Early Cretaceous South Atlantic breakup, we intend to illustrate the different rifting stages that occurred since the Early Mesozoic. We refer to Frizon De Lamotte et al. (2015) for a review of the initial Pangea breakup and the Late Paleozoic rifting which remains out of the scope of this study.

6.5.1 Triassic-Early Jurassic Rifting

In this first stage we have put together all rifting taking place throughout the Triassic (indicated by purple faults in Fig. 6.7) and until the Earliest Jurassic (red faults in Fig. 6.7 indicate extensional activity in the Late Triassic-Early Jurassic). We highlight three depocenters a series of aligned depocenters in Patagonia, in the SW Gondwana retroarc and two orthogonal features. The retroarc depocenters (1 in Fig. 6.7) include the Cuyo, Bermejo, Neuquén, Deseado basin and possibly some extension into the Malvinas basin area. The other two extensional features at high angles with the margin are: the axis formed by the Santa María (Brazil) and the Waterberg and Mid-Zambezi basins extending into East Africa as part of the Karoo I system (2 in Fig. 6.7) sensu Frizon De Lamotte et al. (2015); and the Permian-Early Triassic Cape fold-and thrust belt, and its extension into South America known as the Ventania system, reactivated throughout the Mesozoic (3 in Fig. 6.7).

Because of changes in subduction dynamics, the SW margin of Gondwana experienced different stages of extension throughout the Mesozoic. Following a period of flat slab

subduction that lasted between the Late Carboniferous and the Early Permian (Ramos and Folguera, 2009), slab steepening and possibly slab detachment produced the rhyolitic flare of the Choiyoi Magmatic Province, widely distributed in Central Chile and Argentina (Llambias et al., 2003). Subduction was probably continuous since the Triassic. In central Chile, the volcanic arc was established since the Early-Middle Triassic in the Domeyko Range (Fig. 6.7), and migrated to the west (towards the trench) to the Coastal Cordillera in the Early Jurassic (Oliveros et al., 2018; Fig. 6.8). In northern Chile, the Triassic arc is present in the Coastal Cordillera (Maksaev et al., 2014). The presence of a Triassic arc and its trench-ward migration until the Early Jurassic was also observed in the Antarctic Peninsula (Fig. 6.7) by Storey et al. (1992), who linked these observations to a steepening of the subducting plate and highlighted the importance of subduction-plate boundary forces in the initial stages of Gondwana breakup.

A series of extensional basins developed in the retroarc, product of slab-steepening. The Bermejo and the Cuyo basins in western Argentina have been related to the evolution of the Gondwanide active margin (Zerfass et al., 2004). U-Pb zircon ages for the Cuyo basin and indicate several pulses of rifting throughout the Middle Triassic (Spalletti et al., 2008; Barredo et al., 2012). An Early Triassic age is suggested for rift initiation in the Bemejo basin (Stipanicic and Bonaparte, 1979). Recent U-Pb zircon ages from tuffs interbedded in the late synrift units (sensu Milana and Alcober, 1994) indicate Middle to Late Triassic ages of 236-234 Ma (Marsicano et al., 2016). The location and the orientation of these basins is a consequence of crustal heterogeneities as they were emplaced in the hanging wall of the sutures between Paleozoic terranes (Ramos and Kay, 1991). Triassic depocenters develop as well in central and northern Chile (see Mpodozis and Ramos, 2008; and Espinoza et al., 2018)

In Patagonia, the Central Patagonia Batholith (Rapela et al., 1991), and the Chonos Metamorphic Complex of Late Triassic-Early Jurassic age (Hervé and Fanning, 2001; Willner et al., 2000) were associated with active subduction along this segment (Fig. 6.1; (Rapela et al., 2005; Zaffarana et al., 2014). However, Kay (1993) interpreted the Central Patagonian Batholith as extension-related, and there is still debate on the batholith arc nature. Further east, in the Deseado massif, the Mid-Late Triassic El Tranquilo basin was a NNW-oriented rift filled with fossil-rich continental deposits interbedded with volcanic rocks (Haller, 2002). The El Tranquilo basin probably developed as a late stage of the Permian extension recorded in the Deseado massif by the La Golondrina rifting (Homovc and Constantini, 2001). Offshore, the

San Julián and Malvinas basins might record a similar stratigraphy. Depocenters of both basins remain unexplored.

Moving to the intracratonic area, Zerfass et al. (2005) proposed the correlation of the Triassic Santa Maria with the Waterberg and Mid-Zambezi Karoo I basins in Africa. Guillocheau et al. (2018) extended this correlation for other basins in Eastern Africa, India and Australia. There seems to be a relationship between these Karoo I depocenters and the rifting and successive breakup in the Central Atlantic between NW Africa and eastern North America, both because of the geometrical sub-parallel relationship and the synchronicity (see Fig. 6.1).

Following the end-of-compression in the Cape fold belt in the Early Triassic, negative inversion of the compressive structures has been identified in Africa by De Wit and Ransome (1992) both onshore on the Cape fold belt itself, and towards the south, in the Outeniqua basin. The chronology of this extensional reactivation is poorly constrained. Offshore in Outeniqua, the oldest datable marine sediments are of Late Jurassic age, but onshore the sedimentary infill indicates more proximal environments, the Enon Fm. conglomerates of largely Late Triassic-Jurassic age (Dingle, 1973). Reactivation took place probably in several pulses (Fig. 6.6). Extensional reactivation of previously compressive structures has been identified offshore Argentina, in the Colorado basin, by Pángaro and Ramos (2012) and Lovecchio et al. (2018) and below the Orange basin by Paton et al. (2016).

In the Neuquén basin, Late Triassic to Early Jurassic rifting is recorded by the Precuyano cycle. Depocenters filling seems diachronous, older in the north, becoming younger towards the south (Fig. 6.4; D'Elia et al., 2015). In the southern Neuquén basin extension reactivates E-W-oriented Late Paleozoic structures (Fig. 6.7), associated with the Patagonia collision, in the Huincul ridge area (Mosquera and Ramos, 2006). This Late Triassic-Early Jurassic rifting event was correlated with the extensional reactivation of the offshore extension of the Ventania-Cape fold belt in the Colorado basin by Lovecchio et al. (2018).

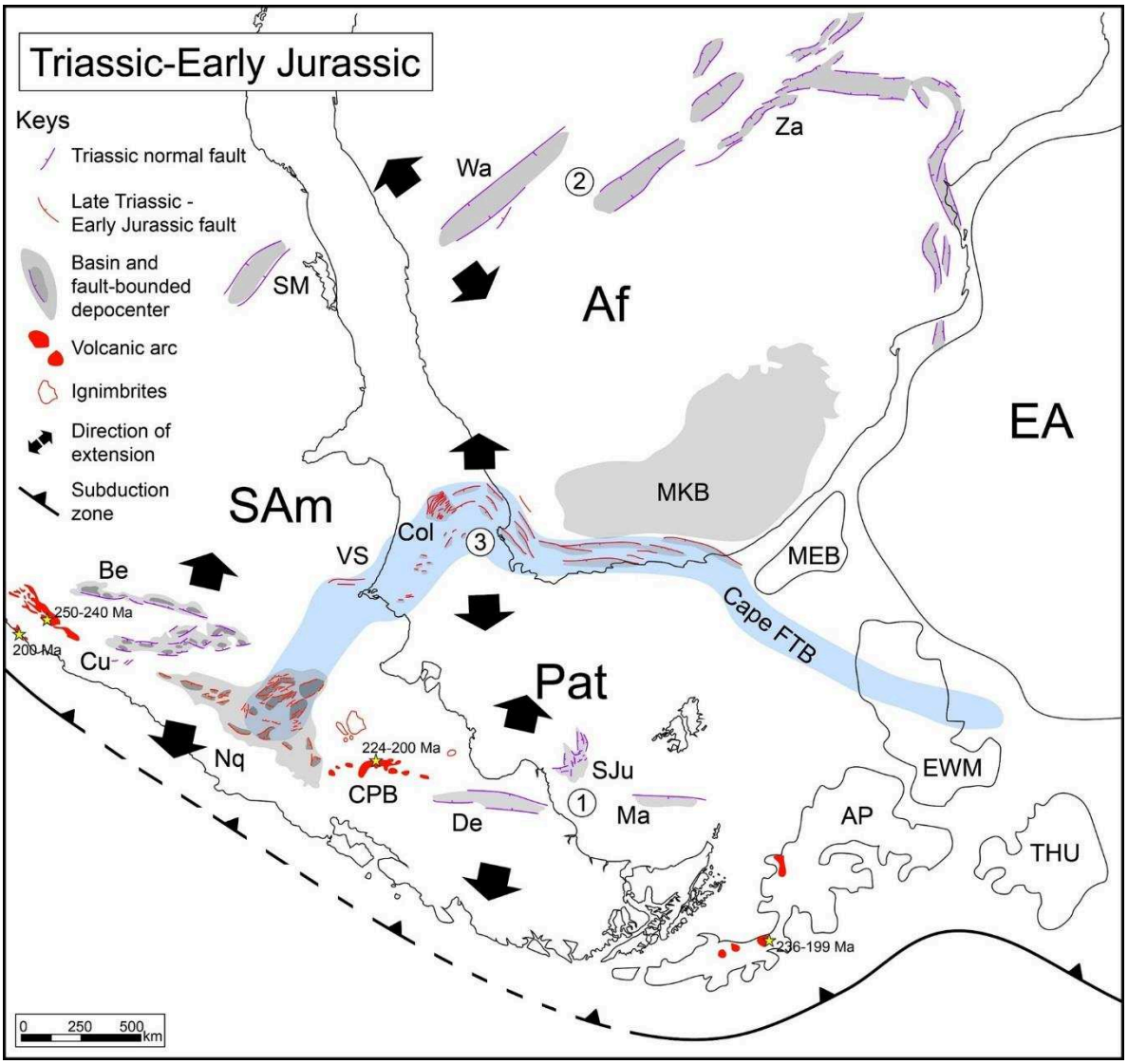

Figure 6.7: Paleo-tectonic reconstruction of SW Gondwana at 200 Ma. Africa in its present-day position. Gondwana fit after Dalziel et al. (2013). Triassic volcanic arc in Central Chile after Oliveros et al. (2018), Central Patagonian Batholith (CPB, age after Rapela et al., 2005). Volcanic arc in the Antarctic Peninsula after Storey et al. (1992) Basins develop in a back-arc: Cuyo (Cu), Bermejo (Be), faults after Uliana et al. (1995); or intracratonic setting: Santa Maria (SM), Waterberg (Wa), Zambezi (Za), after Zerfass et al. (2004), San Julián (SJ, after Micucci et al., 2011a). Late Triassic-Early Jurassic basins: Neuquén (Nq, Precuyano cycle, faults after Bechis et al., 2014), Deseado (De) and Malvinas (Ma) basins after Uliana et al. (1989). The previously compressive faults of the Ventania (VS) - Cape Permian-Early Triassic fold and thrust belt (FTB, in blue) have been extensionally reactivated in the Colorado (Col) and Cape (Cap) area (Lovecchio et al., 2018; Mosquera et al., 2011; Mosquera and Ramos, 2006; Paton, 2006). MKB: Main Karoo basin. Tectonic blocks: South America (Sam), Patagonia (Pat), Africa (Af), Maurice Ewing Bank (MEB), Eastern Antarctica (EA), Ellsworth-Whitmore Mountains (EWM), Antarctic Peninsula (AP), Thurston Island–Eights Coast (THU). 1, 2 and 3 are different groups of basins referred in the text.

6.5.2 Early - Middle Jurassic Rifting

In the second stage represented in figure 6.8, we put together two key events: the Karoo II rifting (sensu Frizon De Lamotte et al., 2015), consequence of the impact of the Karoo mantle plume in East Africa, and the effect of the Chon Aike magmatic province in the SW Gondwana margin retroarc (sensu Pankhurst et al., 1998).

We have mapped the maximum extension of the Karoo volcanics (Fig. 6.8) and obtained a diameter of influence of the mantle plume of about 2,000 km, consistent with suggestions of White and Mckenzie (1989). According to Frizon De Lamotte et al. (2015), various evidences such as regional doming and volcanism preceding rifting, are evidence of an active rifting process, with plume impingement being the triggering mechanism for the Karoo II event. The presence of a potential triple junction in East Africa (Fig. 6.8) has increased the debate. Jourdan et al. (2004) suggests that the Jurassic Karoo igneous dykes were emplaced along reactivated Proterozoic mobile belts between cratons, and thus the variety of dykes' orientations would not be due to a triple junction, but conditioned by the basement fabric. Anyhow, the Limpopo area remains the geographic center of volcanic activity and ENE seems to be the predominant orientation of rifts. Some authors relate the Karoo rifting to subduction process, a rifting that would have been accentuated, but not triggered by the Karoo plume (Storey et al., 1992).

In the Mozambique basin area (Fig. 6.8), rifting evolved and succeeded throughout the Early - Middle Jurassic, with SDR emplacement in the Bathonian and normal oceanic crust accretion since the Callovian (Mueller and Jokat, 2017).

On the southwestern margin of Gondwana, a new phase of extension is recorded in the Neuquén basin during the Early Jurassic: the Cuyano cycle. This extension is associated with larger depocenters formed by reactivation of some Precuyano structures (Vergani et al., 1995). The Neuquén basin and the Chubut basin, further south, developed behind the same Early Jurassic magmatic arc, represented by the Subcordilleran Batholith (Fig. 6.8).

Huge magmatic volumes where extruded during the Early to Middle Jurassic in Patagonia and form the Chon Aike magmatic province (Fig. 6.8; Pankhurst et al., 2000). For the Early Jurassic, acidic volcanism is coeval with arc volcanism in the Subcordilleran Batholith (Rapela et al., 2005), which is emplaced westward from the Triassic Central Patagonian Batholith (see Fig. 6.7). This implies arc migration towards the paleo-pacific trench, which is

consistent with slab retreat (Mpodozis and Ramos, 2008). Suárez and Márquez (2007) proposed that the Toarcian Chubut basin developed in the former forearc region of the Upper Triassic magmatic arc given by the Central Patagonian Batholith, and in the retroarc of the coetaneous Early Jurassic, easterly subduction-related arc, indicated by the Subcordilleran Batholith. According to these authors, the closure of the Chubut basin in the Middle Jurassic coincides with a new westward migration of the magmatic arc, from a position in central extra-Andean Patagonia and a NNW orientation, to a location in the Patagonian Cordillera and a north-south orientation.

Slab retreat is also coherent with the extensional regime in the retroarc observed in other extensional basins of this age that developed further south. If we interpret the orientation of the mafic dykes in the Malvinas (Falkland) Islands as indicators of stress orientation (sigma 3) for the Early Jurassic. We observe a diachronism between these structures and the Middle Jurassic synrift infill, dated in the Austral (Magallanes) basin (Pankhurst et al., 2000). Thermochronological data from the Malvinas (Falkland) islands (Thomson et al., 2002) indicate exhumation in the Early-Middle Jurassic, consistent with shoulder uplift, respect to the Malvinas basin. Further west, in the Austral (Magallanes) basin, Malkowski et al. (2015) highlight diachronism of rifting initiation and bimodal volcanism towards the northwest, as well as diachronism of oceanic crust accretion in the Late Jurassic for the Rocas Verdes back-arc basin, which also becomes younger towards the north (see Fig. 6.9).

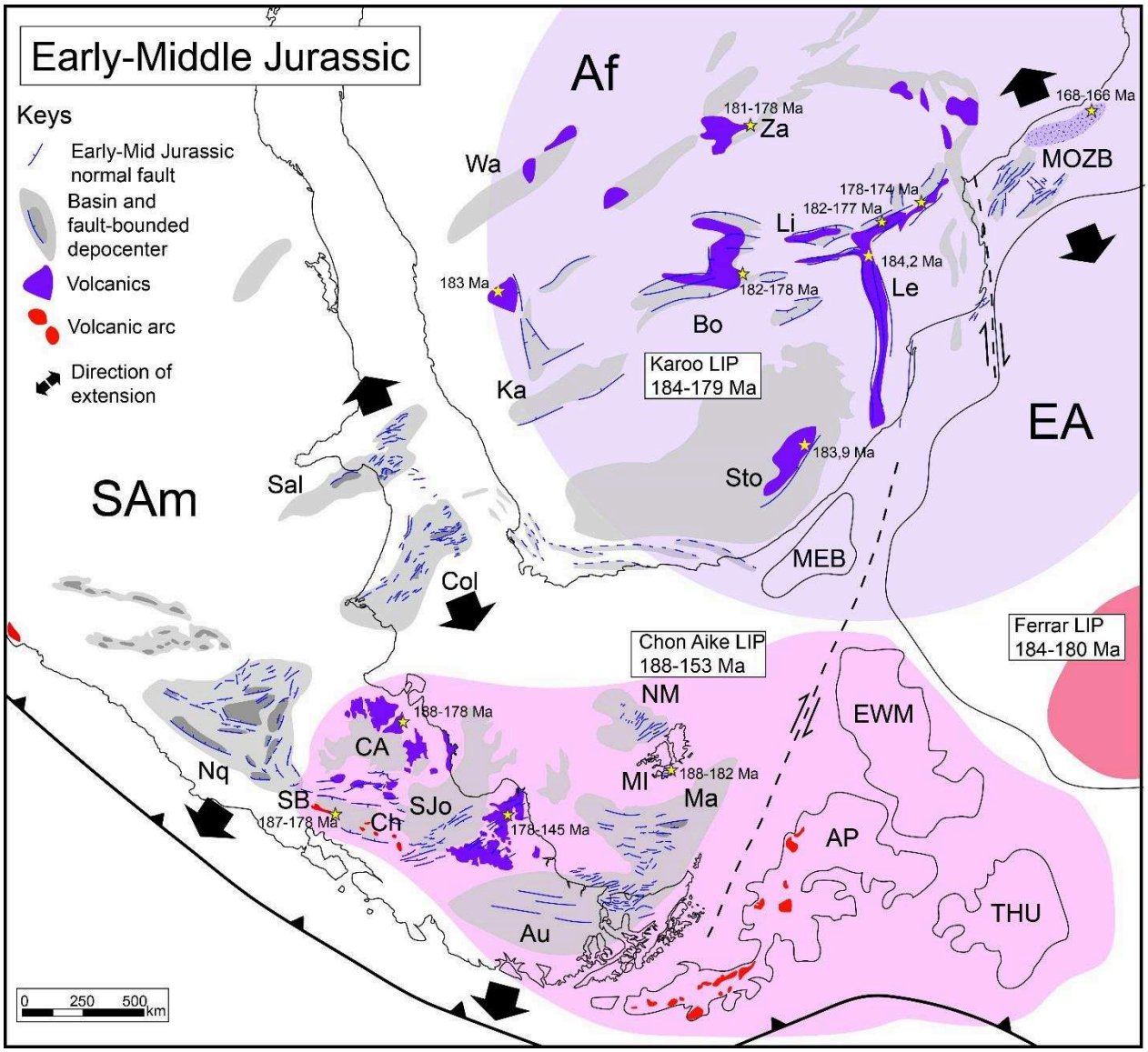

Figure 6.8: Paleo-tectonic reconstruction of SW Gondwana in the Early-Mid Jurassic. Gondwana fit after Dalziel et al. (2013). Eastern Africa and Eastern Antarctica are impacted by the Karoo mantle plume (purple), coeval with the Ferrar LIP (red) and Chon Aike LIP (pink, Pankhurst et al., 2000). Karoo rifts: Kalahari (Ka), Botswana (Bo), Limpopo (Li), Lebombo (Le), Stormberg (Sto), Mozambique (MOZB), ages from Jourdan et al. (2005), and Mueller and Jokat (2017). In South America, this is a period of intense rifting in the Colorado (Col), Salado (Sal) and Neuquén basins (Nq, Cuyano cycle). Also in the Cañadón Asfalto (CA) and San Jorge (SJ) basins. The Liassic Chubut basin (Ch) is a back-arc basin for the arc-related Subcordilleran Batholith (SB, age after Rapela et al. (2005). Dikes of this age reported in the Malvinas islands (MI; Ramos et al., 2017). The Tobífera Series in the Malvinas (Ma) and Austral (Au) basins also developed at this time (Pankhurst et al., 2000; Uliana et al., 1989).

For the Antarctic Peninsula, Storey et al. (1992) observe a westward migration of the Jurassic arc compared to the Triassic arc (see Fig. 6.7 and 6.8 for comparison) and development of back-arc extension and magmatism. The Early Jurassic magmatism in the Antarctic

Peninsula has been also correlated with the subduction-related Subcordilleran Batholith in Patagonia by Riley et al. (2016).

The Colorado and Salado basins are located between, but presumably outside, the areas affected by magmatism of the Karoo and the Chon Aike LIPs (Fig. 6.8). This Early-Middle Jurassic rifting stage has been interpreted responsible for the formation of the main depocenters of the Colorado and Salado rifts (Lovecchio et al., 2018). This event is associated with SW-NE to N-S extension in present-day South America. In a paleo-tectonic perspective (Fig. 6.8), these basins are aligned with the ENE-oriented Karoo II Kalahari, Botswana, Limpopo and Mozambique rifts in Africa. The Colorado and Salado rifts could be the westernmost extension of the Karoo II rift basins (Fig. 6.8).

6.5.3 Late Jurassic

In the Late Jurassic, oceanic crust accretion was already occurring in the Mozambique channel in East Africa. In order to accommodate relative displacement of Antarctica (East Gondwana) with respect to South America and Africa (West Gondwana) during the opening of the channel, König and Jokat (2006) propose firstly the establishment of a dextral strike-slip deformation zone, precursor of the Weddell Sea (here represented at its early stage in Fig. 6.8). Once East and West Gondwana became completely detached, continental dispersal initiated and the deeply-rooted strike-slip zone started acting as an oceanic ridge, giving birth to the Weddell Sea (Fig. 6.9). There are multiple possible scenarios regarding the origin and evolution of the Weddell Sea, mainly due to the lack of geological information (Ghidella et al., 2002). One of the conjugate margins, on Western Gondwana (present-day southern South America) was consumed by subduction under the Scotia plate during the Cenozoic. The other conjugate, on Eastern Gondwana, is covered by ice most of the year in the Antarctic territories, and difficult to access and study. Magnetic data from the present-day Weddell Sea were documented by Ghidella et al. (2002) and König and Jokat (2006). A possible SDR wedge associated with the Gondwana breakup is also illustrated (Explora wedge, Hinz, 1981; Kristoffersen et al., 2014).

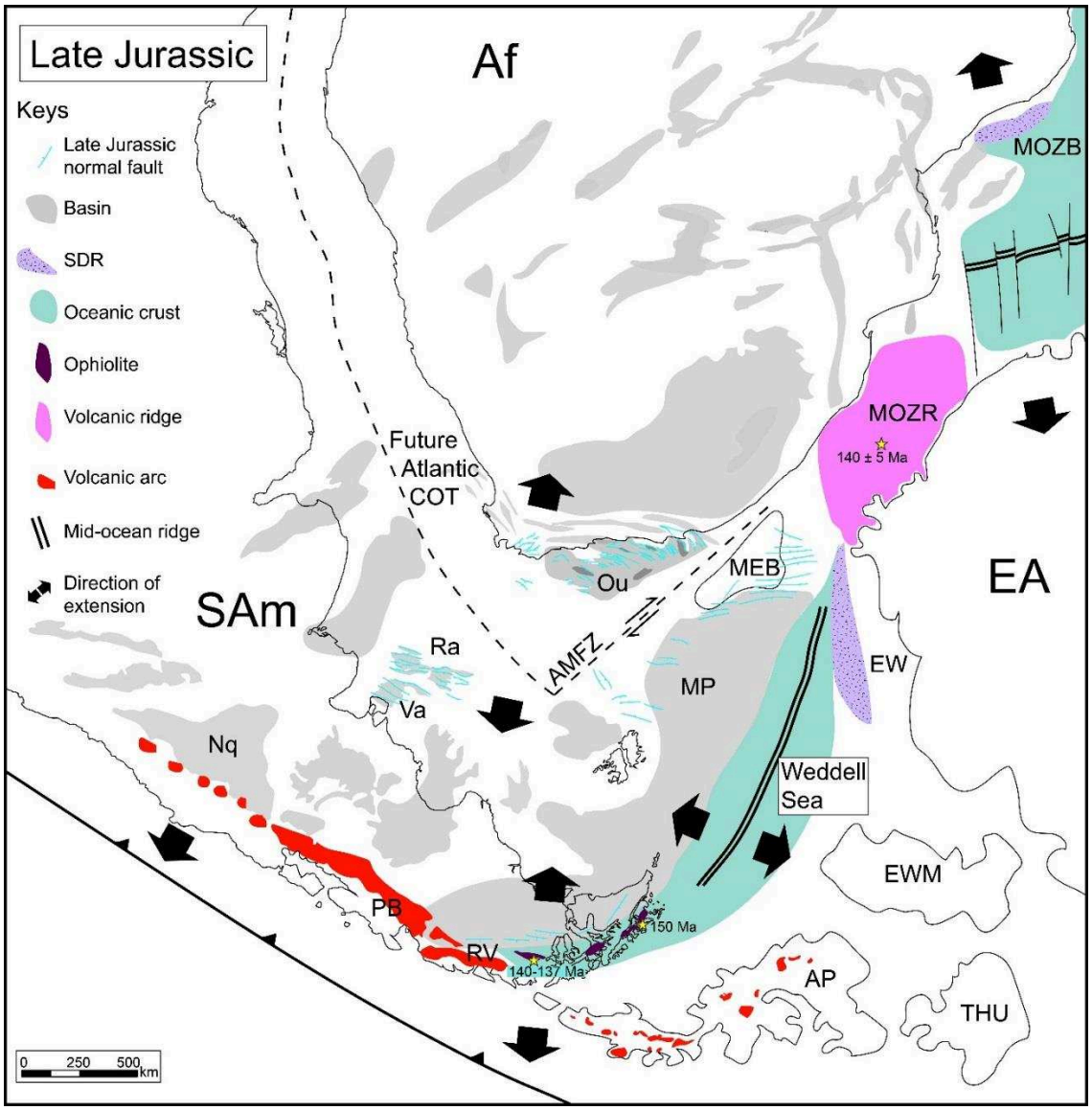

Figure 6.9 (previous page): Paleo-tectonic reconstruction of SW Gondwana in the Late Jurassic. Gondwana fit after König and Jokat (2006). The Mozambique channel opens as Antarctica moves south. Wrenching along the South America-Antarctica limit ends with seafloor spreading and the origin of the Weddell sea. Mozambique ridge (MOZR) age after Mueller and Jokat (2017). The Rocas Verdes (RV) back-arc basin develops to the west of the Austral basin. Schematic Patagonian Batholith (OB) after Rapela et al. (2005). Oceanic crust ages after Mukasa and Dalziel (1996) and Stern et al. (1992). Oblique rifting produced the formation of the Rawson/Valdés (Ra/Va) and Outeniqua (Ou) basins in the core of the Late Paleozoic Gondwanides orogen. Wrenching along the future Agulhas-Malvinas fracture zone (AMFZ) will release South America from Africa and produce the breakup along the Neoproterozoic orogenic belt.

On the Pacific margin, arc migration to the west continued in central Patagonia, with the establishment of the Andean Patagonian batholith in the Late Jurassic (Fig. 6.9). It involves westerly migration and clockwise rotation of the arc, suggesting differential rollback of the subducted slab (Rapela et al., 2005).

Rifting associated with opening of the Rocas Verdes back-arc basin in the Late Jurassic is represented by bi-modal magmatism, and the successive onset of oceanic crust accretion (Calderon et al., 2016). The Rocas Verdes was probably a N-S elongated basin (possibly not originally curved, see Vérard et al., 2012). The marine connection between this back-arc basin and the Weddell Sea seems possible, however, tectonically these basins are related to two independent mechanisms. Opposite to Diraison et al. (2000), who suggested a connection of the mid-oceanic ridges of the Rocas Verdes basin and the Weddell Sea via a system of transform faults, we favor a solution as the one proposed by Vérard et al. (2012), by having two independent oceanic basins: the Rocas Verdes back-arc basin produced by negative roll-over of the subducting plate, and the Weddell Sea generated by normal oceanic accretion on both sides of an active oceanic ridge. However, we disagree with some aspects of the reconstructions presented by Vérard et al. (2012), especially regarding the N-S extent of the Rocas Verdes back-arc basin, the amount of extension (final width) and shape (they favor a N-S elongated back-arc basin all along the margin). Rocas Verdes was an asymmetric basin, where rifting started earlier in the south (Malkowski et al., 2015), thus producing more cumulative extension than in the north, generating an asymmetric, triangular shaped basin (also consistent with clock-wise rotation of the arc). The northernmost obducted oceanic crust outcrops south of 51°S (Sarmiento Complex), suggesting that the back-arc basin could not have reached the 48°S latitude (Fig. 6.3 and 6.9). The impact of the Patagonian orocline in curving the remnants of the Rocas Verdes basin in the south, plays an important role and remains a matter of discussion out of the scope of this study (Ghiglione and Cristallini, 2007; Torres Carbonell et al., 2016). In our reconstruction (Fig. 6.9) we present the Patagonian orocline and the Fuegian Andes in their present-day position.

In Africa, Late Jurassic marine sediments are recorded in the Outeniqua basin. In a paleo-tectonic perspective (Fig. 6.9), regardless the continental fit used, fault orientation in the Outeniqua and in the Rawson/Valdés basins in South America seem rather parallel, consistent with largely present-day N-S extension for Africa (ENE extension for present-day South America). As suggested by Continanzia et al. (2011), we associate both basins with a single oblique rifting event initiated in the Late Jurassic. The extensional faults observed around the Maurice Ewing Bank (MEB in Fig. 6.9), and the faults associated with the Malvinas (Falkland) Plateau possibly belong to the same rifting event.

6.5.4 Early Cretaceous

The main tectonic event taking place in the Early Cretaceous is the opening of the South Atlantic Ocean, related to E-W extension between Africa and South America. This process has been interpreted to be diachronous, initiating in the south and progressively propagating northwards (Nürnberg and Müller, 1991). The southern South Atlantic is a volcanic (or magma-rich) margin. These margins are characterized by the presence of SDRs on the continental-oceanic transition domain (COT), an area where normal continental crust passes to oceanic crust, with a gradient in crustal thickness and composition. Volcanic margins have been related to high extension rates (Frizon De Lamotte et al., 2015). The northwards migration of rifting and ocean spreading took place in segments. Both conjugate margins, South American and African, present a strong segmentation. The structures limiting the different segments are fracture zones (FZ), which have been interpreted to be active at least since SDR emplacement (Franke, 2013; Franke et al., 2007). For reference on the segmentation of the South Atlantic margin, we refer to Clemson et al. (1997), Franke et al. (2007), and Blaich et al. (2009). Several models have been published regarding the origin of SDR and possible mechanisms of emplacement (Hinz, 1981; Planke et al., 2000; Talwani and Abreu, 2000; Pindell et al., 2014; Quirk et al., 2014; Paton et al., 2017; Clerc et al., 2018; among others) and remain out of the scope of this study. We intend to characterize however the architecture of the margin to better understand the rifting evolution.

It is interesting to note the apparent absence of SDR in the southernmost segment of the southern South Atlantic, where the Argentina and Cape basins develop, an area bracketed between the Agulhas-Malvinas (Falkland) FZ and the Colorado-Cape FZ (Fig. 6.3 and 6.5). For the South American margin, the lack of SDRs in the southernmost segment had been interpreted, considering the influence of the Agulhas-Malvinas FZ, as part of a transform margin offshore Argentina (Becker et al., 2012). Another characteristic to analyze is the difference in length (N-S) of the magma-poor segment on both sides of the South Atlantic (see Fig. 6.10): 380 km north of the AMFZ offshore South America (Franke et al., 2010) and approximately 460 km between the AMFZ and the first occurrence of SDRs offshore South Africa. This difference was interpreted by Koopmann et al. (2014) as a product of a pre-breakup extensional regime. Following Heine et al. (2013), they suggest that extension started initiated in the Late Jurassic, with N-S extension that produced the Outeniqua and Rawson and successively turned clockwise towards an E-W direction.

Besides the SDRs, directly related to continental breakup, we present in Fig. 6.10 the Atlantic basins on the African margin and the main depocenter-bounding faults. Most of these structures are oriented parallel to the African present-day coastline and the COB. In the Orange basin, some half-grabens developed on continental crust, most of them bounded by seaward-dipping faults (as the AJ; see Broad et al., 2012). On the South American conjugate margin, Stica et al. (2014) presented a series of continentalward-dipping faults as bounding both synrift depocenters and SDR wedges. The nature of the SDRs bounding surfaces, either SDR-bounding faults (sensu Stica et al., 2014) or feeder dykes for the SDR volcanic layers (Quirk et al., 2014), remains under debate. We propose that even if they might not behave as standard normal faults, their strike is directly associated with the stress regime at the time of SDR emplacement.

In the Colorado and Salado segments, Lovecchio et al. (2018) present a series of mostly continentward-dipping normal faults, oriented parallel or slightly oblique to the COB, and restricted to the outer 200 km of continental crust (Fig. 6.10). The North Rift of the North Malvinas (Falkland) basin develops at this stage (Lohr and Underhill, 2015), and its northern appendix connecting to the Atlantic rift, as introduced by Becker et al. (2012).

The COT in the segments between the Colorado/Cape FZ and the Salado/Orange FZ are characterized by along-strike asymmetry in width of the SDR wedges. The COT on the Argentinean margin is narrower and decreases in width northward towards the Salado FZ, while on the African margin the COT is wider and underwent significant thinning (Blaich et al., 2011).

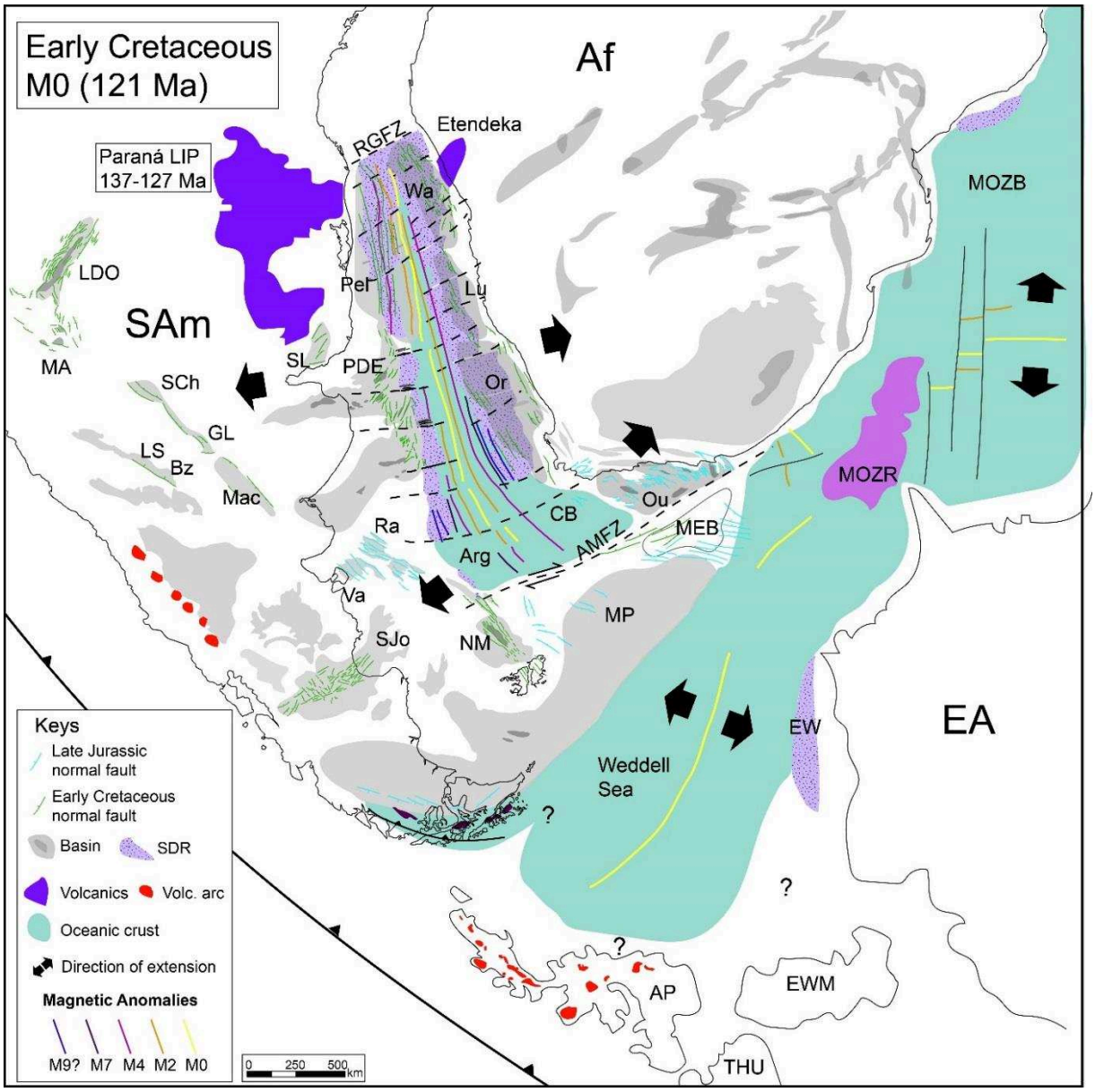

Figure 6.10: Paleo-tectonic reconstruction of SW Gondwana in the Early Cretaceous (at 121 Ma). The South Atlantic opening is presented at an evolved stage. South America-Africa fit after Blaich et al. (2011), Antarctica blocks after König and Jokat (2006). Antarctica continues to drift south. Wrenching along the AMFZ allows the opening of the South Atlantic Ocean. The southernmost segment lacking SDRs, probably due to lower velocities. Southwards, the North Malvinas graben is an extension of the Atlantic rift (Becker et al. (2012). Faults after Lohr and Underhill (2015). Dykes in the Malvinas Islands indicate an Early Cretaceous age (see Ramos et al., 2017). Extension is recorded on both margins in a narrow rift on both sides of the present-day COTs. SDRs develop on the other segments norths of Rawson. South American basins: Punta del Este (PDE); Santa Lucía (SL), Pelotas (Pel). African basins: Outeniqua (Ou), Orange (Or, age from biostratigraphy in the Kudu well, Erlank et al., 1990), Luderitz (Lu) and Walvis (Wa). Ancient basement structures are extensionally reactivated producing the Macachín (Mac), Sierras Chicas (SCh, ages from Lagorio, 2008), Las Salinas (LS) and Beazley basins of San Luis, Metán-Alemanía (MA) and Lomas de Olmedo basins (LDO, age after Galliski and Viramonte, 1988). The Paraná-Etendeka LIP extrudes during this period (Pinto et al., 2011). Structures and depocenters after

Uliana et al., 1989; Ramos and Turic, 1996; Gladczenko et al., 1997; Jungslager, 1999; Franke et al., 2007; Starck, 2011; Broad et al., 2012; Stica et al., 2014; Koopmann et al., 2014; Figari et al., 2015; Lohr and Underhill, 2015; and Lovecchio et al. (2018).

E-W oriented rifting might have started in the Berriasian-Valanginian (undetermined as the southernmost segments remains underexplored and the magnetic anomalies mapping available at the time of preparation of this work do not include much detail). Breakup (first oceanic crust) initiated in the south possibly in the Valanginian. The unconformity between synrift I and II in the Outeniqua basin is dated mid-Valanginian and is related to strike-slip movement along the Agulhas-Malvinas (Falkland) FZ due to E-W extension. Breakup progressively advanced north (Nürnberg and Müller, 1991). Plate kinematic models indicate a top Hauterivian age for the initiation of normal oceanic crust accretion at the Colorado/South Orange segment, and Aptian in the northern Pelotas/Walvis segment (Heine et al., 2013). Rifting and successive breakup were thus diachronous from source to north and evolved in segments bounded by fracture zones that accommodated the relative displacement.

Onshore Argentina, a series of aligned Cretaceous basins developed on the western edge of the Rio de la Plata craton (Macachín, General Levalle, Sierras Chicas, etc.) and another trend to the west of that one (Las Salinas, Beazley, etc.; Uliana et al., 1989). The Santa Lucia basin develops within the Rio de la Plata craton, possibly associated with strike-slip as suggested by (Veroslavsky, 1999). In the San Jorge Gulf basin, a Neocomian phase of extension is responsible for a series of depocenters across the basin and extending to the west into the Rio Senguerr, Rio Mayo, and Rio Guenguel sub-basins (Iannizzotto et al., 2004; Mpodozis and Ramos, 2008). In northern Argentina, the three-branched NW Argentina basin opened at this stage, with the N-S oriented Metán/Alemanía and Tres Cruces sub-basins, and the E-W directed Lomas de Olmedo sub-basin.

6.6 Discussion

We have shown in our reconstructions a model that explains the occurrence and timing of Mesozoic rifting in SW Gondwana. Basement structural inheritance played a key role in conditioning faults and depocenters emplacement across the Mesozoic. In the Triassic, for instance, the Cuyo basin developed on a the hanging wall of an extensionally reactivated suture between terranes accreted to the SW margin of Gondwana during the Paleozoic (Ramos and Kay, 1991). In the Cretaceous, a series of N-S oriented basins developed along the boundary of

the Río de la Plata craton and the Pampia cratonic block (Macachín, General Levalle, Sierras Chicas, etc.).

Regarding the mechanisms triggering rifting, we follow the rationale of Frizon De Lamotte et al. (2015). Besides the active rifting process produced by plume inception (Dewey and Burke, 1974), recent studies suggest that in some cases rifting precedes volcanism (Buiter and Torsvik, 2014) and subduction-related slab rollback instability is presumed to be a major trigger of continent dispersal (Bercovici and Long, 2014). We have highlighted this effect since the Triassic for SW Gondwana (Cuyo, Bermejo, Neuquén basins). In addition, Riel et al. (2018) suggest a counter-clockwise rotation of Pangea between 260 and 230 Ma as the cause for initiation of extension in the SW Gondwana margin. On the other hand, the presence of intracratonic rifts associated with the Karoo I event in central Gondwana (Santa Maria, Waterberg, etc.) could be related to far-field stresses associated with the Central Atlantic rifting.

The Early Jurassic Karoo event (Karoo II) is an exception. Regional doming and volcanic activity prior to rifting confirm an active rifting mechanism (Frizon De Lamotte et al., 2015), that triggered the opening of the Mozambique channel and the breakup of Eastern from Western Gondwana. We associate the Karoo II event with the formation of the Colorado and Salado basins, offshore Argentina. Even if these basins surround the area of influence of the plume-related volcanic activity, in their paleo-tectonic position (Fig. 6.8) they are aligned with other Karoo II depocenters in Africa and could then be coeval with the Cuyo Group rifting in the Neuquén basin (Vergani et al., 1995).

Out of the area of influence of the Karoo plume, towards the SW Gondwana margin, the Chon Aike magmatic province, one of the silicic igneous provinces known, played a major role, as it is intrinsically related to diachronic extension in Patagonia, the Antarctic Peninsula and other Antarctic territories (Pankhurst et al., 2000). Rapela et al. (2005) propose the development of the Subcordilleran Batholith volcanic arc, coeval with the Chon Aike LIP, emplaced under crustal extension. The southwestward clockwise migration of the arc between the Late Triassic Central Patagonian Batholith and the Early Jurassic Subcordilleran Batholith has been associated with differential slab rollback (Echaurren et al., 2017). Extension related to the Chon Aike LIP has been linked to the formation of the Cañadón Asfalto, Malvinas and Austral basins (Uliana et al., 1985), to which we add, following Ramos et al. (2017), the South Rift of the North Malvinas (Falkland) basin.

Rifting in the Mozambique basin since the Early-Mid Jurassic (Karoo II rifting), and the successive opening of the Mozambique channel, could not have been accomplished without lateral slip along the proto-Weddell fracture zone that mechanically released Eastern from Western Gondwana (as suggested by König and Jokat, 2006). The separation between both semi-continents of Gondwana was a no-turning-back-point in the Gondwana dispersal process. Moreover, it allowed the acceleration of retro-arc extension on Western Gondwana, with the progressive formation of the Malvinas and Austral basins in the Middle Jurassic, a process that culminated in the Late Jurassic with the opening of the Rocas Verdes back-arc basin. Slab steepening was suggested by Mpodozis and Ramos (2008) and Echaurren et al. (2017) as the triggering mechanism of retroarc extension in the Late Jurassic. Moreover, we relate this extension to rifting in the Outeniqua and Rawson Valdés basins, a rifting that is presumed to have been oblique to the future South Atlantic COB, but that seems rather parallel to the paleo-tectonic orientation of the northern Rocas Verdes basin (Fig. 6.9). The area affected by the Outeniqua-Rawson/Valdés rifting is presumably the core of the Gondwanides orogen (Fig. 6.2), an area subjected to compression in the Late Paleozoic collision of Patagonia but that remains poorly studied. A good analog to better understand the Rawson/Valdés – Outeniqua segment could be the Gulf of Aden (Leroy et al., 2012, 2010; Mohriak and Leroy, 2013). Both settings seem to be related with oblique rifting and evolve through a lateral third branch at almost 90° (the South Atlantic Ocean, and the Red Sea respectively). There is a difference, however, regarding the rift-to-drift transition. In the case of the Gulf of Aden, the system evolved to an oceanic basin as the stress regime remained oblique to the structural grain. In the case of the South Atlantic, the oblique rifting was aborted, as the stress regime presumably changed from N-S to almost E-W in a short period of time (Heine et al., 2013). The Agulhas-Malvinas (Falkland) lineation evolved, under the new stress regime, as a dextral shear zone at least since the Valanginian (Baby et al., 2018). The Agulhas-Malvinas FZ could be another case of structural inheritance, as it could be related to the subduction zone between the Deseado Massif and Northern Patagonia (Pankhurst et al., 2006). Although there are differences regarding plume impingement in the Afar, in our understanding the Afar triple junction could work as a good analog for the early evolution of the AMFZ/South Atlantic 'elbow', originating the Argentina and Cape basins.

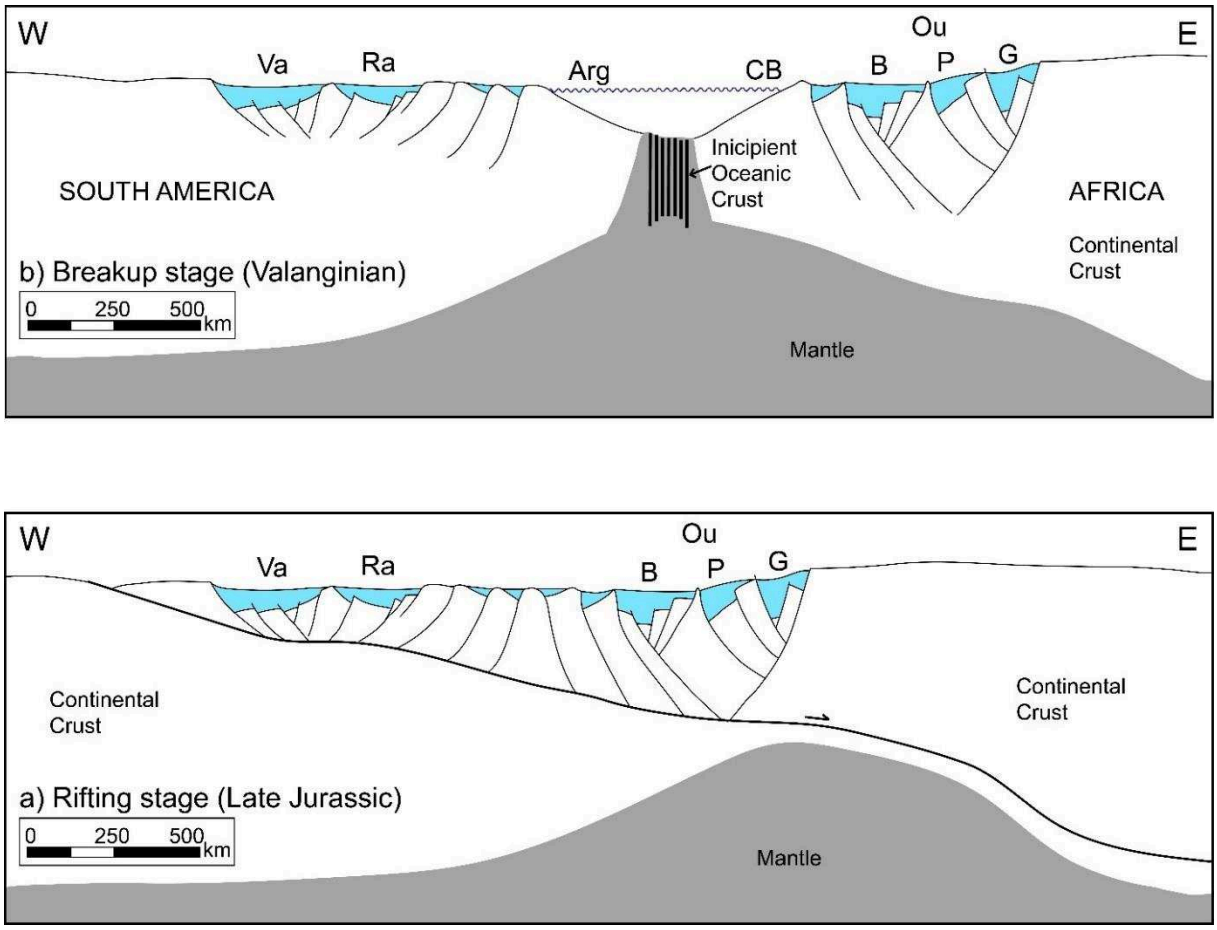

Figure 6.11: Schematic sections across the Rawson/Valdés-Outeniqua segment. a) Rifting stage (Late Jurassic), the Rawson/Valdés and Outeniqua basins evolve synchronously with a common detachment level dipping to the East. Modified after Ramos (1996), Continanzia et al. (2011) and Broad et al. (2012). b) Breakup stage in the Early Cretaceous (Valanginian), with incipient oceanic crust accretion (magma-poor segment).

As it has recently been suggested from numerical modeling, oblique rifting seems to facilitate continental breakup, as it requires less force to reach the plastic yield limit as compared to rift-perpendicular extension (Brune et al., 2012a). In our study case, we propose that a first phase of oblique rifting in the Rawson/Valdés – Outeniqua segment, might have been effective in thinning the lithosphere since the Late Jurassic (Fig. 6.11a). Thus, in the Early Cretaceous, lithosphere had already been thinned in the southernmost segment of the South Atlantic and when subjected to E-W extension, was the first segment to break-up, without large volumes of volcanics forming SDRs (Fig. 6.11b). The southernmost segment behaves in our opinion, and until new data is available, as a magma-poor margin.

The breakup along the Atlantic rift occurred in segments delimited by fracture zones (FZ). Mechanics of rift propagation across the different segments have been postulated by several authors, notably Franke et al. (2007), Franke (2013), Blaich et al. (2013), and

Koopmann et al. (2014). Regarding the E-W oriented extension since at least the Mid-Valanginian, we agree with the model presented by Blaich et al. (2011) who introduced a two-phase breakup process, with first a continental rifting phase (crustal thinning) forming a 500-km wide Atlantic rift system (Lovecchio et al., 2018), followed by the breakup phase itself with SDR emplacement and successive oceanic crust accretion. Both phases could take place as part of a continuum process. We present in figure 6.12-I a paleo-tectonic reconstruction at the time of active rifting in the South Atlantic (presumable Early Valanginian). At this stage, oceanization had already started in the southernmost Rawson/Valdés – Outeniqua segment (Fig. 6.12-IIa). The Colorado FZ is a major feature at this stage, accommodating oceanic crust accretion to the south, and continental rifting to the north. In the Colorado-Orange segment (Fig. 6.12-IIb), the areas affected by older rifting stages (Late Triassic to Early-Mid Jurassic) remain out of the area of active rifting (in a thermal subsidence phase, Lovecchio et al., 2018). We believe this is an important observation to be considered in future thermo-mechanical modeling of the South Atlantic breakup at the Colorado segment, the older rifts forming the Central and Eastern Colorado depocenters should not be modelled as part of the same Early Cretaceous South Atlantic opening. Figures 6.12-IIc and 6.12-IId are schematic transects across the South Atlantic Rift in the Salado/Orange and Pelotas/Walvis segments. For all segments, following Ramos (1996) we interpret an east-dipping detachment, which is consistent with the no-reactivation of structures in the Colorado basin at this stage and the wider development of Early Cretaceous rifts and SDRs on the African conjugate margin.

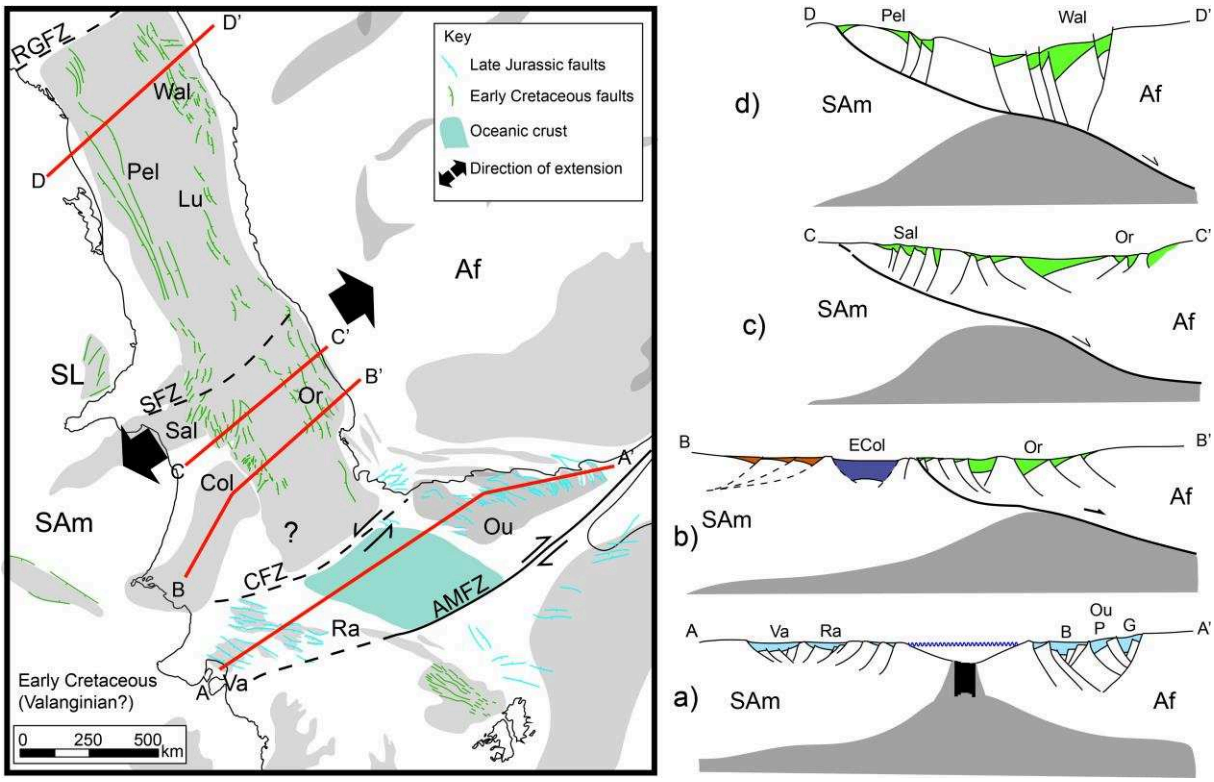

Figure 6.12: I: Paleo-tectonic reconstruction of the South Atlantic Rift for the Early Cretaceous, at the time of breakup in the southern Rawson/Valdés – Outeniqua segment (Early Valanginian?). North of the Colorado fracture zone (CFZ), the South Atlantic rift has an approximate width of 500 km. Faults are oriented approximately parallel to the future Atlantic COB, which indicate the paleo-stress regime (near E-W extension). II: Schematic cross sections across the South Atlantic rift. A) Rawson-Valdés/Outeniqua segment already at the breakup stage at this stage; b) Colorado/Southern Orange segment. Note the presence of the older rift infills in the Colorado basin, west of the area affected by Early Cretaceous extension; c) South Salado/Orange segment; d) Pelotas/Walvis conjugate segment.

The South Atlantic Rift followed basement weakness zones, formed in the Neoproterozoic Brasiliano-Panafrican Orogeny. These weakness zones could have been either sutures (Hartnady et al., 1985) or, as recently suggested by Will and Frimmel (2018), the long axis of Neoproterozoic back-arc basins (the Marmora basin, Namibia). We believe that basement inheritance certainly played an important role, but what was key for the orientation of the South Atlantic rift was the rotation of the stress regime in the Early Cretaceous to a more orthogonal position with respect to this basement structural fabric. This configuration would have allowed the rapid propagation of the Rift following precursor weakness zones, north of the already rifted Rawson-Valdés/Outeniqua segment. Wrenching along the Agulhas-Malvinas fracture zone was necessary to accommodate extension to the north of it and allow continent separation. Early Cretaceous rifting is present, however, south of the Agulhas-Malvinas FZ. The North Branch of the North Malvinas (Falkland) basin and some minor rifts seem to connect

the land-locked rifts to the South Atlantic Rift to the north (Becker et al., 2012; Lohr and Underhill, 2015). For some reason, probably related to plate rotation, breakup favored wrenching along the Agulhas-Malvinas FZ instead of continuing propagation to the south (through the nowadays aborted North Malvinas graben).

6.7 Conclusions

The opening of the South Atlantic in the Early Cretaceous was only the final stage of the complex rifting process of SW Gondwana. The Central Atlantic was the locus of the Triassic rifting, however intracontinental rifts also developed in Africa and South America at this stage (Karoo I). Triassic-Earliest Jurassic depocenters are also found on the SW Gondwana margin (Cuyo, Bermejo, Precuyano of Neuquén, and the Deseado basins) and are related to retro-arc extension.

In the Early Jurassic, rifting on Eastern Africa was triggered by the impact of the Karoo plume, which produced the formation of a network of Karoo II depocenters in Africa. The Colorado and Salado basins in the Argentinean shelf formed at this stage, together with the Cuyano cycle of the Neuquén basin. Rifting in East Africa ultimately produced the breakup of Eastern from Western Gondwana in the Middle Jurassic. In Patagonia, the Chon Aike silicic large igneous province occurred at this time, in the retroarc of the Subcordilleran Batholith. Retroarc extension, due to slab rollback, is responsible for the formation of the Cañadón Asfalto, Austral and Malvinas basins, and possibly the southern rift of the North Malvinas (Falkland) basin.

Retro-arc extension continued and, subsequent slab steepening produced in the Late Jurassic the opening of the Rocas Verdes back-arc basin. Rifting in the Outeniqua and Rawson/Valdés basins took place at this stage, possibly oblique to the future South Atlantic COB. The Late Jurassic rifting affected the orogenic core of the Gondwanides orogen and is precursor to South Atlantic opening.

The Early Cretaceous South Atlantic Rift possibly took advantage of crustal weakness zones (Precambrian mobile belts) but is related to a rotation of the stress field to a present-day E-W direction. Rifting occurred diachronically from south to north, and started during or before the Valanginian. The southernmost segment, between the Colorado-Cape and the Agulhas-Malvinas (Falkland) fracture zone, had already been affected by crustal thinning during the Late

Jurassic oblique rifting. This could explain the lack of SDRs in this segment. North of the Colorado-Cape fracture zones, rifting and SDR emplacement took place in segments bounded by fracture zones. We presented a schematic cross-section across the margin showing a westward-dipping detachment fault associated with depocenter formation on both margins, followed by SDR emplacement asymmetrically on both margins and eventually oceanic crust inception diachronically along the margin, between Hauterivian and Aptian times.

PART III: POST-BREAKUP EVOLUTION OF THE ARGENTINEAN MARGIN

Chapter 7. Post-breakup evolution of the Colorado basin and the northern Argentinean passive margin

7.1 Introduction

In this Chapter, the Argentinean passive margin dynamics are assessed, especially in the Colorado basin where a complete dataset allowed a detailed extraction of subsidence maps using the stratigraphic architecture (“surface approach”). These results are then compared with previously published data produced with a different methodology ("deep approach", Dressel et al., 2017).

A general summary of factors conditioning subsidence in passive margin is presented in Chapter 1, section 1.5.

An introduction to the Colorado basin stratigraphy is presented in Chapter 3, sections 3.2.2 and 3.2.3. The Colorado basin’s post-breakup stratigraphy is better constrained than the synrift infill, both from well data and seismic facies. Marine sediments form the Campanian to recent sedimentary deposits and are suitable for dating with biostratigraphic methods. A recent biostratigraphic and paleoenvironmental review of the Colorado and Salado/Punta del Este basins was carried out during the development of this thesis, in collaboration between YPF and Y-TEC (YPF Laboratories; Pérez Panera et al., 2018; Ronchi et al., 2016). The results of these studies were incorporated in the present thesis as biostratigraphic markers used for seismic interpretation calibration.

The pre-Campanian section has poor age constrain. This section is composed of red-beds interpreted as fluvial deposits from the cutting and electric log data of hydrocarbon exploration wells (e.g. Pejerrey, Cruz del Sur, Puelche, Ranquel). Moreover, the recovered rock samples were barren for biostratigraphic material.

7.2 Post-breakup seismic stratigraphy of the Colorado basin

Lithosphere breakup for the Colorado basin segment, understood as end of SDR emplacement and onset of oceanic crust accretion, is interpreted to occur near the Hauterivian-Barremian boundary (Franke, 2013). The breakup unconformity (BU) develops between the time of breakup and the onset of sediment deposition in the drift or passive margin stage. With the onset of oceanic crust accretion and the development of an incipient mid-ocean ridge, the first marine transgression occurs. Sediments will tend to deposit where accommodation creation allows. For the Colorado basin, the first marine transgression is interpreted to be of Aptian age, but has not been drilled. Source rock deposition is interpreted at this stage, as sedimentary supply tends to be low at the early drift, allowing concentration of organic matter in condensed sections. Potential marine source rocks of good quality have been described at this age in the conjugate African margin (Bralower et al., 1994; Hartwig et al., 2012).

A margin-dip section along the Colorado basin axis, is displayed in Fig. 7.2 (see location in basement Fig. 7.1). Four main megasequences of second order are shown. In the continental crust domain under the shelf, a package of Jurassic synrift and pre-breakup sag developed below the BU in discrete depocenters (colored in blue in Fig. 7.2). The SDR wedges, shown in purple, are emplaced during breakup and also precede the BU on the continent-ocean domain. Above the BU (interpreted of Barremian/Aptian age), a thick post-Aptian, Cretaceous Drift Megasequence develops along the line. Clinoforms associated with a shelf-break occur above the External High. These clinoforms are located nearby the abrupt step produced by the change from continental to transitional crust (Fig. 5.1). On the shelf, the Late Cretaceous reflectors display a subparallel character. Where it has been drilled, the Late Cretaceous usually displays sand-rich red beds, that have been interpreted as fluvial deposits of the Colorado Fm (Gerster et al., 2011; Juan et al., 1996; Lesta et al., 1978). Discontinuous seismic facies, continentward from the shelf-break, support this interpretation. The overall aggradational stacking pattern observed for the Late Cretaceous drift indicated a relative balance between accommodation and sediment supply throughout this stage. In the continent-ocean transition (COT), the lower drift

reflectors clearly onlap the steep BU. Marine onlap of deepwater facies is interpreted in seismic data.

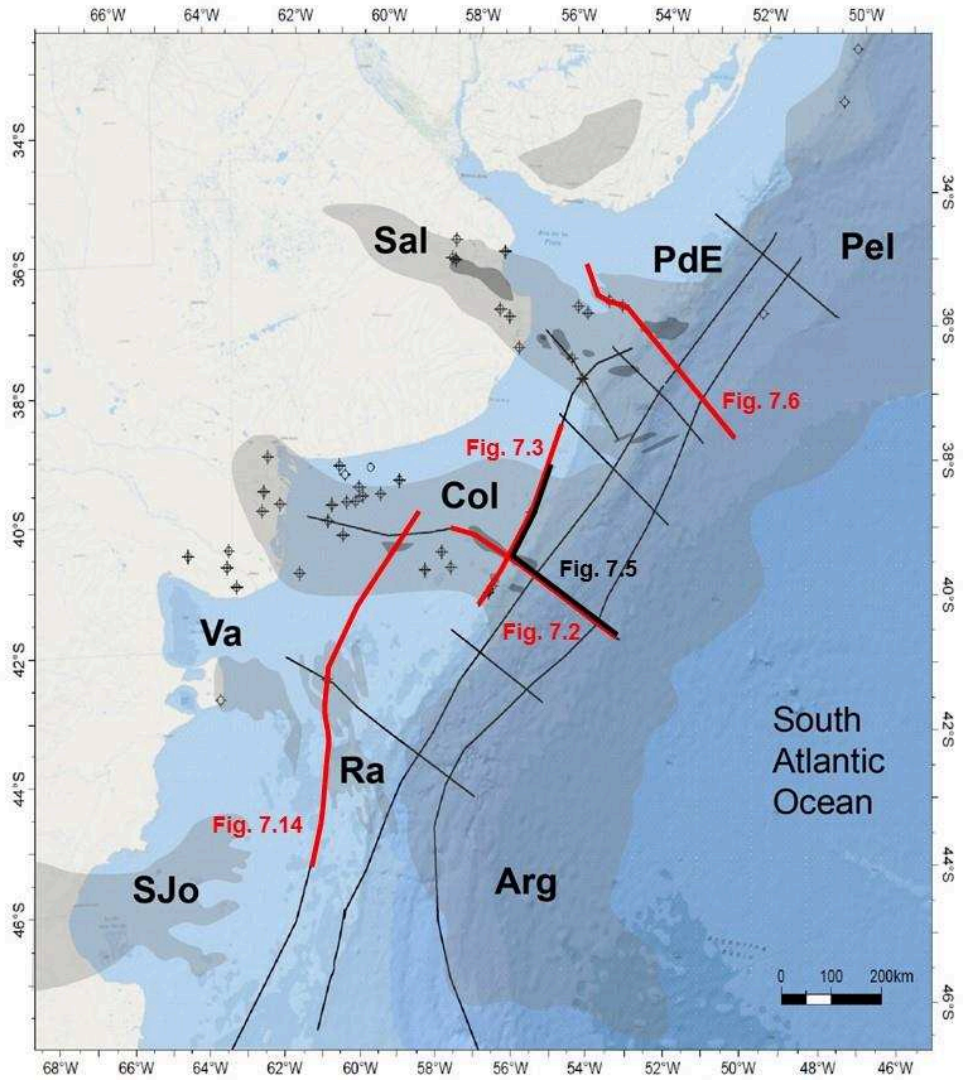

Figure 7.1: Basemap of the northern Argentinean Atlantic margin. Note the location of the Colorado (Col), Salado (Sal), Punta del Este (PdE), Pelotas (Pel), Rawson (Ra), Valdés (Va), San Jorge Gulf basin (SJo) and the Argentina basin (Arg)

A regional marine transgression flooded the Colorado basin in the Late Cretaceous to Early Paleocene (Campanian to Danian; Lesta et al., 1978; Ottone et al., 2018; Appendix 1). This flooding even reached the Neuquén basin (Fig. 3.12; (Aguirre-Urreta et al., 2011; Camacho, 1967). A regional unconformity marks the top of the marine shales deposited during this transgression and is referred to as the NTK (Near Top Cretaceous) horizon.

The Paleogene Megasequence develops between the NTK unconformity and the Top Oligocene (Pal horizon). It is a rather thin section on the shelf (Fig. 7.3), which thins out towards

the former shelf-break. I thickens up on the slope with plastered drift contourites. It is also present in the deepwater basin with thick contourite – turbidite deposits. Shaly and carbonate facies characterize this package in the wells drilled on the shelf (see Fig. 3.10).

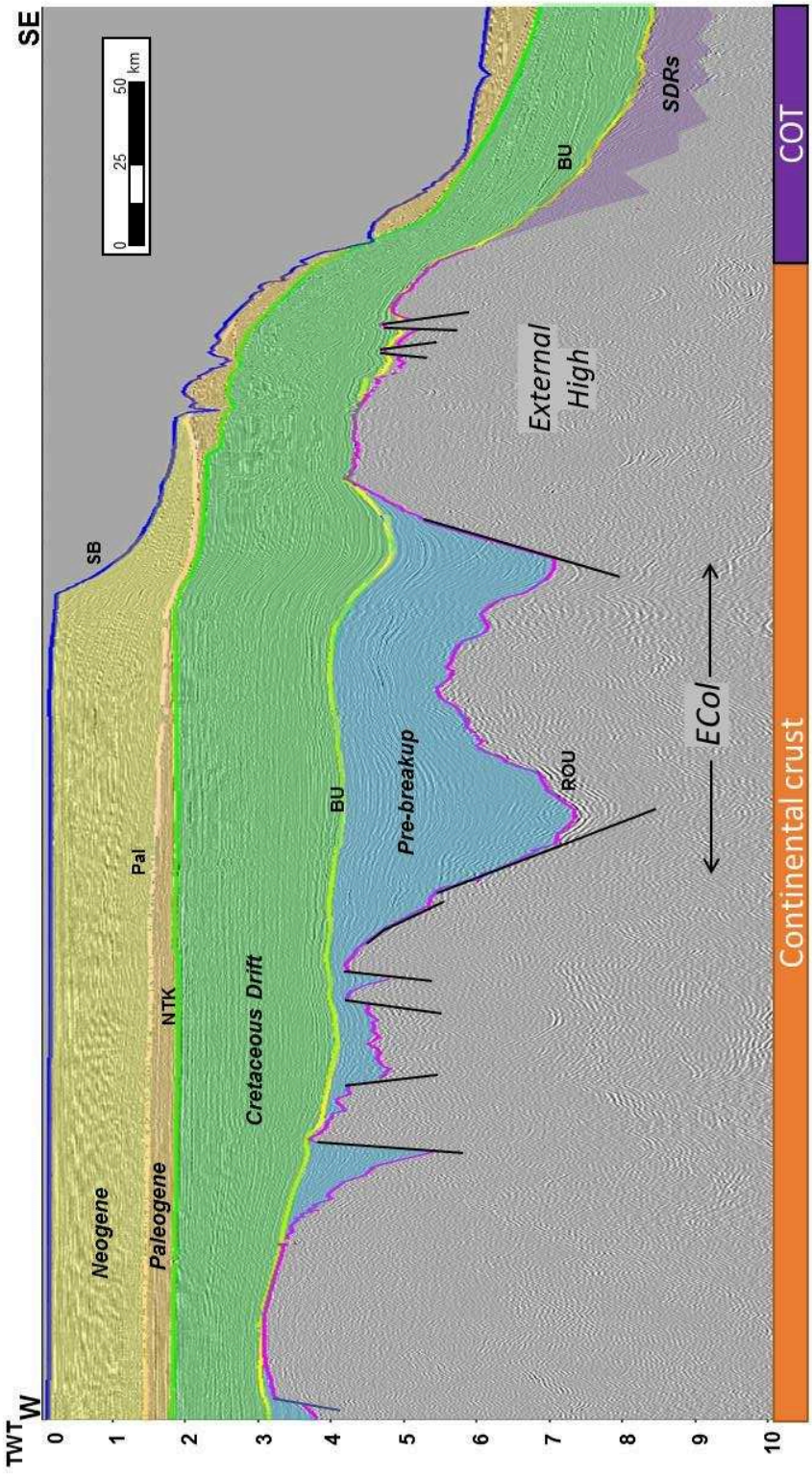

Figure 7.2: Dip seismic line along the Colorado basin axis. Vertical scale TWT (in seconds).

The Neogene Megasequence is a thick overall flat package (although with internal geometries). Note that it primarily develops on the shelf and that the present-day shelf break does not reach the position of the Late Cretaceous shelf-break, indicating the development of a platform sensu Helland-Hansen et al. (2012) on the shelf (Fig. 1.28).

A seismic line parallel to the margin-strike, and across the Eastern Colorado depocenter (ECol, developed on continental crust), is presented in figure 7.3 (see location in Fig. 7.1). The Late Cretaceous Drift Megasequence pinches-out towards the south and north. Lateral coastal onlap terminations, towards the northern Tandilia and southern Rawson highs, are observed for the reflectors forming the Late Cretaceous Drift. Note that the thickest depozone coincides with the synrift ECol depocenter, and that as the older reflectors pinch-out, the younger beds extend over larger areas. These are typical geometrical characteristics of thermal subsidence.

The Paleogene Megasequence, however is thicker towards the north, and thins out towards the south. Internally, progradations from north to south (apparent) are observed. The Neogene Megasequence, on the other hand, seems to be thicker towards the south and clinoforms on the apparent direction of this seismic line, seem to prograde towards the north.

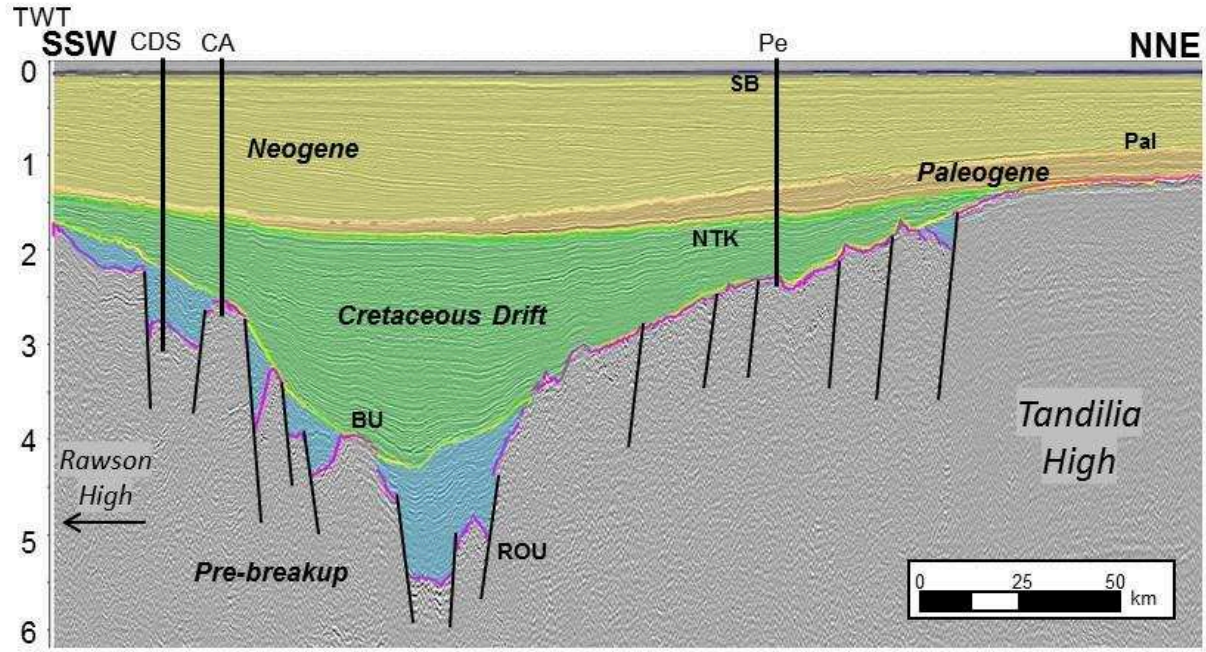

Figure 7.3: Srike seismic line across the Colorado basin (ECol depocenter). Vertical scale TWT (in seconds).

An isopach map of the total post-breakup sedimentary cover (BU to sea bottom, SB) is presented in Figure 7.4. It sums up the thickness of the Cretaceous, Paleogene and Neogene

Megasequences. The thickening of the drift units in above the Western, Central and Eastern Colorado depocenters. The NNE-trending shelf-break towards the east is also illustrated on the isopach map.

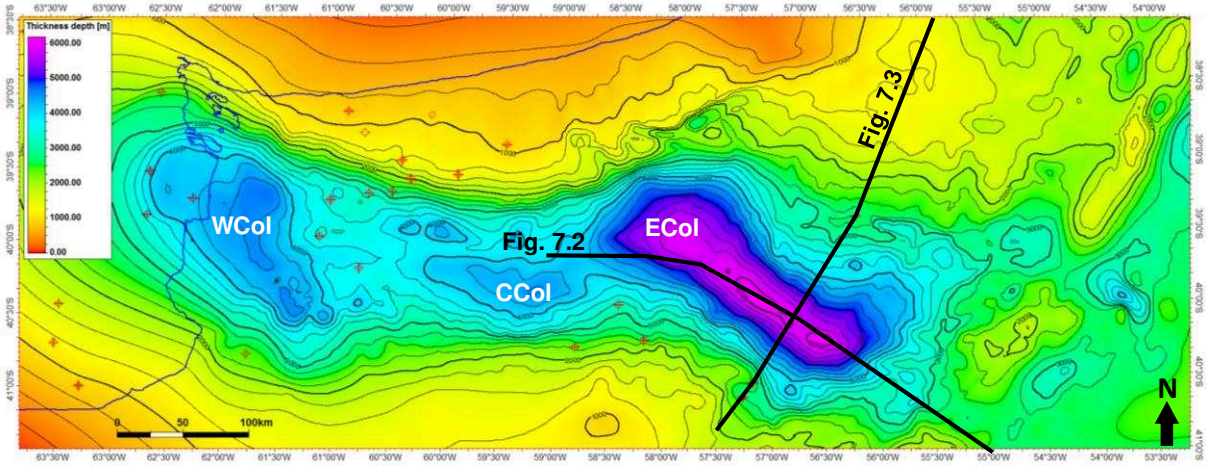

Figure 7.4: Total thickness map (in meters) of the post-breakup cover (BU-SB) in the Colorado basin area. The location of figures 7.2 and 7.3 is depicted.

The E-W orientation of the Colorado basin axis, at a very high angle with respect to the COT, makes difficult to establish a coastal onlap curve for the Colorado basin. This is because the reflectors usually continue subparallel to the west along the basin axis (Fig. 7.2) instead of terminating against the margin. Moreover, the western part of the basin has a low quality and poorly covered seismic database. A composite seismic transect was then prepared, using the clinoforms and deepwater section of figure 7.2, and the onlap against the Tandilia High towards the north (Fig. 7.3). This composite seismic transect is presented in figure 7.5.

The main horizons (mostly sequence boundaries) addressed in this chapter are presented in Fig. 7.5a. These horizons are the ones used to create the surfaces to produce the isopach maps presented in this chapter, and the in the forward stratigraphic model. Figure 7.5b is the same seismic transect but with a detailed seismic stratigraphic interpretation. That is provided to illustrate the description that follows. Note that sequence between 125Ma (BU) and 115 Ma is preserved in the Eastern Colorado depocenter (ECol), and on the external, where it is eroded in the seaward direction. In the basin, it onlaps the BU. This first post-breakup sequence is interpreted as Aptian, including the Aptian transgression deposits (Fig. 7.23).

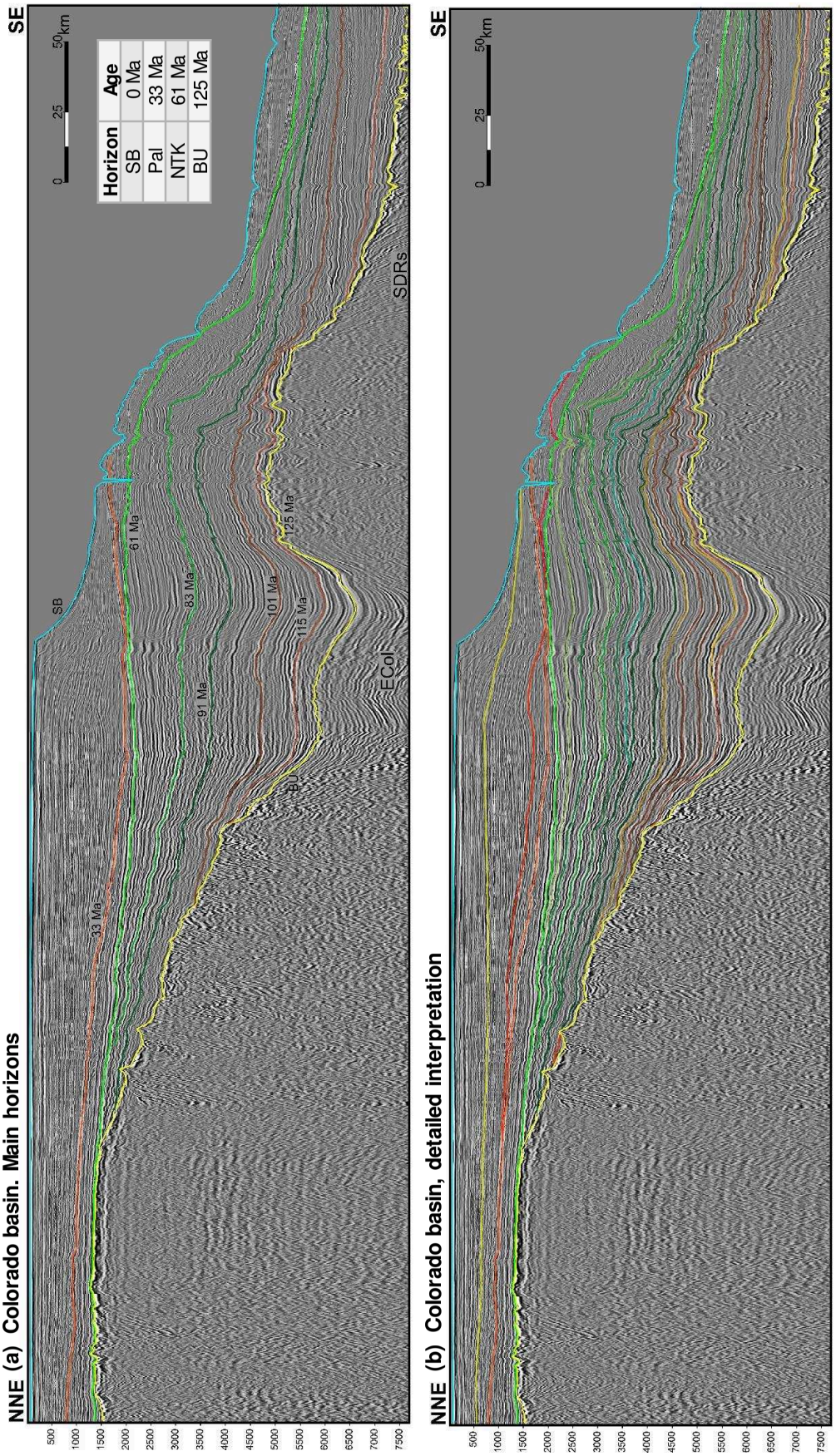

Figure 7.5: seismic transect in the Colorado basin: a) Main horizons used in this study, b) high resolution seismic interpretation.

The sequence between the 115 Ma and 101 Ma horizons (Aptian-Albian) corresponds to the nucleation phase of shelf formation, characterized by basinward progradation of the shelf-break (Helland-Hansen et al., 2012). Between the 101 and 91 Ma horizons, rapid aggradation of the shelf is observed. The basinward progradation of the slope break is compensated slope failure processes and the erosve action of contour currents, that deposit plastered drifts as the ono observed at this interval at the toe of slope. Between the 91 and 83 Ma horizons, the shelf displays aggradation but also a seaward shift in the shelf-break position. For the sequences below the 83 Ma horizon, note the discontinuous seismic facies in the landward direction, interpreted as fluvial system deposits. The interval between 83 and 61 Ma (NTK unconformity) represents the Campanian-Danian transgression, a thick succession of continuous, high amplitude reflectors above the shelf. An internally deformed contourite deposit thickens on the slope and is sometimes referred as a 'healing phase' (Catuneanu, 2006). The Paleogene Megasequence (defined between 61 and 33 Ma, the Danian is confined below the NTK horizon) shows a thickening trend in the landward direction and shows as well the development of a plastered drift contourite deposit near the shelf-break. Finally, the Neogene Megasequence (actually corresponds to the Neogene plus the Quaternary systems) shows low angle progradations and some convex-up features produced by progradation of shelf clinoforms towards the north (perpendicular to the axis of the transect, see Fig. 7.3.

7.3 Regional post-breakup evolution of the northern Argentinean margin

7.3.1 Introduction

The variations observed in the Colorado basin along its post-breakup evolution, made necessary the extrapolation of these observations to a larger study area. The Salado and Punta del Este basins, to the north, were incorporated into the study area. The horizons bounding the megasequences of interest were extended across this region. Some observations were also made in the Rawson basin area, to the south of the Colorado basin. The main objective was to better constrain the overall stratigraphic architecture in the southern part of the Colorado basin. Only scarce data from this region was finally available. It was not considered for the mapping presented in this section, but seismic lines were used to established referenced cross-sections.

7.3.2 Results

The Salado basin is an extensional basin emplaced north of Colorado, on the Río de la Plata craton. The main depocenter of the Salado basin is placed onshore (Fig. 4.1) where no seismic data was acquired. Rifting has been interpreted in this study as Early-Mid Jurassic (see Chapter 4). Towards the east, the Punta del Este basin separated from the Salado basin by the Martín García High. The Early Cretaceous rifting, related to the South Atlantic opening, is interpreted to have influenced the eastern part of the Salado and Punta del Este basins, where faults present a NE to NNE strike (Fig. 4.1). The main references regarding the Salado basin structure and stratigraphy are from Stoakes et al. (1991), Tavella and Wright (1996), Raggio et al. (2011), and Morales et al. (2017).

A dip seismic section across the Punta del Este basin is presented in Fig. 7.6 (location displayed in Fig. 7.1). The transition from continental to transitional crust (COT) in the Salado/Punta del Este segment seems more gradual compared to the Colorado basin (Fig. 7.3),. Half-grabens associated with the Early Cretaceous Atlantic rifting are associated with crustal thinning along the slope.

Regarding the synrift infill, it is possible to differentiate two types of depocenters. Northwestwards, towards the Río de la Plata craton, a graben is perched in the continental crust domain. This graben would be related to the Jurassic rifting. Outboard, a series of half-grabens bounded by continentward dipping normal faults are observed (at least three). The faults limiting these depocenters dip towards the continent, as the faults bounding the inner SDRs.

The Cretaceous Drift Megasequence thins out towards the craton. The thickest section is associated with stacking of shelf-break clinoforms, near the outer end of continental crust and the pass to the COT. The top of this megasequence, the NTK horizon is interpreted at the top of the Maastrichtian-Danian transgression. In the Salado-Punta del Este basins, the transgression seems to have started only in the Maastrichtian (no marine Campanian deposits have been encounter on the shelf, Ronchi et al., 2016).

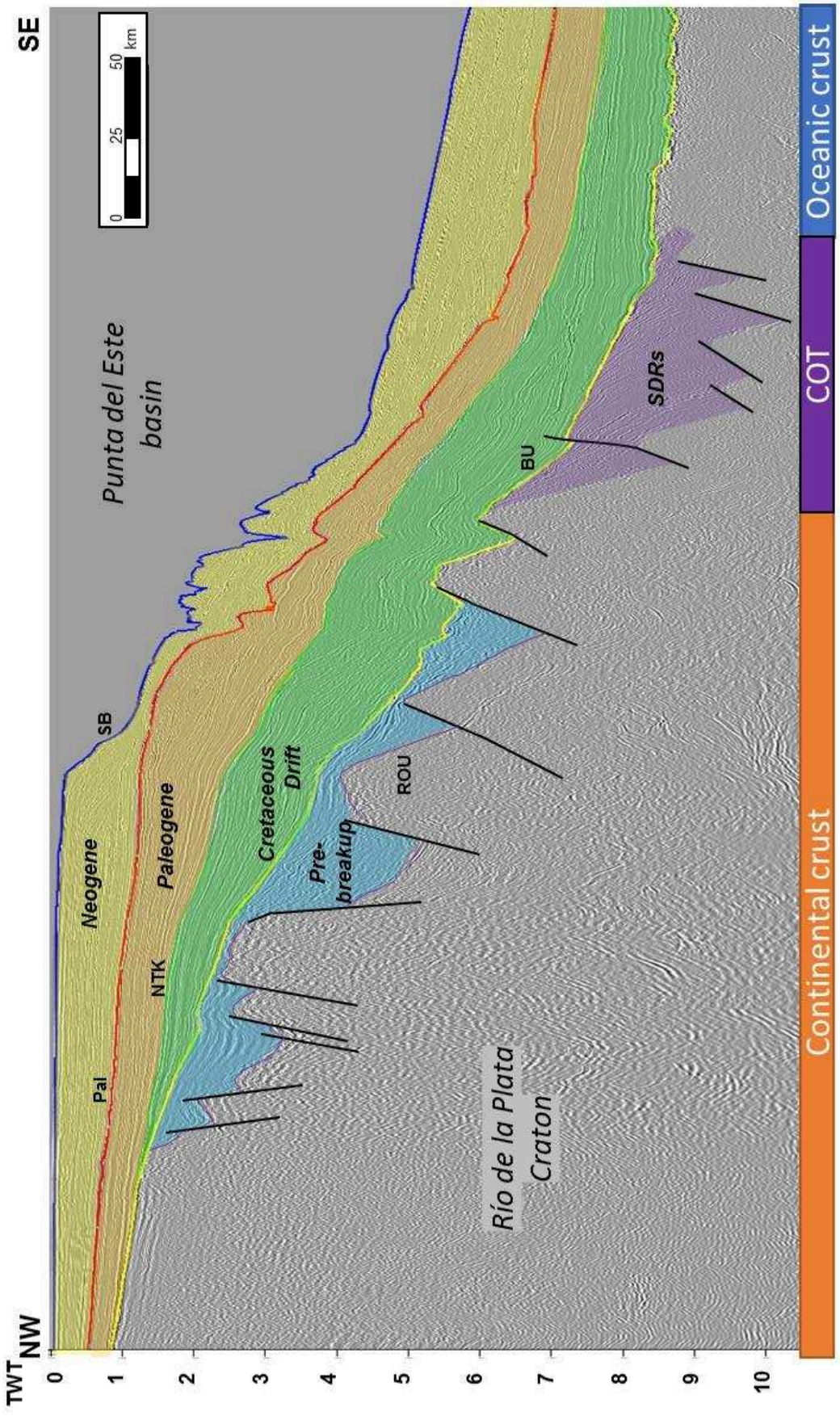

Figure 7.6: Dip seismic line in the Punta del Este basin. Vertical scale TWT (in seconds)

The Paleogene Megasequence (colored in orange in figure 7.6), is thicker that in the Colorado basin (compare Figs. 7.6 to 7.1). At least three progradational packages are identified within this Megasequence and have been interpreted as Late Paleocene, Eocene, and Oligocene respectively in the Punta del Este basin. The later displays quite steep curved clinoforms interpreted as affected by the action of bottom contour currents.

The Neogene Megasequence develops on the shelf, slope and basin. Similarly to the Colorado basin, the position of the present-day shelf-break is inboard compared to the Cretaceous shelf-break. This is interpreted as produced by larger accommodation creation overpassing the sediment supply. On the slope, the Neogene package is deeply incised. A thick Neogene package is interpreted outboard the Punta del Este basin in the deepwater setting. This is similar to what is observed in the Pelotas basin, where a thick Neogene cover has been described (Abreu, 1998; Contreras et al., 2010; Morales et al., 2017).

For a more complete assessment of the passive margin evolution of the northern Argentinean Atlantic margin, thickness maps were built for the main stages of evolution. The grids that originated these maps could not be converted to depth because the 3D velocity model created in this study (Chapter 3) is only available for the Colorado basin and does not extend into the Salado/Punta del Este area. Nevertheless, the main trends in passive margin evolution can be clearly deduced from the isochron maps presented here. Maps were generated for the shelf only, because of larger uncertainties in the interpretation and the scarcity of seismic data in the basin at the time of this study.

A isochron map of the synrift interval is presented in figure 7.7. This map gathers all synrift depocenters, regardless their time of formation (Late Triassic, Jurassic, Early Cretaceous) and is defined between the top prerift (ROU) and the top synrift (BU) unconformities. No synrift depocenter is depicted for the Western Colorado (WCol) depocenters because the bad seismic quality does not allow the determination of fault bounded depocenters. The Central and Eastern Colorado fault controlled depocenters are clearly observed.

In the Salado basin area, the available seismic data only allowed mapping in the offshore area. No reflection seismic data has been acquired onshore the Salado basin. Some NW-trending depocenters can be interpreted (Fig. 7.7). The Martín García basement High separates the Salado and Punta del Este synrift depocenters. Towards the east, in the area affected by the

Early Cretaceous rifting (see figure 4.1), several E-W and NE-oriented depocenters are interpreted from the isochron map, and are associated with normal faults (Fig. 4.1).

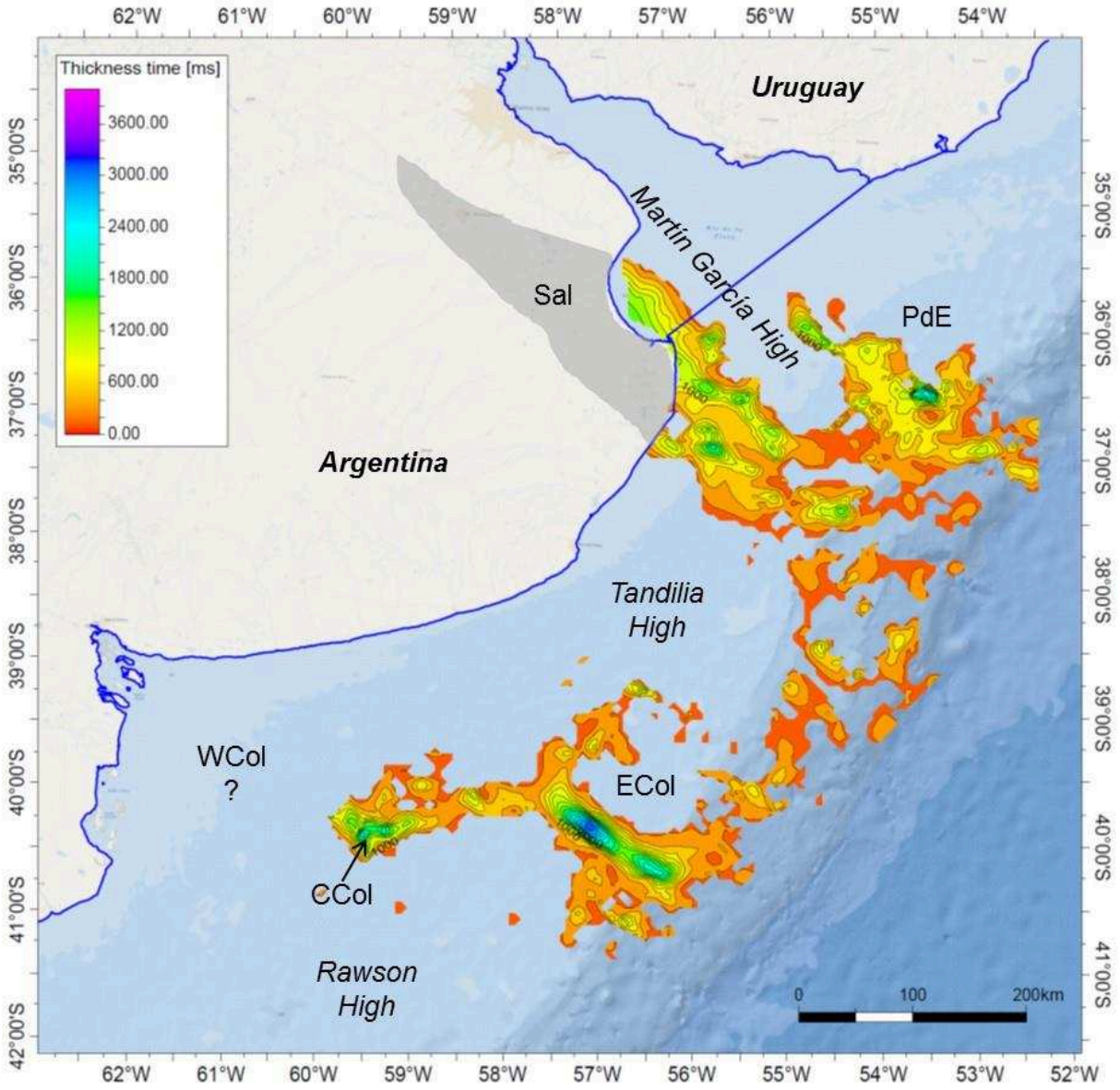

Figure 7.7: Isochron map of the Synrift Megasequence (ROU-BU), in the northern Argentinean margin.

The isochron map of the Cretaceous Drift Megasequence in the Colorado/Salado/PdE basins area (Fig. 7.8) shows the development of the early drift depocenters under a strong influence of the older rifting event. The areas where this unit is thicker coincide with the synrift depocenters (Fig. 7.7), especially Eastern Colorado. The basement highs bounding the basins, e.g. Tandilia, Rawson highs, remain under erosion or no-deposition during this stage (Fig. 7.8).

Only the Martín García High, between the Salado and Punta del Este basins, seems to display a Cretaceous cover as it plunges to the SE.

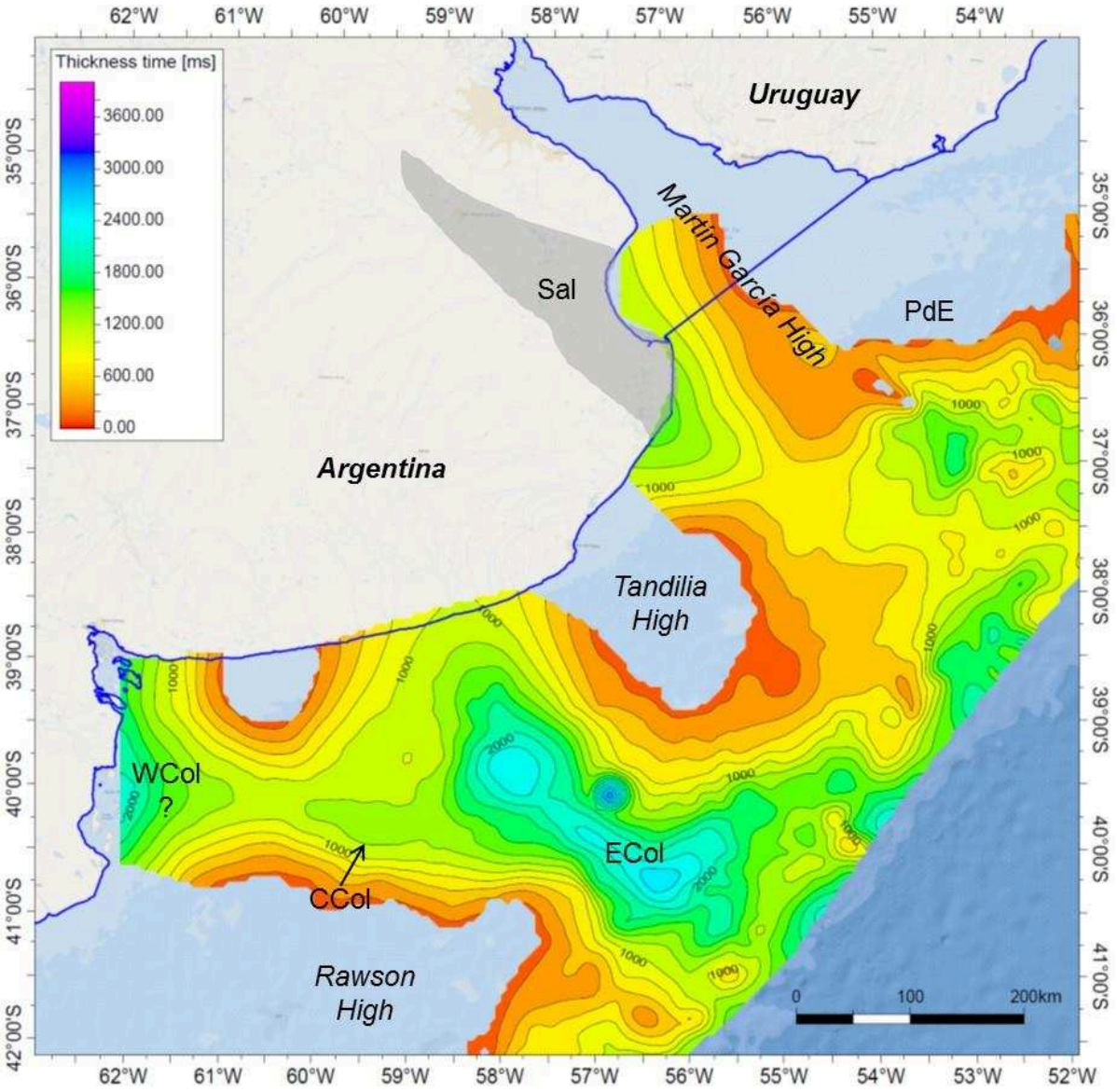

Figure 7.8: Isochron map of the Cretaceous Drift Megasequence (BU-NTK).

A paleogeographic reconstruction for the Late Cretaceous in the Argentinean margin is presented in Fig. 7.9. Fluvial systems developed in the Colorado and Salado/Punta del Este basins, over large fluvial plains developing across the shelf, with a coastline near the shelf-break location. They correspond to the Colorado Fm and the General Belgrano Fm in the Colorado and Salado basins respectively. The Tandilia High still continued to divide the

Colorado from Salado basin. The southern Rawson and San Jorge Gulf basin were also included in the paleogeographic map (see Fig. 7.5). Fluvial systems are also interpreted to drain the Rawson basin. The NNE-striking normal faults might have exerted some structural control on the drainage system (this is an interpretation that remains to be tested with more seismic data). The San Jorge Gulf basin is endorreic during the Late Cretaceous, with some influence of the Andes uplift towards the west (not included in Fig. 7.9). Sediment transfer into the deepwater basin was important during the Late Cretaceous. The shelf-edge in the Colorado and Salado basins stacks near the step produced at the outer limit of the oceanic crust. Figures 7.2 and 7.3 show thick packages of post-breakup Cretaceous drift deposits in the deepwater basin. Sedimentary supply would have exceeded accommodation during this stage, transferring large amounts of sediments to the basin, with the development of turbidite systems (Figure 7.9).

Besides the Late Cretaceous fluvial deposits, the isochron map of Fig. 7.8 comprehends as well the shaly deposits of the marine transgression that started in the Campanian in the Colorado basin, and in the Maastrichtian in the Salado basin (Ottone et al., 2018; Pérez Panera et al., 2018; Ronchi et al., 2016) and finished in the Danian (early Paleocene). The horizon that defines the top of this Megasequence is named NTK (Near Top Cretaceous). It is here considered at the top of the transgression that ended in the Danian as it would be difficult to interpret the real top Cretaceous horizon, with the scarce well data available within the overall transgressive package. This Campanian-Danian marine transgression occurred synchronously with the extrusion of the Ranquel volcanic field south of the Colorado basin, on the Rawson high, under subaqueous conditions (Lesta et al., 1978; Lovecchio et al., 2017, Appendix 2).

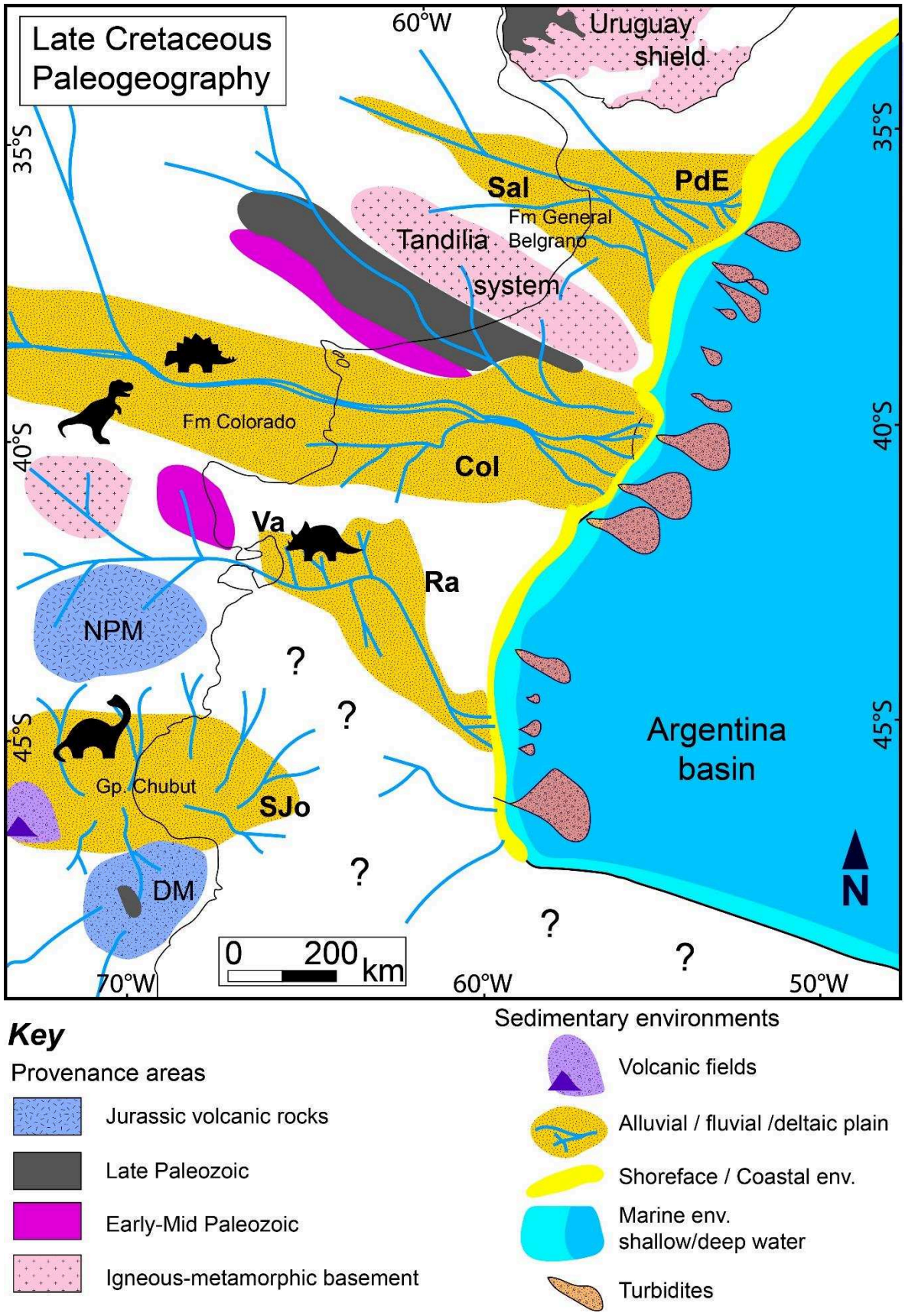

Figure 7.9: Paleogeographic reconstruction of the Argentinean margin during the Late Cretaceous. Present-day coastline is indicated in black. Basin indications as in Fig. 7.1. NPM: North Patagonian Massif, DM: Deseado Massif.

Figure 7.10 is a paleogeographic reconstruction at the time of the Campanian-Danian transgression. The Colorado and Salado basins are flooded. Flooding through the Colorado basin even reached the Neuquén basin to the west, where it deposited the carbonate-rich Malargüe Gr (Aguirre-Urreta et al., 2011; Camacho, 1967). Further south, the San Jorge Gulf basin records its first Atlantic transgression (it had been previously flooded from the Pacific during the Early Cretaceous, Fitzgerald et al., 1990; Sylwan, 2001).

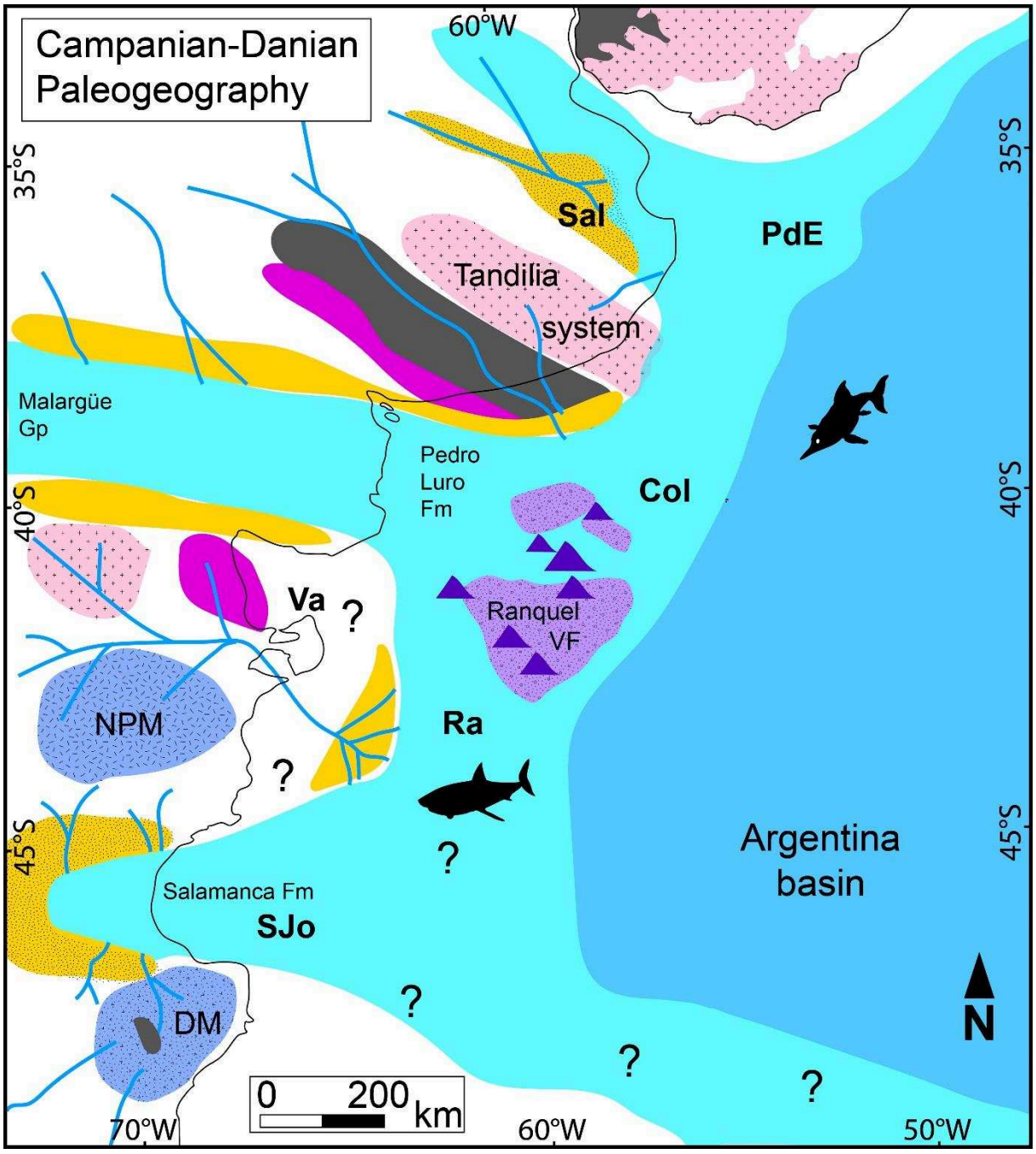

Figure 7.10: Paleogeographic reconstruction of the Argentinean margin during the Campanian-Danian transgression (submerged area after Camacho, 1967; volcanic field after Lovecchio et al., 2017). See keys in Fig. 7.9.

Figure 7.11 displays the isochron map of the Paleogene Megasequence. A major change in the thickness trend is observed for this interval. The thicker depocenter is restricted to the Salado and Punta del Este basins. A thicker Paleogene section is also observed in the Salado/Punta del Este basins when comparing the seismic sections presented in figures 7.6 and 7.3. Three stacked prograding units were observed within this megasequence in the Punta del Este basin (Fig. 7.7), while this unit is rather thin in the Colorado basin (Fig. 7.3) and thins out to the south, towards the Rawson high (Fig. 7.3). Carbonate facies are described in the Eocene Elvira formation (Fig. 3.10), possibly indicating lack, or low sedimentary supply in the Colorado basin. The area where the Ranquel Volcanic Field (RVF) developed in the Latest Cretaceous displays a lack of preserved thickness, which is interpreted as influence of the paleorelief inherited from the buildup of large volcanoes (Lovecchio et al., 2017).

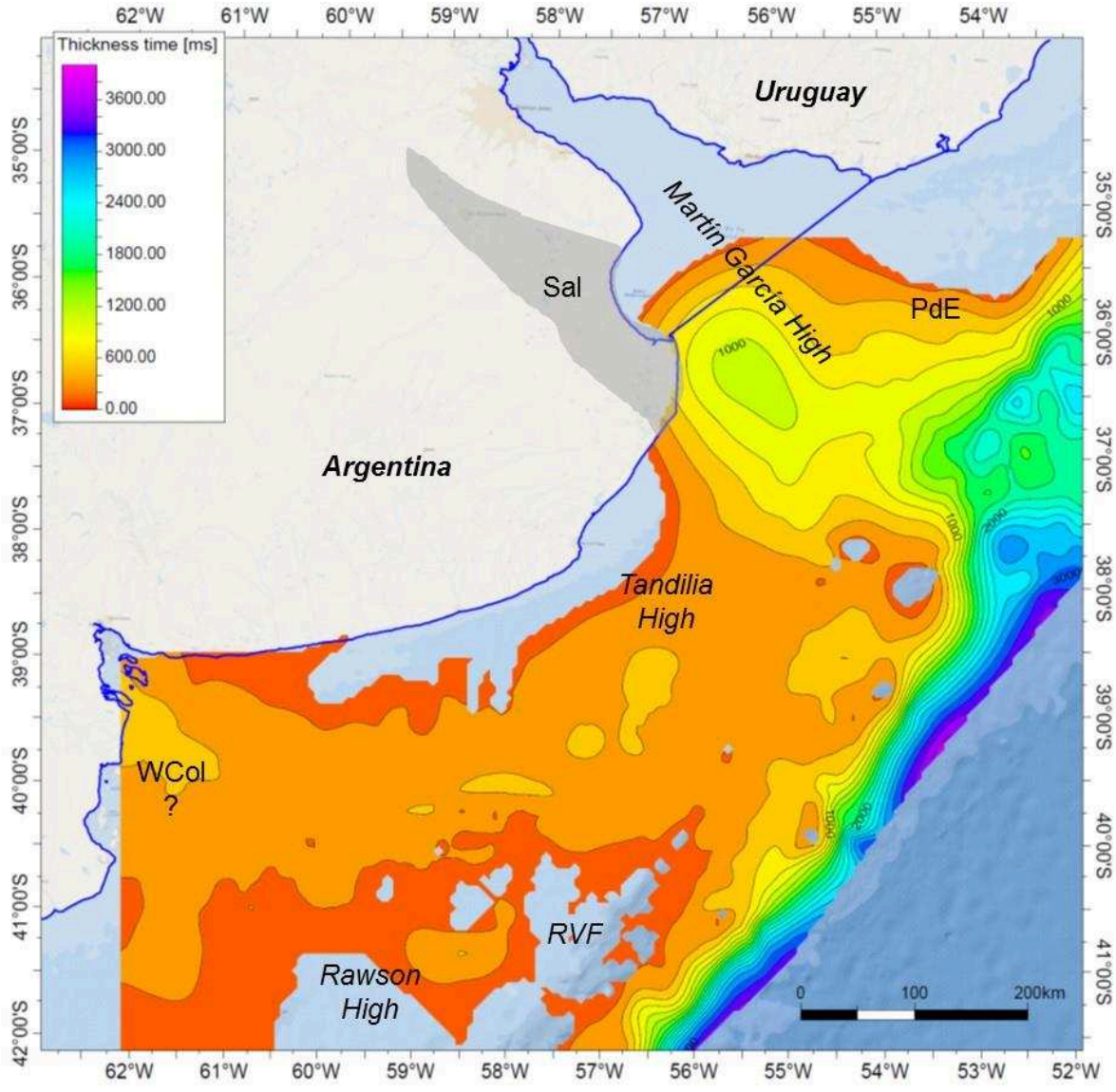

Figure 7.11: Isochron map of the Paleogene Megasequence.

A paleogeographic reconstruction for the Paleogene Megasequence is displayed in Figure 7.12. It mostly refers to the Eocene. A prograding deltaic system is represented in the Salado/Punta del Este basin. The Tandilia High is fully flooded since the latest Cretaceous and shallow marine conditions developed. The thin sedimentary cover is characterized by a carbonate-dominated depositional environment (Elvira Fm). In the Colorado basin. Towards the south, the Ranquel volcanic field in the Rawson high, probably remained as a positive feature under erosion.

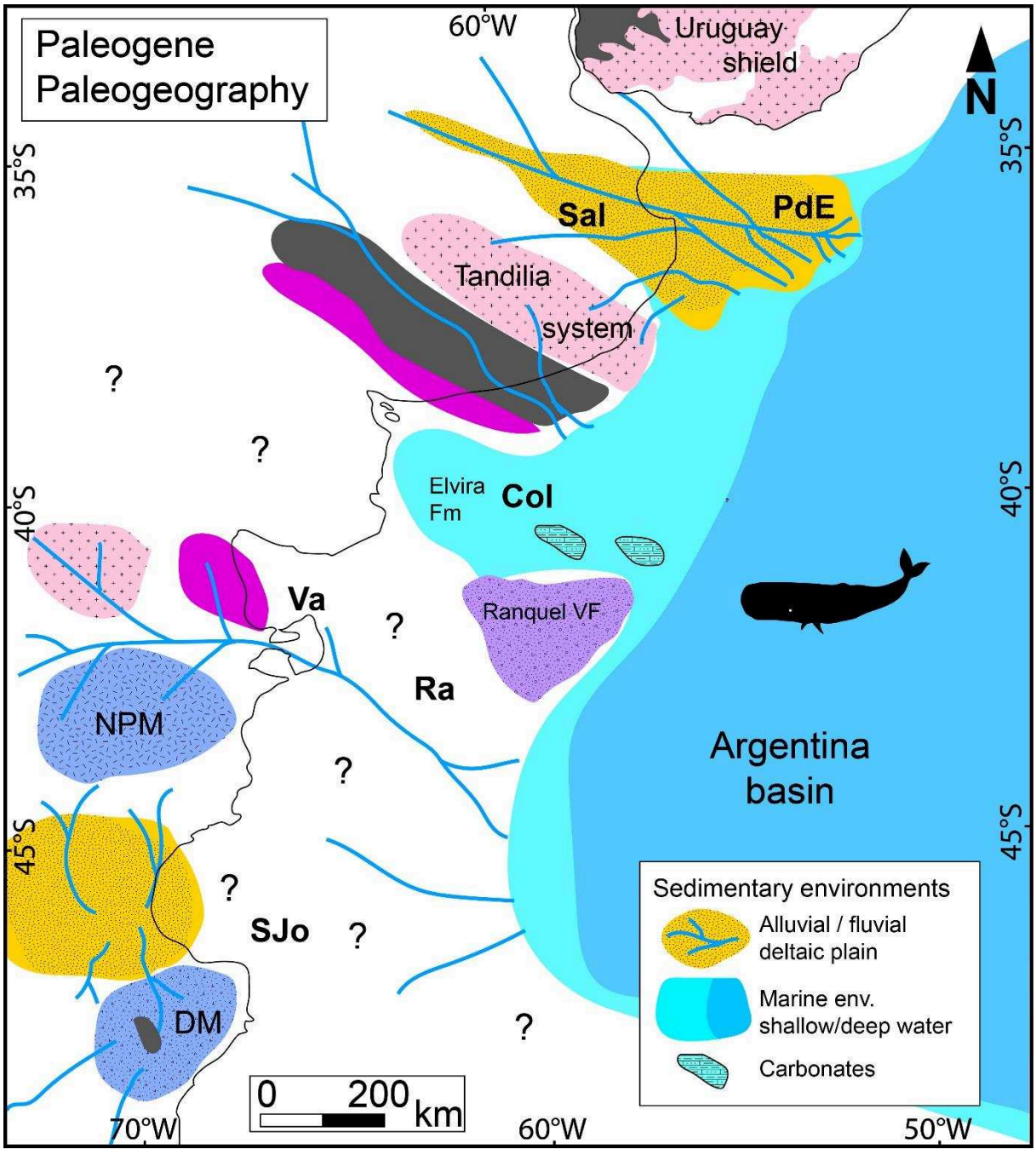

Figure 7.12: Paleogeographic reconstruction of the Argentinean margin during the Paleogene.

In the map presented in Fig. 7.12, the paleogeography is less constrained towards the south, although the Paleogene seems absent in the Rawson area (no Paleogene could be determined in the only exploration well drilled so far (Continanzia et al., 2011).

The isochron map of the Neogene Megasequence is presented in figure 7.13. Continuous deposits are observed all over the shelf. The ancient Tandilia and Rawson highs (especially the area of the Ranquel volcanic field, RVF) display however lower thicknesses. The thicker depocenters seem to be influenced by the E-W oriented Colorado basin axis, although the fingerprint of the individual synrift depocenters is not further detectable. Similarly, a depocenter is inferred in the SE end of the Salado basin.

A sharp NNE-striking shelf-edge in the Colorado basin, associated with a rapid decrease in thickness is observed on the slope of the Neogene Megasequence. In the Salado segment, the shelf-break seems to display a different strike, it is oriented NE, while in Colorado is NNE. This shift in the shelf-break direction occurs in the transition between the Tandilia High and the Salado basin (Fig. 7.13), which is however an area with scarce seismic coverage. In the Salado area, the shelf-break seems to be preserved landward compared to the Colorado basin. An additional increase in thickness on the slope corresponds to a plastered drift, produced by bottom contour currents (see Fig. 7.6, Hernández-Molina et al., 2016).

In the Colorado basin, clinoforms with a southern provenance and downlapping towards the northern flank of the basin, were observed in Fig. 7.3. A seismic line along the shelf strike covering the Rawson basin, and extending into the Colorado basin was interpreted to better characterize the system responsible for the deposition of the Neogene Megasequence in the Colorado basin. The Neogene is formed of mostly shaly facies and is formally referred to as the Barranca Final and Belén Fms (Fig. 3.13) interpreted to be deposited in a marine environment on the shelf.

In the interpreted seismic line presented in Figure 7.14, the depocenters of the Rawson basin are presented, perched on the continental crust and topped by a flat NTK unconformity. Within the depocenters it is difficult to identify internal surfaces, and it was impossible to differentiate a Synrift Megasequence from a Cretaceous Drift Megasequence. Towards the northern end of the line, the Central Colorado depocenter (CCol) is illustrated, with a thick Cretaceous Drift cover. The pinchout of the Paleocene Megasequence can be interpreted to the south of the Colorado basin, onto the Rawson High. Within the Neogene Megasequence, several

surfaces were interpreted. Notably, above the Rawson depocenters, some convex-up bodies, with flanks dipping to the south and north respectively, were interpreted as submarine deltaic lobes for which a western provenance is interpreted. To the southern end of the line presented in Fig. 7.14, thickness decreases. The deltaic lobes or fans in the Rawson area seem to nest and prograde mainly towards the north (towards the Colorado basin).

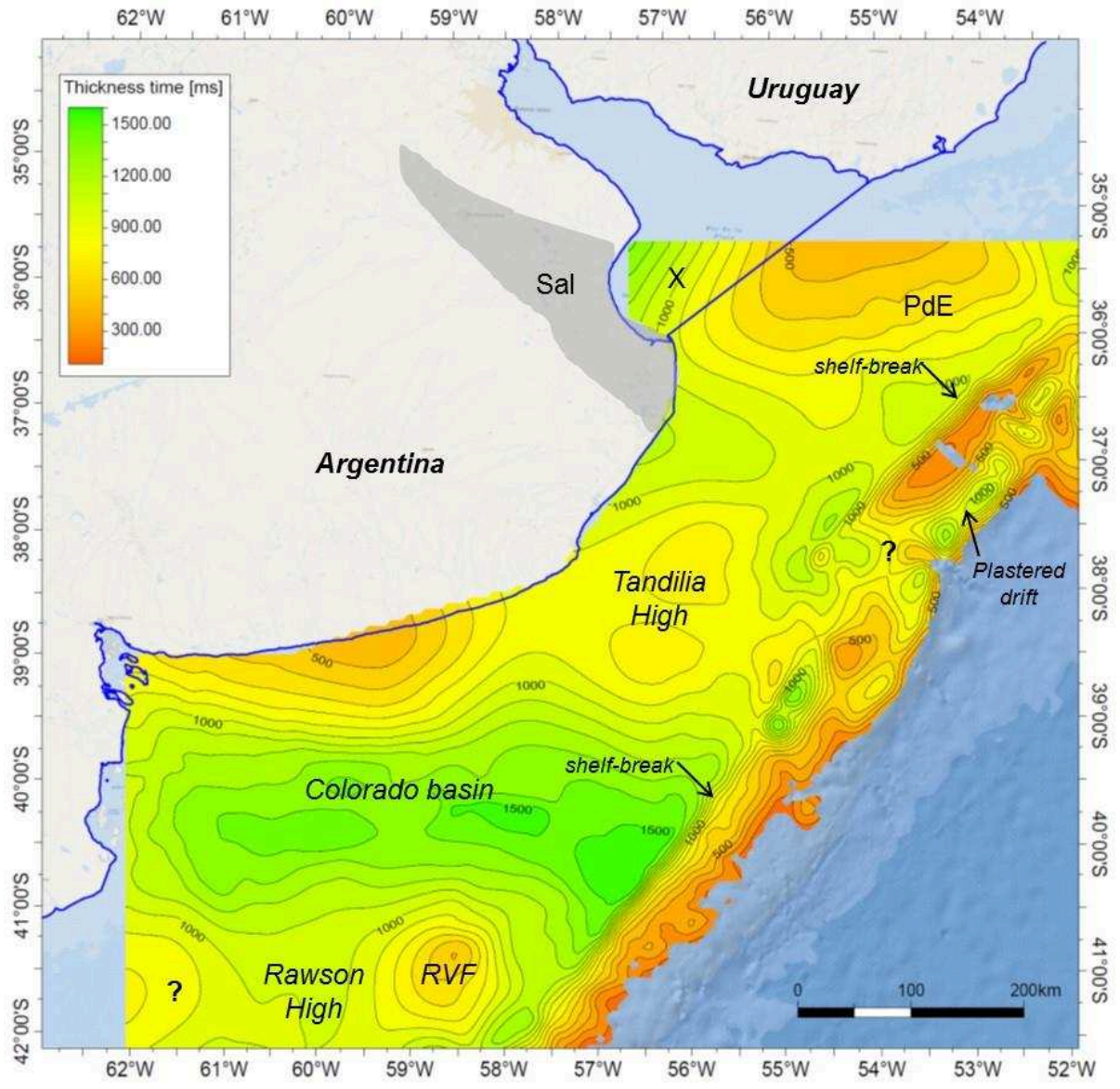

Figure 7.13: Isochron map of the Neogene Megasequence.

Figure 7.15 is a paleogeographic reconstruction for the Neogene Megasequence, especially for the Miocene. The full Argentinean shelf is flooded. The Colorado and Salado basins in particular are fully flooded and operated as marine sea-ways through which the Atlantic floods the pampas. Only the Tandilia and Ventania systems, and parts of the Northern Patagonian and Deseado Massifs remain under subaerial conditions as isolated isles.

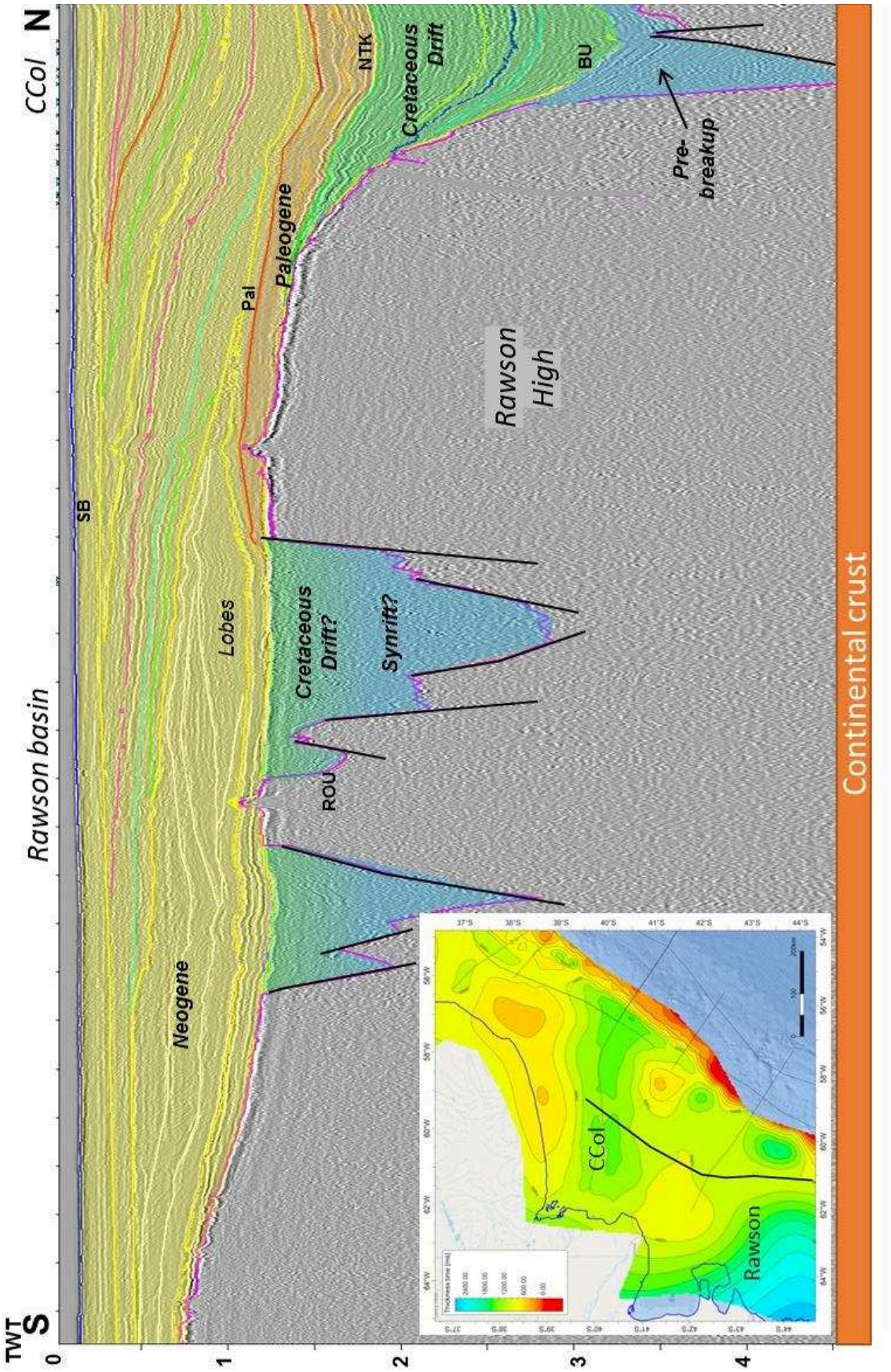

Figure 7.14: Seismic line across the Rawson and Colorado basin. Vertical scale TWT (in seconds)

The lobate features observed on the shelf in the Rawson basin (Fig. 7.14) are interpreted to record a major active sediment source in the western vicinity (deltaic lobes). A fluvial system is then interpreted westward from the Rawson area. These deltaic lobes seem to migrate northwards, which is interpreted as the record of shelf contour currents enhanced after the Eocene by the opening of the Drake Passage and installation of the circum-Antarctic current (Dalziel et al., 2013; Hernández-Molina et al., 2010).

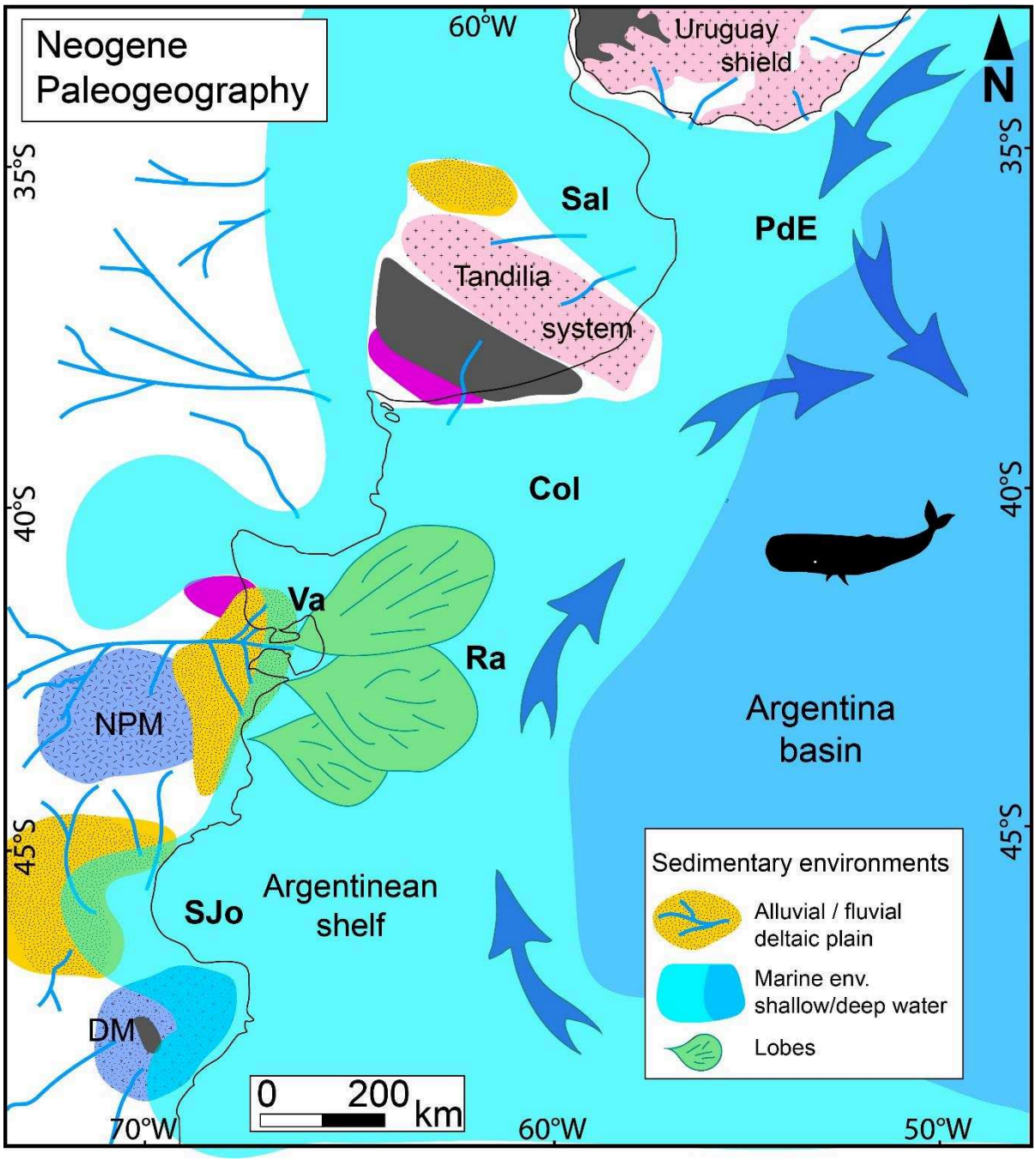

Figure 7.15: Paleogeographic reconstruction of the Argentinean margin during the Neogene (after Camacho, 1967). Blue arrows indicate bottom contour currents.

7.3.3 Discussion

The post-breakup evolution of the Argentinean Atlantic margin has been divided in three main stages that display a variable behavior. The synrift depocenters, formed during the Mesozoic breakup of Gondwana in the Jurassic to Early Cretaceous, were grouped in a unique map of pre-breakup deposits and were displayed in this chapter (Fig. 7.7) to highlight their influence in the successive passive margin stages.

The Cretaceous Drift Megasequence corresponds to the interval between the breakup unconformity (BU) and the end of the Danian (Early Paleocene) transgression marked by the NTK unconformity. Accommodation creation during this stage is larger above the main synrift depocenters, notably Eastern Colorado, but also Central Colorado and the depocenters of the Salado and Punta del Este basin (Fig. 7.8). A combined influence of thermal subsidence and differential compaction of the synrift sedimentary column, is interpreted to play a key role in accommodation creation during this stage.

During the Paleogene, the main depocenter corresponds to the Salado/Punta del Este basin, while the Colorado remained at shallow water depths, probably associated with a low subsidence over this stage. The development of the Ranquel volcanic field (interpreted as product of intra-plate volcanism, Lovecchio et al., 2017) in the Campanian-Danian could have produced a thermal anomaly responsible for uplift of the area (Rawson high and the southern flank of the Colorado basin) that may have continued during the Paleogene. Carbonate facies in the Eocene Elvira Fm of the Colorado basin, are interpreted to indicate a starved basin and a shallow water setting. A large sediment supply system is interpreted for the Salado/Punta del Este basin. Sediment supply occasionally exceeded accommodation, resulting in three stacked cycles of progradation. Some progradational packages delivered from the Salado/Punta del Este basin reached the Colorado basin along its northern edge (Fig. 7.3). For the multiple events recorded here, the margin behaved asymmetrically in the Salado/Punta del Este, Colorado and Rawson basins during the Paleogene. Subsidence is observed in the Salado/Punta del Este basin area towards the north of the study area, a phenomenon that might have been accentuated by increased sediment supply (e.g. a paleo-Paraná river system catching drainage systems sourcing in the Andean foothills). The Rawson area experienced uplift, that is interpreted to be related to a thermal anomaly associated the Late Cretaceous-Early Paleocene volcanism. Uplift in the Rawson basin is evidenced, not only through the absence of the Paleogene Megasequence (at

least in the area with seismic data available to this study), but also in the strong erosive, flat-lying, unconformity affecting the top of the synrift/Cretaceous undifferentiated unit. The Colorado basin is in an intermediate position during this period of time. It seems to have been characterized by a shallow water sea, with a southern exhumed flank (towards the Ranquel volcanic field) and very weak sedimentary supply from the north (Tandilia High/Salado basin).

The Neogene Megasequence displays a different setting, with accommodation being created all over the shelf. Increased thickness is observed along the Colorado and Salado basins axis. The Argentinean shelf is finally a single, continuous system. A sediment entry point is determined near the Rawson basin. Although the seismic facies indicate shaly sediments, the lobate shapes are interpreted as distal deltaic systems. Sediment drift towards the north is then interpreted for the Rawson-Colorado segment, with clinoforms downlapping the northern flank of the Colorado basin (Fig. 7.3). It is worth to highlight that all these systems develop on the shelf, with a shelf-break that does not reach the position of the Late Cretaceous shelf-break (previous to the transgression that initiated in the Campanian). Two possible interpretations were envisaged. First, the sediment supply could have been lower than the accommodation creation and thus the platform (sensu Helland-Hansen et al., 2012) progrades without reaching its maximum capacity (with the slope reached, sediments would be transferred to the basin). Second, the bottom contour currents, known to be very important since the Eocene opening of the Drake passage, continuously redistributed the sediments and shaped the platform, not allowing its maximum development.

The Argentinean margin shows a changing character throughout its post-breakup evolution. Accommodation creation during the Cretaceous seems to be controlled by thermal subsidence above the main synrift depocenters. At the end of the Cretaceous, the volcanism observed in the Rawson area could have produced uplift that continued during the Paleogene. The Salado/Punta del Este area displays accommodation during the Paleogene. It is not clear if this could be related to a flexural effect potentially associated with the Rawson uplift, but whatever the origin, subsidence was probably enhanced by an exceeding sediment supply (which at the same time could be related to drainage catchment of the drainage systems that previously supplied the now uplifted Colorado area). Oppositely, during the Neogene the margin shows a more cylindrical behavior, with accommodation being created all along the shelf (although increased in the Colorado and Salado basins axis). The explanation for the accommodation creation remains uncertain, however this period coincides with a pulse of the

Andean orogeny (Alicia Folguera et al., 2015), that could have also produced additional dynamic subsidence in the study area (as suggested by Dávila and Lithgow-Bertelloni, 2013).

7.4 Stratigraphic modeling

7.4.1 Introduction

With the objective of quantifying the subsidence evolution of the Colorado basin, a forward stratigraphic model was carried out for the study area (Fig. 7.16) using the DionisosFlow software (Granjeon, 1997; Granjeon and Joseph, 1999). DionisosFlow had previously been used in the Colorado basin back in 2001, over a smaller area near the shelf-break (Fig. 7.16). At that time, the objective was to assess facies distribution regarding potential source rocks and reservoirs, to perform afterwards petroleum system modelling (Beicip, 2001; Mancilla et al., 2002).

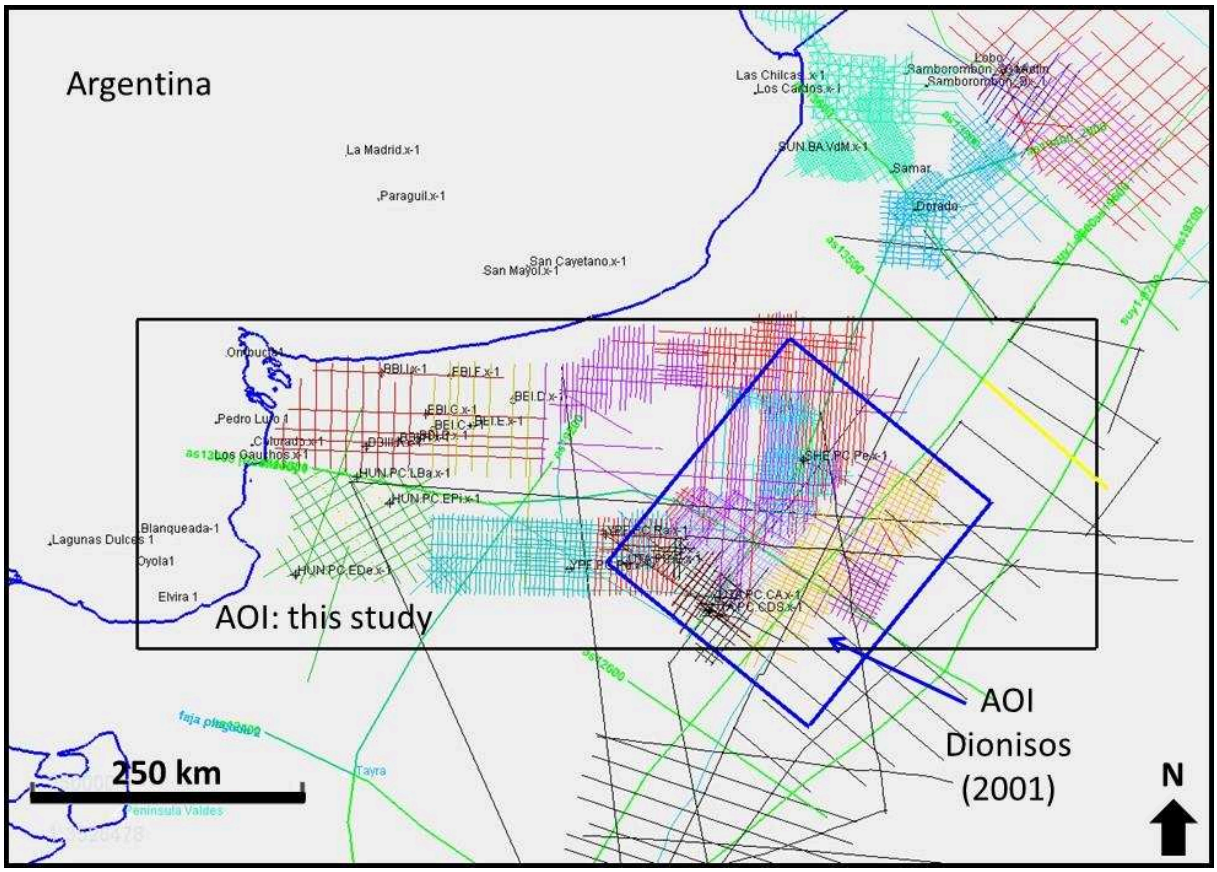

Figure 7.16: Basemap for the Colorado basin Area of Interest (AOI) defined for this study, compared with the DionisosFlow model carried out in 2001 (Beicip, 2001).

In the approach presented in this PhD study, the objective was to evaluate the post-breakup subsidence history of the Colorado basin, from a seismic stratigraphic approach. The model is limited to the Colorado basin (and does not cover the whole northern Argentinean margin) because the velocity model (see Chapter 3) is restricted to this area of 270,000 km^2 (Area of Interest, AOI: 900 x 300 km). Depth-converted grids are used to produce thickness maps that will be incorporated in the subsidence estimations.

A previous subsidence history analysis for the Colorado basin has recently been produced by Dressel et al. (2017), from a set of structural grids published by Autin et al. (2013). Dressel et al. (2017) divided the post-breakup succession in seven layers, and carried out backward modelling by calculating the amount of sediment load subsidence produced by each layer. From a crustal thickness map, the authors calculated a stretching (β) factor map and were able to predict thermal subsidence for each post-breakup phase. They used the obtained thermal subsidence maps to correct the backstripped surfaces and produced paleobathymetry maps for seven time-steps (25, 40, 55, 70, 90, 98, and 125 Ma). However, these paleobathymetry maps are not consistent with the sedimentary environments observed in well and seismic data. The range of error seems to be larger towards the deeper units. For example, for 98 Ma Dressel et al. (2017) present a paleobathymetry map with deepwater conditions all along the Colorado basin axis (Fig. 7.17), while well and seismic data indicate that the Colorado basin was under subaerial conditions during the Late Cretaceous, with fluvial systems occupying the basin axis and a coastline near the shelf-break, towards the east of the basin (Fig. 7.9).

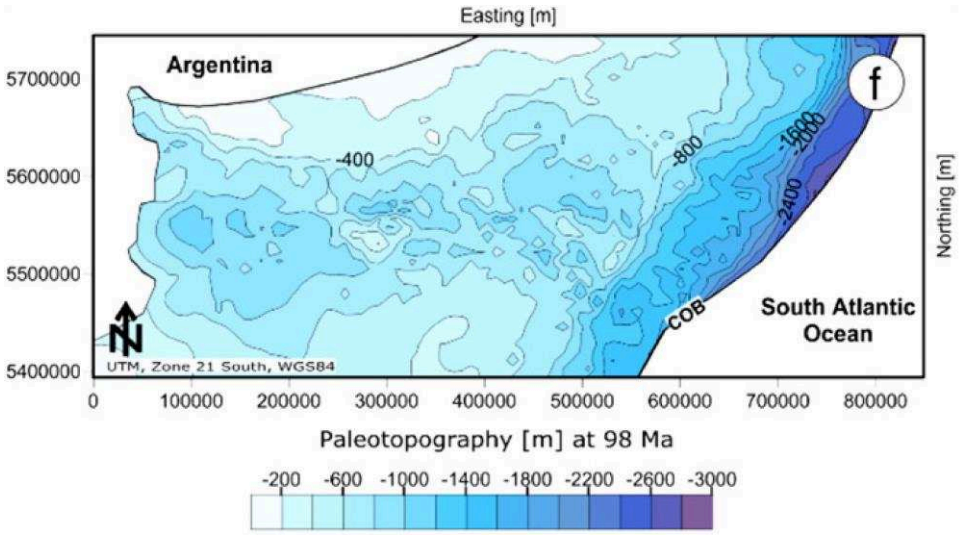

Figure 7.17: Estimated Paleobathymetry at 98 Ma in the Colorado basin (from Dressel et al., 2017).

In this study, the subsidence history was approached from a completely different approach. Paleobathymetry maps were produced, respecting lithologies and sedimentary environments determined in the exploration wells (e.g. red-beds, marine shales), seismic facies (e.g. discontinuous fluvial facies, transgressive coastal ridges), the shelf-break position, bathymetry inferred from biostratigraphic data (available for the Campanian-recent section; Pérez Panera et al., 2018).

Paleobathymetry maps, together with thickness maps for the modeled units, were used to estimate subsidence for each stage of passive margin evolution. The model was adjusted until it calibrated the sedimentary thickness and respected the stratigraphic architectures. New subsidence rate maps were produced for each stage and are compared in the following sections. The approach can be defined as a "surface approach" when compared to the "deep approach" used by Dressel et al. (2017).

7.4.2 Model setup

A six-layer forward stratigraphic model was generated using DionisosFlow (version 2017.5). Due to its largest thickness, the Cretaceous Drift unit was sub-divided into four layers: 125-101 Ma, 101-91 Ma, 91-83 Ma, and 83-61 Ma (the latest corresponding to the Campanian-Danian transgression). One layer for the Paleogene unit (61-33 Ma), and one for the Neogene unit (33-0 Ma, Fig. 7.18).

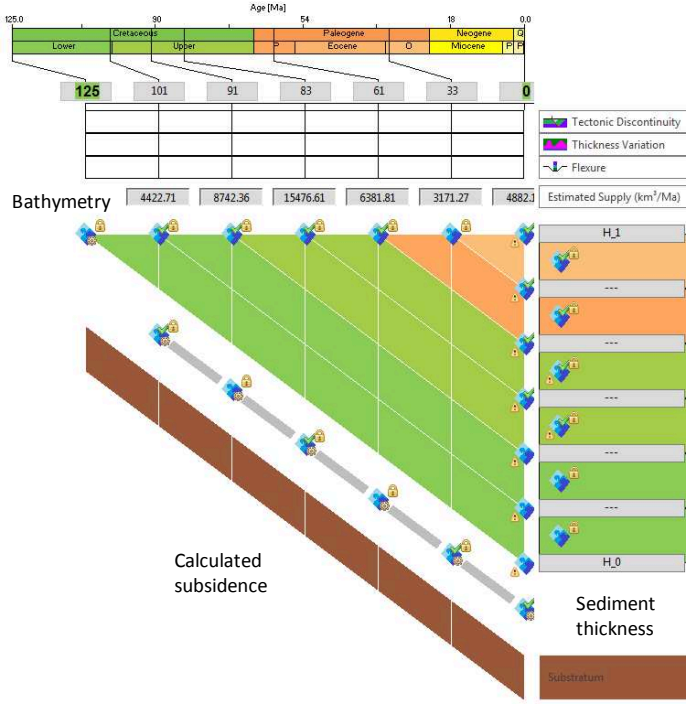

Figure 7.18: Structural evolution diagram for the Colorado basin model as defined in DionisosFlow. The paleobathymetry maps are loaded on the horizontal (time) axis, while the thickness maps for each unit are loaded on the vertical (depth) axis.

The paleobathymetry maps that were used in the forward stratigraphic modeling are presented in figure 7.19. Note that for the Cretaceous layers, most of the Colorado basin is under subaerial conditions and only the eastern edge is flooded. Figure 7.19d represents the paleobathymetry just before the onset of the Campanian-Danian transgression. Figure 7.19e is the estimated bathymetry at the end of the Campanian-Danian transgression, with all the study area under marine conditions. Figure 7.19g is present-day bathymetry, note the calibration with the coastline (that is used as a reference in all maps).

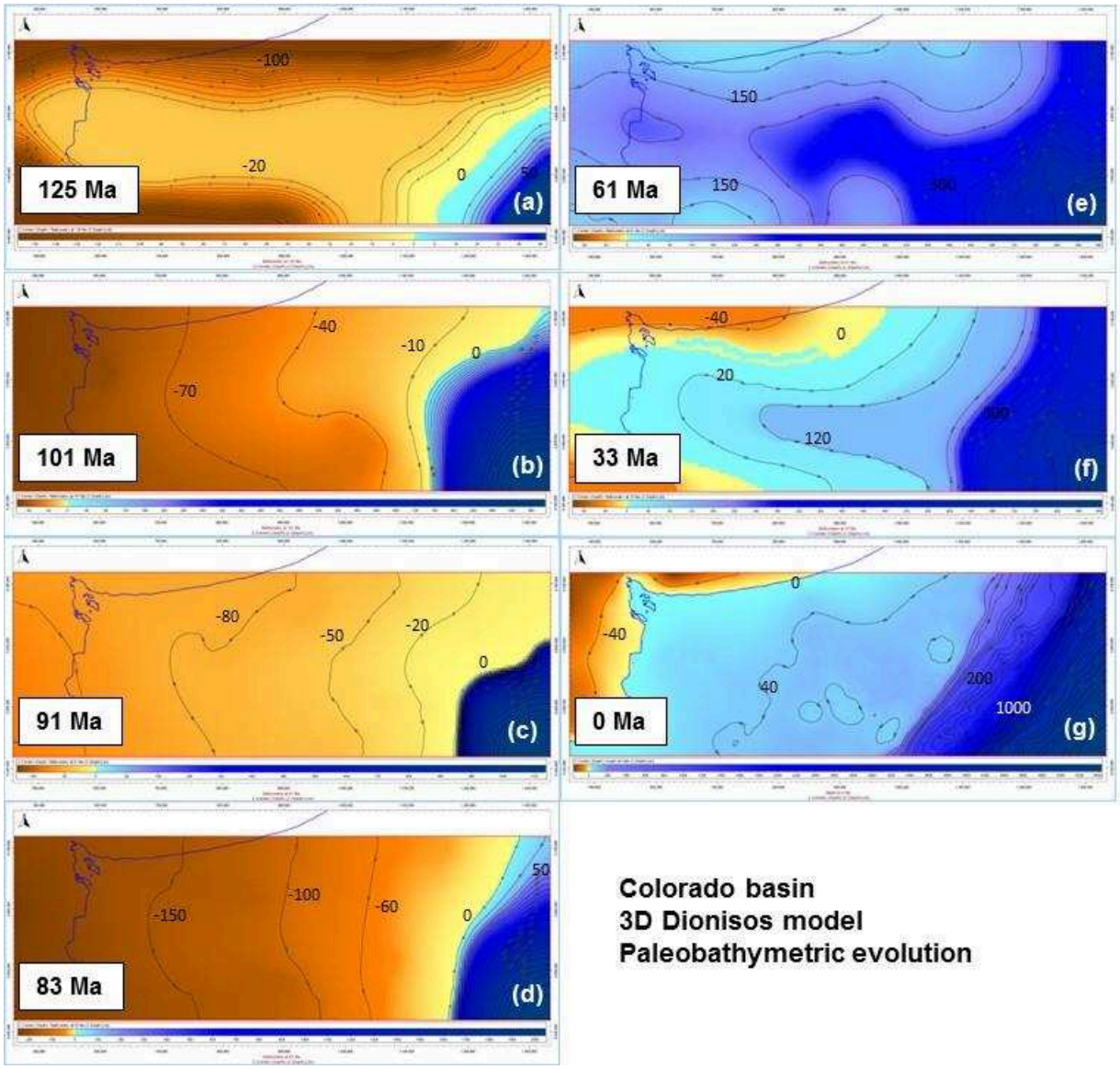

Figure 7.19: Paleobathymetry maps used in the stratigraphic model: a) Paleobathymetry at 125 Ma, b) Paleobathymetry at 101 Ma, c) Paleobathymetry at 91 Ma, d) Paleobathymetry at 83 Ma, e) Paleobathymetry at 61 Ma, f) Paleobathymetry at 33 Ma, g) Paleobathymetry at present-day (0 Ma).

Five sediment sources were defined to supply the necessary sediment to fill the accommodation created. Their locations were established using the paleogeographic maps previously presented in this chapter. One main sediment source (S1) was defined in the west, interpreted as a major axial fluvial system draining into the basin. Two sediment sources were distributed on each flank of the basin to reproduce the lateral sediment input from the Tandilia high to the north and the Rawson high to the south (S2 and S3 in the north, and S4 and S5 in the south, Fig. 7.20). Two sediment classes were defined to restore the grain size distribution known at wells: sand and shale. Table 7.1 displays the sedimentary fluxes and water discharges used at each time step in the model.

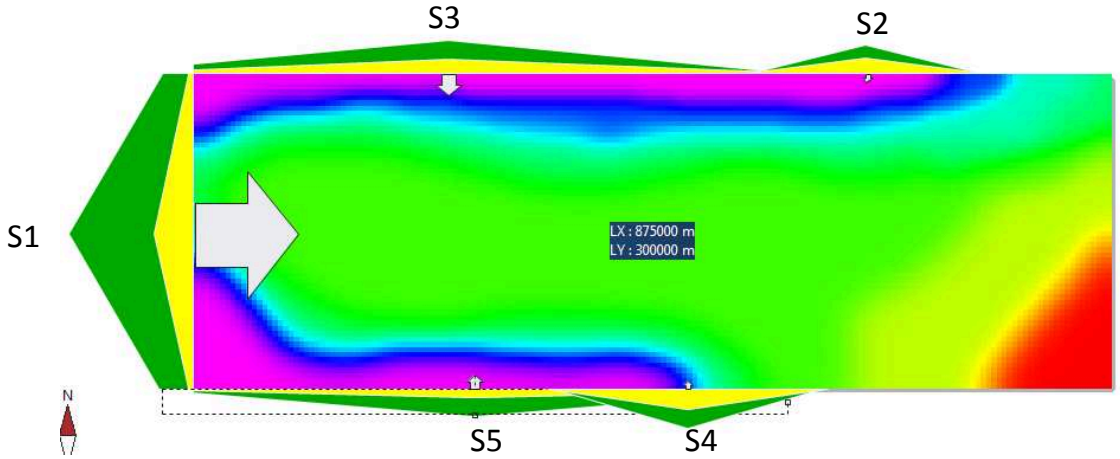

Figure 7.20: Sediment sources defined for the Colorado basin DionisosFlow model.

	Average											
Age (Ma)		125	120	113	101	97	91	83	65	61	33	10
Estimated Supply (km³/Ma)		-	-	-	-	-	-	-	-	-	-	-
Total Supply (km³/Ma)	4212.12	4542.2	4530.9	4464.4	10000	11000	14000	3000	0	2900	4000	4700
Total Fluvial Discharge (m³/s)	4078.79	18200	18600	22200	33000	50000	31000	10000	0	13000	4200	3800
Rain Fall (mm/year)	0	0	0	0	0	0	0	0	0	0	0	0
Evaporation (mm/year)	0	0	0	0	0	0	0	0	0	0	0	0
◢ Sources List												
S1	1290.91	2159.4	2108.8	2023.6	3729.8	3666.6	6533.3	1428.5	0	900	1200	1500
S3	921.21	938.98	938.98	938.98	1730.6	1833.3	2800	714.29	0	900	800	1200
S5	2000	751.18	790.82	809.46	1491.9	1833.3	2800	714.29	0	100	2000	2000
s4	0	432.69	432.69	432.69	1523.8	1833.3	933.33	71.43	0	0	0	0
s2	0	259.62	259.62	259.62	1523.8	1833.3	933.33	71.43	0	1000	0	0

Table 7.1: Sediment supply summary chart.

The DionisosFlow software is an advecto-diffusive model where the sediment transport is function of the ground slope and the water discharge (Granjeon & Joseph, 1999). Transport coefficients were established according the mean expected slope and are presented in Table 7.2. 95% water driven transport (5% gravity driven). The sea level variations were estimated from

Haq et al. (1988) and adapted to calibrate the model using as a guideline the corrections of the Beicip (2001) report (Fig. 7.21).

Simulation was carried out step by step, iterating and calibrating each stage, before moving forward to the next stage. A two million years-time step was used for the modelling in DionisosFlow (version 2017.5).

	Sand	Shale
Gravity-Driven Diffusion Coefficient : Kgravity		
Continental (km²/kyr)	12.2099	27.3022
Marine (km²/kyr)	0.4083	2.0413
Water-Driven Diffusion Coefficient : Kwater		
Continental (km²/kyr)	231.9881	518.7411
Marine (km²/kyr)	7.0000	39.0000
Wave Diffusion Coefficient : Kwave		
Kwave (km²/kyr)	5.3222	11.9007
Slope Failure Model		
Critical Slope Failure (m/km)	60.0000	60.0000

Table 7.2: Transport coefficients used for the Colorado basin DionisosFlow model.

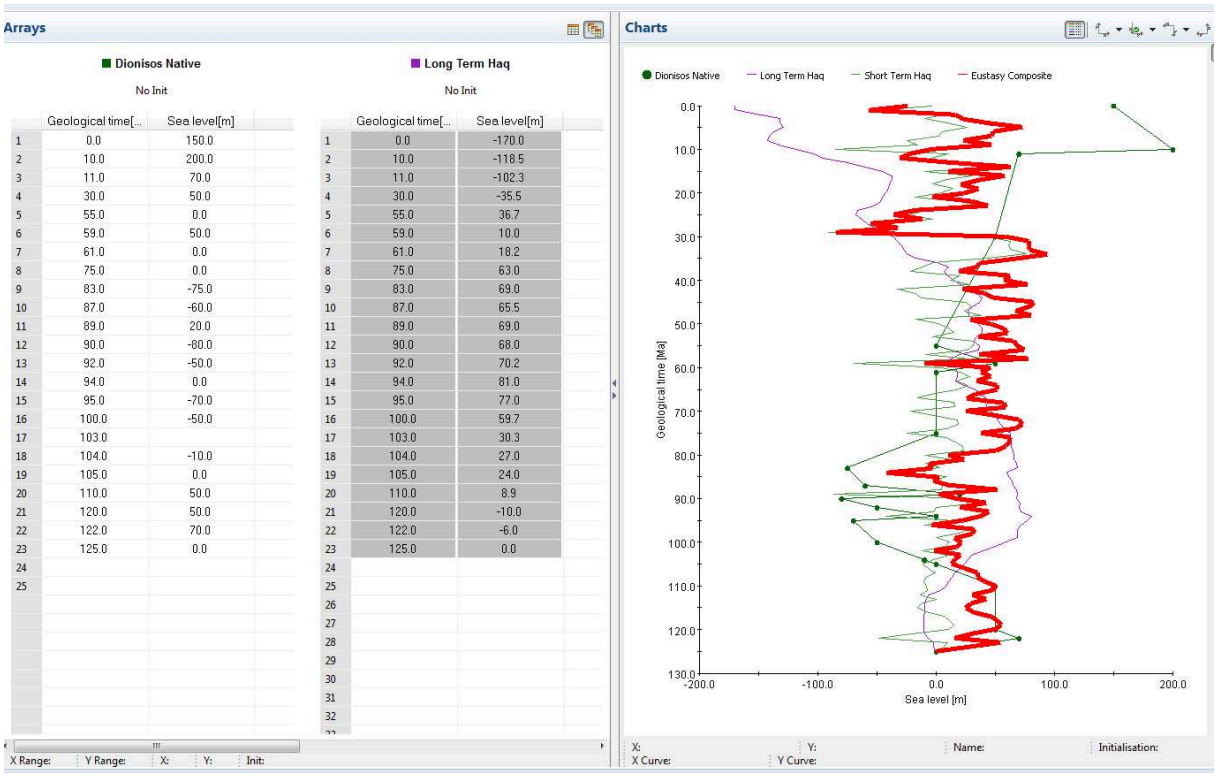

Figure 7.21: Eustatic curve obtained after editing the Long and Short Term Haq sea level curve (Haq et al., 1988). The red curve on the right is the resulting composite eustatic curve used by the model.

7.4.3. Results

With the input presented in the previous section, a DionisosFlow model was generated, honoring some key stratigraphic observations in the Colorado basin. Figure 7.22 displays a 3D view of the Colorado basin model, at 73 Ma. Note that the basin is flooded, during the Campanian-Danian transgression developing at this time. Just below this level, the Late Cretaceous fluvial systems can be identified (orange and yellow colors represent subaerial environments, highlighted with negative bathymetries). The Cretaceous Drift presents a mostly aggrading stacking pattern, although with onlaps against the BU in the marine domain (Fig. 7.22). The cross-section on the edge of the 3D block presented in Fig. 7.22 is at a similar position as the seismic line presented in Fig. 7.3. Towards the east (right of the image), the fluvial systems pass to marine conditions and clinoforms develop above and downlap on the External High (Fig. 7.22).

Near the base of the system, just above the breakup unconformity (interpreted here as the 125 Ma horizon), the first marine transgression occurred and flooded the Eastern Colorado depocenter, as it has been proposed by Mancilla et al. (2002) and Gerster et al. (2011). A bathymetry map recovered from the model at the time of the Aptian transgression is presented in Fig. 7.23.

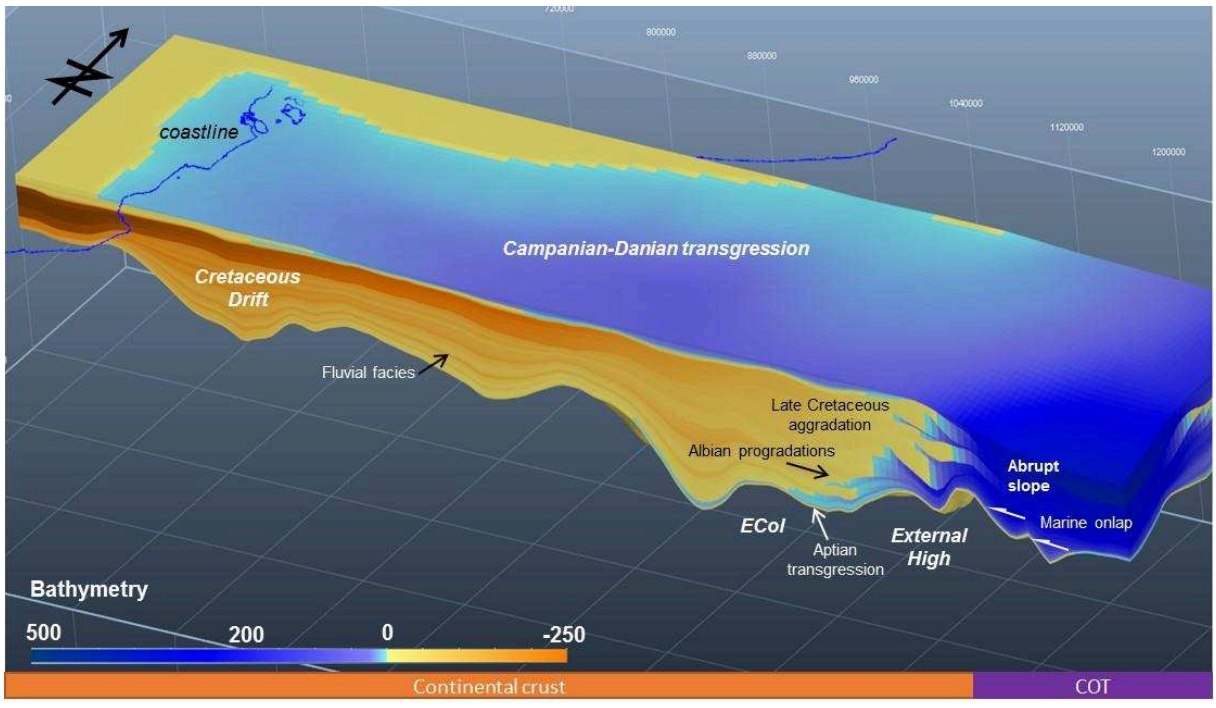

Figure 7.22: 3D perspective of the Colorado basin DionisosFlow model at 73 Ma during the Campanian-Danian transgression. Color scale indicates bathymetry at the time of deposition.

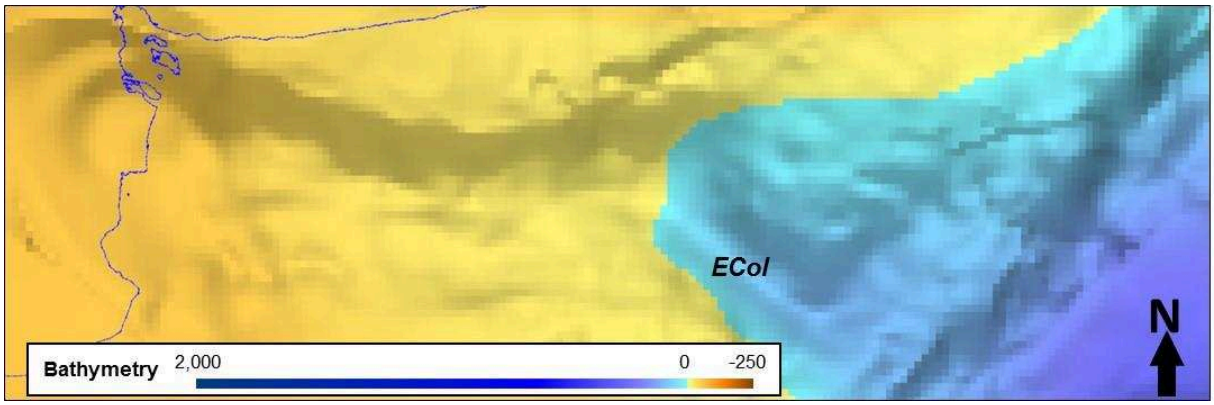

Figure 7.23: Modeled bathymetry at 123 Ma (Aptian), most of the ECol depocenter is flooded.

After maximum flooding is achieved, the system begins to prograde and the shelf nucleation process (sensu Helland-Hansen et al., 2012) initiates. The first progradations are characterized by low slope angles (indicated in Fig. 7.22 as "Albian" progradations, although no age control is available for these sequences). The later progradations display a more aggradational stacking pattern. The system progrades until reaching the structural slope, on the COT, that defines an abrupt slope. The equivalent early drift sequences in the basin, display marine onlaps against the BU (on the slope).

Fig. 7.24 presents the sand-to-shale ratio distribution along a key section. The Cretaceous Drift Megasequence is sandier in the lower section (typically fluvial in the position of this section, similar to the seismic line presented in Fig. 7.3). Sand content of the basal units increases towards the basin flanks, where lower accommodation favors sand body amalgamation. The Campanian-Danian transgression appears here as a shale-rich unit, thicker in the center above the depocenter and thinner towards the flanks. The thin Paleogene Megasequence is representing as a low angle wedge, subtly prograding towards the south (downlap is indicated with arrows). The Neogene Megasequence, on the other hand, appears as a thick package of prograding clinoforms migrating towards the NNE. The overall stratigraphic architecture identified from the seismic data is well represented by the numerical model.

The software calculates cumulative subsidence maps from input layer thicknesses and paleo-bathymetry variations. These maps can then be adjusted in the process of model calibration. A set of corrected cumulative subsidence maps were obtained from DionisosFlow results. These maps where then back-stripped to compute the subsidence at each stage, which was then divided by the time lapse of the stage, to obtain the subsidence rate maps (in m/Ma)

presented in Fig. 7.25. The advantage of subsidence rate maps comparatively to total subsidence maps is that they facilitate comparison and analysis of subsidence evolution though time. Note that the SE sector of the maps, corresponding to the COT and oceanic basin, were removed (white triangles) because uncertainties in these areas are too large. Figures 7.25a, b, c and d correspond to the Cretaceous Drift unit. A clear trend of enlarging area of subsidence is observed in Fig. 7.25a, b and c, that could be related to thermal subsidence. Note in Fig. 7.25b, the NE oriented depozone, indicating the shelf-break, where larger subsidence induced by sediment load is expected. Fig. 7.25c (interval 91-83 Ma) displays the largest and more widely distributed subsidence. It is worth to mention, however, that these first three sequences do not have age control (ages are interpreted from the stratigraphic record), and this larger subsidence rate could be an artifact of the shorter time interval (8 Ma). Subsidence is however more widely distributed, and the NE area (eastern extension of the Tandilia High) displays larger subsidence rates at this time.

Figure 7.25d displays the subsidence rate for the Campanian-Danian transgression at the top of the Cretaceous Drift Megasequence. The maximum (but smaller) subsidence rate seems to be located along the Colorado basin axis.

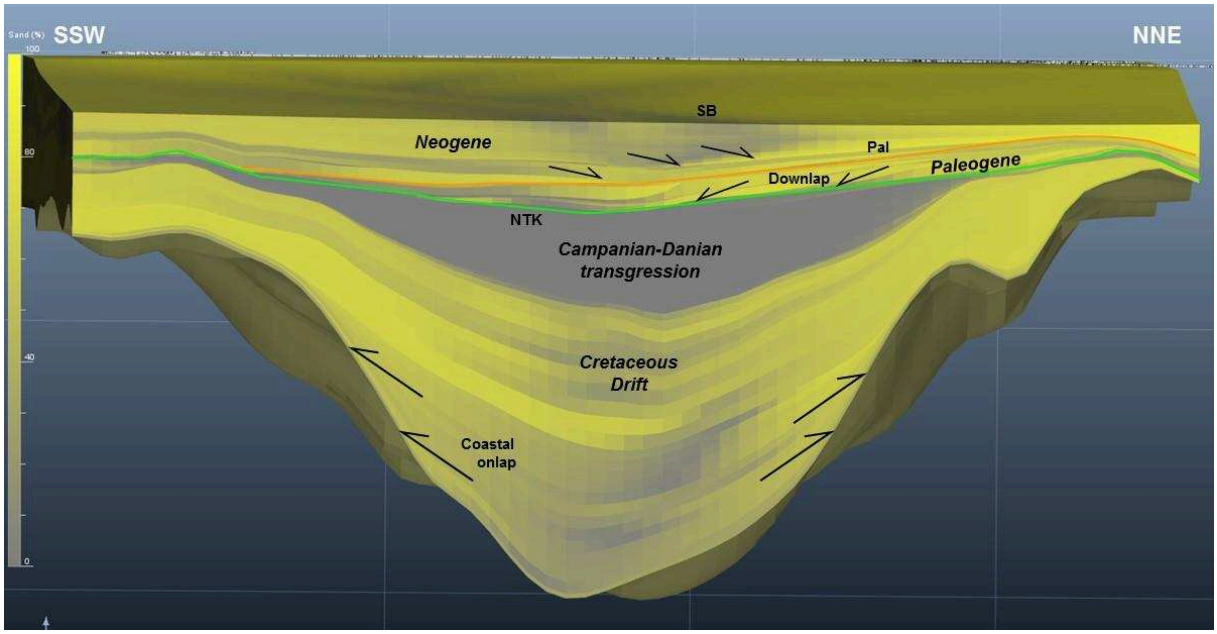

Figure 7.24: NNE-SSW cross-section across the ECol depocenter (equivalent to the seismic line presented in Fig. 7.3). Color scale represents the relative proportion in sand (yellow) and shale (grey).

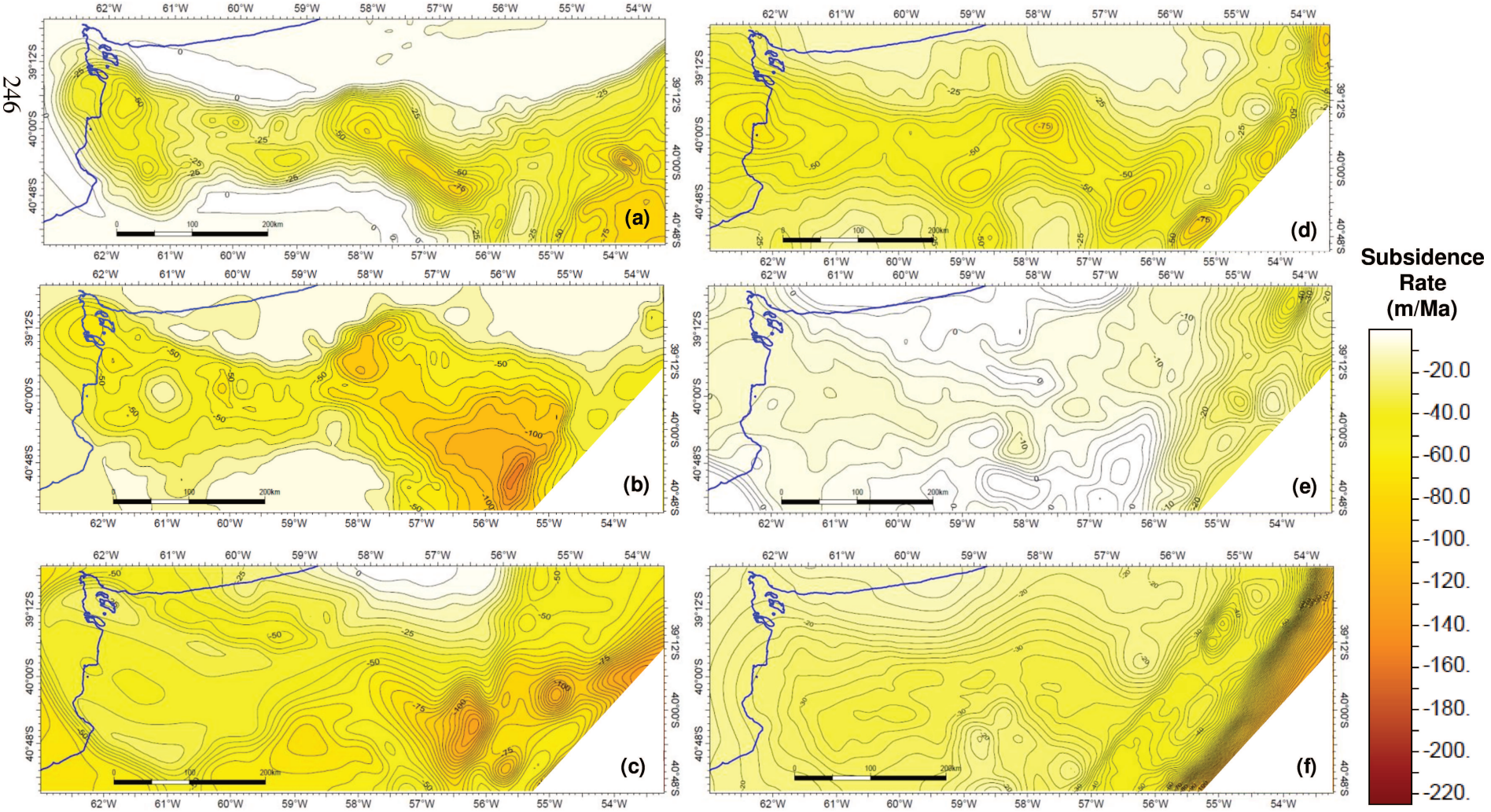

Figure 7.25: Subsidence rate maps (in m/Ma) for the six intervals modeled: a) 121-101 Ma; b) 101-91 Ma; c) 91-83 Ma; d) 83-61 Ma; f) 33-0 Ma. Blue line corresponds to the present-day coastline. Color scale is the same for all maps.

The Paleocene Megasequence (Fig. 7.25e) presents the lowest subsidence rate values, with no subsidence in the southern Colorado basin flank and the Rawson high. The subsidence rate increases for the Neogene Megasequence (Fig. 7.25f), especially along the Colorado basin axis and the shelf-break but also all over the shelf.

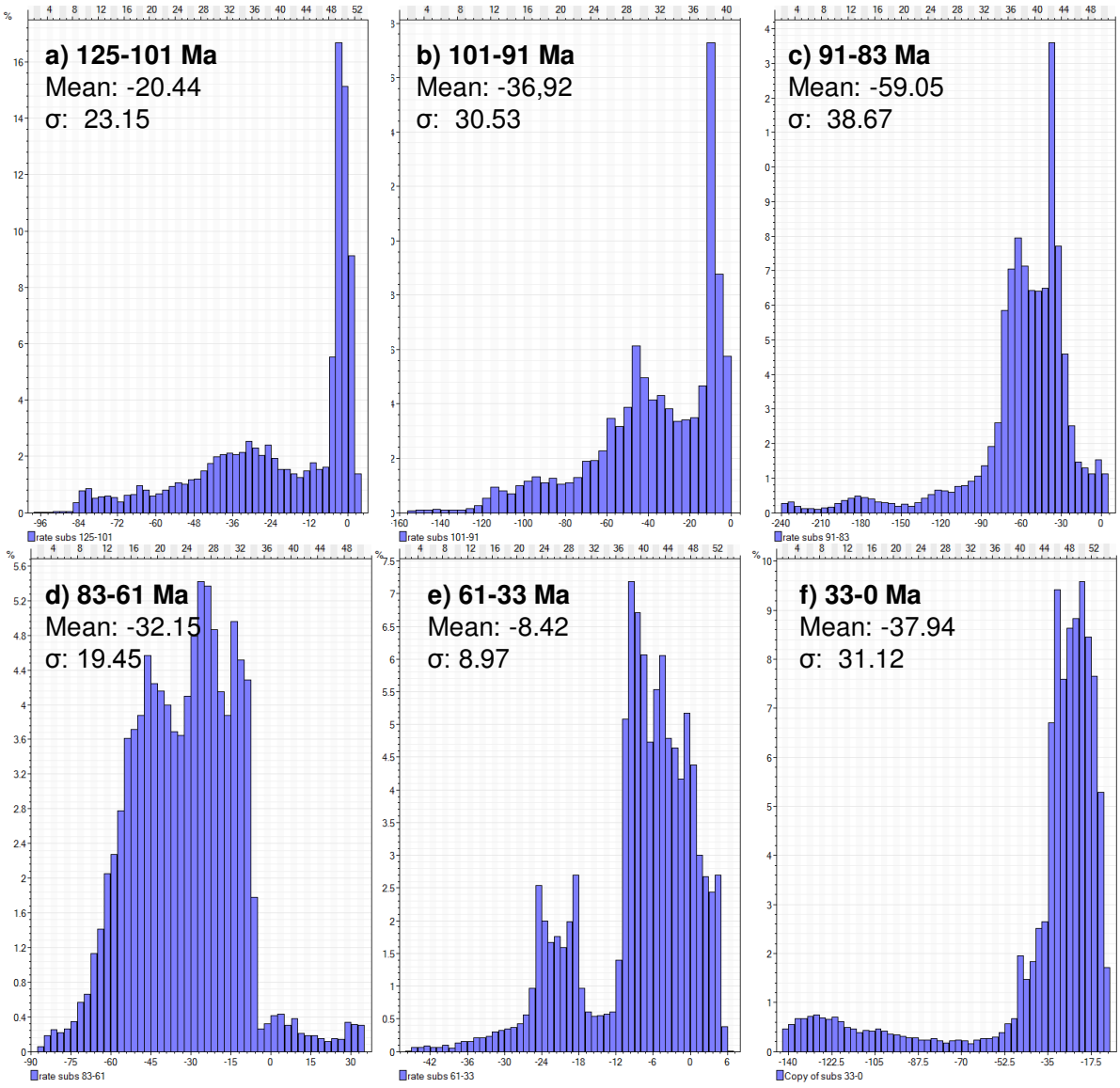

Figure 7.26: Histograms of subsidence rate (in m/Ma) for the six modeled intervals: a) 121-101 Ma; b) 101-91 Ma; c) 91-83 Ma; d) 83-61 Ma; e) 61-33; f) 33-0 Ma. Note that the horizontal scales vary between histograms.

Figure 7.26 displays the histograms of subsidence rate frequency for each time interval and the statistic mean and standard deviation σ, that were computed with Petrel. Note that the horizontal (subsidence rate) scales vary from one histogram to the other. The mean values suggest of the acceleration in subsidence rate observed between 125 and 83 Ma, and a deceleration observed in the Campanian-Danian interval (83-61 Ma), with minimum mean subsidence during the Paleogene and renewed subsidence in the Neogene. Note also that for the Paleogene, for example, two populations can be identified (Fig. 7.26e). We interpret these two populations as one representing the low subsidence in the Colorado basin, and the other, the higher subsidence observed to the northeast, towards the Salado depocenter (Fig. 7.25e). In general terms, these values are in the same order of magnitude than on the shelf of the Pelotas basin as computed by Contreras et al. (2010). The same trend with a major decrease in subsidence rate towards the Cretaceous / Paleogene transition is documented in the Pelotas, Santos and Campos basins to the north of our studied area (Contreras et al., 2010), suggesting that the volcanism and potential related uplift documented in the Rawson area during the Paleogene is part of a larger, probably plate-scale process.

7.4.5 Final remarks

A complete set of subsidence rate maps was obtained from forward stratigraphic modeling with the DionisosFlow software for the Colorado basin. These maps were used to quantify subsidence throughout the post-breakup evolution in the Colorado basin. The Cretaceous Drift Megasequence shows a trend of increasing subsidence rate and increasing area under subsidence in the first three stages considered in the model (125-101, 101-91, and 91-83 Ma). The 83-61 Ma stage (Campanian-Danian transgression) shows a deceleration in subsidence rate that reaches a minimum in the Paleogene. Renewed subsidence is observed in the Neogene.

Forward stratigraphic modelling demonstrated to be a useful tool to quantify subsidence in a passive margin basin. These subsidence values are directly inverted from the stratigraphic record and have been obtained honoring the geological and geophysical data.

These newly obtained subsidence values unfortunately, could not be compared with the subsidence calculations of Dressel et al. (2017), because these authors used a different set of

horizons and time frame, and did not represent the subsidence values as rates (m/Ma), but as subsidence over the time interval (in meters). Moreover, these authors do not show total subsidence, but independent maps for calculated thermal and sediment load induced subsidence. The Paleobathymetry estimations produced by Dressel et al. (2017) overestimate the bathymetry reconstructed with geological and seismic data. A new iteration in the back-stripping subsidence estimation using the "deep approach" introduced by Dressel et al. (2017, 2015) should be carried out to better assess the subsidence history, and the mechanisms triggering subsidence at each stage.

Conclusions and Perspectives

Passive margins were, and are still nowadays, the locus of major scientific and industrial interest. Historically, studies of passive margins have focused on characterization of the crustal structure, their breakup history (e.g. kinematic reconstructions, analog and numerical modeling), or their stratigraphic evolution (using sequence stratigraphy techniques to understand the relationship between accommodation creation and sediment supply). The discovery of important hydrocarbon resources in deep and ultra-deep waters has brought the interest of the industry leading to a better imaging of the passive margin's structure and basin fill. The South Atlantic Ocean is an ideal laboratory for understanding the evolution of passive margins, as it provides the full spectrum of phenomena related to continental breakup and passive margin formation (i.e. magma-poor, magma-rich, transform margins), and because of the huge petroleum resources that draw the world's attention (e.g. the pre-salt plays along the Brazilian and African margins, stratigraphic plays along the equatorial margins of Ghana and Guyana). To the south, the Argentinean margin, and the conjugate Namibian and South African margins remain as an exploration frontier still poorly characterized but with enormous potential. In the last few years, the South Atlantic has been the target of both scientific projects and hydrocarbon exploration strategies, extending frontiers with growing datasets and challenging paradigms.

The complex rifting history that preceded the extensional event leading to the opening of the new ocean, in this case the South Atlantic, has so far been disregarded. Precursor rifting history is important not only due to its impact on structural inheritance, but it also influences the passive margin evolution. This problematic has been explored in this thesis, with a focus on the effect of rifting history on passive margin development, in both inducing structural heterogeneities for the successive breakup, and in conditioning the stratigraphic response.

Three main findings should be highlighted from this study.

1. Passive margin initiation: complex superimposed extensional events evidenced in the Colorado basin.

The first question addressed in this PhD was dedicated to the initiation of passive margin. Many controversies were still debated regarding the integration of the Argentinean basins in the dynamic of the south Atlantic opening. The Argentinean passive margin, in particular, displays a unique complexity. Several aborted rift basins developed on the present-day shelf, throughout the Mesozoic extensional evolution of the supercontinent of Gondwana. The multistage rifting history observed in the Colorado basin and in the Argentinean margin, has proved to influence its stratigraphic development, both during extension and after, in the passive margin stage. Different synrift depocenters, produced by different rifting events, host sedimentary infill of different ages, deposited under different climatic settings. This explains why some depocenters may host source rock intervals and others may not. Multistage rifting has also played a key role regarding the post-breakup stratigraphic evolution during the passive margin stage.

The interpretation of a large seismic dataset from the Colorado basin area, leads to the identification of several generations of faults with cross-cutting relationships, superimposed in a complex area marked by the development of a late Paleozoic to Early Triassic fold-and-thrust belt between Patagonia and the Gondwana cratonic core, as part of the Gondwanides orogen. Three independent rifting settings were identified in the Colorado basin area. The oldest extensional event was related to the negative inversion of the Ventania-Cape fold-and-thrust belt, with an extensional reactivation of the Late Paleozoic thrusts, originating a system of tilted blocks over a listric detachment, as clearly seen in the northern flank of the Colorado basin, and the half-grabens north of the Central Colorado depocenter. By correlation with the Precuyano cycle of the neighboring Neuquén basin (to the west, also coincident with the northern boundary of Patagonia) the negative inversion of the fold-and-thrust belt was interpreted to have occurred in the Late Triassic-Early Jurassic. A second rifting event is represented by faults that intersect the later and form the main depocenters of the Colorado basin (Eastern and Central Colorado), and possibly the adjacent Salado basin. Deep industrial seismic lines, allowed the interpretation of these steeper faults down to deep crustal levels near the Moho. This second rifting event, associated with the E-W to SE-NW oriented depocenters (highly oblique with respect to the NNE-trending South Atlantic COB), had been previously recognized in the area, and largely

interpreted as Jurassic. We have correlated this second and main rifting event in the Colorado basin to the Early-Middle Jurassic Cuyano cycle of the Neuquén basin, and to the coeval Karoo rifting in Africa. Moreover, we were able to discriminate the faults directly associated with the South Atlantic opening in this part of the margin for the first time. Faults related to the Early Cretaceous South Atlantic rifting and breakup are restricted to a 200-km wide strip inboard of the SDRs that develop on the continent-ocean transition. Most of these faults are subparallel to the SDR wedges-bounding faults and tend to dip towards the continent. By classifying and mapping these faults, we have constrained the width of the South Atlantic rift system (at least on its western side) that evolved to lithosphere breakup, with SDR emplacement, and the successive opening of the ocean.

2. Multistage rifting in the Colorado basin. A local peculiarity or a Rosetta stone for the complex SW Gondwana Mesozoic rifting jigsaw?

Polyphase rifting is common in the evolution of sedimentary basins, but the identification for the first time of three superimposed rifting setting in a single area in the South Atlantic, motivated the extrapolation of these results to other basins in SW Gondwana.

The second main point addressed in this PhD was then, to extrapolate the Colorado basin results throughout the Southern South Atlantic realm, by considering the onshore Mesozoic basins in South America (Argentina, Uruguay, Brazil, and southern Africa). The objective was to assess the effect of the large-scale triggers of rifting (e.g. plume impingement, retroarc subduction-related extension).

In the southernmost end of South America, the opening of the Malvinas basin (offshore southern Patagonia) in the Early-Middle Jurassic rifting event was partially coeval with the second and main rifting stage in the Colorado basin area. Patagonia experienced intense volcanism during the Jurassic with the emplacement of the Chon Aike silicic Magmatic Province (Kay et al., 1989; Pankhurst et al., 2000), and particularly profuse rhyolitic volcanism during the Mid-Jurassic. The Chon Aike Magmatic Province has been related to retroarc synextensional volcanism along NW- to NNW-trending structures. The first two U-Pb on zircon ages for the Malvinas basin were presented in this thesis, which permitted dating the prerift and the top of the synrift units. A Late Triassic age is reported for the first time in the Malvinas basin. A crystallization age of 215 Ma (U-Pb in zircon) was obtained from a volcanic breccia that was correlated with the Central Patagonian Batholith (in the North Patagonian Massif) and

the coeval El Tranquilo basin (Deseado Massif). This new Late Triassic age within the prerift constrains the age of rifting.

The Malvinas basin's synrift is grouped with the Serie Tobífera unit, which has been included within the Chon Aike Magmatic Province. The correlation between the age of the Tobífera in the Austral (Magallanes) basin and the Malvinas basin has been confirmed with the Middle Jurassic age of 169 Ma (U-Pb in zircon) obtained from a tuff layer close to the top of Serie Tobífera in the Río Chico High area. This Middle Jurassic age also confirms the link between rifting in the Malvinas basin and the Chon Aike Magmatic Province. The main depocenters of the Malvinas basin, bounded by NNW-directed faults, have been seismically characterized with two deep regional seismic transects. Retroarc volcanism and extension (increasing towards the south), associated with trenchward arc clockwise rotational migration has recently been attributed to differential slab rollback. These observations were incorporated into a regional model, that suggests the presence of a sub-vertical slab tear between present-day Patagonia and Antarctica, active since the latest Triassic and across the Jurassic. This tear would have allowed the decoupling of the Panthalassa subducting slab, below the Patagonian and Antarctic segments. The slab tear model, which was generated after the submission of the paper presented in chapter 6 and was not yet incorporated in the Gondwana reconstructions, also provides an explanation for the thermal anomaly that triggered the opening of the Weddell Sea in the Late Jurassic between Western (South America + Africa) and Eastern Gondwana (Antarctica + other blocks).

The integration of the pre-Atlantic rifting events into the Mesozoic rifting history of SW Gondwana allowed the correlation of coeval rift basins in South America and Africa. By producing paleotectonic reconstructions it was possible to correlate, for example, the Colorado and Salado basins, to the Karoo II rifting onshore west Africa (e.g. Kalahari basin). Mesozoic rifting of SW Gondwana started in the Triassic. The Central Atlantic was the locus of the Triassic rifting, however intracontinental rifts also developed in Africa and South America at this stage (Karoo I). Correlation of the Triassic Santa María basin (Brazil) with the Watersberg basin and other Karoo I depocenters in Africa was suggested (Zerfass et al., 2003). Triassic-Early Jurassic depocenters are also found on the SW Gondwana margin (Cuyo, Bermejo, Precuyano of Neuquén, and the Deseado basins) and are related to retro-arc extension.

In the Early Jurassic, rifting on Eastern Africa was triggered by the Karoo plume impingement, which produced the formation of a network of Karoo II depocenters in Africa

(Frizon De Lamotte et al., 2015). The Colorado and Salado basins in the Argentinean shelf formed at this stage, coetaneous with a reactivation of extension in the Neuquén basin, recorded by the Cuyano cycle. In Patagonia, the Chon Aike silicic large igneous province occurred simultaneously, behind the volcanic arc represented by the Early Jurassic Subcordilleran Batholith (Rapela et al., 2005). Retroarc extension, due to differential slab rollback (Echaurren et al., 2017; Mpodozis and Ramos, 2008), is responsible for the formation of the Cañadón Asfalto, Austral and Malvinas basins, in the Early-Middle Jurassic. The slab tear model introduced in this thesis would have played a major role in explaining the clockwise rotation extension observed in Patagonia. Rifting in East Africa ultimately produced the breakup between East Antarctica and Africa along the Mozambique channel, and the connection to the Weddell Sea. The slab tear model is a new way to explain the origin of the thermal anomaly that triggered the Weddell Sea opening between East and West Gondwana in the Late Jurassic. In the Gondwana margin, the Late Jurassic retroarc extension and volcanism is concentrated towards the west, in the present-day Andean foothills, and ultimately produced the opening of the Rocas Verdes back-arc basin.

Rifting in the Outeniqua and Rawson/Valdés basins is interpreted to have initiated in the Late Jurassic in the orogenic core of the Late Paleozoic Gondwanides orogen. In the Late Jurassic paleotectonic reconstruction, the orientation of the Rawson/Valdés faults, and those of the different Outeniqua depocenters is rather parallel. However, these structures are oriented at a certain angle with respect to the South Atlantic COB. The southernmost South Atlantic sub-segment, that corresponds to the Rawson/Valdés and Outeniqua basins, hosts the oldest South Atlantic magnetic anomalies and is interpreted to be first to open. Oblique rifting is suggested to facilitate continental breakup (Brune et al., 2012b). In this thesis, we suggest that the lack of SDRs in this southernmost sub-segment could be explained by the existence of a relatively ductile lithospheric mantle (remnant of the Gondwanides orogen) that was subjected to extension and thinning during the Late Jurassic Rawson/Valdés-Outeniqua basins rifting and that, at the time of breakup in the Latest Jurassic-Early Cretaceous, when the stress field rotated to E-W (Koopmann et al., 2016), extended in a magma-poor style.

It is still a matter of debate, if the Early Cretaceous South Atlantic rift took advantage of older crustal weakness zones (e.g. Precambrian mobile belts, Buiter and Torsvik, 2014; Will and Frimmel, 2018). After opening occurred in the magma-poor though abrupt southernmost sub-segment, north of the Colorado-Cape fracture zones rifting and SDR emplacement occurred

in a deeply segmented margin. The other source of crustal heterogeneities, previous rift basins, seems not to have played a key role in the South Atlantic emplacement. The Salado and Colorado basins, that we have correlated to the Karoo rifting in this thesis, remained perched on the South American plate. The near E-W Early Cretaceous direction of extension may have played a role in favoring reactivation of certain structures. The Colorado and Salado basins are oriented subparallel to this extension and this may be the reason why they were not reactivated.

Another group of basins are certainly Atlantic and formed during the Early Cretaceous rifting. The conjugate Cape and Argentina basins in the southernmost sub-segment, or the Pelotas and the conjugate Luderitz and Walvis basins in the northernmost sub-segment of the Southern South Atlantic, are examples. This aspect should be considered when studying the asymmetry of the conjugate margins in the future. Asymmetry in breakup and passive margin evolution is not only conditioned by the asymmetric emplacement of SDRs on either margin. The previous crustal structure (i.e. rift basins presence inboard from the COT) will also play a key role in the successive passive margin dynamics. This is the case of the Colorado-Orange conjugate margins, that so far have been studied using 2D cross sections across the margin (e.g. Blaich et al., 2013; Marcano et al., 2013). The 3D perspective and the multistage evolution needs to be considered to properly evaluate the factors conditioning passive margin evolution.

Finally, another major contribution from this thesis is the supra-regional evaluation of the SW Gondwana rifting. This study highlights the major controlling role of subduction-related processes in triggering retroarc extension in relatively wide domains throughout the Mesozoic. Far field forces, related to sub-horizontal stress originating in plate borders (i.e. roll-back, ridge-push, etc.) have been called to be the more common origin of extensional forces producing rifting. Plume impingement, a process that seems less common than originally proposed by Sengör and Burke (1978), could have, nevertheless, played an important role in Gondwana breakup (Frizon De Lamotte et al., 2015). The supercontinent dispersal, that initiated in the Triassic, was definitely accentuated by the Karoo rifting, which has been attributed to the impingement of the Karoo plume in the Early Jurassic. The opening of the Mozambique channel, between East Africa and East Antarctica, was followed by the opening of the Weddell Sea in the Late Jurassic, and was a point of not-return in the supercontinent dispersal process. The factors triggering the opening of the South Atlantic Ocean are still under debate. Very recently Dal Zilio et al. (2018) has suggested that once again, it could be subduction-related mechanisms that triggered rifting in the interior of Western Gondwana. We have demonstrated

in this thesis, that the area where the South Atlantic Ocean emplaced, was the core of the Late Paleozoic Gondwanides orogen, and was deeply affected by Late Triassic and Jurassic extension.

3. After the continental breakup, how was the passive margin evolution along the Argentinean Atlantic margin? Did the margin behave cylindrically?

The third main point addressed in this PhD was the characterization of basin evolution after the Atlantic breakup. Related to previous Jurassic rifting, the Colorado and Salado basin are oriented at a high angle regarding the NNE-striking Atlantic COB. The question is then, what was the influence of the Jurassic rift basins in the passive margin evolution. To address this question, the post-breakup stratigraphy of the Colorado basin (provided with a complete dataset) was first characterized and then modeled to assess subsidence dynamics, and the potential influence of previous rifting. Stratigraphic forward modeling (DionisosFlow), was carried out to calibrate the subsidence history in the Colorado basin. The model reproduced key stratigraphic observations made in the characterization of the post-breakup stratigraphic evolution of the basin. These results were also integrated in a larger perspective, into the passive margin evolution of the Rawson-to-Punta del Este basin basins segment.

Three main Megasequences were determined in the characterization of the Colorado basin post-breakup evolution. These three Megasequences, that roughly coincide with Cretaceous, Paleogene and Neogene systems, display striking differences that illustrate the changing nature of passive margin evolution. While the Cretaceous Megasequence development was restricted to the individual basins (i.e. Colorado, Salado), the basement highs that separate these basins (i.e. Tandilia, Rawson) continued to act as watersheds, bounding the depocenters. The Cretaceous drift Megasequence is characterized by the development of continental systems, mostly fluvial, throughout the Colorado and Salado basins, with a coastline and shelf-break towards the east, near the outer end of the continental crust domain and the continent-ocean transition (COT). Marine onlap against the breakup unconformity (BU) is interpreted as an abrupt basement slope, occurring on the COT domain, and probably induced by the continuous subsidence of the newly generated oceanic crust immediately to the east. On the shelf, we focused on the Colorado and Salado basins, which developed entirely on the continental crust domain. The Cretaceous Drift Megasequence is restricted to the Colorado and Salado basins axis with its depocenters roughly coinciding with the synrift depocenters. The depocenters were independent, and an exceeding sediment supply compared to accommodation

pushed the shelf-break seaward and was effective in transferring sediments to the deep-water basin. In the forward stratigraphic model, carried out to quantify the subsidence necessary to explain the Colorado basin preserved thickness, the Cretaceous Drift Megasequence was divided into four layers: 121-101 Ma, 101-91 Ma, 91-83 Ma, and 83-61 Ma, the latter representing the Campanian-Danian transgression deposits. The Colorado basin shows increasing subsidence rates between 125 and 91 Ma. The preservation of the Cretaceous Drift Megasequence along the Colorado and Salado basin axis seems to have been controlled by thermal induced subsidence and eventual compaction of the synrift infill continuously developing through the Cretaceous. The influence of lower crustal high-density bodies in inducing part of this subsidence is not discarded (Dressel et al., 2017). Davila et al. (2017) have suggested that subduction-related dynamic subsidence could play a key part, as an Andean compressive event occurred in the Late Cretaceous (Folguera and Ramos, 2011).

The Paleogene Megasequence shows a depocenter in the Salado basin, while in the Colorado basin it thins out towards the south (Rawson High) and records carbonate facies, usually indicative or low sediment supply. The Tandilia High was probably fully flooded since Maastrichtian and thus, the Salado and Colorado basins were connected during the Paleocene. A non-cylindrical behavior of the margin is observed, subsiding in the north (Salado/Punta del Este) and being uplifted in the south (Rawson). The uplift of the Rawson High was interpreted in part as an effect of thermal uplift produced by the Campanian-Danian volcanism observed in the area to the south of the Colorado basin (Lovecchio et al., 2017; Appendix 2). In the Colorado basin, the subsidence rates for the Paleogene interval (61-33 Ma), that were inverted from the forward stratigraphic model, are the lowest subsidence rate values observed in the whole post-breakup evolution. When taking a more regional perspective, a similar trend was identified in the Pelotas basin (Contreras et al., 2010), pointing to a more regional, plate-scale phenomenon.

The Neogene Megasequence is present all along the study area. The thickness map for this unit shows increased thickness along the Colorado basin axis, and a sharp limit to the southeast, indicative of the shelf-break. It is worth to mention that the Neogene shelf-break is retracted landward compared to the Cretaceous most-seaward shelf-break. Two cases are envisaged to explain this situation, either accommodation creation rate exceeds sedimentary supply, or an erosive effect of bottom contour currents. The subsidence rate obtained from forward stratigraphic modeling indicates a new pulse of increasing subsidence after the

Paleogene quiescence. The margin seems to cylindrically subside during the Neogene. The ancient basin-bounding highs are completely flooded (although show less subsidence) and the Argentinean shelf is fully integrated. Sediment entry points were determined south of Colorado in the Rawson area. Sediment is redistributed in the shelf by bottom contour currents that, in the area of study, show a northward flow.

It has been demonstrated that passive margins do not necessarily display cylindrical dynamics throughout their post-breakup evolution. In the study area, the pre-Atlantic rift basins played a key role during the Cretaceous. The margin shows clear asymmetric subsidence during the Paleogene and renewed cylindrical behavior during the Neogene. The influence of the Andean orogenic events and their effects on dynamic subsidence must be considered in future studies in the Argentinean margin. We would highlight also the importance of using the geological and geophysical surface data to constrain geophysical models, even if they focus in the deep crustal structure of the margin.

The intrinsic differences in crustal structure and rifting evolution between the Argentinean and the conjugate Namibian margin must be considered when comparing the conjugate passive margin evolution. Subsidence history in the Colorado area has proved to be strongly different from the Orange basin evolution, especially because the Colorado rift basin is perched in the continental crust domain, and evolved in a different way comparatively to the oceanic crust domain.

This work has produced three congress presentations, one published paper (Multistage rifting evolution of the Colorado basin, Terra Nova, October 2018) and two submitted papers (Rifting evolution of the Malvinas basin, Offshore Argentina, submitted to the Journal of South American Earth Sciences; and Mesozoic breakup of SW Gondwana and basin formation along the Argentinean Atlantic margin, submitted to Basin Research). One other paper, carried out in collaboration with biostratigraphers of Y-TEC Laboratories and the University of Buenos Aires has been published (A new dinoflagellate form the Late Cretaceous of the Colorado basin, Offshore Argentina, Ameghiniana, Appendix 1). Finally, the results on the post-breakup evolution of the Argentinean margin will be integrated to produce a publication.

Several collaborations were also established during the development of is PhD. The biostratigraphic review of the Colorado and Salado Punta del Este with the team of the Biostratigraphy Lab at Y-TEC, and G. Ottone (palynologist at the University of Buenos Aires,

UBA). Core and thin sections descriptions of the Ranquel volcanic rocks were performed by Elisabeth Rodríguez (Y-TEC). Seismic interpretation in the Malvinas basin was carried out by my colleagues at the Offshore Team at YPF. The zircon dating was carried out in collaboration with M. Naipauer (UBA) and V. Valencia (Washington State University)

Perspectives

Amongst the results summarized in the conclusions, several observations open new research lines. Future studies should address:

1. Higher resolution and subsidence quantification

In this thesis, we have studied the large regional scale dynamics of the Argentinean passive margin and assessed the accommodation of large stratigraphic envelops. The next step is to go into higher detail, perform high resolution sequence stratigraphy to better calibrate the models. The Colorado and Salado basins have a dataset that allows this higher resolution interpretation.

2. Stratigraphic modeling of the entire margin segment: quantification and comparison with "deep" model results

The observations made in this study, and the results that were obtained, should be integrated in a source-to-sink study of the whole Argentinean and Southern South Atlantic margin. This source-to-sink study should take into account sediment provenance characterization, sediment routing systems, thermochronology of both the provenance areas and main structures of the margin (e.g. Ventania, Tandilia, the North Patagonian Massif), and a detailed set of depth-converted grids for the shelf and deepwater basin. Forward stratigraphic modeling of the full Argentinean passive margin, should be a tool to assess passive margin dynamics, and hydrocarbon play fairways.

Bibliographie

Abreu, V. dos S., 1998. Geologic evolution of conjugate volcanic pasive margins. Pelotas basin (Brazil) and Offshore Namibia (Africa); Implications for global sea-level changes. Rice University.

Abreu, V.S., Feldman, H.R., Pederson, K.H., Neal, J.E., 2010. Sequence Stratigraphy of Siliciclastic Systems, First. ed. SEPM. Concepts in Sedimentology and Paleontology 9.

Adie, R.J., 1952. Representatives of the Gondwana System in the Falkland Islands. Symp. sur le Ser. Gondwana, 19th Int. Geol. Congr. 385–392.

Aguirre-Urreta, B., Tunik, M., Naipauer, M., Pazos, P., Ottone, E., Fanning, M., Ramos, V.A., 2011. Malargüe Group (Maastrichtian-Danian) deposits in the Neuquén Andes, Argentina: Implications for the onset of the first Atlantic transgression related to Western Gondwana break-up. Gondwana Res. 19, 482–494. https://doi.org/10.1016/j.gr.2010.06.008

Aguirre, C., Blanco, S., Corbari, S., Ferraresi, P., Rodriguez Schelotto, M.L., 2001. Estudio Petrografico y Geocronologico Sondeo: UTA.PC.CA.x-1, Muestra: 3309-3390 mbbp. R1328/01. Buenos Aires.

Aldiss, D.T., Edwards, E.J., 1999. The Geology of the Falkland Islands. British Geological Survey Technical Report. WC/99/10.

Alessandretti, L., Philipp, R.P., Chemale, F., Brückmann, M.P., Zvirtes, G., Matté, V., Ramos, V.A., 2013. Provenance, volcanic record, and tectonic setting of the Paleozoic Ventania Fold Belt and the Claromecó Foreland Basin: Implications onsedimentation and volcanism along the southwestern Gondwana margin. J. South Am. Earth Sci. 47, 12–31. https://doi.org/10.1016/j.jsames.2013.05.006

Allen, P.A., Allen, J.R., 2013. Basin Analysis - Principles and Application to Petroleum Play Assessment, Third. ed. John Wiley & Sons Ltd, Chichester, West Sussex, UK.

Allen, P.A., Allen, J.R., 2005. Basin Analysis - Principls and Application, Second edi. ed. Blackwell Science Ltd, Malden, MA, USA.

Amante, C., Eakins, B.W., 2009. ETOPO1 1 Arc-Minute Global Relief Model: Procedures, Data Sources and Analysis.

Anderson, D.L., 1994. Superplumes or supercontinents? Geology 22, 39–42.

Andreis, R.R., Japas, M.S., 1996. Cuencas Sauce Grande y Colorado, in: El Sistema Pérmico En La República Argentina y En La República Oriental Del Uruguay. Academia Nacional de Ciencias, Córdoba, pp. 45–64.

Antobreh, A.A., Faleide, J.I., Tsikalas, F., Planke, S., 2009. Rift-shear architecture and tectonic development of the Ghana margin deduced from multichannel seismic reflection and potential field data. Mar. Pet. Geol. 26, 345–368. https://doi.org/10.1016/j.marpetgeo.2008.04.005

Arbe, H., Fernandez Bell Fano, F.J., 2002. Los reservorios de la Fm Springhill en el Area costa afuera, in: Schiuma, M., Hinterwimmer, G., Vergani, G. (Eds.), Rocas Reservorio de Las Cuencas Productivas de Argentina. Instituto Argentino del Petróleo y del Gas, Buenos Aires, pp. 75–90.

Archangelsky, S., Gamerro, J.C., 1980. Palinomorfos pérmicos del subsuelo de la Cuenca Colorado, en la plataforma del Mar Argentino, provincia de Buenos Aires. BOl. IG. Inst. Geociências, USP. 5, 120–124.

Arecco, M.A., Ruiz, F., Pizarro, G., Giménez, M., Martínez, P., Ramos, V.A., 2016. Gravimetric determination of the continental-oceanic boundary of the Argentine continental margin (from 36°S to 50°S). Geophys. J. Int. 204, 366–385. https://doi.org/10.1093/gji/ggv433

Aslanian, D., Moulin, M., Olivet, J.L., Unternehr, P., Matias, L., Bache, F., Rabineau, M., Nouzé, H., Klingelheofer, F., Contrucci, I., Labails, C., 2009. Brazilian and African passive margins of the Central Segment of the South Atlantic Ocean: Kinematic constraints. Tectonophysics 468, 98–112. https://doi.org/10.1016/j.tecto.2008.12.016

Autin, J., Bellahsen, N., Leroy, S., Husson, L., Beslier, M.O., d'Acremont, E., 2013. The role of structural inheritance in oblique rifting: Insights from analogue models and application to the Gulf of Aden. Tectonophysics 607, 51–64.

https://doi.org/10.1016/j.tecto.2013.05.041

Autin, J., Scheck-Wenderoth, M., Loegering, M.J., Anka, Z., Vallejo, E., Rodriguez, J.F., Dominguez, F., Marchal, D., Reichert, C., di Primio, R., Götze, H.J., 2013. Colorado Basin 3D structure and evolution, Argentine passive margin. Tectonophysics 604, 264–279. https://doi.org/10.1016/j.tecto.2013.05.019

Autin, J., Scheck-wenderoth, M., Loegering, M.J., Anka, Z., Vallejo, E., Rodriguez, J.F., Marchal, D., Dominguez, F., Reichert, C., Primio, R., 2011. Crustal structure of the Colorado Basin from 3D gravity modelling 13, 2928. https://doi.org/10.1016/j.marpetgeo.2009.1006.1009.Moulin

Baby, G., Guillocheau, F., Boulogne, C., Robin, C., Dall'Asta, M., 2018. Uplift history of a transform continental margin revealed by the stratigraphic record : The case of the Agulhas transform margin along the Southern African Plateau. Tectonophysics 731–732, 104–130. https://doi.org/10.1016/j.tecto.2018.03.014

Balarino, M.L., 2012. Palinología del Pérmico de la Cuenca Claromecó-Colorado, Argentina. Ameghiniana 49, 343–364.

Balarino, M.L., 2009. Palinoestratigrafía del Paleozoico Superior de la cuenca Colorado, República Argentina y su correlación con áreas relacionadas. Universidad Nacional de La Plata.

Baldi, J.E., Nevistic, A.V., 1996. Cuenca costa afuera del Golfo de San Jorge, in: Ramos, V.A., Turic, M.A. (Eds.), Geología y Recursos Naturales de La Plataforma Continental Argentina. Asociación Geológica Argentina; Instituto Argentino del Petróleo, Buenos Aires, pp. 171–192.

Baristeas, N., Anka, Z., di Primio, R., Rodriguez, J.F., Marchal, D., Dominguez, F., 2013. New insights into the tectono-stratigraphic evolution of the Malvinas Basin, offshore of the southernmost Argentinean continental margin. Tectonophysics 604, 280–295. https://doi.org/10.1016/j.tecto.2013.06.009

Barker, P.F., 1999. Evidence for a volcanic rifted margin and oceanic crustal structure for the Falkland Plateau Basin. J. Geol. Soc. London. 156, 889–900.

https://doi.org/10.1144/gsjgs.156.5.0889

Barredo, S., Chemale, F., Marsicano, C., Ávila, J.N., Ottone, E.G., Ramos, V.A., 2012. Tectono-sequence stratigraphy and U–Pb zircon ages of the Rincón Blanco Depocenter, northern Cuyo Rift, Argentina. Gondwana Res. 21, 624–636. https://doi.org/10.1016/j.gr.2011.05.016

Basile, C., Mascle, J., Guiraud, R., 2005. Phanerozoic geological evolution of the Equatorial Atlantic domain. J. African Earth Sci. 43, 275–282. https://doi.org/10.1016/j.jafrearsci.2005.07.011

Bechis, F., Cristallini, E.O., Giambiagi, L.B., Yagupsky, D.L., Guzmán, C.G., García, V.H., 2014. Transtensional tectonics induced by oblique reactivation of previous lithospheric anisotropies during the Late Triassic to Early Jurassic rifting in the Neuquén basin: Insights from analog models. J. Geodyn. 79, 1–17. https://doi.org/10.1016/j.jog.2014.04.010

Becker, K., Franke, D., Schnabel, M., Schreckenberger, B., Heyde, I., Krawczyk, C.M., 2012. The crustal structure of the southern Argentine margin. Geophys. J. Int. 189, 1483–1504. https://doi.org/10.1111/j.1365-246X.2012.05445.x

Beicip, 2001. Petroleum system analysis of the Colorado basin, Offshore Argentina. Rueil-Malmaison, France.

Bellahsen, N., Husson, L., Autin, J., Leroy, S., d'Acremont, E., 2013. The effect of thermal weakening and buoyancy forces on rift localization: Field evidences from the Gulf of Aden oblique rifting. Tectonophysics 607, 80–97. https://doi.org/10.1016/j.tecto.2013.05.042

Bellosi, E.S., Jalfin, G.A., 1989. Cuencas Neopaleozoicas de la Patagonia Extraandina e Islas Malvinas, in: Cuencas Sedimentarias Argentinas. pp. 379–393.

Ben-Avraham, Z., Hartnady, C.J.H., Kitchin, K.A., 1997. Structure and tectonics of the Agulhas-Falkland fracture zone. Tectonophysics 282, 83–98.

Benedetto, J.L., 2012. El continente de Gondwana a través del tiempo: Una introducción a la Geología Histórica, First. ed. Academia Nacional de Ciencias, Córdoba.

Beniest, A., Koptev, A., Burov, E., 2017. Numerical models for continental break-up: Implications for the South Atlantic. Earth Planet. Sci. Lett. 461, 176–189. https://doi.org/10.1016/j.epsl.2016.12.034

Bercovici, D., Long, M.D., 2014. Slab rollback instability and supercontinent dispersal 1–8. https://doi.org/10.1002/2014GL061251.Abstract

Biddle, K.T., Snavely, P.D.I., Uliana, M.A., 1996. Plateau de Malvinas, in: Ramos, V.A., Turic, M.A. (Eds.), Geología y Recursos Naturales de La Plataforma Continental Argentina1. Asociación Geológica Argentina; Instituto Argentino del Petróleo, pp. 225–252.

Bigot-Cormier, F., Basile, C., Poupeau, G., Bouillin, J.P., Labrin, E., 2005. Denudation of the Côte d'Ivoire-Ghana transform continental margin from apatite fission tracks. Terra Nov. 17, 189–195. https://doi.org/10.1111/j.1365-3121.2005.00605.x

Blaich, O.A., 2006. Northeastern Brazilian margin: Regional tectonic evolution based on integrated analysis of seismic reflection and potential field data and modelling. University of Oslo. https://doi.org/10.1016/j.tecto.2008.02.011

Blaich, O.A., Faleide, J.I., Tsikalas, F., 2011. Crustal breakup and continent-ocean transition at South Atlantic conjugate margins. J. Geophys. Res. Solid Earth 116, 1–38. https://doi.org/10.1029/2010JB007686

Blaich, O.A., Faleide, J.I., Tsikalas, F., Franke, D., León, E., 2009. Crustal-scale architecture and segmentation of the Argentine margin and its conjugate off South Africa. Geophys. J. Int. 178, 85–105. https://doi.org/10.1111/j.1365-246X.2009.04171.x

Blaich, O.A., Faleide, J.I., Tsikalas, F., Gordon, A.C., Mohriak, W.U., 2013. Crustal-scale architecture and segmentation of the South Atlantic volcanic margin, in: Mohriak, W.U., Danforth, A.L., Post, P.J., Brown, D.E., Tari, G.C., Nemcok, M., Sinha, S.T. (Eds.), Conjugate Divergent Margins. Geological Society Special Publication 369, pp. 167–183.

Blaich, O.A., Tsikalas, F., Faleide, J.I., 2008. Northeastern Brazilian margin: Regional tectonic evolution based on integrated analysis of seismic reflection and potential field data and modelling. Tectonophysics 458, 51–67. https://doi.org/10.1016/j.tecto.2008.02.011

Blakey, R.C., 2008. Gondwana paleogeography from assembly to breakup—A 500 m.y.

odyssey. Geol. Soc. Am. Spec. Pap. 441, 1–28. https://doi.org/10.1130/2008.2441(01).

Bracaccini, O.I., 1980. Cuenca de Salado. pp. 879–918.

Bralower, T.J., Arthur, M. a, Leckie, R.M., Sliter, W. V, Allard, D.J., Schlanger, S.O., 1994. Timing and paleoceanography of oceanic dysoxia/anoxia in the late Barremian to early Aptian (early Cretaceous). Palaios 9, 335–369. https://doi.org/10.2307/3515055

Brandsen, P.J.E., Burges, P., Durham, M.J., Hall, J.G., 1999. Evidence for multi-phase rifting in the North Falklands Basin, in: Cameron, N.R., Bate, R.H., Clure, V.S. (Eds.), The Oil and Gas Habitats of the South Atlantic. Geological Society of London Special Publications 153, pp. 425–442.

Braun, J., Deschamps, F., Rouby, D., Dauteuil, O., 2013. Flexure of the lithosphere and the geodynamical evolution of non-cylindrical rifted passive margins: Results from a numerical model incorporating variable elastic thickness, surface processes and 3D thermal subsidence. Tectonophysics 604, 72–82. https://doi.org/10.1016/j.tecto.2012.09.033

Broad, D.S., Jungslager, E.H.A., McLachlan, I.R., Roux, J., Van der Spuy, D., 2012. South Africa's offshore Mesozoic basins, Regional Geology and Tectonics. https://doi.org/10.1016/B978-0-444-56357-6.00014-7

Brown, L.F., Benson, J.M., Brink, G.J., Doherty, S., Jollands, A., Jungslager, E.H.A., Keenan, J.H.G., Muntingh, A., van Wyk, N.J.S., 1995. Perspective and General Information, in: Sequence Stratigraphy in Offshore South African Divergent Basins, AAPG Studies in Geology 41. pp. 1–18.

Brune, S., Heine, C., Clift, P.D., Pérez-Gussinyé, M., 2017. Rifted margin architecture and crustal rheology: Reviewing Iberia-Newfoundland, Central South Atlantic, and South China Sea. Mar. Pet. Geol. 79, 257–281. https://doi.org/10.1016/j.marpetgeo.2016.10.018

Brune, S., Heine, C., Pérez-Gussinyé, M., Sobolev, S. V., 2014. Rift migration explains continental margin asymmetry and crustal hyper-extension. Nat. Commun. 5, 1–9. https://doi.org/10.1038/ncomms5014

Brune, S., Popov, A.A., Sobolev, S. V., 2012a. Modeling suggests that oblique extension

facilitates rifting and continental break-up. J. Geophys. Res. Solid Earth 117. https://doi.org/10.1029/2011JB008860

Brune, S., Popov, A.A., Sobolev, S. V, 2012b. Modeling suggests that oblique extension facilitates rifting and continental break-up 117, 1–16. https://doi.org/10.1029/2011JB008860

Bry, M., White, N., Singh, S., England, R., Trowell, C., 2004. Anatomy and formation of oblique continental collision: South Falkland basin. Tectonics 23, 1–20. https://doi.org/10.1029/2002TC001482

Buck, W.R., 2017. The role of magmatic loads and rift jumps in generating seaward dipping reflectors on volcanic rifted margins. Earth Planet. Sci. Lett. 466, 62–69. https://doi.org/10.1016/j.epsl.2017.02.041

Buiter, S.J.H., Torsvik, T.H., 2014. A review of Wilson Cycle plate margins: A role for mantle plumes in continental break-up along sutures? Gondwana Res. 26, 627–653. https://doi.org/10.1016/j.gr.2014.02.007

Bulhoes, É.M., Nogueira de Amorim, W., 2005. Princípio da SismoCamada Elementar e sua aplicação à Técnica Volume de Amplitudes (tecVA), in: 9th International Congress of the Brazilian Geophysical Society & EXPOGEF. Brazilian Geophysical Society, Salvador de Bahía, pp. 1–6. https://doi.org/10.1190/sbgf2005-275

Bullard, E.C., Everett, J.E., Smith, A.G., 1965. The fit ofthe continents around the Atlantic. Symposium on Continental Drift. Philos. Trans. R. Soc. London 258 Ser. A, pp. 41–51. Philos. Trans. R. Soc. London 258, 41–51.

Burov, E., Poliakov, A., 2001. Erosion and reology controls on synrift and postrift evolution: Verifying old and new ideas using a fully coupled nomerical model. J. Geophys. Res. 106, 16461–16481.

Burov, E., Toussaint, G., 2007. Surface processes and tectonics: Forcing of continental subduction and deep processes. Glob. Planet. Change 58, 141–164. https://doi.org/10.1029/2003TC001604

Calderon, M., Herve, F., Fuentes, F., Fosdick, J.C., Sepulveda, F., Galaz, G., 2016. Tectonic

Evolution of Paleozoic and Mesozoic Andean Metamorphic Complexes and the Rocas Verdes Ophiolites in Southern Patagonia, in: Ghiglione, M.C. (Ed.), Geodynamic Evolution of the Southernmost Andes. Springer International Publishing, Switzerland, pp. 7–36. https://doi.org/10.1007/978-3-319-39727-6

Calderón, M., Prades, C.F., Hervé, F., Avendaño, V., Fanning, M., Massonne, H.J., Theye, T., Simonetti, A., 2013. Petrological vestiges of the Late Jurassic–Early Cretaceous transition from rift to back-arc basin in southernmost Chile: New age and geochemical data from the Capitán Aracena, Carlos III, and Tortuga ophiolitic complexes. Geochem. J. 47, 201–217. https://doi.org/10.2343/geochemj.2.0235

Camacho, H.H., 1967. Las Transgresiones del Cretacico Superior y Terciario de la Argentina.pdf. Rev. la Asoc. Geol. Argentina 22, 253–280.

Caminos, R., 1999. Geologia Argentina, Servicio Geologico Minero Argentino.

Cartwright, J., Swart, R., Corner, B., 2012. Conjugate margins of the South Atlantic: Namibia-Pelotas. Reg. Geol. Tectonics. https://doi.org/10.1016/B978-0-444-56357-6.00005-6

Catuneanu, O., 2006. Principles of Sequence Stratigraphy, First. ed. Elsevier, Oxford, UK.

Catuneanu, O., 2002. Sequence stratigraphy of clastic systems: Concepts, merits, and pitfalls. J. African Earth Sci. 35, 1–43. https://doi.org/10.1016/S0899-5362(02)00004-0

Catuneanu, O., Abreu, V., Bhattacharya, J.P., Blum, M.D., Dalrymple, R.W., Eriksson, P.G., Fielding, C.R., Fisher, W.L., Galloway, W.E., Gibling, M.R., Giles, K.A., Holbrook, J.M., Jordan, R., Kendall, C.G.S.C., Macurda, B., Martinsen, O.J., Miall, A.D., Neal, J.E., Nummedal, D., Pomar, L., Posamentier, H.W., Pratt, B.R., Sarg, J.F., Shanley, K.W., Steel, R.J., Strasser, A., Tucker, M.E., Winker, C., 2009. Towards the standardization of sequence stratigraphy. Earth-Science Rev. 92, 1–33. https://doi.org/10.1016/j.earscirev.2008.10.003

Catuneanu, O., Wopfner, H., Eriksson, P.G., Cairncross, B., Rubidge, B.S., Smith, R.M.H., Hancox, P.J., 2005. The Karoo basins of south-central Africa. J. African Earth Sci. 43, 211–253. https://doi.org/10.1016/j.jafrearsci.2005.07.007

Cawood, P.A., 2005. Terra Australis Orogen: Rodinia breakup and development of the Pacific

and Iapetus margins of Gondwana during the Neoproterozoic and Paleozoic. Earth-Science Rev. 69, 249–279. https://doi.org/10.1016/j.earscirev.2004.09.001

Chaboureau, A.-C., 2012. Impact du climat et de la tectonique sur la dynamique des systèmes sédimentaires pendant l ' ouverture de l'Atlantique Sud. Université Rennes 1.

Chaboureau, A.C., Guillocheau, F., Robin, C., Rohais, S., Moulin, M., Aslanian, D., 2013. Paleogeographic evolution of the central segment of the South Atlantic during Early Cretaceous times: Paleotopographic and geodynamic implications. Tectonophysics 604, 191–223. https://doi.org/10.1016/j.tecto.2012.08.025

Chalmers, J.A., 2012. Labrador Sea, Davis Strait, and Baffin Bay, in: Regional Geology and Tectonics. pp. 384–435. https://doi.org/10.1016/B978-0-444-56357-6.00010-X

Chebli, G., Spalletti, L.A., 1989. Cuencas Sedimentarias Argentinas, First. ed. Universidad Nacional de Tucumán, San Miguel de Tucuman.

Chebli, G.A., Cortiñas, J.S., Spalletti, L.A., Legarreta, L., Vallejo, E. (Eds.), 2005. Frontera Exploratoria de la Argentina.

Chebli, G.A., Gebhard, J., Menzel, M., 1976. Estratigrafía y magmatismo en la zona de la Estancia La Juanita y alrededores (departamento Deseado, prov. de Santa Cruz), in: Actas Del Sexto Congreso Geológico Argentino. Asociación Geológica Argentina, Buenos Aires, pp. 357–373.

Chemale, F., Ramos, V.A., Naipauer, M., Girelli, T.J., Vargas, M., 2018. Age of basement rocks from the Maurice Ewing Bank and the Falkland/Malvinas Plateau. Precambrian Res. 314, 28–40. https://doi.org/10.1016/j.precamres.2018.05.026

Cingolani, C.A., 2011. The Tandilia system of Argentina as a southern extension of the Río de la Plata craton: An overview. Int. J. Earth Sci. 100, 221–242. https://doi.org/10.1007/s00531-010-0611-5

Cingolani, C.A., Varela, R., 1976. Investigaciones geologicas y geocronologicas en el extremo sur de la isla Gran Malvina, sector Cabo Belgrano (Cabo Meredith), Islas Malvinas, in: Actas Del Sexto Congreso Geológico Argentino. Asociación Geológica Argentina, Bahía Blanca, pp. 457–473.

Clavijo, R., 1986. Estratigrafia del cretacico inferior en el sector occidental de la cuenca Golfo San Jorge. Bol. Inf. Pet. 15–32.

Clemson, J., Cartwright, J., Booth, J., 1997. Structural segmentation and the influence of basement structure on the Namibian passive margin. J. Geol. Soc. London. 154, 477–482. https://doi.org/10.1144/gsjgs.154.3.0477

Clemson, J., Cartwright, J., Swart, R., 1999. The Namib Rift: a rift system of possible Karoo age, offshore Namibia. Geol. Soc. London, Spec. Publ. https://doi.org/10.1144/GSL.SP.1999.153.01.23

Clerc, C., Jolivet, L., Ringenbach, J.C., 2015. Ductile extensional shear zones in the lower crust of a passive margin. Earth Planet. Sci. Lett. 431, 1–7. https://doi.org/10.1016/j.epsl.2015.08.038

Clerc, C., Ringenbach, J., Jolivet, L., Ballard, J., 2018. Rifted margins: Ductile deformation , boudinage , continentward-dipping normal faults and the role of the weak lower crust. Gondwana Res. 53, 20–40. https://doi.org/10.1016/j.gr.2017.04.030

Cloetingh, S., Burov, E., 2011. Lithospheric folding and sedimentary basin evolution : a review and analysis of formation mechanisms. Basin Res. 23, 257–290. https://doi.org/10.1111/j.1365-2117.2010.00490.x

Cloetingh, S., Burov, E., Matenco, L., Beekman, F., Roure, F., Ziegler, P.A., 2013. The Moho in extensional tectonic settings: Insights from thermo-mechanical models. Tectonophysics 609, 558–604. https://doi.org/10.1016/j.tecto.2013.06.010

Collier, J.S., McDermott, C., Warner, G., Gyori, N., Schnabel, M., McDermott, K., Horn, B.W., 2017. New constraints on the age and style of continental breakup in the South Atlantic from magnetic anomaly data. Earth Planet. Sci. Lett. 477, 27–40. https://doi.org/10.1016/j.epsl.2017.08.007

Colombi, C.E., Santi-Malnis, P., Correa, G.A., Martínez, R.N., Fernandez, E., Abelín, D., Pradeiro, A., Apaldetti, C.G., Alcober, O., Drovandi, J., 2015. La Formación Balde de Leyes, una nueva unidad estratigráfica de la Cuenca Triásica de Marayes-El Carrizal, San Juan. Rev. la Asoc. Geol. Argentina 72, 445–455.

Continanzia, J., Manceda, R., Covellone, G., Gavarrino, A., 2011. Cuencas de Rawson y Valdés: Síntesis del conocimiento exploratorio - Visión Actual, in: Kozlowsky, E., Legarreta, L., Boll, A., Marshall, P. (Eds.), Simposio Cuencas Argentinas Visión Actual: VIII Congreso de Exploración y Desarrollo de Hidrocarburos. Instituto Argentino del Petróleo y del Gas, pp. 47–63.

Contreras, J., Zühlke, R., Bowman, S., Bechstädt, T., 2010. Seismic stratigraphy and subsidence analysis of the southern Brazilian margin (Campos, Santos and Pelotas basins). Mar. Pet. Geol. 27, 1952–1980. https://doi.org/10.1016/j.marpetgeo.2010.06.007

Corti, G., 2009. Continental rift evolution: From rift initiation to incipient break-up in the Main Ethiopian Rift, East Africa. Earth-Science Rev. 96, 1–53. https://doi.org/10.1016/j.earscirev.2009.06.005

Courtillot, V., 1982. Propagating rifts and continental break-up. Tectonics 1, 239–250.

Coward, M.P., 1986. Heterogeneous stretching, simple shear and basin development. Earth Planet. Sci. Lett. 80, 325–336.

Cuneo, R., Ramezani, J., Scasso, R., Pol, D., Escapa, I., Zavattieri, A.M., Bowring, S.A., 2013. High-precision U-Pb geochronology and a new chronostratigraphy for the Canadon Asfalto Basin, Chubut, central Patagonia: Implications for terrestrial faunal and floral evolution in Jurassic. Gondwana Res. 24, 1267–1275. https://doi.org/10.1016/j.gr.2013.01.010

Curtis, M., 2001. Tectonic history of the Ellsworth Mountains, West Antarctica: Reconciling a Gondwana enigma. Geol. Soc. Am. Bull. 113, 939–958.

D'Elia, L., Bilmes, A., Franzese, J.R., Veiga, G.D., Hernández, M., Muravchik, M., 2015. Early evolution of the southern margin of the Neuquén Basin, Argentina: Tectono-stratigraphic implications for rift evolution and exploration of hydrocarbon plays. J. South Am. Earth Sci. 64, 42–57. https://doi.org/10.1016/j.jsames.2015.09.004

Dailly, P., Henderson, T., Hudgens, E., KAnschat, K., Lowry, P., 2013. Exploration for Cretaceous stratigraphic traps in the Gulf of Guinea, West Africa and the discovery of the Jubilee Field: a play opening discovery in the Tano basin, Offshore Ghana, in: Mohriak,

W.U., Danforth, A.L., Post, P.J., Brown, D.E., Tari, G.C., Nemcok, M., Sinha, S.T. (Eds.), Conjugate Divergent Margins. Geological Society Special Publication 369, London, pp. 235–248.

Dal Zilio, L., Faccenda, M., Capitanio, F., 2018. The role of deep subduction in supercontinent breakup. Tectonophysics 1–13. https://doi.org/10.1016/j.tecto.2017.03.006

Dalziel, I.W.D., 1981. Back-arc extension in the southern Andes: a review and critial reapprisal. Philosofical Trans. R. Soc. London A300, 319–335.

Dalziel, I.W.D., Lawver, L.A., Norton, I.O., Gahagan, L.M., 2013. The Scotia Arc: Genesis, Evolution, Global Significance. Annu. Rev. Earth Planet. Sci. 41, 767–793. https://doi.org/10.1146/annurev-earth-050212-124155

Dávila, F.M., Lithgow-Bertelloni, C., 2013. Dynamic topography in South America. J. South Am. Earth Sci. 43, 127–144. https://doi.org/10.1016/j.jsames.2012.12.002

Davila, F.M., Lithgow-Bertelloni, C., Martina, F., Avila, P., Nobile, J., Collo, G., Ezpeleta, M., Canelo, H., Sachez, F., 2018. Mantle Influence on Andean and Pre-Andean Topography, in: Folguera, A. et al. (Ed.), The Evolution of the Chilean-Argentinean Andes. Springer International Publishing, pp. 363–385.

Davila, F.M., Martina, F., Avila, P., 2017. Mantle-driven dynamic subsidence and formation of post-rift sequences: an example from mesozoic basins of Argentina, in: XX Congreso Geológico Argentino. pp. 75–76.

Davison, I., Steel, I., 2018. Geology and hydrocarbon potential of the East African continental margin: a review. Pet. Geosci. 24, 57–91. https://doi.org/10.1144/petgeo2017-028

Davison, I., Steel, I., 2016. The Final Atlantic Margin Frontier. GeoExPro 56–58.

de Elorriaga, E.E., 2010. Evaluacion de los depocentros de la cuenca de Macachin, provincias de La Pampa y Buenos Aires. Universidad Nacional del Sur.

De Swardt, A.M.J., McLachlan, I.R., 1982. Petroleum exploration in the South African offshore: the geological framework and hydrocarbon potential, in: Glen, H.W. (Ed.), Proceedings of the 12th CMMI Congress. South Africa Inst. Min. Metall., Johannesburg,

pp. 147–161.

De Wit, M.J., Ransome, I.G.D., 1992. Inversion tectonics of the Cape Fold Belt, Karoo and Cretaceous basins of Southern Africa, Proceedings of the Conference on Inversion Tectonics of the Cape Fold Belt. Balkema, Roderdam.

Delvaux, D., 2001. Karoo rifting in western Tanzania: precursor of Gondwana break-up?, in: Contributions to Geology and Palaeontology of Gondwana, in Honour of Helmut Wopfner. pp. 111–125.

Dewey, J.F. (State U. of new Y. at A., Burke, K. (State U. of new Y. at A., 1974. Hot Spots and Continental Break-up : Implications for Collisional Orogeny. Geology 2, 57–60.

Dickson, G.O., Pitman III, W.C., Heirtzler, J.R., 1968. Magnetic anomalies in the South Atlantic and ocean floor spreading. J. Geophys. Res. 93, 10408–10420.

Dingle, R. V., 1973. Mesozoic Paleogeography of the Southern Cape, South Africa. Palaeogeogr. Palaeoclimatol. Palaeoecol. 13, 203–213.

Diraison, M., Cobbold, P.R., Gapais, D., Rossello, E.A., Corre, C. Le, 2000. Cenozoic crustal thickening , wrenching and rifting in the foothills of the southernmost Andes. Tectonophysics 316, 91–119.

Dominguez, F., Marchal, D., Sigismondi, M., Espejón, C., Vallejo, E., 2011. Caracterizacion de Dominios Estructurales e Influencia de Estructuras Preexistentes en Hemigrábenes de Rift en el Sector Centro-Norte de la Plataforma Contiental Argentina, in: XVIII Congreso Geologico Argentino. p. 2 p.

Doran, H., Manatschal, G., 2017. Breaking up is never easy. The Complexities That Create Opportunities in the Distal Domain. GeoExPro 58–61.

Dressel, I., Scheck-Wenderoth, M., Cacace, M., 2017. Backward modelling of the subsidence evolution of the Colorado Basin, offshore Argentina and its relation to the evolution of the conjugate Orange Basin, offshore SW Africa. Tectonophysics 716, 168–181. https://doi.org/10.1016/j.tecto.2016.08.007

Dressel, I., Scheck-Wenderoth, M., Cacace, M., Lewerenz, B., Götze, H.J., Reichert, C., 2015.

Reconstruction of the southwestern African continental margin by backward modeling. Mar. Pet. Geol. 67, 544–555. https://doi.org/10.1016/j.marpetgeo.2015.06.006

du Toit, A., 1979. The Mesozoic history of the Agulhas Bank in terms of the plate-tectonic theory, in: Anderson, A.M., van Biljon, W.J. (Eds.), Some Sedimentary Basins and Associated Ore Deposits of South Africa. Special Publication of the Geological Society of South Africa 6, Johannesburg, South Africa, pp. 197–203.

du Toit, A., 1937. Our wandering continents. An hypothesis of Continental Drifting. Oliver & Boyd, London.

du Toit, A., 1927. A geological comparison of South America with Africa. Publication of the Carnegie Institute 381.

Duncan, R.A., Hooper, P.R., Rehacek, J., Marsh, J.S., Duncan, A.R., 1997. The timing and duration of the Karoo igneous event, southern Gondwana 102, 127–138.

Eagles, G., 2007. New angles on South Atlantic opening. Geophys. J. Int. 168, 353–361. https://doi.org/10.1111/j.1365-246X.2006.03206.x

Echaurren, A., Oliveros, V., Folguera, A., Ibarra, F., Creixell, C., Lucassen, F., 2017. Early Andean tectonomagmatic stages in North Patagonia: Insights from field and geochemical data. J. Geol. Soc. London. https://doi.org/10.1144/jgs2016-087

Eldholm, O., Skogseid, J., Planke, S., Gladczenko, T.P., 1995. Volcanic Margin Concepts. Rift. Ocean. Boundaries 1–16. https://doi.org/10.1007/978-94-011-0043-4_1

Eldholm, O., Thiede, J., Taylor, E., 1987. Proceedings of the Ocean Drilling Program. Initial Reports, 104. College Station, TX. https://doi.org/https://doi.org/10.2973/odp.proc.sr.104.1987

Elliott, G.M., Berndt, C., Parson, L.M., 2009. The SW African volcanic rifted margin and the initiation of the Walvis Ridge, South Atlantic. Mar. Geophys. Res. 30, 207–214. https://doi.org/10.1007/s11001-009-9077-x

Emery, K.O., Uchupi, E., 1984. The Geology of the Atlantic Ocean. Springer, New York.

Erlank, A.J., Roex, A.P., Harris, C., Miller, R.M., McLachlan, I., 1990. Preliminary note on the geochemistry of basalt samples from the Kudu boreholes. Commun. Geol. Surv. Namib 6, 63–65.

Espinoza, M., Montecino, D., Oliveros, V., Astudillo, N., Vazquez, P., Reyes, R., Celis, C., González, R., Contreras, J., Creixell, C., Martínez, A., 2018. The synrift phase of the early Domeyko Basin (Triassic, northern Chile): Sedimentary, volcanic and tectonic interplay in the evolution of an ancient subduction-related rift basin. Basin Res. https://doi.org/10.1111/bre.12305

Ewing, J.I., Ludwig, W.J., Ewing, M., Eitreim, S.L., 1971. Structure of the Scotia Sea and Falkland Plateau. J. Geophys. Res. 76, 7118–7137.

Ewing, M., Eittreim, S.L., Ewing, J.I., Le Pichon, X., 1971. Sediment transport and distribution in the Argentine basin, 3, Nepheloid layer and processes of sedimentation, in: Ahrens, L.H., Press, F., Runcorn, S.K., Urey, H.C. (Eds.), Physics and Chemistry of the Earth. Pergamon, New York, NY, USA, pp. 49–89.

Ewing, M., Lonardi, A.G., 1971. Sedimentary structure of the Argentine margin, basin and related provinces, in: Ahrens, L.H., Press, F., Runcorn, S.K., Urey, H.C. (Eds.), Physics and Chemistry of the Earth. Pergamon, New York, NY, USA, pp. 123–252.

Ewing, M., Ludwig, W.J., 1965. The Sediments of the Argentine Basin, in: Anales. Academia Brasileira de Ciencias, pp. 31–61.

Ewing, M., Ludwig, W.J., Ewing, J.I., 1964. Sediment distribution in the oceans: The Argentine Basin. J. Geophys. Res. 69, 2003–2032.

Ewing, M., Ludwig, W.J., Ewing, J.I., 1963. Geophysical investigations in the submerged Argentine coastal plain, 1, Buenos Aires to Peninsula Valdez. Geol. Soc. Am. Bull. 74, 275–292.

Fennell, L.M., Folguera, A., Naipauer, M., Gianni, G., Rojas Vera, E.A., Bottesi, G., Ramos, V.A., 2015. Cretaceous deformation of the southern Central Andes: synorogenic growth strata in the Neuquén Group (35° 30′–37° S). Basin Res. 29, 1–22. https://doi.org/10.1111/bre.12135

Figari, E.G., Cid de la Paz, M., Laffitte, G.A., 1997. Modelos de hemigrabenes en el neocomiamo del sector occidental de la cuenca del Golfo San Jorge, Argentina: sistemas petroleros, origen e inversión tectónica. Bol. Inf. Pet. 4–17.

Figari, E.G., Scasso, R., Cuneo, R., Escapa, I., 2015. Estratigrafía y evolución geológica de la Cuenca de Cañadón Asfalto , provincia del Chubut. Lat. Am. J. Sedimentol. 22.

Figueiredo, A.M.F., Miranda, A.P., Ferreira, R., Zalán, P.V., 1996. Cuenca de San Julián, in: Ramos, V.A., Turic, M.A. (Eds.), Geología y Recursos Naturales de La Plataforma Continental Argentina. Asociación Geológica Argentina; Instituto Argentino del Petróleo, Buenos Aires, pp. 193–212.

Figueroa, D., Marshall, P., Prayitno, N., 2005. Cuencas Atlánticas de aguas profundas: Principales Plays, in: Chebli, G.A., Cortiñas, J.S., Spalletti, L.A., Legarreta, L. (Eds.), CHEBLI, G.A., CORTIÑAS, J.S., SPALLETTI, L.A., LEGARRETA, L., VALLEJO, E.L. (Eds.). "Frontera Exploratoria de La Argentina". VI Congreso de Exploración y Desarrollo de Hidrocarburos. Instituto Argentino del Petróleo y del Gas, Mar del Plata, pp. 325–335.

Fitzgerald, M.G., Mitchum, R.M., Uliana, M.A., Biddle, K.T., 1990. Evolution of the San Jorge Basin, Argentina. Am. Assoc. Pet. Geol. Bull. 74, 879–920.

Flament, N., Gurnis, M., Williams, S., Seton, M., Skogseid, J., Heine, C., Dietmar Müller, R., 2014. Topographic asymmetry of the South Atlantic from global models of mantle flow and lithospheric stretching. Earth Planet. Sci. Lett. 387, 107–119. https://doi.org/10.1016/j.epsl.2013.11.017

Flint, S.S., Hodgson, D.M., Sprague, A.R., Brunt, R.L., Van der Merwe, W.C., Figueiredo, J., Prélat, A., Box, D., Di Celma, C., Kavanagh, J.P., 2011. Depositional architecture and sequence stratigraphy of the Karoo basin floor to shelf edge succession, Laingsburg depocentre, South Africa. Mar. Pet. Geol. 28, 658–674. https://doi.org/10.1016/j.marpetgeo.2010.06.008

Folguera, A., Bottesi, G., Duddy, I., Martín-González, F., Orts, D., Sagripanti, L., Rojas Vera, E., Ramos, V.A., 2015. Exhumation of the Neuquén Basin in the southern Central Andes (Malargüe fold and thrust belt) from field data and low-temperature thermochronology. J.

South Am. Earth Sci. 64, 381–398. https://doi.org/10.1016/j.jsames.2015.08.003

Folguera, A., Ramos, V.A., 2011. Repeated eastward shifts of arc magmatism in the Southern Andes: A revision to the long-term pattern of Andean uplift and magmatism. J. South Am. Earth Sci. 32, 531–546. https://doi.org/10.1016/j.jsames.2011.04.003

Folguera, A., Zárate, M., Tedesco, A., Dávila, F., Ramos, V.A., 2015. Evolution of the Neogene Andean foreland basins of the Southern Pampas and Northern Patagonia (34°-41°S), Argentina. J. South Am. Earth Sci. 64, 452–466. https://doi.org/10.1016/j.jsames.2015.05.010

Ford, D., Golonka, J., 2003. Phanerozoic paleogeography, paleoenvironment and lithofacies maps of the circum-Atlantic margins, Marine and Petroleum Geology. https://doi.org/10.1016/S0264-8172(03)00041-2

Fourché, J., Bate, K.J., van der Merwe, R., 1992. Plate tectonic setting of the Mesozoic Basins, southern offshore, South Atlantic: A review, in: de Wit, M., Ransome, I.G.D. (Eds.), Inversion Tectonics of the Cape Fold Belt, Karoo and Cretaceous Basins of Southern Africa. Balkema, Rotterdam, pp. 33–45.

Franke, D., 2013. Rifting, lithosphere breakup and volcanism: Comparison of magma-poor and volcanic rifted margins. Mar. Pet. Geol. 43, 63–87. https://doi.org/10.1016/j.marpetgeo.2012.11.003

Franke, D., Ladage, S., Schnabel, M., Schreckenberger, B., Reichert, C., Hinz, K., 2010. Birth of a volcanic margin off Argentina, South Atlantic. Geochemistry Geophys. Geosystems 11, 1–20.

Franke, D., Neben, S., Hinz, K., 2002. Deep crustal structure of the Argentine continental margin from seismic wide-angle and multichannel reflection seismic data. … Habitat Volcan. … 1998–2001. https://doi.org/10.1111/j.1365-246X.2004.02391.x

Franke, D., Neben, S., Ladage, S., Schreckenberger, B., Hinz, K., 2007. Margin segmentation and volcano-tectonic architecture along the volcanic margin off Argentina/Uruguay, South Atlantic. Mar. Geol. 244, 46–67. https://doi.org/10.1016/j.margeo.2007.06.009

Franke, D., Neben, S., Schreckenberger, B., Schulze, A., Stiller, M., Krawczyk, C.M., 2006.

Crustal structure across the Colorado Basin, offshore Argentina. Geophys. J. Int. 165, 850–864. https://doi.org/10.1111/j.1365-246X.2006.02907.x

Franzese, J., Spalletti, L., Pérez, I.G., Macdonald, D., 2003. Tectonic and paleoenvironmental evolution of Mesozoic sedimentary basins along the Andean foothills of Argentina (32°-54°S). J. South Am. Earth Sci. 16, 81–90. https://doi.org/10.1016/S0895-9811(03)00020-8

Franzese, J.R., Spalletti, L.A., 2001. Late triassic- Early jurassic continental extension in SouthWestern Gondwana: Tectonic segmentation and pre-break-up rifting. J. South Am. Earth Sci. 14, 257–270. https://doi.org/10.1016/S0895-9811(01)00029-3

Fraticelli, C.M., Yezerski, D.J., Mercer, J.A., Yusri, Y., Salamoff, S., Reece, J., Hyde, E.R., Bova, J., 2016. Rift basin characteristics derived from antecedents tectonic events: intricacies of the Falkland plateau, in: AAPG Annual Convention and Exhibition 2016. Houston.

Frizon De Lamotte, D., Fourdan, B., Leleu, S., Leparmentier, F., De Clarens, P., 2015. Style of rifting and the stages of Pangea breakup. Tectonics 34, 1009–1029. https://doi.org/10.1002/2014TC003760

Fryklund, B., Marshall, A., Stevens, J., 1996. Cuenca del Colorado, in: Ramos, V.A., Turic, M.A. (Eds.), XIII Congreso Geologico Argentino y III Congreso de Exploracion de Hidrocarburos. p. 135.

Fryklund, R., Stevens, J., 1994. Cruz del Sur.x-1 Final Well Report.

Galeazzi, J.S., 1998. Structural and Stratigraphic Evolution of the Western Malvinas Basin, Argentina. Am. Assoc. Pet. Geol. Bull. 82, 596–636. https://doi.org/10.1306/1D9BC5C5-172D-11D7-8645000102C1865D

Galliski, M.A., Viramonte, J.G., 1988. The Cretaceous paleorift in northwestern Argentina : A petrologic approach. J. South Am. Earth Sci. I, 329–342.

Gebhard, I., 2005. Aspectos exploratorios de la Cuenca del Colorado, in: de Barrio, R.E., Etcheverry, R.O., Caballé, M.F., Llambías, E.J. (Eds.), Geología y Recursos Minerales de La Provincia de Buenos Aires. Asociación Geológica Argentina, La Plata, pp. 447–458.

Geoffroy, L., 2005. Volcanic passive margins. Comptes Rendus - Geosci. 337, 1395–1408. https://doi.org/10.1016/j.crte.2005.10.006

Geoffroy, L., 2001. The structure of volcanic margins: some problematics from the North-Atlantic / Labrador - Baffin system. Mar. Pet. Geol. 18, 463–469.

Geoffroy, L., Burov, E.B., Werner, P., 2015. Volcanic passive margins: another way to break up continents. Nat. Publ. Gr. 5, 12. https://doi.org/10.1038/srep14828

Gerster, R., Welsink, H., Ansa, A., Raggio, F., 2011. Cuenca de Colorado. VIII Congr. Explor. y Desarro. Hidrocarburos Simp. Cuencas Argentinas visión actual 65–80.

Ghidella, M.E., Yáñez, G., LaBrecque, J.L., 2002. Revised tectonic implications for the magnetic anomalies of the western Weddell Sea. Tectonophysics 347, 65–86. https://doi.org/10.1016/S0040-1951(01)00238-4

Ghiglione, M.C., Cristallini, E.O., 2007. Have the southernmost Andes been curved since Late Cretaceous time? An analog test for the Patagonian Orocline. Geology 35, 13–16. https://doi.org/10.1130/G22770A.1

Giacosa, R.E., 1998. Hoja Geológica 4766-III-IV Puerto Deseado. SEGEMAR Bulletin 240. Buenos Aires.

Giacosa, R.E., Márquez, M.M., Panza, J.L., 2002. Basamento Paleozoico Inferior del Macizo del Deseado, in: Haller, M.J. (Ed.), Geología y Recursos Naturales de Santa Cruz. Asociación Geológica Argentina, pp. 33–44.

Gianni, G., Navarrete, C., Orts, D., Tobal, J., Folguera, A., Giménez, M., 2015. Patagonian broken foreland and related synorogenic rifting: The origin of the Chubut Group Basin. Tectonophysics 649, 81–99. https://doi.org/10.1016/j.tecto.2015.03.006

Gianni, G.M., Navarrete, C.G., Folguera, A., 2015. Synorogenic foreland rifts and transtensional basins: A review of Andean imprints on the evolution of the San Jorge Gulf, Salta Group and Taubat?? Basins. J. South Am. Earth Sci. 64, 288–306. https://doi.org/10.1016/j.jsames.2015.08.004

Gillard, M., Autin, J., Manatschal, G., Sauter, D., Munschy, M., Schaming, M., 2015.

Tectonomagmatic evolution of the final stages of rifting along the deep conjugate Australian-Antarctic magma-poor rifted margins: Constraints from seismic observations Morgane. Tectonics 34, 753–783. https://doi.org/10.1002/2015TC003850.Received

Gladczenko, T.P., Hinz, K., Eldholm, O., Meyer, H., Neben, S., Skogseid, J., 1997. South Atlantic volcanic margins. J. Geol. Soc. London. 154, 465–470. https://doi.org/10.1144/gsjgs.154.3.0465

Gladczenko, T.P., Skogseid, J., Eldhom, O., 1998. Namibia volcanic margin. Mar. Geophys. Res. 20, 313–341. https://doi.org/10.1023/A:1004746101320

Gonzalez, P.D., Tortello, M.F., Damborenea, S.E., Naipauer, M., Sato, A.M., Varela, R., 2013. Archaeocyaths from South America: review and a new record. Geol. J. 48, 114–125.

Granjeon, D., 1997. Modelisation stratigraphique deterministe – conception et applications d'un modele diffusif 3D multilithologique. Rennes, France.

Granjeon, D., Joseph, P., 1999. Concepts and applications of a 3-D multiple lithology, diffusive model in stratigraphic modeling, in: Harbaugh, J.W. et al (Ed.), Numerical Experiments in Stratigraphic and Sedimentologic Computer Simulations. SEPM Special Publication 62, pp. 197–210.

Gray, D.R., Foster, D.A., Meert, J.G., Goscombe, B.D., Armstrong, R., Trouw, R.A.J., Passchier, W., 2008. A Damara orogen perspective on the assembly of southwestern Gondwana. Geol. Soc. London, Spec. Publ. 294, 257–278. https://doi.org/10.1144/SP294.14

Green, P.F., Duddy, I.R., Japsen, P., Bonow, J.M., Malan, J.A., 2017. Post-breakup burial and exhumation of the southern margin of Africa. Basin Res. 29, 96–127. https://doi.org/10.1111/bre.12167

Green, P.F., Japsen, P., Chalmers, J.A., Bonow, J.M., Duddy, I.R., 2018. Post-breakup burial and exhumation of passive continental margins : Seven propositions to inform geodynamic models. Gondwana Res. 53, 58–81. https://doi.org/10.1016/j.gr.2017.03.007

Guillocheau, F., Robin, C., Liget-Le Roux, A., 2018. Les rifts Karoo en Afrique: Leur signification à l'échelle du Gondwana et de la subduction de la Panthalassa. Géochronique

145, 52–56.

Guillocheau, F., Rouby, D., Robin, C., Helm, C., Rolland, N., Le Carlier de Veslud, C., Braun, J., 2012. Quantification and causes of the terrigenous sediment budget at the scale of a continental margin: a new method applied to the Namibia-South Africa margin. Basin Res. 24, 3–30. https://doi.org/10.1111/j.1365-2117.2011.0511.x

Gust, D.A., Biddle, K.T., Phelps, D.W., Uliana, M.A., 1985. Associated Middle to Late Jurassic Volcanism and Extension in Southern South America. Tectonophysics 116, 223–253.

Hälbich, I.., 1983. A tectogenesis of the Cape Fold Belt, in: Söhnge, A.P.G., Hälbich, I.W. (Eds.), Geodynamics of the Cape Fold Belt. The Geological Society of South Africa, Special Publication, 12, pp. 165–175.

Hall, S.A., Bird, D.E., McLlean, D.J., Towle, P.J., Grant, J. V, Danque, H.A., 2018. New constraints on the age of the opening of the South Atlantic basin. Mar. Pet. Geol. 95, 50–66. https://doi.org/10.1016/j.marpetgeo.2018.03.010

Haller, M.J., 2002. La Cuenca Triásica de El Tranquilo, in: Haller, M.J. (Ed.), Geología y Recursos Naturales de Santa Cruz. Asociación Geológica Argentina, Buenos Aires, pp. 83–87.

Hansma, J., Tohver, E., Schrank, C., Jourdan, F., Adams, D., 2016. The timing of the Cape Orogeny : New 40 Ar / 39 Ar age constraints on deformation and cooling of the Cape Fold Belt , South Africa. Gondwana Res. 32, 122–137. https://doi.org/10.1016/j.gr.2015.02.005

Haq, B.U., Hardenbol, J.A.N., Vail, P.R., 1988. Mesozoic and Cenozoic chronostratigraphy and cycles of sea-level change, in: Sea-Level Changes: And Integrated Approach. SEPM Special Publication 42, pp. 71–108.

Harrington, H.J., 1980. Sierras Australes de la provincia de Buenos Aires, in: Turner, J.C.M. (Ed.), Segundo Simposio de Geologia Regional Argentina, Vol. 2. Academia Nacional de Ciencias, Córdoba, pp. 967–983.

Hartnady, C.J.H., Joubert, P., Stowe, C., 1985. Proterozoic crustal evolution in southwestern Africa. Episodes 8, 236–244.

Hartwig, A., di Primio, R., Anka, Z., Horsfield, B., 2012. Source rock characteristics and compositional kinetic models of Cretaceous organic rich black shales offshore southwestern Africa. Org. Geochem. 51, 17–34. https://doi.org/10.1016/j.orggeochem.2012.07.008

Heine, C., Zoethout, J., Müller, R.D., 2013. Kinematics of the South Atlantic rift. Solid Earth 4, 215–253. https://doi.org/10.5194/se-4-215-2013

Helland-Hansen, W., Steel, R.J., Somme, T.O., 2012. Shelf genesis revisited. J. Sediment. Res. 82, 133–148. https://doi.org/10.2110/jsr.2012.15

Hernández-Molina, F.J., Paterlini, M., Somoza, L., Violante, R., Arecco, M.A., de Isasi, M., Rebesco, M., Uenzelmann-Neben, G., Neben, S., Marshall, P., 2010. Giant mounded drifts in the Argentine Continental Margin: Origins, and global implications for the history of thermohaline circulation. Mar. Pet. Geol. 27, 1508–1530. https://doi.org/10.1016/j.marpetgeo.2010.04.003

Hernández-Molina, F.J., Soto, M., Piola, A.R., Tomasini, J., Preu, B., Thompson, P., Badalini, G., Creaser, A., Violante, R.A., Morales, E., Paterlini, M., De Santa Ana, H., 2016. A contourite depositional system along the Uruguayan continental margin: Sedimentary, oceanographic and paleoceanographic implications. Mar. Geol. 378, 333–349. https://doi.org/10.1016/j.margeo.2015.10.008

Heron, P.J., Lowman, J.P., 2011. The effects of supercontinent size and thermal insulation on the formation of mantle plumes. Tectonophysics 510, 28–38. https://doi.org/10.1016/j.tecto.2011.07.002

Hervé, F., Calderón, M., Fanning, C.M., Kraus, S., Pankhurst, R.J., 2010. SHRIMP chronology of the Magallanes Basin basement, Tierra del Fuego: Cambrian plutonism and Permian high-grade metamorphism. Andean Geol. 37, 253–275.

Hervé, F., Fanning, C.M., 2001. Late Triassic detrital zircons in meta-turbidites of the Chonos Metamorphic Complex, southern Chile. Andean Geol. 28, 91–104.

Heuret, A., Lallemand, S., 2005. Plate motions , slab dynamics and back-arc deformation. Phys. Earth Planet. Inter. 149, 31–51. https://doi.org/10.1016/j.pepi.2004.08.022

Hinz, K., 1981a. A hypothesis on terrestrial catastrophes_wedges of very thick oceanward dipping layers beneath Passive continental margins. Geol. Jb. 3–28.

Hinz, K., 1981b. A hypothesis on terrestrial catastrophes. Wedges of very thick Oceanward Dipping Layers beneath Passive Continental Margins. Their origin and paleoenvironmental significance. Geol. Jb. 22, 3–28.

Hinz, K., Neben, S., Schreckenberger, B., Roeser, H.A., Block, M., Meyer, H., 1999. The Argentine continental margin north of 48°S:sedimentary successions, volcanic activity during breakup. Mar. Pet. Geol. 16, 1–25.

Holbrook, W.S., Purdy, G.M., Sheridan, R.E., Glover, L., Talwani, M., 1994. Seismic structure of the US Mid-Atlantic continental margin. J. Geophys. Res. 99, 17871–17891.

Hole, M.J., Ellam, R.M., Macdonald, D.I.M., Kelley, S.P., 2015. Gondwana break-up related magmatism in the Falkland Islands. J. Geol. Soc. London 173, 108–126.

Homovc, J.F., Constantini, L., 2001. Hydrocarbon exploration potential within intraplate shear-related depocenters: Deseado and San Julián basins, southern Argentina. Am. Assoc. Pet. Geol. Bull. 85, 1795–1816.

Horn, B., 2015. Access and exploration opportunities – A view of the potential in frontier and mature basins. First Break 33, 85–93.

Hudec, M.R., Jackson, M.P.A., 2012. De Re Salica: Fundamental principles of salt tectonics, in: Regional Geology and Tectonics. pp. 18–41. https://doi.org/10.1016/B978-0-444-56357-6.00001-9

Huismans, R.S., Beaumont, C., 2008. Complex rifted continental margins explained by dynamical models of depth-dependent lithospheric extension. Geology 36, 163–166. https://doi.org/10.1130/G24231A.1

Iannizzotto, N.F., Folguera, A., Leal, P.R., Iaffa, D., 2004. Control tectónico de las secuencias volcaniclásticas neocomianas y paleogeografía en la zona del Lago La Plata (45°S). Sector interno de la faja plegada y corrida de los lagos La Plata y Fontana. Rev. la Asoc. Geol. Argentina 59, 655–670. https://doi.org/10.2307/198976

Iñiguez, A.M., Andreis, R.R., Zalba, P.E., 1988. Eventos piroclásticos en la Formación Tunas (Pérmico) Sierras Australes, provincia de Buenos Aires, República Argentina, in: Segundas Jornadas Geológicas Bonaerenses. Bahía Blanca, pp. 383–395.

Introcaso, A., Ramos, V.A., 1984. La cuenca de Salado_un modelo de evolucion aulacogenica, in: IX Congreso Geológico Argentino. San Carlos de Bariloche, pp. 27–46.

Jackson, M.P.A., Cramez, C., Fonck, J.M., 2000. Role of subaerial volcanic rocks and mantle plumes in creation of South Atlantic margins: Implications for salt tectonics and source rocks. Mar. Pet. Geol. 17, 477–498. https://doi.org/10.1016/S0264-8172(00)00006-4

Jacobs, J., Thomas, R.J., Armstrong, R.A., Henjes-Kunst, F., 1999. Age and thermal evolution of the Mesoproterozoic Cape Meredith Complex, West Falkland. J. Geol. Soc. London. 156, 917–928. https://doi.org/10.1144/gsjgs.156.5.0917

Jenchen, U., Rosenfeld, U., 2002. Continental Triassic in Argentina: Response to tectonic activity. J. South Am. Earth Sci. 15, 461–479. https://doi.org/10.1016/S0895-9811(02)00049-4

Jokat, W., 2003. Timing and geometry of early Gondwana breakup. J. Geophys. Res. 108, 1–15. https://doi.org/10.1029/2002JB001802

Jolivet, L., Menant, A., Sternai, P., Rabillard, A., Arbaret, L., Augier, R., Laurent, V., Beaudoin, A., Grasemann, B., Huet, B., Labrousse, L., Le Pourhiet, L., 2015. The geological signature of a slab tear below the Aegean Laurent. Tectonophysics 659, 166–182. https://doi.org/10.1016/j.tecto.2015.08.004

Jolivet, L., Tamaki, K., Fournier, M., 1994. Japan Sea: opening history and mechanism: a synthesis. J. Geophys. Res. Solid Earth 99, 22237–22259.

Jourdan, F., Bertrand, H., Watkeys, M.K., 2007. From flood basalts to the inception of oceanization: Example from the 40 Ar/ 39 Ar high-resolution picture of the Karoo large igneous province. Geochemistry Geophys. Geosystems 8, 20. https://doi.org/10.1029/2006GC001392

Jourdan, F., Féraud, G., Bertrand, H., Kampunzu, A.B., Tshoso, G., Le Gall, B., Tiercelin, J.J., Capiez, P., 2004. The Karoo triple junction questioned : evidence from Jurassic and

Proterozoic 40 Ar / 39 Ar ages and geochemistry of the giant Okavango dyke swarm (Botswana). Earth Planet. Sci. Lett. 222, 989–1006. https://doi.org/10.1016/j.epsl.2004.03.017

Jourdan, F., Féraud, G., Bertrand, H., Kampunzu, A.B., Tshoso, G., Watkeys, M., Le Gall, B., 2005. Karoo large igneous province: Brevity , origin , and relation to mass extinction questioned by new 40Ar/39Ar age data. Geology 33, 745–748. https://doi.org/10.1130/G21632.1

Juan, R. del C., de Jager, J., Russel, J., Gebhard, I., 1996. Geologia del flanco norte de la cuenca del Colorado.

Jungslager, E.H.A., 1999. Petroleum habitats of the Atlantic margin of South Africa. Geol. Soc. London, Spec. Publ. 153, 153–168. https://doi.org/10.1144/GSL.SP.1999.153.01.10

Jungslager, E.H.A., 1996. Geological evaluation of the remaining prospectivity for oil and gas of the pre-1At1 “synrift” succession in Block 9, Republic of South Africa.

Kaasschieter, J.P.H., 1965. Geologia de la cuenca del Colorado.

Kaasschieter, J.P.H., 1963. Geology of the Colorado basin. Tulsa Geol. Soc. Dig. 31, 177–187.

Karl, M., Glasmacher, U.A., Kollenz, S., Franco-Magalhaes, A.O.B., Stockli, D.F., Hackspacher, P.C., 2013. Evolution of the South Atlantic passive continental margin in southern Brazil derived from zircon and apatite (U-Th-Sm)/He and fission-track data. Tectonophysics 604, 224–244. https://doi.org/10.1016/j.tecto.2013.06.017

Kay, S.M., 1993. Late Paleozoic tectonics in Southern South America: a global perspective, in: Douzieme Congres International de La Stratigraphie et Geologie Du Carbonifere et Permien, Comptes Rendus I. Buenos Aires, pp. 109–122.

Kay, S.M., Ramos, V.A., Mpodozis, C., Sruoga, P., 1989. Late Paleozoic to Jurassic silicic magmatism at the Gondwana margin: Analogy to the Middle Proterozoic in North America? Geology 17, 324–328.

Keeley, M.L., Light, M.P.R., 1993. Basin Evolution and Prospectivity of the Argentine Continental Margin. J. Pet. Geol. 16, 451–464. https://doi.org/10.1111/j.1747-

5457.1993.tb00352.x

Keidel, J., 1916. La Geología de las Sierras de la Provincia de Buenos Aires y sus relaciones con las montañas de Sudáfrica y los Andes. Buenos Aires.

Kelemen, J.A., Holbrook, W.S., 1995. Origin of thick, high-velocity igneous crust along the U.S. East Coast Margin. J. Geophys. Res. 100, 10077–10094.

Kimbell, G.S., Richards, P.C., 2008. The three-dimensional lithospheric structure of the Falkland Plateau region based on gravity modelling. J. Geol. Soc. London. 165, 795–806.

Klausen, M.B., 2009. The Lebombo monocline and associated feeder dyke swarm: Diagnostic of a successful and highly volcanic rifted margin? Tectonophysics 468, 42–62. https://doi.org/10.1016/j.tecto.2008.10.012

Kokogian, D., Mancilla, O.H., 1989. Análisis Estratigráfico Secuencial de la Cuenca Cuyana, in: Chebli, G.A., Spalletti, L. (Eds.), Cuencas Sedimentarias Argentinas. Instituto Superior de Correlación Geológica, San Miguel de Tucuman, pp. 169–201.

Kollenz, S., 2015. Long-term landscape evolution, cooling and exhumation history of the South American passive continental margin in NE Argentina and SW Uruguay. University of Heidelberg.

König, M., Jokat, W., 2006. The Mesozoic breakup of the Weddell Sea. J. Geophys. Res. Solid Earth 111, 1–28. https://doi.org/10.1029/2006JB004035

Koopmann, H., Brune, S., Franke, D., Breuer, S., 2014a. Linking rift propagation barriers to excess magmatism at volcanic rifted margins. Geology 42, 1071–1074. https://doi.org/10.1130/G36085.1

Koopmann, H., Franke, D., Schreckenberger, B., Schulz, H., Hartwig, A., Stollhofen, H., di Primio, R., 2014b. Segmentation and volcano-tectonic characteristics along the SW African continental margin, South Atlantic, as derived from multichannel seismic and potential field data. Mar. Pet. Geol. 50, 22–39. https://doi.org/10.1016/j.marpetgeo.2013.10.016

Koopmann, H., Schreckenberger, B., Franke, D., Becker, K., Schnabel, M., 2016. The late

rifting phase and continental break-up of the southern South Atlantic: the mode and timing of volcanic rifting and formation of earliest oceanic crust. Geol. Soc. London, Spec. Publ. 420, 315–340. https://doi.org/10.1144/SP420.2

Kostadinoff, J., Llambías, E., 2002. Cuencas sedimentarias en el subsuelo de la Provincia de La Pampa, in: 5 Congreso de Exploración y Desarrollo de Hidrocarburos. Instituto Argentino del Petróleo y del Gas, p. 9.

Kozlowsky, E., Legarreta, L., Boll, A., Marshall, P., 2011. Simposio Cuencas Argentinas, Visión Actual. Instituto Argentino del Petróleo y del Gas, Buenos Aires.

Kristoffersen, Y., Hofstede, C., Diez, A., Blenkner, R., Lambrecht, A., Mayer, C., Eisen, O., 2014. Reassembling Gondwana: A new high quality constraint from vibroseis exploration of the sub-ice shelf geology of the East Antarctic continental margin. J. Geophys. Res. Solid Earth 119, 1–12. https://doi.org/10.1002/2014JB011479.Received

Kukla, P.A., Strozyk, F., Mohriak, W.U., 2018. South Atlantic salt basins – Witnesses of complex passive margin evolution. Gondwana Res. 53, 41–57. https://doi.org/10.1016/j.gr.2017.03.012

Ladd, J.W., 1974. South Atlantic seafloor spreading and Caribbean tectonics. Columbia University, New York.

Lagorio, S.L., 2008. Early Cretaceous alkaline volcanism of the Sierra Chica de Córdoba (Argentina): Mineralogy, geochemistry and petrogenesis. J. South Am. Earth Sci. 26, 152–171. https://doi.org/10.1016/j.jsames.2008.05.003

Lagorio, S.L., Vizán, H., Geuna, S.E., 2016. Early Cretaceous Volcanism in Central and Eastern Argentina During Gondwana Break-Up.

Larsen, H.C., Dahl-Jensen, T., Hopper, J.R., 1998. Crustal structure along the leg 152 drilling transect, in: Proceedings of the Ocean Drilling Program, Scientific Results, 152. Ocean Drilling Program, Texas A&M University, College Station, TX, pp. 463–475.

Larson, R.L., Pitman III, W.C., Goloychenko, X., Cande, S.C., Dewey, J.F. (State U. of new Y. at A., Haxby, W.F., LaBrecque, J.L., 1985. The Bedrock Geology of the World. Freeman, New York, NY, USA.

Lavier, L.L., Manatschal, G., 2006. A mechanism to thin the continental lithosphere at magma-poor margins. Nature 440, 324–328. https://doi.org/10.1038/nature04608

Lavier, L.L., Steckler, M.S., Brigaud, F., 2000. An Improved Method for Reconstructing the Stratigraphy and Bathymetry of Continental Margins: Application to the Cenozoic Tectonic and An Improved Method for Reconstructing the Stratigraphy and Bathymetry of Continental Margins : Application to the Cenozo. Am. Assoc. Pet. Geol. Bull. 84, 923–939. https://doi.org/10.1306/A9673B6C-1738-11D7-8645000102C1865D

Le Pichon, X., Sibuet, J.-C., 1981. Passive margins: A model of formation. J. Geophys. Res. 86, 3708–3720.

Legarreta, L., Uliana, M.A., 1996. The Jurassic succession in west-central Argentina: stratal patterns, sequences and paleogeographic evolution. Palaeogeogr. Palaeoclimatol. Palaeoecol. 120, 303–330. https://doi.org/10.1016/0031-0182(95)00042-9

Leleu, S., Hartley, A.J., van Oosterhout, C., Kennan, L., Ruckwied, K., Gerdes, K., 2016. Structural, stratigraphic and sedimentological characterisation of a wide rift system: The Triassic rift system of the Central Atlantic Domain. Earth-Science Rev. 158, 89–124. https://doi.org/10.1016/j.earscirev.2016.03.008

Leroy, S., Lucazeau, F., D'Acremont, E., Watremez, L., Autin, J., Rouzo, S., Bellahsen, N., Tiberi, C., Ebinger, C., Beslier, M.O., Perrot, J., Razin, P., Rolandone, F., Sloan, H., Stuart, G., Lazki, A. Al, Al-Toubi, K., Bache, F., Bonneville, A., Goutorbe, B., Huchon, P., Unternehr, P., Khanbari, K., 2010. Contrasted styles of rifting in the eastern Gulf of Aden: A combined wide-angle, multichannel seismic, and heat flow survey. Geochemistry, Geophys. Geosystems 11. https://doi.org/10.1029/2009GC002963

Leroy, S., Razin, P., Autin, J., Bache, F., d'Acremont, E., Watremez, L., Robinet, J., Baurion, C., Denèle, Y., Bellahsen, N., Lucazeau, F., Rolandone, F., Rouzo, S., Kiel, J.S., Robin, C., Guillocheau, F., Tiberi, C., Basuyau, C., Beslier, M.O., Ebinger, C., Stuart, G., Ahmed, A., Khanbari, K., Al Ganad, I., de Clarens, P., Unternehr, P., Al Toubi, K., Al Lazki, A., 2012. From rifting to oceanic spreading in the Gulf of Aden: A synthesis. Arab. J. Geosci. 5, 859–901. https://doi.org/10.1007/s12517-011-0475-4

Lesta, P.J., Turic, M.A., Mainardi, E., 1978. Actualizacion de la informacion estratigrafica en

la Cuenca de Colorado_Lesta et al_1978.pdf, in: VII Congreso Geológico Argentino. Neuquén, pp. 701–713.

Light, M.P.R., Keeley, M.L., Maslanyj, M.R., Urien, C.M., 1993. The Tectono-Stratigraphic Development of Patagonia, and Its Relevance To Hydrocarbon Exploration. J. Pet. Geol. 16, 465–482. https://doi.org/10.1111/j.1747-5457.1993.tb00353.x

Linares, E., 1978. Informe sobre datación radimétrica K-Arpozo YPF.CCM-I.Pu.x-1 (Puelche). Buenos Aires.

Linol, B., Wit, M.J. De, 2016. Origin and Evolution of the Cape Mountains and Karoo Basin.

Llambias, E.J., Quenardelle, S., Montenegro, T., 2003. The Choiyoi Group from central Argentina: a subalkaline transitional to alkaline association in the craton adjacent to the active margin of the Gondwana continent. J. South Am. Earth Sci. 16, 243–257. https://doi.org/10.1016/S0895-9811(03)00070-1

Loegering, M.J., Anka, Z., Autin, J., di Primio, R., Marchal, D., Rodriguez, J.F., Franke, D., Vallejo, E., 2013. Tectonic evolution of the Colorado Basin, offshore Argentina, inferred from seismo-stratigraphy and depositional rates analysis. Tectonophysics 604, 245–263. https://doi.org/10.1016/j.tecto.2013.02.008

Lohr, T., Underhill, J.R., 2015. Role of rift transection and punctuated subsidence in the development of the North Falkland Basin. Pet. Geosci. 21, 85–110. https://doi.org/10.1144/petgeo2014-050

Lopez-Gamundi, O.R., Conaghan, P.C., Rossello, E.A., Cobbold, P.R., 1995. The Tunas Formation (Permian) in the Sierras Australes foldbelt, East Central Argentina: evidence for syntectonic sedimentation in a foreland basin. J. South Am. Earth Sci. 8, 129–142.

Lopez-Gamundi, O.R., Rosello, E.A., 1998. Basin fill evolution and paleotectonic patterns along the Samfrau geosyncline: the Sauce Grande basin-Ventana foldbelt (Argentina) and Karoo basin-Cape foldbelt (South Africa) revisited. Geol. Rundsch 86, 819–834.

Lorenzo, J.M., Wessel, P., 1997. Flexure across a continent-ocean fracture zone: the northern Falkland/Malvinas Plateau, South Atlantic. Geo-Marine Lett. 17, 110–118. https://doi.org/10.1007/s003670050015

Lovecchio, J.P., Kress, P.R., Rodríguez, E., Flores, G., Gerster, R., Bolatti, N., Rohais, S., Ramos, V.A., 2017. Caracterización del Campo Volcánico Campaniano-Paleoceno de la Cuenca del Colorado, Plataforma Continental Argentina, in: Grosse, P., Petrinovic, I. (Eds.), XX Congreso Geológico Argentino, ST8. Asociación Geológica Argentina, San Miguel de Tucuman, pp. 74–80.

Lovecchio, J.P., Rohais, S., Joseph, P., Bolatti, N., Kress, P.R., Gerster, R., Ramos, V.A., 2018. Multistage rifting evolution of the Colorado basin (offshore Argentina): Evidence for extensional settings prior to the South Atlantic opening. Terra Nov. 30, 359–368. https://doi.org/10.1111/ter.12351

Ludwig, W.J., Ewing, J.I., Ewing, M., 1968. Structure of Argentine Continental Margin. Am. Assoc. Pet. Geol. Bull. 52, 2337–2368.

Lundin, E.R., Redfield, T.F., Péron-Pevindic, G., 2014. Rifted Continental Margins: Geometric Influence on Crustal Architecture and Melting, in: Pindell, J., Horn, B., Rosen, N., Weimer, P., Dinkleman, M., Lowrie, A., Fillon, R., Granath, J., Kennan, L. (Eds.), Sedimentary Basins: Origin, Depositional Histories, and Petroleum Systems. GCSSEPM, pp. 1–36. https://doi.org/https://doi.org/10.5724/gcs.14.33

Macdonald, D., Gomez-Perez, I., Franzese, J., Spalletti, L., Lawver, L., Gahagan, L., Dalziel, I., Thomas, C., Trewin, N., Hole, M., Paton, D., 2003. Mesozoic break-up of SW Gondwana: Implications for regional hydrocarbon potential of the southern South Atlantic. Mar. Pet. Geol. 20, 287–308. https://doi.org/10.1016/S0264-8172(03)00045-X

Mahanjane, E.S., 2012. A geotectonic history of the northern Mozambique Basin including the Beira High - A contribution for the understanding of its development. Mar. Pet. Geol. 36, 1–12. https://doi.org/10.1016/j.marpetgeo.2012.05.007

Maksaev, V., Munizaga, F., Tassinari, C., 2014. Timing of the magmatism of the paleo-Pacific border of Gondwana: U-Pb geochronology of Late Paleozoic to Early Mesozoic igneous rocks of the north Chilean Andes between 20° and 31° S. Andean Geol. 41, 447–506. https://doi.org/10.5027/andgeoV41n3-a01

Malkowski, M.A., Grove, M., Graham, S.A., 2015. Unzipping the Patagonian Andes — Long-lived influence of rifting history on foreland basin evolution 1–7.

https://doi.org/10.1130/L489.1

Mancilla, O.H., Salinas, A., Soubies, E.D., Debarre, R., Granjeon, D., 2002. Exploration of a Frontier Area Using Numerical Stratigraphical Modeling , Application to the Offshore Colorado Basin of Argentina, in: AAPG Annual Meeting. AAPG, Houston, Texas, p. 90007.

Mann, P., Gahagan, L., Gordon, M.B., 2001. Tectonic setting of the world's giant oil fields. World Oil 42–50.

Marcano, G., Anka, Z., di Primio, R., 2013. Major controlling factors on hydrocarbon generation and leakage in South Atlantic conjugate margins: A comparative study of Colorado, Orange, Campos and Lower Congo basins. Tectonophysics 604, 172–190. https://doi.org/10.1016/j.tecto.2013.02.004

Marshall, J.E.A., 1994a. The Falkland Islands: A key element in Gondwana paleogeography. Tectonics 13, 631–636.

Marshall, J.E.A., 1994b. The Falkland Islands and the early fragmentation of Gondwana: implications for hydrocarbon exploration in the Falkland Plateau. Mar. Pet. Geol. 11, 631–636. https://doi.org/10.1016/0264-8172(94)90073-6

Marsicano, C.A., Irmis, R.B., Mancuso, A.C., Mundil, R., Chemale, F., 2016. The precise temporal calibration of dinosaur origins, in: Proceedings of the National Academy of Sciences. pp. 509–513. https://doi.org/10.1073/pnas.1512541112

Martin, A.K., 1984. Propagating rifts: Crustal extension during continental rifting. Tectonics 3, 611–617. https://doi.org/10.1029/TC003i006p00611

Martins-Neto, M.A., Catuneanu, O., 2012. Rift sequence stratigraphy, in: Phanerozoic Rift Systems and Sedimentary Basins. Elsevier B.V., pp. 59–70. https://doi.org/10.1016/B978-0-444-56356-9.00003-1

McDermott, C., Lonergan, L., Collier, J.S., McDermott, K.G., Bellingham, P., 2018. Characterization of seaward-dipping reflectors along the S . American Atlantic margin and implications for continental breakup. Tectonics in press. https://doi.org/10.1029/2017TC004923

McHone, J.G., 2000. Non-plume magmatism and rifting during the opening of the central Atlantic Ocean. Tectonophysics 316, 287–296. https://doi.org/10.1016/S0040-1951(99)00260-7

McKenzie, D., 1978. Some remarks on the development of sedimentary basins. Earth Planet. Sci. Lett. 40, 25–32.

McMillan, I.K., 2003. Foraminiferally defined biostratigraphic episodes and sedimentation pattern of the Cretaceous drift succession (Early Barremian to Late Maastrichtian) in seven basins on the South African and southern Namibian continental margin. S. Afr. J. Sci. 99, 537–576.

McMillan, I.K., 1990. Foraminiferal biostratigraphy of the Barremian to Miocene rocks of the Kudu 9A-1 , 9A-2 and 9A-3 boreholes. Communs Geol. Surv. Namib 6, 25–32.

Merle, O., 2011. A simple continental rift classification. Tectonophysics 513, 88–95. https://doi.org/10.1016/j.tecto.2011.10.004

Micucci, E., Continanzia, J., Manceda, R., Gavarrino, A., 2011a. Cuenca de San Julián: Síntesis del Conocimiento Exploratorio - Visión Actual, in: Simposio Cuencas Argentinas Visión Actual: VIII Congreso de Exploración y Desarrollo de Hidrocarburos. Instituto Argentino del Petróleo y del Gas, pp. 17–46.

Micucci, E., Continanzia, J., Manceda, R., Gavarrino, A., 2011b. CUENCA DE SAN JULIAN: SÍNTESIS DEL CONOCIMIENTO EXPLORATORIO – VISION ACTUAL, in: Simposio Cuencas Argentinas Visión Actual: VIII Congreso de Exploración y Desarrollo de Hidrocarburos. Instituto Argentino del Petróleo y del Gas, Buenos Aires, pp. 17–46.

Milana, J.P., Alcober, O., 1994. Modelo tectosedimentario de la cuenca triásica de Ischigualasto (San Juan, Argentina). Rev. la Asoc. Geol. Argentina 49, 217–235.

Miller, W., Wit, M.J. De, Linol, B., Armstrong, R., 2016. New Structural Data and U/Pb Dates from the Gamtoos Complex and Lowermost Cape Supergroup of the Eastern Cape Fold Belt, in Support of a Southward Paleo-Subduction Polarity, in: Linol, B., de Wit, M. (Eds.), Origin and Evolution of the Cape Mountains and Karoo Basin. Springer, Cham, pp. 35–44. https://doi.org/10.1007/978-3-319-40859-0

Milner, S.C., Duncan, A.R., Whittingham, A.M., Ewart, A., 1995. Trans-Atlantic correlation of eruptive sequences and individual silicic volcanic units within the Paran??-Etendeka igneous province. J. Volcanol. Geotherm. Res. 69, 137–157. https://doi.org/10.1016/0377-0273(95)00040-2

Mitchum, R.M., Vail, P.R., Thompson, S., 1977. Seismic Stratigraphy and Global Changes of Sea Level, Part 2: The Depositional Sequence as a Basic Unit for Stratigraphic Analysis, in: Payton, C.E. (Ed.), Seismic Stratigraphy: Applications to Hydrocarbon Exploration. AAPG Memoir 26, Tulsa, Oklahoma, pp. 53–62.

Mohriak, W.U., 2003. Bacias sedimentares da Margem Continental Brasileira, in: Bizzi, L.A. (Ed.), Geologia, Tectonica e Recursos Minerais Do Brasil. Servicio Geologico Brasileiro, pp. 87–165.

Mohriak, W.U., Leroy, S., 2013. Architecture of rifted continental margins and break-up evolution: insights from the South Atlantic, North Atlantic and Red Sea–Gulf of Aden conjugate margins. Geol. Soc. London, Spec. Publ. 369, 497–535. https://doi.org/10.1144/SP369.17

Mohriak, W.U., Nemcok, M., Enciso, G., 2008. South Atlantic divergent margin evolution : Rift-border uplift and salt tectonics in basins of SE Brazil, in: Pankhurst, R.J. (Ed.), West Gondwana: Pre-Cenozoic Correlations across the South Atlantic Region. Geological Society of London, Special Publication 294, pp. 365–398.

Morales, E., Chang, H.K., Soto, M., Correa, F.S., Veroslavsky, G., De Santa Ana, H., Conti, B., Daners, G., 2017. Tectonic and stratigraphic evolution of the Punta del Este and Pelotas basins (offshore Uruguay). Pet. Geosicence 23, 415–426. https://doi.org/10.1144/petgeo2016-059

Moreira, P., Fernández, R., Hervé, F., Fanning, C.M., Schalamuk, I.A., 2013. Detrital zircons U-Pb SHRIMP ages and provenance of La Modesta Formation, Patagonia Argentina. J. South Am. Earth Sci. 47, 32–46. https://doi.org/10.1016/j.jsames.2013.05.010

Mosquera, A., Ramos, V.A., 2006. Intraplate deformation in the Neuquén Embayment. Geol. Soc. Am. Spec. Pap. 407, 97–123. https://doi.org/10.1130/2006.2407(05).

Mosquera, A., Silvestro, J., Ramos, V.A., Alarcón, M., Zubiri, M., 2011. La estructura de la Dorsal de Huincul, in: Leanza, H.A., Arregui, C., Carbone, O., Danieli, J.C., Vallés, J.M. (Eds.), Geología y Recursos Naturales de La Provincia de Neuquén. Asociación Geológica Argentina, Neuquén, pp. 385–398.

Moulin, M., 2003. Étude géologique et géophysique des marges continentales passives: exemple du Zaïre et de l'Angola. Univesité de Bretagne Occidentale, Brest.

Moulin, M., Aslanian, D., 2010. Corrigendum to "A new starting point for the South and Equatorial Atlantic Ocean" [Earth Science Reviews 98 (2010), 1-37]. Earth-Science Rev. 103, 197–198. https://doi.org/10.1016/j.earscirev.2010.10.001

Moulin, M., Aslanian, D., Olivet, J.L., Contrucci, I., Matias, L., Géli, L., Klingelhoefer, H.N., Réhault, J.P., Unternehr, P., 2005. Geological constraints on the evolution of the Angolan margin based on reflection and refraction seismic data (ZaïAngo project). Geophys. J. Int. 162, 793–810.

Moulin, M., Aslanian, D., Rabineau, M., Patriat, M., Matias, L., 2013. Kinematic keys of the Santos – Namibe basins. Geol. Soc. London, Spec. Publ. 369, 91–107. https://doi.org/10.1144/SP369.3

Moulin, M., Aslanian, D., Unternehr, P., 2010. A new starting point for the South and Equatorial Atlantic Ocean. Earth-Science Rev. 98, 1–37. https://doi.org/10.1016/j.earscirev.2009.08.001

Mpodozis, C., Ramos, V.A., 2008. Tectónica Jurásica en Argentina y Chile: Extensión, subducción oblicua, rifting, deriva y colisiones? Rev. la Asoc. Geol. Argentina 63, 481–497.

Mueller, C.O., Jokat, W., 2017. Geophysical evidence for the crustal variation and distribution of magmatism along the central coast of Mozambique. Tectonophysics 712–713, 684–703. https://doi.org/10.1016/j.tecto.2017.06.007

Mukasa, S.B., Dalziel, I.W.D., 1996. Southernmost Andes and South Georgia Island, North Scotia Ridge : Zircon U-Pb and muscovite 40Ar / 39Ar age constraints on tectonic evolution of Southwestern Gondwanaland. J. South Am. Earth Sci. 9, 349–365.

Müller, R.D., Hassan, R., Gurnis, M., Flament, N., Williams, S.E., 2018. Dynamic topography of passive continental margins and their hinterlands since the Cretaceous. Gondwana Res. 53, 225–251. https://doi.org/10.1016/j.gr.2017.04.028

Müller, R.D., Sdrolias, M., Gaina, C., Roest, W.R., 2008. Age, spreading rates, and spreading asymmetry of the world's ocean crust. Geochemistry Geophys. Geosystems 9, 1–19. https://doi.org/10.1029/2007GC001743

Mutter, J.C., Talwani, M., Stoffa, P.L., 1982. Origin of seaward-dipping reflectors in oceanic crust off the Norwegian margin by "subaerial sea-floor spreading." Geology 10, 353–357.

Naipauer, M., Garcia Morabito, E., Manassero, M., Valencia, V. V, Ramos, V.A., 2018. A Provenance Analysis from the Lower Jurassic Units of the Neuqu é n Basin. Volcanic Arc or Intraplate Magmatic Input?, in: Folguera, A., et al. (Eds.), The Evolution of the Chilean-Argentinean Andes. Springer International Publishing, pp. 191–222.

Nairn, A.E.M., Lerche, I., Iliffe, J.E., 1991. Geology, basin analysis, and hydrocarbon potential of Mozambique and the Mozambique Channel. Earth Sci. Rev. 30, 81–123. https://doi.org/10.1016/0012-8252(91)90014-7

Nelson, K., De Jesus, M., Chakhmakhchev, A., Manning, M., 2013. Deepwater operators look to new frontiers. Offshore Mag.

Nemčok, M., 2016. Rifts and Passive Margins, First ed. ed. Cambridge University Press, New York, NY, USA.

Nivière, B., Messager, G., Carretier, S., Lacan, P., 2013. Geomorphic expression of the southern Central Andes forebulge (37°S, Argentina). Terra Nov. 25, 361–367. https://doi.org/10.1111/ter.12044

Nürnberg, D., Müller, R.D., 1991. The tectonic evolution of the South Atlantic from Late Jurassic to present. Tectonophysics 191, 27–53. https://doi.org/10.1016/0040-1951(91)90231-G

Olivero, E.B., 1987. Cefalopodos y bivalvos Titonianos y Hauterivianos de la Formación Lago La Plata, Chubut. Ameghiniana 24, 181–202.

Olivero, E.B., Aguirre-Urreta, M.B., 2002. Sucesion de amonoideos de la Formacion Katterfeld (Valanginiano-Hauteriviano) en su area tipo, Lago Fontana, Chubut, in: XV Congreso Geologico Argentino. El Calafate.

Oliveros, V., González, J., Espinoza Vargas, M., Vásquez, P., Rossel, P., Creixell, C., Sepúlveda, F., Bastias, F., 2018. The Early Stages of the Magmatic Arc in the Southern Central Andes, in: Folguera, A., Contreras-Reyes, E., Heredia, N., Encinas, A., Iannelli, S.B., Oliveros, V., Dávila, F., Collo, G., Giambiagi, L., Maksymowicz, A., Iglesia Llanos, M.P., Turienzo, M., Naipauer, M., Orts, D., Litvak, V., Álvarez, O., Arriagada, C. (Eds.), The Evolution of the Chilean-Argentinean Andes. Springer Nateure, pp. 165–190.

Otis, R.M., Schneidermann, N., 2000. A failed hydrocarbon system - Rawson Basins, Argentina, in: Petroleum Systems of South Atlantic Margins. AAPG Memoir 73. pp. 417–428.

Ottone, E.G., Angelozzi, G.N., 2015. Informe Palinológico Pozo Cruz del Sur x-1, Cuenca del Colorado. Ensenada, Argentina.

Ottone, E.G., Lovecchio, J.P., Pérez-panera, J.P., Ronchi, D., 2018. A new dinoflagellate form the Late Cretaceous of the Colorado basin, Offshore Argentina. Ameghiniana 55, 343–349.

Pángaro, F., 2013. Las cuencas paleozoicas episuturales del margen atlántico de la provincia de Buenos Aires y su control sobre la apertura atlántica. Universidad de Buenos Aires.

Pángaro, F., Ramos, V.A., 2012. Paleozoic crustal blocks of onshore and offshore central Argentina: New pieces of the southwestern Gondwana collage and their role in the accretion of Patagonia and the evolution of Mesozoic south Atlantic sedimentary basins. Mar. Pet. Geol. 37, 162–183. https://doi.org/10.1016/j.marpetgeo.2012.05.010

Pángaro, F., Ramos, V.A., Pazos, P.J., 2016. The Hesperides basin: a continental-scale upper Palaeozoic to Triassic basin in southern Gondwana. Basin Res. 28, 685–711. https://doi.org/10.1111/bre.12126

Pankhurst, R.J., Leat, P.T., Sruoga, P., Rapela, C.W., Márquez, M., Storey, B.C., Riley, T.R., 1998. The Chon Aike province of Patagonia and related rocks in West Antarctica: a silicic

large igneous province. J. Volcanol. Geotherm. Res. 81, 113–136. https://doi.org/10.1016/S0377-0273(97)00070-X

Pankhurst, R.J., Rapela, C., Marquez, M., 1993. Geocronologia y petrogenesis de los granitoides jurasicos del noreste del Macizo del Deseado, in: XII Congreso Geologico Argentino, Actas IV. Mendoza, pp. 134–141.

Pankhurst, R.J., Rapela, C.W., Fanning, C.M., Márquez, M., 2006. Gondwanide continental collision and the origin of Patagonia. Earth-Science Rev. 76, 235–257. https://doi.org/10.1016/j.earscirev.2006.02.001

Pankhurst, R.J., Rapela, C.W., Loske, W.P., Márquez, M., Fanning, C.M., 2003. Chronological study of the pre-Permian basement rocks of southern Patagonia. J. South Am. Earth Sci. 16, 27–44. https://doi.org/10.1016/S0895-9811(03)00017-8

Pankhurst, R.J., Riley, T.R., Fanning, C.M., Kelley, S.P., 2000. Episodic silicic volcanism in Patagonia and the Antarctic Peninsula: Chronology of magmatism associated with the break-up of Gondwana. J. Petrol. 41, 605–625. https://doi.org/10.1093/petrology/41.5.605

Panza, J.L., Haller, M.J., 2002. El volcanismo Jurásico, in: Haller, M.J. (Ed.), Geología y Recursos Naturales de Santa Cruz. Asociación Geológica Argentina, Buenos Aires, pp. 89–101.

Parsiegla, N., Stankiewicz, J., Gohl, K., Ryberg, T., Uenzelmann-Neben, G., 2009. Southern African continental margin: Dynamic processes of a transform margin. Geochemistry, Geophys. Geosystems 10. https://doi.org/10.1029/2008GC002196

Paton, D.A., 2006. Influence of crustal heterogeneity on normal fault dimensions and evolution : southern South Africa extensional system. J. Struct. Geol. 28, 868–886. https://doi.org/10.1016/j.jsg.2006.01.006

Paton, D.A., Mortimer, E.J., Hodgson, N., Van Der Spuy, D., 2016. The missing piece of the South Atlantic jigsaw - when continental break-up ignores crustal heterogeneity. Pet. Geosci. West Africa Margin, Geol. Soc. London, Spec. Publ. 438. https://doi.org/http://doi.org/10.1144/SP438.8

Paton, D.A., Pindell, J., Mcdermott, K., Bellingham, P., Horn, B., 2017. Evolution of seaward-

dipping reflectors at the onset of oceanic crust formation at volcanic passive margins : Insights from the South Atlantic 439–442. https://doi.org/10.1130/G38706.1

Paton, D.A., Underhill, J.R., 2004. Role of crustal anisotropy in modifying the structural and sedimentological evolution of extensional basins: the Gamtoos Basin, South Africa. Basin Res. 16, 339–359. https://doi.org/10.1111/j.1365-2117.2004.00237.x

Pérez-Díaz, L., Eagles, G., 2014. Constraining South Atlantic growth with seafloor spreading data. Tectonics 33, 1–26. https://doi.org/10.1002/2014TC003644.Received

Pérez-Gussinyé, M., 2013. A tectonic model for hyperextension at magma-poor rifted margins: an example from the West Iberia – Newfoundland conjugate margins. Geol. Soc. London, Spec. Publ. 369, 403–427. https://doi.org/10.1144/SP369.19

Pérez Panera, J.P., Ronchi, D., Angelozzi, G.N., Lovecchio, J.P., Calvo-Marcilese, L., Hiriart, M.L., Tortora, L., Calaramo, N., Cuciniello, C.D., 2018. Synthesis of the Colorado basin, Argentine Offshore integrated Biostrarigraphic and Paleoenvironmental Analysis. Berisso.

Peron-Pinvidic, G., Manatschal, G., Osmundsen, P.T., 2013. Structural comparison of archetypal Atlantic rifted margins: A review of observations and concepts. Mar. Pet. Geol. 43, 21–47. https://doi.org/10.1016/j.marpetgeo.2013.02.002

Picarelli, A., Abreu, V., 2015. Sequence Stratigraphy Applied to Continental Rift Basins: Example from Recô ncavo Basin, Brazil. Lacustrine sandstone Reserv. Hydrocarb. Syst. AAPG Mem. 95 347–366. https://doi.org/10.1306/13291396M953453

Pindell, J., Graham, R., Horn, B., 2014. Rapid outer marginal collapse at the rift to drift transition of passive margin evolution, with a Gulf of Mexico case study. Basin Res. 26, 701–725. https://doi.org/10.1111/bre.12059

Pindell, J.L., Dewey, J.F. (State U. of new Y. at A., 1982. Permo-Triassic reconstructions of western Pangea and the evolution of the Gulf of Mexico/Caribbean region. Tectonics 1, 179–211.

Pinto, V.M., Hartmann, L.A., Santos, J.O.S., McNaughton, N.J., Wildner, W., 2011. Zircon U-Pb geochronology from the Paraná bimodal volcanic province support a brief eruptive

cycle at ~135Ma. Chem. Geol. 281, 93–102. https://doi.org/10.1016/j.chemgeo.2010.11.031

Planke, S., Symonds, P.A., Alvestad, E., Skogseid, J., 2000. Seismic volcanostratigraphy of large-volume basaltic extrusive complexes on rifted margins. J. Geophys. Res. Solid Earth 105, 19335–19351. https://doi.org/10.1029/1999JB900005

Price, G.D., Gröcke, D.R., 2002. Strontium-isotope stratigraphy and oxygen- and carbon-isotope variation during the Middle Jurassic-Early Cretaceous of the Falkland Plateau, South Atlantic. Palaeogeogr. Palaeoclimatol. Palaeoecol. 183, 209–222. https://doi.org/10.1016/S0031-0182(01)00486-2

Quirk, D.G., Shakerley, A., Howe, M.J., 2014. A mechanism for construction of volcanic rifted margins during continental breakup. Geology 42, 1079–1082. https://doi.org/10.1130/G35974.1

Rabinowitz, P.D., LaBreque, J., 1979. The Mesozoic South Atlantic Ocean and Evolution of its Conjugate MArgins. J. Geophys. Res. 84, 5973–6002.

Raggio, F., Gerster, R., Welsink, H., 2011a. Cuencas del Salado y Punta del Este. VIII Congr. Explor. y Desarro. Hidrocarburos Simp. Cuencas Argentinas visión actual 80–87.

Raggio, F., Welsink, H., Fiptiani, N., Prayitno, W., Gerster, R., 2011b. Cuenca Malvinas. VIII Congr. Explor. y Desarro. Hidrocarburos Simp. Cuencas Argentinas visión actual 1–16.

Ramos, V., 1999. Rasgos estructurales del territorio argentino. Geol. Argentina 29, 70.

Ramos, V.A., 2010. The tectonic regime along the Andes: Present-day and Mesozoic regimes. Geol. J. 45, 2–25. https://doi.org/10.1002/gj.1193

Ramos, V.A., 2010. Pampia : A large cratonic block missing in the Rodinia supercontinent. https://doi.org/10.1016/j.jog.2010.01.019

Ramos, V.A., 2008. Patagonia: A paleozoic continent adrift? J. South Am. Earth Sci. 26, 235–251. https://doi.org/10.1016/j.jsames.2008.06.002

Ramos, V.A., 2002. Evolucion Tectonica, in: Haller, M.J. (Ed.), Geología y Recursos Naturales

de Santa Cruz. Asociación Geológica Argentina, El Calafate, pp. 365–387.

Ramos, V.A., 1996. Evolucion tectonica de la plataforma continental, in: Ramos, V.A., Turic, M.A. (Eds.), Geología y Recursos Naturales de La Plataforma Continental Argentina. pp. 385–404.

Ramos, V.A., Chemale, F., Naipauer, M., Pazos, P.J., 2014. A provenance study of the Paleozoic Ventania System (Argentina): Transient complex sources from Western and Eastern Gondwana. Gondwana Res. 26, 719–740. https://doi.org/10.1016/j.gr.2013.07.008

Ramos, V.A., Cingolani, C., Junior, F.C., Naipauer, M., Rapalini, A., 2017. The Malvinas (Falkland) Islands revisited: The tectonic evolution of southern Gondwana based on U-Pb and Lu-Hf detrital zircon isotopes in the Paleozoic cover. J. South Am. Earth Sci. 76, 320–345. https://doi.org/10.1016/j.jsames.2016.12.013

Ramos, V.A., Folguera, A., 2009. Andean flat-slab subduction through time, in: Murphy, J.B., Keppie, J.D., Hynes, A.J. (Eds.), Ancient Orogens and Modern Analogs. Geological Society of London SP 327. pp. 31–54.

Ramos, V.A., Kay, S.M., 1991. Triassic rifting and associated basalts in the Cuyo basin, central Argentina 79–92. https://doi.org/10.1130/SPE265-p79

Ramos, V.A., Palma, M.A., 1996. Tectónica del Pérmico de Argentina, in: Archangelsky, S. (Ed.), El Sistema Pérmico En La República Argentina y En La República Oriental Del Uruguay. Academia Nacional de Ciencias, Córdoba, pp. 239–254.

Ramos, V.A., Turic, M.A., 1996. Geología y Recursos Naturales de la Plataforma Continental Argentina, First. ed. Asociación Geológica Argentina; Instituto Argentino del Petróleo, Buenos Aires.

Rapela, C.W., Días, G.F., Franzese, J.R., Alonso, G., Benvenuto, A.R., 1991. El Batolito de la Patagonia Central: Evidencias de un magmatismo Triásico-Jurásico asociado a fallas transcurrentes. Rev. Geológica Chile 18, 121–138.

Rapela, C.W., Pankhurst, R.J., Fanning, C.M., Herve, F., 2005. Pacific subduction coeval with the Karoo mantle plume : the early Jurassic subcordilleran belt of northwestern Patagonia.

Geol. Soc. 217–239. https://doi.org/10.1144/GSL.SP.2005.246.01.07

Renne, P.R., Glen, J.M., Milner, S.C., Duncan, A.R., 1996. Age of Etendeka flood volcanism and associated intrusions in southwestern Africa. Geology 24, 659–662. https://doi.org/10.1130/0091-7613(1996)024<0659:AOEFVA>2.3.CO;2

Richards, P.C., Fannin, N.G.T., 1997. Geology of the North Falkland Basin. J. Pet. Geol. 20, 165–183. https://doi.org/10.1111/j.1747-5457.1997.tb00771.x

Richards, P.C., Hillier, B. V., 2000. Post-drilling analysis of the North Falkland Basin-Part 1: Tectono-stratigraphic framework. J. Pet. Geol. 23, 253–272. https://doi.org/10.1111/j.1747-5457.2000.tb01019.x

Richards, P.C., Stone, P., Kimbell, G.S., McIntosh, W.C., Phillips, E.R., 2013. Mesozoic magmatism in the Falkland Islands (South Atlantic) and their offshore sedimentary basins. J. Pet. Geol. 36, 61–73. https://doi.org/10.1111/jpg.12542

Riel, N., Jaillard, E., Martelat, J.-E., Guillot, S., Braun, J., 2018. Permian-Triassic Tethyan realm reorganization: Implications for the outward Pangea margin. J. South Am. Earth Sci. 81, 78–86. https://doi.org/10.1016/j.jsames.2017.11.007

Riley, T.R., Flowerdew, M.J., Pankhurst, R.J., Curtis, M.L., Millar, I.L., Fanning, C.M., Whitehouse, M.J., 2016. Early Jurassic magmatism on the Antarctic Peninsula and potential correlation with the Subcordilleran plutonic belt of Patagonia. J. Geol. Soc. London. https://doi.org/10.1144/jgs2016-053

Ritsema, J., van Heijst, H.J., Woodhouse, J.H., 1999. Complex shear wave velocity structure imaged beneath Africa and Iceland. Science (80-.). 286, 1925–1928.

Roberts, D.G., Bally, A.W., 2012. From rifts to passive margins: A continuum of extension, Regional Geology and Tectonics: Phanerozoic Rift Systems and Sedimentary Basins. Elsevier B.V. https://doi.org/10.1016/B978-0-444-56356-9.00001-8

Robinson, S.A., Murphy, D.P., Vance, D., Thomas, D.J., 2010. Formation of “Southern Component Water” in the Late Cretaceous: Evidence from Nd-isotopes. Geology 38, 871–874. https://doi.org/10.1130/G31165.1

Ronchi, D., Angelozzi, G.N., Pérez Panera, J.P., Calvo-Marcilese, L., Tortora, L., Calaramo, N., Lovecchio, J.P., Cuciniello, C.D., Hiriart, M.L., Ottone, G., 2016. Synthesis of the Salado and Punta del Este basins, Argentine Offshore integrated Biostrarigraphic and Paleoenvironmental Analysis. Ensenada.

Rosenbaum, G., Gasparon, M., Lucente, F.P., Peccerillo, A., Miller, M.S., 2008. Kinematics of slab tear faults during subduction segmentation and implication for Italian magmatism. Tectonics 27, 16. https://doi.org/10.1029/2007TC002143

Ross, J.G., Pinchin, J., Griffin, D.G., Dinkelman, M.G., Turic, M.A., Nevistic, A.V., 1996. Cuenca de Malvinas Norte, in: Ramos, V.A., Turic, M.A. (Eds.), Geología y Recursos Naturales de La Plataforma Continental Argentina. Asociación Geológica Argentina; Instituto Argentino del Petróleo, Buenos Aires, pp. 253–271.

Rouby, D., Braun, J., Robin, C., Dauteuil, O., Deschamps, F., 2013. Long-term stratigraphic evolution of Atlantic-type passive margins: A numerical approach of interactions between surface processes, flexural isostasy and 3D thermal subsidence. Tectonophysics 604, 83–103. https://doi.org/10.1016/j.tecto.2013.02.003

Roux, J., 1997. Potential outlined in southern Outeniqua Basin off S Africa. Oil Gas J.

Saunders, A.D., Fitton, J.G., Kerr, A.C., Norry, M.J., Kent, R.W., 1997. The North Atlantic igneous province, in: Mahoney, J.J., Coffin, M.F. (Eds.), Large Igneous Provinces: Continental, Oceanic, Amd Planetary Flood Volcanism. AGU Geophysical Monography 100, Washington, pp. 45–93.

Schiuma, M., 2012. Provincia de Buenos Aires, Cuenca de Claromeco. Buenos Aires.

Schmidt, C.J., Astini, R.A., Costa, C.H., Gardini, C.E., Kraemer, P.E., 1995. Cretaceous rifting, alluvial fan sedimentation, and Neogene inversion , Southern Sierras Pampeanas, Argentina, in: Tankard, A., Suarez-S., R., Welsink, H.J. (Eds.), Petroleum Basins of South America. AAPG Memoir 62, pp. 341–358.

Schnabel, M., Franke, D., Engels, M., Hinz, K., Neben, S., Damm, V., Grassmann, S., Pelliza, H., Dos Santos, P.R., 2008. The structure of the lower crust at the Argentine continental margin, South Atlantic at 44°S. Tectonophysics 454, 14–22.

https://doi.org/10.1016/j.tecto.2008.01.019

Schwarz, E., Veiga, G.D., Spalletti, L.A., Massaferro, J.L., 2011. The transgressive infill of an inherited-valley system: The Springhill Formation (lower Cretaceous) in southern Austral Basin, Argentina. Mar. Pet. Geol. 28, 1218–1241. https://doi.org/10.1016/j.marpetgeo.2010.11.003

Sengör, A.M.C., Burke, K., 1978. Relative timing of rifting and volcanism on Earth and its tectonic implications. Geophys. Res. Lett. 5, 419–421.

Shirley, K., 2010. Deepwater Exploration and Production. Baker Hughes White Paper.

Smith, R.M.H., Eriksson, P.G., Botha, W.J., 1993. A review of the stratigraphy and sedimentary environments of the Karoo-aged basins of Southern Africa. J. African Earth Sci. 16, 143–169. https://doi.org/10.1016/0899-5362(93)90164-L

Soto, M., Morales, E., Veroslavsky, G., de Santa Ana, H., Ucha, N., Rodríguez, P., 2011. The continental margin of Uruguay: Crustal architecture and segmentation. Mar. Pet. Geol. 28, 1676–1689. https://doi.org/10.1016/j.marpetgeo.2011.07.001

Spalletti, L., Fanning, C.M., Rapela, C.W., 2008. Dating the Triassic continental rift in the southern Andes : the Potrerillos Formation, Cuyo Basin, Argentina. Geol. Acta 6, 267–283.

Spikings, R., Reitsma, M.J., Boekhout, F., Mi, A., Ulianov, A., Chiaradia, M., Gerdes, A., Schaltegger, U., 2016. Characterisation of Triassic rifting in Peru and implications for the early disassembly of western Pangaea 35, 124–143. https://doi.org/10.1016/j.gr.2016.02.008

Starck, D., 2011. Cuenca Cretácica-Paleógena del Noroeste Argentino, in: Kozlowsky, E., Legarreta, L., Boll, A., Marshall, P. (Eds.), Simposio Cuencas Argentinas Visión Actual: VIII Congreso de Exploración y Desarrollo de Hidrocarburos. Instituto Argentino del Petróleo y del Gas, Buenos Aires, pp. 407–454.

Steckler, M.S., Watts, A.B., 1978. Subsidence of the Atlantic-type continental margin off New York. Earth Planet. Sci. Lett. 42, 1–13.

Steckler, M.S., Watts, A.B., Thorne, J.A., 1988. Subsidence and basin modeling at the U.S. Atlantic passive margin, in: Sheridan, R.E., Grow, J.A. (Eds.), The Atlantic Continental Margin, U.S. Geological Society of America, pp. 399–416.

Stern, C.R., Mukasa, S.B., Fuenzalida, R., 1992. Age and petrogenesis of the Sarmiento ophiolite complex of southern Chile. J. South Am. Earth Sci. 6, 97–104.

Stica, J.M., Zalán, P.V., Ferrari, A.L., 2014. The evolution of rifting on the volcanic margin of the Pelotas Basin and the contextualization of the Paraná-Etendeka LIP in the separation of Gondwana in the South Atlantic. Mar. Pet. Geol. 50, 1–21. https://doi.org/10.1016/j.marpetgeo.2013.10.015

Stipanicic, P.N., 2001. Antecedentes geológicos y paleontológicos, in: Artabe, A.E., Morel, E.M., Zamuner, A.B. (Eds.), El Sistema Triásico En La Argentina. Fundación Museo de la Plata "Francisco Pascasio Moreno," La Plata, pp. 1–21.

Stipanicic, P.N., Bonaparte, J.F., 1979. Cuenca Triasica de Ischigualasto-Villa Unión (Provincias de La Rioja y San Juan), in: Segundo Simposio de Geología Regional Argentina I. pp. 523–576.

Stoakes, F.A., Campbell, C. V., Cass, R., Ucha, N., 1991. Seismic stratigraphic analysis of the Punta del Este Basin, offshore Uruguay, South America. Am. Assoc. Pet. Geol. Bull.

Stollhofen, H., Gerschütz, S., Stanistreet, I.G., Lorenz, V., 1998. Tectonic and volcanic controls on Early Jurassic rift-valley lake deposition during emplacement of Karoo flood basalts, southern Namibia. Palaeogeogr. Palaeoclimatol. Palaeoecol. 140, 185–215. https://doi.org/10.1016/S0031-0182(98)00029-7

Stone, P., Richards, P.C., Kimbell, G.S., Esser, R.P., Reeves, D., 2008. Cretaceous dykes discovered in the Falkland Islands: implications for regional tectonics in the South Atlantic. J. Geol. Soc. London. 165, 1–4. https://doi.org/10.1144/0016-76492007-072

Storey, B.C., Alabaster, T., Hole, M.J., Pankhurst, R.J., Wever, H.E., 1992. Role of subduction-plate boundary forces during the initial stages of Gondwana break-up: evidence from the proto-Pacific margin of Antarctica, in: Magmatism and the Causes of Continental Break-up, Geological Society Special Publication. Geological Society, London, pp. 149–163.

https://doi.org/10.1144/GSL.SP.1992.068.01.10

Suárez, M., Márquez, M., 2007. A Toarcian retro-arc basin of Central Patagonia (Chubut), Argentina: Middle Jurassic closure, arc migration and tectonic setting. Rev. Geológica Chile 34, 63–79.

Sylwan, C.A., 2001. Geology of the Golfo San Jorge Basin, Argentina. 1. J. Iber. Geol. 27, 123–157.

Talwani, M., Abreu, V., 2000. Inferences regarding initiation of oceanic crust formation from the U.S. east coast margin and conjugate South Atlantic margins. Atl. Rift. Cont. margins. 115, 211–233. https://doi.org/10.1029/GM115p0211

Talwani, M., Ewing, J.I., Sheridan, R.E., Holbrook, W.S., Glover, L., 1995. The EDGE experiment and the US Coast Magnetic anomaly, in: Banda, E., Talwani, M., Torne, M. (Eds.), NATO/AR Series Book "Rift Ocean-Contient Boundaries." pp. 155–181.

Tankard, A.., Uliana, M.A., Welsink, H.J., Ramos, V.A., Tunik, M., Franca, A.B., Milani, E.J., de Brito Neves, B.B., Eyles, N., Skarmeta, J., Santa Ana et al., H., 1995. Structural and tectonic controls of basin evolution in southwestern Gondwana during the Phanerozoic. Tecton. Control. basin Evol. Southwest. Gondwana, A.J. Tankard, R. Suarez S., H.J. Weslsink, Pet. basins South Am. AAPG Mem. 62 5–52.

Tankard, A., Welsink, H., Aukes, P., Newton, R., Stettler, E., 2009. Tectonic evolution of the Cape and Karoo basins of South Africa, Marine and Petroleum Geology. https://doi.org/10.1016/j.marpetgeo.2009.01.022

Tavella, G.F., 2005. Cuenca del Salado, in: de Barrio, R.E., Etcheverry, R.O., Caballé, M.F., Llambías, E.J. (Eds.), Geología y Recursos Minerales de La Provincia de Buenos Aires. Asociación Geológica Argentina, La Plata, pp. 459–472.

Tavella, G.F., Wright, C.G., 1996. Cuenca del Salado, in: Ramos, V.A., Turic, M.A. (Eds.), Geología y Recursos Naturales de La Plataforma Continental Argentina. Buenos Aires, pp. 95–116.

Thomas, C.R., 1949. Geology and Petroleum Exploration in Magallanes Province, Chile. Am. Assoc. Pet. Geol. Bull. 33, 1553–1578.

Thomas, R.J., Henjes-Kunst, F., Jacobs, J., 1998. Pre-lamprophyre mafic dykes of the Cape Meredith Complex, West Falkland. Geol. Mag. 135, 495–500.

Thomson, K., Hegarty, K.A., Marshallsea, S.J., Green, P.F., 2002. Thermal and tectonic evolution of the Falkland Islands: Implications for hydrocarbon exploration in the adjacent offshore region. Mar. Pet. Geol. 19, 95–116. https://doi.org/10.1016/S0264-8172(02)00005-3

Torres Carbonell, P.J., Guzmán, C., Yagupsky, D., Dimieri, L. V., 2016. Tectonic models for the Patagonian orogenic curve (southernmost Andes): An appraisal based on analog experiments from the Fuegian thrust – fold belt. Tectonophysics 671, 76–94. https://doi.org/10.1016/j.tecto.2016.01.020

Torsvik, T.H., Rousse, S., Labails, C., Smethurst, M.A., 2009. A new scheme for the opening of the South Atlantic Ocean and the dissection of an Aptian salt basin. Geophys. J. Int. 177, 1315–1333. https://doi.org/10.1111/j.1365-246X.2009.04137.x

Trubitsyn, V.P., Mooney, W.D., Abbott, D.H., 2003. Cold cratonic roots and thermal blanckets: how continents affect mantle convection. Int. Geol. Rev. 45, 479–496.

Tugend, J., Gillard, M., Manatschal, G., Nirrengarten, M., Harkin, C., Epin, M., Sauter, D., Autin, J., Kusznir, N., McDermott, K., 2018. Reappraisal of the magma-rich versus magma-poor rifted margin archetypes, in: McClay, K.R., Hammerstein, J.A. (Eds.), Passive Margins: Tectonics, Sedimentation and Magmatism. Geological Society of London, Special Publication 476, London.

Turic, M.A., Nevistic, A. V., Rebay, G., 1996. Geologia y recursos naturales de la plataforma continental, in: Ramos, V.A., Turic, M.A. (Eds.), Geología y Recursos Naturales de La Plataforma Continental Argentina. pp. 405–423.

Turner (Ed.), 1980. Geologia Regional Argentina, First. ed. Academia Nacional de Ciencias, Cordoba.

Uliana, M.A., Arteaga, M.E., Legarreta, L., Cerdan, J.J., Peroni, G.O., 1995. Inversion structures and hydrocarbon occurence in Argentina, in: Buchanan, J.G., Buchanan, P.G. (Eds.), Basin Inversion. Geological Society Special Publication 88, pp. 211–233.

Uliana, M.A., Biddle, K., Cerdán, J., 1989. Mesozoic extension and the formation of Argentina sedimentary basins. Extensional tectonics Stratigr. North Atl. Margin, AAPG Mem., 46 599–613.

Uliana, M.A., Biddle, K.T., Phelps, D.W., Gust, D.A., 1985. Significado del vulcanimso y extensión Mesojurasicos en el extremo meridional de Sudamérica. Rev. la Asoc. Geol. Argentina 40, 231–253.

Unternehr, P., Curie, D., Olivet, J.L., Goslin, J., Beuzart, P., 1988. South Atlantic fits and intraplate boundaries in Africa and South America. Tectonophysics 155, 169–179.

Urien, C.M., Zambrano, J.J., 1973. The geology of the basins of the Argentine continental margin and Malvinas Plateau, in: Nairn, A.E.M., Stehli, F.G. (Eds.), The Ocean Basins and Its Margins. Plenum, New York, pp. 135–169.

Urien, C.M., Zambrano, J.J., Martins, L.R., 1981. The basins of Southestern South America (Southern Brazil, Uruguay and Eastern Argentina) including the Malvinas Plateau and Southern South Atlantic Paleogeographic Evolution, in: Volkheimer, W., Mussachio, E.A. (Eds.), Cuencas Sedimentarias Del Jurásico y Cretácico de América Del Sur. Comité Sudamericano del Jurásico y Cretácico, Buenos Aires, pp. 45–125.

Urien, C.M., Zambrano, J.J., Yrigoyen, M.R., 1995. Petroleum basins in southern South America: an overview. Pet. basins South Am. 62, 63–78.

Vail, P.R., 1987. Seismic Stratigraphy Interpretation using Sequence Stratigraphy, in: Bally, A.W. (Ed.), Atlas of Seismic Stratigraphy. AAPG Studies in Geology 27, Tulsa, Oklahoma, pp. 1–10.

Vail, P.R., Mitchum, R.M., Thompson, S., 1977a. Seismic Stratigraphy and Global Changes of Sea Level, Part 3: Relative Changes of Sea Level from Coastal Onlap, in: Payton, C.E. (Ed.), Seismic Stratigraphy: Applications to Hydrocarbon Exploration. AAPG Memoir 26, Tulsa, Oklahoma, pp. 63–81.

Vail, P.R., Mitchum, R.M., Thompson, S., 1977b. Seismic Stratigraphy and Global Changes of Sea Level, Part 4: Global Cycles of Relative Changes of Sea Level, in: Payton, C.E. (Ed.), Seismic Stratigraphy: Applications to Hydrocarbon Exploration. AAPG Memoir 26,

Tulsa, Oklahoma, pp. 83–97.

Valicenti, V.H., Stephens, J.M., 1984. Ostracodes from the Upper Valanginian and Upper Hauterivian of the Sundays River Formation, Algoa Basin, South Africa. Rev. Española Micropaleontol. 16, 171–239.

van Hinsbergen, D.J.J., Langereis, C.G., Meulenkamp, J.E., 2005. Revision of the timing , magnitude and distribution of Neogene rotations in the western Aegean region. Tectonophysics 396, 1–34. https://doi.org/10.1016/j.tecto.2004.10.001

Van Wagoner, J.C., R.M., M., Campion, K.M., Rahmanian, V.D., 1990. Siliciclastic Sequence Stratigraphy in Well Logs, Cores, and Outcrops: Concepts for High-Resolution Correlation of Time and Facies, AAPG Methods in Exploration Series 7. https://doi.org/0-89181-657-7

Varela, R., Pezzuchi, H., Genini, A., Zubia, M., 1992. Dataciones en el Jurásico inferior de rocas magmáticas del noroeste del Macizo del Deseado, Santa Cruz. Rev. la Asoc. Geol. Argentina 46, 257–262.

Vaughan, A.P.M., Pankhurst, R.J., 2008. Tectonic overview of the West Gondwana margin. Gondwana Res. 13, 150–162. https://doi.org/10.1016/j.gr.2007.07.004

Vaughan, A.P.M., Storey, B.C., 2007. A new supercontinent self-destruct mechanism: evidence from the Late Triassic-Early Jurassic. J. Geol. Soc. London. 164, 383–392. https://doi.org/10.1144/0016-76492005-109

Veevers, J.J., 1981. Morphotectonics of rifted continental margins in Embryo (East Africa), Youth (Africa-Arabia), and Maturity (Australia). J. Geol. 89, 57–82.

Veevers, J.J., Cole, D.I., Cowan, E.J., 1994. Southern Africa: Karoo Basin and Cape Fold Belt, in: Veevers, J.J., Powell, C.. (Eds.), Permian-Triassic Pangean Basins and Foldbelts Along the Panthalassan Margin of Gondwanaland. Geological Society of America, Boulder, Colorado, pp. 223–279. https://doi.org/10.1130/MEM184-p223

Vérard, C., Flores, K., Stampfli, G., 2012. Geodynamic reconstructions of the South America-Antarctica plate system. J. Geodyn. 53, 43–60. https://doi.org/10.1016/j.jog.2011.07.007

Vergani, G.D., Tankard, A.J., Belotti, H.J., Welsink, H.J., 1995. Tectonic Evolution and Paleogeography of the Neuquén Basin, Argentina. Pet. basins South Am. 1904, 383–402. https://doi.org/10.1306/7834F6E1-1721-11D7-8645000102C1865D

Veroslavsky, G., 1999. Geologia da Bacia de Santa Lucia - Uruguai. Universidade Estadual Paulista.

Viera, R., Pezzuchi, H., 1976. Presencia de sedimentitas Pérmicas en contacto con rocas del "Complejo Metamórfico" de la Patagonia Extrandina, estancia Dos Hermanos, provincia de Santa Cruz. Rev. la Asoc. Geol. Argentina 31, 274–285.

Vink, G.R., 1982. Continental rifting and the implication for plate tectonics reconstructions. J. Geophys. Res. 87, 10677–10688.

Visser, D.J.L., 1998. The Geotectonic Evolution of South Africa and Offshore Areas. Pretoria.

Voigt, S., Jung, C., Friedrich, O., Frank, M., Teschner, C., Hoffmainn, J., 2013. Tectonically restricted deep-ocean circulation at the end of the Cretaceous greenhouse. Earth Planet. Sci. Lett. 369–370, 169–177.

Volkheimer, W., Quattrocchio, M.E., Cabaleri, N.G., Narváez, P.L., Rosenfeld, U., Scafati, L., Melendi, D.L., 2015. Environmental and climatic proxies for the Cañadón asfalto and Neuquén Basins (Patagonia, Argentina): Review of middle to upper jurassic continental and near coastal sequences. Rev. Bras. Paleontol. 18, 71–82. https://doi.org/10.4072/rbp.2015.1.04

Wagner, T., Petsh, T., 1999. Tectono-sedimentary controls on Cretaceous black shale deposition along the opening Equatorial Atlantic Gateway (ODP Leg 159), in: Cameron, N.R., Bate, R.H., Clure, V.S. (Eds.), The Oil and Gas Habitats of the South Atlantic. Geological Society of London Special Publications 153, London, England, pp. 241–265.

Watts, A.B., 2012. Models for the evolution of passive margins, Regional Geology and Tectonics: Phanerozoic Rift Systems and Sedimentary Basins. Elsevier B.V. https://doi.org/10.1016/B978-0-444-56356-9.00002-X

Watts, A.B., 1989. Lithospheric flexure due to prograding sediment loads: implication for the origin of onlap/offlap patterns in sedimentary basins. Basin Res. 2, 133–144.

Watts, A.B., 1988. Gravity anomalies, crustal structure and flexure of the lithosphere at the Baltimore canyon trough. Earth Planet. Sci. Lett. 89, 221–238.

Watts, A.B., Ryan, W.B.F., 1976. Flexure of the lithosphere and continental margin basins. Tectonophysics 36, 25–44.

Webster, R.E., Chebli, G.A., Fischer, J.F., Webster, R.E., Oil, H., Field, R., 2004. General Levalle basin , Argentina : A frontier Lower Cretaceous rift basin 5, 627–652.

Welsink, H.J., 2010. Regional Tectono-Stratigraphic Framework. Offshore Argentina. Buenos Aires.

Wernicke, B., 1985. Uniform-sense normal simple shear of the continental lithosphere. Can. J. Earth Sci. 22, 108–125. https://doi.org/10.1139/e85-009

Wernicke, B., 1981. Low-angle normal faults in the Basin and Range province: nappe tectonics in anextending orogen. Nature 291, 645–648.

White, R.S., Mckenzie, D., 1989. Magmatism at rift zones: The generation of volcanic continental margins and flood basalts. J. Geophys. Res. Solid Earth 94, 7685–7729.

Whitmarsh, R.B., Manatschal, G., 2012. Evolution of magma poor continental margins: From rifting to the onset of seafloor spreading, in: Regional Geology and Tectonics. pp. 326–341. https://doi.org/10.1016/B978-0-444-56357-6.00008-1

Will, T.M., Frimmel, H.E., 2018. Where does a continent prefer to break up ? Some lessons from the South Atlantic margins. Gondwana Res. 53, 9–19. https://doi.org/10.1016/j.gr.2017.04.014

Willner, A.P., Herve, F., Massonne, H.J., 2000. Mineral Chemistry and Pressure – Temperature Evolution of Two Contrasting High- pressure – Low-temperature Belts in the Chonos Archipielago, Southern Chile. J. Petrol. 41, 309–330.

Withjack, M., Schlisde, R., Olsen, P., 1999. Diachronus rifting, drifting, and inversion on the passive margin of eastern North America: An analog for other passive margins. AAPG Bullettin 82, 817–835. https://doi.org/10.1306/1D9BC60B-172D-11D7-8645000102C1865D

Withjack, M.O., Schlische, R.W., Olsen, P.E., 2012. Development of the passive margin of Eastern North America: Mesozoic rifting, igneous activity, and breakup, Regional Geology and Tectonics: Phanerozoic Rift Systems and Sedimentary Basins. Elsevier B.V. https://doi.org/10.1016/B978-0-444-56356-9.00012-2

Yrigoyen, M.R., 1975. Geologia del subsuelo y la plataforma continental, in: Geología de La Provincia de Buenos Aires, 6th Argentinean Geological Congress, Bahía Blanca. pp. 139–168.

Zaffarana, C.B., Somoza, R., López De Luchi, M.G., 2014. The Late Triassic Central Patagonian Batholith: Magma hybridization , 40Ar/39Ar ages and thermobarometry. J. South Am. Earth Sci. 55, 94–122. https://doi.org/10.1016/j.jsames.2014.06.006

Zambrano, J.J., 1980. Comarca de la cuenca cretacica de Colorado. pp. 1033–1070.

Zambrano, J.J., Urien, C.M., 1970. Geological outline of the basins in southern Argentina and their continuation off the Atlantic. J. Geopysical Res. 75, 1363–1369.

Zborowski, M., 2018. ExxonMobil's Eighth Discovery off Guyana adds another development possibility. J. Pet. Technol.

Zerfass, H., Chemale, F., Lavina, E., 2005. Tectonic control of the Triassic Santa Maria supersequence of the Paraná Basin, southernmost Brazil, and its correlation to the Waterberg Basin, Namibia. Gondwana Res. 8, 163–176. https://doi.org/10.1016/S1342-937X(05)71115-1

Zerfass, H., Chemale, F., Schultz, C.L., Lavina, E., 2004. Tectonics and sedimentation in Southern South America during Triassic. Sediment. Geol. 166, 265–292. https://doi.org/10.1016/j.sedgeo.2003.12.008

Zerfass, H., Lavina, E.L., Schultz, C.L., Garcia, A.J.V., Faccini, U.F., Chemale, F., 2003. Sequence stratigraphy of continental Triassic strata of Southernmost Brazil: A contribution to Southwestern Gondwana palaeogeography and palaeoclimate. Sediment. Geol. 161, 85–105. https://doi.org/10.1016/S0037-0738(02)00397-4

Zhang, N., Dang, Z., Huang, C., Li, Z.-X., 2018. The dominant driving force for supercontinent breakup : Plume push or subduction retreat? Geosci. Front. 1–11.

https://doi.org/10.1016/j.gsf.2018.01.010

Zou, H., Fan, Q., Yao, Y., 2008. U-Th systematics of dispersed young volcanoes in NE China: astenosphere upwelling caused by pilling up and upward thickening of stagnant Pacific slab. Chem. Geol. 255, 134–142.

.

Table des illustrations

Table des tableaux

APPENDIX 1

AMEGHINIANA
A GONDWANAN PALEONTOLOGICAL JOURNAL

A NEW DINOFLAGELLATE FROM THE LATE CRETACEOUS OF THE COLORADO BASIN, OFF SHORE ARGENTINA

EDUARDO G. OTTONE[1]
JUAN P. LOVECCHIO[2]
JUAN P. PÉREZ-PANERA[3]
DIANA RONCHI[4]

[1]CONICET - Universidad de Buenos Aires. Instituto de Estudios Andinos Don Pablo Groeber (IDEAN). Departamento de Ciencias Geológicas, Facultad de Ciencias Exactas y Naturales, Pabellón II Ciudad Universitaria, C1428EHA, Buenos Aires, Argentina.
[2]YPF S.A., Gerencia de Exploración Offshore, Av. Macacha Güemes 515, Puerto Madero, C1106BKK Buenos Aires, Argentina.
[3]CONICET - Laboratorio de Bioestratigrafía, Gerencia de Geociencias, YPF Tecnología S.A., Avenida del Petróleo Argentino s/n entre 129 y 143, CP 1923, Berisso, Buenos Aires - Cátedra de Micropaleontología, División Paleozoología Invertebrados, Museo de La Plata, Paseo del Bosque s/n, La Plata, CP 1900, Buenos Aires, Argentina.
[4]GEMA SRL - Laboratorio de Bioestratigrafía, Gerencia de Geociencias, YPF Tecnología S.A., Avenida del Petróleo Argentino s/n entre 129 y 143, CP 1923, Berisso, Buenos Aires, Argentina.

Submitted: June 29th, 2017 - **Accepted:** January 10th, 2018 - **Published online:** February 9th, 2018

To cite this article: Eduardo G. Ottone, Juan P. Lovecchio, Juan P. Pérez-Panera, and Diana Ronchi (2018). A new dinoflagellate from the Late Cretaceous of the Colorado Basin, off shore Argentina. *Ameghiniana* 55: 343–349.

To link to this article: http://dx.doi.org/10.5710/AMGH.10.01.2018.3129

AMEGHINIANA - 2018 - Volume 55 (3): 343–349 PALEONTOLOGICAL NOTES

ISSN 0002-7014

A NEW DINOFLAGELLATE FROM THE LATE CRETACEOUS OF THE COLORADO BASIN, OFF SHORE ARGENTINA

EDUARDO G. OTTONE[1], JUAN P. LOVECCHIO[2], JUAN P. PÉREZ-PANERA[3], AND DIANA RONCHI[4]

[1]CONICET - Universidad de Buenos Aires. Instituto de Estudios Andinos Don Pablo Groeber (IDEAN). Departamento de Ciencias Geológicas, Facultad de Ciencias Exactas y Naturales, Pabellón II Ciudad Universitaria, C1428EHA, Buenos Aires, Argentina. *ottone@gl.fcen.uba.ar*

[2]YPF S.A., Gerencia de Exploración Offshore, Av. Macacha Güemes 515, Puerto Madero, C1106BKK Buenos Aires, Argentina. *juan.lovecchio@ypf.com*

[3]CONICET - Laboratorio de Bioestratigrafía, Gerencia de Geociencias, YPF Tecnología S.A., Avenida del Petróleo Argentino s/n entre 129 y 143, CP 1923, Berisso, Buenos Aires – Cátedra de Micropaleontología, División Paleozoología Invertebrados, Museo de La Plata, Paseo del Bosque s/n, La Plata, CP 1900, Buenos Aires, Argentina. *juan.p.panera@ypftecnologia.com*

[4]GEMA SRL - Laboratorio de Bioestratigrafía, Gerencia de Geociencias, YPF Tecnología S.A., Avenida del Petróleo Argentino s/n entre 129 y 143, CP 1923, Berisso, Buenos Aires, Argentina. *dianaines.ronchi@set.ypf.com*

An extensive search for new source rocks and hydrocarbon accumulations has been carried out over the past 50 years by different oil companies in the main southwest Atlantic basins. To achieve this exploration prospect, a lot of boreholes have been drilled, mostly offshore, in the Colorado and the Salado and Punta del Este basins (Fig. 1). In this framework, several biostratigraphic studies were carried out to the better understand of the different phases of the depositional history and the evolution of these basins. The purpose of this contribution is to improve the palynological knowledge of the Colorado Basin and to introduce a new species that is considered important from a biostratigraphic point of view.

GEOLOGICAL BACKGROUND

The Colorado Basin, as other Southwest Atlantic basins (*e.g.*, Punta del Este, Salado and Rawson basins), was originated in relation to the breakup of Gondwana during the Jurassic–Early Cretaceous (Fryklund *et al.*, 1996; Juan *et al.*, 1996; Gerster *et al.*, 2011). The breakup unconformity (dated Barremian–Aptian) marks the onset of the passive margin stage, with some thermal subsidence that was accentuated in a west-east oriented trough, which was, in turn, controlled by synrift depocenters (Fig. 1). In the areas known by means of hydrocarbon exploration drilling, the sedimentation throughout the Late Cretaceous took place in fluvial to coastal and marine-shelf environments (sandstones from the Colorado Formation). A major marine transgression is recorded in the overlying marine shales of the Pedro Luro Formation, interbedded with volcanic rocks of the Ranquel Formation on the southern margin of the basin (Lesta *et al.*, 1978; Lovecchio *et al.*, 2017).

BIOSTRATIGRAPHIC SETTING

The biostratigraphy (dinocysts and calcareous nannofossils) of the YPF.BB-I-B.x-1, Bahía Blanca well and YPF.CCMI.Ra.x-1, Ranquel well are shown in Fig. 2.

The main previously published palynological contributions dealing with Cenozoic dinoflagellate cysts assemblages from the Colorado Basin include: Gamerro and Archangelsky (1981), Guerstein (1990, a, b), Archangelsky (1996), Quattrocchio and Sarjeant (1996), Guerstein and Guler (2000), Guerstein and Junciel (2001), Guerstein *et al.* (2001) and Daners *et al.* (2016).

Late Cretaceous–Paleocene dinoflagellate cysts from the Pedro Luro Formation have been documented in the papers by Gamerro and Archangelsky (1981), Archangelsky (1996), Quattrocchio and Sarjeant (1996), Guerstein and Junciel (2001) and Guerstein *et al.* (2005).

No palynological publications dealing with the Colorado Formation are known.

MATERIALS AND METHODS

This paper is based on the analysis of cutting and core

samples recovered from the YPF.BB-I-B.x-1, Bahía Blanca well, and the YPF.CCMI.Ra.x-1, Ranquel well, both drilled on the Argentine continental shelf (Fig. 1).

The herein studied material from the Colorado Formation was mainly recovered from cutting samples 2560–2570 m, and 2950–2665 m from the YPF.BB-I-B.x-1, Bahía Blanca well, and 2279–2291 m of the YPF.CCMI.Ra.x-1, Ranquel well. Laboratory procedures followed conventional practices. Carbonates and silicates were removed by a hydrochloric and hydrofluoric acid treatment. Residues were sieved on a 10 µm mesh and mounted in unstained glycerin jelly on glass slides. Specimens were examined under a Leitz Orthoplan binocular microscope. Photomicrographs were taken with a Sony Cyber-shot DSC-P93A camera. Palynological slides are prefixed YT.RMP. The illustrated specimens are identified with a slide number and England Finder coordinates. The slides are stored at the Biostratigraphy Laboratory, Geoscience Management, YPF Tecnología. The terms used for the characterization for the shape and indexes of the dinoflagellate archeopyle follow the schemes by Evitt (1985).

SYSTEMATIC PALEONTOLOGY

Division Dinoflagellata (Bütschli, 1885) Fensome *et al.*, 1993
Subdivision Dinokaryota Fensome *et al.*, 1993
Class Dinophyceae Pascher, 1914
Subclass Peridiniphycidae Fensome *et al.*, 1993
Order Peridiniales Haeckel, 1894
Suborder Peridiniineae Autonym
Family Peridiniaceae Ehrenberg, 1831
Subfamily Deflandreoideae Bujak and Davies, 1983

Genus ***Andalusiella*** Riegel, 1974 emend.
Masure *et al.*, 1996

Type species. *Andalusiella mauthei* Riegel, 1974.

Andalusiella guersteiniae sp. nov.
Figure 3.1–4

Derivation of name. Named after Dr. Raquel Guerstein, in recognition of her contribution to the knowledge of fossil dinoflagellates.

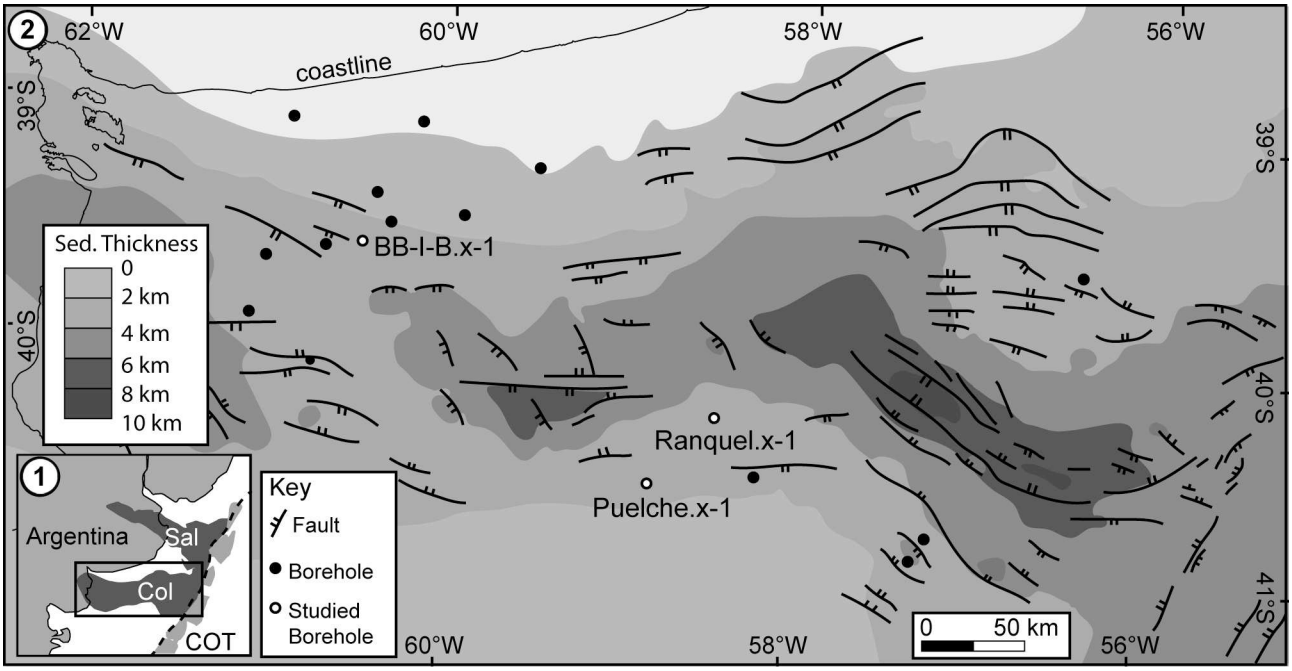

Figure 1. 1, The Colorado (**Col**) and Salado (**Sal**) basins. **COT,** Continental-Oceanic crust Transition zone. **2,** Basemap for the Colorado basin depicting the main depocenters and the location of the Bahía Blanca.B.x-1 well, Puelche.x-1 well and Ranquel.x-1 well. Modified after Lovecchio *et al.* (in press).

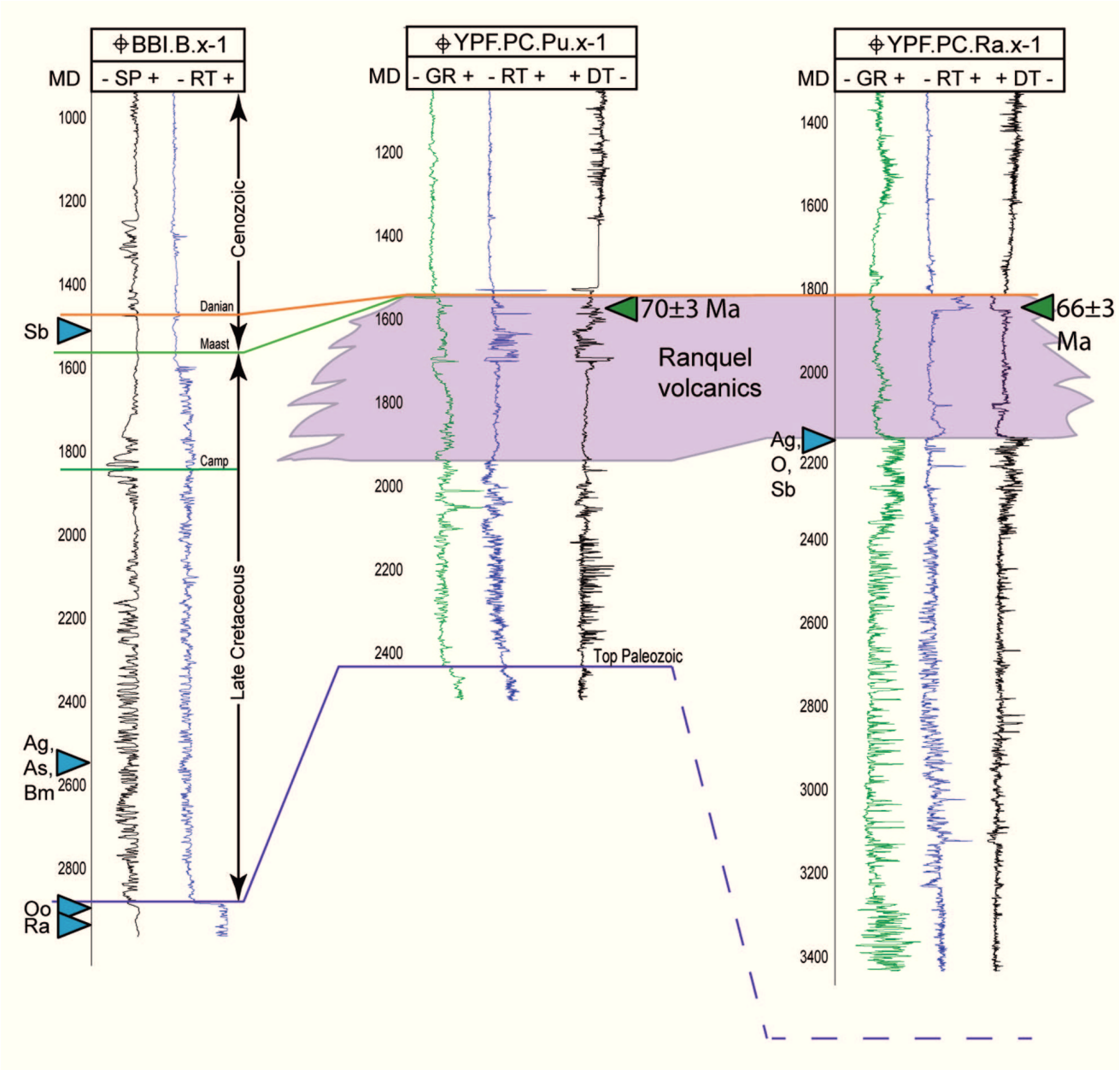

Figure 2. Schematic stratigraphic sections of the Bahía Blanca.B.x-1 well, Puelche.x-1 well and Ranquel.x-1 well, showing the last occurrence (left arrows) of *Andalusiella guersteinae* sp. nov.; Abbreviations: **Ag,** and key associated species (dinocysts and calcareous nannofossils: **Sb,** *Senegalinium bicavatum*; **As,** *Acuturris scouts*; **Bm,** *Biscutum magnum*; **Oo,** *Odontochitina operculata*; **Ra,** *Reinhardtites anthophorus*; **O,** *Odontochitina* spp.), radiometric ages (right arrows) and tentative correlations. **MD,** Measured Depth; **SP,** Spontaneous Potential; **RT,** Resistivity Log; **GR,** Gamma Ray; **DT,** Sonic Log; **Danian,** top Danian; **Maast,** top Maastrichtian; **Camp,** top Campanian. Modified from Lovecchio *et al.* (2017).

Type material. Well: YPF.BB-I-B.x-1, Bahía Blanca (2560–2570 m), slide: YT.RMP– P.000002.17(1), England Finder Graticule: O41/0.

Geographic occurrence. Bahía Blanca.B.x-1 well, and Ranquel.x-1 well, Colorado Basin.

Stratigraphic occurrence. Late Campanian–Early Maastrichtian of the Colorado Formation.

Diagnosis. Proximate, acrocavate organic-walled dinoflagellate cyst, with a rhomboidal to ellipsoidal central body lengthened by a long apical horn and a single undivided an-

tapical horn. Wall composed of a periphragm and an endophragm, the latter extends into the horns. A peridinioid paratabulation is suggested by the intercalary 2a hexa isodeltaform archeopyle and a paracingulum. Parasulcus with a flagellar scar.

Description. Long cyst with a rhomboidal to ellipsoidal central body. The apical horn is longer than the single undivided antapical horn which is the left one. The periphragm is smooth to chagrinate and markedly thinner than the endophragm. The endophragm develops thickenings in horn areas. The wall of the endophragm is smooth. The periphragm and the endophragm are closely pressed on the central body. The paracingulum is currently bordered by folds. The parasulcus bears a flagellar scar. Intercalary archeopyle 2a hexa, iso-deltaform. The operculum is adherent or free.

Dimensions. (19 specimens) Overall length 185 (196) 208 µm, overall width 70 (81) 91 µm, apical horn 41–67 µm, antapical horn 36–38 µm, overall length/wide ratio ≈ 2.5–2.8, endophragm length/wide ratio ≈ 1.2–1.6, apical/antapical horns ratio ≈ 1.1–1.7, archeopyle ratio (**AR**) ≈ 1, archeopyle signum (**AS**) = 0.3–0.6, transverse archeopyle index = 0.5, longitudinal archeopyle index = 0.7.

Comparisons. *Andalusiella guersteiniae* sp. nov. is distinguishable from most species that have two or divided antapical horns as described by Masure *et al.* (1996) and Srivastava (1995). In contrast, *Andalusiella guersteiniae* sp. nov. should be compared to species that only have a single undivided antapical horn as: *A. rhomboides, A. spinosa* and *A. basita.* All these species have shorter horns that are proportional to the central body, however, *A. rhomboides* and *A. spinosa* show an ornamented periphragm, verrucose in *A. rhomboides,* spiny in *A. spinosa*. *Andalusiella guersteiniae* sp. nov. differs from *A. basita* by virtue of its much more thickened endophragm, its apical and antapical horns of unequal length, the presence of a paracingulum and of a distinct flagellar scar, and by reaching a markedly larger size. Close comparison of *A. guersteiniae* sp. nov. with specimens from the Campanian of offshore Mauritania, referred to as *A. polymorpha* by Malloy (1972) is hindered by the fact that the African material has not been described.

BIOSTRATIGRAPHICAL RESULTS

In the YPF.BB-I-B.x-1, Bahía Blanca well and YPF.CCMI. Ra.x-1, Ranquel well, the stratigraphic associated species to *Andalusiella guersteiniae* sp. nov. (Fig. 2) that have the following ranges include: *Odontochitina costata* (Early San-

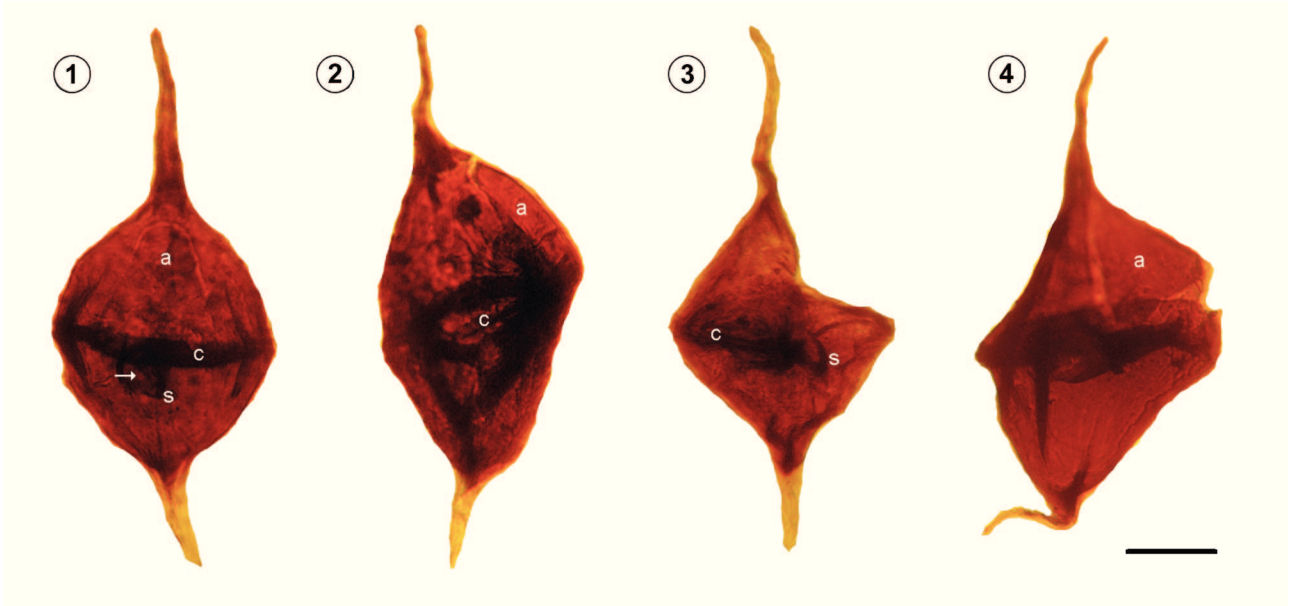

Figure 3. ***Andalusiella guersteiniae*** sp. nov. **1,** YT.RMP–P.000002.17(1) O41/0, Holotype (Bahía Blanca.B.x-1 well, 2560–2570 m). **2,** YT.RMP–P.000002.17(1) A24/4 (Bahía Blanca.B.x-1 well, 2950–2965 m). **3,** YT.RMP–P.000002.17(7) K41/0, the epicyst of this specimen is broken (Bahía Blanca.B.x-1 well, 2560–-2570 m). **4,** YT.RMP–P.000001.10(1) C39/0 (Ranquel.x-1 well, 2279–2291 m). **a,** archeopyle; **s,** parasulcus; **c,** paracingulum; arrow indicates the flagellar scar. Scale bar= 40 µm.

tonian–Early Maastrichtian: Costa and Davey, 1992), *O. operculata* (Aptian–Early Maastrichtian: Helby *et al.*, 1987; Roncaglia *et al.*, 1999), *O. spinosa* (Santonian–Early Maastrichtian: Wilson, 1984; Roncaglia *et al.*, 1999); *Senegalinium bicavatum* (Campanian–Danian: Jain and Millepied, 1973; Slimani *et al.*, 2010). The stratigraphic range of the species associated to *A. guersteiniae* sp. nov. suggests a Middle Campanian–Early Maastrichtian age.

At the Bahía Blanca.B.x.1 well, the last occurrences (**LO**) of the calcareous nannofossils *Acuturris scotus* and *Biscutum magnum* stand at 2560–2570 m, and the **LO** of *Reinhardtites anthophorus* at 2950–2965 m (recovered with *O. operculata* from the same Paleozoic horizon as a product of cutting contamination by caving during drilling), are of an Early Maastrichtian and Late Campanian age, respectively. At the Ranquel x.1 well, a poorly preserved assemblage of calcareous nannofossils, including *Micula staurophora* and *M. concava* of Santonian–Maastrichtian age was recovered. Conversely, the nannofossil and foraminifer assemblages related to the Late Maastrichtian, overlie the *A. guersteiniae* sp. nov.-bearing horizons at the Bahía Blanca.B.x.1 well (Fig. 2).

Other microfossils recovered from the same stratigraphic levels include a diverse assemblage of agglutinated foraminifers that are typical of the early Maastrichtian of the Salado, the Colorado and the eastern Austral basins (Malumián and Masiuk, 1976; Malumián and Náñez, 1990, 1996; Náñez and Malumián, 2008; Pérez Panera, 2012).

At the Ranquel.x-1 well, the core sample 2156-2162 m (Lovecchio *et al.*, 2017), lacks *A. guersteiniae* sp. nov., but yields *Diconodinium lurense*, an index species from the Late Maastrichtian–Early Danian in southern South America (Guerstein *et al.*, 2005). The last occurrence of *A. guersteiniae* sp. nov., *O. operculata* and *O. spinosa* stand at 2165–2168 m (Fig. 2).

CONCLUSION

Andalusiella guersteiniae sp. nov. is a new species from the Upper Cretaceous of the Colorado Formation, at the Colorado Basin. In account of the restricted, Middle Campanian to Early Maastrichtian, stratigraphic range of key species of palynomorphs, foraminifers and nannofossils associated to *A. guersteiniae* sp. nov., a Middle Campanian–Early Maastrichtian age is suggested for the new species. A $^{40}K/^{40}Ar$ study from the volcanic intercalations of the Ranquel Formation suggests an age of 66 ± 3 Ma. On the other hand, from the same horizons, at the Puelche.x-1 well, a $^{40}Ar/^{39}Ar$ age of 74 ± 0.3 Ma was obtained from a core sample of a trachyandesitic composition (Lovecchio *et al.*, 2017, figs. 1, 2). Therefore, a Late Campanian–Maastrichtian age (66-74 Ma) is assigned to the volcanic Ranquel Formation. As the Ranquel Formation overlies the *A. guersteiniae* sp. nov.-bearing horizons, the species herein described is of Middle Campanian to Early Maastrichtian age. The restricted stratigraphic range of this form, if confirmed in more sections, would make *A. guersteiniae* sp. nov. a good local index species.

ACKNOWLEDGEMENTS

We express our gratitude to YPF S.A. and Y-TEC for allowing the publication of this work. The authors would also thank the suggestions of the editor D. Pol, the reviewer E. Masure and a second anonymous reviewer, who helped improve the quality of this contribution. This research was partially supported by the grants 112 – 201501 – 00613 – CO (Consejo Nacional de Investigaciones Científicas y Técnicas) and Y-TEC IB – 620 (YPF Tecnología, Laboratorio de Bioestratigrafía). This is the contribution R-246 of the Instituto de Estudios Andinos Don Pablo Groeber.

Taxa lists

Dinoflagellate cysts:

Andalusiella basita Slimani *et al.*, 2012

A. rhomboides (Boltenhagen, 1977) Lentin and Williams, 1980 emend. Masure *et al.*, 1996

A. spinosa Guler *et al.*, 2005

Diconodinium lurense Guerstein *et al.*, 2005

Odontochitina costata Alberti, 1961

O. operculata (Wetzel, 1933) Deflandre and Cookson, 1955

O. spinosa Wilson, 1984

Senegalinium bicavatum Jain and Millepied, 1973

Calcareous nannofossils:

Acuturris scotus (Risatti, 1973) Wind and Wise in Wise and Wind, 1977

Biscutum magnum Wind and Wise in Wise and Wind, 1977

Micula staurophora (Gardet, 1955) Thierstein, 1974

M. concava (Stradner in Martini and Stradner, 1960) Verbeek, 1976

Reinhardtites anthophorus (Deflandre, 1959) Perch-Nielsen, 1968

REFERENCES

Alberti, G. 1961. Zur Kenntnis mesozoischer und alttertiärer Dinoflagellaten und Hystrichosphaerideen von Nord- und Mitteldeutschland sowie einigen anderen Europäischen Gebieten. *Palaeontographica, Abteilung A* 116: 1–58.

Archangelsky, S. 1996. Palinoestratigrafía de la plataforma continental. In: V.A. Ramos, and M.A. Turic (Eds.), *Geología y recursos naturales de la plataforma continental argentina. Relatorio del 13° Congreso Geológico Argentino y 3° Congreso de Exploración de Hidrocarburos* (Buenos Aires), p. 67–72.

Boltenhagen, E. 1977. *Microplancton du Cretacé supérieur du Gabon*. Cahiers de Paléontologie CNRS, Paris, 150 p.

Bujak, J.P., and Davies, E.H. 1983. *Modern and fossil Peridiniieae*. American Association of Stratigraphic Palynologists, Contribution Series 13, Dallas, 203 p.

Bütschli, O. 1885. Erster Band. Protozoa. In: *Dr. H.G. Bronn's Klassen und Ordnungen des Their-Reichs, wissenschafaftlich dargestellt in Wort und Bild.* C.F. Winter'sche Verlagshandlung, Leipzig and Heidelberg, p. 865–1088.

Costa, L.I., and Davey, R.J. 1992. Dinoflagellate cysts of the Cretaceous System. In: A.J. Powell (Ed.), *A stratigraphic index of dinoflagellate cysts*, Kluwer Academic Publishers, Dordrecht, p. 99–153.

Daners, G., Guerstein, G.R., Amenábar, C.R., and Morales, E. 2016. Dinoflagelados del Eoceno medio a tardío de las cuencas Punta del Este y Colorado, latitudes medias del atlántico sudoccidental. *Revista Brasileira de Paleontologia* 19: 281–300.

Deflandre, G. 1959. Sur les nannofosiles calcaires et leur systématique. *Revue de Micropaléontologie* 2: 127–152.

Deflandre, G., and Cookson, I.C. 1955. Fossil microplankton from Australian late Mesozoic and Tertiary sediments. *Australian Journal of Marine and Freshwater Research* 6: 242–313.

Ehrenberg, C.G. 1831. Zoologica II, *Phytozoa*, Icones et descriptiones animalium evertebratorum sepositis insectis. In: F.C. Hemprich, and C.G. Ehrenberg (Eds.), *Symbolae physicae seu icons et descriptiones corporum naturalium novorum aus minus cognitorum quae ex itineribus per Libiam Aegyptum Nubiam Dongalam Syriam Arabiam et Abessiniam.* Berlin, 128 p.

Evitt, W.R. 1985. *Sporopollenin dinoflagellate cysts: their morphology and interpretation.* American Association of Stratigraphic Palynologists Foundation, Dallas, 333 p.

Fensome, R.A., Taylor, F.J.R., Norris, G., Sarjeant, W.A.S., Wharton, D.I., and Williams, G.L. 1993. *A classification of living and fossil dinoflagellates.* Micropaleontology Special Publication 7, Salem, viii, 351 p.

Fryklund, B., Marshall, A., and Stevens, J. 1996. Cuenca del Colorado. In: V.A. Ramos, and M.A. Turic (Eds.), *Geología y Recursos Naturales de la Plataforma Continental Argentina. Relatorio del 13° Congreso Geológico Argentino y 3° Congreso de Exploración de Hidrocarburos* (Buenos Aires): 135–158.

Gamerro, J.C., and Archangelsky, S. 1981. Palinozonas neocretácicas y terciarias de la plataforma continental argentina en la Cuenca del Colorado. *Revista Española de Micropaleontología* 13: 119–140.

Gardet, M. 1955. Contribution à l'étude des coccolithes des terrains néogènes de l'Algérie. *Publications du Service de La Carte Géologique de l'Algérie (Nouvelle Série)* 5: 477–550.

Gerster, R., Welsink, H., Ansa, A., and Raggio, F. 2011. Cuenca de Colorado. In: E. Kozlowsky, L. Legarreta, A. Boll, and P. Marshall (Eds.), *Simposio Cuencas Argentinas. 8° Congreso de Exploración y Desarrollo de Hidrocarburos*, *IAPG* (Mar del Plata): 65–80.

Guerstein, G.R. 1990a. Palinología estratigráfica del Terciario de la Cuenca del Colorado, República Argentina. Parte II : Especies marinas de la perforación Nadir N.° 1. *Revista Española de Micropaleontología* 22: 167–182.

Guerstein, G.R. 1990b. Palinología estratigráfica del Terciario de la Cuenca del Colorado, República Argentina. Parte III : Estudio sistemático y estadístico de la perforación Puerto Belgrano N.° 20. *Revista Española de Micropaleontología* 22: 459–480.

Guerstein, G.R., and Guler, M.V. 2000. Bioestratigrafía basada en quistes de dinoflagelados del Eoceno-Mioceno del pozo (YPF) Ombucta x-1, Cuenca del Colorado, Argentina. *Ameghiniana* 37: 81–90.

Guerstein, G.R., and Junciel, G.L. 2001. Quistes de dinoflagelados del Cenozoico de la Cuenca del Colorado, Argentina. *Ameghiniana* 38: 299–316.

Guerstein, G.R., Williams, G.L., and Fensome, R.A. 2001. *Cannosphaeropsis quattrocchiae*, a new species of dinoflagellate cyst from the mid Cenozoic of the Colorado Basin, Argentina. *Micropaleontology* 47: 155–167.

Guerstein, G.R., Junciel, G.L., Guler, M.V., and Daners, G. 2005. *Diconodinium lurense* sp. nov., a late Maastrichtian to Danian dinoflagellate cyst from southwest Atlantic basisn. *Ameghiniana* 42: 329–338.

Guler, M.V., Guerstein, G.R., and Casadío, S. 2005. New dinoflagellate cyst species from the Calafate Formation (Maastrichtian), Austral Basin, Argentina. *Ameghiniana* 42: 419–428.

Haeckel, E. 1894. *Systematische Phylogenie. Entwurf eines natüralischen Systems der Organismen auf Grund ihrer Stammegeschichte, I. Systematische Phylogenie der Protisten und Pflanzen.* Reimer, Berlin, xv, 400 p.

Helby, R., Morgan, R., and Partridge, A.D. 1987. A palynological zonation of the Australian Mesozoic. *Memoirs of the Association of Australasian Palaeontologists* 4: 1–94.

Jain, K.P., and Millepied, P. 1973. Cretaceous microplankton from Senegal Basin, N.W. Africa. I. Some new genera species and combinations of dinoflagellates. *The Palaeobotanist* 20: 22–35.

Juan, R.C., De Jager, J., Russell, J., and Gebard, I. 1996. Flanco norte de la Cuenca del Colorado. In: V.A. Ramos, and M.A. Turic (Eds.), *Geología y Recursos Naturales de la Plataforma Continental Argentina. Relatorio del 13° Congreso Geológico Argentino y 3° Congreso de Exploración de Hidrocarburos* (Buenos Aires): 117–133.

Lentin, J.K., and Williams, G.L. 1980. *Dinoflagellate provincialism with emphasis on Campanian Peridiniaceans.* American Association of Stratigraphic Palynologists, Contribution Series 7, Dallas, 47 p.

Lesta, P.J., Turic, M.A., and Mainardi, E. 1978. Actualización de la información estratigráfica en la Cuenca del Colorado. *7° Congreso Geológico Argentino* (Neuquén), *Actas* 1: 701–713.

Lovecchio, J.P., Kress, P.R., Rodríguez, E., Flores, G., Gerster, R., Bolatti, N.D., Rohais, S., and Ramos, V.A. 2017. Caracterización del campo volcánico Ranquel, Cuenca de Colorado, Plataforma Continental Argentina. *20° Congreso Geológico Argentino* (San Miguel de Tucumán), *Actas* (Sección Técnica 8 Volcanología): 74–80.

Lovecchio, J.P., Rohais, S., Joseph, P., Bolatti, N., Kress, P., Gerster, R., and Ramos, V.A. in press. Multi-stage rift evolution of the Colorado basin (offshore Argentina): Evidence for extensional settings prior to the South Atlantic opening. *Terra Nova.*

Malloy, R.E. 1972. An Upper Cretaceous dinoflagellate cyst lineage from Gabon, West Africa. *Geoscience and Man* 4: 57–65.

Malumián, N., and Masiuk, V. 1976. Foraminíferos de la Formación Cabeza de León (Cretácico Superior, Tierra del Fuego, Rep. Argentina). *Revista de la Asociación Geológica Argentina* 31: 180–202.

Malumián, N., and Náñez, C. 1990. Foraminíferos aglutinados del Cretácico Superior de cuenca Austral (Provincia de Santa Cruz), Argentina. In: W. Volkheimer (Ed.), *Bioestratigrafía de los Siste-*

mas regionales del Jurásico y Cretácico de América del Sur. Comité Sudamericano del Jurásico y Cretácico 2, Mendoza, p. 497–55.

Malumián, N., and Náñez, C. 1996. Microfósiles y nanoplancton calcáreo de la Plataforma Continental. In: V.A. Ramos, and M.A. Turic (Eds.), *Geología y Recursos Naturales de la Plataforma Continental Argentina. Relatorio del 13° Congreso Geológico Argentino y 3° Congreso de Exploración de Hidrocarburos* (Buenos Aires): 73–93.

Martini, E., and Stradner, H. 1960. Nannotetraster, eine stratigraphisch bedeutsame neue Discoasteriden gattung. *Erdöel-Zeitschritf* 76: 266–270.

Masure, E., Tea, J., and Yao, R. 1996. The dinoflagellate *Andalusiella*: emendation of the genus, revision of species, *A. ivoriensis* Masure, Tea and Yao, *sp. nov. Review of Palaeobotany and Palynology* 91: 171–186.

Náñez, C., and Malumián, N. 2008. Paleobiogeografía y paleogeografía del Maastrichtiense marino de la Patagonia, Tierra del Fuego y la Plataforma Continental Argentina, según sus foraminíferos bentónicos. *Revista Española de Paleontología* 23: 273–300.

Pascher, A. 1914. Über Flagellaten und Algen. *Berichte der Deutsche Botanische Gesellschaft* 32: 136–160.

Perch-Nielsen, K. 1968. Der Feinbau und die Klassifikation der Coccolithen aus dem Maastrichtien von Dänemark. *Detkongelige Danske Videnskabernes Selskab Biologiske Skrifter* 16: 1–93.

Pérez-Panera, J.P. 2012. Nanofósiles calcáreos y bioestratigrafía del Cretácico del sudeste de la Cuenca Austral, Patagonia, Argentina. *Ameghiniana* 49: 137–163.

Quattrocchio, M.E., and Sarjeant, W.A.S. 1996. Early Palaeocene (Danian) dinoflagellates from the Colorado Basin Argentina. *Revista Española de Micropaleontología* 38: 111–138.

Riegel, W. 1974. New forms of organic-walled microplankton from an Upper Cretaceous assemblage in southern Spain. *Revista Española de Micropaleontología* 6: 347–386.

Risatti, J.B. 1973. Nannoplankton biostratigraphy of the Upper Bluffport Marl-Lower Prairie Bluff Chalk interval (upper Cretaceous) in Mississippi. In: L.A. Smith, and J. Hardenbol (Eds.) *Proceedings of the Symposium on Calcareous Nannofossils. Gulf Coast Section, SEPM (Society for Sedimentary Geology) Special Publication*: 8–57.

Roncaglia, L., Field, B.D., Raine, J.L., Schiøler, P., and Wilson, G.J. 1999. Dinoflagellate biostratigraphy of Piripauan–Hamurian (Upper Cretaceous) sections from northeast South Island, New Zealand. *Cretaceous Research* 20: 271–314.

Slimani, H., Louwye, S., and Toufiq, A. 2010. Dinoflagellate cysts from the Cretaceous–Paleogene boundary at Ouled Haddou, southeastern Rif, Morocco: biostratigraphy, paleoenvironments and paleobiogeography. *Palynology* 34: 90–124.

Slimani, H., Louwye, S., and Toufiq, A. 2012. New species of organic-walled dinoflagellate cysts from the Maastrichtian–Danian boundary interval at Ouled Haddou, northern Morocco. *Alcheringa* 36: 341–358.

Srivastava, S.K. 1995. Dinocyst biostratigraphy of Santonian–Maastrichtian formations of the Western Gulf Coastal Plain, southern United States. *The Palaeobotanist* 42: 249–362.

Thierstein, H.R. 1974. Calcareous nannoplankton - Leg 26, Deep Sea Drilling Project. *Initial Reports of the Deep Sea Drilling Project* 26: 619–667.

Verbeek, J.W. 1976. Upper Cretaceous nannoplankton zonation in a composite section near El Kef, Tunisia. *Proceedings of the Koninklijke Nederlandse Akademie van Wetenschappen B* 79: 129–148.

Wetzel, O. 1933. Die in organischer Substanz erhaltenen Mikrofossilien des baltischen Kreide-Feuersteins mit einem sediment-petrographischen und stratigraphischen Anhang. *Palaeontographica, Abteilung A* 78: 1–110.

Wilson, G.J. 1984. Some new dinoflagellate species from the New Zealand Hamurian and Pripauan Stages (Santonian-Maastrichtian, Late Cretaceous). *New Zealand Journal of Botany* 22: 549–556.

Wise, S.W., and Wind, F.H. 1977. Mesozoic and Cenozoic calcareous nannofossils recovered by DSDP Leg 36 drilling on the Falkland Plateau, south-west Atlantic sector of the Southern Ocean. *Initial Reports of the Deep Sea Drilling Project* 36: 269–491.

doi: 10.5710/AMGH.10.01.2018.3129

Submitted: June 29th, 2017
Accepted: January 10th, 2018
Published online: February 9th, 2018

APPENDIX 2

CARACTERIZACIÓN DEL CAMPO VOLCÁNICO CAMPANIANO-PALEOCENO DE LA CUENCA DEL COLORADO, PLATAFORMA CONTINENTAL ARGENTINA

Juan Pablo LOVECCHIO[1], Pedro R. KRESS[1], Elizabeth RODRÍGUEZ[2], Gonzalo FLORES[1], Ricardo GERSTER[1], Néstor D. BOLATTI[1], Sébastien ROHAIS[3], Víctor A. RAMOS[4]

[1] YPF S.A. Gerencia de Exploración Offshore. E-mail: juan.lovecchio@ypf.com
[2] Y-TEC. Laboratorio de Sedimentología y Petrografía
[3] IFPEN, Direction Géosciences
[4] IDEAN, UBA-CONICET

RESUMEN

El campo volcánico de Ranquel, emplazado en el flanco sur de la cuenca de Colorado está compuesto de rocas volcánicas y volcaniclásticas, intercaladas con los depósitos marinos transgresivos de la Formación Pedro Luro (Campaniano-Paleoceno). Se describieron facies de peperitas, que registran procesos de interacción de lava con sedimentos marinos someros inconsolidados. Los análisis geoquímicos permiten asignar estas rocas a basaltos alcalinos de intraplaca, emplazados durante la fase de *sag* de la cuenca.

Palabras clave: Peperita, basalto, volcanismo, subácueo, Cretácico.

ABSTRACT

Characterization of the Ranquel volcanic field, Colorado basin, Argentinian continental shelf. The Ranquel volcanic field, located on the southern flank of the Colorado basin is formed of volcanic and volcaniclastic rocks, interbedded within the marine transgressive deposits of the Pedro Luro Formation (Campanian-Paleocene). Peperite facies were described, recording processes of interaction between lava and unconsolidated shallow-marine sediments. The geochemical analyses relate these rocks to alkaline within-plate basalts, emplaced during the sag phase.

Keywords: Peperite, basalt, volcanism, subaqueous, Cretaceous.

INTRODUCCIÓN

La cuenca de Colorado es una cuenca extensional emplazada en la plataforma y talud continental argentinos. Tiene una orientación general E-O, desarrollándose entre los 39° y 41° latitud Sur y entre 56° y 63° de longitud Oeste. Está limitada al norte por el alto de Tandilia y al sur por el alto de Rawson (Fig. 1). Consta de tres depocentros principales (occidental, central y oriental), de los cuales el oriental es el más profundo, alcanzando 12 km de espesor sedimentario total.

Esta cuenca de rift mesozoica se emplazó sobre un sustrato previo de edad paleozoica tardía (Lesta et al. 1978), producto de esfuerzos extensionales ocurridos con anterioridad a la apertura del Atlántico Sur (Gerster et al. 2011). Se distinguen al menos dos eventos extensionales (Lovecchio et al. 2016). La última fase de *sag* habría sido interrumpida por la discordancia de ruptura continental *(break-up unconformity)* que inició la apertura del océano Atlántico Sur en el Barremiano-Aptiano. A partir de ese momento se desarrolla la fase de deriva (*drift)*, marcada por subsidencia térmica en los depocentros principales. El relleno estratigráfico corresponde a secuencias mayormente continentales fluviales, con una línea de costa ubicada en la parte oriental, en transición a facies marinas. La estratigrafía sísmica permitió detectar distintas transgresiones. A partir del Campaniano se registra una transgresión marina mayor (Fig. 1b) que, en varios pulsos, se extiende hasta el Paleoceno temprano (Daniano). Estas condiciones se mantuvieron el resto del Cenozoico.

El hallazgo de rocas piroclásticas y basaltos intercalados con los depósitos de la transgresión Campaniana-Daniana de la Formación Pedro Luro fue informado por Lesta et al. (1978). En una revisión de la estratigrafía de la cuenca, describieron el hallazgo de rocas extrusivas en la perforación de los pozos Puelche y Ranquel, perforados por YPF en 1977 en el flanco sur (Fig. 1). El objetivo de dichos sondeos estaba marcado por anomalías con tope convexo identificadas en las líneas sísmicas dispo-

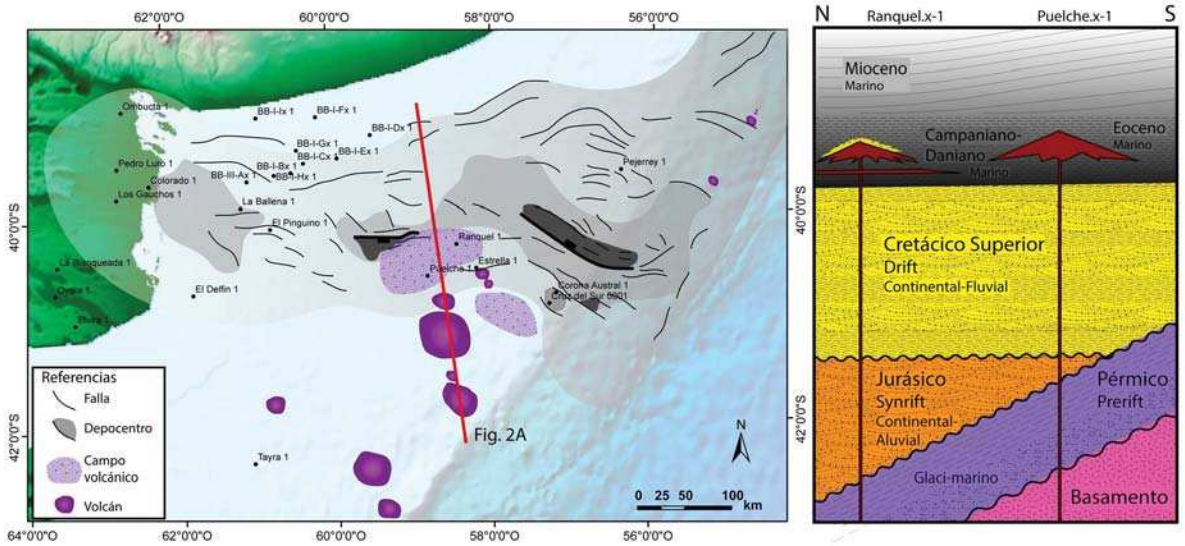

Figura 1. a) Mapa de la cuenca del Colorado, mostrando los principales depocentros y el desarrollo del campo volcánico de Ranquel en el flanco sur de la cuenca: b) Esquema geológico del flanco Sur de la cuenca del Colorado, en la zona investigada por los pozos Puelche y Ranquel.

nibles, que se interpretaron como posibles arrecifes. Sin embargo, al ser perforadas, dichas anomalías resultaron ser cuerpos volcánicos formados por basaltos, aglomerados volcánicos, tobas y hialoclastitas, que fueron denominadas Formación Ranquel (Lesta et al. 1978). Las dataciones K/Ar de basaltos del pozo Ranquel arrojaron una edad de 66 ± 3 Ma (Linares 1977), mientras que se obtuvo una edad de 70 ± 3 Ma para un basalto del pozo Puelche (Linares 1978). Ambas edades se muestran en la correlación de la Figura 3. Recientemente, Pángaro y Ramos (2012) presentaron un mapa de la distribución del campo volcánico de Ranquel, en un trabajo donde discuten la influencia de la fábrica del basamento en la evolución de la cuenca.

METODOLOGÍA

Se llevó a cabo la interpretación de toda la información sísmica de reflexión TWT 2D disponible, calibrada con datos de los pozos Puelche y Ranquel (Fig. 1). Como complemento se generó un atributo sísmico similar a TecVA (Bulhões y Amorin 2005) para las líneas de interés, a través del cálculo del atributo instantáneo de la envolvente de la señal compleja (obtenida por medio de la transformada de Hilbert), luego se rotó la fase para llevarla de fase cero a mínima, y finalmente se sumaron la sección sísmica original con la resultante del proceso mencionado. Por otro lado, se correlacionaron los perfiles eléctricos de los sondeos, se describieron coronas, redescribieron cortes delgados disponibles en el Archivo Técnico de YPF y se realizaron análisis químicos y dataciones Ar/Ar de muestras de basaltos de los pozos Puelche y Ranquel.

RESULTADOS

Dado que el campo volcánico se encuentra completamente cubierto por sedimentos cenozoicos, la interpretación sísmica resulta una herramienta fundamental para extender el conocimiento del evento volcánico de Ranquel en el subsuelo. El trabajo con información de subsuelo permitió generar un nuevo mapa del campo volcánico de Ranquel que se presenta en la Figura 1.

El alto contraste de impedancia al tope de las volcanitas (cubiertas por areniscas o pelitas marinas terciarias) facilitó la interpretación. Los cuerpos volcánicos presentan una arquitectura variable. En posiciones más internas del depocentro (pozos Puelche y Ranquel), se observa una acumulación más mantiforme, con presencia de algunos cuerpos volcánicos encima que presentan un relieve positivo (Fig. 2B). Estos cuerpos corresponden al campo volcánico de Ranquel que tiene un área de 500 km^2. Está compuesto mayormente por tobas y cubiertos por una delgada capa de basalto en la posición de los pozos.

A pesar de la escasa cobertura sísmica, hacia el borde sur del depocentro, sobre el Alto de Rawson, se detectaron grandes aparatos volcánicos con diámetros de hasta 40 km y relieves de unos 400 m, (500 ms TWT) emplazados sobre el paleo-fondo oceánico y posteriormente cubiertos por sedimentos marinos (con geometría de *onlap*). Se detectaron al menos ocho conos volcánicos sobre el Alto de Rawson, a partir de información sísmica que se vuelve más escasa al salir del ámbito de los depocentros. También se observaron conos volcánicos, aunque de menores dimensiones, en intervalos estratigráficos equivalentes en sísmica sobre el margen norte de la cuenca (al este del pozo Pejerrey, Fig. 1).

La correlación realizada entre los pozos Puelche.x-1

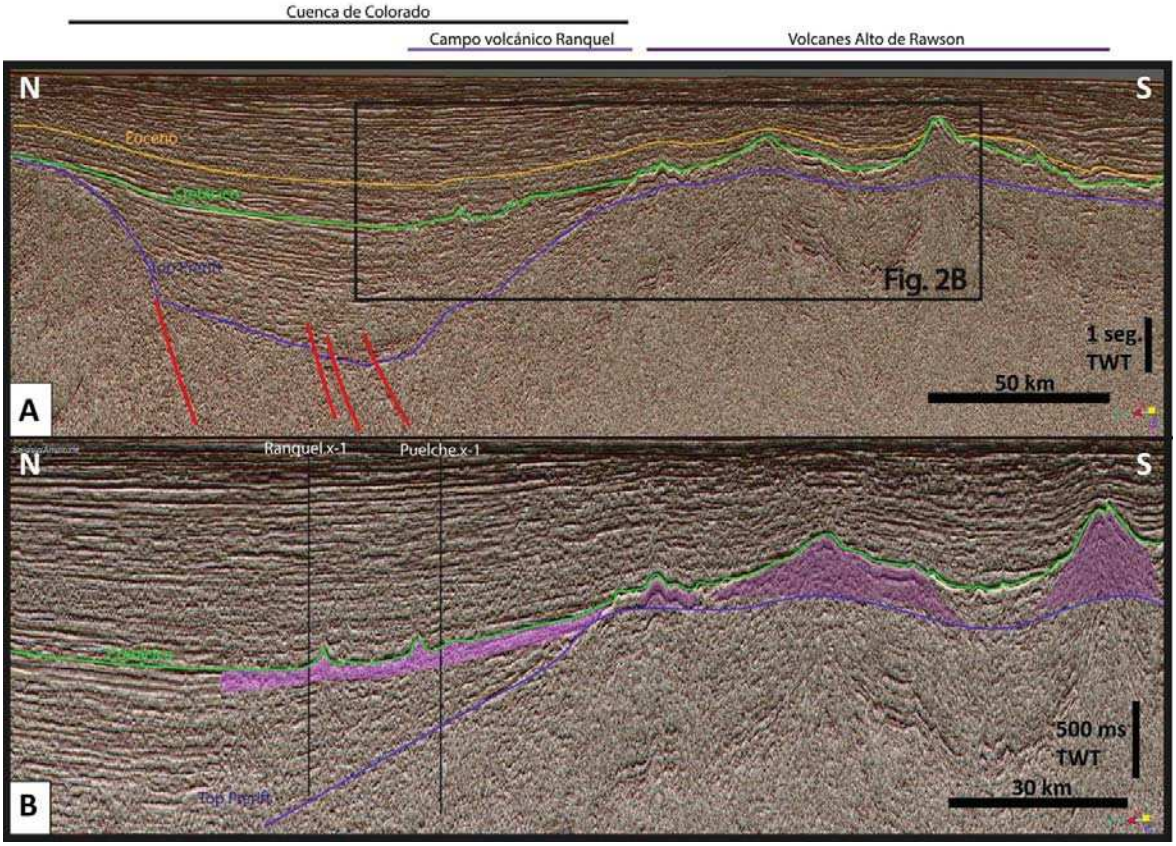

Figura 2. a) Línea sísmica 2D (atributo TecVA) mostrando el desarrollo del campo volcánico de Ranquel en el flanco sur de la cuenca de Colorado y la extensión hacia el sur sobre el Alto de Rawson. Véase ubicación en Fig. 1. b) Zoom sobre la figura 2a donde se resaltaron las formas correspondientes a los cuerpos volcánicos; se muestran también los pozos Puelche y Ranquel proyectados.

y Ranquel.x-1 (Fig. 3) muestra que en el pozo Ranquel las secuencias volcánicas se encuentran a cotas estructurales más bajas que en Puelche dado que el depocentro profundiza hacia el norte (Fig. 1). Las facies volcánicas y volcaniclásticas de la Formación Ranquel apoyan sobre las pelitas transgresivas de la Formación Pedro Luro (Campaniano-Daniano) y son cubiertas por sedimentos eocenos, por lo que su edad queda comprendida entre el Campaniano y el Eoceno. La facies mejor desarrollada en la zona de los pozos es la de tobas, que presentan colores gris verdosos a blanquecinos y son a veces arenosas. El tope de la Formación Ranquel en ambos pozos se caracteriza por una capa de basalto amigdaloide, que en Puelche se intercala con facies de aglomerados volcánicos con extraclastos, venillas rellenas por calcita. En la zona de los pozos, la Formación Ranquel presenta espesores totales del orden de 350 m (Fig. 3).

Petrografía

Un corte delgado de testigo corona del pozo Puelche (1587 m MD *(measured depth)* se describió como un basalto con olivino, compuesto por microfenocristales de clinopiroxeno (augita) y olivino con rebordes de óxido de hierro o reemplazo total por óxido y alteración a calcita, en una pasta con microcristales de plagioclasa prismática intercrecida con piroxeno, óxido de hierro y minerales opacos indiferenciados, vidrio volcánico intersticial recristalizado o alterado a clorita, y epidoto como alteración de cristales y de minerales de la pasta.

Para el pozo Ranquel.x-1 se analizaron tres cortes delgados de la corona situada entre 1816 y 1826 m MD, en los que pudieron identificarse procesos de interacción lava-sedimento a partir de la observación de contactos irregulares entre una roca volcánica básica amigdaloide alterada, clasificada petrográficamente como basalto y una sedimentita muy fina micritizada. En el contacto entre ambas facies son abundantes las autobrechas, engolfamientos, proyecciones del basalto dentro del sedimento, además de vesículas irregulares con rellenos de calcita microcristalina, minerales secundarios y posible sedimento alterado. Además, en el sedimento se observaron clastos juveniles de volcanitas. Una muestra presenta además vidrio volcánico de color amarillento, brechado, perlitizado y alterado, con rebordes teñidos por óxidos, que se interpretó como una hialoclastita (Fig. 4a y b).

Las sedimentitas que forman parte de las peperitas son *mudstones* micríticos (posiblemente producidos por

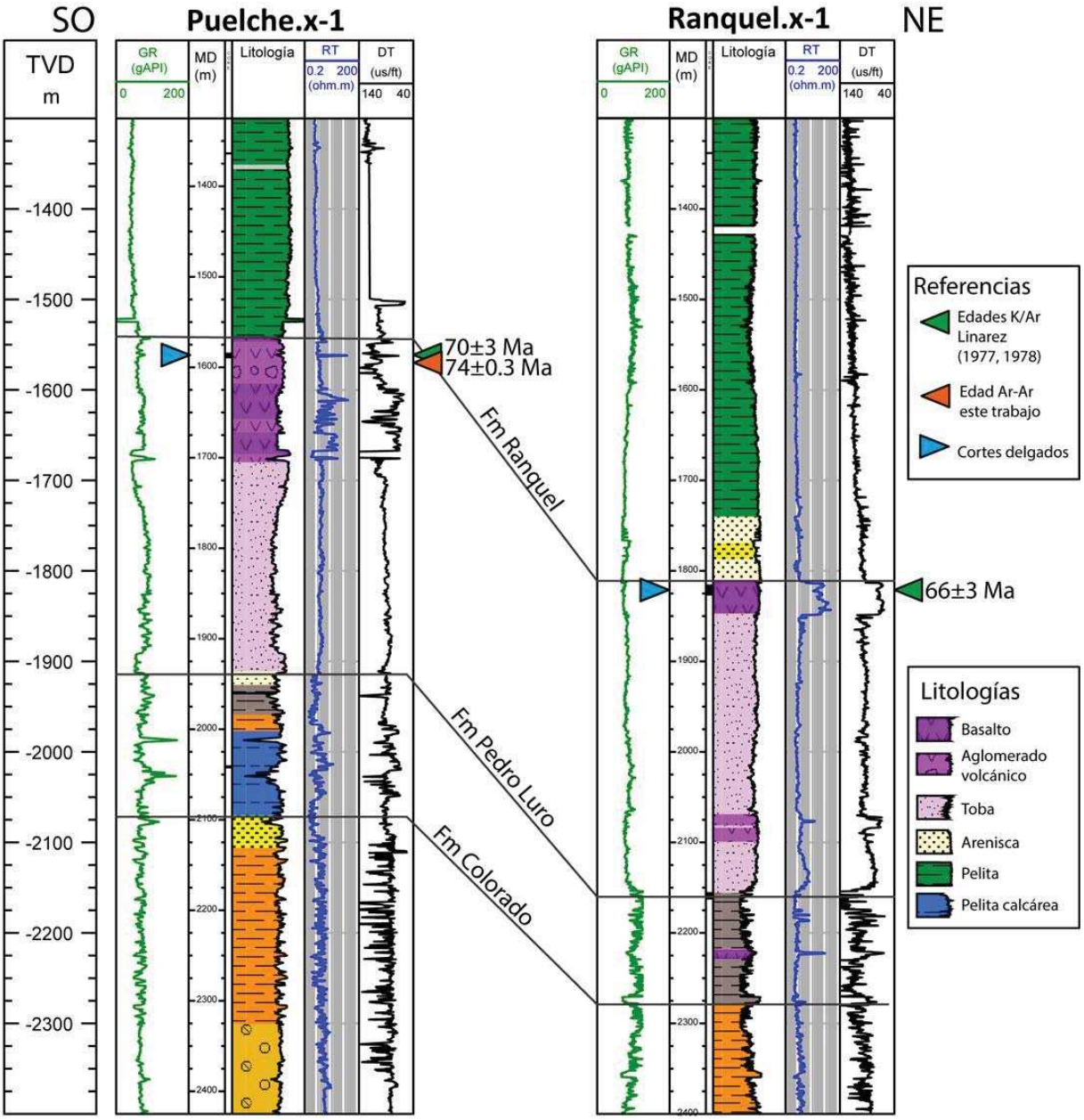

Figura 3. Correlación de los pozos Puelche y Ranquel, en el flanco sur de la cuenca de Colorado. Véase ubicación de los pozos en Fig. 1.

alteración de fangolitas [Scholle 1978], Fig. 4a) y bioclásticos (Fig. 4b y c), donde se reconocieron foraminíferos, briozoarios, braquiópodos; ostrácodos, pelecípodos y posibles intraclastos carbonáticos reemplazados por calcita y fosfatos, clastos de vidrio volcánico alterado y clastos juveniles oscuros vesiculares. Los bioclastos retransportados y mezclados reconocidos en estas sedimentitas permiten interpretar que estos procesos se originaron en aguas poco profundas cercanas a la costa.

La íntima asociación de rocas sedimentarias marinas con basaltos reconocidas en el pozo Ranquel conformando peperitas, evidencia la mezcla mecánica de lava basáltica con sedimento húmedo (Skilling et al. 2002), en coincidencia con las observaciones realizadas por Menzel (1977). Este mecanismo origina las abundantes amígdalas irregulares, ameboidales rellenas por sedimentos dentro del basalto, las vesículas en las rocas sedimentarias, los vidrios perlitizados y los clastos juveniles.

Geoquímica

Una muestra tomada de facies extrusivas de un testigo corona del pozo Puelche (1588 m MD) se hizo analizar geoquímicamente para elementos mayoritarios, minoritarios y trazas (DTP Laboratorios 2014). Los resultados indican una composición de traquiandesita, en la se-

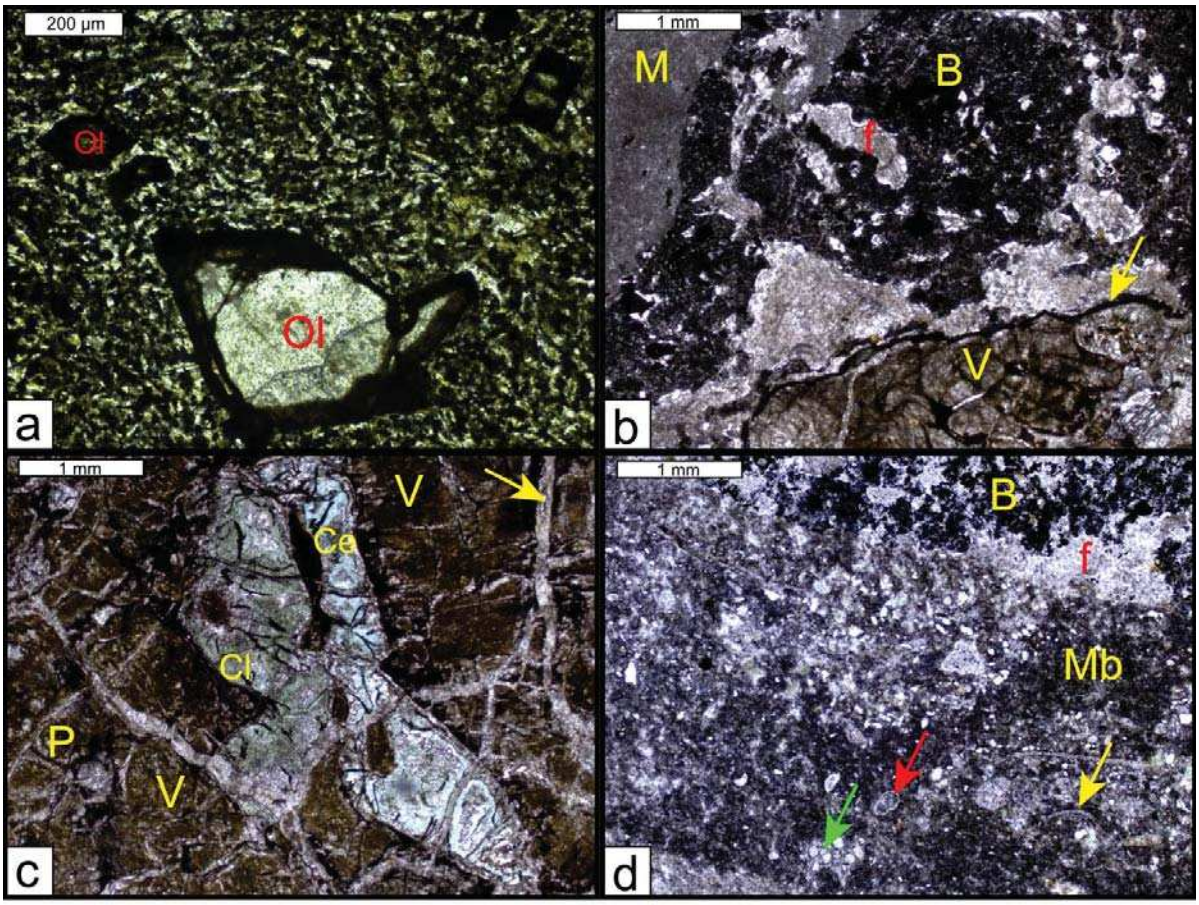

Figura 4. a) Puelche.x-1, 1587 m MD: Basalto, microfenocristales de olivino (Ol) con borde de óxidos de hierro, a veces alterados a óxidos en pasta afanítica con microlitos de plagioclasa, vidrio alterado, piroxeno y óxidos (nicoles cruzados). b) Ranquel.x-1, 1824,1 m MD: Peperita, detalle del contacto entre vidrio volcánico perlitizado (V), lava básica amigdaloide con forma globular y engolfamientos (B) y sedimentita muy fina micritizada (M); reborde de óxidos en el vidrio sobreenfriado (flecha), amígdalas por fluidización (f), nicoles paralelos (n.p.). c) Ranquel.x-1 1824,1 m MD: Hialoclastita, vidrio volcánico teñido por óxido y perlitizado (V) con fracturas rellenas por calcita (flecha), alteración a clorita (Cl) y celadonita (Ce) y fracturas perlíticas (P), n.p. d) Ranquel.x-1 1824,1 m MD: Peperita, contacto irregular entre lava básica sobreenfriada, engolfada (B) y mudstone bioclástico (Mb), fluidización (f), granos de feldespato y bioclastos: briozoarios (flecha verde), foraminíferos (flecha roja), pelecípodos (flecha amarilla), n.p.

rie alcalina (diagrama TAS, Fig. 5a). El diagrama de Wood (1980) permite caracterizar su origen como basalto alcalino de intraplaca (Fig. 5b).

Al representar la composición de la muestra en el diagrama de tierras raras (Fig. 5c) puede observarse que la misma presenta una distribución que se asemeja a la de los basaltos de islas oceánicas (OIB), salvo por mayores valores de Rb, Ba y K; y menores concentraciones de tierras raras pesadas.

La misma muestra del pozo Puelche (1588m MD) arrojó una edad de 74 ± 0,3 Ma al ser datada por el método $^{40}Ar/^{39}Ar$ (DTP Laboratorios 2015). Dicha edad corresponde al Campaniano, sin embargo, determinaciones micropaleontológicas recientes realizadas en las tobas que infrayacen al basalto datado, indicarían edades potencialmente más jóvenes (Maastrichtianas). Futuros trabajos podrán esclarecer la edad precisa del volcanismo y sus distintos pulsos. Es interesante destacar que en el Atlántico Sur existen otras localidades con volcanismo de la misma época. Particularmente se han encontrado edades similares en el Alto de Río Grande (Geraldes et al. 2013), relacionadas genéticamente a la pluma de Tristan da Cunha que presenta un quimismo similar a las volcanitas de este trabajo (Wood 1980).

CONCLUSIONES

La cuenca de Colorado presenta en su flanco sur un extenso campo volcánico de edad campaniana-daniana. El mismo fue investigado por dos pozos exploratorios en 1977 a partir de los cuales se definió la Formación Ranquel (Lesta et al. 1978), una secuencia volcánica-volcaniclástica de 350 m de espesor (en la zona de los sondeos). La geoquímica permitió caracterizar las rocas afaníticas como traquiandesitas, que tendrían un origen asociado a basaltos alcalinos de intraplaca. La petrogra-

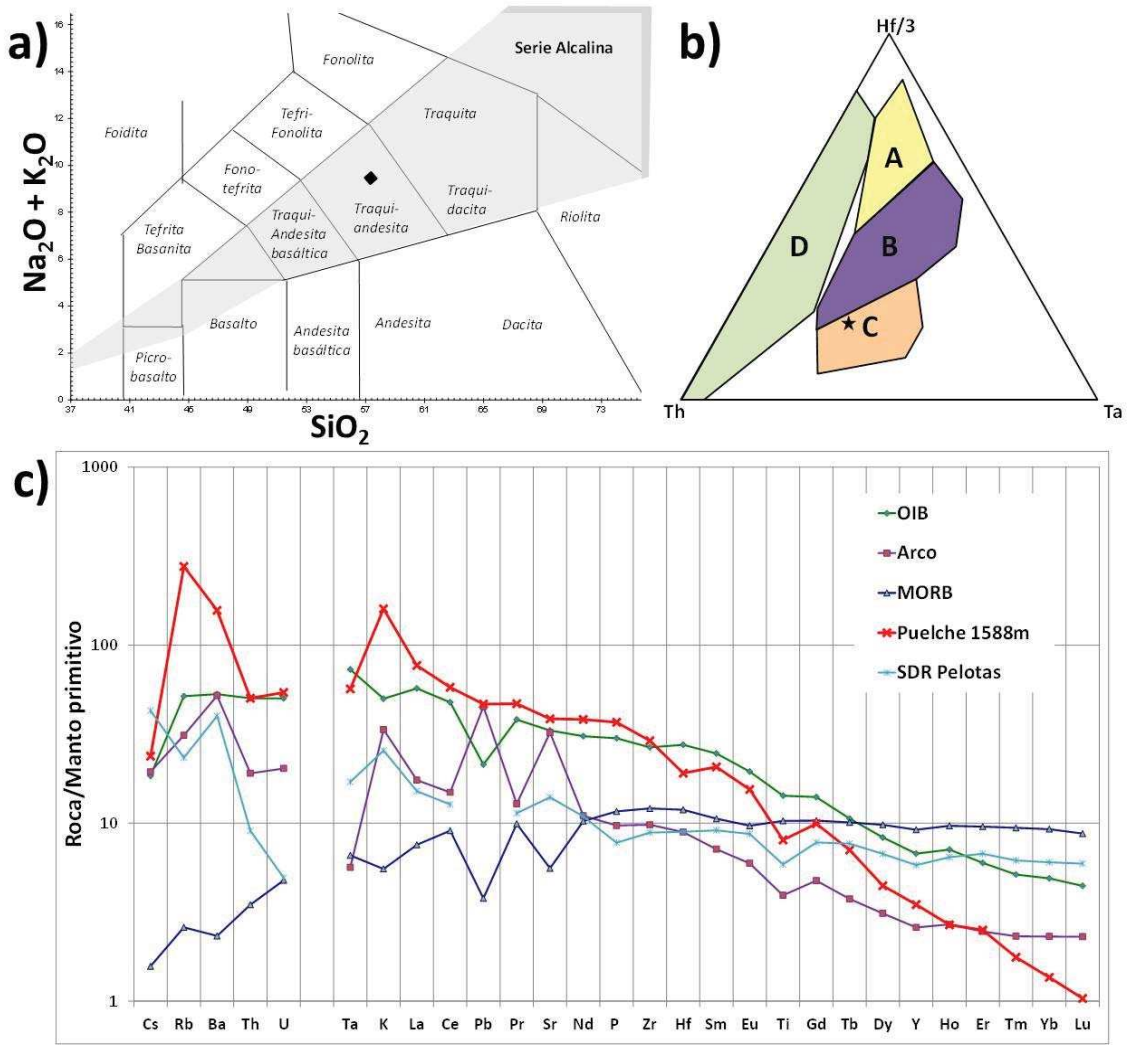

Figura 5. a) Diagrama TAS: la muestra del pozo Puelche (1588 m MD) cae en el campo de las traquiandesitas. b) Diagrama de Wood (1980), A: MORB tipo N, B: MORB tipo E y basaltos toleíticos de intraplaca, C: basaltos alcalinos de intraplaca, D: basaltos de márgenes convergentes. c) Distribución de REE normalizado a manto primitivo para distintos arquetipos de rocas volcánicas: OIB (Ocean Island Basalt), Arco magmático, MORB (MidOcean Ridge Basalt), SDR (Seaward Dipping Reflectors) de la cuenca de Pelotas, y la comparación con la muestra del pozo Puelche (1588 m MD).

fía muestra procesos de interacción lava-sedimento, con producción de peperitas, facies que se relacionan a volcanismo subácueo consistente con el momento de transgresión marina que sufría la cuenca de Colorado al momento de la instalación del volcanismo.

AGRADECIMIENTOS

Los autores agradecen a YPF S.A. la posibilidad de presentar estos datos, a Guadalupe Hernández Fuda por su colaboración en la preparación del mapa y a Juan Presta por sus comentarios y recomendaciones.

LISTA DE TRABAJOS CITADOS EN EL TEXTO

Bulhões, E.M. y Amorim, W.N. 2005. Princípio da SismoCamada Elementar e sua aplicação à técnica de volume de amplitudes (tecVA). Ninth International Congress of the Brazilian Geophysical Society: 1382-1387, Salvador.

DTP Laboratorios 2014. Geoquímica de rocas volcánicas de la cuenca del Colorado. Pozos Ranquel.x-1 y Puelche.x-1. Informe preparado para YPF, 16 p., Buenos Aires.

DTP Laboratorios 2015. Edades Argón-Argón en testigos de pozos Puelche y Ranquel, cuenca del Colorado, Argentina. Informe preparado para YPF, 14 p., Buenos Aires.

Geraldes, M.C., Motoki, A., Costa, A. Mota, C.A. y Mohriak, W.U. 2013. Geochronology (Ar/Ar and K-Ar) of the South Atlantic post-break-up magmatism. En: Mohriak, W.U., Post, P.J., Brown, D.E., Tari, G.C., Nemcok, M. y Sinha, S.T. (Eds.) Conjugate Divergent Margins. Geological Society of London Special Publications 369: 41-74.

Gerster, R., Welsink, H., Ansa, A. y Raggio, F. 2011. Cuenca de Colorado. En Simposio de Cuencas Argentinas: visión actual, 8º Congreso de Exploración y Desarrollo de Hidro-

carburos: 65-80, Buenos Aires.

Lesta, P.J., Turic, M.A. y Mainardi, E. 1978. Actualización de la información estratigráfica en la Cuenca del Colorado. 7º Congreso Geológico Argentino, Actas 1: 701-713, Neuquén.

Linares, E. 1977. Informe sobre datación radimétrica del pozo Ranquel. Instituto de Geocronología y Geología Isotópica. Universidad de Buenos Aires, inédito, 1 p., Buenos Aires.

Linares, E. 1978. Informe sobre datación radimétrica del pozo Puelche. Instituto de Geocronología y Geología Isotópica. Universidad de Buenos Aires, inédito, 1 p., Buenos Aires.

Lovecchio, J.P., Rohais, S., Ramos, V.A. y Joseph, P. 2016. Evolución de la cuenca de Colorado: rifting multi-episódico en el contexto de la ruptura de Gondwana. VI Jornadas de Geociencias de YPF, 1 p., Buenos Aires

Menzel, M. 1977. Estudio petrográfico de testigos del pozo YPF CCMI.Ra.es-1. Informe interno de YPF, 10 p., Buenos Aires.

Pangaro, F. y Ramos, V.A. 2012. Paleozoic crustal blocks of onshore and offshore central Argentina: New pieces of the southwestern Gondwana collage and their role in the accretion of Patagonia and the evolution of Mesozoic South Atlantic sedimentary basins. Marine and Petroleum Geology 37: 162–183.

Scholle, P. 1978. A color illustrated guide to carbonate rock constituents, textures, cements, and porosities. AAPG Memoir 27, 241 p., Tulsa

Skilling, I., White, J.D.I. y Mcphie, J. 2002. Peperite. Processes and products of magma – sediment mingling. Elsevier, 255 p., Amsterdam

Wood, D.A. 1980. The application of a Th-Hf-Ta diagram to problems of tectonomagmatic classification and to establishing the nature of crustal contamination of basaltic lavas of the British Tertiary Volcanic Province. Earth and Planetary Science Letters, 50: 11-30